PB82-230715

Effects of Fuel Properties and Atomization Parameters on NOx Control for Heavy Liquid Fuel Fired Package Boilers

Energy and Environmental Research Corp.
Santa Ana, CA

Prepared for

Industrial Environmental Research Lab.
Research Triangle Park, NC

Apr 82

U.S. Department of Commerce
National Technical Information Service
NTIS

EPA 600/7-82-029
April 1982

PB82-230715

EFFECTS OF FUEL PROPERTIES AND ATOMIZATION PARAMETERS ON NO_x CONTROL FOR HEAVY LIQUID FUEL FIRED PACKAGE BOILERS

Prepared for

W. S. Lanier

U. S. Environmental Protection Agency
Research Triangle Park, NC 27711

FINAL REPORT

EPA Contract No.68-02-2624

Prepared by

G. C. England
D. W. Pershing
M. P. Heap
J. E. Cichanowicz

Energy and Environmental Research Corporation
8001 Irvine Boulevard
Santa Ana, California 92705

REPRODUCED BY
NATIONAL TECHNICAL
INFORMATION SERVICE
U.S. DEPARTMENT OF COMMERCE
SPRINGFIELD, VA. 22161

TECHNICAL REPORT DATA

(Please read Instructions on the reverse before completing)

1. REPORT NO. EPA-600/7-82-029

2. ORD Report

3. RECIPIENT'S ACCESSION NO. PB82 230715

4. TITLE AND SUBTITLE **Effects of Fuel Properties and Atomization Parameters on NOx Control for Heavy Liquid Fuel Fired Package Boilers**

5. REPORT DATE April 1982

6. PERFORMING ORGANIZATION CODE

7. AUTHOR(S) G. C. England, D. W. Pershing, M. P. Heap, and J. E. Cichanowicz

8. PERFORMING ORGANIZATION REPORT NO.

9. PERFORMING ORGANIZATION NAME AND ADDRESS
Energy and Environmental Research Corporation
8001 Irvine Boulevard
Santa Ana, California 92705

10. PROGRAM ELEMENT NO.

11. CONTRACT/GRANT NO. 68-02-2624

12. SPONSORING AGENCY NAME AND ADDRESS
EPA, Office of Research and Development
Industrial Environmental Research Laboratory
Research Triangle Park, NC 27711

13. TYPE OF REPORT AND PERIOD COVERED Final; 1/77-1/79

14. SPONSORING AGENCY CODE EPA/600/13

15. SUPPLEMENTARY NOTES IERL-RTP project officer is W. Steven Lanier, Mail Drop 65, 919/541-2432.

16. ABSTRACT
The report gives information necessary for development and generalization of low-NOx oil burner technology for package firetube boilers. It gives results of experiments at two scales: 20 kW and 1.08 MW heat input. At 20 kW, effects of fuel properties were examined in tests of 3 distillate oils, 13 petroleum-derived residual fuel oils, 3 alternate liquid fuels, and 14 doped and/or blended liquid fuels. The tests included systematic variation of excess air and drop size distribution, normal and staged combustion conditions, and separation of fuel NOx from total NOx. At 1.08 MW, experiments concentrated on the interaction between spray characteristics and the combustion aerodynamic flowfield. Spray characteristics were varied by using different commercial atomizing nozzles and by adjusting nozzle operating conditions. Combustion flowfield was varied by modifying the swirl level on the combustion air. The 1.08 MW tests also examined fuel property, flue gas recirculation, and staged combustion effects on NOx and smoke emissions. Test results at both scales indicate a strong influence of fuel properties, atomization quality, and mixing characteristics on NOx emissions. They also show that each of these parameters interacts in a complex manner; e.g., increased drop size decreases NOx for fuel-lean combustion, but increases NOx for staged combustion. Further testing is needed.

17. KEY WORDS AND DOCUMENT ANALYSIS

a. DESCRIPTORS		b. IDENTIFIERS/OPEN ENDED TERMS	c. COSATI Field/Group	
Pollution	Oil Burners	Pollution Control	13B	
Fire Tube Boilers	Nozzles	Stationary Sources	13A	13G
Nitrogen Oxides	Atomizing	Staged Combustion	07B	13H,07A
Smoke	Drops (Liquids)		21B	07D
Combustion	Stoichiometry			
Residual Oils	Swirling		21D,11H	

18. DISTRIBUTION STATEMENT Release to Public

19. SECURITY CLASS *(This Report)* Unclassified

20. SECURITY CLASS *(This page)* Unclassified

21. NO. OF PAGES

22. PRICE

EPA Form 2220-1 (9-73)

TYPING GUIDE SHEET
BEGIN FIRST LINE OF TEXT HERE
CENTER OF PAGE
TOP OF IMAGE AREA
DROPPED HEAD: BEGIN SECTIONS HERE

ABSTRACT

This report provides information necessary for development and generalization of low NO_x oil burner technology for package firetube boilers. Results are reported from experimental studies conducted at two scales (20 kW and 1.08 MW heat input). In the small scale studies, effects of fuel properties were examined in tests of three distillate oils, thirteen petroleum derived residual fuel oils, three alternate liquid fuels and fourteen doped and/or blended liquid fuels. These tests included systematic variation of excess air and drop size distribution, normal and staged combustion conditions as well as separation of fuel NO_x from total NO_x. In the larger scale tests, experimentation concentrated on the interaction between spray characteristics and the combustion aerodynamic flowfield. Spray characteristics were varied by using different commercial atomizing nozzles and by adjusting the nozzle operating conditions. Combustion flowfield variation was achieved by modifying the swirl level on the combustion air. The large scale tests also examined fuel property effects, flue gas recirculation and staged combustion effects on NO_x and smoke emissions. Results from testing at both scales indicate a strong influence of fuel properties, atomization quality and mixing characteristics on NO_x emissions. Further, it is shown that each of these parameters interacts in a complex manner. For example, increased drop size decreases NO_x for fuel lean combustion, but increases NO_x for staged combustion conditions. The need for further testing, especially under staged combustion conditions, is indicated.

BEGIN LAST LINE OF TEXT
BOTTOM OF IMAGE AREA; OUTSIDE DIMENSION FOR TABLES AND ILLUSTRATIONS
3/8"

PAGE NUMBER
EPA-287 (Cin.)
(4-76)

TABLE OF CONTENTS

Section		Page
1.0	INTRODUCTION	1-1
	1.1 Background	1-1
	1.2 Purpose and Scope	1-3
	1.3 Overall Approach	1-4
	1.4 Report Organization	1-5
	References	**1-7**
2.0	PILOT-SCALE ATOMIZER SELECTION	2-1
	2.1 Summary	2-1
	2.2 The Influence of Atomizer Design on Pollutant Emissions	2-1
	2.3 Atomizer Selection	2-10
	2.4 Atomizer Characterization	2-18
3.0	FUEL SELECTION	3-1
	3.1 Summary	3-1
	3.2 Fuel Selection Criteria	3-3
	3.3 Characteristics of the Fuels Tested	3-8
4.0	SMALL-SCALE RESULTS	4-1
	4.1 Summary	4-1
	4.2 Combustion Facility	4-4
	4.3 Results - Excess Air Conditions	4-11
	4.4 Results - Staged Combustion Conditions	4-78
	References	**4-106**
5.0	PILOT-SCALE STUDIES	5-1
	5.1 Summary	5-1
	5.2 Experimental Systems	5-2
	5.3 Phase I Investigations - Problem Definition	5-9
	5.4 Phase II Experimental Results	5-39
6.0	CONCLUSIONS	6-1
	6.1 Fuel Properties	6-1
	6.2 Flow Field Effects	6-1

TABLE OF CONTENTS (Cont.)

Section	Page
APPENDIX I - Atomizer Characterization	A1-1
1.0 INTRODUCTION	A1-1
2.0 EXPERIMENTAL SYSTEMS	A1-2
2.1 Spray Rig	A1-2
2.2 Laser Diffraction Droplet Size Analysis	A1-5
2.3 Physical Limitations	A1-10
2.4 Velocity Effects	A1-14
3.0 ATOMIZER CHARACTERISTICS	A1-20
3.1 Mass Distribution and Shape of the Spray	A1-20
3.2 Droplet Size Distribution	A1-27
3.3 Axial Distance Effect	A1-48
4.0 DISCUSSION	A1-64
4.1 Spray Shape and Mass Distribution	A1-64
4.2 Air Pressure and Oil Flow Effect of Spray Characteristics	A1-64
4.3 Actual Droplet Size Distribution in Operating Conditions	A1-68
4.4 Axial Distance Effect	A1-68
4.5 Suitability of the Laser Diffraction Technique for Spray Analysis	A1-77
5.0 GENERAL CONCLUSIONS	A1-81
References	A1-82
APPENDIX II - Liquid Fuel Characteristics	A2-1
1.0 TRENDS IN LIQUID FUEL USAGE	A2-1
2.0 MODERN REFINERY PRACTICE	A2-2
3.0 FUEL OIL CHARACTERIZATION	A2-7

LIST OF TABLES

Table		Page
1-1	Conversion of English Units to SI Units	1-6
2-1	Classification of Commercial Atomizers	2-13
3-1	Summary of Fuels Tested	3-2
3-2	Liquid Fuels Tested	3-9
4-1	Analytical Instrumentation	4-11
5-1	Atomizers which were Selected for this Study and the Test Conditions for Each	5-41
5-2	Test Matrix for Fuel Composition Effects Test Series	5-100
5-3	Summary of Experimental Conditions - Staged Combustion Studies	5-137

LIST OF FIGURES

Figure		Page
2-1a	Typical Package Boiler Burners - Firetube Boiler Burner.	2-2
2-1b	Typical Paciage Boiler Burners - Register Burner for Watertube Boilers.	2-3
2-2	Effect of Oil Atomization Method and Excess Oxygen Level on the Total Nitrogen Oxides Emissions. (After Cato et al[7])	2-5
2-3	(a) NO_x and Smoke Emissions as a Function of Excess Air Level and Atomization Medium and (b) The Influence of Atomization Fluid and Pressure Pollutant Emissions from Oil Flames (17 percent Excess Air, 3.4 X 10^6 Btu/hr).	2-6
2-4	(a) Emission Characteristics of Fuel Oil Flames (5 percent Excess Air, 300°C Preheat, Primary Swirl Vanes 30°) and (b) The Effect of Fuel Oil Temperature on NO_x Emissions.	2-7
2-5	(a) Dropsize Distribution for the Atomizers used in Figure b (b) Solid Emissions from a Refinery Heater as a Function of Fuel Load.	2-9
2-6	Droplet Size Distribution in Operating Conditions for Six Atomizers.	2-19

LIST OF FIGURES

Figure		Page
3-1	Major Sources of Residual Fuel Oil Supply for the U.S. by P.A.D. Districts.	3-4
3-2	Fuel Nitrogen Versus Sulfur Content.	3-13
3-3	Fuel Nitrogen Versus API Gravity.	3-14
3-4	Fuel Nitrogen Versus C/H Ratio.	3-15
3-5	Fuel Nitrogen Versus Asphaltene Content.	3-16
3-6	Vacuum Distillation Results - Mass Evolved.	3-19
3-7	Vacuum Distillation Results - Nitrogen Evolved.	3-20
3-8	Viscosity of Fuels Tested.	3-21
3-9	DTA Analysis of Eight Fuel Oils.	3-22

LIST OF FIGURES

Figure		Page
4-1	Details of the Tunnel Furnace System.	4-5
4-2	Cross Section Drawing of Furnace.	4-6
4-3	Flow System.	4-8
4-4	New Oil Gun.	4-10
4-5	Emissions from Pure Fuels Burned in $Ar/O_2/CO_2$.	4-12
4-6	Kinetic Modeling Predictions on the Effect of $Ar/O_2/CO_2$ Under Fuel-Rich Conditions.	4-14
4-7	Influence of Oxidant Composition on Response of Chemiluminescent Analyzer.	4-15
4-8	Comparison of Fuel NO_x Determination Methods - Distillate Oil.	4-17
4-9	Comparison of Fuel NO_x Determination Methods - Residual Oil.	4-18
4-10	Typical Data on Fuel and Thermal NO_x.	4-19
4-11	Influence of Excess O_2 - Alaskan Diesel.	4-21
4-12	Influence of Excess O_2 - West Texas Diesel.	4-22
4-13	Influence of Excess O_2 - California No. 2.	4-23
4-14	Influence of Fuel Sulfur on Fuel and Thermal NO_x Formation.	4-24
4-15	Influence of Excess O_2 - 0.36% N, 2.43% S Doped Distillate.	4-25
4-16	Influence of Excess O_2 - 0.8% N Doped Distillate.	4-26
4-17	Influence of Excess O_2 - 0.76% N, 2.3% S Doped Distillate.	4-27
4-18	Influence of Excess O_2 - 1.2% N Doped Distillate.	4-28
4-19	Influence of Excess O_2 - 1.14% N, 2.3% S Doped Distillate.	4-29
4-20	Essex County Oil - Standard Test Conditions.	4-31
4-21	Middle Eastern Oil - Standard Test Conditions.	4-32

LIST OF FIGURES

Figure		Page
4-22	Low Sulfur Oil - Standard Test Conditions.	4-33
4-23	Indo/Malaysian Oil - Standard Test Conditions.	4-34
4-24	Desulfurized Venezuelan Oil - Standard Test Conditions.	4-35
4-25	Pennsylvania Oil - Standard Test Conditions.	4-36
4-26	Gulf Coast Oil - Standard Test Conditions.	4-37
4-27	Venezuelan Oil - Standard Test Conditions.	4-38
4-28	Alaskan North Slope Oil - Standard Test Conditions.	4-39
4-29	California Oil #1 - Standard Test Conditions.	4-40
4-30	California Oil #2 - Standard Test Conditions.	4-41
4-31	California Oil #3 - Standard Test Conditions.	4-42
4-32	California Oil #4 - Standard Test Conditions.	4-43
4-33	Desulfurized Venezuelan Oil Doped to Simulate the Venesuelan Oil.	4-45
4-34	Desulfurized Venesuelan Oil Doped to Simulate the Alaskan Oil.	4-46
4-35	Desulfurized Venesuelan Oil Doped to 0.80% N.	4-47
4-36	Desulfurized Venesuelan Oil Doped to Simulate the California Oils.	4-48
4-37	DFM - Standard Test Conditions.	4-49
4-38	Crude Shale Oil - Standard Test Conditions.	4-50
4-39	75% Shale Blend - Standard Test Conditions.	4-51
4-40	50% Shale Blend - Standard Test Conditions.	4-52
4-41	26% Shale Blend - Standard Test Conditions.	4-53
4-42	90% Synthoil Blend - Standard Test Conditions.	4-54
4-43	80% Synthoil Blend - Standard Test Conditions.	4-55

LIST OF FIGURES

Figure		Page
4-44	Influence of Excess O_2 - Methane Doped with NH_3.	4-57
4-45	Effect of Excess O_2 on Fuel NO_x.	4-58
4-46	Effect of Excess O_2 on Total NO_x.	4-60
4-47	Effect of Fuel Nitrogen Content on Total and Fuel NO_x.	4-61
4-48	Effect of Fuel Nitrogen Content on Percent Conversion to NO_x.	4-62
4-49	Composite Fuel Nitrogen Conversion to NO_x as a Function of Fuel Nitrogen Content.	4-64
4-50	Results of Shale Oil Blending Studies.	4-66
4-51	Thermal NO_x vs. API Gravity.	4-67
4-52	Influence of Fuel Viscosity - Middle Eastern Oil.	4-68
4-53	Influence of Fuel Viscosity - Indo/Malaysian Oil.	4-69
4-54	Influence of Fuel Viscosity - Desulfurized Venesuelan Oil.	4-70
4-55	Influence of Fuel Viscosity - Gulf Coast Oil.	4-71
4-56	Influence of Bulk Flame Temperature.	4-73
4-57	Droplet Size Distribution Data - Ultrasonic Nozzle Used in the Tunnel Furnace.	4-75
4-58	Influence of Drop Size on Thermal and Fuel NO_x Formation - Shale Oil.	4-76
4-59	The Effect of Drop Size on Total and Fuel NO_x Production.	4-77
4-60	Effect of Mean Drop Size on Percent Fuel N Conversion.	4-79
4-61	Effect of Mean Drop Size on Thermal NO_x Formation.	4-80
4-62	Influence of Atomizer Design on Thermal NO_x.	4-81
4-63	Influence of Atomizer Design on Fuel NO_x.	4-82
4-64	Typical Staged Combustion Results.	4-83

LIST OF FIGURES

Figure		Page
4-65	Influence of Primary Zone Stoichiometry.	4-85
4-66	Influence of Primary Zone Residence Time.	4-86
4-67	Staging Results - Alaskan Diesel.	4-88
4-68	Staging Results - Essex County Oil.	4-89
4-69	Staging Results - Indo/Malaysian Oil.	4-90
4-70	Staging Results - Port 4 - Gulf Coast Oil.	4-91
4-71	Staging Results - Port 8 - Gulf Coast Oil.	4-92
4-72	Staging Results - Alaskan Oil.	4-94
4-73	Staging Results - Shale Crude.	4-95
4-74	Staging Results - CH_4/NH_3.	4-96
4-75	Influence of Fuel Nitrogen Content on Minimum NO_x Emissions Staged.	4-97
4-76	HCN Yield as a Function of Pyrolysis Temperature.	4-99
4-77	Staging Efficiency and Fuel Nitrogen Volatility.	4-100
4-78	Effect of Drop Size on Staged Emissions - Alaskan Oil.	4-101
4-79	Effect of Mean Drop Size on Minimum Staged Emissions - Indo/Malaysian Oil.	4-103
4-80	Effect of Mean Drop Size on Minimum Staged Emissions - Essex County Oil.	4-104
4-81	Influence of Droplet Size Under Staged-Combustion Conditions.	4-105

LIST OF FIGURES

Figure		Page
5-1	Experimental Firetube Combustor.	5-4
5-2	Multichannel Continuously Variable Swirl Generator - Rear View and Exit Geometry.	5-5
5-3	Multichannel Continuously Variable Swirl Generator - Details.	5-6
5-4	Double Concentric Swirl Burner with Refractory Sleeve.	5-8
5-5	The Effect of Spray Angle on NO_x/Smoke Emissions with Kerosene, HN and LN Air Patterns, Hollow Spray Cone.	5-12
5-6	The Effect of Spray Angel on NO_x/Smoke Emissions with Distillate Fuel; HN and LN Air Patterns, Hollow Spray Cone.	5-13
5-7	The Effect of Spray Angle on NO_x/Smoke Emissions with Doped Distillate Fuel; HN and LN Air Patterns, Hollow Spray Cone.	5-14
5-8	The Effect of Spray Angle on NO_x/Smoke Emissions with No. 6 Fuel; HN and LN Patterns, Hollow Cone Spray.	5-15
5-9	The Effect of Spray Pattern on NO_x/Smoke Emissions for Kerosene Fuel; HN and LN Air Pattern.	5-18
5-10	The Effect of Spray Pattern on NO_x/Smoke Emissions with Distillate Fuel; HN and LN Air Patterns, Hollow and Solid Spray Cone.	5-19
5-11	The Effect of Spray Pattern on NO_x/Smoke Emissions with Doped Distillate Fuel; HN and LN Air Patterns, Hollow and Solid Spray Cones.	5-20
5-12	The Effect of Spray Pattern on NO_x/Smoke Emissions with No. 6 Fuel; HN and LN Air Patterns, Hollow and Solid Spray Cones.	5-21
5-13	The Effect of Nozzle Design Capacity on NO_x/Smoke Emissions with Kerosene; HN Air Pattern.	5-23
5-14	The Effect of Nozzle Design Capacity on NO_x/Smoke Emissions with Kerosene; LN Air Pattern.	5-24
5-15	The Effect of Nozzle Design Capacity on NO_x/Smoke Emissions, Distillate Fuel, HN Air Pattern.	5-25
5-16	The Effect of Nozzle Design Capacity on NO_x/Smoke Emission with Distillate Fuel; LN Air Pattern.	5-26

LIST OF FIGURES

Figure		Page
5-17	The Effect of Nozzle Design Capacity on NO$_x$/Smoke Emission; Doped Distillate Fuel, HN Air Pattern.	5-28
5-18	The Effect of Nozzle Design Capacity on NO$_x$/Smoke Emission with Doped Distillate Fuel, LN Air Pattern.	5-29
5-19	The Effect of Nozzle Design Capacity on NO$_x$/Smoke Emission with No. 6 Fuel; HN Air Pattern.	5-30
5-20	The Effect of Nozzle Size on NO$_x$/Smoke Emission with No. 6 Fuel; LN Air Pattern.	5-31
5-21	The Effect of Nozzle Size on NO$_x$/Smoke Emissions with No. 6 Fuel; High Fuel Temperature.	5-32
5-22	NO$_x$ Emissions from Doped Distillate Fuel; with the Monarch Atomizers; Air Atomization, HN and LN Airflow Patterns.	5-34
5-23	NO$_x$ and Emissions with Doped Distillate Fuel from the Monarch Atomizers; Steam Atomization; HN and LN Airflow Patterns.	5-36
5-24	NO$_x$ Emissions from Residual Fuel Oil with the Monarch Atomizers; Air Atomization; HN and LN Airflow Patterns.	5-37
5-25	NO$_x$ Emissions from Residual Fuel Oil with the Monarch Atomizers; Steam Atomization; HN and LN Airflow Patterns.	5-38
5-26	Atomizer Screening Tests - Sonicore 250T Atomizer with 45° Swirl Vanes.	5-42
5-27	Atomizer Screening Tests - Sonicore 250T Atomizer with 30° Swirl Vanes.	5-43
5-28	Atomizer Screening Tests - Todd CDS Atomizer with 45° Swirl Vanes.	5-44
5-29	Atomizer Screening Tests - Todd CDS Nozzle with 30° Swirl Vanes.	5-45
5-30	Atomizer Screening Tests - Todd CDS Atomizer with 15° Swirl Vanes.	5-46
5-31	Atomizer Screening Tests - Todd CDS Atomizer with 0° Swirl Vanes.	5-47
5-32	Atomizer Screening Tests - Peabody 6-102-55 with 45° Swirl Vanes.	5-48
5-33	Atomizer Screening Tests - Peabody 6-102-55 with 30° Swirl Vanes.	5-49

LIST OF FIGURES

Figure		Page
5-34	Atomizer Screening Tests - Peabody 6-102-55 with 15° Swirl Vanes.	5-50
5-35	Atomizer Screening Tests - Peabody 6-086-55 with 45° Swirl Vanes.	5-51
5-36	Atomizer Screening Tests - Peabody 6-086-55 with 30° Swirl Vanes.	5-52
5-37	Atomizer Screening Tests - Peabody 6-096-55 with 15° Swirl Vanes.	5-53
5-38	Atomizer Screening Tests - Peabody 6-052-70 with 45° Swirl Vanes.	5-54
5-39	Atomizer Screening Tests - Peabody 6-052-70 with 30° Swirl Vanes.	5-55
5-40	Atomizer Screening Tests - Peabody 6-052-70 with 15° Swirl Vanes.	5-56
5-41	Atomizer Screening Tests - Cleaver Brooks with 45° Swirl Vanes.	5-57
5-42	Atomizer Screening Tests - Cleaver Brooks with 15° Swirl Vanes.	5-58
5-43	Atomizer Screening Tests - Delavan "Swirl Air" with 45° Swirl Vanes.	5-59
5-44	Atomizer Screening Tests - Delavan "Swirl Air" with 30° Swirl Vanes.	5-60
5-45	Atomizer Screening Tests - Delavan "Swirl Air" with 15° Swirl Vanes.	5-61
5-46	Atomizer Screening Tests - Delavan "Airo" with 45° Swirl Vanes.	5-62
5-47	Atomizer Screening Tests - Delavan "Airo" with 30° Swirl Vanes.	5-63
5-48	Atomizer Screening Tests - Delavan "Airo" with 15° Swirl Vanes.	5-64
5-49	Atomizer Screening Tests - Delavan "Airo" with 45° Swirl Vanes.	5-65
5-50	Atomizer Screening Tests - Delavan "Airo" with 15° Swirl Vanes.	5-66
5-51	Atomizer Screening Tests - Industrial Combustion with 15° Swirl Vanes.	5-67

LIST OF FIGURES

Figure		Page
5-52	Atomizer Screening Tests - Industrial Combustion with 45° Swirl Vanes.	5-68
5-53	Atomizer Screening Tests - Industrial Combustion with 30° Swirl Vanes.	5-69
5-54	Atomizer Screening Tests - Industrial Combustion with 15° Swirl Vanes.	5-70
5-55	Atomizer Screening Tests - Monarch 30 gph with 30° Swirl Vanes.	5-71
5-56	Atomizer Screening Tests - Monarch 30 gph with 15° Swirl Vanes.	5-72
5-57	Atomizer Screening Tests - Monarch 60 gph with 45° Swirl Vanes.	5-73
5-58	Atomizer Screening Tests - Monarch 60 gph with 30° Swirl Vanes.	5-74
5-59	Atomizer Screening Tests - Monarch 60 gph with 15° Swirl Vanes.	5-75
5-60	Atomizer Screening Tests - Monarch 100 gph with 45° Swirl Vanes.	5-76
5-61	Atomizer Screening Tests - Monarch 100 gph with 30° Swirl Vanes.	5-77
5-62	Atomizer Screening Tests - Monarch 100 gph with 15° Swirl Vanes.	5-78
5-63	Effect of Atomizer with Weak Swirl.	5-80
5-64	Effect of Atomizer with Intermediate Swirl.	5-81
5-65	Effect of Atomizer with Strong Swirl.	5-82
5-66	Effect of Atomizing Pressure - Weak Swirl.	5-83
5-67	Effect of Atomizing Pressure - Strong Swirl.	5-84
5-68	Effect of Atomizing Pressure - Intermediate Swirl.	5-86
5-69	Effect of Atomizing Pressure - Todd CDS Atomizer.	5-87
5-70	Effect of Atomizing Pressure - Monarch 100 gph Atomizer.	5-88
5-71	Effect of Swirl Upon NO_x Emissions.	5-89
5-72	Effect of Swirl - Delavan "Airo" Atomizer.	5-90
5-73	Effect of Swirl - Sonicore 250T Atomizer.	5-91

LIST OF FIGURES

Figures		Page
5-74	Effect of Swirl - Delavan "Swirl Air" Atomizer.	5-92
5-75	Effect of Swirl with Peabody 6-086-55 Atomizer.	5-93
5-76	Effect of Swirl with Peabody 6-102-55 Atomizer.	5-94
5-77	Effect of Swirl with Todd CDS Atomizer.	5-95
5-78	Effect of Swirl Upon Bacharach Smoke Number.	5-97
5-79	Effect of Flue Gas Recirculation.	5-98
5-80	Fuel Composition Studies - Middle Eastern Oil with Monarch Atomizers.	5-102
5-81	Fuel Composition Studies - Middle Eastern Oil with Peabody Atomizer.	5-103
5-82	Fuel Composition Studies - Middle Eastern Oil with Todd Atomizer.	5-104
5-83	Fuel Composition Studies - Middle Eastern Oil with Sonicore Atomizers.	5-105
5-84	Fuel Composition Studies - Indo/Malaysian Oil with Monarch Atomizer.	5-106
5-85	Fuel Composition Studies - Indo/Malaysian Oil with Sonicore Atomizer.	5-107
5-86	Fuel Composition Studies - Shale Derived Diesel Fuel Marine Todd Atomizer.	5-108
5-87	Fuel Composition Studies - Gulf Coast Oil with Sonicore Atomizers.	5-109
5-88	Fuel Composition Studies - Alaskan Bunker C Oil with Monarch Atomizer.	5-110
5-89	Fuel Composition Studies - Alaskan Bunker C Oil with Peabody Atomizers.	5-111
5-90	Fuel Composition Studies - Alaskan Bunker C Oil with Todd Atomizers.	5-112
5-91	Fuel Composition Studies - Alaskan Bunker C Oil with Sonicore Atomizers.	5-113

LIST OF FIGURES

Figure — Page

5-92 Fuel Composition Studies - California Oil with Monarch Atomizers. 5-114

5-93 Fuel Composition Studies - California Oil with Peabody Atomizers. 5-115

5-94 Fuel Composition Studies - California Oil with Todd Atomizer. 5-116

5-95 Fuel Composition Studies - California Oil with Sonicore Atomizers. 5-117

5-96 Fuel Composition Studies - Parho Process Shale Oil with Sonicore and Monarch Atomizers. 5-118

5-97 Effect of Fuel Type on NO$_x$ Emissions. 5-119

5-98 Effect of Fuel Nitrogen Content Petroleum Fuels. 5-121

5-99 Effect of Fuel Nitrogen Content - Shale Derived Oil. 5-122

5-100 Effect of Swirl Upon Fuel Nitrogen Dependence. 5-124

5-101 Effect of Swirl - Middle Eastern Oil. 5-125

5-102 Effect of Swirl - Indo/Malaysian Oil. 5-126

5-103 Effect of Swirl - Alaskan Bunker C Oil. 5-127

5-104 Effect of Swirl - California Oil. 5-128

5-105 Effect of Fuel on Bacharach Smoke Number. 5-130

5-106 Effect of Fuel on Smoke Emissions. 5-131

5-107 Effect of Atomizer on Smoke Emissions for Four Fuels. 5-132

5-108 Effect of FGR - Middle Eastern Oil and Indo/Malaysian Oil. 5-133

5-109 Effect of FGR - Alaskan and California Oil. 5-134

5-110 Effect of FGR Upon NO$_x$ Emissions. 5-135

5-111 Typical Staging Results - Indo/Malaysian Oil with Sonicore Atomizer. 5-139

LIST OF FIGURES

Figure		Page
5-112	Effect of Overall Stoichiometry - Delavan "Airo" Atomizer, Weak Swirl.	5-140
5-113	Effect of Overall Stoichiometry - Monarch Atomizer, Strong Swirl.	5-141
5-114	Effect of Overall Stoichiometry - Monarch Atomizer, Intermediate Swirl.	5-142
5-115	Effect of Overall Stoichiometry - Monarch Atomizer, Weak Swirl.	5-143
5-116	Effect of Primary Zone Residence Time, Intermediate Swirl.	5-144
5-117	The Influence of Primary Zone Residence Time - No Swirl.	5-145
5-118	Effect of Primary Zone Residence Time.	5-146
5-119	Comparison of Staged NO_x Emissions with and without Refractory Liner.	5-147
5-120	Staged Combustion Studies - Indo/Malaysian Oil with Sonicore Atomizers.	5-148
5-121	Staged Combustion Studies - Indo/Malaysian Oil with Monarch Atomizer.	5-149
5-122	Staged Combustion Studies - Indo/Malaysian Oil with Peabody Atomizer.	5-150
5-123	Staged Combustion Studied - Indo/Malaysian Oil with Todd Atomizer.	5-151
5-124	Comparison of Nozzle Performance Under Staged Combustion Conditions - Weak Swirl.	5-152
5-125	Comparison of Nozzle Performance Under Staged Combustion Intermediate Swirl.	5-153
5-126	Comparison of Nozzle Performance Under Staged Combustion Conditions - Strong Swirl.	5-154
5-127	Effect of Steam Atomization - Sonicore Atomizer, Normal Combustion.	5-155
5-128	Effect of Steam Atomization - Sonicore Atomizer, Staged Combustion.	5-156
5-129	Effect of Steam Atomization - Todd Atomizer.	5-157

LIST OF FIGURES

Figure		Page
5-130	The Influence of FGR on Emissions Under Staged Combustion Conditions.	5-158
5-131	Effect of Primary Zone Stoichiometry with Conical Spreader Secondary Air Injector.	5-159
5-132	Staged Combustion Studies - Alaskan Diesel Oil.	5-160
5-133	Staged Combustion Studies - Alaskan Bunker C Oil.	5-161
5-134	Staged Combustion Studies - Crude Shale Oil.	5-162

LIST OF FIGURES

Figure		Page
6-1	Relative Volatility of Nitrogen Species in Residual Oils.	6-2
6-2	The Effect of Spray Flow Field Interactions.	6-3
6-3	NO_x Emissions as a Function of Dropsize.	6-5
6-4	Influence of Droplet Size Under Staged-Combustion Conditions - Tunnel Furnace.	6-6
6-5	Influence of Atomizer Design - Package-Boiler Simulator - Light Oil.	6-7
6-6	Influence of Atomizer Design - Package-Boiler Simulator - Heavy Oil.	6-8
6-7	Comparison of Experimental Systems.	6-10

1.0 INTRODUCTION

1.1 Background

Although the increased utilization of coal provides a partial solution to the United States energy crisis, the realities of retrofit capability and process limitations necessitate that in the future many industrial users will continue to burn liquid fuels. Refinery operations will probably be geared to the production of premium fuels for transportation and industry and therefore industrial users will be required to burn heavy petroleum, coal, and shale-derived, residual fuels. Since these liquid fuels have relatively high nitrogen contents and low hydrogen-to-carbon ratios, their use could cause adverse environmental impact due to the emission of combustion-generated pollutants unless appropriate control techniques are applied(1,2). The two pollutants of primary concern are nitrogen oxides (NO_x) and fine particulate matter. The production of NO_x and particulates in turbulent-diffusion flames is thought to be controlled by the fuel composition and by the fuel/air contacting process. The latter is dependent upon the complex interaction of the liquid-fuel spray and the combustion-airflow field.

It is generally recognized that the major fraction of the nitrogen oxides produced in residual fuel oil flames results from the oxidation of nitrogen contained in the fuel. Laboratory studies on distillate oil doped with various nitrogen compounds(3) have demonstrated the potential importance of fuel nitrogen. Bench-scale studies in which the combustion air was replaced with argon/oxygen have shown that fuel nitrogen oxidation is significant even at high temperatures(4) where thermal fixation impacts emissions. Pilot-scale studies using flue gas recirculation in an actual package boiler have also suggested the importance of fuel nitrogen in practical systems(5). Field testing results(6,7) have shown that flue gas recirculation is not extremely effective in controlling NO_x emissions from many residual, oil-fired systems. Thus, there exists strong, indirect evidence regarding the importance of fuel nitrogen; however, its role has not been directly documented.

The influence of fuel composition on NO_x formation is ill-understood. Doped distillate oil experiments in laboratory furnaces have suggested that the percentage fuel nitrogen conversion decreases significantly with increasing nitrogen content(3), and that the conversion to NO_x is the same for all nitrogen compounds irrespective of molecular type(5). However, these experiments were somewhat limited because the added nitrogen was contained in low boiling point compounds, and therefore the doped nitrogen was extremely light relative to the nitrogen actually present in residual fuel oils. Pilot-scale data with a limited number of residual fuel oils indicates that percent conversion of fuel nitrogen to NO_x may be an unexplained function of fuel composition(5).

The fraction of fuel nitrogen which is converted to NO_x appears to be strongly dependent on the availability of oxygen during the thermal decomposition of the liquid droplets. Laboratory studies have indicated that fuel/air ratio nonuniformities significantly affect the conversion(8). Pilot-scale studies(9) have demonstrated the importance of mixing between the liquid spray, the internal recirculation zone, and the combustion air. Work on the structure of confined flames(10) has shown that a typical spray consists of large fuel droplets whose velocities are primarily governed by the fuel nozzle characteristics, and of clouds of smaller fuel droplets, which respond relatively quickly to the ambient gas velocity.

Recent large-scale studies at the Central Electricity Generating Board (CEGC/England) on the combustion of residual oil have indicated that NO_x formation is strongly dependent on air temperature and fuel flow rate, but weakly dependent on oil temperature and excess oxygen. Flue gas recirculated to the combustion air or to the early part of the flame caused marked reduction of NO_x formation, but when added after completion of combustion had negligible effect(11).

Nitrogen oxide emissions from stationary combustors can be reduced by combustion modification techniques which involve staging the fuel/air mixing and heat release processes. However, the application of these techniques to residual fuel oil-fired combustors has been only partly successful because of a trade-off in pollutants; a decrease in NO_x emissions is quite often accompanied by an increase in particulate emissions. Early research studies in a laboratory furnace(3) and a pilot-scale package boiler(5) demonstrated the viability of external staging for NO_x control. These results were subsequently expanded in pilot-scale(2) and field testing studies(6,7). Recent laboratory experiments with doped distillate oil have indicated the importance of nitrogen intermediates(12) (e.g., HCN and NH_3); however, the optimization of staged combustion techniques to control NO_x emissions from liquid fuel-fired combustors has proved difficult because the controlling phenomena are not well-understood.

Particulate matter produced in residual fuel oil flames consists of trace amounts of inorganic ash; soot, which is produced from the gas-phase species; and two other constituents, cenospheres and coke, which are associated with the multi-component nature of the fuel and the characteristics of droplet combustion. The formation of these latter two components can be attributed to the occurrence of liquid-phase, thermal cracking, because of high droplet temperatures. Soot formation, which occurs in three distinct phases: nucleation, surface growth, and coagulation, is associated with the existence of fuel-rich zones within the flame. Unfortunately, these are the exact types of conditions which appear to be beneficial in terms of NO_x control.

Thus, the local stoichiometry which is controlled by the turbulent mixing processes, and which is spray/flow field dependent plays a dominant role in the formation of both NO_x and particulate matter. Previous work has identified the overall parameters of major importance; however, the mechanisms of pollutant formation and the exact influence of fuel composition and burner design parameters remain poorly understood.

1.2 Purpose and Scope

The overall goal of this study was to provide the information necessary for the development and generalization of low NO_x oil burner technology for application to package, firetube boilers. Results obtained under a previous contract (EPA No. 68-02-1500) indicated that emissions from a 0.71 percent nitrogen oil could be reduced from approximately 500 ppm to 220 ppm without undue smoke emission by use of a distributed mixing burner system (delayed air addition); however, the results could not be generalized due to the limited number of fuels and atomizers which were considered. The primary purpose of the work reported herein was to investigate the influence of spray properties and fuel composition on the formation of thermal and fuel NO_x in liquid fuel flames. The specific objectives of the research were:

- To relate the formation of nitrogen oxides in liquid fuel flames to the chemical and physical characteristics of the liquid fuel and to atomizer design.
- To investigate the interaction between liquid sprays and the airflow pattern for conditions typical of package boilers under normal and staged conditions.

Both NO_x and particulate emissions were considered throughout the study, because of the need for total environmental optimization.

1.3 Overall Approach

The technical approach in this study was primarily experimental, and it involved a variety of different test facilities. The combustion studies were carried out in two furnaces of different scales. A specially designed 20 kW (70,000 Btu/hr), refractory wall, tunnel furnace was used to assess the influence of fuel chemistry, flame temperature, and droplet size on the formation of fuel and thermal NO_x emissions under carefully controlled combustion conditions. The furnace design and the small-scale made it possible to minimize the spray/flow field interactions. A 900 kW (3,000,000 Btu/hr) combustor, which directly simulated the firetube of a package boiler, was used to define the overall effects of fuel composition and nozzle design on the formation of NO_x, CO, and particulate matter under conditions typical of real systems. The work focused primarily on 13 different petroleum-derived, heavy fuel oils, but it also included consideration of three different distillate oils, four shale oil blends, and two coal-derived liquids.

A wide variety of specialized experimentation was conducted to support the combustion studies in the small-scale tunnel furnace and the package boiler. Several of the nozzles used in the combustion experiments were studied by the International Flame Research Foundation in a cold-flow spray characterization rig using a laser diagnostic technique. These data allowed each nozzle to be characterized in terms of droplet-size distribution and approximate mass distribution.

The chemical and physical properties of the fuels used throughout this work were also evaluated by an independent testing laboratory. Data were obtained on the:

- Ultimate chemical composition;
- Physical properties;
- Thermal gravimetric analysis; and
- Nitrogen volatility.

1.4 Report Organization

This report contains a comprehensive discussion of all of the activities conducted under Contract 68-02-2624. The major results and conclusions are available in a separate, brief summary volume. The purpose of this report is to provide complete details of the actual experimental systems and to present all of the experimental data in either tabular or graphic form.

Section 2 contains a comprehensive discussion of the atomizers which were selected for use in this study. Section 3 discusses the fuels which were selected for this study and presents detailed data on their chemical and physical properties. Sections 4 and 5 summarize the combustion results obtained in the small-scale tunnel furnace and the firetube package boiler, respectively. Each of the major sections contains a brief summary of the results at the beginning for the convenience of the reader. Finally, Section 6 concludes the report by discussing the research needed prior to a field demonstration. The experimental procedures used by the International Flame Research Foundation to characterize the drop-size distribution from each atomizer are described in Appendix I.

This report has been prepared using SI units wherever possible. In the event that conversion to English engineering units is required, Table 1-1 provides a list of some common conversion factors.

Appendix II summarizes a review of trends in liquid fuel usage, refinery processing, and crude feedstock characterizations which was used in determining which fuels were to be selected for testing in this program.

Table 1-1. Conversion of English Units to SI Units

TO OBTAIN	FROM	MULTIPLY BY
mg/MJ	lb/10^6 Btu	430
m	ft	0.3048
cm	in	2.54
m^2	ft^2	0.0929
m^3	ft^3	0.02832
kg	lb	0.4536
Celsius	Fahrenheit	$t_c = 5/9\ (t_F - 32)$
Kelvin	Fahrenheit	$t_K = 5/9\ (t_F - 32) + 273$
Pa	psig	$P_{pa} = (P_{psig} + 14.7)(6.895 \times 10^3)$
Pa	iwg (39.2 F)	$P_{pa} = (P_{iwg})(249.1)$
MW	10^6 Btu/hr	0.293

REFERENCES

1. Mansour, M. N and M. Gerstein, "Correlation of Fuel Nitrogen Conversion to NO_x During Combustion of Shale Oil Blends in a Utility Boiler," Symposium on Combustion of Coal and Synthetic Fuels, American Chemical Society, March 1978.

2. Heap, M. P. et al., "Control of Pollutant Emissions from Oil-Fired Package Boilers," Proceedings of the Stationary Source Combustion Symposium, EPA-600/2-76-1526, NTIS, Springfield, VA (1976).

3. Martin, G. B. and E. E. Berkau, "An Investigation of the Conversion of Various Fuel Nitrogen Compounds to NO in Oil Combustion," AIChE Symposium Series No. 126, 68 (1972).

4. Pershing, D. W., G. B. Martin and E. E. Berkau, "Influence of Design Variables on the Production of Thermal and Fuel NO from Residual Oil and Coal Combustion," AIChE Symposium Series No. 148, 71 (1975).

5. Turner, D. W., R. L. Andrews and C. W. Siegmund, "Influence of Combustion Modification and Fuel Nitrogen Content on Nitrogen Oxide Emissions from Fuel-Oil Combustion," AIChE Symposium Series No. 126, 68 (1972).

6. Cato, G. A. et al., "Field Testing: Application of Combustion Modifications to Control Pollutant Emissions from Industrial Boilers--Phase II," EPA-600/1-76-086a, April 1976.

7. Cato, G. A., L. J. Muzio and R. E. Hall, "Influence of Combustion Modifications on Pollutant Emissions from Industrial Boilers," Proceedings of the Stationary Source Combustion Symposium, EPA-600/2-76-1526, NTIS, Springfield, VA (1976).

8. Appleton, J. P. and J. B. Heywood, "The Effects of Imperfect Fuel-Air Mixing in a Burner on NO Formation from Nitrogen in the Air and the Fuel," Fourteenth Symposium (International) on Combustion, The Combustion Institute, Pittsburgh, PA (1973).

9. Heap, M. P., "NO_x Emissions from Heavy-Oil Combustion," International Flame Research Foundation Report for Contract 68-02-0202, IJmuiden, Holland (1977).

10. Owen, F. K. et al., "Effects of Inlet Air Swirl and Fuel Volatility on the Structure of Confined Spray Flames," Seventeenth Symposium (International) on Combustion, The Combustion Institute, Pittsburgh, PA (1979).

11. Cunningham, A. T. S. and P. J. Jackson, "The Reduction of Atmospheric Pollutants During the Burning of Residual Fuel Oil in Large Boilers," J. Institute of Fuel, 20, March 1978.

12. Gerhold, B. W., C. P. Fenimore and P. K. Dederick, "Two-Stage Combustion of Plain and N-Doped Oil," Seventeenth Symposium (International) on Combustion, The Combustion Institute, Pittsburgh, PA (1979).

2.0 PILOT-SCALE ATOMIZER SELECTION

2.1 Summary

One of the goals of this program was to assess the impact of atomizer characteristics on pollutant production under both excess air and staged combustion conditions. This section describes the atomizer selection procedure and the results of a separate study to characterize several of the atomizers used in the combustion studies. Commercial atomizers were selected for use in a 3 x 10^6 Btu/hr test burner with well defined and variable air flow conditions. Both assist fluid and pressure atomizers were selected. The characteristics of the spray produced by six of the atomizers were determined in a cold flow test rig using a laser diffraction droplet size analyzer. These studies indicate that both atomizer design and operational parameters control the spray characteristics.

2.2 The Influence of Atomizer Design on Pollutant Emissions

The combustion of fuel oils in package boilers requires that the liquid be broken into droplets in order to enhance mixing with the combustion flow field. An atomizer serves two functions: 1) it breaks the liquid jet into a spray of fine droplets and 2) it directs this spray into the combustion air stream so as to provide for ignition stability and complete combustion. Figure 2-1 illustrates the two major types of oil burners used in package boilers. The liquid fuel is supplied through an axial oil gun in both burners, however the method of combustion air delivery is different. In the watertube boiler burner (Figure 2-1b) air supplied from a windbox through a register which acts both as a control damper and a means of imparting tangential momentum to the air stream and a diffuser attached to the oil gun provides for ignition stability by promoting the formation of an axial recirculation zone. Firetube boilers have cylindrical combustion chambers with typical length to diameter ratios of greater than five, and the burner must produce a flame whose shape is compatible with the combustion chamber space, therefore, the air flow is mainly axial. The performance of both burners is dependent upon the combustion of air flow and spray patterns to provide optimum conditions for combustion in the available space.

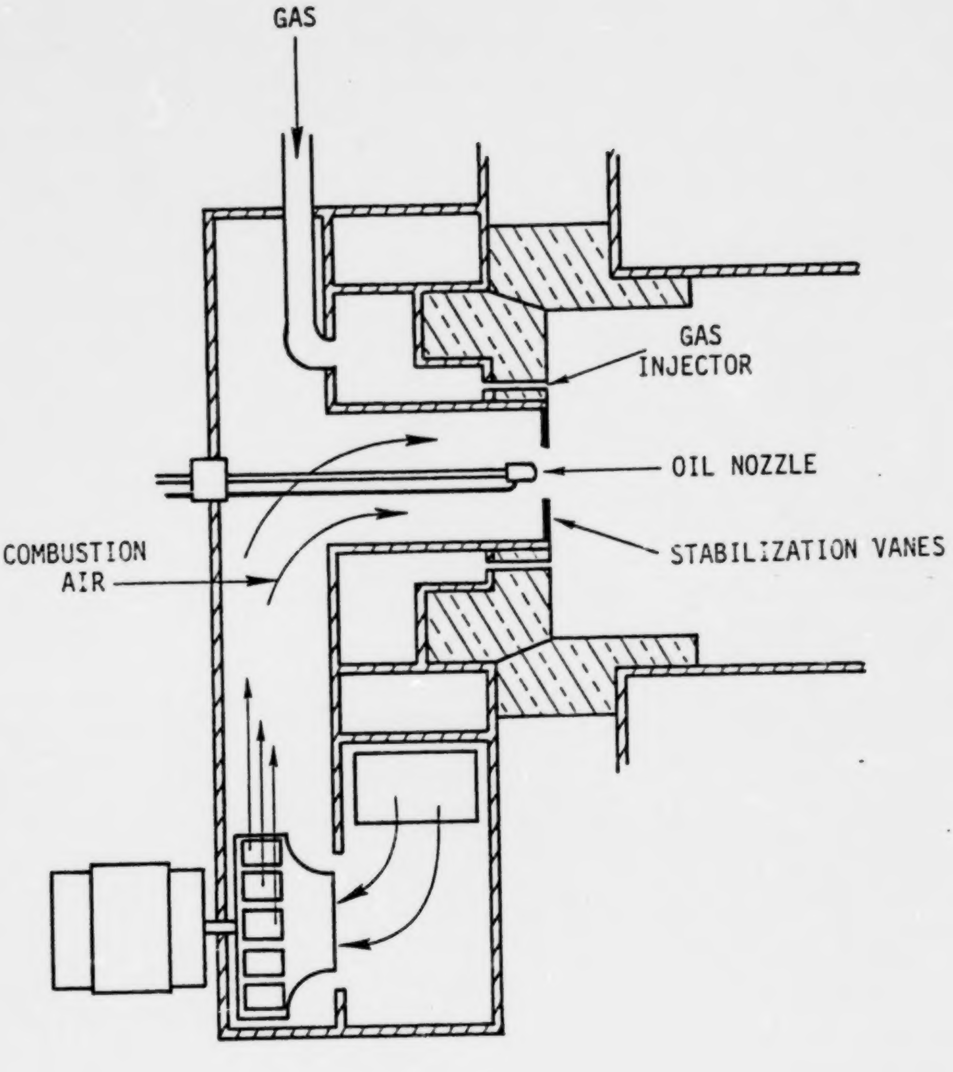
GAS
GAS INJECTOR
OIL NOZZLE
STABILIZATION VANES
COMBUSTION AIR

(a)

Figure 2-1a. Typical Package Boiler Burners - Firetube Boiler Burner.

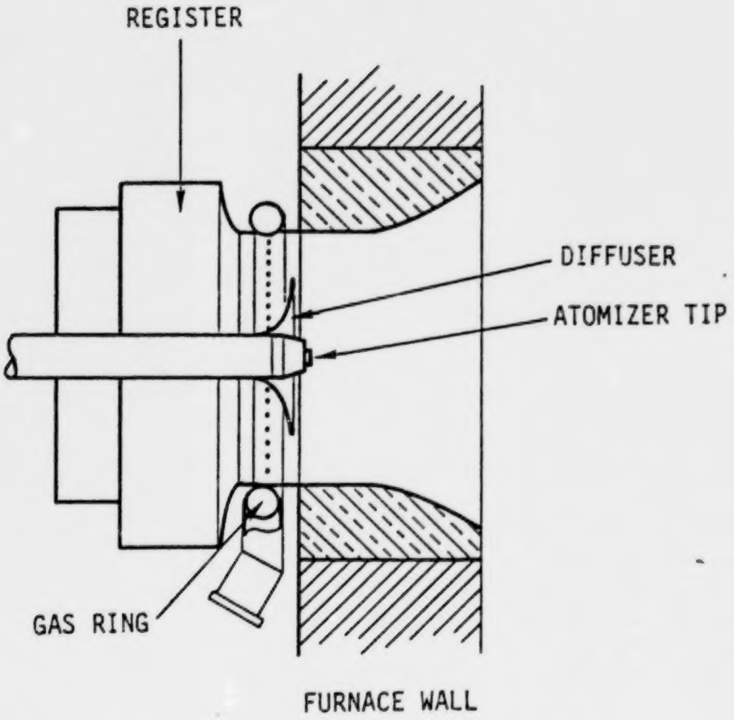
REGISTER
DIFFUSER
ATOMIZER TIP
GAS RING
FURNACE WALL

(b)

Figure 2-1b. Typical Package Boiler Burners - Register Burner for Watertube Boilers.

A review of the available literature concerning the influence of atomization parameters on pollutant emissions from oil-fired equipment produces conflicting evidence concerning the importance of these parameters. Cato et al.[7] concluded that a well-maintained oil burner operating at near its design point will produce about the same level of nitrogen oxides and particulate emissions regardless of the atomization method used, and that boiler efficiency was unaffected to any significant degree by the type of atomization employed. For a given oil burner the oil atomization method that produced the lowest nitrogen oxide emissions usually produced the highest particulate emissions. Figure 2-2 summarizes a series of field tests on one boiler with two No. 6 oils (nitrogen contents of 0.44 and 0.14) and a No. 2 oil. It can be seen that with the nitrogen-containing fuel steam atomization tended to give higher NO_x emissions, however, this trend was reversed with the No. 2 fuel oil. Figure 2-3 compares NO_x emissions from a laboratory combustor with one nozzle and one fuel as a function of atomization fluid and pressure. These results indicate that at a given atomization pressure, steam atomization gives lower NO_x emissions than air atomization. However, this conclusion is not independent of pressure.

Nitrogen oxide production in heavy fuel oil flames is very strongly dependent upon local stoichiometry because the conversion efficiency of fuel bound nitrogen is strongly dependent upon oxygen availability, which is controlled by the combined influence of atomizer properties and combustion air flow distribution. Therefore, it is not surprising that the influence of certain atomizer design parameters on NO_x emissions may vary depending upon overall burner design.

EPA-supported investigations at the IFRF[9] showed a dramatic effect of atomizer design on NO_x emissions. This investigation was carried out in a refractory tunnel furnace with a double concentric swirl burner and compared NO_x emissions from various atomizer designs and characteristics (steam assist, mechanical spray angle) for a given firing rate and fuel oil. The results presented in Figure 2-4 show that NO_x emissions can be reduced from approximately 230 ppm to around 100 ppm by fitting a distributor tip over a normal Y-jet atomizer in order to divide the flame. The distributor tip divides the spray

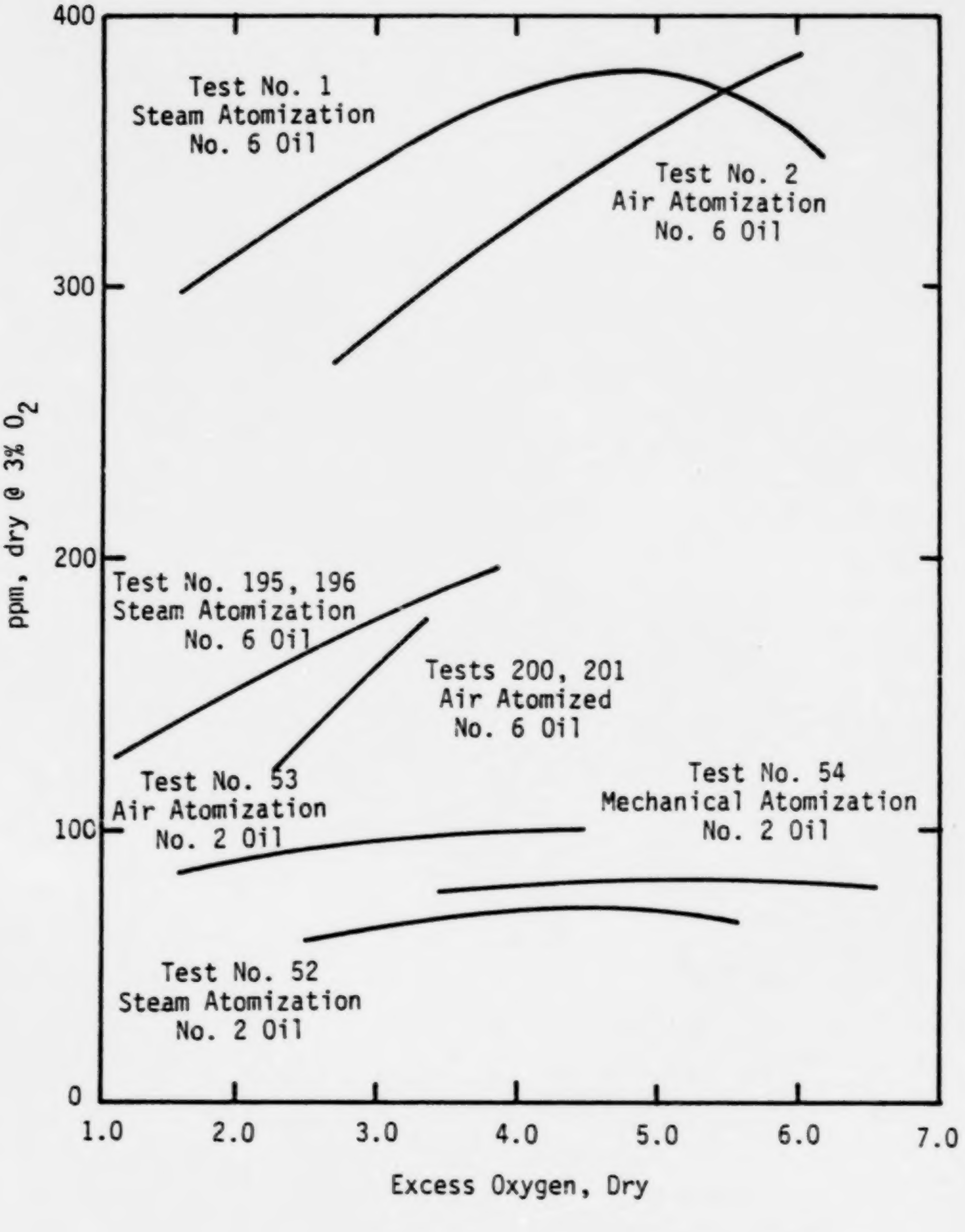

Figure 2-2. Effect of Oil Atomization Method and Excess Oxygen Level on the Total Nitrogen Oxides Emissions. (After Cato et al.[7])

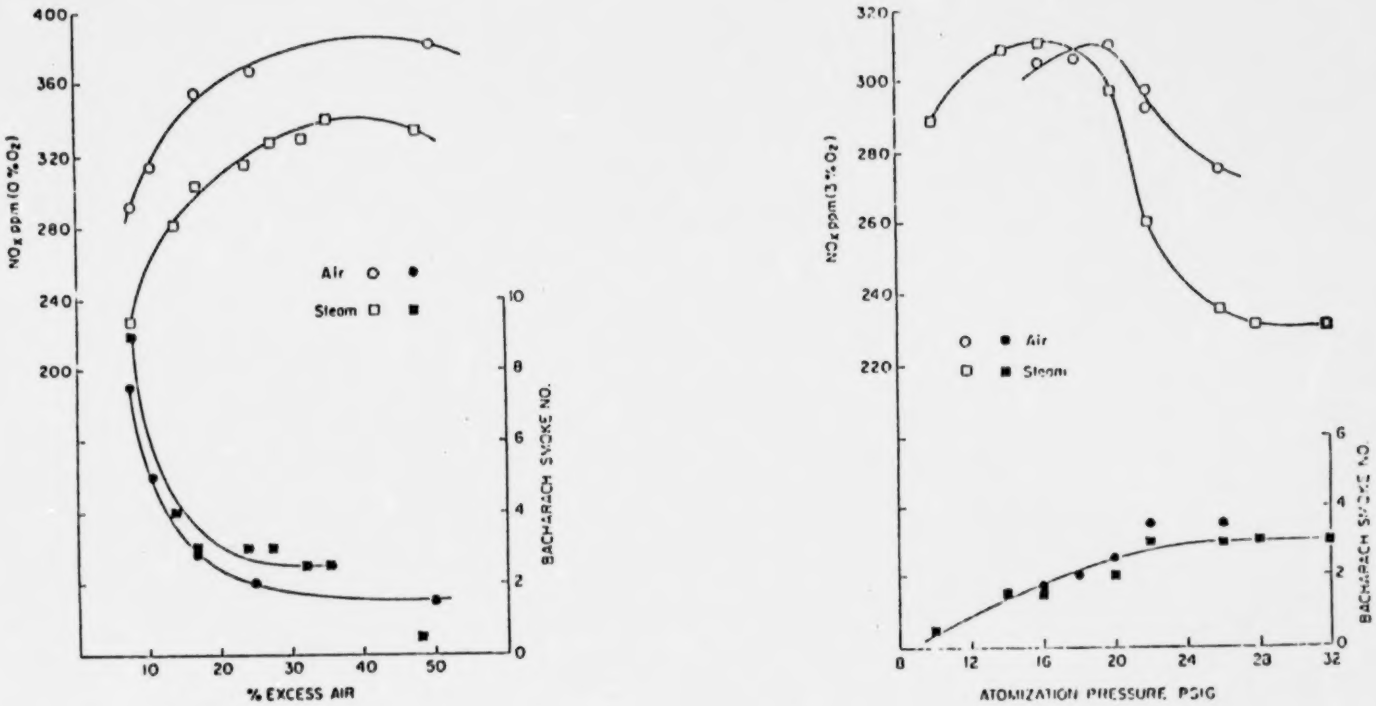

(a)

(b)

Figure 2-3. (a) NO_x and Smoke Emissions as a Function of Excess Air Level and Atomization Medium and (b) The Influence of Atomization Fluid and Pressure Pollutant Emissions from Oil Flames (17 percent Excess Air, 3.4 X 10^6 Btu/hr).

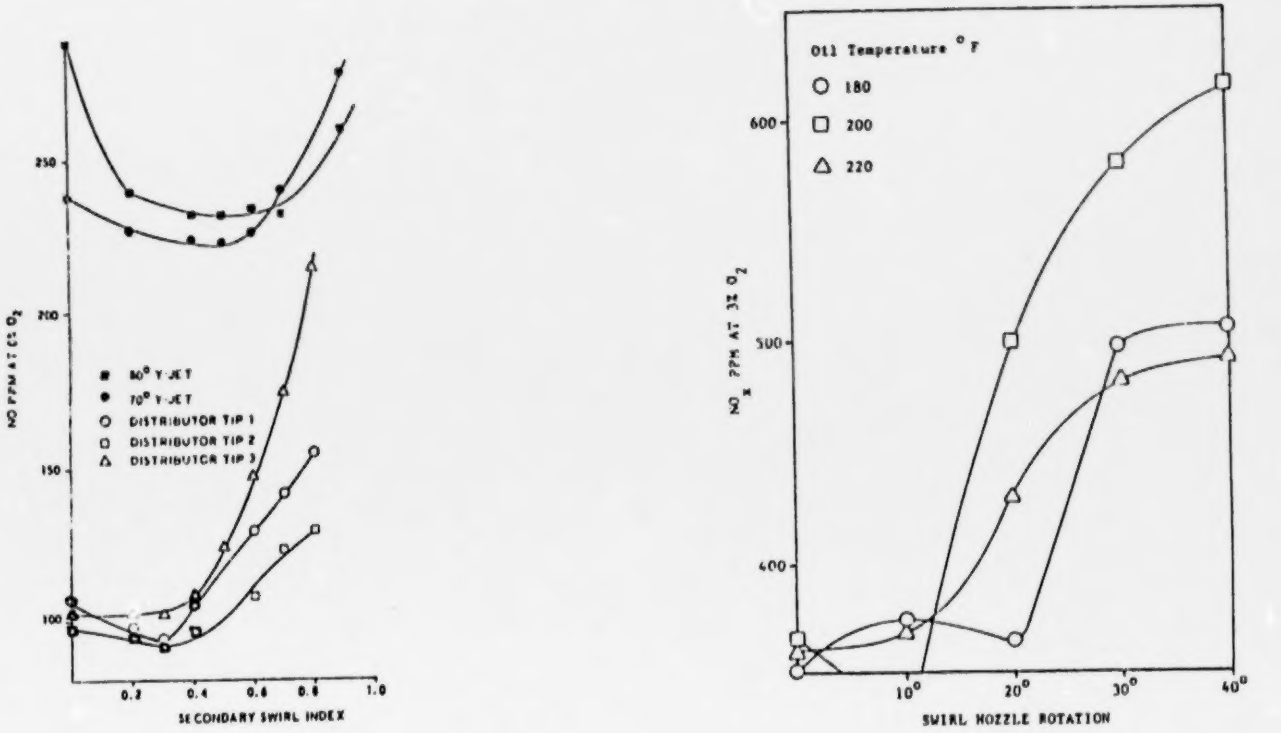

Figure 2-4. (a) Emission Characteristics of Fuel Oil Flames (5 percent Excess Air, 300°C Preheat, Primary Swirl Vanes 30°) and (b) The Effect of Fuel Oil Temperature on NO$_x$ Emissions.

into a series of fuel jets which form individual flames contrasting with the single brush produced without the distributor tip. One possible explanation for those results is that NO_x emissions are reduced because the individual flames will provide fuel-rich conditions within the flame jet, thus minimizing fuel nitrogen oxidation. Placing the distributor tip on the nozzle could also have increased entrainment of furnace gasses into the flame and the fuel residence time within the flame by changing the spray momentum, mean droplet diameter and/or size distribution. These investigations were carried out under relatively high wall temperature conditions atypical of package boilers (although the volumetric heat release rate was low) and it could be argued that this type of atomizer would tend to produce smoke if used in a cold wall combustion chamber since local stoichiometry also affects smoke and particulate formation.

Van Breugal et al.[11] investigated the influence of atomizer design and fuel oil throughput on solid emissions from a refinery furnace. A pressure jet atomizer (mechanical atomization) gave the highest particulate emissions, although emissions were reduced as the atomization pressure was reduced. The lowest particulate emissions were obtained with a steam atomized L-type nozzle which gave a relatively flat dropsize distribution (Figure 2-5). Comparing dropsize distribution with particulate emissions, it can be seen that there is not a simple relationship between the two. Van Breugal argues that those atomizers which produce a narrow drop size distribution will concentrate the fuel in a particular area, whereas the atomizer with a relatively flat distribution can lay the fuel droplets throughout the combustion air stream, thus increasing the rate of fuel/air mixing.

The preceeding discussion was not intended to provide an exhaustive review of information on the impact of atomizer properties on NO_x and particulate formation in fuel oil flames. However, it does serve to illustrate the following points:

- For a given burner the atomizer design can have a strong influence on both NO_x and particulate emissions.
- The influence of atomization parameters cannot easily be separated from the effect of the flow field on the fuel oil spray.
- There is a lack of information on the influence of atomizer parameters under staged combustion conditions.

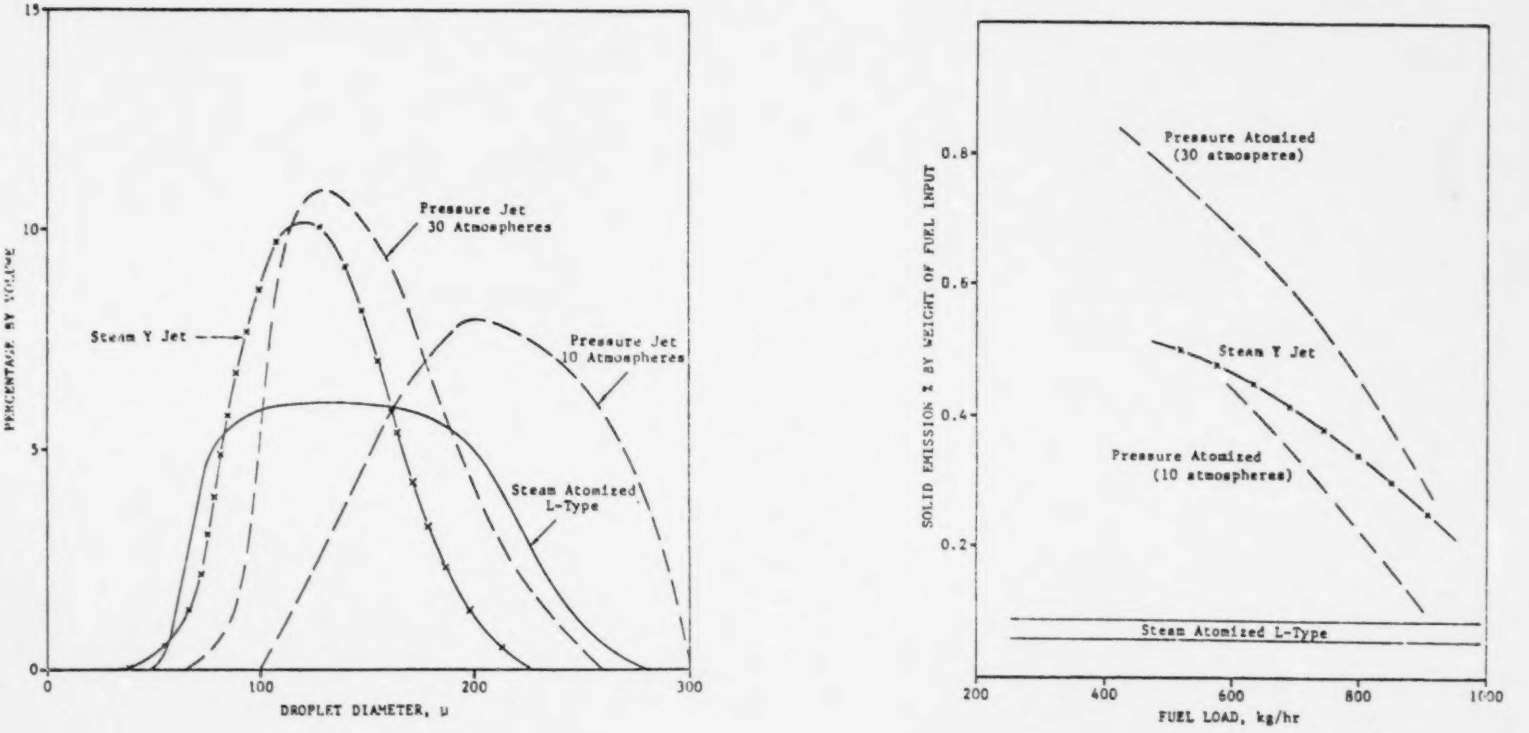

(a)

(b)

Figure 2-5(a) and (b). Dropsize Distribution for the Atomizers used in Figure b (b) Solid Emissions from a Refinery Heater as a Function of Fuel Load.

One of the goals of this research program was to compare the performance of several commercial atomizers under well defined conditions and to relate the pollutant production to the atomizer characteristics. The selection of the atomizers and their characterization will be discussed in the following sections.

2.3 Atomizer Selection

2.3.1. Classification of Atomizers

The basic principle of disintegration of a liquid into a spray requires continual change in the form of the liquid such that the total surface area is increased until the liquid volume becomes unstable and disintegrates. The various atomizer designs primarily transpose bulk liquid into thin liquid sheets. The process by which drops are produced from the liquid stream and the resulting dropsize distribution depends upon the nature of flow in the atomizer, i.e., whether laminar or turbulent, the way in which the energy is imparted to the liquid, the physical properties of the liquid to be disintegrated, and the characteristics of the environment into which the liquid is injected.

The complex process of atomization can be divided into four distinct stages. Initially the fuel oil film is subject to forces which cause instability resulting in the growth of small perturbations on the surface of the liquid film. During the second stage these perturbations grow into spikes on the surface, and subsequently break off as ligaments. The third stage consists of the disintegration of these relatively large ligaments into smaller drops, and includes any secondary atomization due to shattering of these drops by interaction with the flow field. The fourth and final stage is concerned with the formation of the spray and the distribution of dropsize as coalescence and diffusion of the smaller drops takes place forming the final spray configuration. Peskin and Lawler presented a detailed account of the atomization process based upon this four-step approach. They indicate that the spray characteristics can be related to either the initial fuel instability of the first stage, or the relative motion of the fluid in the ambient atmosphere characteristic of the second stage, and that this relationship is dependent upon the source of energy employed for atomization. Therefore, it is convenient to classify atomizers by the source of energy used for disintegration.

The energy used for atomization may be derived from:

- the fuel alone,
- a second atomizing fluid,
- a combination of the above,
- an external device, either directly or indirectly through the action of a fuel and/or a second fluid.

This overall classification can be further subdivided between the various sorts of energy supplies and the ways they can be transformed into kinetic energy which is used to accelerate the liquid field, or liquid droplets. The different types of energy involved in atomizers are:

- potential (static) pressure energy of the fluid,
- kinetic energy of the fluid,
- kinetic energy of a solid structure (rotation, translation, vibration),
- electrostatic energy,
- ultrasonic energy pressure fluctuations.

The majority of fuel oil atomizers can be classified into three groups: liquid pressure energy; centrifugal energy; and assist fluid pressure energy.

- Liquid pressure energy. When the energy is contained in the fuel itself it is in the form of potential energy, and the fuel enters the atomizer gun at low velocity. Such atomizers operate typically with pressures ranging from 5 to 450 psig (136 to 3204 kPa), depending upon the application.
- Centrifugal energy refers to the forces that are applied to a volume of liquid on a disc or cup that has a high rotational velocity. The velocity at the periphery of these devices is typically between 30 and 183 m/sec.

- Assist fluid pressure energy. When a gas or vapor is the only atomizing agent, pressure energy can be transformed either into kinetic energy through an orifice or a venturi, or into ultrasonic energy via a resonating chamber. Contact between the atomizing medium and the liquid to be atomized may take place either within the atomizer (internal mixing) or external to the atomizer as the jets impinge upon each other. Depending upon the particular application, liquid pressure and mixing chamber design, the assist fluid pressure can range from less than 1 psig (108 kPa) to over 100 psig (791 kPa).

It is also possible to classify atomizers in terms of the general type of spray pattern they produce, distinguishing between hollow and solid cone sprays. In the former, droplets are concentrated on the periphery of a cone, while in the latter the whole volume of the spray cone is filled with an almost evenly distributed mass of droplets. Some designs of atomizers are also used to produce flat or fan sprays in which the drops are distributed in a narrow bank, although these are used generally to satisfy special heating requirements. For most applications, and particularly in boilers, the hollow cone spray pattern is used almost universally.

Atomizers relying upon centrifugal energy (e.g., rotary cup) were not considered for this study because they are not widely used commercially in firetube or watertube boilers. Table 2-1 summarizes commercial atomizers as either assist or pressure atomizers.

Pressure energy nozzles are classified into either one of two categories referred to as a swirl cap and swirl cavity type. This classification stems from the two methods available for generating a swirling liquid flow in the discharge orifice. In the swirl cap concept, the tangential momentum is imparted to the liquid as it flows through the tangential or helical passages formed by grooves milled in the swirl cap and the swirl cap head. A pintle is sometimes used with this design. The concept is utilized in commercial nozzles manufactured by at least five companies and is particularly common for low flowrates. In the swirl cavity concept, tangential momentum is imparted to the flow by an arrangement of tangential fuel inlets directed into an internal cavity. The liquid feed flows to the

Table 2-1. Classification of Commercial Atomizers

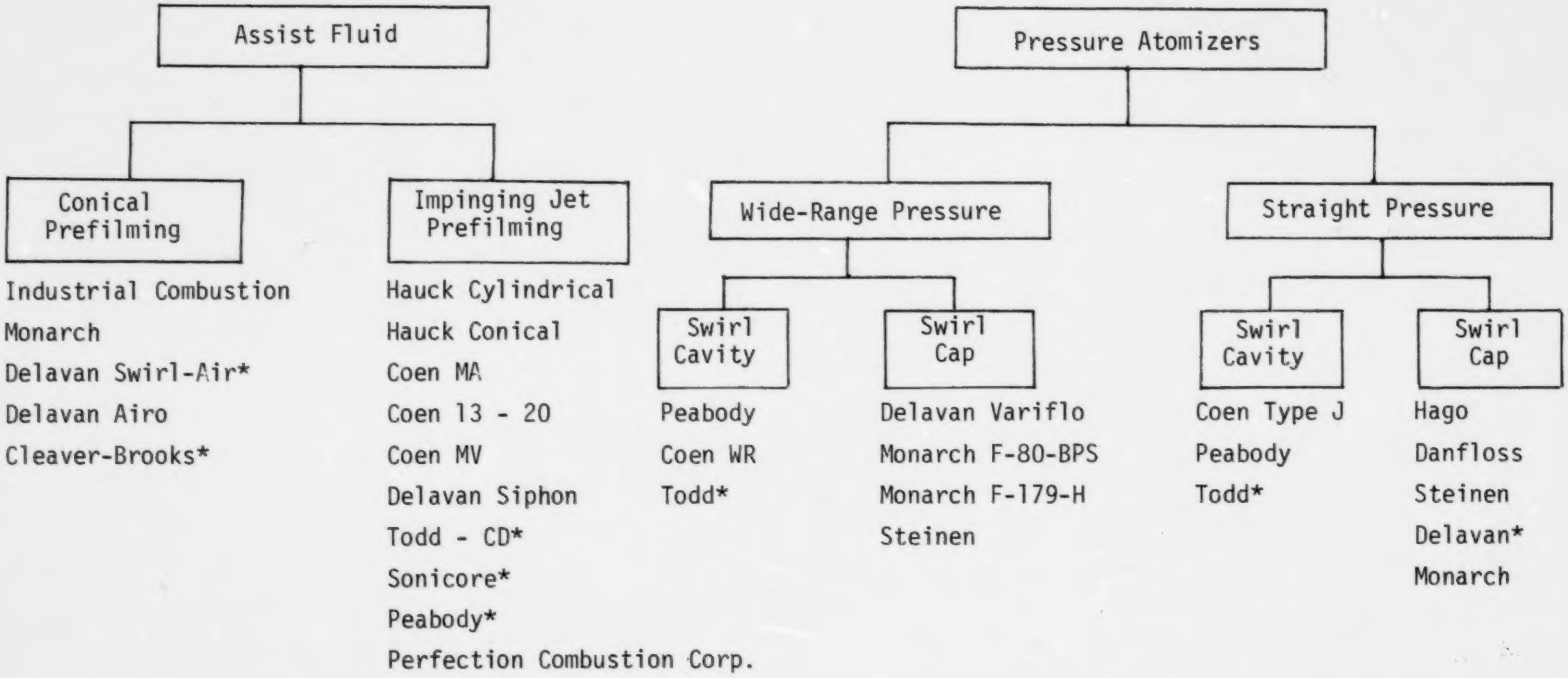
Assist Fluid
Conical Prefilming
Industrial Combustion
Monarch
Delavan Swirl-Air*
Delavan Airo
Cleaver-Brooks*
Impinging Jet Prefilming
Hauck Cylindrical
Hauck Conical
Coen MA
Coen 13 - 20
Coen MV
Delavan Siphon
Todd - CD*
Sonicore*
Peabody*
Perfection Combustion Corp.
Pressure Atomizers
Wide-Range Pressure
Swirl Cavity
Peabody
Coen WR
Todd*
Swirl Cap
Delavan Variflo
Monarch F-80-BPS
Monarch F-179-H
Steinen
Straight Pressure
Swirl Cavity
Coen Type J
Peabody
Todd*
Swirl Cap
Hago
Danfloss
Steinen
Delavan*
Monarch

discharge orifice in a conical sheet, the geometry of which is bounded by the swirl cavity wall on one side and the free surface on the other.

Assist-fluid atomizers can also be categorized into at least two classes and these are also shown in Table 2-1. A prefilming type of atomizer can be distinguished where the liquid to be disintegrated is treated in a manner similar to the mechanical atomizer to create a thin liquid sheet. The assist fluid is brought into contact with the liquid prior to or within the swirl cap or swirl cavity assembly. The pressure of the assist fluid imparts additional tangential momentum to the liquid, and aids in the disintegration of the liquid sheet outside the nozzle. The other class of assist fluid atomizers is the impinging jet atomizer. This class of assist fluid atomizer is characterized by the impingement of the liquid to be atomized and the assist fluid in a premixing chamber or a venturi section. The assist fluid/liquid fuel emulsion usually enters a secondary mixing chamber where it undergoes additional disintegration and finally emerges from the nozzle cap at a spray angle determined by the orientation of the several discharge orifices.

2.3.2 Atomizer Selection Criteria

The atomizers selected for testing are shown with an asterisk in Table 2-1. The criteria used in the nozzle section were:

- applicability of the nozzle for use in package boilers;
- size range suitable for the experimental program;
- suitable for a wide range of fuel properties;
- the types of nozzles chosen must include examples of different atomization principles;
- the selection should include different nozzle designs based upon the same atomization principle;
- the selection must cover a range of fuel pressures, atomizer fluid pressure flow rate and type;
- the nozzles must provide a range of spray characteristics such as spray angle, droplet size and droplet penetration.

The initial approach was to make the selection on the basis of satisfying these criteria with the minimum number of nozzles. Certain manufacturers were eliminated from consideration because their nozzles were not available with a design capacity compatible with the pilot-scale combustor (0.9 Mw). The following discussion describes the rationale of the selection process and the selected atomizers.

2.3.2.1 Pressure (Mechanical) Atomizers

- Swirl Cap Design

  The Delavan line of atomizers was selected for the pilot-scale studies although they are similar in design to other units. Delavan has characterized their nozzles with a photographic technique to determine droplet size, although the characterization was not carried out under practical conditions (i.e., usually with water and in a quiescent atmosphere) however, such information was useful in providing initial information on the effect of nozzle operating conditions on spray characteristics. The disadvantage of using the Delavan line for the pilot-scale studies was the limited number of available spray pattern types compared to Hago or Steinen.

- Swirl Cavity Design

  The Todd straight mechanical nozzle was selected for the pilot-scale testing as representative of the swirl cavity type of nozzle. Todd and Peabody both make similar nozzles of this type, but Todd nozzles were available in the firing rate of the pilot-scale combustor with several interchangeable orifice plate inserts to allow a variation in fuel delivery pressure. The Peabody and the Coen Type-J nozzles were not available at the design capacity of the pilot-scale combustor.

- Wide-Range Pressure Atomizer.

  All of the wide-range pressure atomizers considered are essentially a sophisticated pressure atomizer capable of achieving the practical requirement of high turndown ratio. A survey of nozzle operating characteristics indicated that as the firing rate changes the fuel delivery pressure and spray angle would change. The purpose of the wide-range pressure atomizers is to tailor the fuel delivery conditions for "proper" combustion over the range of loads for industrial boiler operation and not to provide one set of specified spray characteristics at one set of specified input condition. A Todd wide-range atomizer was used to provide a comparison between straight atomizers operating at design conditions and a return atomizer operating over a range of flow rates.

2.3.2.2 Assist Fluid Atomizers

- Impinging Jet.

  The Hauck cylindrical and Hauck conical low pressure air atomized nozzles were selected as representative of impinging jet nozzles. Liquid disintegration is achieved by the impingement of a liquid fuel jet and the atomizing agent at right angles in the venturi section of the atomizer. The spray then leaves the nozzle.

- Internal Mixing Impinging Jet.

  The Todd-CEA "CD" atomizer and Peabody assist-fluid atomizer were chosen as representatives of the impinging jet category which utilize an additional mixing chamber for secondary atomization. The Todd-CEA "CD" atomizer utilizes a prefilming process. The fuel passes into a swirl chamber in six discrete tangential jets and impinges at right angles on high velocity assist fluid stream. The resulting fuel oil/assist-fluid mix discharges into a secondary mixing chamber undergoing further aerodynamic disintegration and finally exits from the nozzle through orifices drilled into the cap.

The principle of operation of the Peabody nozzle is similar to that of the Todd atomizer in that a liquid fuel jet issues into a high-velocity assist-fluid stream. The fuel/assist emulsion produced by this prefilming process then enters a secondary mixing chamber for further aerodynamic disintegration and the spray exits the nozzle through discrete orifices.

Final spray characteristics are determined by the number and orientation of the discharge orifices drilled in the caps of both of these atomizers.

- Ultrasonic.

A Sonicore ultrasonic assist-fluid atomizer was recommended for testing and utilizes a unique process of liquid disintegration by a standing shock wave pressure drop. These atomizers are available in a wide range of design flowrates

- Conical Prefilming Twin Fluid Atomizers

The Delavan swirl-air atomizer was recommeded for use in the pilot-scale studies as representative of conical prefilming devices. This unit utilizes a swirling fuel/assist fluid mixture impinging on a discharge pintle plate rather than the normal divergent surface and is similar to the Monarch assist-fluid nozzle. Of particular interest is the capability to use interchangeable internal orifices to vary the fuel delivery pressure, atomizing fluid pressure, atomizing fluid mass flow and fuel spray angle for a constant fuel delivery quantity. Additionally, information was available from Delavan concerning the influence of atomizer operating parameters on droplet size distribution.

The Cleaver Brooks low-pressure nozzle uses the tangential motion of a fuel/assist fluid emulsion generated by a swirl generator to form a prefilmed conical sheet. This sheet is subject to aerodynamic disintegration, not only by the high velocity primary atomization fluid emerging form the nozzle core, but also by the tertiary airflow. This concept is of interest because of the added ability to affect droplet trajectory with the tertiary air stream.

2.4 Atomizer Characterization

Appendix 1 presents a complete description of an investigation carried out in a cold test rig to characterize six of the atomizers used in the combustion studies. These atomizers were:

- the Delavan Siphon;
- the Sonicore Ultrasonic;
- the Monarch Twin Assist Fluid;
- the Todd CD Assist Fluid;
- the Peabody Assist Fluid, and
- the Delavan Swirl Air.

Dropsize distributions were measured as a function of atomizer operating parameters at various axial locations. The laser droplet size measurement system used in these studies is based upon the Fraunhöfer diffraction pattern caused by particles in a light beam.

The data presented in Figure 2-6 summarize the measured droplet size distributions in terms of weight fraction in each size range for the six atomizers studied.

Three groups can be distinguished based upon dropsize distribution:

- Delavan Swirl Air and Monarch, which produced a coarse spray with a significant weight fraction of droplets greater than 100 μm in diameter.
- Peabody, Todd and Delavan Siphon produced a fine spray with no droplets bigger than 100 μm.
- Sonicore 250T, which gave nearly monosize spray of fine droplets; all the droplets are within the range 15 μm to 30 μm.

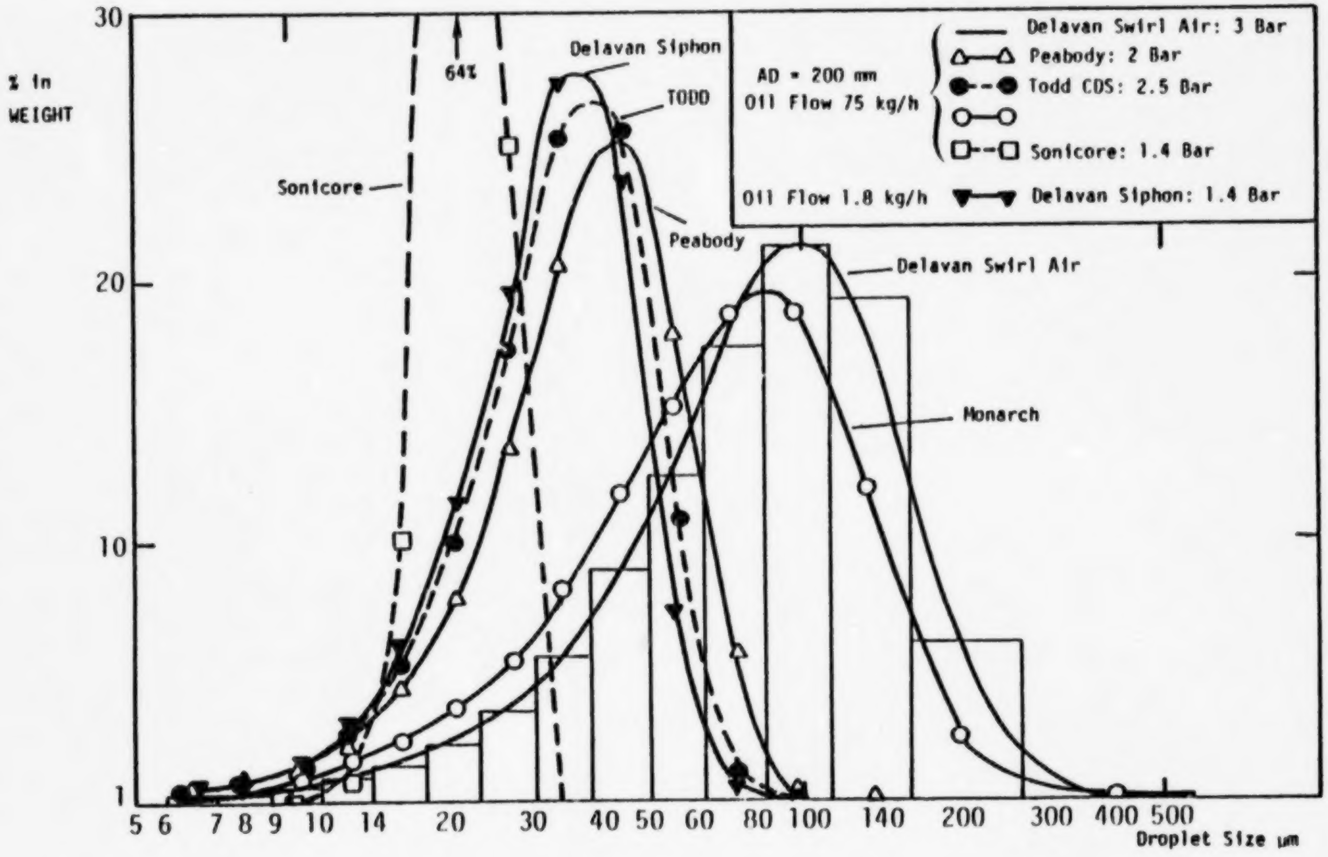

Figure 2-6. Droplet Size Distribution in Operating Conditions for Six Atomizers.

3.0 FUEL SELECTION

This experimental program concerned with the optimization of low NO_x burners for firetube and watertube applications was carried out with a range of fuels typical of those which will be available for industrial use in the next 15 to 20 years. It was decided to test with several fuels since the influence of fuel composition on pollutant emissions cannot be predicted. The two pollutants of major significance in liquid fuel combustion are nitrogen oxides and particulate matter. It is unlikely that combustion modifications can influence SO_2 emissions and the major mode of sulfur control will be its removal from the fuel or the combustion products; however, NO_x and particulate emissions have been shown to be dependent upon both the composition of the fuel (i.e., nitrogen content, boiling range, asphaltene content, etc.) and the conditions under which combustion occurs. In order to include a wide range of fuel properties of interest with respect to pollutant emissions, the test fuels were selected from residual petroleum oils of different origin as well as coal- and shale-derived liquids.

All 19 of the fuels which were selected for this program were tested in the small-scale furnace in order to maximize the amount of information which could be obtained from the sometimes limited quantities of fuel available. Seven of these fuels were available in larger quantities and were thus selected for testing in the pilot-scale combustor.

3.1 Summary

The residual fuel oils used in this program were selected on the basis of importance because of their (1) relationship to major crude oil sources, (2) variability due to different refining processes, and (3) availability. They included a broad spectrum of chemical and physical properties and each oil was characterized in terms of:

- Ultimate chemical composition
- Physical properties
- Distillation characteristics
- Nitrogen distribution

Table 3-1 summarizes the 19 fuels tested during this program. Nitrogen and sulfur contents are shown since these data were of primary interest in the study. Complete fuel analyses are discussed in the following sections.

Table 3-1. Summary of Fuels Tested

Fuel	Nitrogen Content	Sulfur Content
Alaskan Diesel	.007	.31
West Texas Diesel	.026	1.88
Californian Distillate	0.053	0.27
Essex County	.16	.36
Middle East	.18	.67
Low Sulfur Residual	.22	.21
Indo/Malaysian	.24	.22
Desulfurized Venezuelan	.24	.93
Pennsylvanian	.34	2.26
Gulf Coast	.36	2.44
Venezuelan	.22	2.22
Alaskan	.51	1.63
California Residual	.62	1.05
California Residual	.77	1.63
California Residual	.79	1.60
California Residual	.86	.99
Shale (DFM)	.24	.51
Synthoil	1.36	0.8
Shale (Crude)	2.08	.63

Although the major emphasis of this program was upon residual fuels, three distillate oils and three alternate liquid fuels were included for comparison purposes.

3.2 Fuel Selection Criteria

This section of the report describes the development of the criteria which were used in the selection of the test fuels. The program requirements dictated that a reference or "baseline" fuel be chosen for extensive study in both the small-scale, tunnel furnace (70,000 Btu/hr) and in the pilot-scale firetube boiler simulator (3×10^6 BTU/hr). This fuel was to be "representative" of residual fuels in general and to be readily available in large quantities. In addition, at least five other fuels were to be selected so that the test fuels covered the range of petroleum liquids currently being burned in the United States. After consideration of the program requirements, it was decided that the test fuels must meet the following general criteria:

- They should represent residual fuels refined from the major crude oil sources.
- They should provide information on the effect of the refinery processing on the fuel oil properties.
- They must be available for testing.

Each of these criteria is discussed in detail in the following subsections.

3.2.1 Regional Fuel Usage

In order to define the major crude sources, it was necessary to first investigate regional fuel usage patterns because crude sources vary significantly with geographic location. Regional differences such as population, the concentration of industry, and the proximity to domestic fuel oil reserves, alternate fuels, and shipping lanes impact the sources of crudes used by refineries in that area. The Petroleum Administration for Defense (PAD) has identified five regions in the country that are similar in their source and utilization of residual fuel oil. Figure 3-1 defines these regions and shows the major sources of residual fuels for each region. The data in the figure indicate that the two sources of fuel oil primarily used in this country are:

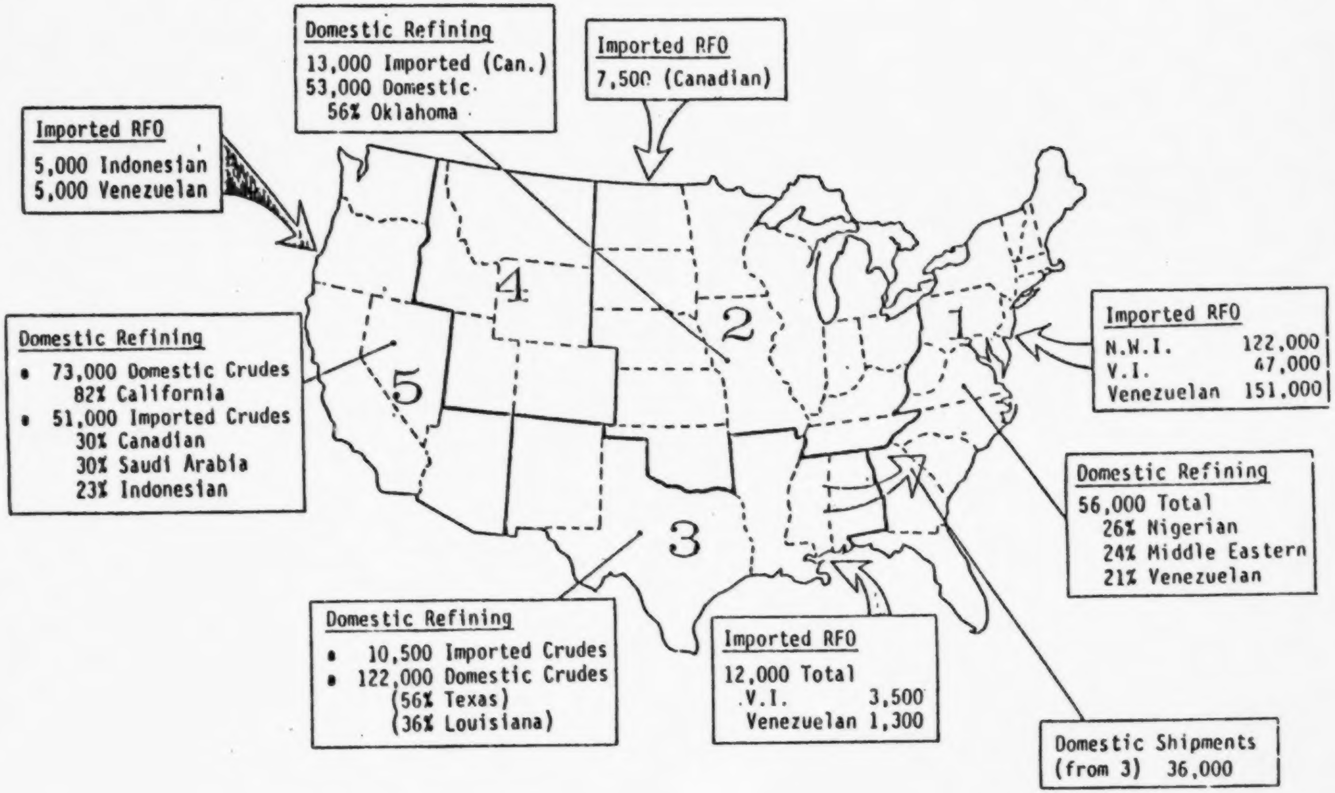
Imported RFO
5,000 Indonesian
5,000 Venezuelan
Domestic Refining
13,000 Imported (Can.)
53,000 Domestic
56% Oklahoma
Imported RFO
7,500 (Canadian)
Domestic Refining
• 73,000 Domestic Crudes
82% California
• 51,000 Imported Crudes
30% Canadian
30% Saudi Arabia
23% Indonesian
4
5
2
3
1
Imported RFO
N.W.I. 122,000
V.I. 47,000
Venezuelan 151,000
Domestic Refining
56,000 Total
26% Nigerian
24% Middle Eastern
21% Venezuelan
Domestic Refining
• 10,500 Imported Crudes
• 122,000 Domestic Crudes
(56% Texas)
(36% Louisiana)
Imported RFO
12,000 Total
V.I. 3,500
Venezuelan 1,300
Domestic Shipments
(from 3) 36,000

Figure 3-1. Major Sources of Residual Fuel Oil Supply for the U.S. by P.A.D. Districts.

- Residual fuel oil imported directly from foreign refineries
- Domestic refineries using either domestic or imported crude oils

Residual fuel oil supplies vary significantly between such diverse regions as the industrial Eastern seaboard (PAD Region 1) and the agricultural South (PAD Region 3). The residual fuel oil supply situation for each region can be summarized as:

- PAD Region 1 - Only 15% of the residual fuel oil used in this district is domestically refined with the remaining 85% imported from foreign refineries. Although the Netherland West Indies and the Virgin Islands are identified as the major sources of imported residual fuel oil, the parent crude for these fuels usually originates in either Venezuela or North Africa. The relatively small quantity of residual fuel oil domestically refined in Region 1 comes primarily from Nigerian, Middle Eastern, and Venezuelan crudes.
- PAD Region 2 - Only a small quantity of residual fuel oil is imported directly into this region (all from Canada); 90% of the supply is refined domestically. Almost all of the imported crude used in domestic refining is Canadian while the largest single source of domestic crude is from Oklahoma.
- PAD Region 3 - Domestic refining supplies 92% of the residual fuel oil and most of the crude used to produce the residual fuel oil originates in Texas and Louisiana.
- PAD Region 4 - Much of the fuel oil used in this region is refined domestically from crude produced in the Western states, particularly Wyoming.
- PAD Region 5 - Imported residual fuel oil shipments are insignificant in comparison to domestic refining. Most of the crude oil used in domestic refining originates from within the U.S. and, of this, over 85% is from California. Imported crudes are mostly Canadian, Saudi Arabian and Indonesian.

Information generated from the Bureau of Mines data for the 1973-74 calendar years indicates that the significant sources of crude oil for production ranked in order of the quantity (MBBLS) of fuel produced are:

North African and Venezuelan (via Carribean)	219,000
Venezuelan (direct)	151,000
Texas	68,000
California	60,000
Louisiana	44,000
Oklahoma	30,000

Although some crude oil sources have changed, the impact of these changes is not considered to be significant at the moment. However, in the future the impact may be more significant. For example, domestic refineries on the West Coast have almost eliminated the importation of Saudi Arabian crudes as Alaska North Slope crudes have become available, and in the future this source is expected to be significant in residual fuel oil production even though many West Coast refineries are not readily adaptable to the use of Alaskan oil as a feedstock. Although shipments of Middle Eastern crudes to the West Coast have decreased, East Coast importation of these and other high sulfur crudes has increased.

3.2.2 Influence of Refining on Residual Oil Properties

Since the refining process can influence the properties of the residual oil produced from a particular crude, it was necessary to review refinery procedures and define potentially significant differences. This subsection of the report summarizes current industrial practice; Appendix 3 contains a detailed discussion of refining practice and fuel specifications.

Although there are many types of refineries, three basic categories can be identified:

- Hydroskimming - crude passes through an atmospheric distillation tower, residual fuel oil feed stream experiences 1 atm pressure, 650+ temperature.
- Conversion/maximize light end - residual fuel oil feed passes through a vacuum distillation tower; experiences pressures less than 1 atm, temperature from 800-1050^{O}F. Lighter ends

(650-800) enter the desulfurization unit and catalytic cracker to maximize gasoline and light end production.

- Conversion/maximize low sulfur residual fuel oil - feed passes from vacuum distillation tower through hydrodesulfurization unit (HDU). The environment within the HDU varies with the details of the process.

The pressure and temperature environments, characteristics of each refining process, could have different influences on the structure of the molecules that contain the trace species and thus pollutant formation. For example, although atmospheric and vacuum distillation processes do not significantly affect the mass of sulfur in the crude, they can influence the class of compounds in which the sulfur is contained. The high temperatures experienced during the distillation process can crack unstable sulfur-containing compounds liberating H_2S which either escapes as a gas or combines with unsaturated hydrocarbons to form new compounds. Hydrodesulfurization significantly reduces the mass of sulfur by affecting primarily the mercaptans; thus, this process changes the distribution of sulfur-containing compounds between the crude and residual fuel oil.

3.2.3 Availability of Fuels

Refineries throughout the United States were contacted as part of a telephone survey to determine the types of residual oil that were for sale and to define their ability to package large and small quantities for shipment to EER. The results indicated that the baseline fuel had to be purchased from a local (California) supplier because of the high cost of shipping large quantities of oil from out-of-state. Refineries in the Northwest, South (primarily Texas), and East were, however, willing to supply smaller quantities of fuels (e.g., two barrels) to be used in the tunnel furnace experiments.

3.2.4 Fuel Selection

The previous subsections described the major sources of United States residual fuel oil, the potential influence of refining conditions on properties and the availability of residual oils. Based on these considerations, it was decided that the baseline and other test fuels must include:

- Residual fuel oils derived from four of the most popular crudes used in the country (North African, Venezuelan, Texas, California)
- Fuels that are expected to be of increased importance in the future (Arabian, Alaska North Slope)
- A wide variation in physical and chemical properties, in particular, oils ranging from the low sulfur, low asphaltene and metal crudes (North African, Indonesian/Malaysian) to the high sulfur, moderate asphaltene and metals (Arabian, West Texas Sour) and the high sulfur, high asphaltene and metals (California, Alaska North Slope and Venezuelan)
- Similar fuels that have gone through different distillation procedures (Indonesian/Malaysian, Venezuelan)

3.3 Characteristics of the Fuels Tested

The characteristics of the fuels tested during this program are presented in Table 3-2. The information presented in this table was generated by an independent testing laboratory. No attempt was made to provide an independent check. However, it is believed that the results are internally consistent. Unidentified samples of the same fuel were analyzed for nitrogen content and the results of four analyses gave 0.24% ± 0.02. The test fuels can be considered in three groups:

1. Distillate Fuels

   Three distillate fuels were tested, these were:

   - D1 Alaskan - very low nitrogen;
   - D2 West Texan - high sulfur (1.88);
   - D3 Californian - relatively high nitrogen (0.05%) level for a distillate oil.

2. Residual Fuels

   A total of 13 residual oils were tested in the bench-scale furnace, and some of these were included in the pilot-scale tests. The residual fuels tested covered a range of nitrogen contents of

Table 3-2. Liquid Fuels Tested

	Alaskan Diesel	W. Texas Diesel	California Distillate	Essex County	Middle East (Exxon)	Low S.* No.6 Oil	Indo/Malay-sian	Venezuelan Desulphurized	DFM (Shale)	Pennsylvania (Amarada Hess)
Ultimate Analysis:										
Carbon, %	86.99	88.09	86.8	86.54	86.78	86.57	86.53	85.92	86.18	84.82
Hydrogen, %	12.07	9.76	12.52	12.31	11.95	12.52	11.93	12.05	13	11.21
Nitrogen, %	0.007	0.026	0.053	0.16	0.18	0.22	0.24	0.24	0.24	0.34
Sulfur, %	0.31	1.88	0.27	0.36	0.67	0.21	0.22	0.93	0.51	2.26
Ash, %	<.001	<.001	<.001	0.023	0.012	0.02	0.036	0.033	0.003	0.067
Oxygen, % (by difference)	0.62	0.24	0.36	0.61	0.41	0.46	1.04	0.83	1.07	1.3
Conradson Carbon Residue, %				2.1	6.0	4.4	3.98	5.1	4.1	12.4
Asphaltene, %				0.34	3.24	0.94	0.74	2.59	0.036	4.04
Flash Point °F				205	350	325	210	176	182	275
Pour Point, °F				50	48	105	61	48	40	66
API Gravity at 60°F	33.1	18.3	32.6	24.9	19.8	25.1	21.8	23.3	33.1	15.4
Viscosity, SSU, at 140°F	33.0	32.0	30.8	131.2	490	222.4	199	113.2	36.1	104.9
at 210°F	29.5	28.8	29.5	45	131.8	69.6	65	50.5	30.7	240
Heat of Combustion:										
Gross Btu/lb			19,330	19,260	19,070	19,110	19,070	18,400	19,430	18,520
Net Btu/lb				18,140	17,980	17,970	17,980	17,300	18,240	7,500
Calcium, ppm				7.1	1.2	9.52	14	8.7	0.13	9.2
Iron, ppm				16	2.6	123.6	16	6.5	6.3	13.2
Manganese, ppm				0.09	0.02	0.46	0.13	0.09	0.06	0.10
Magnesium, ppm				3.7	0.08	2.23	3.6	3.6		3.3
Nickel, ppm				6.7	13	14.10	17	19	0.43	32.7
Sodium, ppm				37	0.98	3.74	57	15	0.09	64.5
Vanadium, ppm				14	25	3.11	2.3	101	<.1	81.5

Table 3-2. Liquid Fuels Tested (cont.)

	"Ultra-Systems" Oil	Gulf Coast	Venezuelan	Alaskan	California #1	California #2	California #3	California #4	Synthoil	Shale (Crude)
Ultimate Analysis:										
Carbon, %	87.68	84.62	85.24	86.04	85.75	85.41	85.33	86.66	86.30	84.5
Hydrogen, %	11.61	10.77	10.96	11.18	11.83	11.44	11.23	10.44	7.44	11.3
Nitrogen, %	0.36	0.36	0.40	0.51	0.62	0.77	0.70	0.86	1.36	2.08
Sulfur, %	0.42	2.44	2.22	1.63	1.05	1.63	1.60	0.99	0.80	0.63
Ash, %	0.02	0.027	0.081	0.034	0.038	0.043	0.032	0.20	1.56	.026
Oxygen, % (by difference)		1.78	1.10	0.61	0.71	0.71	1.02	0.85	2.54	1.36
Conradson Carbon Residue, %		14.8	6.8	12.9		8.72	9.22	15.2	23.9	2.9
Asphaltene, %		7.02	8.4	5.6		5.18	5.18	8.62	16.55	1.33
Flash Point °F	165	155	210	215		---	150	180	210	250
Pour Point °F	80	40	58	38		38	30	42	80	80
API Gravity at 60°F	16.7	13.2	14.1	15.6	19.5	15.4	15.1	12.6	S=1.14	20.3
Viscosity, SSU, at 140°F	950	835	742	1,071	246.1	854	748	720	10,880	97
at 210°F		181	196.7	194	70	129	131.6	200	575	44.1
Heat of Combustion:										
Gross Btu/lb	17,746	18,240	18,400	18,470		18,470	18,460	18,230	16,480	18,290
Net Btu/lb		17,260	17,400	17,580		17,430	17,440	17,230	15,800	17,260
Calcium, ppm		4.4	9.1	6.9		21	14	90.06	1,670	1.5
Iron, ppm		19	11	24		73	53	77.2	109	47.9
Manganese, ppm		0.13	0.09	0.06		0.8	0.1	0.87	6.2	0.17
Magnesium, ppm		0.4	3.8	1.4		5.1	3.8	31.4	170	5.40
Nickel, ppm		29	52	50		65	82	88	2.6	5
Sodium, ppm		3.6	32	37		21	2.6	22.3	148	11.71
Vanadium, ppm		45	226	67		44	53	66.2	6.5	<.3

0.16 to 0.86. If all this nitrogen were to be converted to NO this would correspond to a range of fuel NO of 250 ppm to 1390 ppm at 0% O_2. The residual fuels tested were:

- R1 Essex County - a low sulfur East Coast No. 5 used in an EPA-supported field test of NO_x control studies applied to package boilers;
- R2 Middle East - a residual refined from a Middle Eastern crude;
- R3 Low Sulfur - this low sulfur No. 6 was used in tests carried out by Southern California Edison (Mansour and Jones[1]) with Paraho shale oil (A3);
- R4 Indonesian/Malaysian - this residual formed from a blend of two crudes was chosen for the baseline fuel because of its availability and its nitrogen content was typical of the broad range of fuels being burned throughout the country;
- R5 Desulfurized Venezuelan - the desulfurized version of fuel R8;
- R6 Pennsylvania - an oil used by Brown[2] in a study of coal/oil mixtures;
- R7 Gulf Coast;
- R8 Venezuelan;
- R9 Alaskan - a Bunker C oil produced from a North Slope crude;
- R10 - R13 - examples of residual fuels available in California;
- "Ultrasystems" oil - a blended residual oil used only in the Phase I Pilot Scale Studies (see Section 5.0).

3. Alternative Fuels

Three alternative fuels were procured for testing:

- A1 Shale DFM - a shale-derived diesel fuel marine;
- A2 Synthoil - centrifuged synthoil produced from a West Viriginia coal;
- A3 Crude Shale - Paraho unrefined shale oil

Since the principal objectives of this program were concerned with nitrogen oxide emission control, the nitrogen content of the various oils was of considerable significance. Wendt and co-workers[3] and De Soete[4] have suggested that reactions involving sulfur and nitrogen specie in fuel-rich mixtures can influence fuel NO formation. Consequently, fuel sulfur content could influence fuel nitrogen conversion, particularly under staged combustion conditions, and it was thought that it was necessary to test fuels with a range of sulfur contents. Figure 3-2 shows the nitrogen contents of the fuels tested as a function of fuel sulfur content. It can be seen that the residual fuels fall into three groups: 1) low nitrogen, low sulfur; 2) high nitrogen, intermediate sulfur; and 3) intermediate nitrogen, high sulfur. Within the first group there is an example of fuels with similar nitrogen contents, but a considerable difference in sulfur level.

Figure 3-3 shows the nitrogen content of the fuels tested as a function of API gravity. Nitrogen content increases as the gravity decreases. It should be noted that several of the fuels can be classified as No. 5 oils. Also, the API gravity quoted for the West Texan Diesel (D-2) is uncharacteristically low. A similar (but reverse) distribution can be seen in Figure 3-4 which shows nitrogen content as a function of carbon-to-hydrogen ratio. As before, the properties of D-2 are different from the other distillate fuels.

Asphaltene content of petroleum oils is quite often used as an indicator of their potential for particulate emissions. Figure 3-5 shows the nitrogen content of the fuels tested as a function of their asphaltene content. All fuels with asphaltene contents above four percent show a relatively wide variation in nitrogen content.

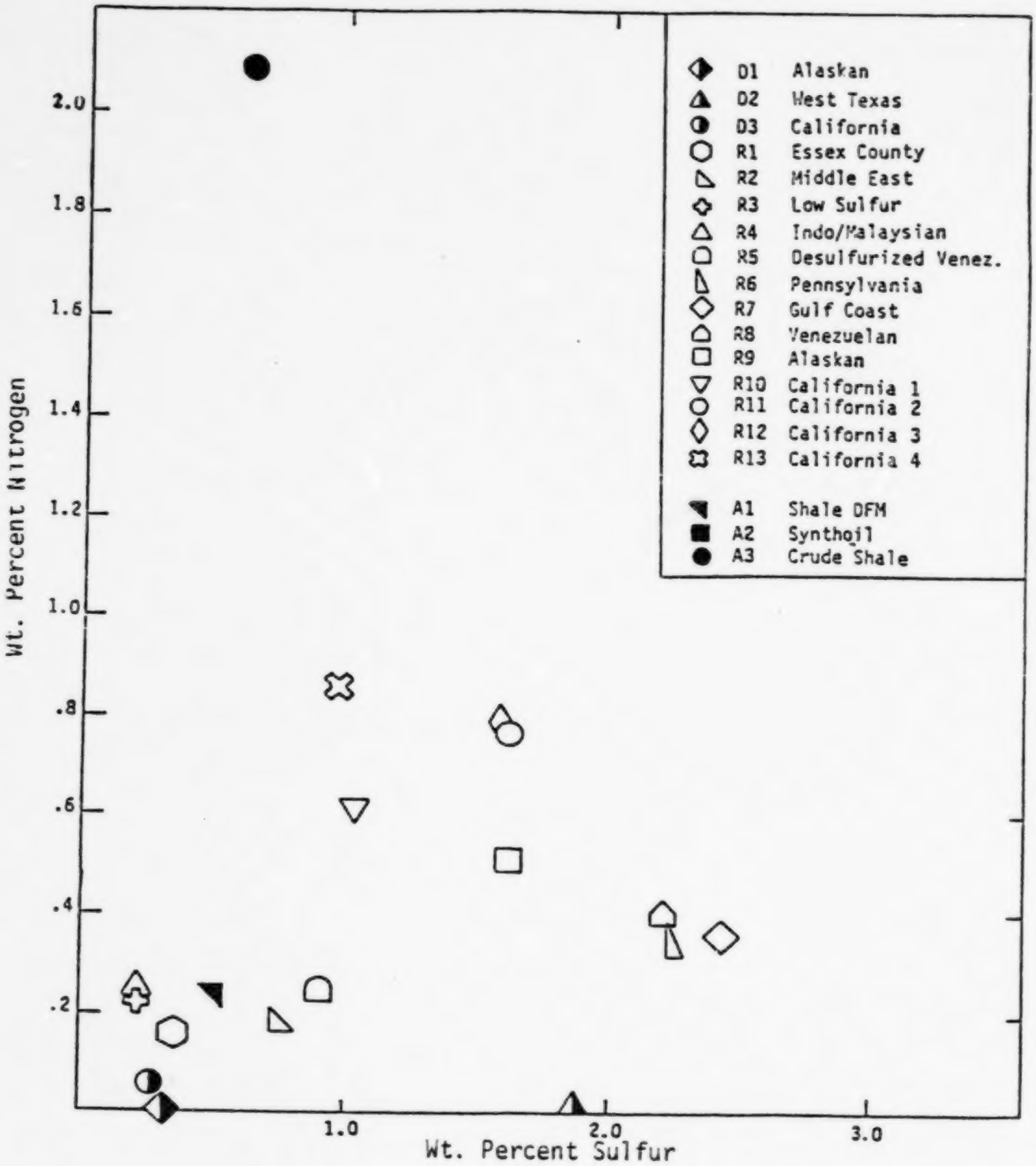

Figure 3-2. Fuel Nitrogen Versus Sulfur Content.

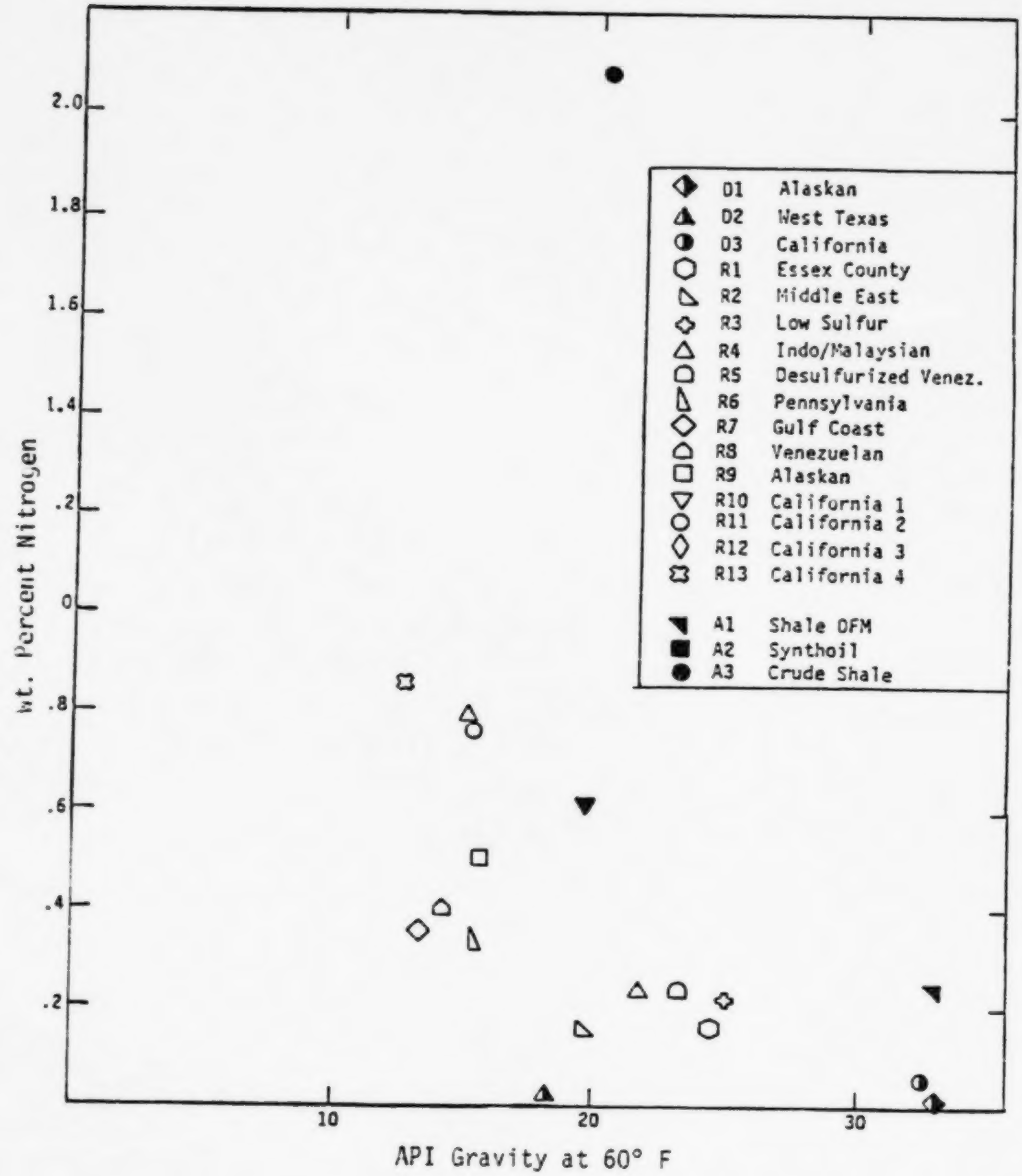

Figure 3-3. Fuel Nitrogen Versus API Gravity.

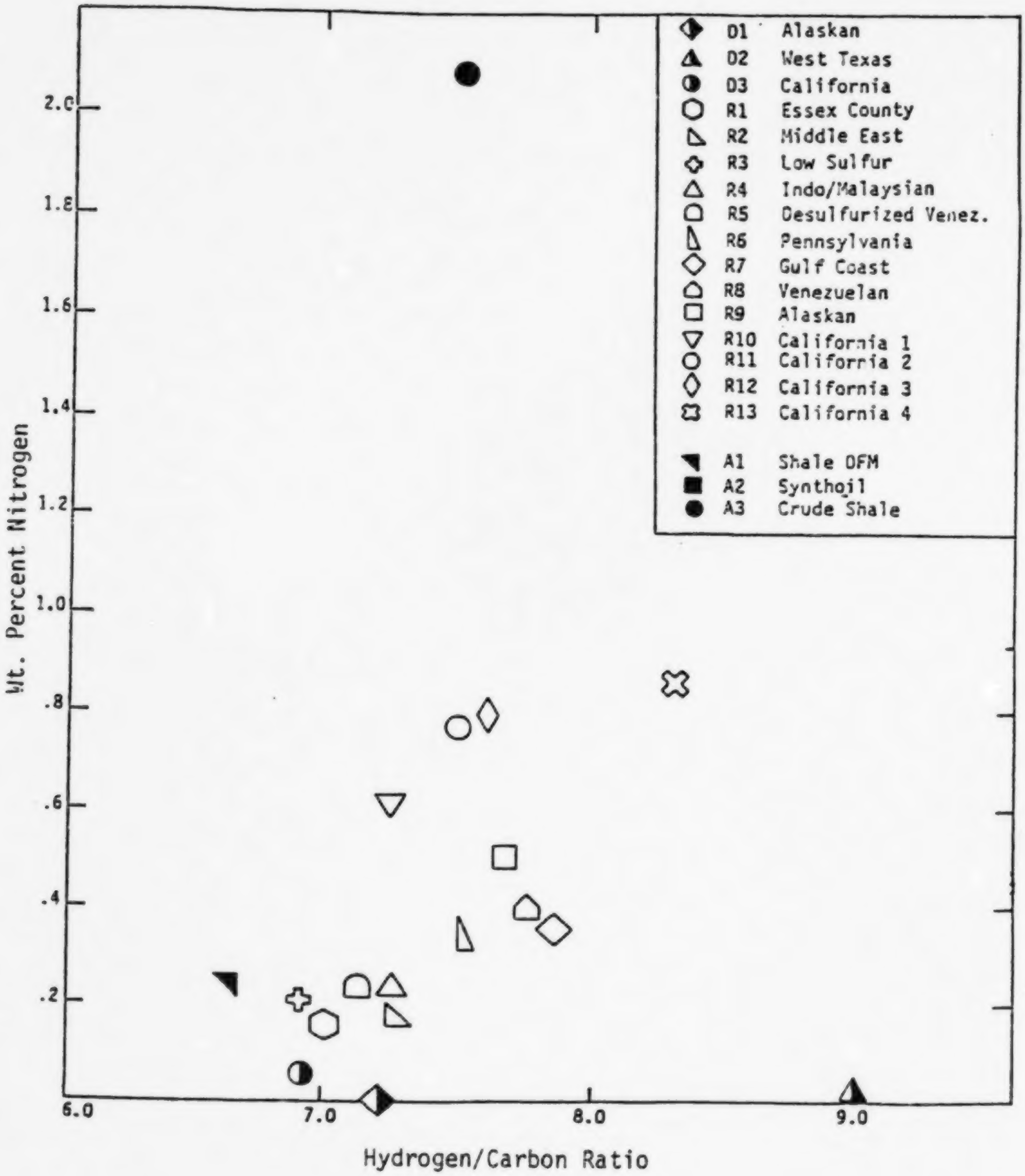

Figure 3-4. Fuel Nitrogen Versus H/C Ratio.

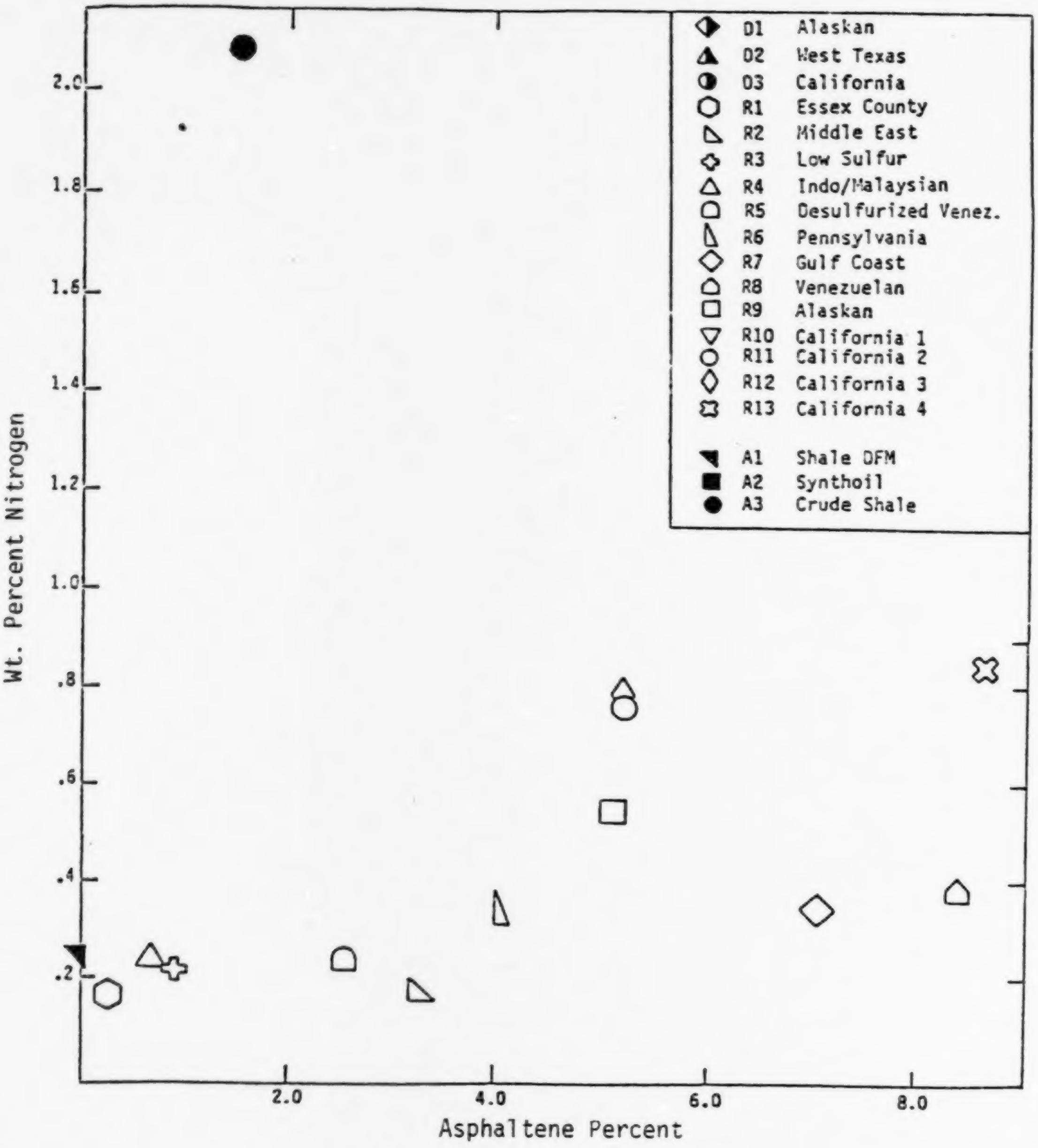

Figure 3-5. Fuel Nitrogen Versus Asphaltene Content.

To quantify the distribution of nitrogen in each of the fuels tested, vacuum distillation data were obtained from an independent testing laboratory. The oil was distilled first at atmospheric pressure and then under vacuum into five fractions and the total mass and nitrogen content of each of these five fractions were determined. Figures 3-6 and 3-7 present the results of these distillations for percent mass loss and percent nitrogen evolved as a function of distillation temperature. The data indicate that there is a large variation in the temperature at which nitrogen is evolved from the various oils. It should be remembered that the temperatures at which nitrogen is evolved will probably be different in flames. However, it is considered that the results obtained with vacuum distillation provide a qualitative ranking for the "refractory" nitrogen content of the various oils.

Oil viscosity has important practical implications because it is a measure of resistance to flow and a minimum viscosity is necessary for efficient atomization. Viscosity in Saybolt Universal Seconds is plotted as a function of temperature in Figure 3-8 together with bands representing the ranges for No.6, heavy No.5 and light No.5 oils. It can be seen that the two shale-derived fuels have low viscosities but the viscosity of the Synthoil is very high. Initially it was not possible to burn this fuel without cutting it with 10 percent light fuel oil.

Several of the fuels tested were also characterized by differential thermogravimetric analysis (DTA). In this analysis procedure a sample of the fuel is placed in a platinum boat which forms one arm of a balance. The boat is contained in a furnace whose rate of temperature rise can be controlled. As the temperature of the furnace is increased the fuel vaporizes and the weight loss as a function of time is recorded. The slope of this curve provides the rate of weight loss. This procedure can be carried out in air or nitrogen and the difference between the curves shown is then indicative of the residuum fraction which will remain in an inert atmosphere, whereas once an ignition point occurs, all the fuel will burn when the analyses is carried out in air. Figure 3-9 compares TGAs for several fuels showing the different character of some of the fuels listed in Table 3-2. It appears that the Indonesian/Malaysian oil contains some middle cut which is completely absent from the Gulf Coast oil, and that the California and Gulf Coast oils have light ends which boil at a similar temperature. This type of information provides a qualitative comparison of the burning rate of the various fuels. Fuels which do not show a weight loss at low temperatures will probably have poor ignition characteristics and will require high internal recirculation rates for flame stabilization. Fuels which show large weight losses at high temperature might well be prone to particulate formation.

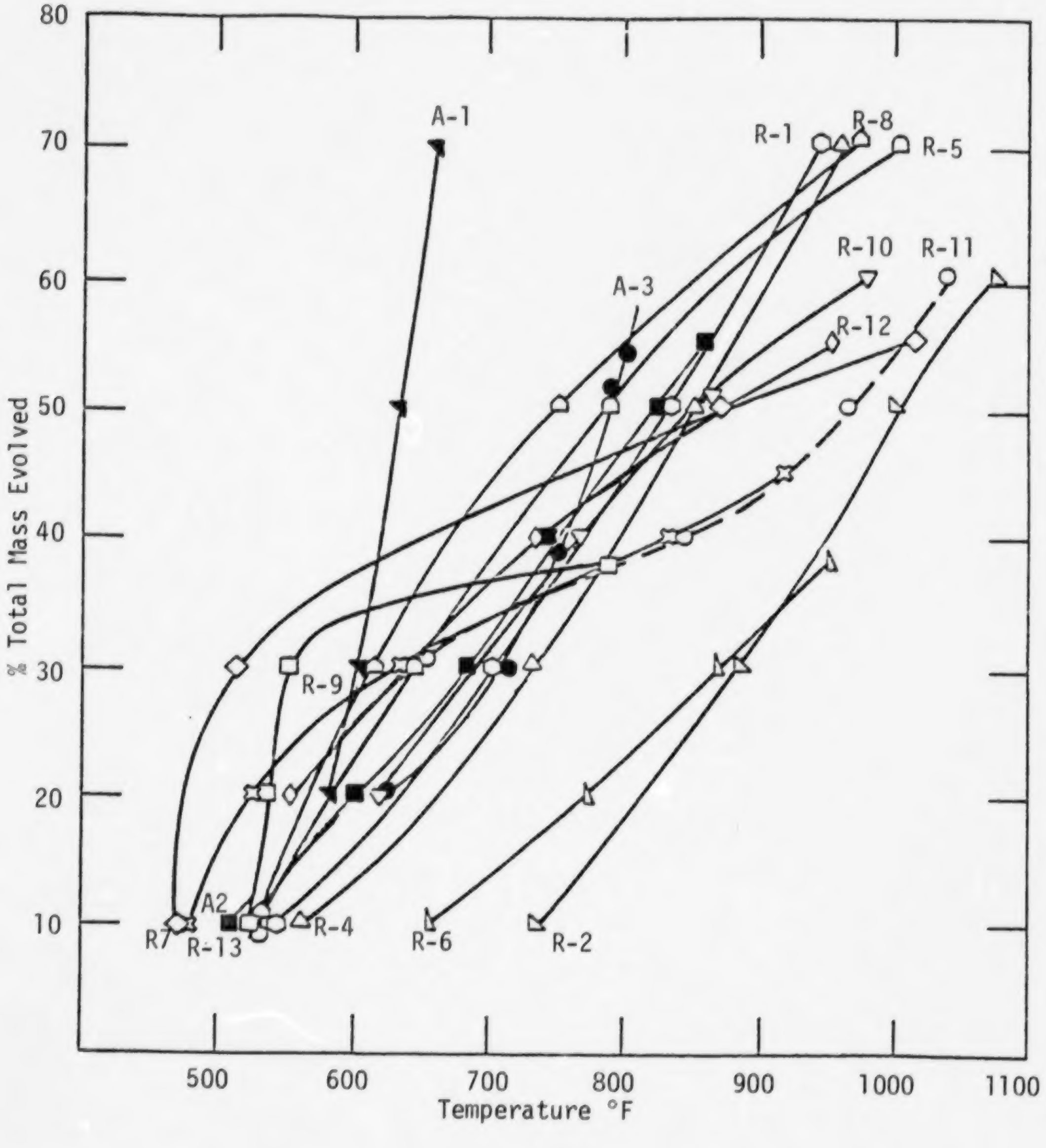

Figure 3-6. Vacuum Distillation Results - Mass Evolved.

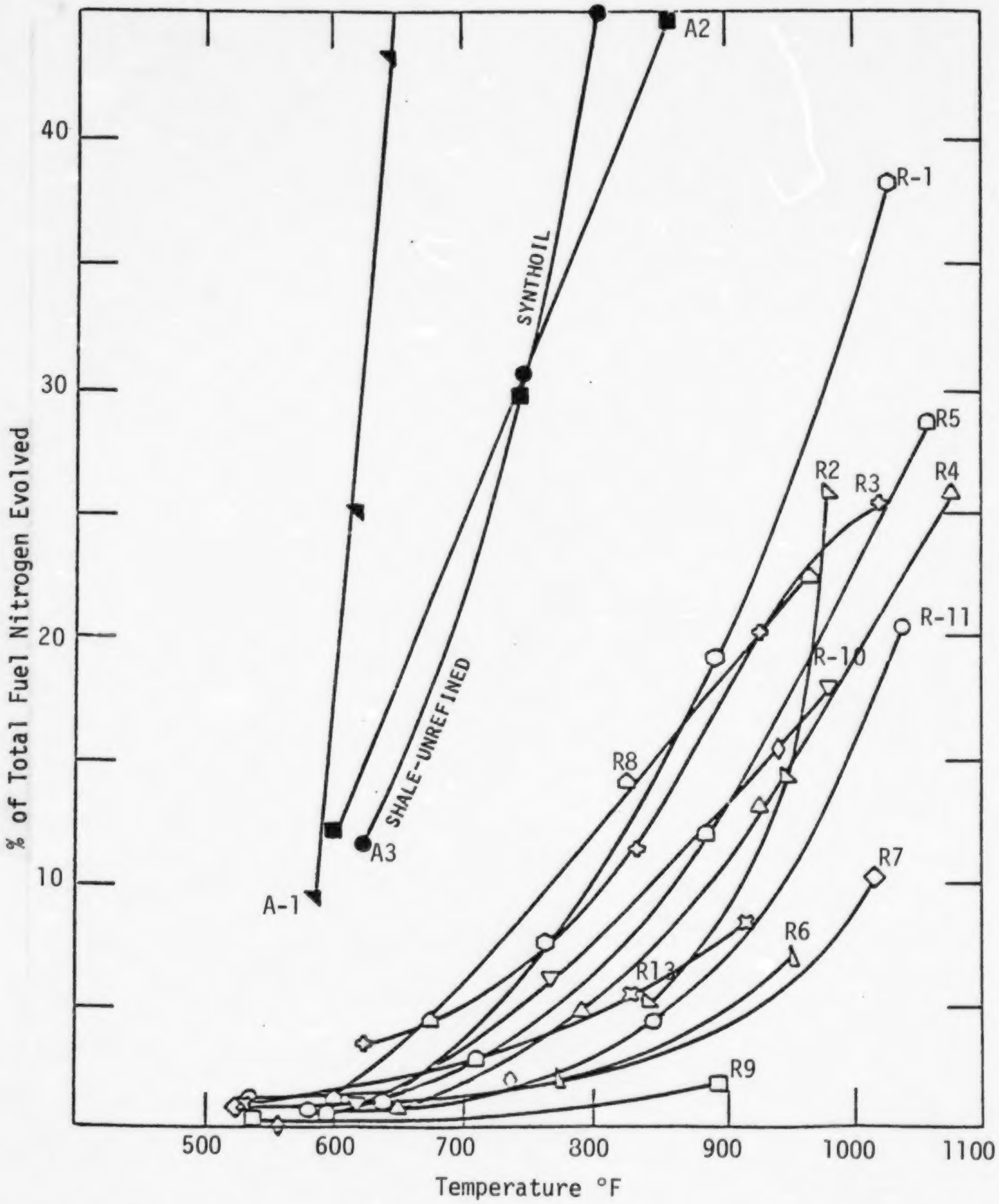

Figure 3-7. Vacuum Distillation Results - Nitrogen Evolved.

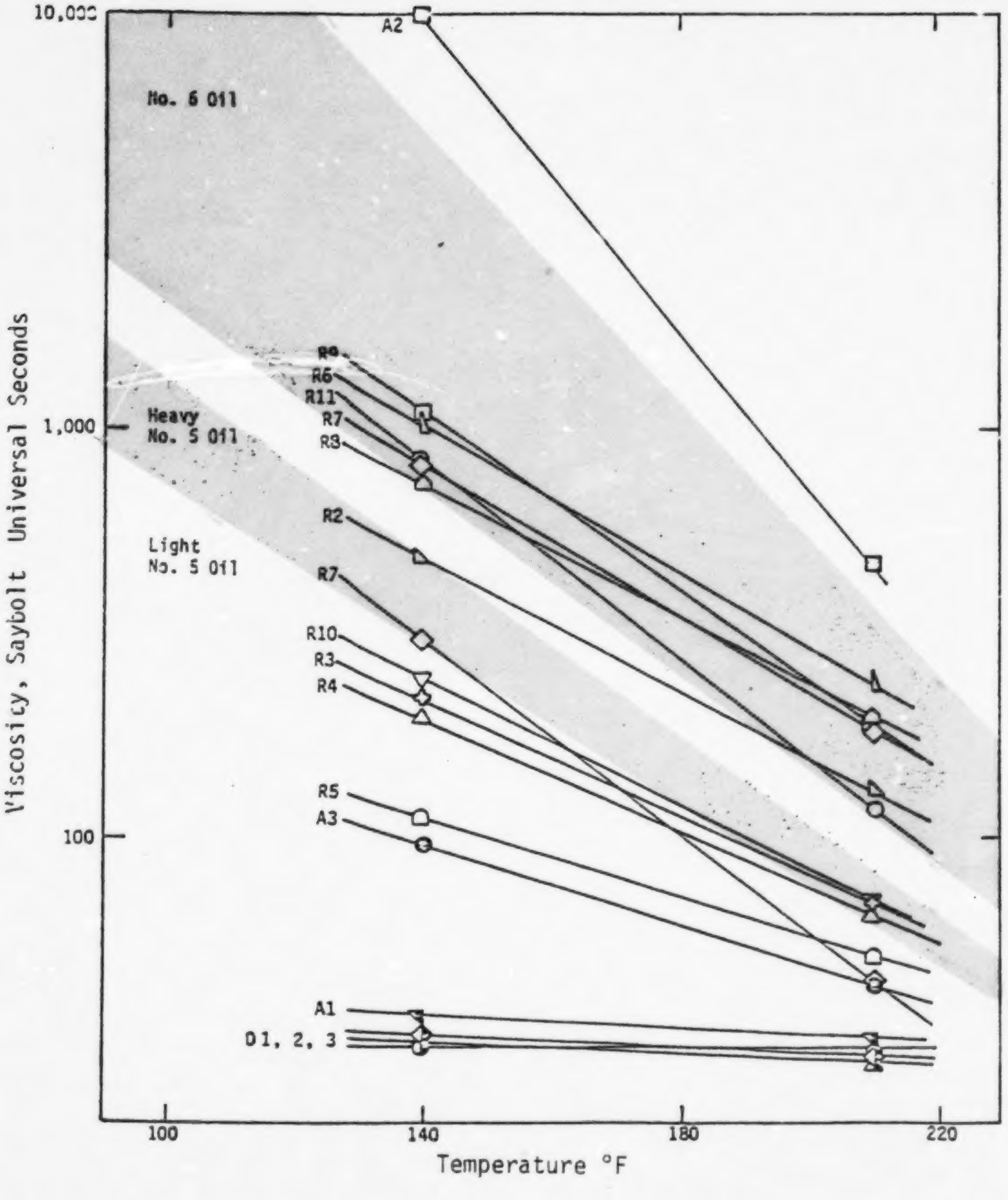

Figure 3-8. Viscosity of Fuels Tested.

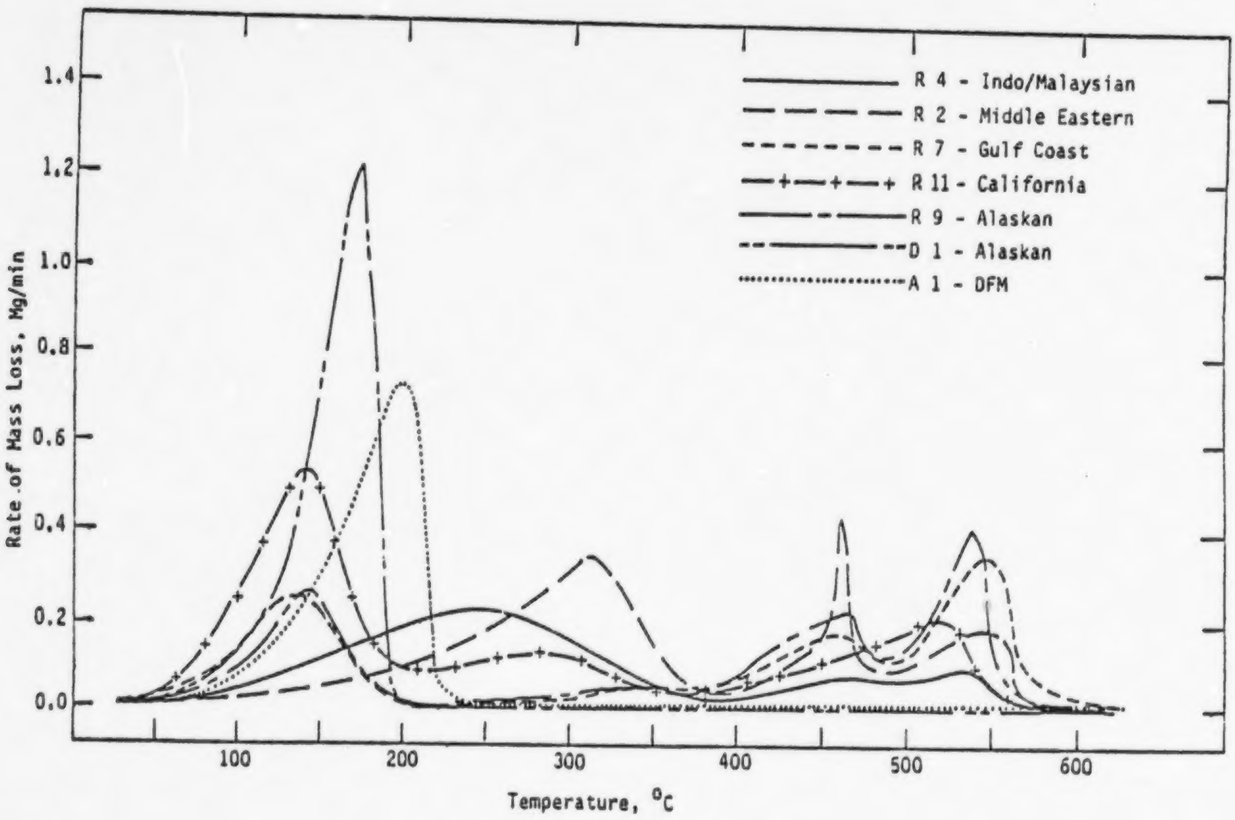

Figure 3-9. DTA Analysis of Eight Fuel Oils.

4.0 SMALL-SCALE RESULTS

4.1 Summary

This portion of the report contains a comprehensive description of the more than 1,050 tests conducted with the small-scale tunnel furnace during this contract. Fuel composition and drop size effects could be more easily examined in the small tunnel furnace because (1) many of the widely different fuels were only available in small quantities; (2) the combustion variables could be more precisely controlled in the tunnel furnace; and (3) fuel and thermal NO_x could be separated in the small-scale. (The pilot-scale testing described in Section 5 focused on atomization because of the wide range of nozzles commercially available for the package boiler simulator and on limited fuel screening based on the small-scale results.)

The small-scale furnace, fuel property studies included investigations of both chemical composition and physical characteristics. Testing was conducted with three distillate oils, 13 petroleum-derived residual fuel oils, three alternate liquid fuels derived from oil shale and coal, and 14 doped and/or blended liquid fuels as described in Section 3.0 of this report. In general, both excess air and staged combustion conditions were considered.

All of the testing was conducted in a 20cm diameter by 2.1m long, tunnel furnace at a nominal thermal input of 20 kW (70,000 Btu/hr). An ultrasonic atomizer was used for most of the testing because it provided excellent atomization (mean drop size 20 μm) of a wide range of heavy liquid fuels at low flow rates (0.5 gal/hr). The exhaust stream was continuously monitored for the combustion gases (CO, CO_2, and O_2) using standard analytical equipment and for NO and NO_x using a chemiluminescent analyzer. Under excess air conditions, fuel NO_x was isolated using an $Ar/O_2/CO_2$ artificial atmosphere. No attempt was made to determine fuel NO_x under staged combustion conditions because of a potential kinetic effect of adding CO_2 into the first stage. Smoke emissions were not routinely measured during the small-scale testing because they were unrealistically low due to the hot refractory walls throughout the furnace. Further, some of the low NO_x conditions studied during the tunnel furnace experiments may not be practical in a cold-wall package due to excessive smoke formation.

4.1.1 Excess Air Conditions

Because of the rapid mixing nature of the small-scale burner and the fine atomization achieved with the ultrasonic nozzle, both total and fuel NO_x were relatively insensitive to the overall excess oxygen under excess air conditions. In general, both total and fuel NO_x increased steadily with increasing fuel nitrogen. The distillate oil, petroleum-derived residual oil, and alternate fuel data all correlated well together, and, infact, under excess air conditions the only first-order composition parameter was total fuel nitrogen content. Doped distillate oils and doped residual oils were found to approximately simulate actual heavy residuals. No significant influence of sulfur content or ash composition was observed. The percent conversion of the fuel nitrogen decreased from approximately 90 percent at zero percent fuel nitrogen to approximately 50 percent at two percent fuel nitrogen. Thermal NO_x was found to be approximately 30 percent higher for the distillate oils than for the heaviest residual fuel oils. This was believed to be the result of an increase in local burning rate which caused higher local temperatures (less time for radiative and convective cooling) in the case of the very volatile distillate oils.

Fuel viscosity was varied between 40 and 200 SSU by altering the fuel temperature at the nozzle. In general, increasing fuel viscosity had little effect on either the fuel or thermal NO_x formation except in one case where the quality of the atomization is believed to have decreased dramatically at the high viscosity condition.

The influence of bulk gas temperature was determined by varying the CO_2 content of the oxidizer stream. Tests with five heavy fuel oils indicated that a 200^oK change in the measured gas temperature had little influence on fuel NO_x formation.

The influences of drop size and size distribution were determined by varying the atomizing air pressure between four and 20 psig. Data taken with both petroleum-derived residual liquids and alternate liquids indicated that as the mean droplet diameter was increased from 20 μm to 200 μm, thermal NO_x formation increased slightly and then decreased by as much as

50 percent. Fuel NO_x formation generally decreased with increasing drop size. It was not possible to investigate the effect of atomizer design in detail during this testing because only two atomizers are commercially available for heavy oil firing in the appropriate size range. Data obtained on these two units did, however, indicate that the atomizer which produced the smallest droplets (20 μm) also produced the highest thermal NO_x emissions under excess air conditions.

4.1.2 Staged-Combustion Conditions

Staged combustion was found to be a very effective means of controlling NO_x emissions. Reductions (relative to excess air conditions) greater than 85 percent were typical for the alternate and petroleum-derived liquid fuels. As the primary zone stoichiometry was decreased from 1.0, the emissions dropped dramatically, went through a minimum, and then increased again, in general. The primary zone stoichiometry required to achieve minimum emissions was found to be a function of both first stage residence time and fuel composition, but it was generally between 0.7 and 0.85. Increasing the first stage residence time decreased the measured exhaust emissions. This effect was most significant below residence times of approximately 700 ms.

In strong contrast to the excess air studies, the minimum NO_x emissions staged were not found to be a simple function of total fuel nitrogen content. More fundamental data are required before definitive conclusions can be reached; however, it appears that the effectiveness of staged combustion conditions is dependent on both the amount of fuel nitrogen and the fraction of that nitrogen which is refractory (nonvolatile) in nature. The shale liquids tend to produce extremely high emissions under excess air conditions because they contain large amounts of fuel nitrogen; however, under staged conditions the emissions are dramatically reduced because the nitrogen is relatively volatile in nature. In contrast, some of the petroleum-derived liquids most notably the Alaskan North Slope oil, were not as easily controlled with staged combustion, because a significant fraction of their fuel nitrogen appears to be relatively heavy in character.

Under staged combustion conditions increasing the mean droplet diameter increased the thermal NO_x formation, but had relatively little effect on fuel NO_x formation.

4.2 Combustion Facility

4.2.1 Tunnel Furnace

The tunnel furnace which was designed and constructed under this contract is illustrated schematically in Figures 4-1 and 4-2. The design allowed commercially available atomizers to be utilized for economical testing of a wide range of liquid fuels, including residual fuel oils, in either natural air or artificial atmospheres. The axisymmetric combustion chamber, constructed of a high-temperature, castable refractory core surrounded by insulating refractories, is 2.1 meters long and 20 cm in inside diameter. The overall outside diameter, including the steel shell, is 81 cm. Ports with quartz windows for sampling, observation, and air injection are located along the length of the furnace. Thermocouples for measurement of wall temperatures are located in each section. The full load firing rate was C.53 cc/sec (0.5 gal/hr) which corresponds to a nominal thermal input of 20 kW (70×10^3 Btu/hr-ft^3) in the burner zone. The furnace was fired continuously on propane gas whenever experiments were not in progress to extend the life of the refractory and reduce time spent waiting for furnace heat-up to operating temperature. A spark-ignited propane pilot was also used to sustain initial ignition. A damper located in the steel exhaust stack allowed slight positive pressure to be maintained in the furnace at all times.

Four auxiliary firing ports were cast in the refractory surrounding the main combustion chamber to allow the furnace to be maintained at adiabatic temperatures. Four up-fired gas pilots were installed with flame detectors and safety systems; however, these were not used because severe cracks quickly developed between the auxiliary ports and main combustion chamber which allowed the combustion products to mix. The auxiliary ports were later plugged with refractory to stop air inleakage.

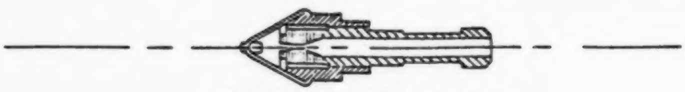

Ultrasonic Twin-fluid Atomizer

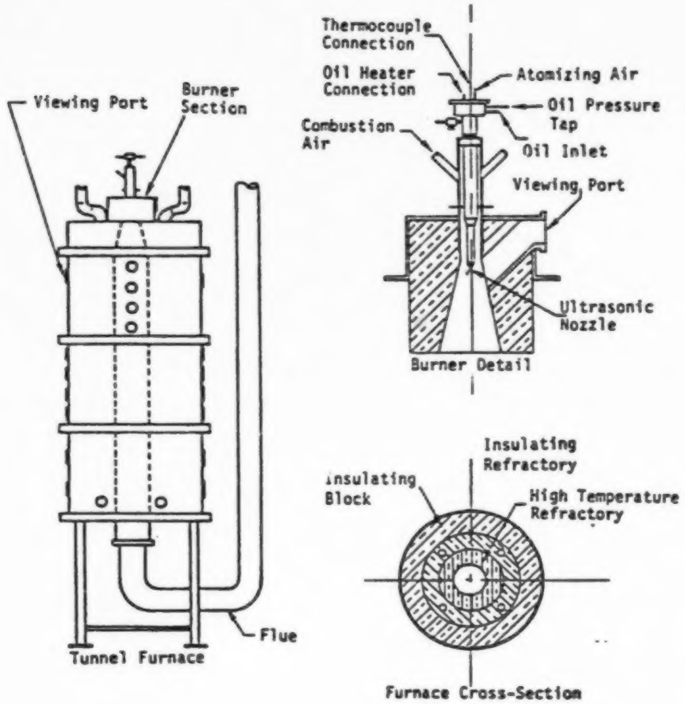
Viewing Port
Burner Section
Flue
Thermocouple Connection
Oil Heater Connection
Atomizing Air
Oil Pressure Tap
Combustion Air
Oil Inlet
Viewing Port
Ultrasonic Nozzle
Insulating Refractory
Insulating Block
High Temperature Refractory

Tunnel Furnace

Burner Detail

Furnace Cross-Section

Figure 4-1. Details of the Tunnel Furnace System.

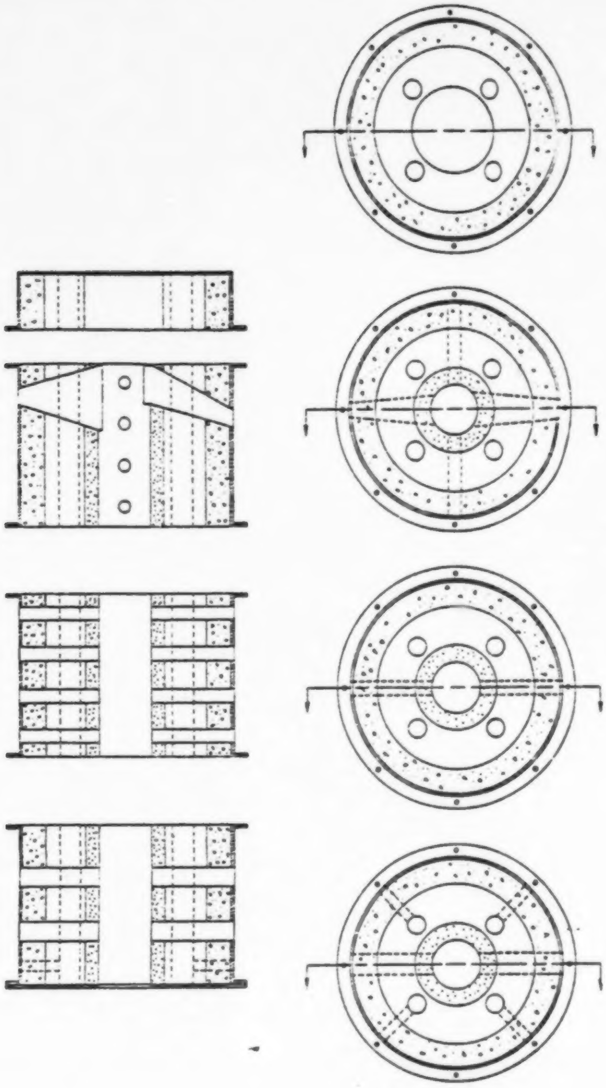

Figure 4-2. Cross Section Drawing of Furnace.

The furnace is capable of utilizing either natural air or artificial oxidants for combustion of the fuels. Figure 4-3 illustrates the air and fuel flow systems. Natural air was supplied from a 690 kPa air compressor and partificial atmospheres were mixed from gases contained in high-pressure cylinders. The gases were mixed in a manifold and the mixture composition was precisely monitored on the analytical instruments. The main combustion "air" was metered with a Brooks high-accuracy 600 mm rotameter and preheated with an electric circulation heater. The atomization "air" was also metered with a 600 mm rotameter but was not preheated.

For those experiments involving two-stage combustion, two water-cooled air injection lances were fabricated which allowed a portion of the combustion air to be added downstream of the fuel injector through any of 10 available sampling ports along the length of the furnace. The tip of the lances was designed to inject the air at a relatively high velocity (21-30 m/sec) normal to the furnace flow resulting in rapid mixing of the secondary air with the combustion products.

The test fuels were electrically heated in a small 19 liter (5 gallon) supply tank and drawn into a precision variable speed gear-type metering pump (Zenith Model BPB-4391-1.168 with Model ZM constant torque drive unit). The oil flow rate was varied by direct mechanical adjustment of the pump speed and electrically heated lines were used wherever feasible to facilitate pumping very viscous fuels.

4.2.2 Burner System

Fuel and primary air entered the combustion chamber through the burner illustrated in Figure 4-1. The combustion air was introduced axially without swirl into a long refractory burner exit of L/D=5. The throat of the burner was 5.1 cm (2.0 inches) in diameter which yields a combustion air velocity at the throat of 5.3 m/sec at 115 percent theoretical air and $405^{\circ}K$ preheat. Due to coke formation on the nozzle tip, a removable sleeve (ID = 4.1 cm) was inserted in the throat to increase the velocity to 8.5 m/sec which displaced the flame front one to two nozzle diameters downstream and alleviated the coking problems. This sleeve was in place throughout the program. A narrow observation slot was located along the divergent to allow the flame front and nozzle tip to be viewed.

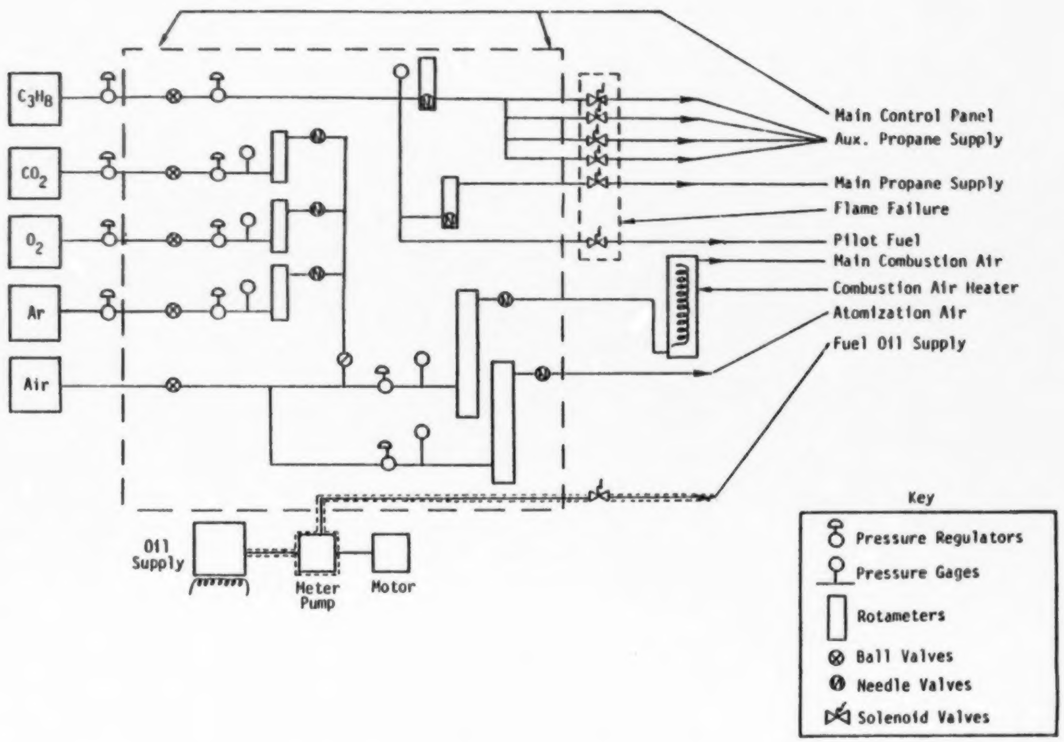
C_3H_8
CO_2
O_2
Ar
Air
Main Control Panel
Aux. Propane Supply
Main Propane Supply
Flame Failure
Pilot Fuel
Main Combustion Air
Combustion Air Heater
Atomization Air
Fuel Oil Supply
Oil Supply
Meter Pump
Motor
Key
Pressure Regulators
Pressure Gages
Rotameters
Ball Valves
Needle Valves
Solenoid Valves

Figure 4-3. Flow System.

The fuel injection system consisted of a 19 mm (3/4 in.) diameter stainless steel tube which contained the atomizing air supply tube, a cartridge heater for final oil temperature control, and a chromel/alumel thermocouple positioned in the injector tip prior to the nozzle for accurate oil temperature measurement. This fuel gun with a commercial air assisted ultrasonic oil atomizer (Sonicore Model 052H, Sonic Development Corporation) was used for the bulk of the test program because it provided excellent atomization of a wide range of heavy liquid fuels at low flow rates. Figure 4-1 illustrates this fuel gun and nozzle.

A second fuel gun was fabricated to allow another commercial atomizer to be used in the tunnel furnace. The fuel gun and nozzle (Delavan, Siphon Nozzle, Model 30610-5) are shown in Figure 4-4. This differs from the one shown in Figure 4-1 since the fuel oil is supplied and heated through the center tube. The tube was constructed of thin-wall, stainless-steel tubing through which a low voltage current was passed causing the tube to act as a controllable heating element. The entire gun was surrounded by a cooling jacket. This gun was used with both the Sonicore or Delavan nozzles since the oil temperature could be very accurately controlled whether the oil is supplied through the central tube or around it. In all cases, the tip of the nozzle was precisely located at the throat of the burner (beginning of the sloping section shown in Figure 4-1). Previous work(1) had indicated that the location of the fuel injector could influence the fuel/air mixing, and hence, the NO_x formation.

4.2.3 Analytical System

The analytical system used for this program allowed for continuous monitoring of NO, NO_x, CO, CO_2, O_2, and SO_2 using the instruments listed in Table 4-1. The same system was employed for both the package boiler simulator and the tunnel furnace. Flue gas was drawn from the appropriate stack through a water-jacketed, stainless-steel probe and immediately into an ice bath water condensor to dry the sample. The sample was then passed through a Pyrex wool filter, a stainless steel/Teflon-lined sample pump, and a stainless steel Balston instrument filter prior to the analytical

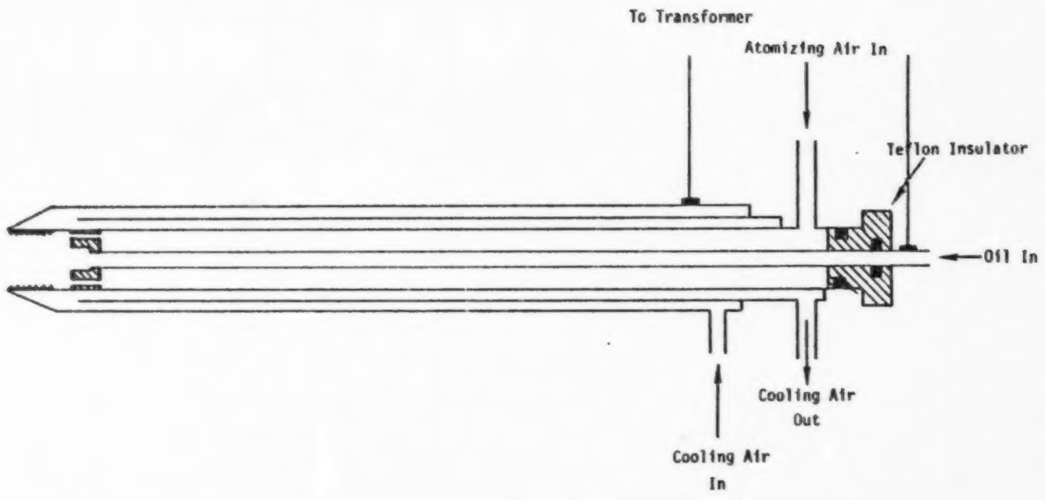
To Transformer
Atomizing Air In
Teflon Insulator
Oil In
Cooling Air Out
Cooling Air In

Figure 4-4. New Oil Gun.

instruments. All fittings were stainless-steel and all sample lines 1/4-inch Teflon tubing.

Table 4-1. Analytical Instrumentation

NO	Thermo Electron Model 10A Chemiluminescence Analyzer
NO_x	TECO Model 10A with Stainless Steel Converter
O_2	Servomex Paramagnetic
CO, CO_2	Anarad Model AR-600 NDIR
SO_2	Thermo Electron Model 40 Pulsed Fluorescence Analyzer

4.3 Results -- Excess Air Conditions

4.3.1 Identification of Fuel NO_x

Throughout this work, fuel NO_x is defined to be the emissions measured when the combustion air was replaced with a synthetic-oxidant mixture containing 21 percent O_2, 20 percent CO_2, and 59 percent argon. It is believed that these measurements approximate the NO_x that results from oxidation of the fuel nitrogen during normal combustion; however, the possibility of fuel-thermal interactions must be acknowledged. To investigate the validity of this technique for determining fuel NO_x emissions, several experiments and calculations were conducted at the beginning of the program.

Propane and methanol were burned in the $Ar/O_2/CO_2$ atmosphere to demonstrate that these compressed gases did not contain significant N_2, and that room air was not leaking into the furnace. Figure 4-5 shows these results and indicates that when there was no nitrogen present in the fuel, the emissions were always less than 10 ppm. (The trace amounts measured with the propane flame may have been due to the commercial-grade propane containing trace N_2.)

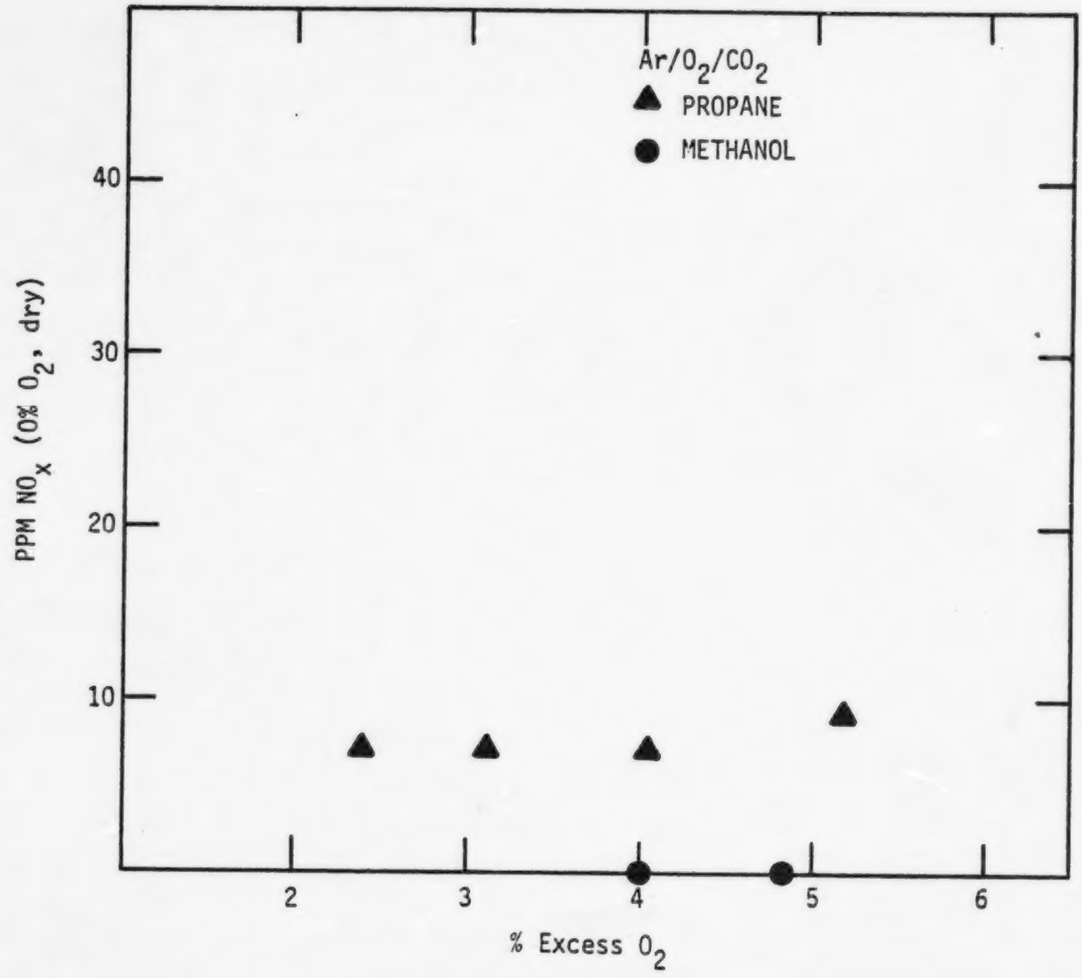

Figure 4-5. Emissions from Pure Fuels Burned in Ar/O$_2$/CO$_2$.

The CO_2 was used with the Argon to allow the theoretical flame temperatures to be approximately matched. Wall temperature measurements confirmed that this was indeed true. Kinetic-modeling studies(11) carried out with $CH_4/NH_3/O_2/N_2/Ar/CO_2$ mixtures in a well-stirred reactor demonstrated that the replacement of N_2 with Ar did not significantly change the distribution of total mass or the gas-phase nitrogen species resulting from typical fuel-nitrogen compounds. CO_2 was also predicted to be inert with respect to fuel-nitrogen chemistry under excess air conditions. This was confirmed by experimental tests(2) which demonstrated that the presence of CO_2 in the oxidizer did not have an appreciable effect on NO formation in an unstaged, pulverized-coal flame. However, under fuel-rich conditions, kinetic modeling studies indicated that the CO_2 tends to enhance fuel NO_x formation. Figure 4-6 shows the results of a 2 msec, well-stirred reactor calculation for a methane feed containing 1300 ppm NH_3. Examination of these calculations indicated that the fuel NO_x formation was enhanced because under fuel-rich conditions the CO_2 acts as an oxidant. Therefore, in this work no attempt was made to isolate fuel NO_x formation under fuel-rich conditions. All of the staged combustion data presented in this report were obtained by burning the liquid fuels in normal air.

Another potential problem was the influence of the artificial atmosphere components on the continuous analysis equipment. Argon and carbon dioxide have a more negative, relative magnetic susceptibility than nitrogen, but resulting error on the paramagnetic O_2 analyzer reading was computed to be less than 4 percent at the primary test condition. The effect of Argon and carbon dioxide on the Thermal Electron chemiluminescent NO analyzer was investigated by Folsom and Courtney(3). Figure 4-7 summarizes their experimental results for both rich and lean conditions. Their data indicate that the use of Argon and carbon dioxide causes the analyzer to read approximately 10 percent lower than the corresponding air case. This is due to differences in both viscosity and third-body quenching efficiency between the N_2 and the Ar/CO_2. Although this effect is certainly believed to be real unless otherwise noted, the fuel NO_x data presented in this report have not been adjusted to account for this measurement difference because:

- The effect is the same order of magnitude as the inherent experimental uncertainty of the testing (10 percent);

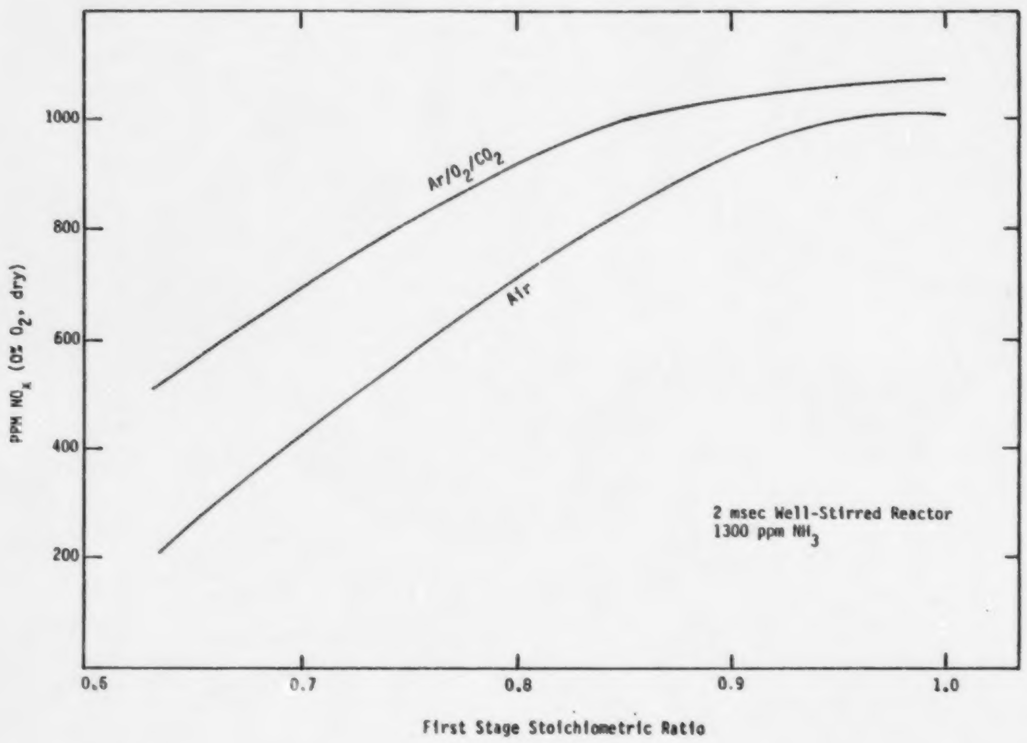

Figure 4-6. Kinetic Modeling Predictions on the Effect of $Ar/O_2/CO_2$ under Fuel-Rich Conditions.

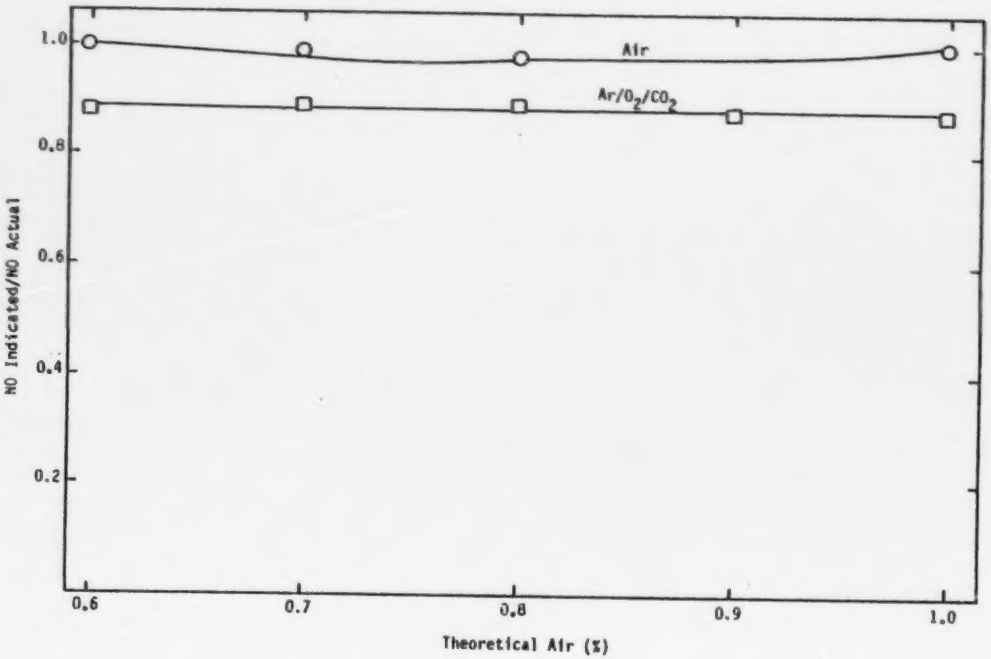

Figure 4-7. Influence of Oxidant Composition on Response of Chemiluminescent Analyzer.

- The effect is opposite and of approximately equal magnitude to predict kinetic differences (Figure 4-6) for fuel-lean stoichiometry.

In addition, the primary focus of this study was on a relative comparison of many different liquid fuels; therefore, it was decided that for reporting purposes the actual experimental results should be presented.

The technique of using $Ar/O_2/CO_2$ replacement to define fuel NO_x was further verified by studies using distillate and residual oils doped with pyridine. Figures 4-8 and 4-9 show the results of this testing. The solid symbols represent the fuel NO_x associated with the added pyridine based on tests in the Argon/oxygen/carbon dioxide atmosphere. (These data have been corrected for the effects of argon and carbon dioxide on the chemiluminescent analyzer.) The other symbols represent the fuel NO_x as determined by subtracting the emissions from the pure distillate oil burning in air from the emissions in the doped case (as suggested by Martin et al.(4)). The distillate oil results (Figure 4-8) indicate that the difference method predicts approximately 10 percent less fuel NO_x than the $Ar/O_2/CO_2$ technique. At present the reason for this difference is not fully understood. Figure 4-9 shows the results of similar testing with the desulfurized Venezuelan residual oil. In this case both methods agree very well.

Thus, in summary, considerable effort was expended to investigate the $Ar/O_2/CO_2$ replacement technique for fuel NO_x definition and although it cannot be absolutely validated, it appears to give a good indication of the amount of fuel nitrogen being oxidized in the flame zone.

Figure 4-10 shows a typical set of experimental results. The upper line (air data) represents the total NO_x emissions measured in the furnace exhaust. The data obtained in $Ar/O_2/CO_2$ indicate the fuel NO_x formation; the difference is then defined to be the thermal NO_x. Clearly, in light of the previous comments, the thermal NO_x data should be viewed as only an estimate of the fraction of the total which is the result of nitrogen fixation. Figure 4-10 shows data obtained over a four-month period and indicates the reproducibility of the experiments.

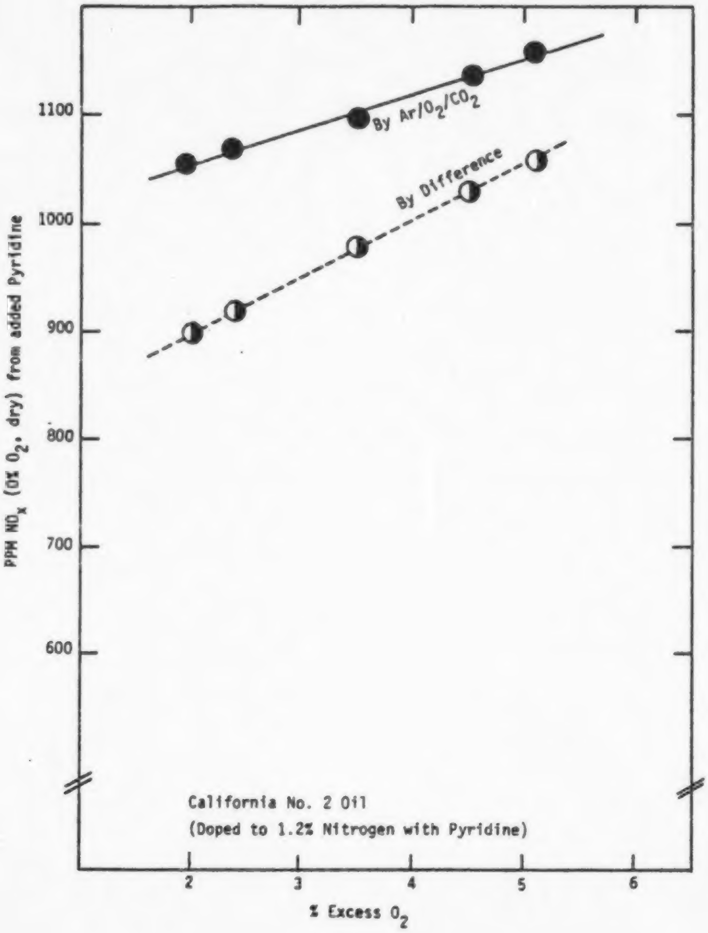

Figure 4-8. Comparison of Fuel NO_x Determination Methods - Distillate Oil.

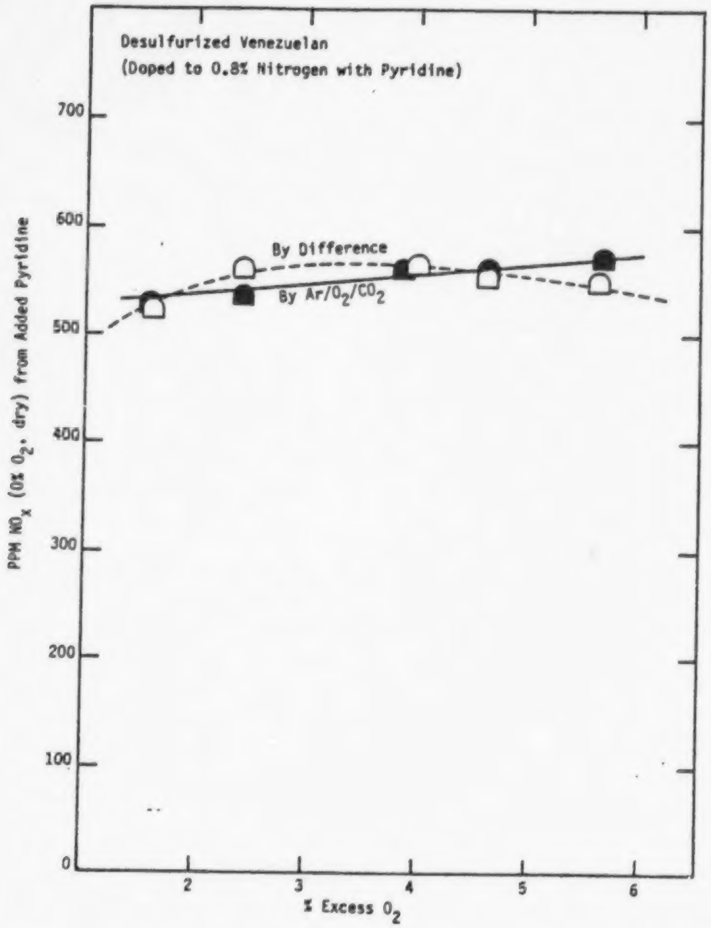

Figure 4-9. Comparison of Fuel NO_x Determination Methods - Residual Oil.

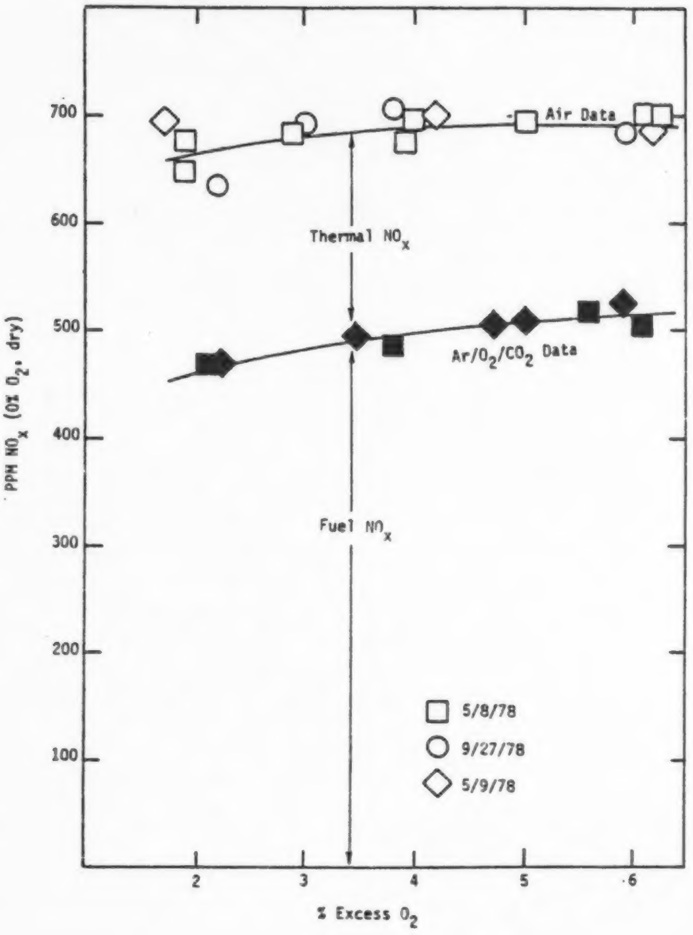

Figure 4-10. Typical Data on Fuel and Thermal NO$_x$.

4.3.2 Fuel Properties -- Chemical

4.3.2.1 Distillate Oils

Figures 4-11 through 4-13 summarize the baseline data obtained with the three distillate oils evaluated in this study. In each case the combustion air preheat was $405 \pm 5^{\circ}K$, the firing rate was 0.55 cc/sec, and the atomizer was the ultrasonic nozzle with 205 kPa (15 psig) atomization pressure. The fuels were not preheated because of their inherently low viscosities; however, the oil temperature at the nozzle was approximately $150^{\circ}F$ due to convective heating of the fuel injector. The upperline (half-shaded symbols) indicates the total NO_x emissions measured as a function of excess oxygen in the tunnel furnace exhaust. Fuel NO_x (lower line, solid symbols) was isolated by replacing the combustion air with the synthetic oxidant mixture containing 21 percent O_2, 20 percent CO_2, and 59 percent Argon.

The Alaskan diesel oil (Figure 4-11) is the No. 2 fuel oil cut from the North Slope crude. It is essentially nitrogen-free (0.006 percent N), and as such, provided a very good fuel for comparison purposes.

The West Texas diesel oil is the No. 2 cut from a sour, West Texas crude. While it is a No. 2 oil in terms of viscosity, its other properties are far more typical of heavy oils (API gravity equal to 18.3, sulfur equal to 1.88 percent).

4.3.2.2 Distillate Oil Doping

Figures 4-14 through 4-19 summarize the data taken during an experimental series where the California No. 2 distillate oil was doped with varying amounts of pyridine and/or thiophene. The particular doping levels were selected to match actual residual fuels, and thereby investigate the suitability of simulating a heavy residual oil with a doped distillate oil. These results are relatively uninteresting by themselves and have only been included here for completeness. The data are discussed in detail in a subsequent section (4.3.2.7) when they are compared to the emissions from the actual residual oils.

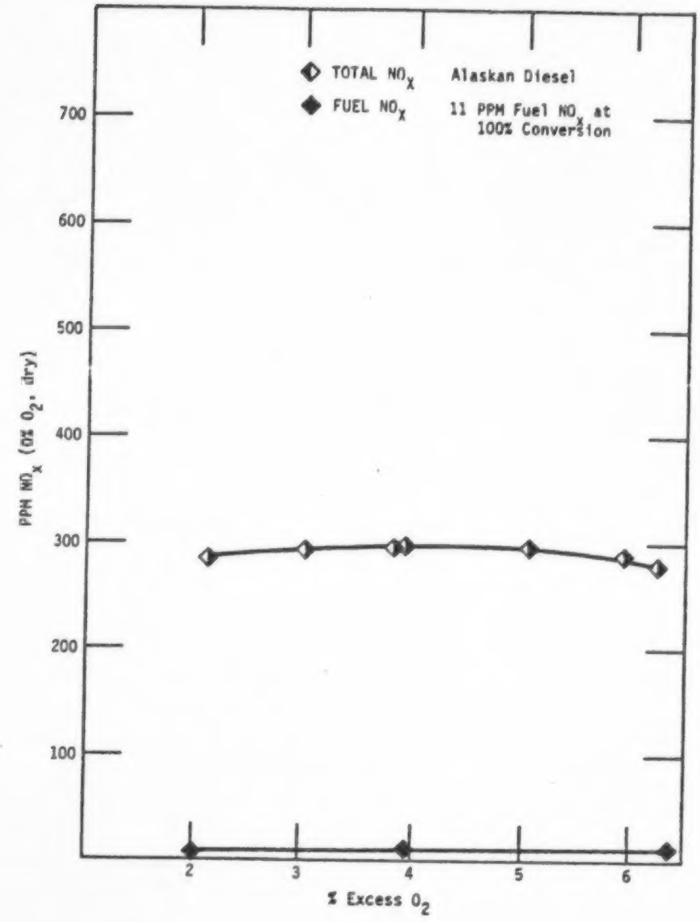

Figure 4-11. Influence of Excess O_2 - Alaskan Diesel.

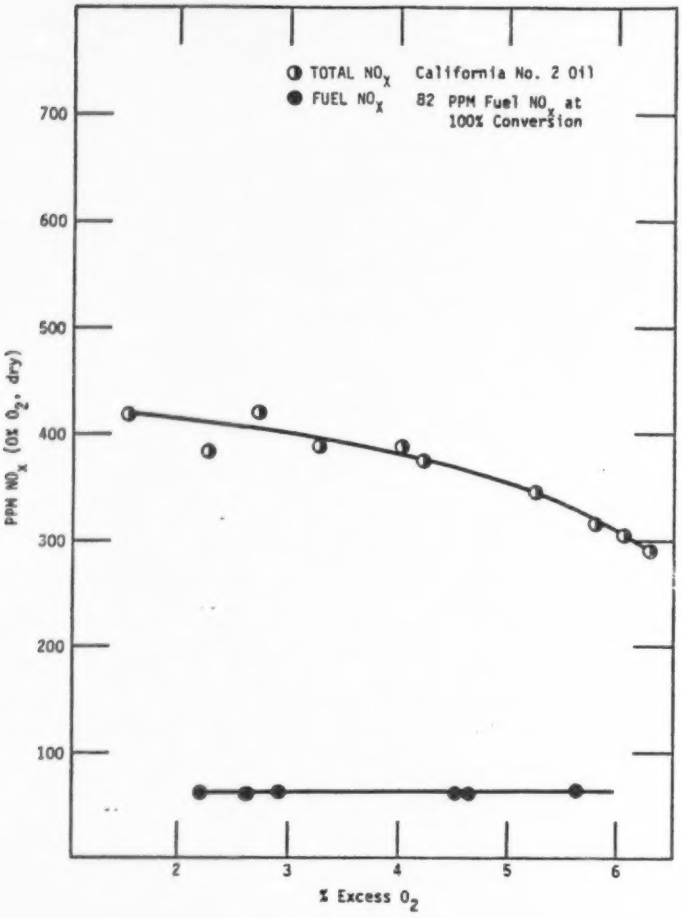

Figure 4-12. Influence of Excess O_2 - Calif. No.2 Oil.

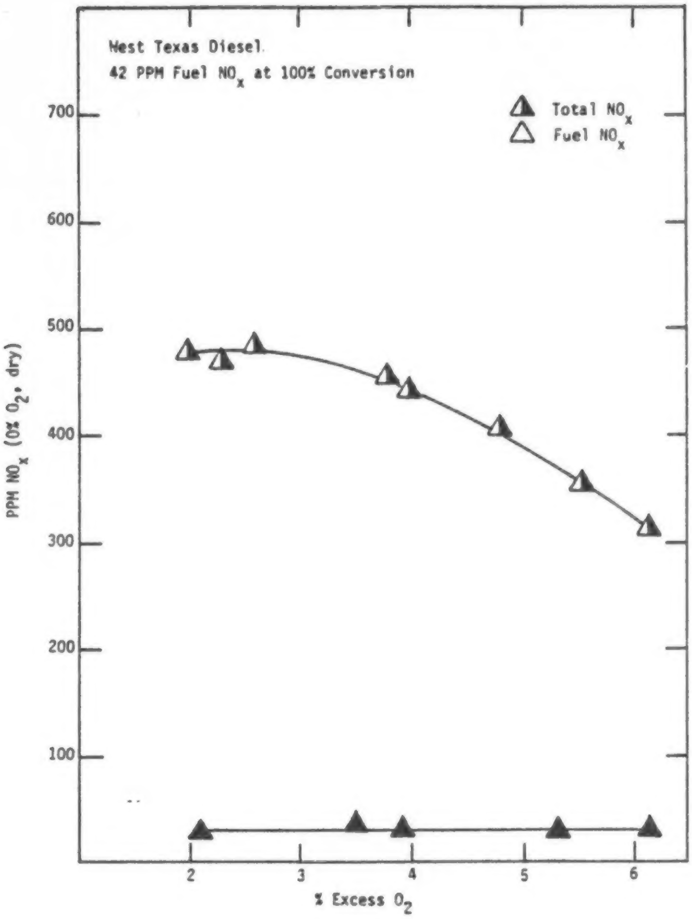

Figure 4-13. Influence of Excess O_2 - West Texas Diesel.

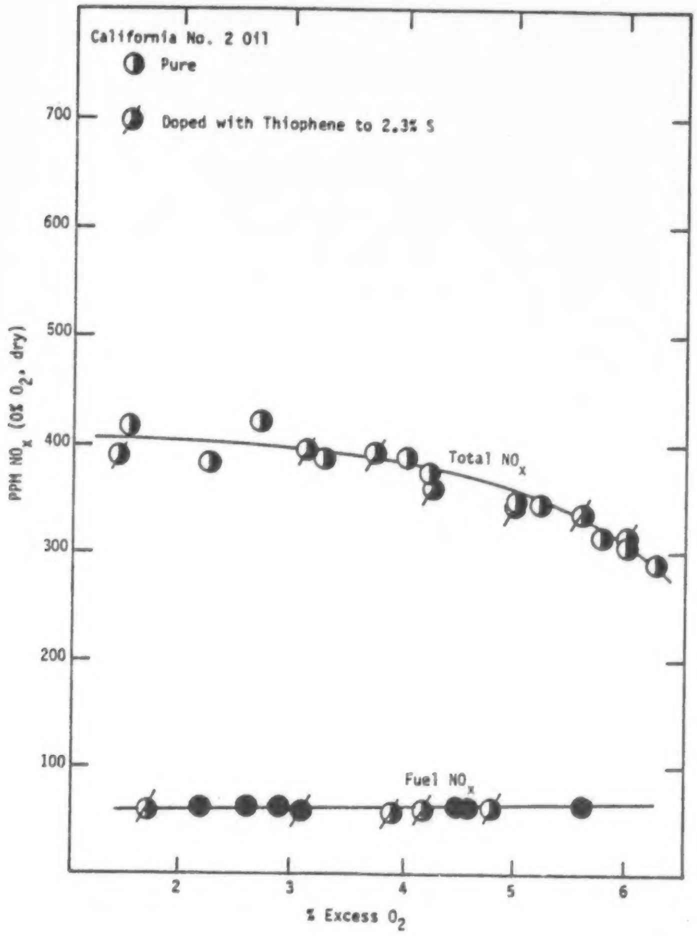

Figure 4-14. Influence of Fuel Sulfur on Fuel and Thermal NO_x Formation.

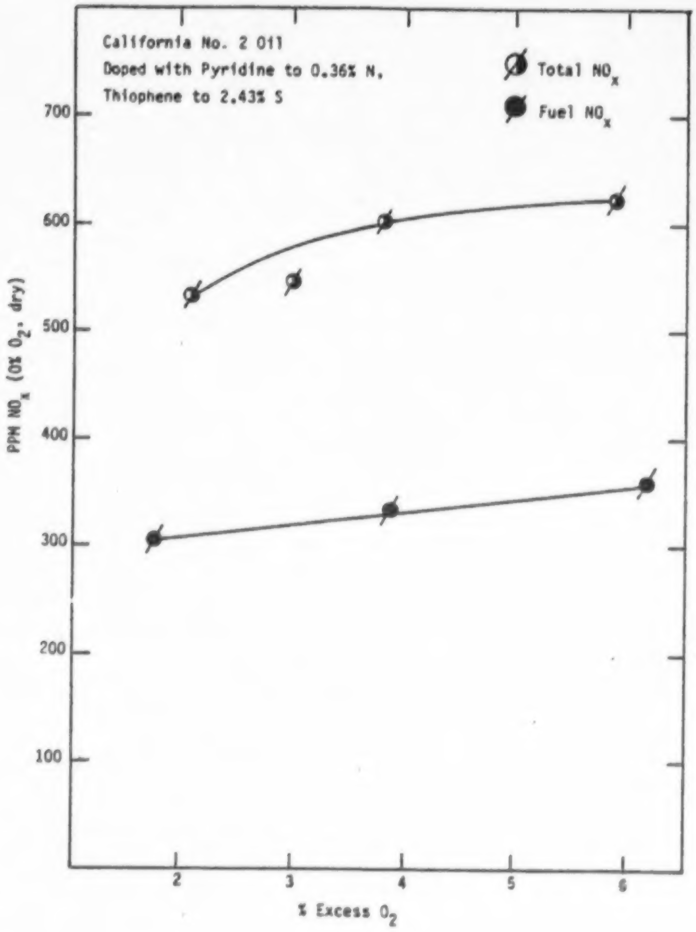

Figure 4-15. Influence of Excess O_2 - 0.36% N, 2.43% S Doped Distillate.

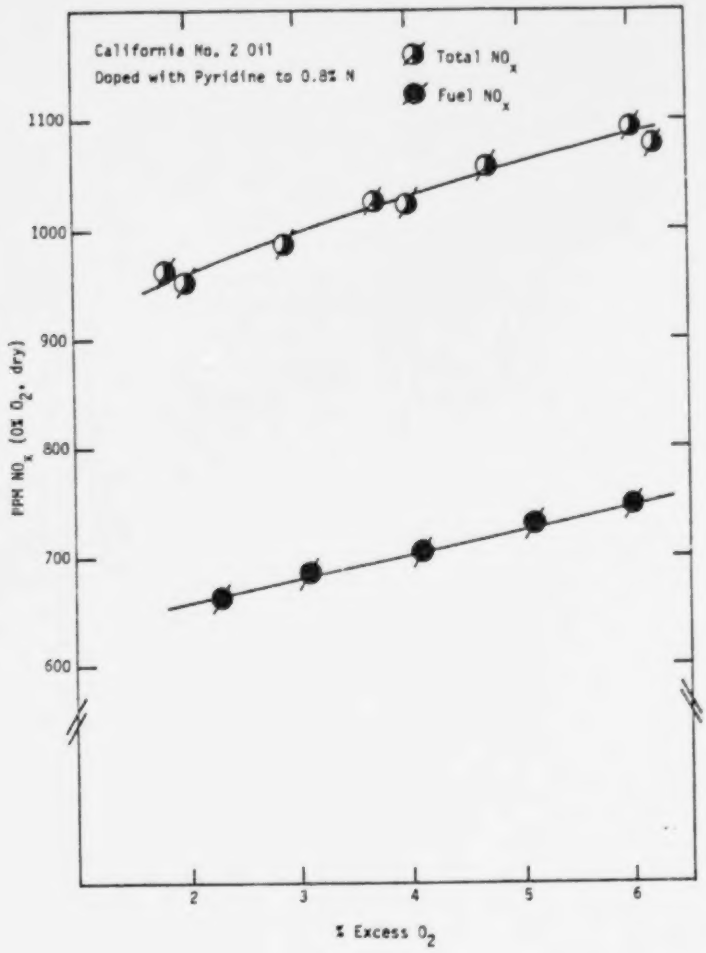

Figure 4-16. Influence of Excess O_2 - 0.8% N Doped Distillate.

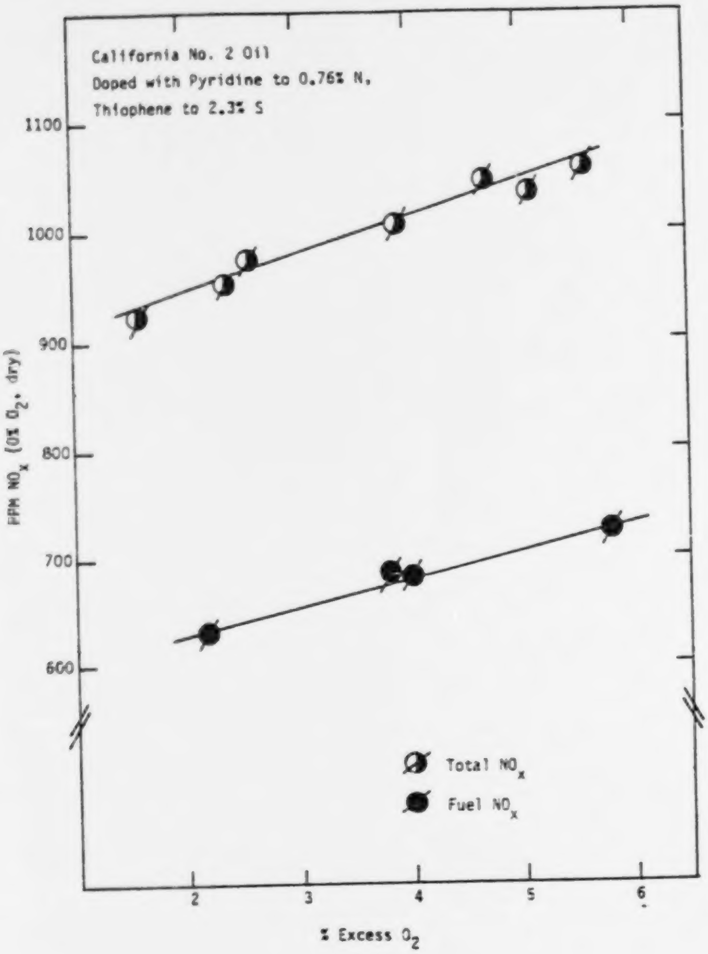

Figure 4-17. Influence of Excess O_2 - 0.76% N, 2.3% S Doped Distillate.

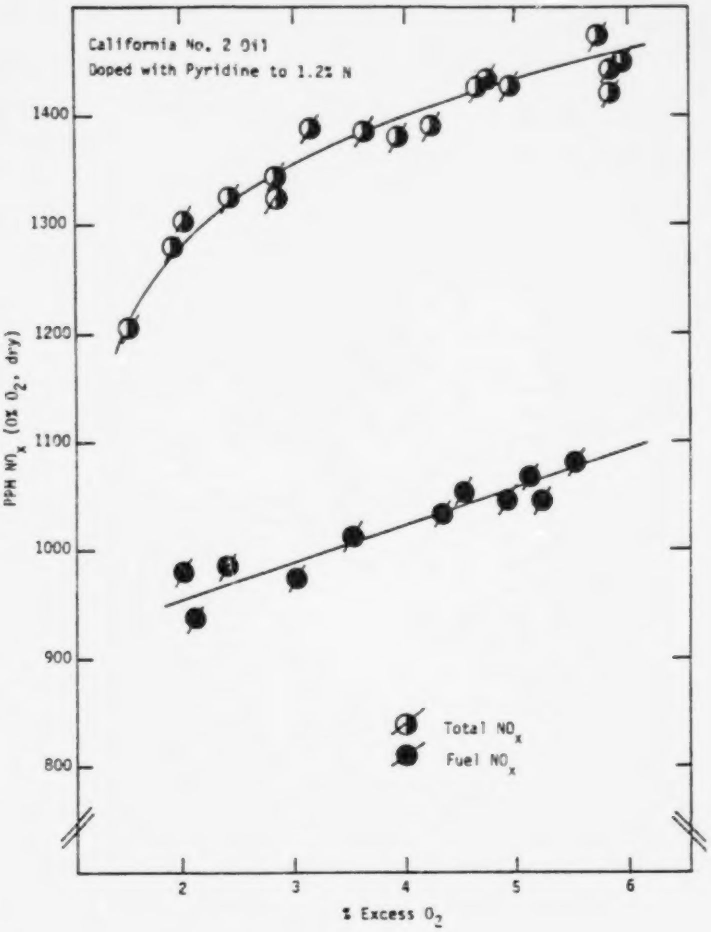

Figure 4-18. Influence of Excess O_2- 1.2% N Doped Distillate.

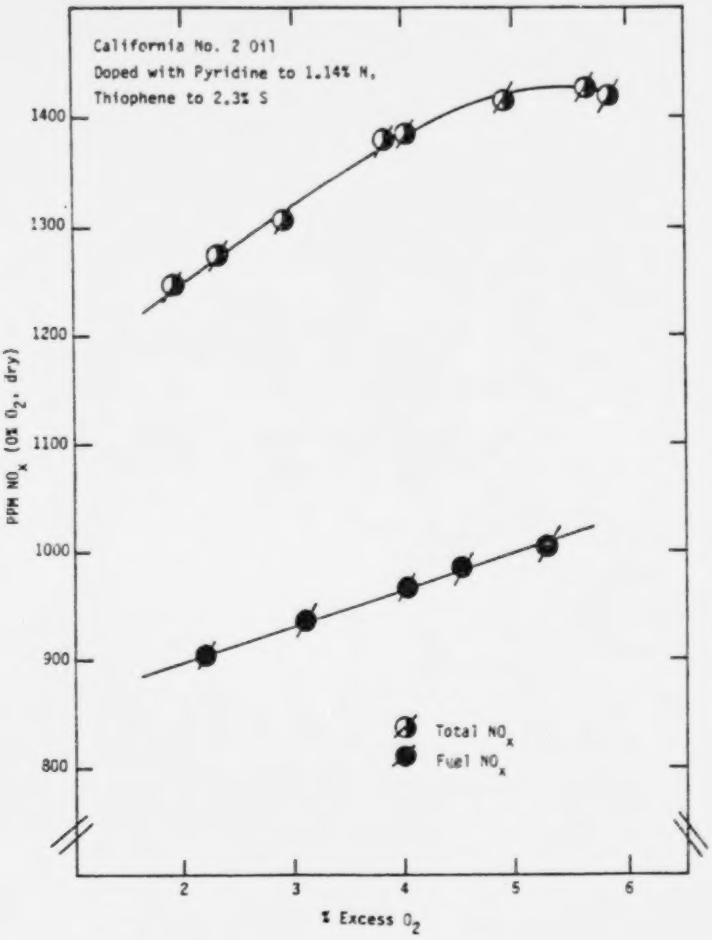

Figure 4-19. Influence of Excess O_2 - 1.14% N, 2.3% S Doped Distillate.

Figure 4-14 shows the California distillate oil emissions with and without 2.3 percent sulfur as thiophene. The data indicate that the presence of a substantial amount of fuel sulfur has little effect on either the formation of fuel or thermal NO_x under rapidly mixed excess air conditions. This is in agreement with the work of Wendt et al. at the University of Arizona(5).

Figure 4-15 shows the total and fuel NO_x formation for the California distillate doped to 0.36 percent nitrogen and 2.43 percent sulfur (to simulate the Gulf Coast residual oil). Figures 4-16 and 4-17 show the California distillate doped to approximately 0.8 percent nitrogen with and without 2.3 percent sulfur (to simulate the California residual oils labeled R2 and R3). Figures 4-18 and 4-19 show similar data with pyridine doping to 1.2 percent nitrogen. Figure 4-18 shows data taken on several different days and again indicates the relative reproducibility of this experimental testing.

4.3.2.3 Residual Oils

Figures 4-20 through 4-32 summarize the total and fuel NO_x emissions data for the 13 petroleum-derived, residual fuels used in this study. In each case the combustion conditions in the tunnel furnace were matched insofar as was possible; the combustion air preheat was 405 $\pm 5^{o}$K, the firing rate was 0.55 cc/sec, and the atomizer was the ultrasonic nozzle operated at an air pressure of 205 kPa. The fuel viscosity was maintained at 14 $\pm$2 cSt by using the appropriate fuel temperature.

In each case the total and fuel NO_x emissions were determined as a function of excess oxygen. As before, the fuel NO_x (Solid symbols, lower line) was isolated with the $Ar/O_2/CO_2$ synthetic oxidant mixture.

The 13 petroleum-derived liquids represent the wide spectrum of liquid fuels currently available throughout the world. Their nitrogen content ranged from 0.16 percent (Essex County--East Coast) to 0.86 percent (California No. 4). The sulfur content varied from 0.21 percent to 2.44 percent. Samples of the Venezuelan oil before and after desulfurization were included to define the effect of fuel processing.

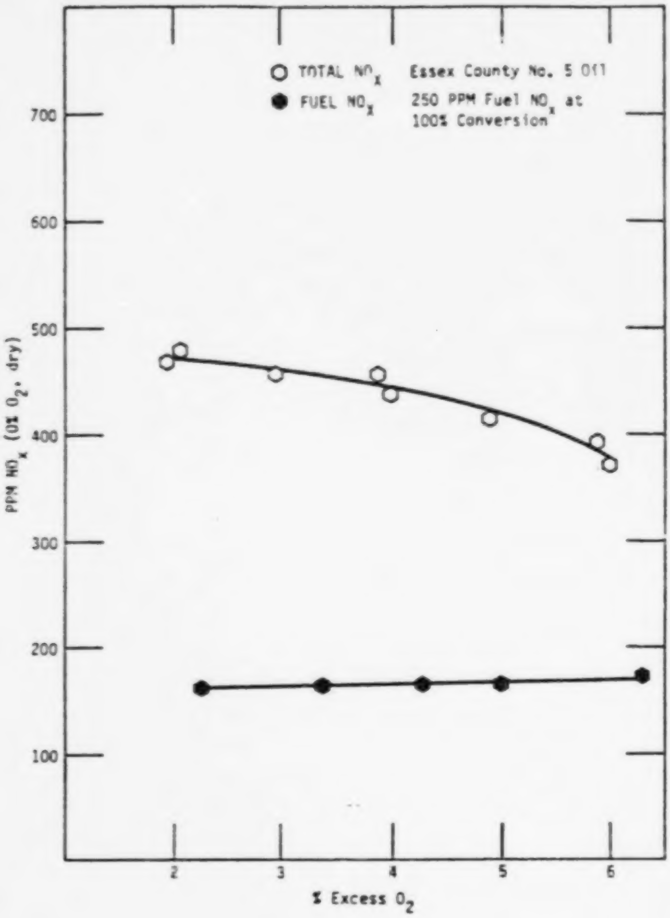

Figure 4-20. Essex County Oil - Standard Test Conditions.

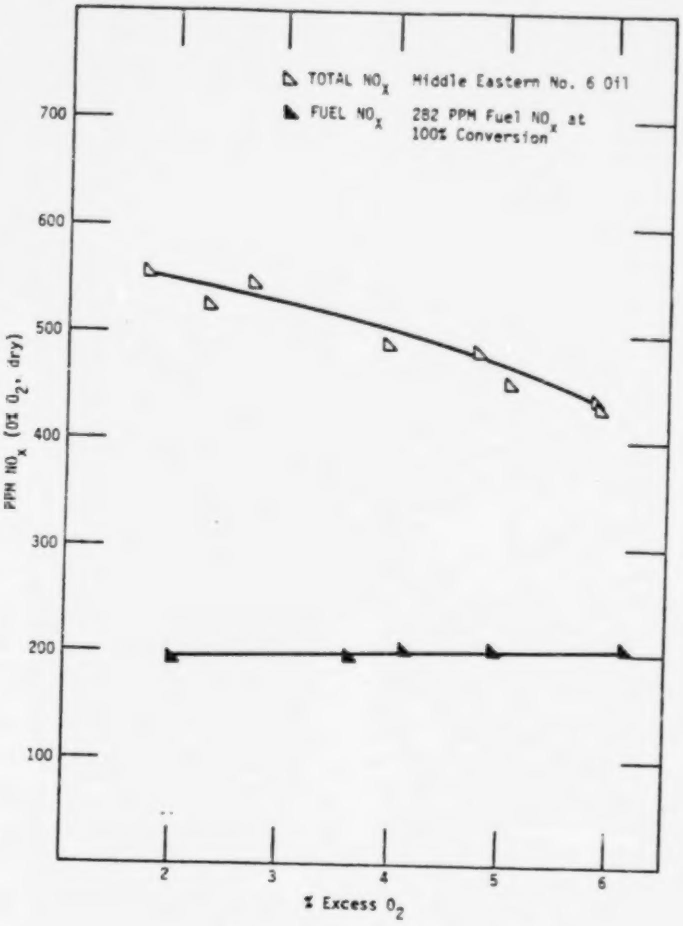

Figure 4-21. Middle Eastern Oil - Standard Test Conditions.

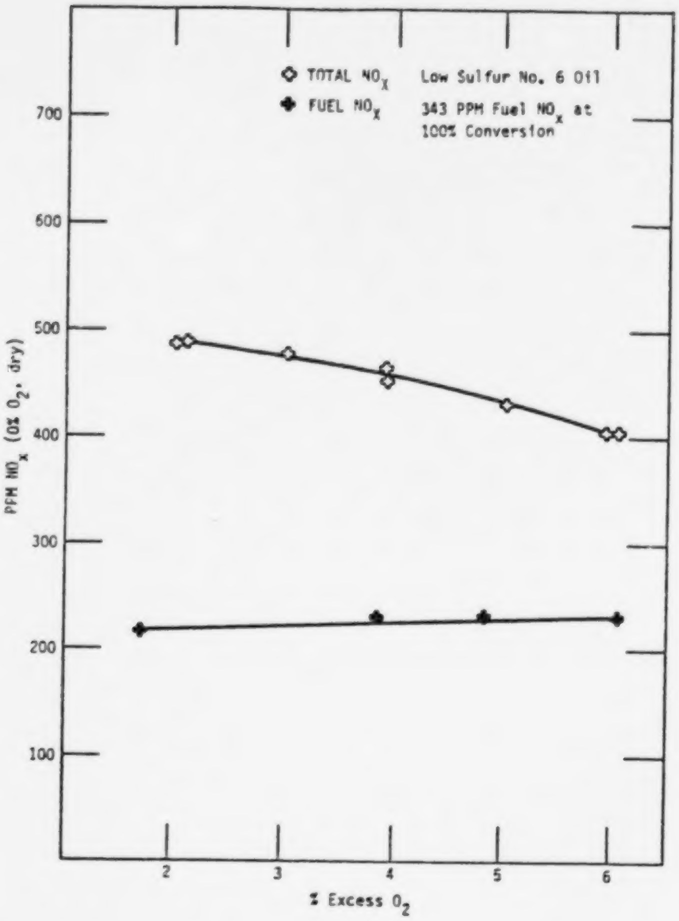

Figure 4-22. Low Sulfur Oil - Standard Test Conditions.

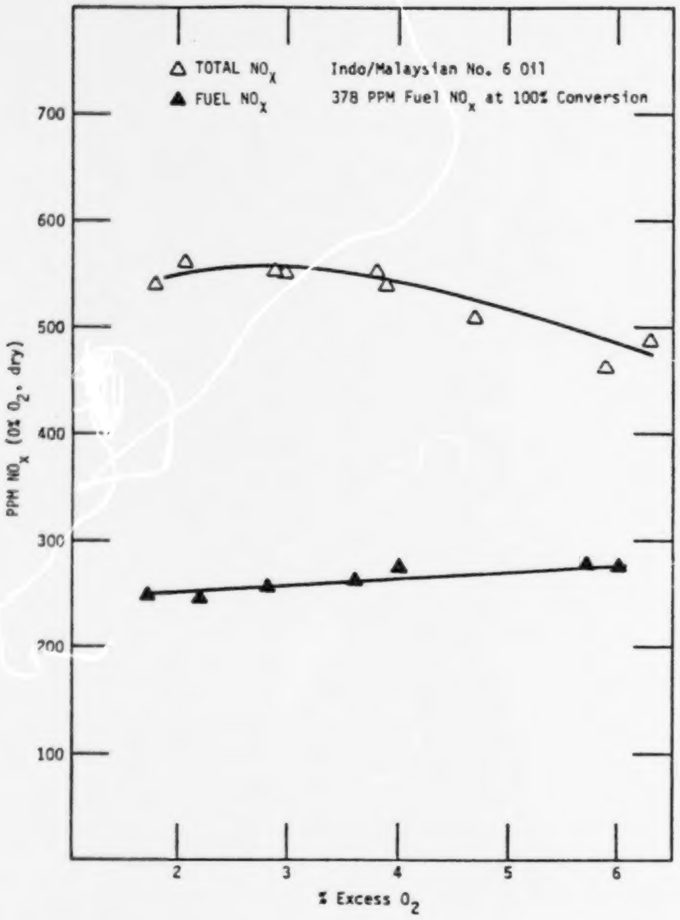

Figure 4-23. Indo/Malaysian Oil - Standard Test Conditions.

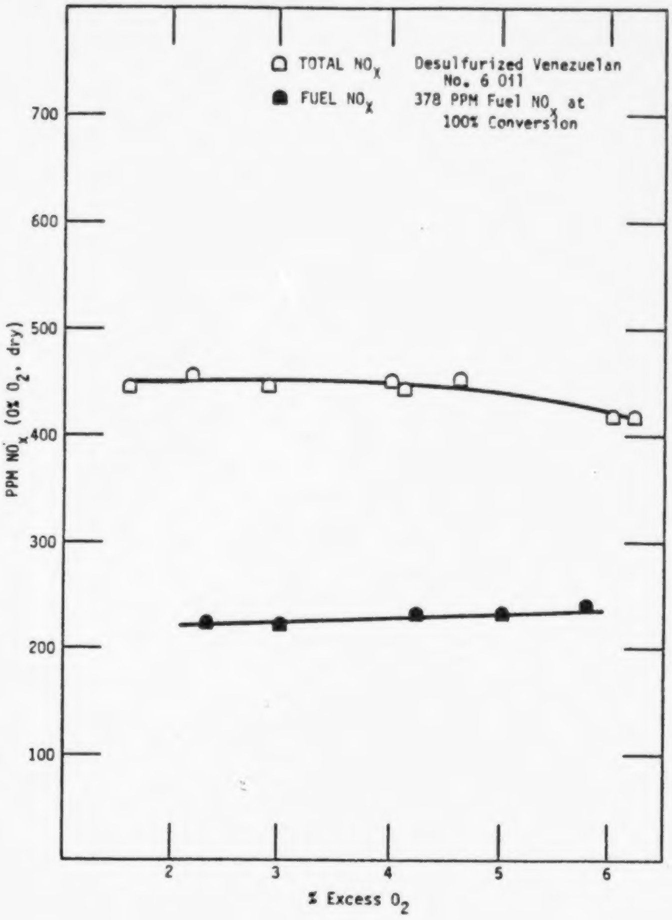

Figure 4-24. Desulfurized Venezuelan Oil - Standard Test Conditions.

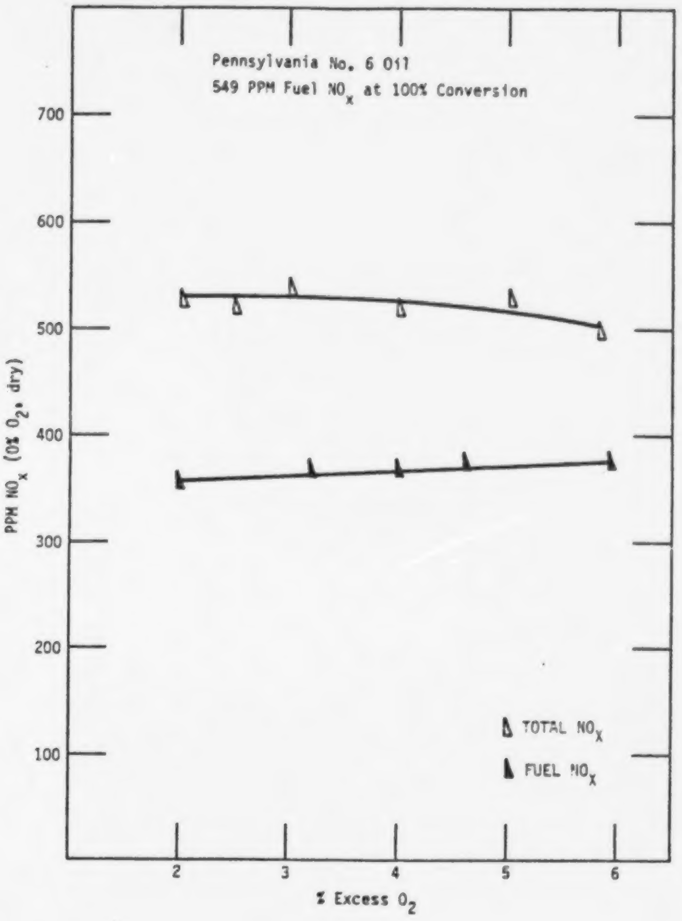

Figure 4-25. Pennsylvania Oil - Standard Test Conditions.

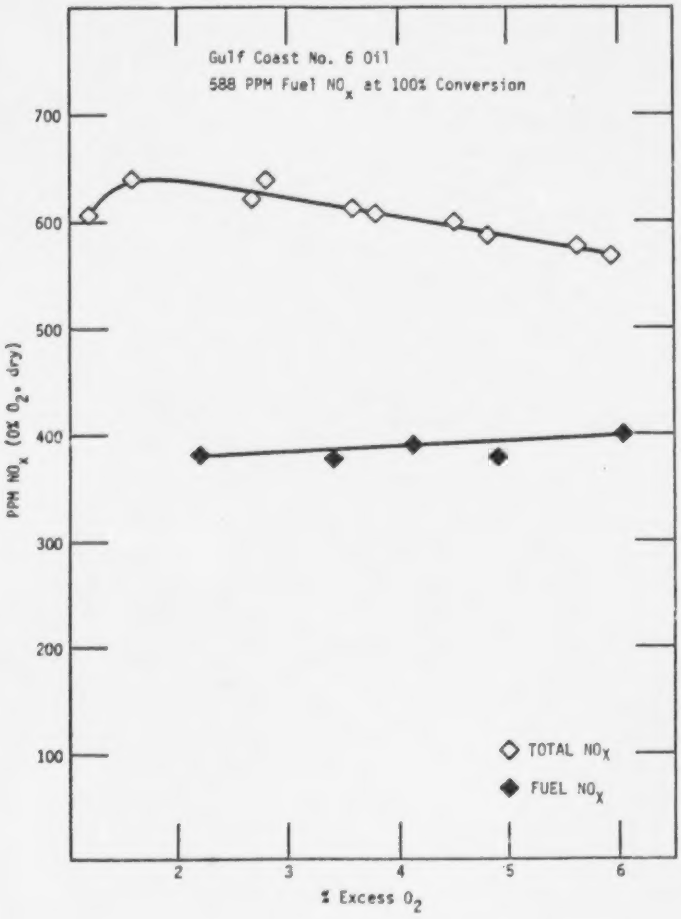

Figure 4-26. Gulf Coast Oil - Standard Test Conditions.

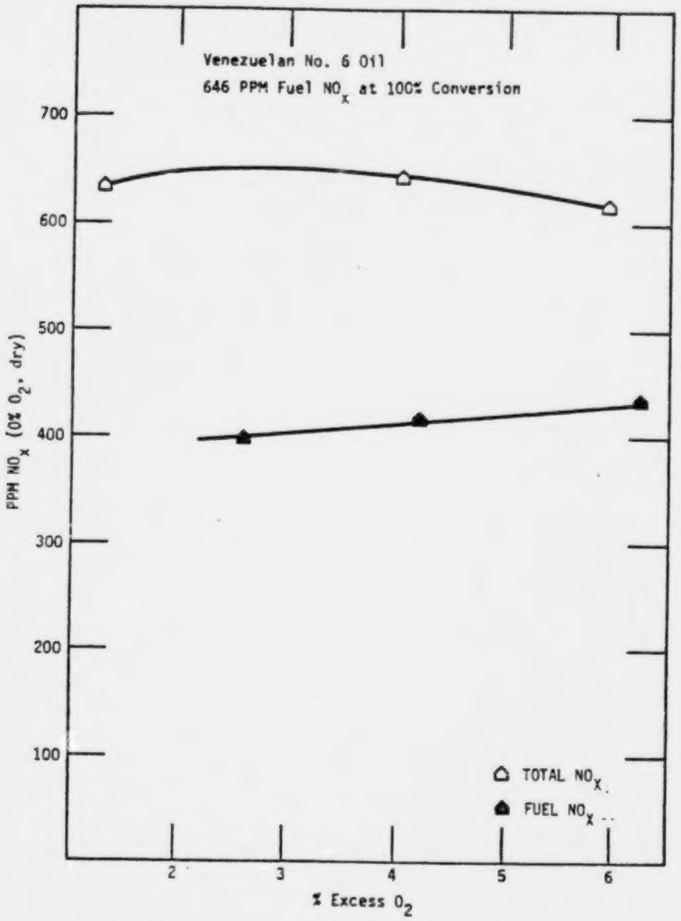

Figure 4-27. Venezuelan Oil - Standard Test Conditions.

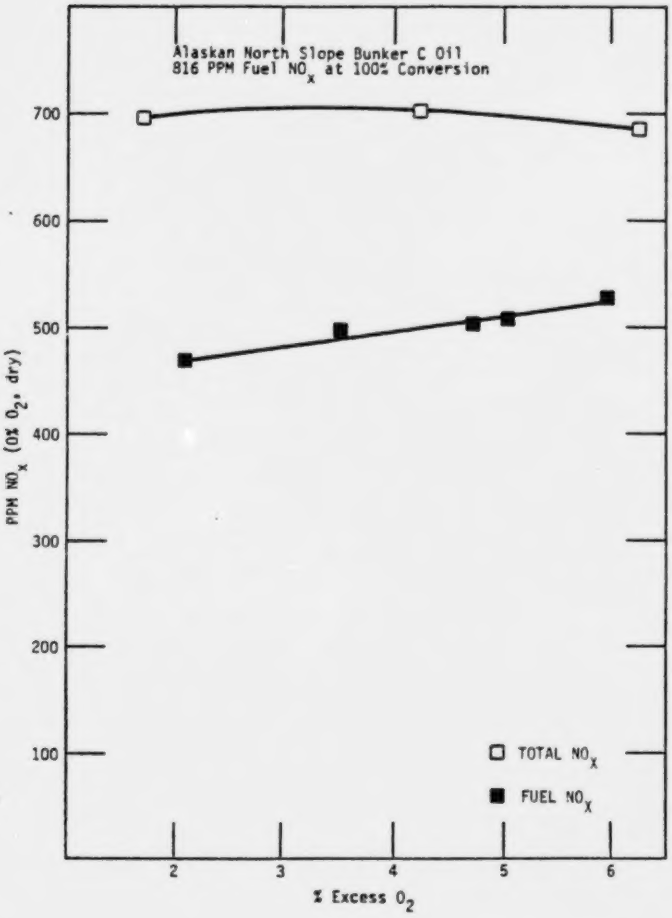

Figure 4-28. Alaskan North Slope Oil - Standard Test Conditions.

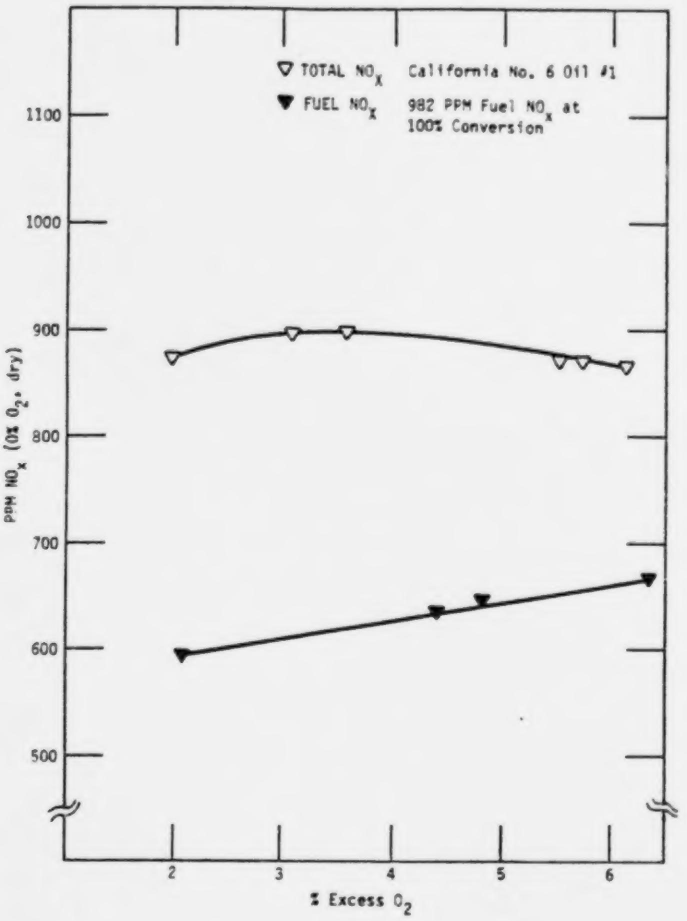

Figure 4-29. California Oil #1 - Standard Test Conditions.

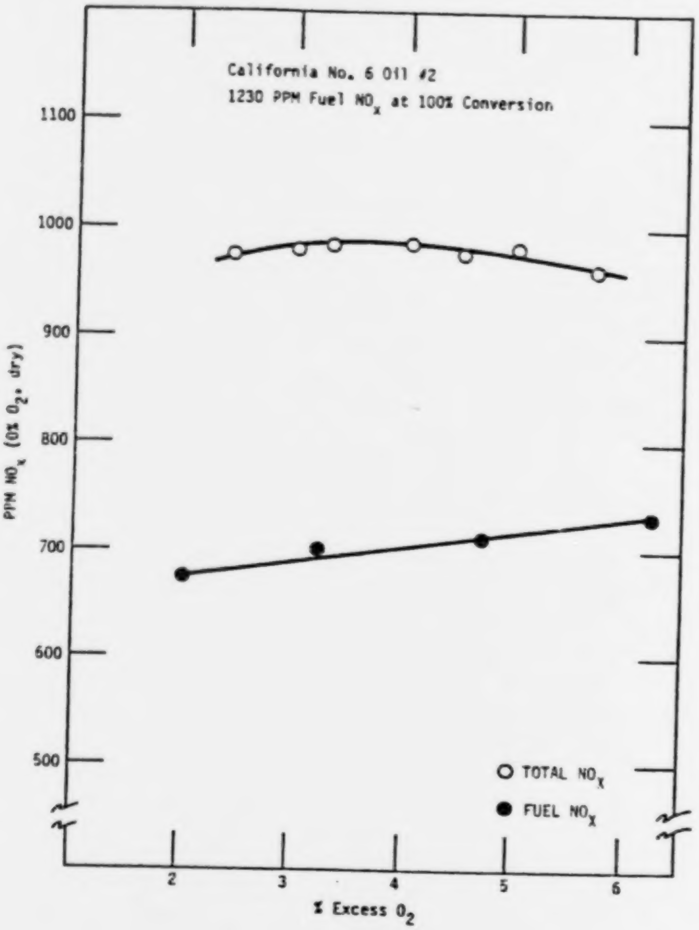

Figure 4-30. California Oil #2 - Standard Test Conditions.

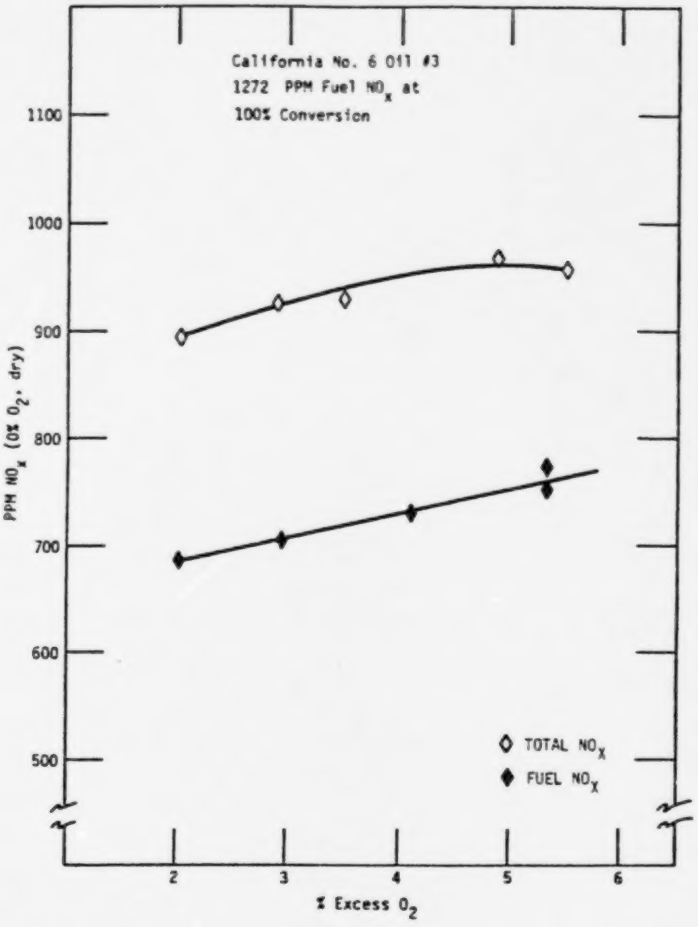

Figure 4-31. California Oil #3 - Standard Test Conditions.

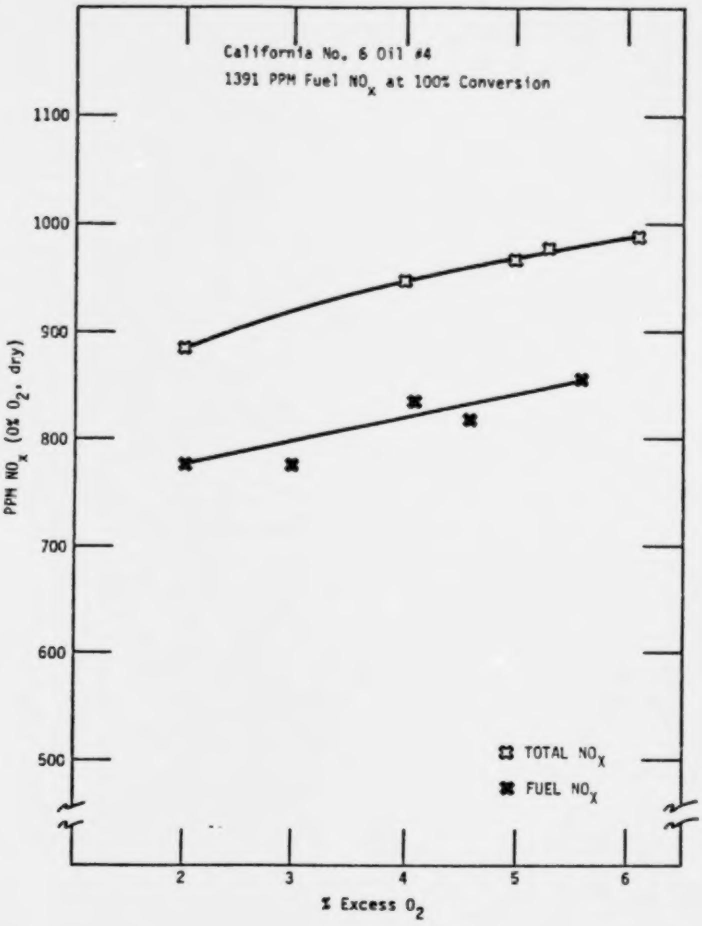

Figure 4-32. California Oil #4 - Standard Test Conditions.

4.3.2.4 Residual Oil Doping

Figures 4-33 through 4-36 summarize the results obtained from an experimental-test series in which the desulfurized Venezuelan No. 6 oil was doped with varying amounts of pyridine and/or thiophene to produce nitrogen and sulfur levels comparable to various other heavy residual oils. These figures present the detailed data obtained and the results are compared in Section 4.3.2.7. In each case, both total NO_x emissions (open symbols, upper line) and fuel NO_x emissions (solid symbols, lower line) were measured. As expected, both total and fuel NO_x increased with increasing nitrogen content.

4.3.2.5 Alternate Liquid Fuels

Figures 4-37 through 4-43 summarize the data taken with alternate liquid fuels. As in the case of the petroleum liquids, the data were obtained in the tunnel furnace with the ultrasonic nozzle operating at an atomization pressure of 205 kPa. The combustion air preheat was 405 $\pm 5^{o}$K, and the firing rate was 0.55 cc/sec. In each case, both the total and fuel NO_x emissions were determined as a function of excess oxygen.

Figure 4-37 presents the results obtained with the light diesel fuel which was derived from the Paraho shale oil. The total and fuel NO_x emissions were rather high for a diesel fuel because this synthetic, light oil contained a substantial amount of fuel nitrogen (0.24 percent).

Figure 4-38 shows the results for the crude Paraho shale as a function of excess oxygen. This liquid fuel produced extremely high NO_x emissions under these conditions because of its very high fuel-nitrogen content (2.08 percent nitrogen).

Figures 4-39 through 4-41 show results for 75 percent, 50 percent, and 26 percent blends of the shale crude with the low sulfur No. 6 petroleum oil. As expected, the NO_x emissions decreased as the fuel-nitrogen content was reduced.

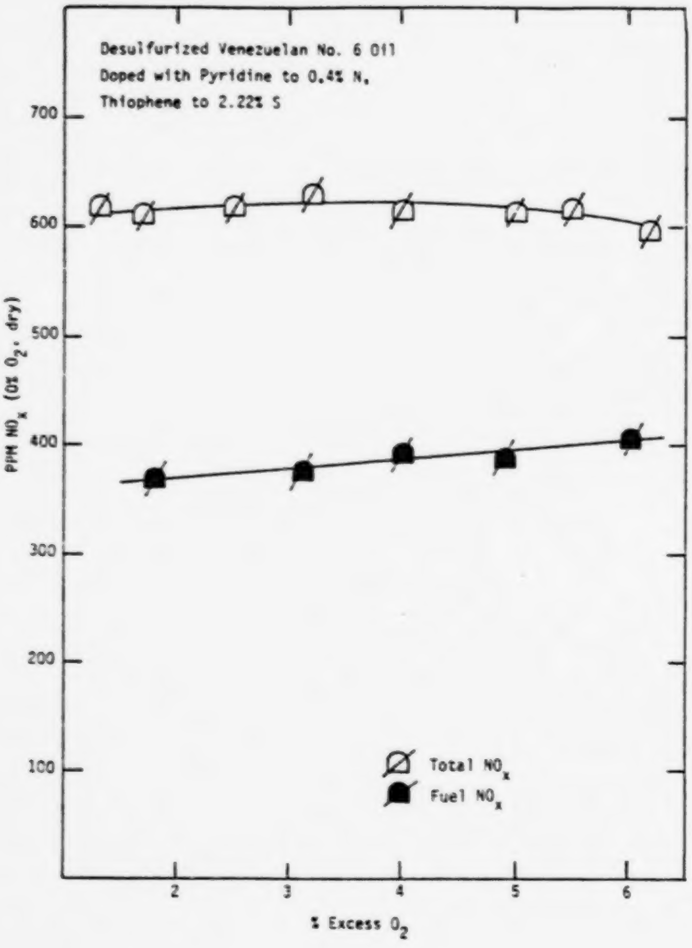

Figure 4-33. Desulfurized Venezuelan Oil Doped to Simulate the Venezuelan Oil.

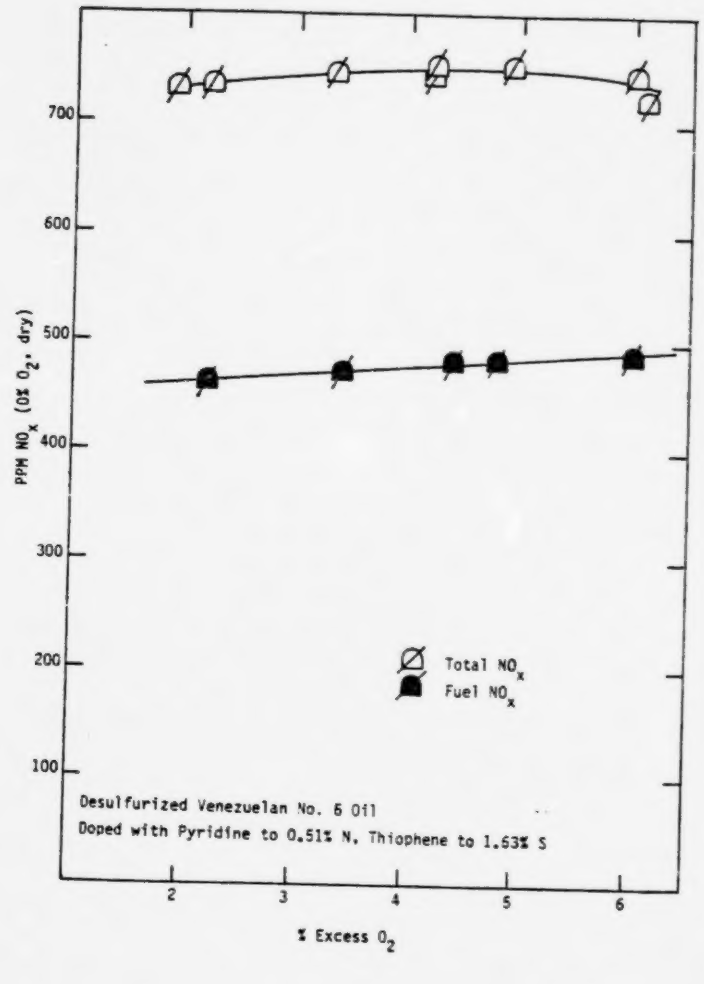

Figure 4-34. Desulfurized Venezuelan Oil Doped to Simulate the Alaskan Oil.

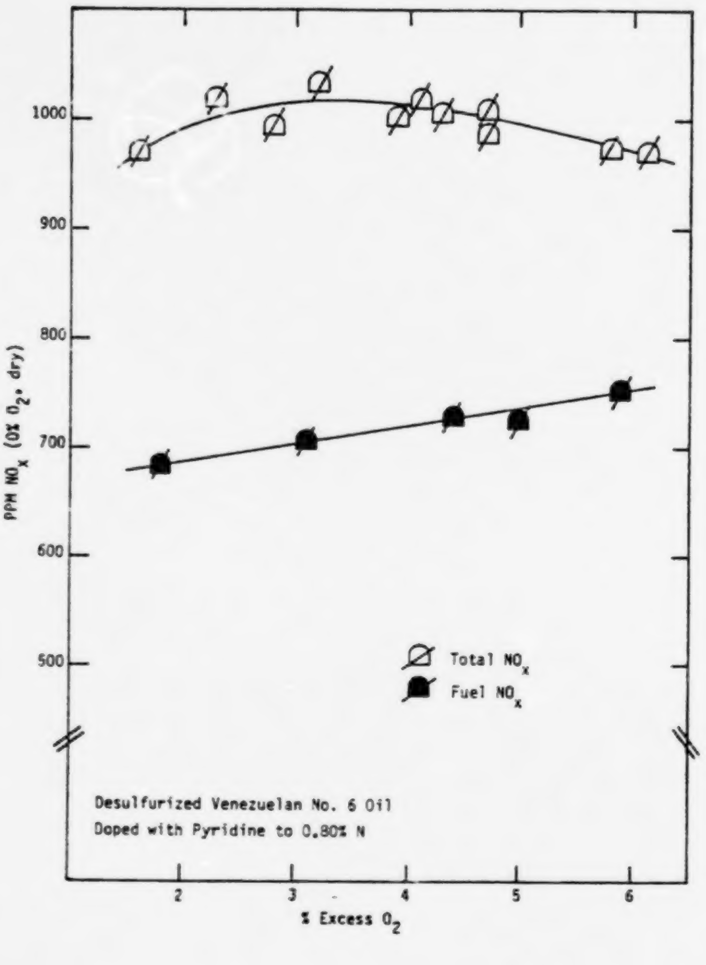

Figure 4-35. Desulfurized Venezuelan Oil Doped to 0.80% N.

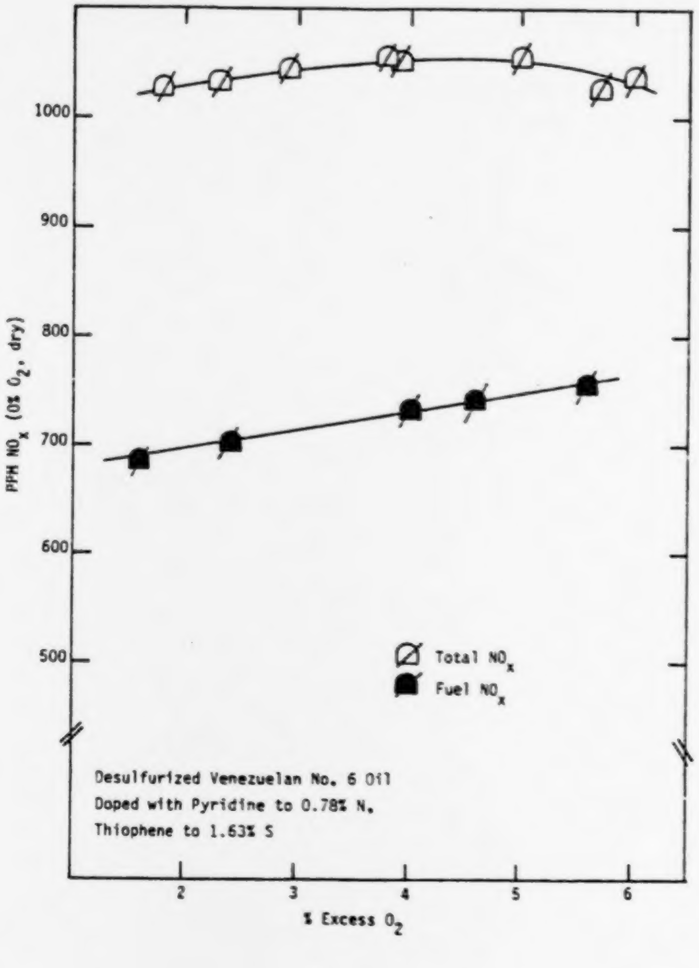

Figure 4-36. Desulfurized Venezuelan Oil Doped to Simulate the California Oils.

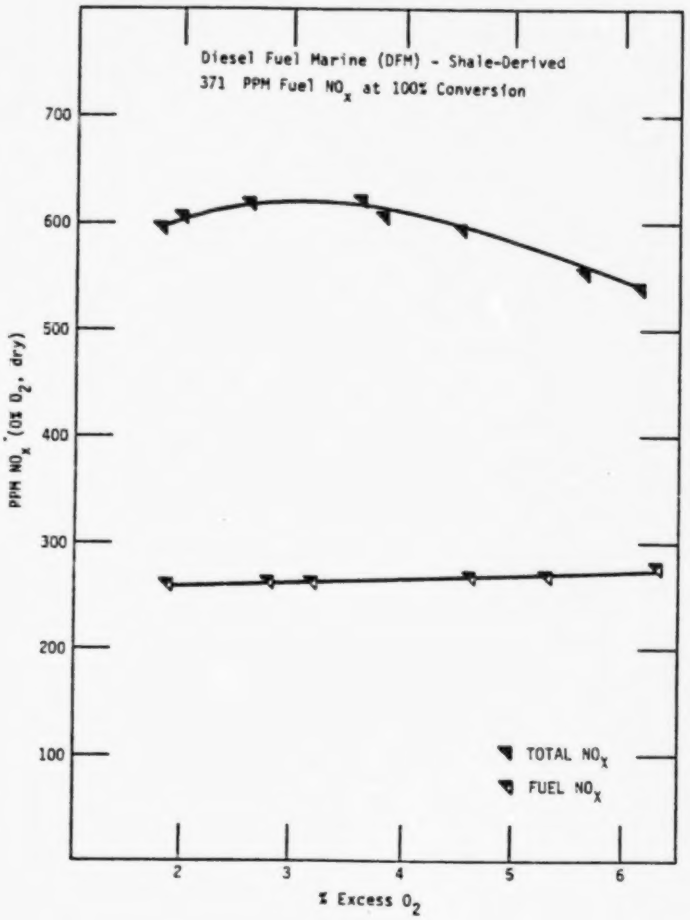

Figure 4-37. DFM - Standard Test Conditions.

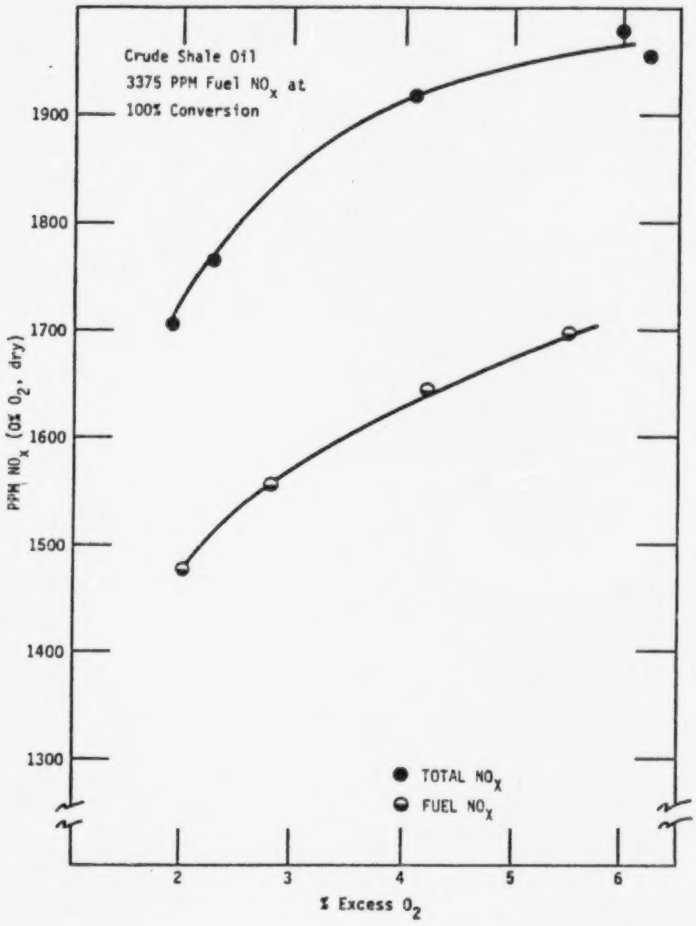

Figure 4-38. Crude Shale Oil - Standard Test Conditions.

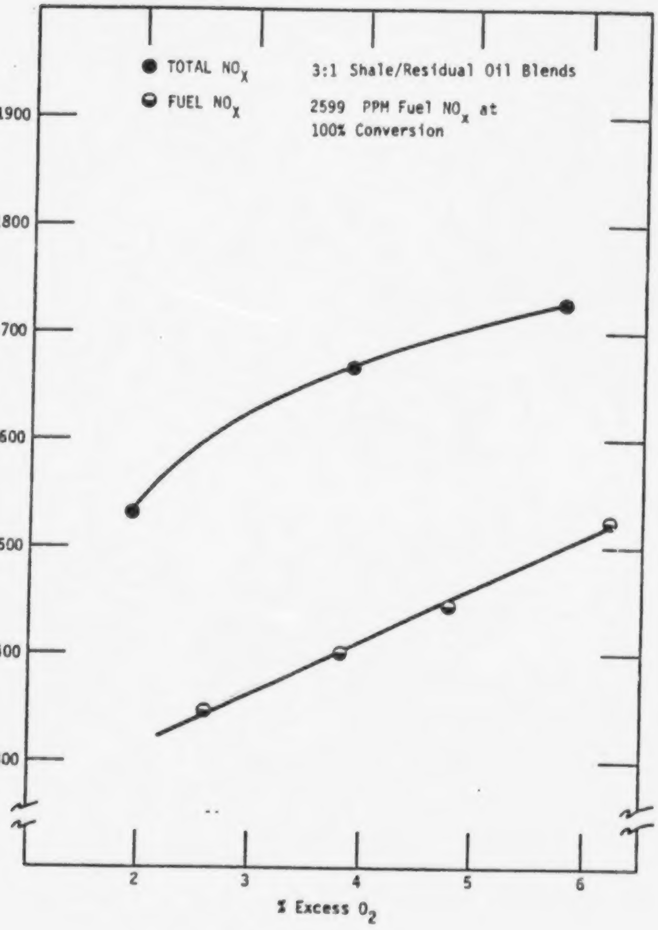

Figure 4-39. 75% Shale Blend - Standard Test Conditions.

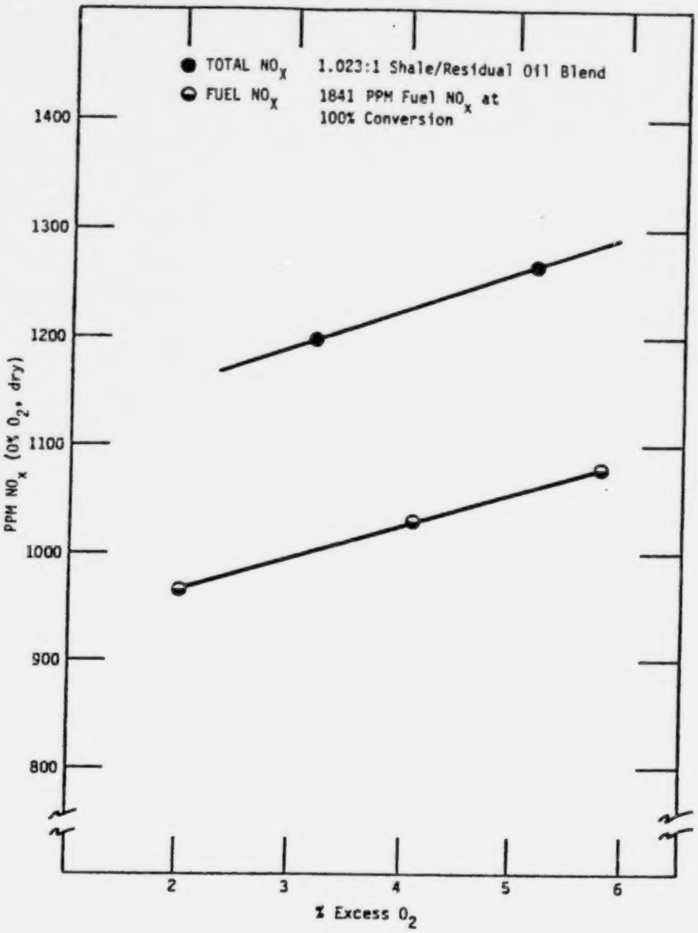

Figure 4-40. 50% Shale Blend - Standard Test Conditions.

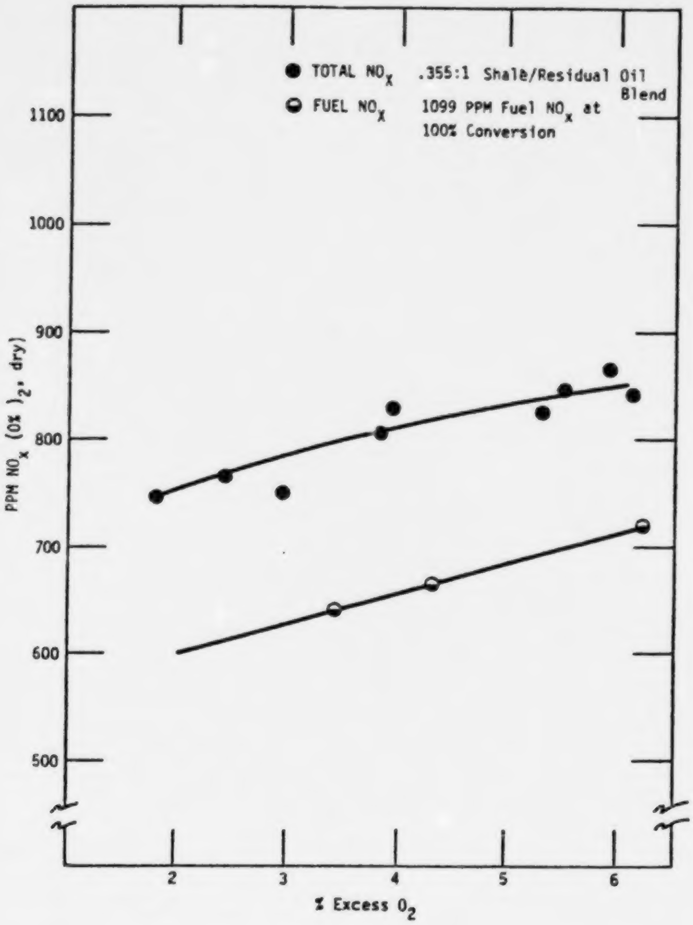

Figure 4-41. 26% Shale Blend - Standard Test Conditions.

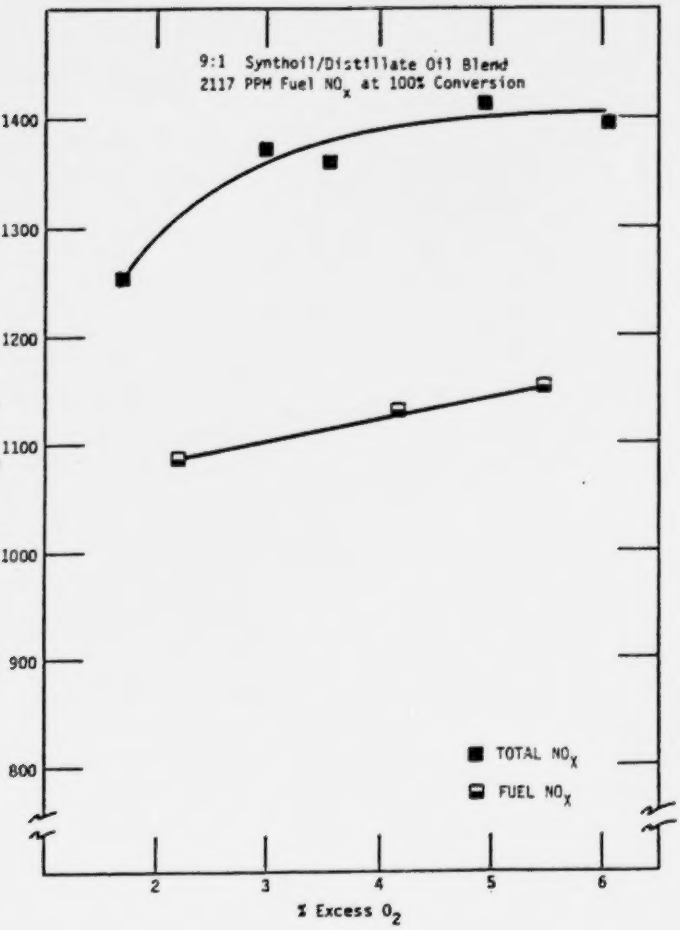

Figure 4-42. 90% Synthoil Blend - Standard Test Conditions.

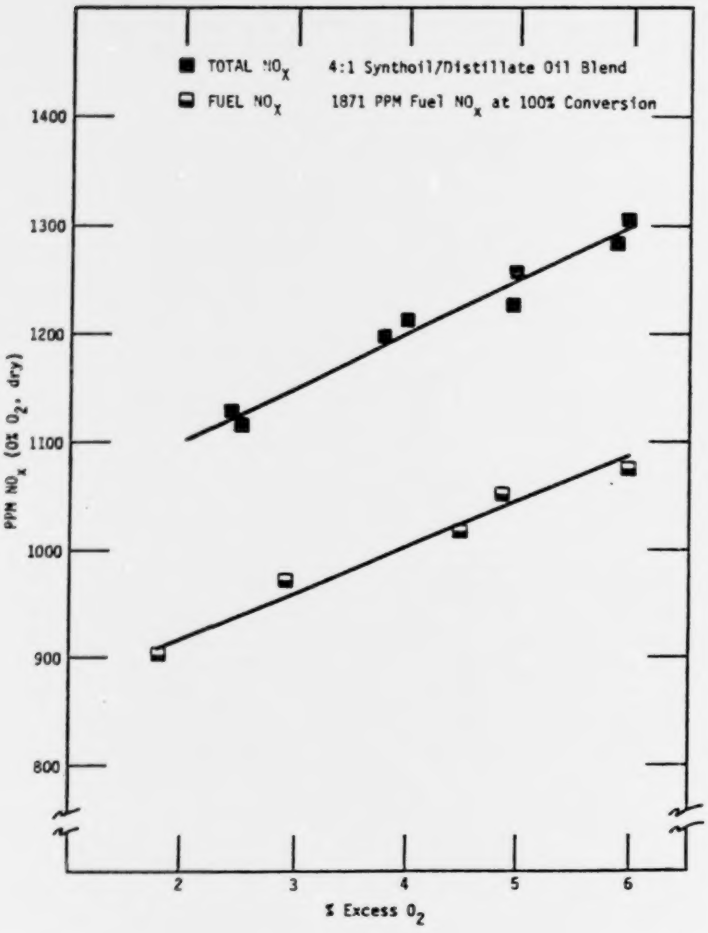

Figure 4-43. 80% Synthoil Blend - Standard Test Conditions.

Figures 4-42 and 4-43 show data obtained with a synthetic coal liquid: Synthoil. These data are for 90 percent and 80 percent blends of the Synthoil with a distillate oil. It was not possible to obtain data on this pure coal liquid because of extreme coking problems. (Small-scale studies are particularly susceptible to nozzle problems due to the small orifice sizes and distances involved.) Like the shale liquids, the Synthoil produced relatively large amounts of fuel and total NO_x emissions because of the high fuel nitrogen content.

4.3.2.6 Doped Gas

Figure 4-44 shows the results of an experimental series in which methane containing 0.87 weight percent nitrogen as ammonia was burned under conditions similar to those used in the previous oil testing. In this case, the methane was fired through the ultrasonic nozzle and the atomizing airflow was held constant at the level used during the oil testing. Figure 4-44 shows the total and fuel NO_x data obtained as a function of excess oxygen. This test series was run to evaluate the effect of instantaneous fuel vaporization.

4.3.2.7 Discussion

Figure 4-45 is a composite plot showing all of the fuel NO_x emissions data for the pure fuels as a function of percent excess O_2. All of the data presented in this graph were obtained by burning the fuels in $Ar/O_2/CO_2$. The half-shaded symbols refer to the distillate fuels, the open symbols are the petroleum liquids, and the solid symbols refer to the alternate fuels. These results indicate that with the burner system used in these experiments, the formation of fuel NO_x in petroleum-liquid flames is relatively insensitive to the overall excess oxygen. This suggests that the fuel and air are relatively well-premixed prior to the formation of the fuel NO_x since early fundamental studies by Sarofim and co-workers(6) indicated a strong dependence of fuel NO_x on overall excess air in poorly mixed diffusion flames. These data also suggest that fuel NO_x formation is relatively insensitive to bulk flame temperature because the bulk temperature decreases as the

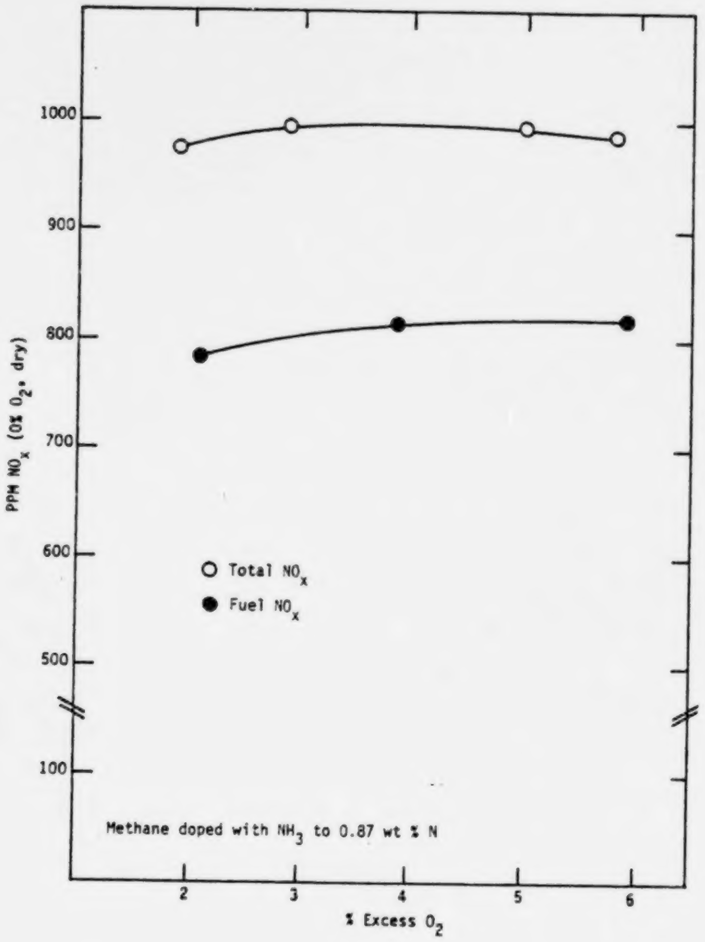

Figure 4-44. Influence of Excess O_2 - Methane Doped with NH_3.

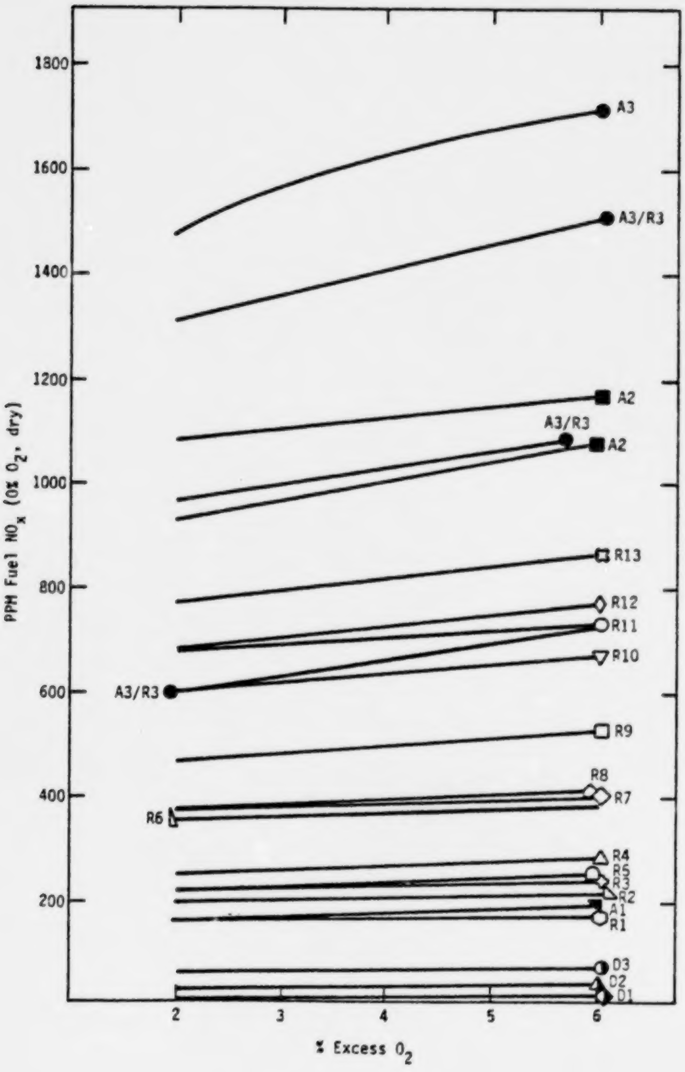

Figure 4-45. Effect of Excess O_2 on Fuel NO_x.

percent excess O_2 is increased. In the case of the alternate liquid fuels there is a stronger dependence of fuel NO_x formation on percent excess oxygen; however, the percentage increase is still relatively small.

Figure 4-46 shows the total NO_x emissions for the various liquid fuels as a function of percent excess O_2. The data for most of the petroleum liquids indicate that total NO_x emissions remain relatively constant or decrease slightly as excess O_2 is increased. This again suggests that the burner is producing a highly pre-mixed flame. (Thermal NO_x increases dramatically with increasing excess O_2 in a pure diffusion flame.)

Figure 4-47 is a composite plot of the total and fuel NO_x emissions vs. weight percent nitrogen in the fuel for the three distillate oils, 13 residual oils, and three alternate liquid fuels investigated in this study. In each case the combustion conditions were approximately identical and the overall excess oxygen was five percent (stoichiometric ratio equal to 1.29). The upper line is data obtained in air (total NO_x) and the lower line is the data obtained in $Ar/O_2/CO_2$ (fuel NO_x). Both total and fuel NO_x emissions increase with increasing fuel nitrogen. Since all of the data is for the tunnel furnace with ultrasonic atomization, which results in very fine oil droplets (about 25 μm) which are well dispersed in the oxidizer, it is not surprising that the fuel NO_x emissions are a strong function of fuel nitrogen content; the lower curve has a slope of approximately 95 ppm NO_x per 0.1 percent nitrogen. Thermal NO_x (the difference between the total and fuel NO_x emissions) appears to be slightly higher for the distillate oils and for some of the alternate fuels than for the petroleum residual fuels.

In general, the NO_x emissions for the alternate fuels correlate very well in terms of fuel nitrogen, compared to those for the petroleum-derived liquids. This suggests that under excess air conditions alternate fuels containing large amounts of fuel nitrogen will result in very high NO_x emissions. Consequently, there is a particularly strong need for control technology for the alternate fuels.

Figure 4-48 shows the fuel NO_x data for the petroleum-derived liquid fuels converted to a percentage conversion basis; i.e., ppm fuel NO_x divided by ppm NO_x if all fuel nitrogen were converted to NO_x. In general, the

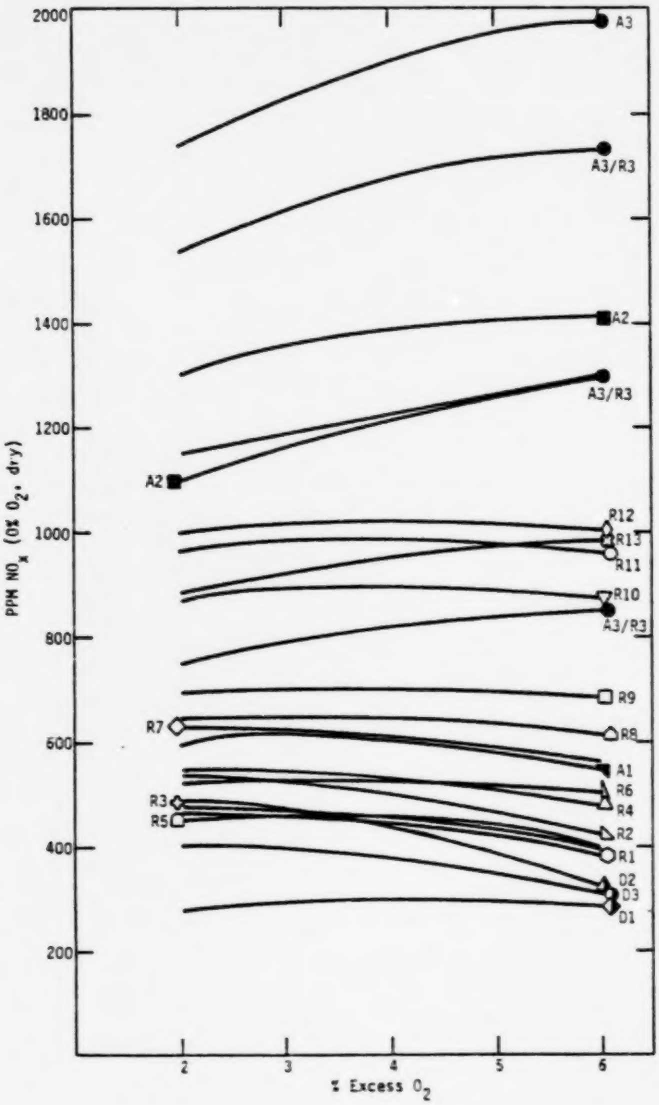

Figure 4-46. Effect of Excess O$_2$ on Total NO$_x$.

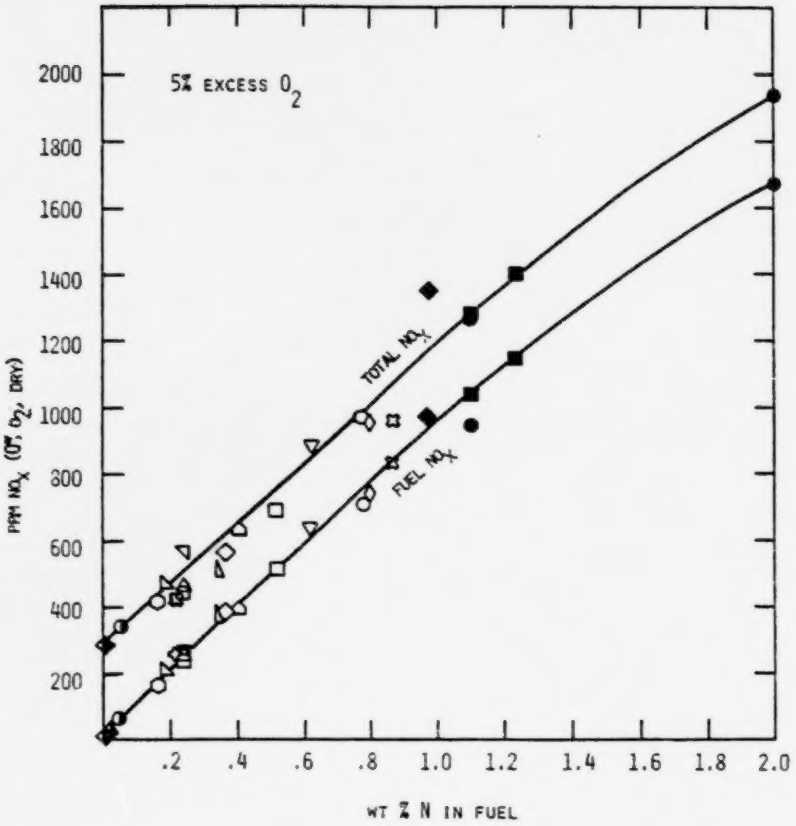

Figure 4-47. Effect of Fuel Nitrogen Content on Total and Fuel NO_x.

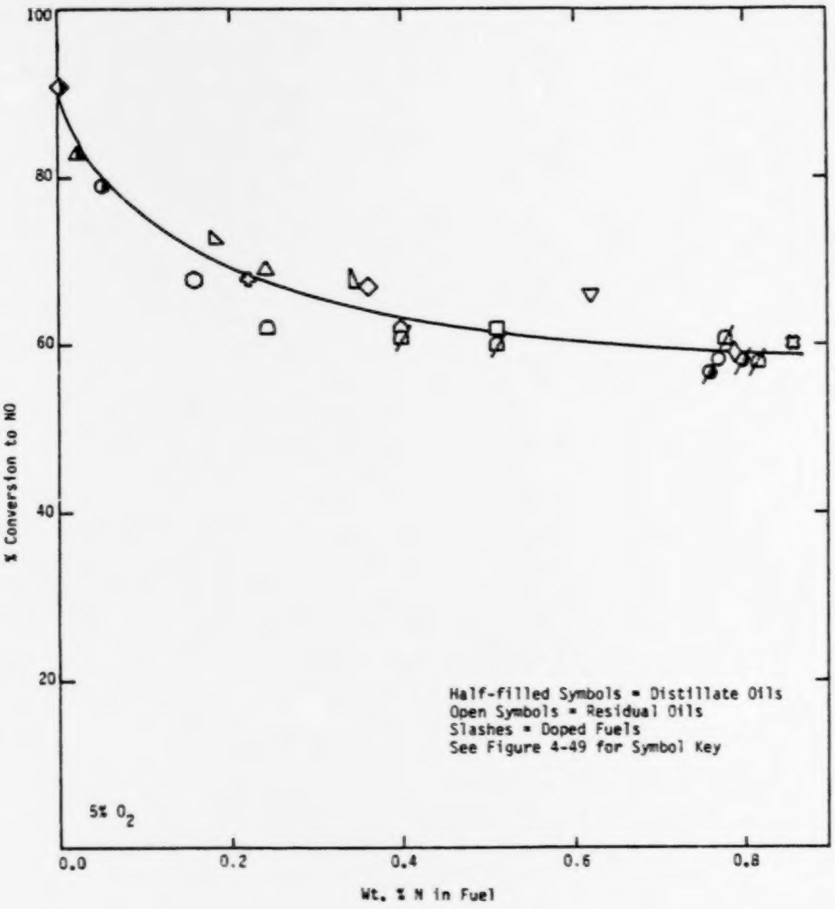

Figure 4-48. Effect of Fuel Nitrogen Content on Percent Conversion to NO_x.

percentage conversion of fuel nitrogen decreases rapidly up to about 0.3 percent nitrogen. Beyond this point only a small decrease was observed and this is consistent with previous work on a limited number of fuels(7). The overall percentage conversions are higher (60 to 80 percent) than are expected in practical systems (25 to 50 percent), because of the rapid fuel/air mixing characteristic of the burner system used in this work.

Figure 4-48 also shows the doping results in comparison with the actual heavy fuel oils which they were simulating. The data from the doped distillate oil (slashed, half-filled symbols) and from the doped residual oil (slashed, open symbols) correlate well with that obtained from the actual heavy fuel oils. Thus, it appears that under excess air conditions with good fuel/air mixing, the only first-order composition parameter is total nitrogen content in the fuel. Variation in other parameters such as fuel sulfur, hydrogen-to-carbon ratio, etc., do not appear to significantly effect the formation of fuel NO_x under these conditions.

Figure 4-49 shows all of the liquid fuel data plotted in terms of percent conversion of the fuel nitrogen to NO_x. All of the data shown in this figure were obtained by burning the liquid fuels in $Ar/O_2/CO_2$. Note that the x-axis has been expanded to 2.0 percent nitrogen to include the alternate liquid fuels, and that the ordinate axis has been expanded to emphasize these variations due to fuel properties. In general, the percent conversion to NO_x decreased as the fuel nitrogen content increased. The alternate fuels follow much the same curve as the petroleum liquids suggesting that, in the case of liquid fuels, the origin of the fuel is not a first-order parameter. Again the data show that the primary composition parameter is total fuel nitrogen, although there appear to be some second-order fuel effects. Consideration of the data obtained with the Venezuelan oil before and after desulfurization indicates that while desulfurication reduces NO_x because some denitrification occurs, there does not appear to be any other substantial sulfur effect.

Figure 4-49 also shows the data obtained with methane doped to 0.8 percent nitrogen with ammonia. The NO_x emissions obtained in this test were somewhat higher than those obtained with the actual liquid fuels suggesting that

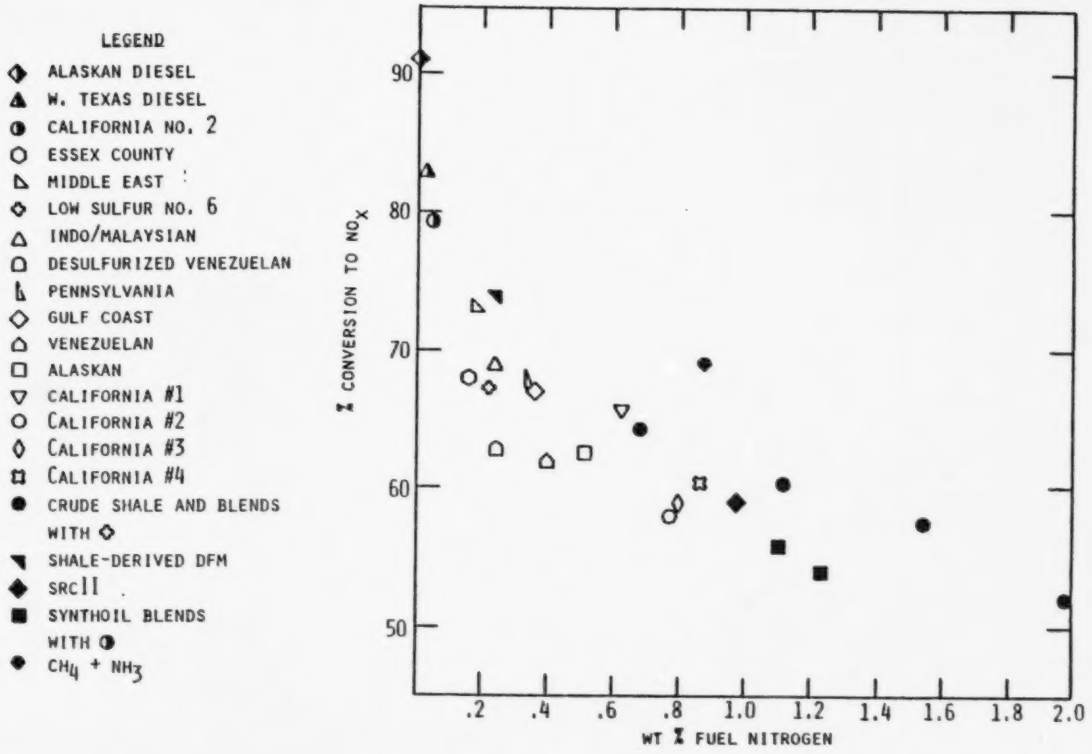

Figure 4-49. Composite Fuel Nitrogen Conversion to NO_x as a Function of Fuel Nitrogen Content.

for equal nitrogen content fuels, the lighter fuels will tend to produce more NO_x. Unfortunately, the actual heavy oil data does not totally substantiate this concept. In general, the data obtained with the shale oil blends were above that obtained with the coal liquid blends; however, both have approximately the same relative nitrogen volatility.

Figure 4-50 summarizes the tests with the crude shale and shale/low sulfur No. 6 oil blends in detail. The data indicated that both the total and fuel NO_x increased uniformly as the nitrogen content of the fuel was increased by the addition of larger amounts of the shale oil. Again, the dominant effects appears to be the weight fraction nitrogen in the liquid fuel.

Figure 4-51 shows a preliminary attempt to correlate the thermal NO_x in terms of fuel properties. Several types of correlation were attempted, but none were particularly successful. In Figure 4-51 the thermal NO_x data (obtained by subtracting the fuel NO_x from the total NO_x) are plotted as a function of the API gravity of the fuel. The data indicate that in general the lighter fuels appear to form more thermal NO_x. This is consistent with the observation that the lighter fuels burn in shorter, more intense flames and, therefore, probably have higher local peak temperatures. Unfortunately, the variations between fuels of a given API gravity cannot be simply explained in terms of relative fuel volatility. It is interesting that the thermal NO_x obtained with the gas flame is significantly below that obtained with distillate oils. This suggests that the thermal NO_x may be partially formed in the early flame zone where droplet effects are still significant. (Of course, the difference could also be due to differences in the fluid mechanics even though both the gas and distillate oil were fired through the same ultrasonic nozzle.)

4.3.3 Fuel Properties -- Physical

Figures 4-52 through 4-55 show the effect of fuel viscosity on both total and fuel NO_x emissions for four different heavy oils. These data were obtained by varying the fuel temperature at the nozzle, and in each case, the actual experimental fuel temperatures are indicated at the top

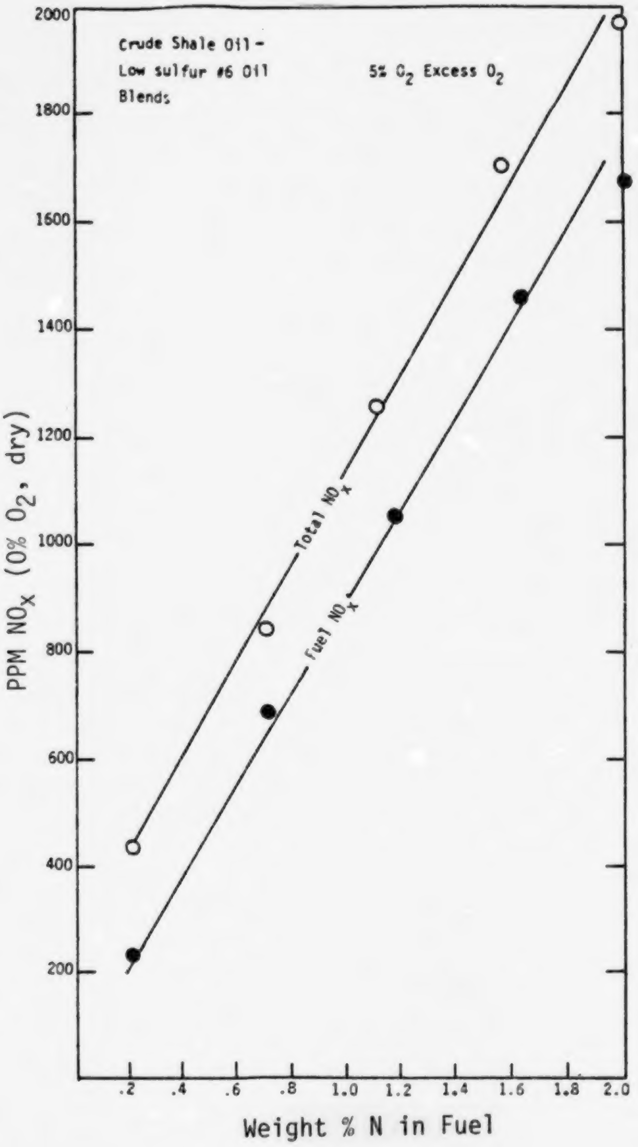

Figure 4-50. Results of Shale Oil Blending Studies.

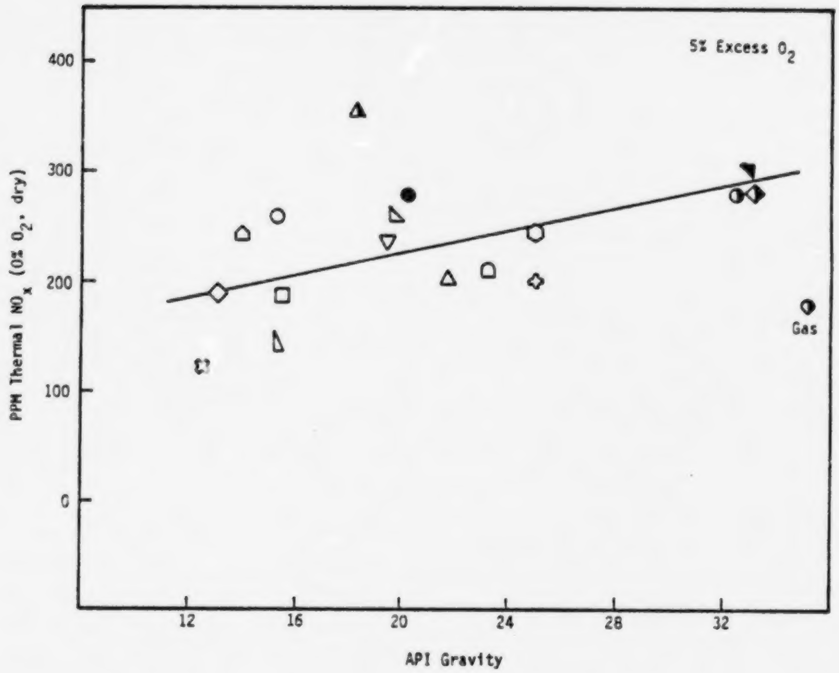

Figure 4-51. Thermal NO_x vs. API Gravity.

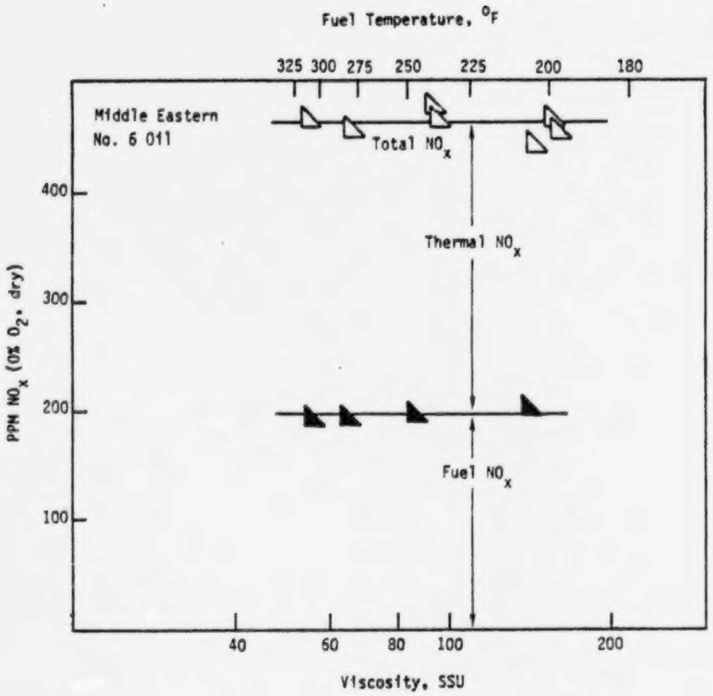

Figure 4-52. Influence of Fuel Viscosity - Middle Eastern Oil.

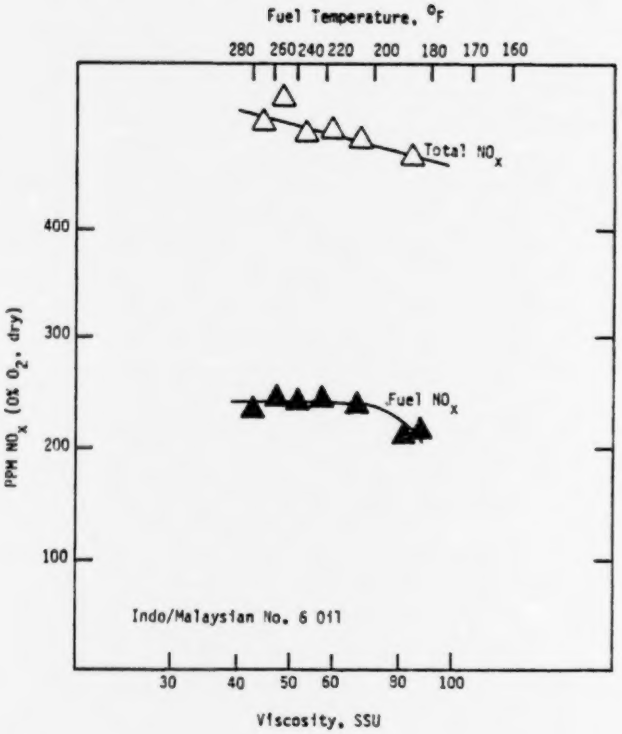

Figure 4-53. Influence of Fuel Viscosity - Indo/Malaysian Oil.

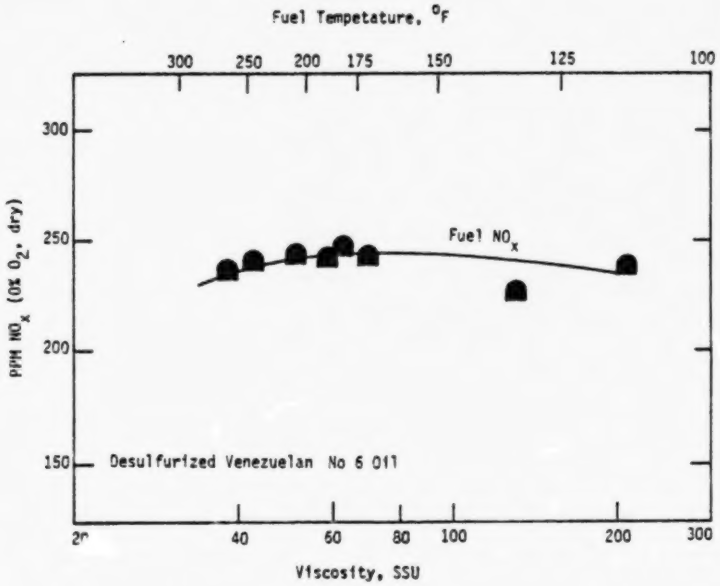

Figure 4-54. Influence of Fuel Viscosity - Desulfurized Venezuelan Oil.

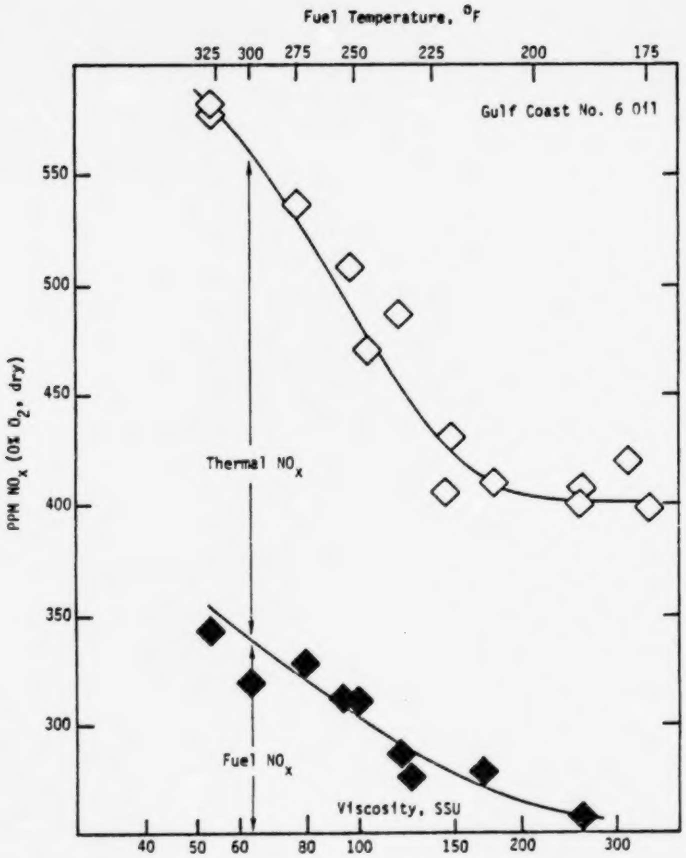

Figure 4-55. Influence of Fuel Viscosity - Gulf Coast Oil.

of the figure. For the first three cases studied (Middle Eastern No. 6 oil, Indonesian/Malaysian No. 6 oil, and the desulfurized Venezuelan No. 6 oil), fuel viscosity had essentially no effect on either the fuel or thermal NO_x formation. This is consistent with the previously reported measurements which indicated that changes in fuel viscosity did not substantially change the mean drop size or size distribution with the ultrasonic nozzle when it was operated at a high atomization pressure. In the final case (the Gulf Coast No. 6 oil), there appeared to be a significant effect of fuel viscosity on the fuel NO_x formation. At present these results cannot be explained. However, in general it appears that so long as the fuel viscosity does not become so high that the atomization dramatically changes, there is little effect of viscosity on fuel or thermal NO_x formation.

4.3.4 Thermal Effects

Figure 4-56 shows the results of flame temperature studies with five residual oils. Adiabatic flame temperature was chosen as the correlating parameter, even though the actual bulk gas and droplet temperatures were probably significantly lower. The adiabatic flame temperatures were calculated using an adiabatic chemical equilibrium model based on a free energy minimization algorithm. In the experimental testing, the theoretical temperature was varied from 2100°K to 2600°K by varying the CO_2 concentration in the oxidizer ($Ar/O_2/CO_2$) and by slight oxygen enrichment of the oxidizer. A suction pyrometer was used to measure the bulk gas temperature approximately 10 cm from the divergent exit. These data, taken with the Alaskan oil and shown in parenthesis in Figure 4-56, revealed that a 400° change in theoretical temperature corresponded to a 200° change in bulk gas temperature.

All of the data shown in Figure 4-56 were taken in argon at three percent excess O_2, 405°K oxidant preheat, 205° kPa atomization pressure, and 14 cSt fuel viscosity. In general, fuel NO_x formation was found to increase only slightly with increasing fuel temperature. However, the Gulf Coast oil

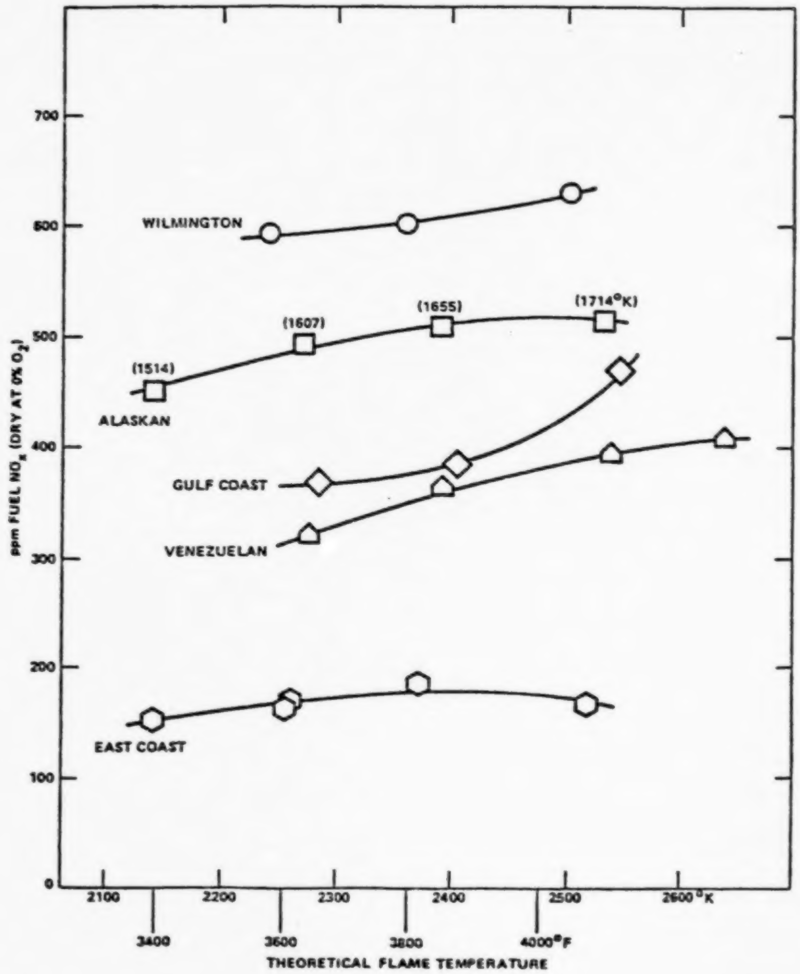

Figure 4-56. Influence of Bulk Flame Temperature.

showed a distinct increase at high flame temperature, behavior analogous to that observed previously with pulverized coal flames(8). Note that this behavior does not relate to any of the particular fuel characteristics discussed in Section 3.

4.3.5 Fuel Atomization

4.3.5.1 Drop Size

Figure 4-57 shows laser diffraction measurements of the droplet size distribution for the ultrasonic nozzle used in a tunnel furnace as a function of the atomizing air pressure. As discussed previously, these data indicate that it is possible to significantly change the size distribution by altering the atomization pressure. Above a pressure of approximately 184 kPa (12 psi), the droplet size distribution becomes extremely narrow due to sonic flow in the nozzle throat. These data further indicate that at the normal operating condition (205 kPa) the nozzle is producing very small droplets. This characteristic was used to investigate the influence of drop size and size distribution on both thermal and fuel NO_x formation.

Figure 4-58 shows the result of varying the droplet size by altering the atomization pressure for the relatively light Indonesian/Malaysian oil and for the Alaskan Bunker C oil. These data indicate that the thermal NO_x increases slightly and then drops dramatically as the mean drop size is increased from 20 to 200 μm. These results are not in agreement with the work of Nizami and Cernansky(9) who found a minimum in thermal NO_x formation at a droplet diameter of 50 μm. It should be noted, however, that these workers were studying monodisperse isopropanol aerosols with a maximum NO_x formation of 20 ppm at SR = 1.0. Thus the difference in results between the two experiments may not be contradictory due to completely different fuel vaporization characteristics, droplet histories, and/or different combustion aerodynamics.

Figure 4-58 also indicates that fuel NO_x was observed to decrease with increasing droplet size. This effect was particularly significant in the case of the heavy Alaskan oil.

Figure 4-59 shows similar results obtained with the crude shale oil at two different excess oxygen levels. These data again show a decrease in both fuel and thermal NO_x formation at large droplet sizes.

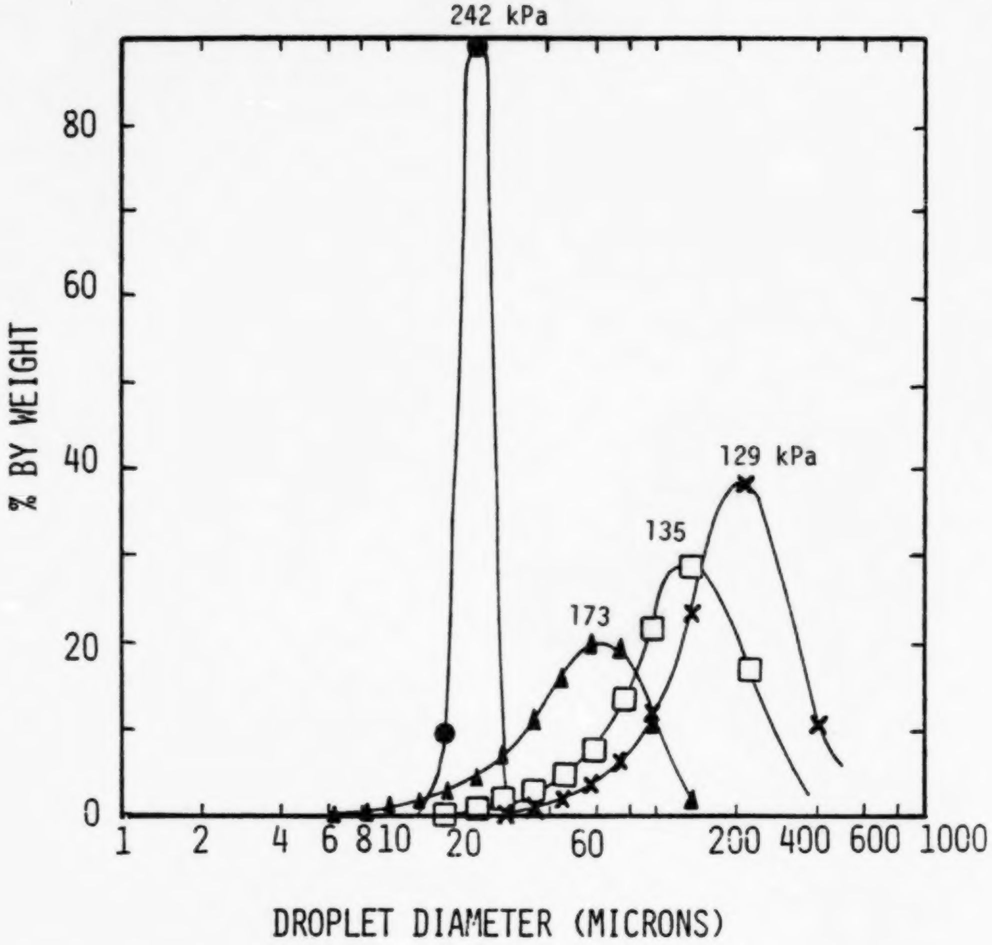

Figure 4-57. Droplet Size Distribution Data - Ultrasonic Nozzle Used in the Tunnel Furnace

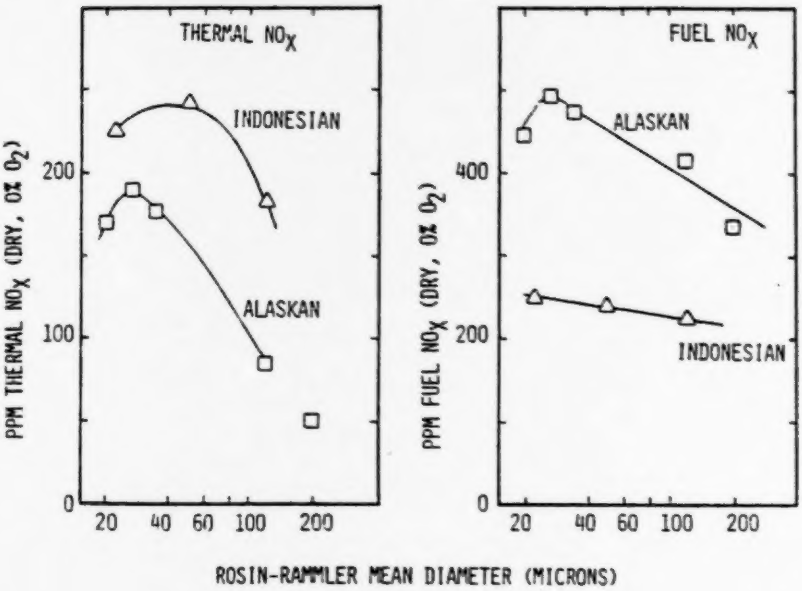

Figure 4-58. Influence of Drop Size on Thermal and Fuel NO$_x$ Formation - Shale Oil.

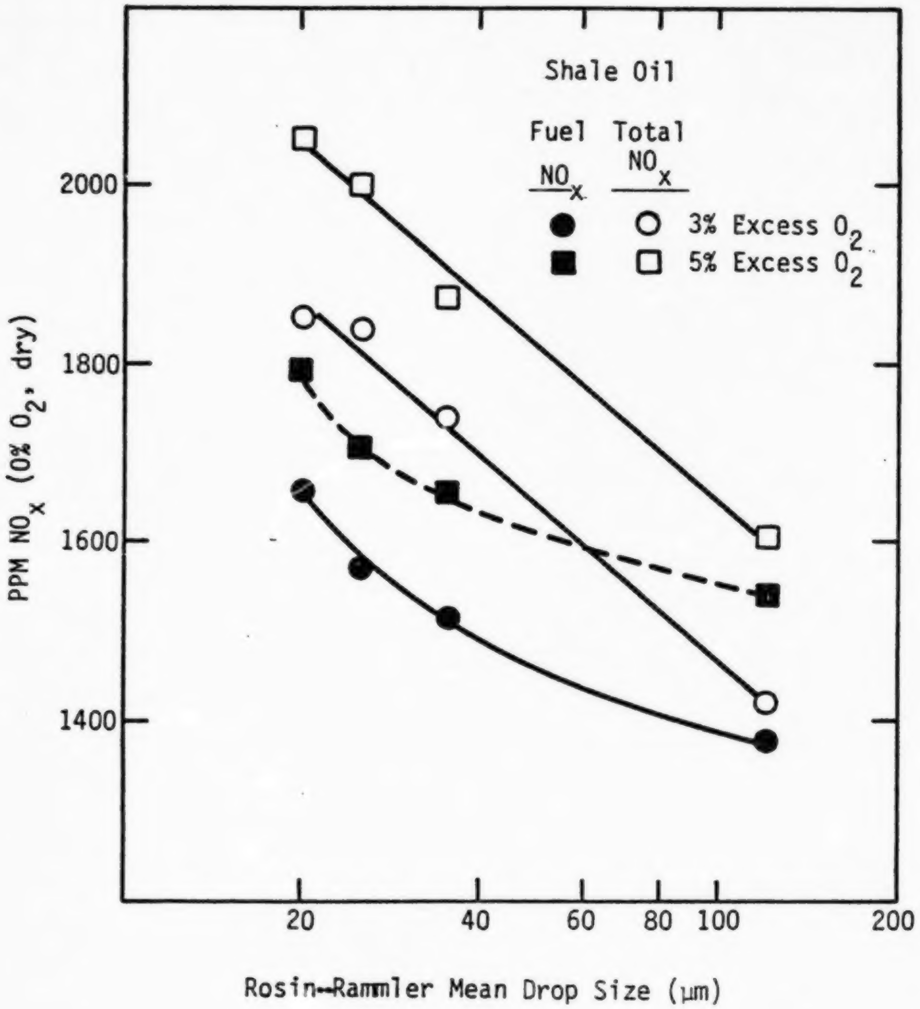

Figure 4-59. The Effect of Drop Size on Total and Fuel NO_x Production.

Figure 4-60 shows the fuel NO_x data plotted on a percent conversion basis as a function of the mean droplet size. This figure also includes data obtained with the coal-derived liquid SRC-II. In general, the coal liquid appears to be less sensitive to the drop size than either the petroleum liquids or the shale oil.

Figure 4-61 shows the corresponding data on thermal NO_x formation. In every case the thermal NO_x increases slightly then decreases as the drop size increases.

4.3.5.2 Nozzle Design

Figure 4-62 shows the effect of nozzle type on thermal NO_x formation with the Alaskan oil. The data shown previously with the ultrasonic nozzle are compared to data obtained with the ultrasonic nozzle after the resonator tip was removed and to that obtained with the Delavan "siphon" nozzle. Drop size measurements indicated that the mean drop size was approximately the same for the ultrasonic nozzle with and without the resonator. However, the mean drop size for the siphon nozzle was approximately 40 μm (double that for the ultrasonic nozzle). Thus, again it appears that increasing the mean drop size has decreased the thermal NO_x formation. However, considering the magnitude of the decrease shown in Figure 4-62, it appears likely that the fluid mechanics have also changed to some extent. Figure 4-63 shows similar data on fuel NO_x formation with the same three nozzle configurations. In this case, there was relatively little effect of nozzle design on the measured emissions (note the expanded ordinate scale).

4.4 Results — Staged Combustion Conditions

4.4.1 First-Stage Stoichiometry

Figure 4-64 shows a typical set of staged combustion results obtained with the Alaskan North Slope Bunker C oil. These data illustrate the effect of primary zone stoichiometric ratio on total NO_x emissions in the exhaust of the furnace.

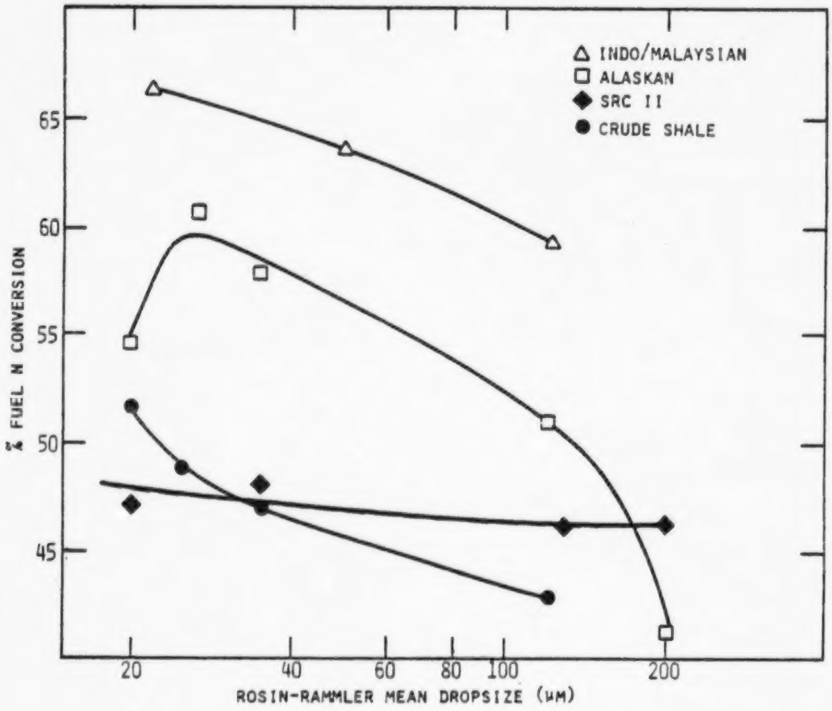

Figure 4-60. Effect of Mean Drop Size on Percent Fuel N Conversion.

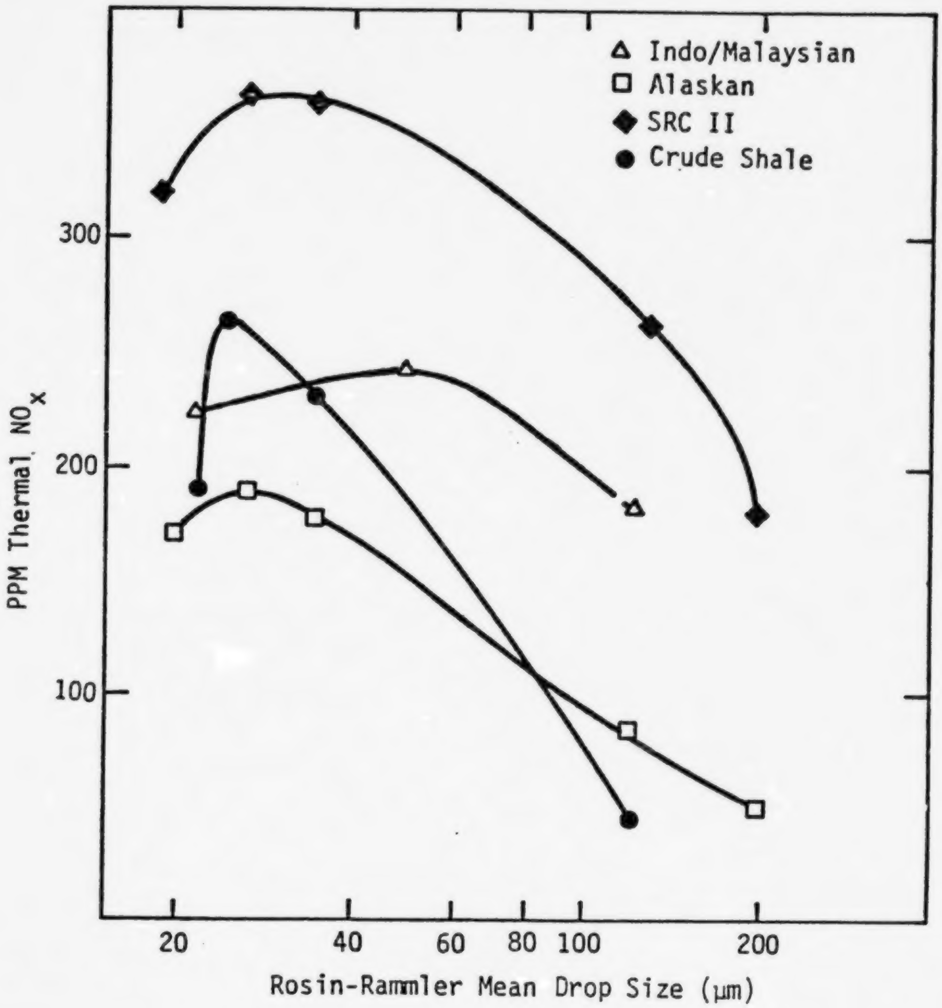

Figure 4-61. Effect of Mean Drop Size on Thermal NO_x Formation

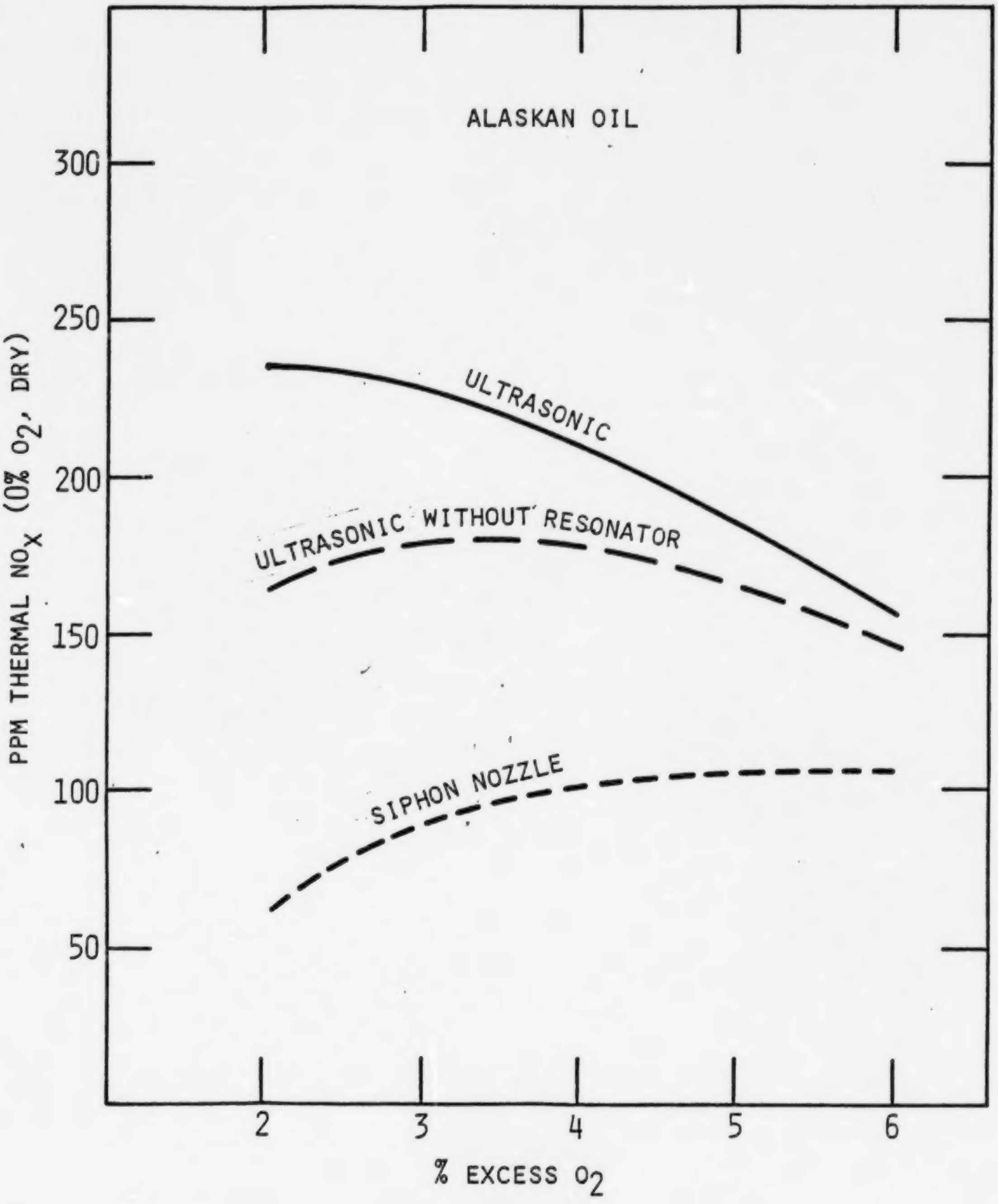

Figure 4-62. Influence of Atomizer Design on Thermal NO_x.

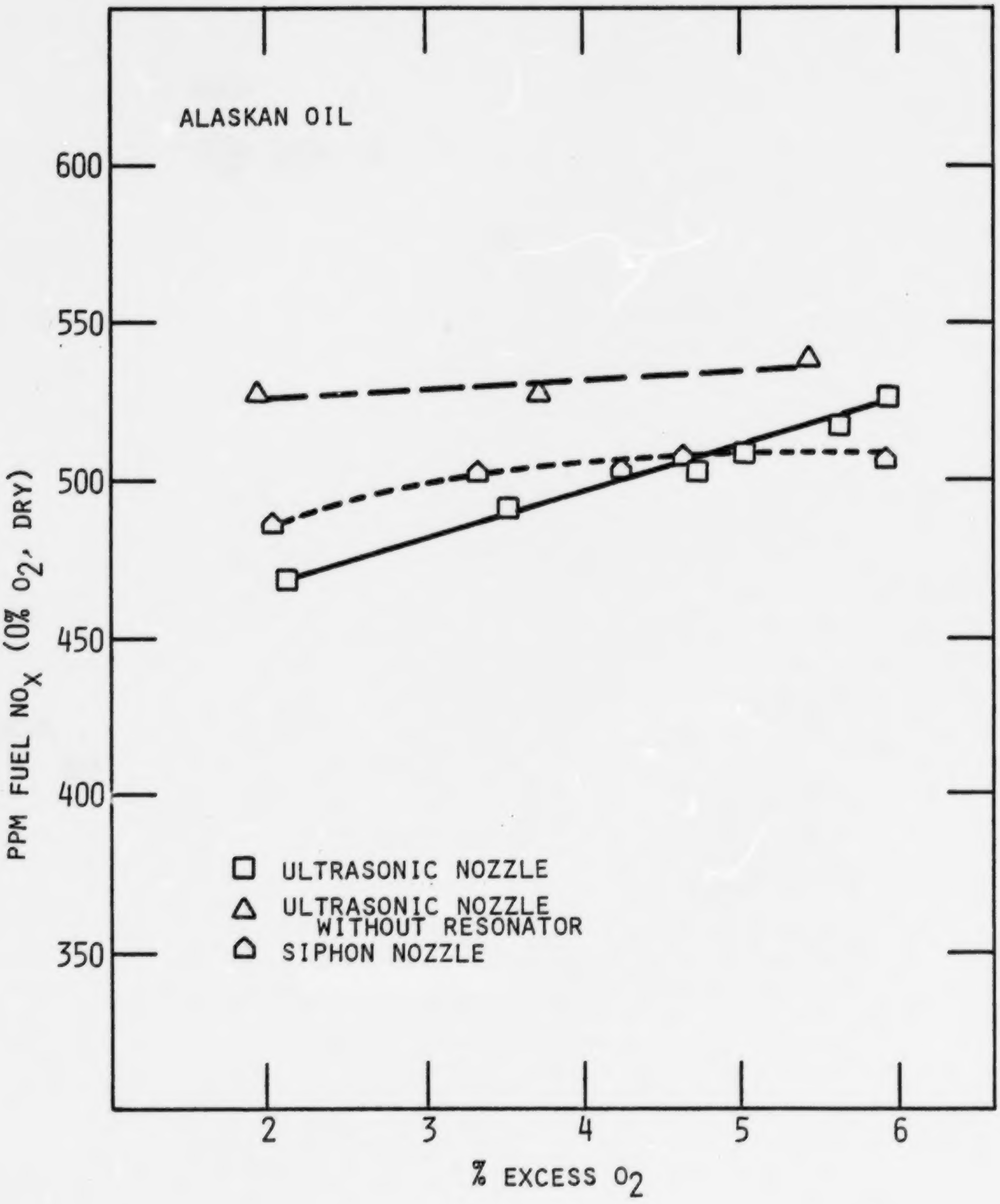

Figure 4-63. Influence of Atomizer Design on Fuel NO$_x$

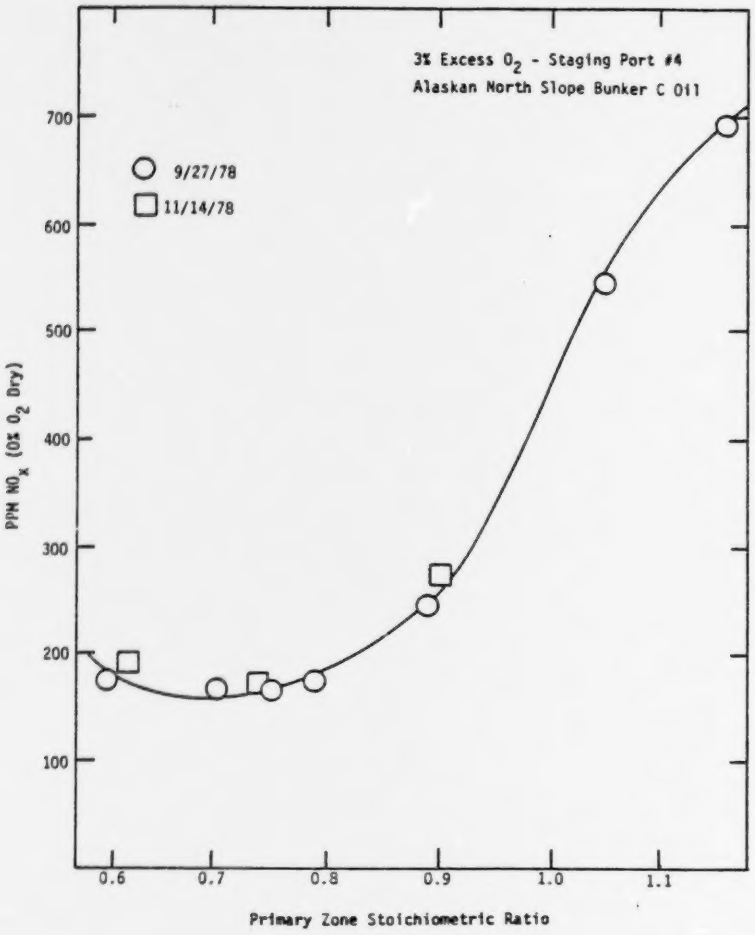

Figure 4-64. Typical Staged Combustion Results.

Throughout the staged combustion testing, the overall excess air was held at a constant value (typically three percent excess O_2), and the primary zone stoichiometry was varied by decreasing the amount of air going through the burner and increasing the amount going through the second-stage air injection lances. In general, the atomization pressure and airflow rate were not changed. Also, all of the staged combustion results were obtained with air as the oxidizer. Because of the complications associated with using $Ar/O_2/CO_2$ under rich combustion conditions, no attempt was made to directly measure fuel NO_x formation.

Figure 4-64 shows that as the primary zone stoichiometric ratio is decreased below 1.0, the total NO_x emissions decrease drastically. Continuing to decrease the primary zone stoichiometry ratio results in a minimum emission level after which the NO_x starts to increase again. While the location of the minimum is a function of both fuel and first-stage residence time, as will be discussed in the following sections, the overall shape of the curve shown in Figure 4-64 is typical of most of the results obtained. Data are also shown for two replicate runs approximately two months apart and these points indicate the type of reproducibility normally achieved.

Figure 4-65 shows similar data obtained at a shorter first-stage residence time. In general, these data were obtained by adding the second-stage air at a particular staging port (constant axial distance from the burner). Thus, as the stoichiometry was decreased the first-stage residence time effectively increased (due to a decreased mass flow). Figure 4-65 also shows data (circles) which have been corrected for this effect by interpolating between data obtained at different axial positions to maintain a constant first stage residence time (400 msec). Comparison of these two curves indicates the importance of both primary zone stoichiometry and primary zone residence time in a staged combustion system.

4.4.2 First-Stage Residence Time

Figure 4-66 illustrates the effect of the first-stage redicence time at various first-stage stoichiometries. The residence times shown are

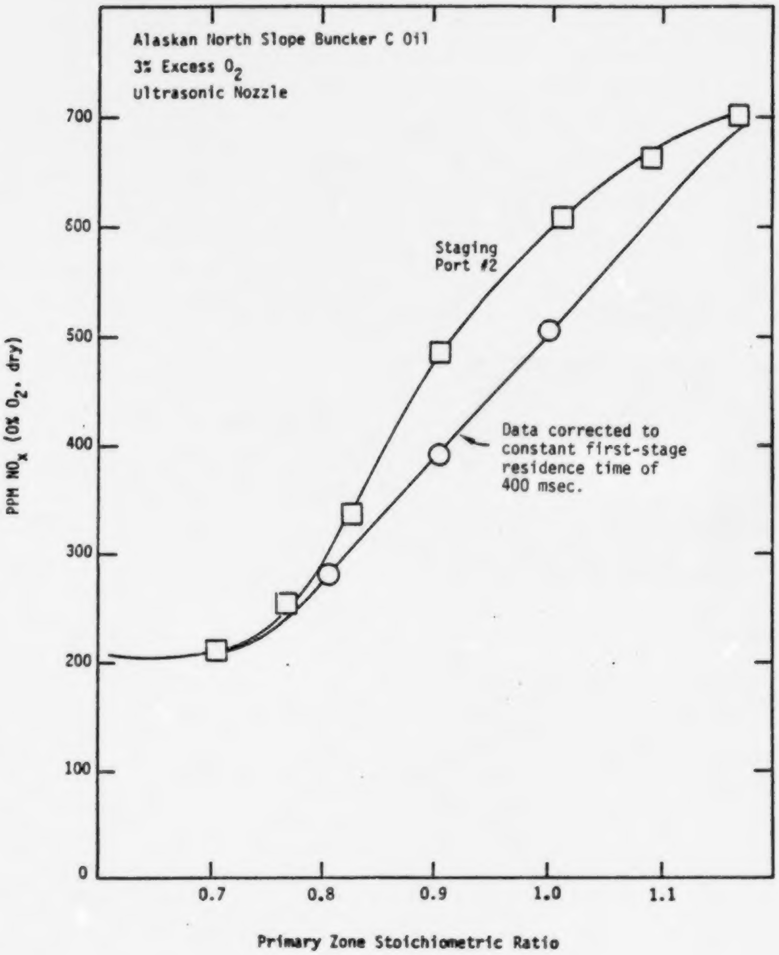

Figure 4-65. Influence of Primary Zone Stoichiometry at Constant τ.

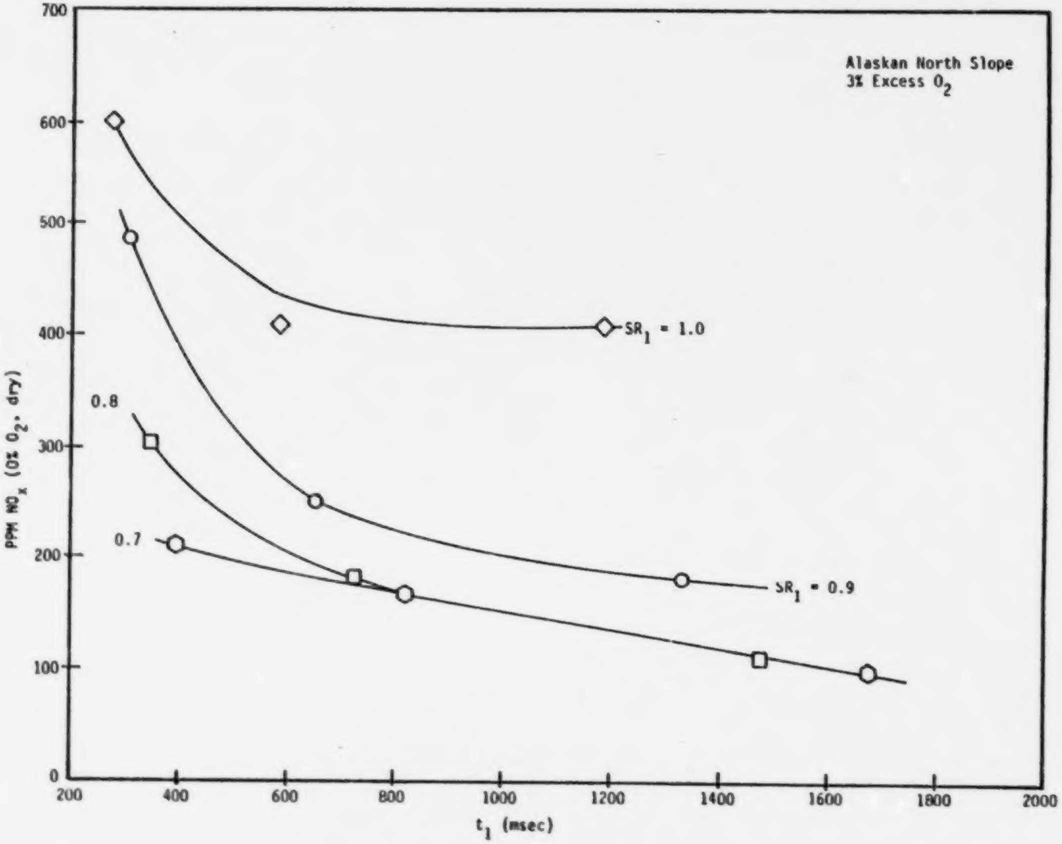

Figure 4-66. Influence of Primary Zone Residence Time.

nominal values calculated on the basis of a plug flow system and constant mean gas temperature. These data indicate that after approximately 600 ms increasing first-stage residence time does little to decrease the measured NO_x. This may be due to the absence of significant hydrocarbon fragments after that point or to a decrease in kinetic rates because of decreased bulk temperatures.

4.4.3 Fuel Properties

Figure 4-67 shows the effect of primary zone stoichiometry and primary zone residence time on the measured NO_x emissions from the Alaskan diesel oil. Since this oil contains essentially no fuel nitrogen, these data represent the influence of staged combustion on thermal NO_x formation. Thus, staged combustion is very effective in controlling NO_x formed via thermal fixation of atmospheric nitrogen if the residence time in the first stage is adequate. (The residence time to staging-port eight at SR_1 equal to 0.9 is approximately 1300 ms.)

Figures 4-68 and 4-69 show the influence of primary zone stoichiometry and primary zone residence time on the NO_x emissions from the Essex County and Indonesian/Malaysian oils. In each case, increasing the primary zone residence time decreases the minimum NO_x emissions achieved and shifts the location of the minimum toward a primary zone stoichiometry of 0.9.

Figures 4-70 and 4-71 show staging results for the heavy Gulf Coast oil at staging ports four and eight, respectively. In each case, data are also shown for a distillate oil simulation of the heavy Gulf Coast oil. This simulation was achieved by doping the California diesel oil with the appropriate amounts of thiophene and pyridine to match the sulfur and nitrogen content of the Gulf Coast oil. The data shown in Figure 4-70 indicate that under excess air conditions the distillate oil simulation is indeed very good; however, under fuel-rich conditions the distillate oil produces less NO_x than the actual Gulf Coast residual oil. This difference, although small in terms of absolute ppm, and nearly within the data scatter, represents a significant percentage decrease and it was found to be consistently reproducible. These data suggest that the minimum emission may be

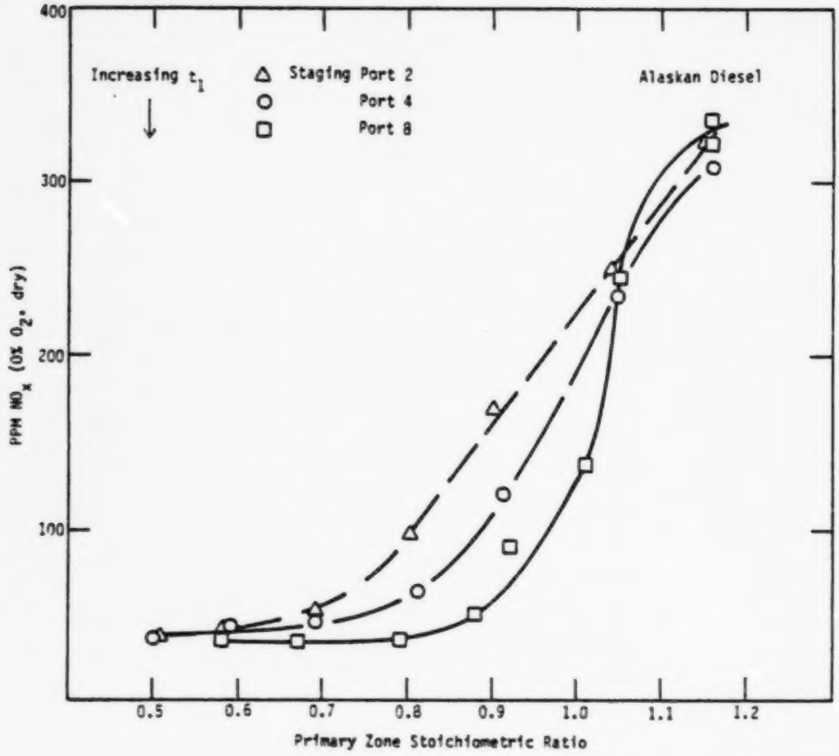

Figure 4-67. Staging Results - Alaskan Diesel.

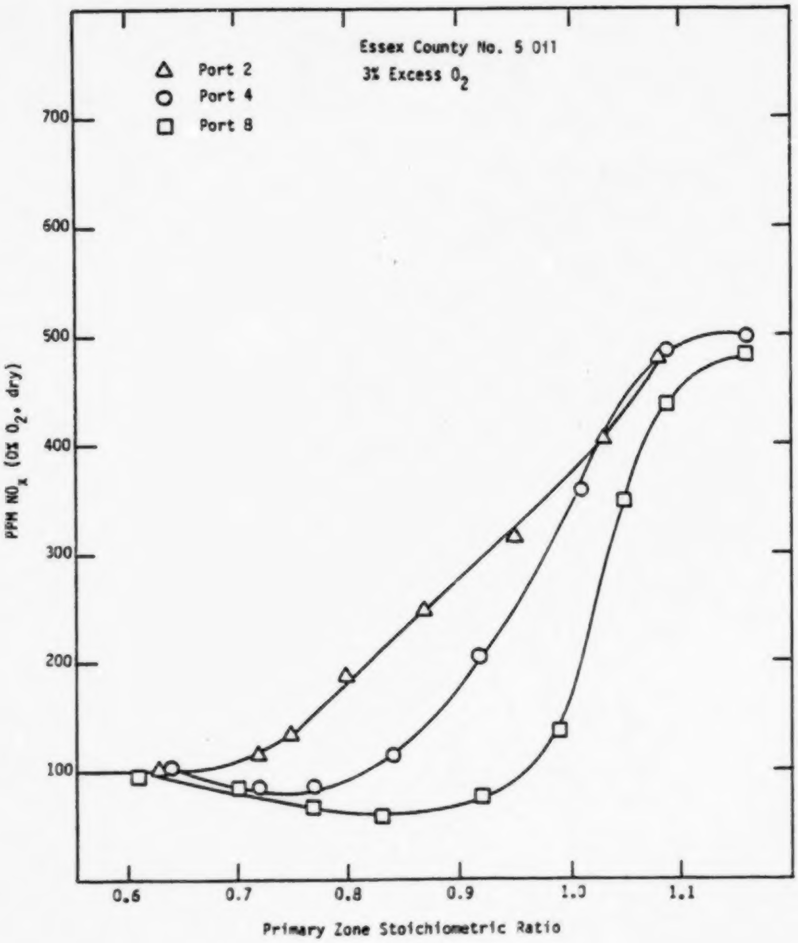

Figure 4-68. Staging Results - Essex County Oil.

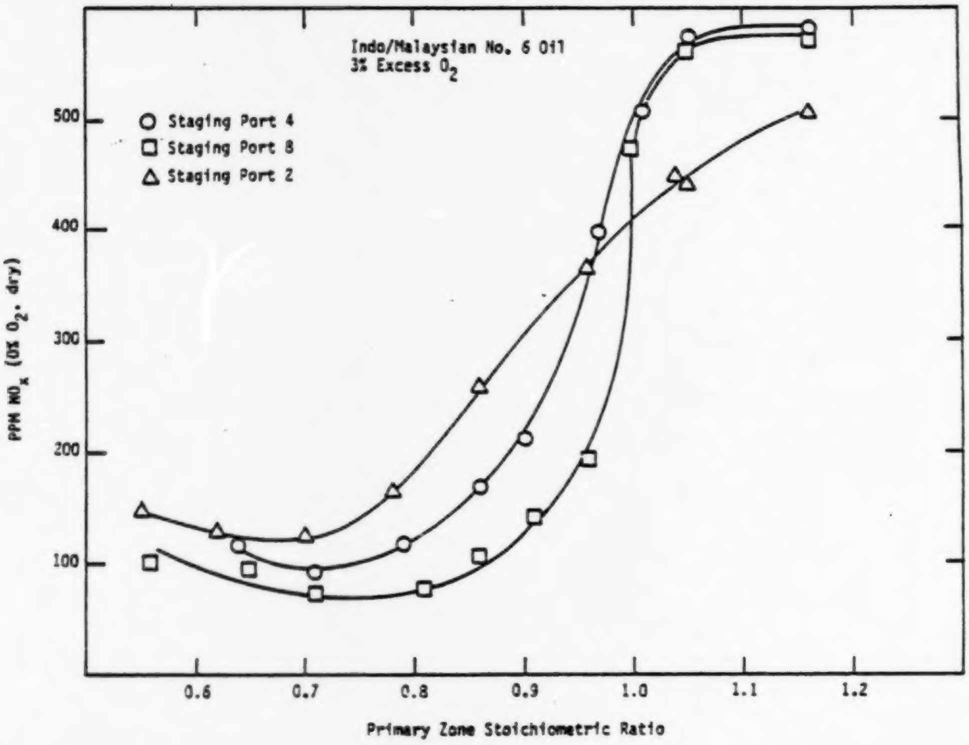

Figure 4-69. Staging Results - Indo/Malaysian Oil.

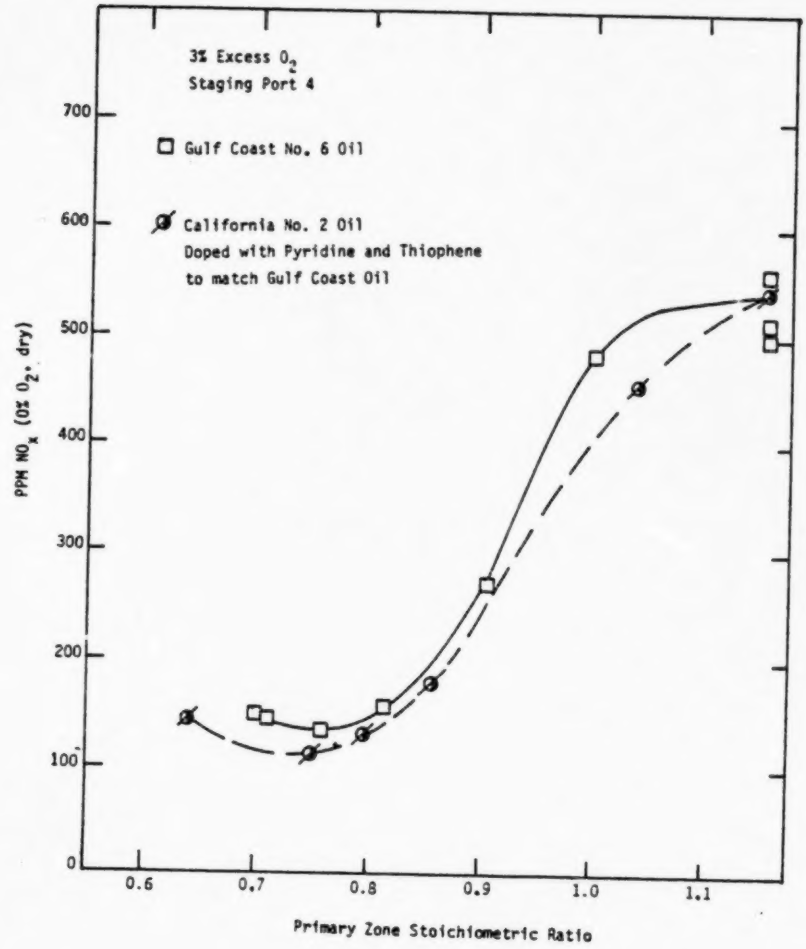

Figure 4-70. Staging Results - Port 4 - Gulf Coast Oil.

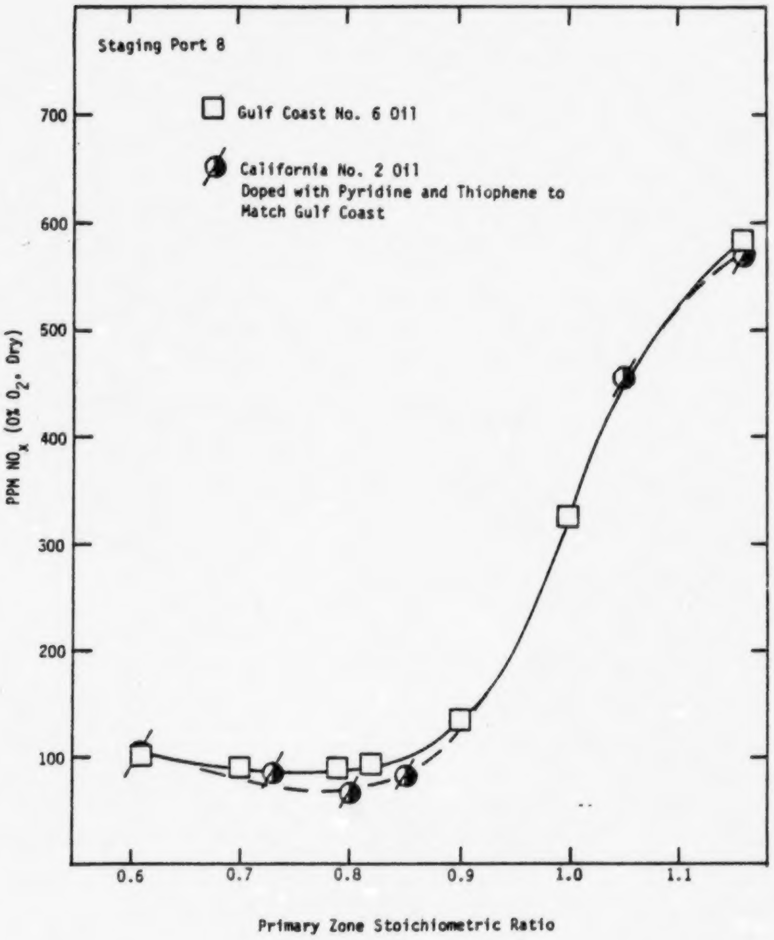

Figure 4-71. Staging Results - Port 8 - Gulf Coast Oil.

influenced by the relative volatility of the fuel, and, in particular, by the relative volatility of the nitrogen.

Figure 4-72 shows the staged combustion data obtained with the Alaskan North Slope oil. Figure 4-73 shows similar data at two overall excess air conditions for the shale oil. These data indicate that the exhaust emissions are insensitive to the overall excess air. This suggests that the formation or reduction of NO_x in the first stage is controlling the exhaust emission level. It is also interesting that while the shale produces very large amounts of NO_x under excess air conditions (due to its high nitrogen content), the emissions under staged conditions are not dramatically above those observed with the petroleum liquids.

Figure 4-74 shows the results of a staged combustion study conducted with methane containing one percent nitrogen as NH_3. These data indicate a very steep dependence of NO_x formation on primary zone stoichiometry, and this is typical of rapidly mixed gas systems. These tests were conducted to investigate the influence of relative fuel volatility; CH_4/ammonia is an approximate simulation of an instantaneously volatilized fuel which tends to be more premixed.

Figure 4-75 summarizes the minimum emission levels observed with the various fuels tested. This figure illustrates that the minimum emission levels observed under staged combustion conditions do not correlate simply with total fuel nitrogen, and this is in direct contrast to the results obtained under excess air conditions. All of the data shown in Figure 4-75 were obtained with the second-stage air injected at the staging-port four, and with the overall excess oxygen at three percent. The data indicate that the doped distillate is significantly lower than the actual residual oil which it simulates. The CH_3/NH_4 emissions were also dramatically lower than the high nitrogen liquid fuels tested. The shale oil does not correlate with the petroleum-derived liquids.

In summary, Figure 4-75 suggests that the effectiveness of staged combustion cannot be simply assessed based on a knowledge of the fuel nitrogen content of a particular liquid fuel.

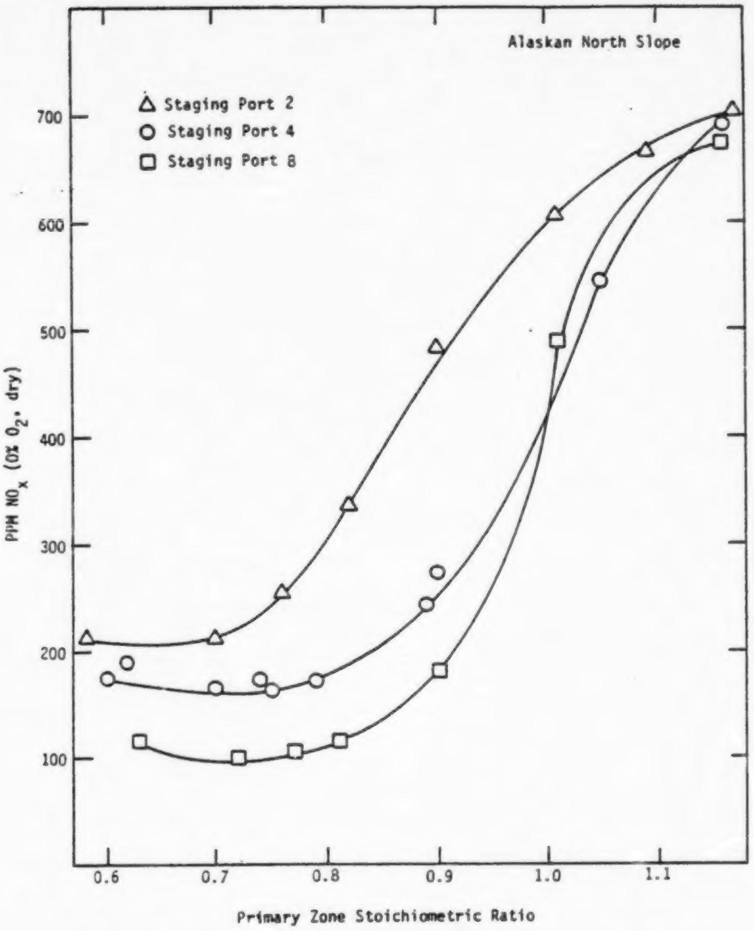

Figure 4-72. Staging Results - Alaskan Oil.

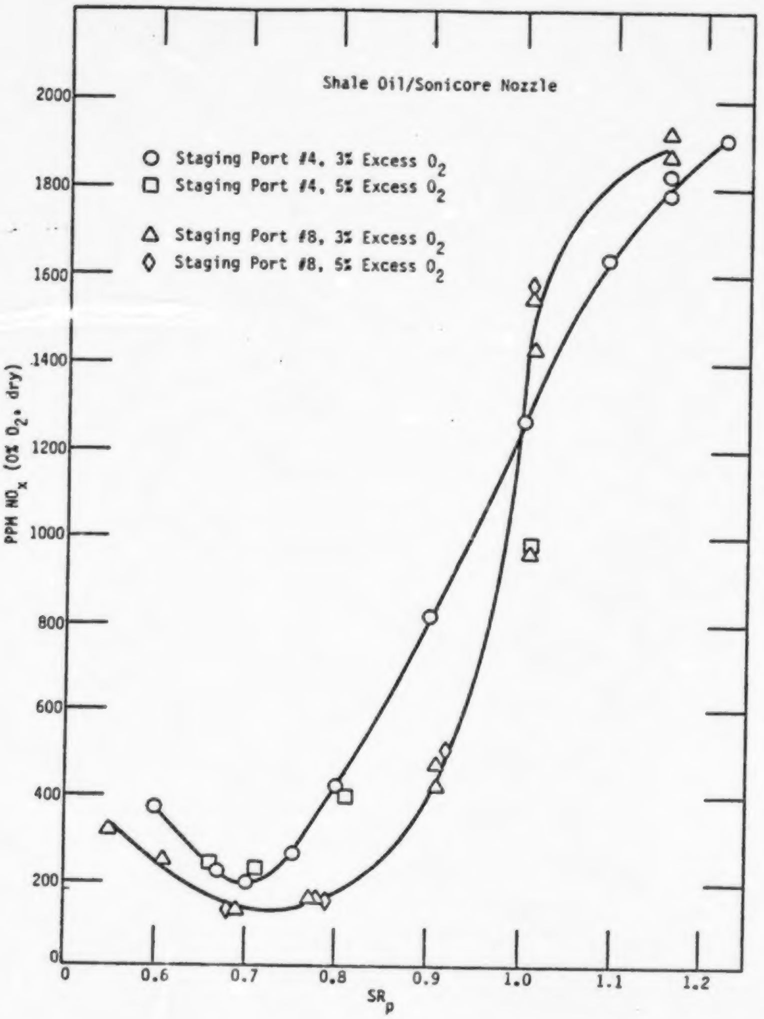

Figure 4-73. Staging Results - Shale Crude.

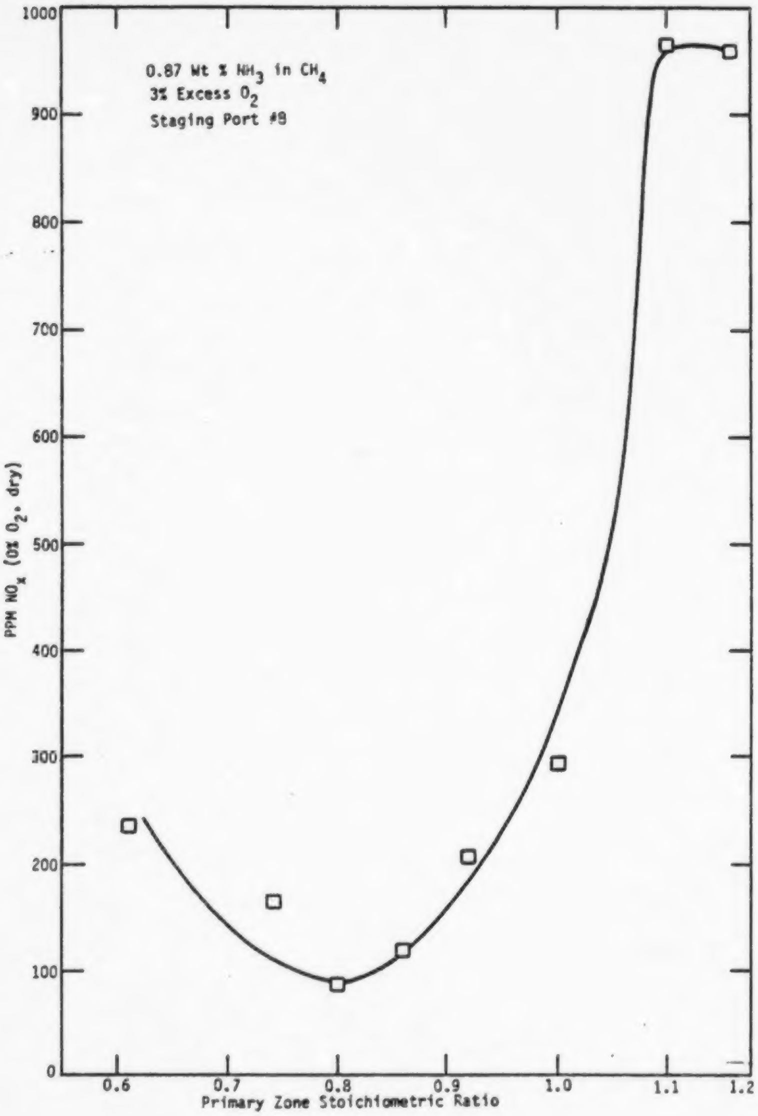

Figure 4-74. Staging Results - CH_4/NH_3

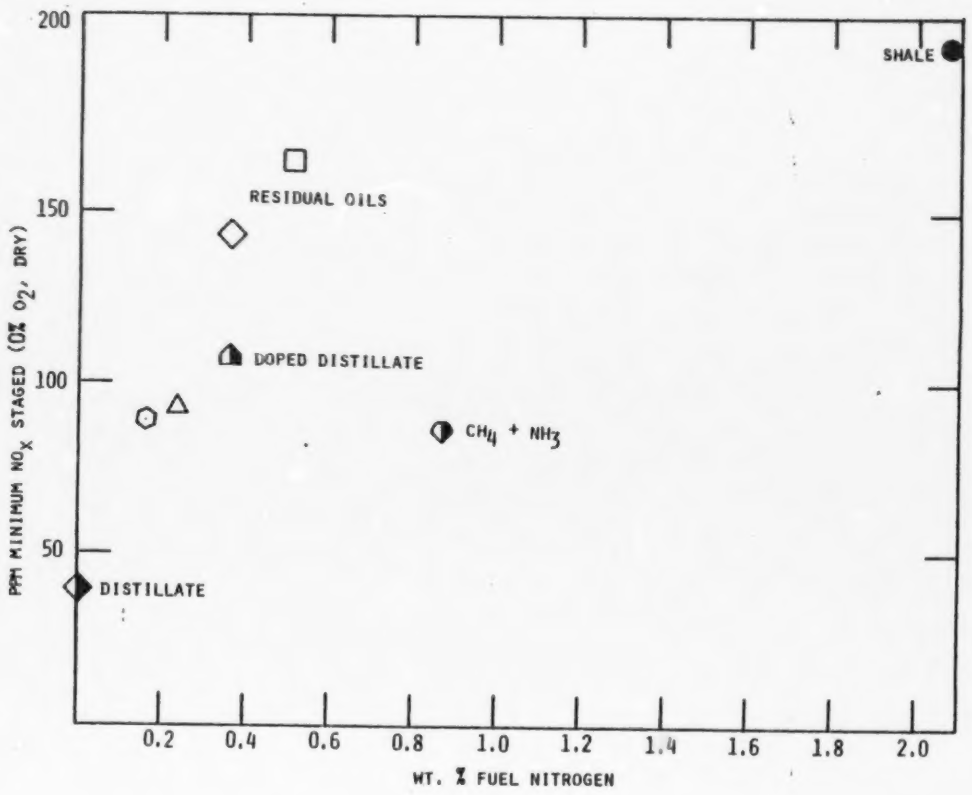

Figure 4-75. Influence of Fuel Nitrogen Content on Minimum NO_x Emissions Staged.

In an effort to try to further understand the controlling parameters under staged combustion conditions, fundamental data was obtained as part of the EPA Fundamental Combustion Research Program.

Figure 4-76 shows the data of Axworthy and Nealy(10) for six of the oils tested in this program. These data show the percentage of the original fuel nitrogen in the oil which is recovered as HCN in a two-stage inert pyrolysis technique. The fuels were rapidly pyrolyzed in the first stage of a quartz reactor over the range of temperatures shown. The reactive volatile nitrogen species evolved were then converted to HCN in the second stage of the reactor at 1100°C and were measured as HCN. These data then are representative of the volatile nitrogen yields from the six-fuel study. Figure 4-77 shows the staged combustion data obtained in the tunnel furnace (plotted as the ratio of minimum emissions to uncontrolled emissions) as a function of the percent of the initial fuel nitrogen recovered as HCN in the Axworthy experiment. This figure illustrates that the data correlate extremely well in terms of this parameter and it strongly suggests that the efficiency of staged combustion in controlling NO_x emissions is directly related to the type of fuel nitrogen present in the liquid. In the case of the Alaskan oil, very little of the fuel nitrogen is volatilized and convertible to HCN. However, in the case of the shale, a significant fraction of the nitrogen appears to be relatively volatile. Thus, to assess the ability of a particular staged combustion system to control NO_x emissions for a given fuel, one must know both the total nitrogen content of the fuel and the relative volatility of that nitrogen. It appears that controlling the emissions from fuels containing large amounts of refractory nitrogen may be extremely difficult.

4.4.4 Fuel Atomization

Figure 4-78 shows the effect of air atomizing pressure on total NO_x emissions as a function of primary zone stoichiometric ratio. As noted previously, varying the atomization pressure from 129 to 205 kPa (4 psi to 14 psi) reduces the mean drop size from 200 μm to 20 μm. The data shown in Figure 4-78 indicate that under staged combustion conditions with the Alaskan North

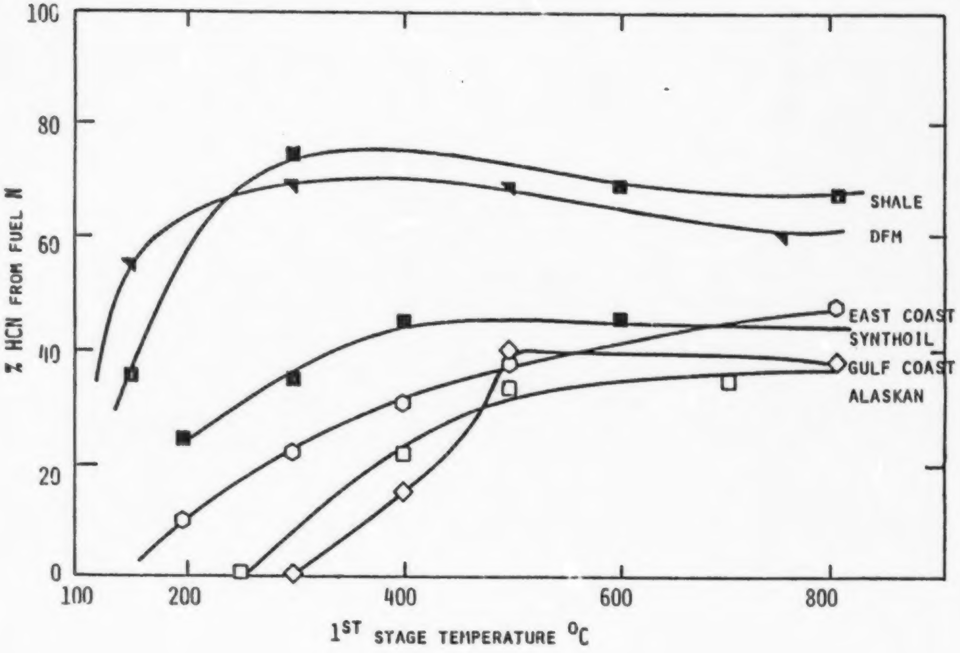

Figure 4-76. HCN Yield as a Function of Pyrolysis Temperature.

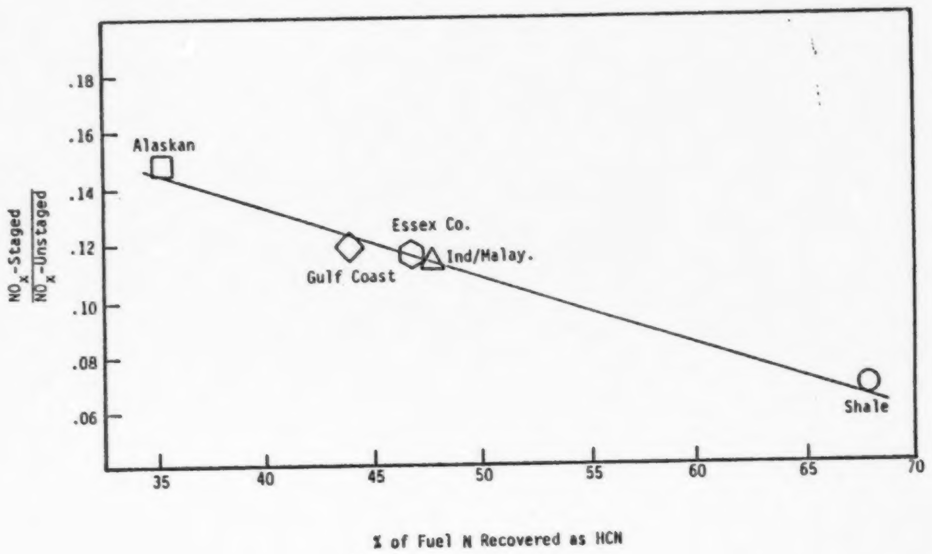

Figure 4-77. Staging Efficiency and Fuel Nitrogen Volatility.

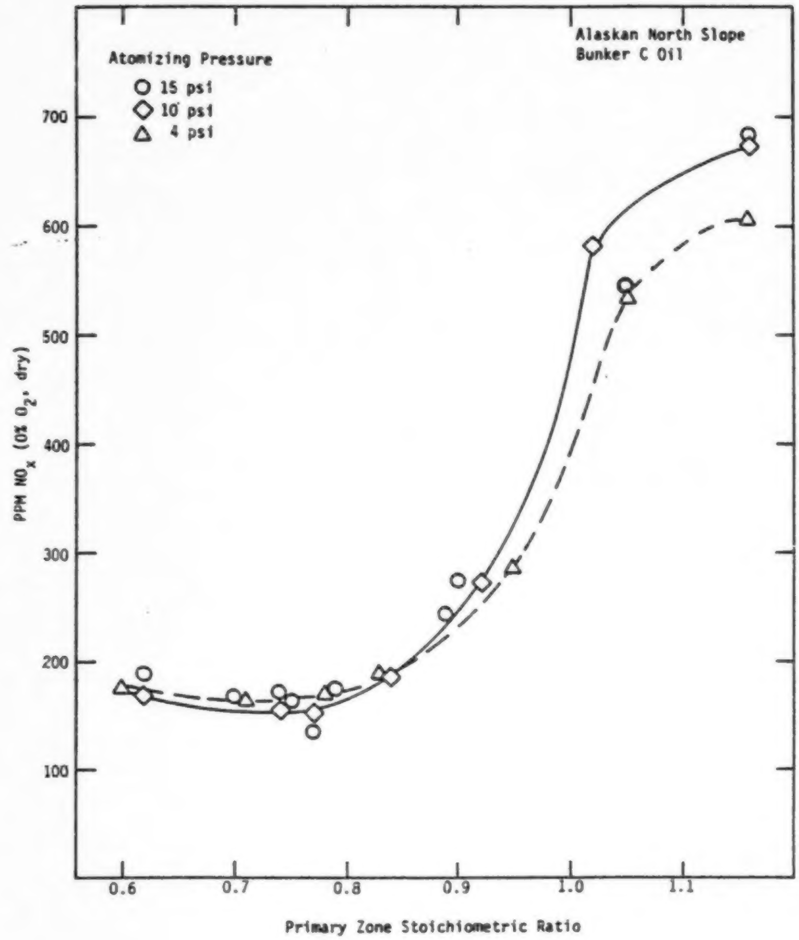

Figure 4-78. Effect of Drop Size on Staged Emissions - Alaskan Oil.

Slope Bunker C oil, the drop size has only a very small effect on NO_x emissions. Figures 4-79 and 4-80 show the influence of mean drop size on minimum staged NO_x emissions for two different first-stage residence times. In general, the minimum emissions increase slightly as the drop size is increased. Figure 4-81 summarizes this data and also shows the influence of drop size on thermal NO_x based on data with the Alaskan diesel oil (essentially nitrogen-free). In general, it appears that under staged combustion conditions increasing drop size increases NO_x with the light oils and has relatively little influence on the minimum NO_x with a heavy oil such as the Alaskan oil.

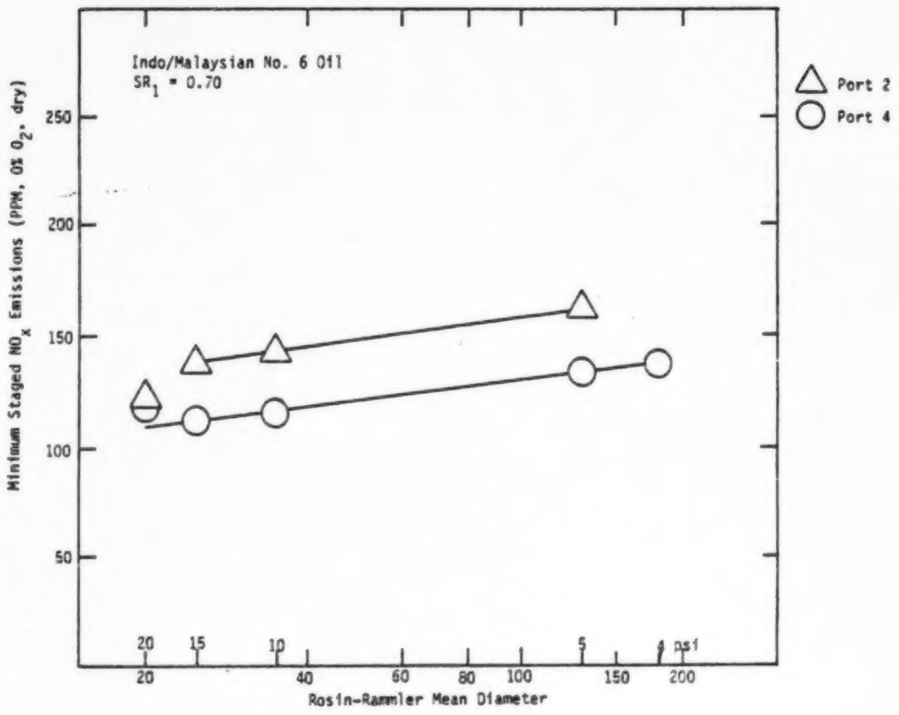

Figure 4-79. Effect of Mean Drop Size on Minimum Staged Emissions - Indo/Malaysian Oil.

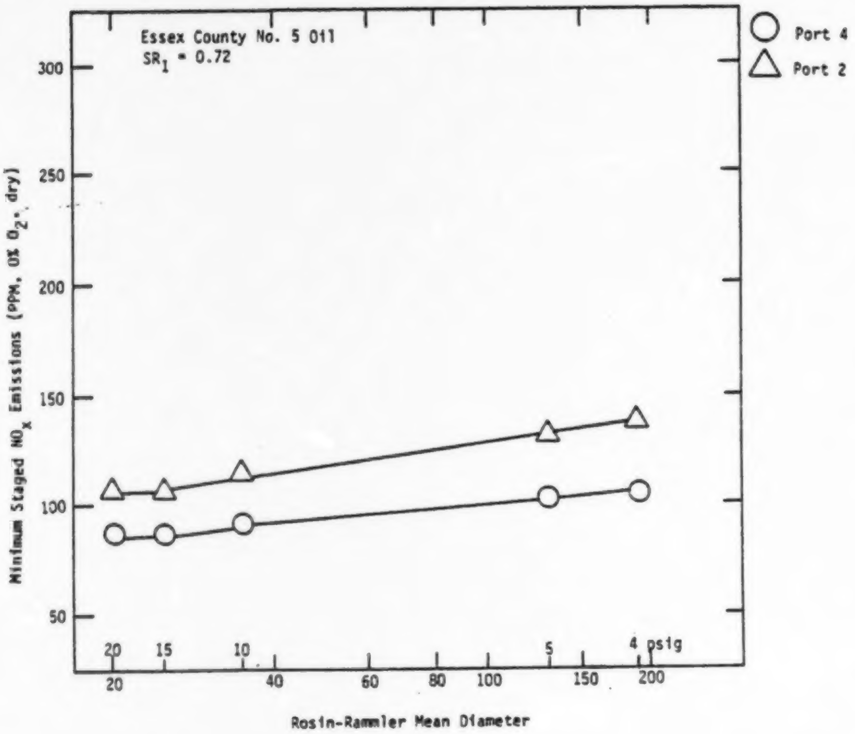

Figure 4-80. Effect of Mean Drop Size on Minimum Staged Emissions - Essex County Oil.

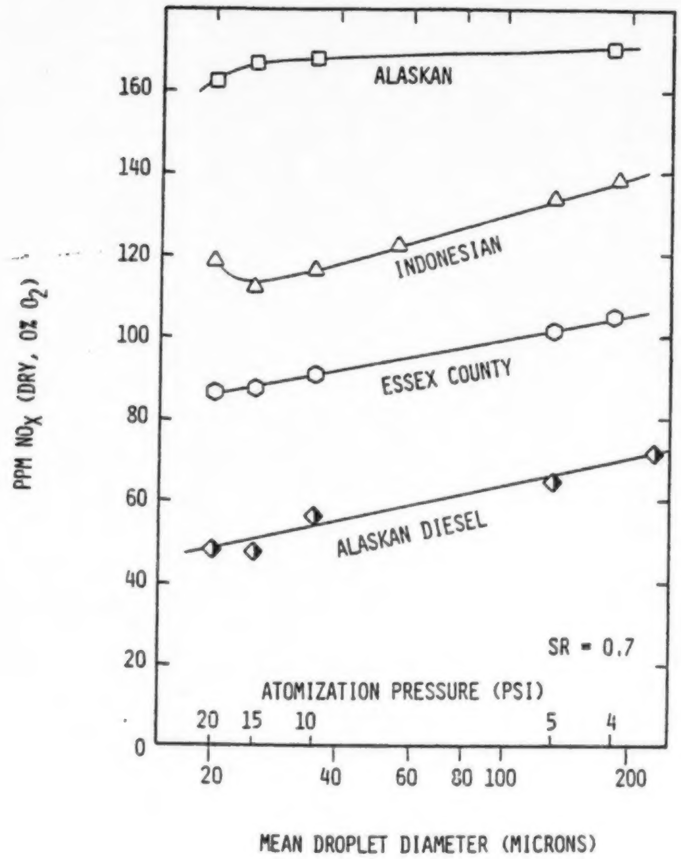

Figure 4-81. Influence of Droplet Size Under Staged-Combustion Conditions.

REFERENCES

1. Heap, M. P., T. M. Lowes, R. Walmsley, and H. Bartelds, "Burner Design Principles for Minimum NO_x Emissions", Proceedings, Coal Combustion Seminar, EPA-650/2-73-021, NTIS, Springfield, Virginia (1973).

2. Pershing, D. W., Ph.D thesis, University of Arizona (1976).

3. Folsom, B. A. and C. W. Courtney, "Chemiluminescent Measurement of Nitric Oxide in Combustion Products", Proceedings of the Third Stationary Source Combustion Symposium, Vol. II, EPA-600/7-79-0506, NTIS, Springfield, Virginia (1979).

4. Martin, G. B. and E. E. Berkau, "An Investigation of the Conversion of Various Fuel Nitrogen Compounds to NO in Oil Combustion", AIChE Symposium Series No. 126, 68 (1972).

5. Wendt, J. O. L., J. T. Morcomb, E. M. Morcomb, and T. L. Corley, "Influence of Fuel Sulfur on Fuel Nitrogen Oxidation Mechanisms", Seventeenth Symposium (International) on Combustion, The Combustion Institute, Pittsburgh, Pennsylvania (1979).

6. Mitchell, R. E. and A. F. Sarofim, "Nitrogen Oxide Formation in Laminar Methane-Air Diffusion Flames", paper presented at the Fall Meeting, WSS-Combustion Institute, Palo Alto, California (1975).

7. Turner, D. W., R. L. Andrews, and C. W. Siegmund, "Influence of Combustion Modification and Fuel Nitrogen Content on Nitrogen Oxide Emissions from Fuel Oil Combustion", AIChE Symposium Series No. 126, 68 (1972).

8. Pershing, D. W. and J. O. L. Wendt, "Pulverized Coal Combustion: The Influence of Flame Temperature and Coal Composition on Thermal and Fuel NO_x", Sixteenth Symposium (International) on Combustion, The Combustion Institute, Pittsburgh, Pennsylvania (1977).

9. Nizami, A. A. and N. P. Cernansky, "NO_x Formation in Monodisperse Fuel Spray Combustion", Seventeenth Symposium (International) on Combustion, The Combustion Institute, Pittsburgh, Pennsylvania (1978).

10. Axworthy, A. E. and C. L. Nealy, paper presented at the Third Stationary Source Combustion Symposium, San Francisco, California, March 1979.

11. Kramlich, J., M. P. Heap, W. R. Seeker, and T. J. Tyson, "Fundamental Combustion Research Applied to Pollution Control - Volume 1: Gas Phase Chemistry", Final Report EPA Contract 68-02-2631, April, 1981.

5.0 PILOT-SCALE STUDIES

5.1 Summary

An axisymmetric calorimetric combustor which simulates the firetube of an industrial package boiler was used in a series of experiments to:

- Investigate the influence of the interaction between the fuel spray and the flow field in the region near the flame base on pollutant production in residual fuel oil flames.
- Investigate the influence of fuel properties, particularly total nitrogen content on pollutant production.
- Assess the impact of both fuel properties and spray parameters on the control of nitrogen oxide emissions by staged combustion.

The majority of these experiments were carried out with a simple double concentric burner with fixed interchangeable annular swirl vanes. The flow field could be modified by changing the swirl vanes which gave swirl numbers of 0.2, 0.45 and 0.8. Spray chracteristics were varied by changing fuel nozzles and by varying fuel pressure.

The addition of cooled combustion products to the combustion air supply flue gas recirculation (FGR) was used as a diagnostic technique to assess the fraction of the total emissions attributable to fuel NO_x formation. Due to the quantities of oxidizer involved it was not possible to use synthetic oxidizers in these tests as was done in the small-scale experiments reported in Section 4.

The addition of FGR minimizes thermal NO_x formation by reducing peak flame temperatures through the addition of inert diluents to the reaction zone. However, the impact of FGR should be interpreted with caution since the total mass flow through the burner is increased, resulting in higher burner air velocities which could cause more intense mixing of fuel and air. Thus, fuel NO_x formation might well be affected by the addition of FGR. This is reflected in certain instances by an increase in NO_x emissions with the application of FGR.

Spray/Flow Field Interaction

Spray parameters such as nozzle type and atomizing fluid pressure were found to have their strongest effects in a flow field produced by weak swirl. Maximum emissions of 350 ppm NO_x were measured at low swirl levels with the Indonesian/Malaysian No. 6 oil (0.24 percent N). Minimum levels of 160 ppm were achieved at all three swirl levels tested. The ranking of emission levels for the various nozzles did not remain constant for the different swirl levels. As an example, one atomizer gave the highest NO_x emissions at the low and intermediate swirl levels, but had almost the lowest emissions characteristics at the high swirl level. Smoke emissions were generally highest at high swirl levels.

Fuel Effects

NO_x emissions were found to increase linearly with fuel nitrogen content for each atomizer and flow field combination. With the exception of one nozzle, emissions at high swirl levels were almost independent of spray characteristics. The addition of FGR to the combustion air did not reduce NO_x emission levels below those achievable with high swirl and unvitiated combustion air for any of the fuels studied.

Staged Combustion Studies

Dividing the total combustion air into two streams and operating the first stage fuel-rich before addition of second stage air for burnout reduced NO_x emissions as expected. Minimum emission levels were achieved at the intermediate swirl level, but the minimum level and the optimum primary zone stoichiometry were found to be dependent upon nozzle design. Under staged combustion conditions the addition of cooled flue gases to the rich first stage increased NO_x emissions slightly, but reduced smoke emissions. Minimum emissions obtained under staged conditions were found to increase with increasing fuel nitrogen content.

5.2 Experimental Systems

The experimental system involved in the pilot-scale investigations consisted of:

- an axisymmetric calorimetric combustor;
- burners which allowed variation of axial and tangential inlet air velocity;
- a variety of commercial fuel nozzles.

The combustion chamber of the axisymmetric calorimetric combustor was designed to simulate the firetube of an industrial firetube package boiler and was used originally as a test bed for the development of low NO_x combustion systems, and has the following nominal specifications:

- load 1.08 MW (3.7×10^6 Btu/hr);
- volumetric heat release rate 1.76 MW/M^3 (170,000 Btu/hr/ft^3);
- a combustor L/D of 3.9;
- fuel capabilities for residual, distillate and gaseous fuels;
- provision for flue gas recirculation and downstream injection for staged combustion air;
- provision for in-flame sampling from the rear or the side;
- access for flame observation from the rear or from the side.

A schematic of the combustor is presented in Figure 5-1. The basic furnace is a cylinder with an inside diameter of 0.58m and a length (not including the end elbow section) of 3.2m. The combustor consists of four sections, each divided into two compartments, thus allowing the heat absorbed by the cooling fluid to be assessed as a function of combustor length. The coolant is Dowtherm G which is circulated at a nominal rate of approximately 379 liters/minute. The first section includes ports for access and flame observation. The combustor includes a convective heat exchanger which allows 40 percent of the combustion gases to be cooled to approximately 204°C during full-load operation. The cooled combustion products are recycled by a separate fan, metered and they can be added to the combustion airflow at separate locations. The total combustion airflow can be divided into several streams, thus allowing control over mean stoichiometry along the length of the combustor. Access is provided at the rear of the combustor for a water-cooled boom which acts either as a support for sampling probes or as an injection point for combustion air. Further details of the design and construction of the axisymmetric calorimetric combustor have been described elsewhere(1).

An initial series tests (Phase I experiments) were carried out with the burner system shown in Figures 5-2 and 5-3. In the multi-channel swirl

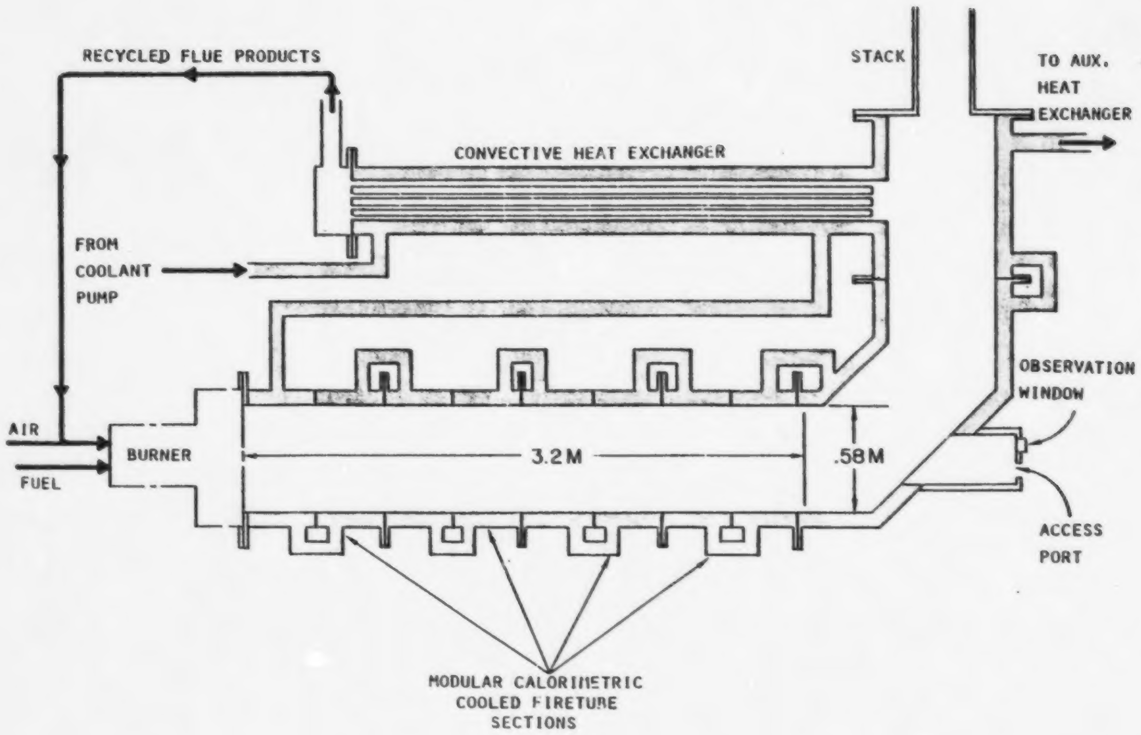
RECYCLED FLUE PRODUCTS
STACK
TO AUX. HEAT EXCHANGER
CONVECTIVE HEAT EXCHANGER
FROM COOLANT PUMP
OBSERVATION WINDOW
AIR
BURNER
FUEL
3.2M
.58M
ACCESS PORT
MODULAR CALORIMETRIC COOLED FIRETUBE SECTIONS

Figure 5-1. Experimental Firetube Combustor.

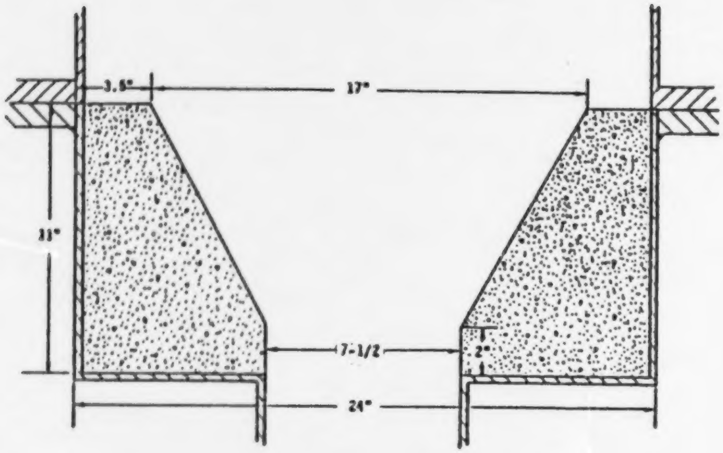
3.5"
17"
11"
7-1/2
2"
24"

Divergent Exit

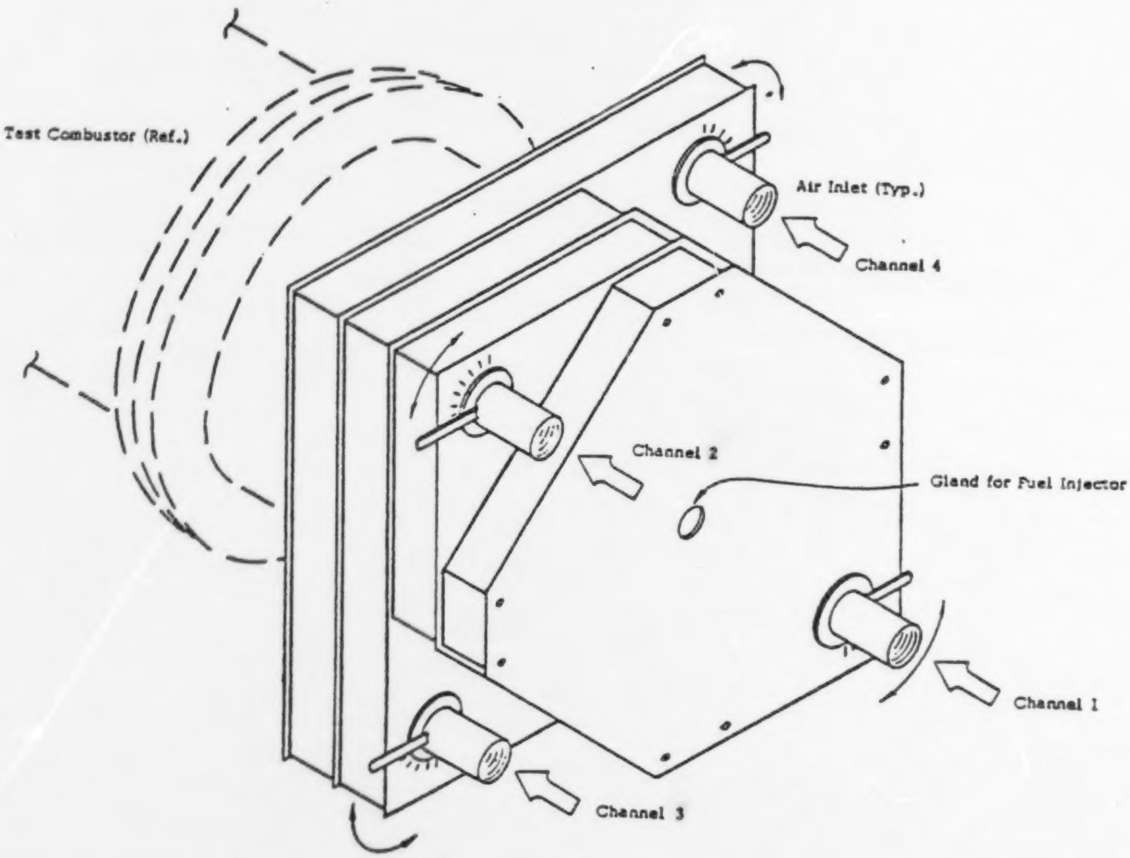
Test Combustor (Ref.)
Air Inlet (Typ.)
Channel 4
Channel 2
Gland for Fuel Injector
Channel 1
Channel 3

Figure 5-2. Multichannel Continuously Variable Swirl Generator - Rear View and Exit Geometry

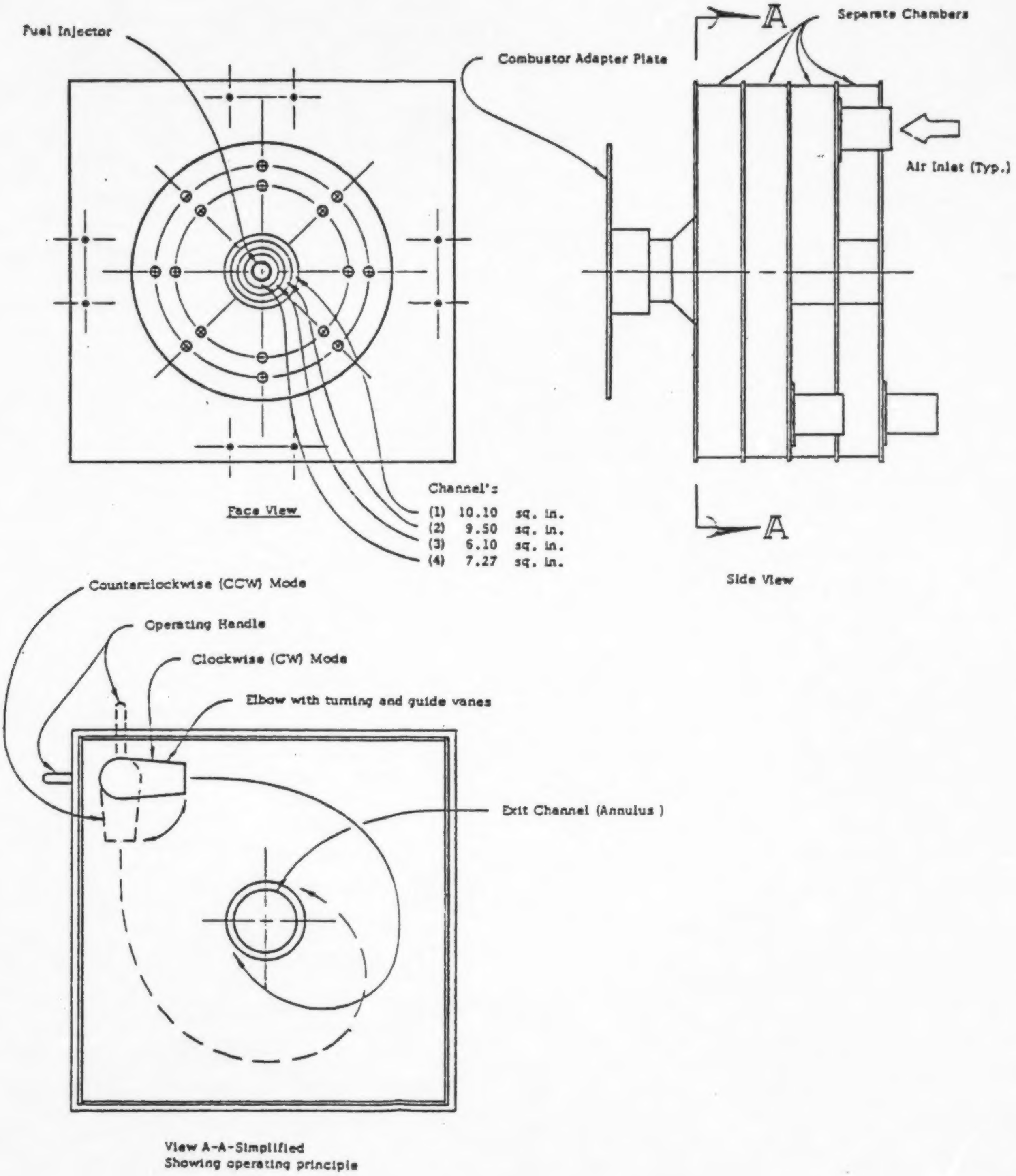
Fuel Injector
Combustor Adapter Plate
A
Separate Chambers
Air Inlet (Typ.)
Face View
Channel's
(1) 10.10 sq. in.
(2) 9.50 sq. in.
(3) 6.10 sq. in.
(4) 7.27 sq. in.
A
Side View
Counterclockwise (CCW) Mode
Operating Handle
Clockwise (CW) Mode
Elbow with turning and guide vanes
Exit Channel (Annulus)
View A-A-Simplified
Showing operating principle

Figure 5-3. Multichannel Continuously Variable Swirl Generator - Details

generator (MCSG) air is supplied to four annular ducts through separate chambers. Combustion air from the delivery manifold enters each chamber through a 90-degree elbow section. The velocity vector of the combustion air may be directed toward the axis of the burner or off-center from the axis by rotating the elbow section as shown in Figure 5-3. When the velocity vector is directed at the axis, the tangential momentum is zero, and the resulting airflow through the annular section is completely axial. By rotating the elbow, tangential momentum is imparted to the airstream, resulting in an airflow with both axial and tangential velocity components. The ratio of axial-to-tangential momenta is dictated by the angle of nozzle rotation and the proportion of total airflow supplied to each annulus. Consequently, it is possible to describe the axial and tangential velocity distribution at the burner throat by specifying the fraction of total airflow in each channel and the corresponding nozzle rotation. The following notation has been used to describe airflow distribution and swirl:

Swirl: 20/10/5/30 refers to the degrees of nozzle rotation in Channels 1, 2, 3 and 4 respectively, with Channel 1 supplying the innermost annulus of the burner.

Airflow Distribution: 50/0/0/50 refers to the percentage of total air supplied through the burner to Channels 1, 2, 3 and 4, respectively.

The major portion of the experimental investigations (Phase II experiments) described in this report were carried out with a more simple burner system, shown in Figure 5-4. Fuel was supplied from an axial oil gun which could be located precisely, and yet allow for rapid exchange of a wide range of oil nozzles. Combustion air was supplied to the single annular stream surrounding the nozzle, and an initial plenum chamber ensured uniform axial velocity of 30 meters per second. Tangential momentum was imparted to the airstream by interchangeable fixed annular swirl vanes with vane angles of 0, 15, 30 and 45, giving swirl numbers of 0, 0.20, 0.45 and 0.80, respectively. A 45-degree half-angle burner exit was normally used. For some

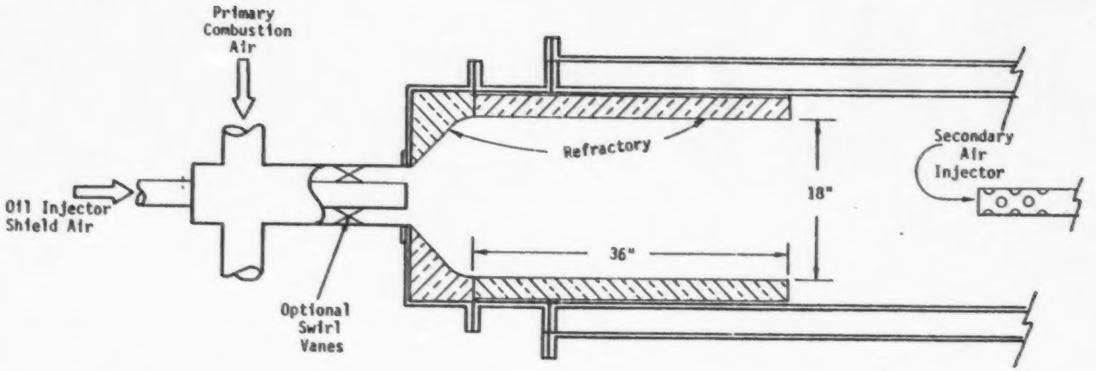
Primary Combustion Air
Oil Injector Shield Air
Optional Swirl Vanes
Refractory
18"
36"
Secondary Air Injector

Figure 5-4. Double Concentric Swirl Burner with Refractory Sleeve.

experiments, a refractory sleeve was inserted at the exit of the divergent to reduce heat loss and increase temperatures in the initial heat release zone. This sleeve was 89 cm long and 46 cm in diameter. Staged combustion air was added downstream of the burner through a water-cooled boom located on the axis. Air was injected radially outward through eight holes in the tip of the boom with velocity of 35 m/sec (113 ft/sec) at a primary zone stoichiometric ratio equal to 0.6. The atomizers used in these studies have been described in Section 2.

The flue gas sampling and analysis system was identical to that utilized for the small-scale experiments.

5.3 Phase I Investigations — Problem Definition

The Phase I test program was planned to satisfy two objectives:

- To define the influence of gross fuel spray properties (initial spray angle, spray pattern, and mean drop size) on flame structure and pollutant emissions.
- To provide a data base to fully characterize the emissions from the Monarch assist fluid atomizers in order to provide a link between the data generated in EPA Contract No. 68-02-1500(2) and the current test program. Previous investigations concerned with the development of low emission burners had shown that the formation of nitrogen oxides was strongly dependent upon atomizer characteristics under both excess air and staged conditions.

5.3.1 Gross Spray Characteristics

Gross spray properties were varied by selecting the appropriate mechanical atomizers to provide the desired spray conditions:

- initial spray angle;
- spray pattern;
- droplet size.

The initial spray angle was varied between 45, 60 and 80 degrees, although limited testing was also carried out at 30, 70 and 90-degree sprays under restricted conditions. The actual spray angle will vary from the initial angle depending upon interaction of the droplet trajectory with the flow field. The spatial distribution of fuel drops within the spray cone is referred to as the spray pattern. For these tests the drops were either confined within a narrow spray sheath (hollow cone) or uniformly distributed within the spray cone (solid cone). The mean drop size is dependent on both physical properties (i.e., viscosity) and fuel delivery pressure. For most of these tests the drop size was varied at a fixed heat input by using different capacity nozzles, and the fuel delivery pressure varied inversely with capacity.

The combustion airflow distribution used for the Phase I tests were the two distributions of axial/tangential momentum that had been identified in previous tests(2) as those which produced very different flame structures which resulted in high and low NO_x emissions. These airflow patterns could be established with two different MCSG air distributions and swirl configurations. A 50/0/0/50 distribution could be used with a 20/-/-/40 swirl configuration to produce an airflow pattern which under combusting conditions resulted in a relatively short flame in which the mixing process was dominated by a strong axial internal recirculation zone. A combustion airflow pattern with completely different mixing characteristics can be established by using a 50/0/0/50 air distribution with a 10/-/-/40 swirl configuration. Under combustion conditions this airflow pattern produced a long narrow flame with delayed fuel/air mixing. These input airflow conditions were selected because they represent two extremes in fuel/air mixing, and are referred to as the high NO_x (HN) and low NO_x (LN) airflow patterns in the following discussion.

It was expected that two fuel properties would have a major impact upon NO_x emissions from liquid fuels. Thermal NO_x (that NO produced from molecular nitrogen) could be expected to be dependent upon fuel volatility. Since combustion is a vapor phase phenomenon the fuel availability will be controlled by the rate of vaporization. The amount and nature of the fuel-bound nitrogen will affect fuel NO formation. The fuels used in the Phase I tests were:

- Kerosene - a relatively volatile, nitrogen-free fuel of low viscosity.
- Distillate Fuel Oil - lower in volatility and higher in viscosity than kerosene; the small nitrogen content (usually less than 0.05 percent) allows the contribution of fuel nitrogen to total NO_x to be neglected.
- Distillate Fuel Doped with Pyridine - the nitrogen added as pyridine is bound to a simple molecule of relatively high volatility, and thus does not accurately simulate the combustion of heavy fuel oil. However, the use of doped distillate fuel is helpful in determining the approximate contribution of fuel-bound nitrogen to total NO_x when comparing mixing conditions.
- Residual Fuel Oil (No. 6) - residual fuel oil of 0.37 percent N content preheated to 93°C. (Referred to as "Ultrasystems" No. 6 fuel oil in Section 3.)

NO_x emissions are reported as measured (dry sample, at 3 percent O_2) and smoke emissions are reported in terms of the Bacharach Smoke Number (BSN). The BSN rating appears next to the appropriate data point for values of three or greater and is not given for values of two or less. Test conditions at which prohibitive smoke emission were measured are indicated by the designation SL (smoke-limited) in addition to the BSN rating of the last test condition not restricted by smoke.

5.3.1.1 The Effect of Spray Angle

The effect of spray angle on NO_x/smoke emissions is shown in Figures 5-5 through 5-8 for kerosene, distillate fuel, distillate fuel with 0.2 percent N as pyridine, and residual fuel oil. Results are compared for both the HN and LN combustion airflow pattern for all fuels. NO_x emissions with kerosene, which differs by approximately 10 ppm between the HN and LN airflow patterns, are

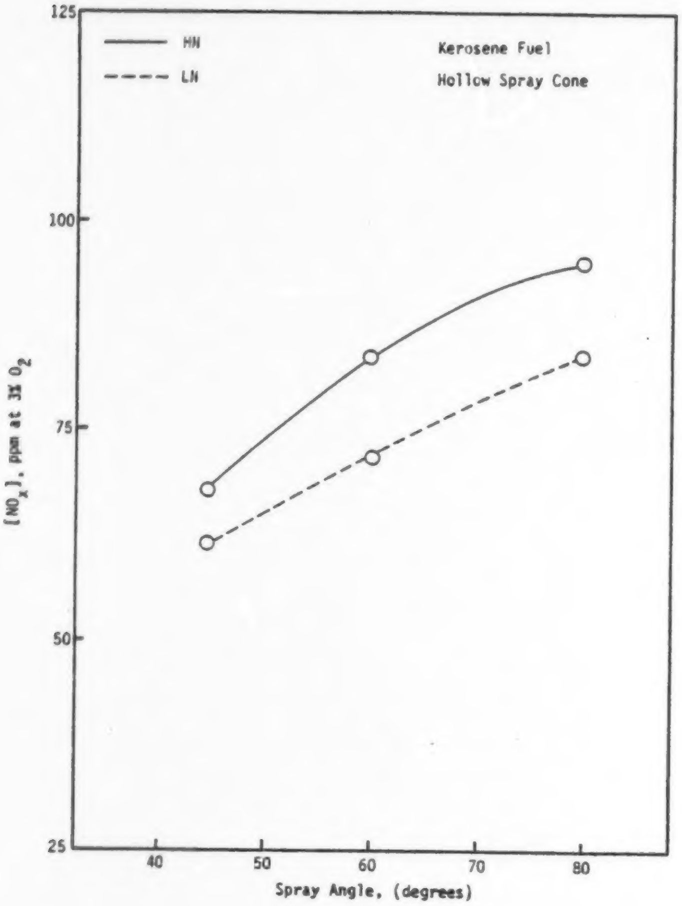

Figure 5-5. The Effect of Spray Angle on NO$_x$/Smoke Emissions with Kerosene, HN and LN Air Patterns, Hollow Spray Cone.

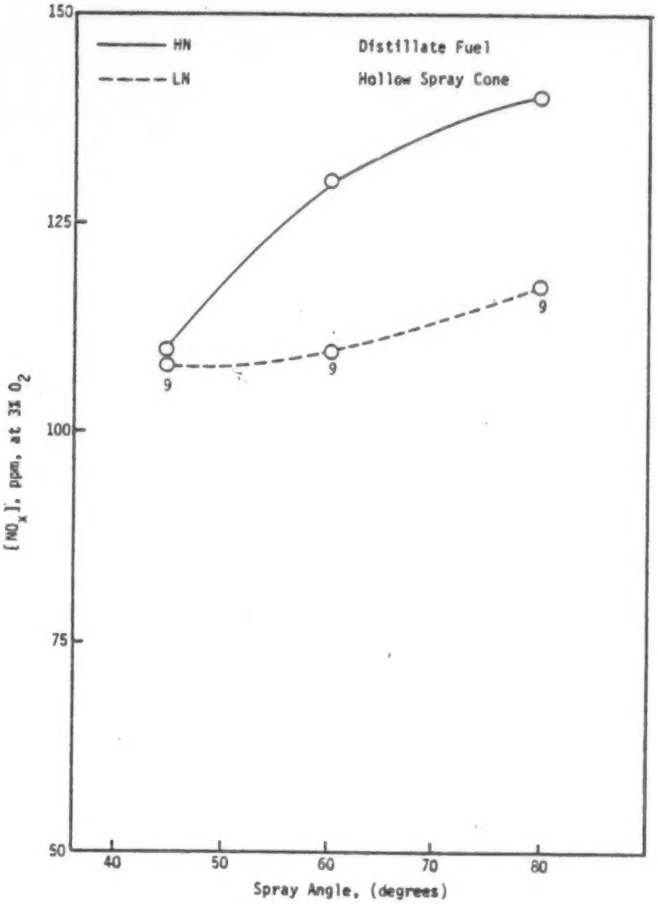

Figure 5-6. The Effect of Spray Angle on NO_x/Smoke Emissions with Distillate Fuel; HN and LN Air Patterns, Hollow Spray Cone.

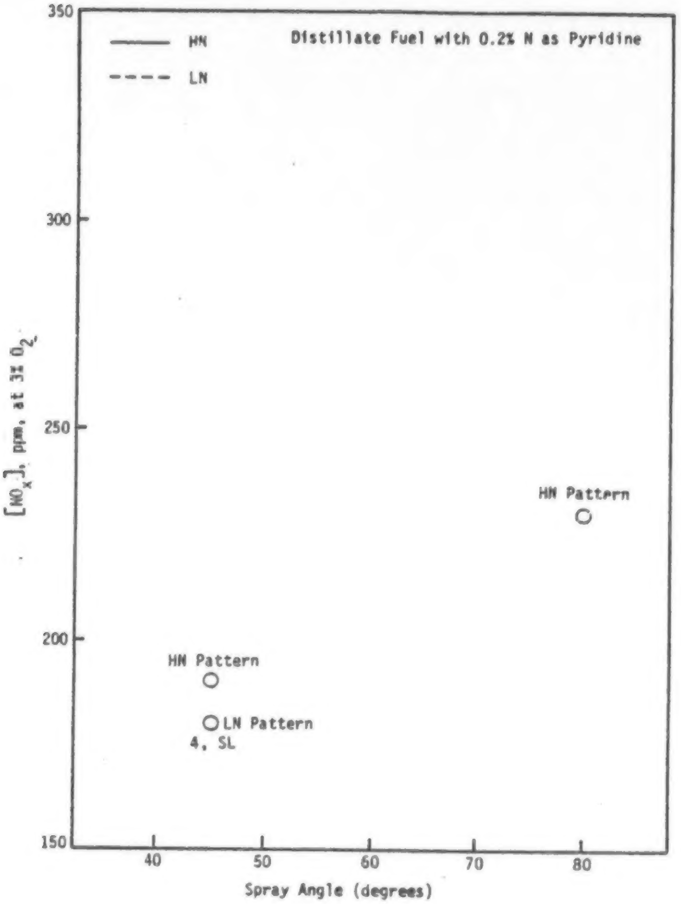

Figure 5-7. The Effect of Spray Angle on NO$_x$/Smoke Emissions with Doped Distillate Fuel; HN and LN Air Patterns, Hollow Spray Cone.

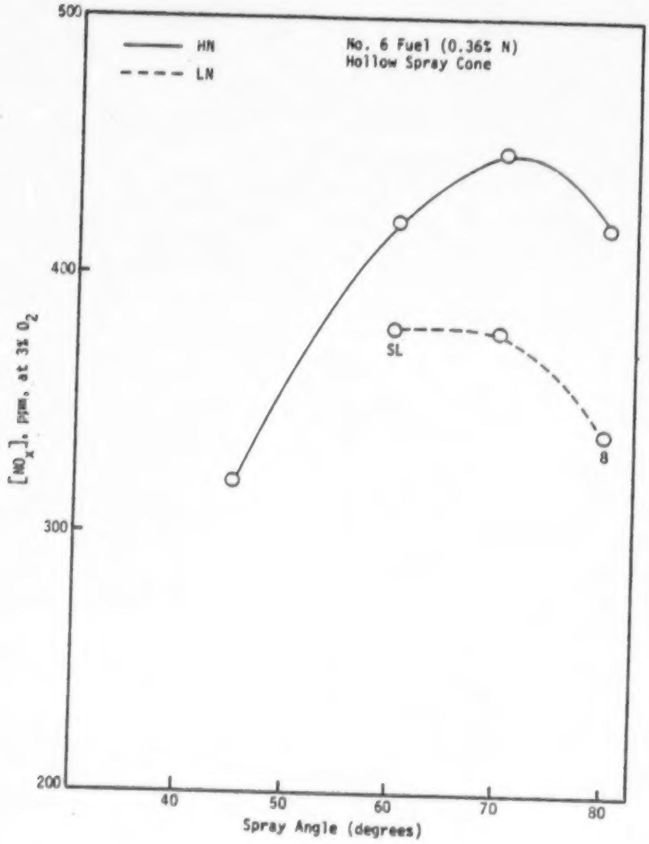

Figure 5-8. The Effect of Spray Angle on NO_x/Smoke Emissions with No. 6 Fuel; HN and LN Patterns, Hollow Cone Spray.

highest at the widest (80-degree) spray angle. The difference in emission levels between the HN and LN pattern is largest at the widest angle and smallest at the narrowest angle. Smoke emissions were negligible for all operating conditions, therefore no effect of spray angle could be detected. NO_x emission from undoped distillate fuel in Figure 5-6 are similar in some ways to those from kerosene, although they are higher in magnitude. The difference in emissions between the HN and LN pattern varies from several ppm at the narrowest spray angle to over 20 ppm at the widest spray angle. The effect of spray angle on NO_x emission is apparently much stronger for the HN airflow pattern. Negligible smoke emissions were measured with the HN case, but very high smoke emission were measured for all conditions of the LN case. The flame pattern with both kerosene and distillate fuel appeared to be dominated by the fuel spray angle and relatively unaffected by the airflow distribution. A short flame was obtained at both air distributions when the wide angle (80-degree) spray was used. When using either the 45- or 60-degree spray, a small difference in flame length could be detected between the HN and LN airflow patterns. The only visible difference between flame patterns from each fuel was the higher luminosity of the distillate oil flame, especially with the LN airflow pattern.

Results from a limited series of tests involving distillate oil doped with pyridine to give 0.2 percent nitrogen are presented in Figure 5-7. Comparison with Figure 5-6 shows that emissions with the doped fuel are almost twice those obtained with the undoped distillate for extreme spray angles. These results show the impact of fuel nitrogen on NO_x emissions. It should be noted that emission measurements at the very wide spray angle with the LN airflow pattern were not possible because of excessive smoke emissions.

NO_x emissions from residual fuel oil are shown in Figure 5-8 as a function of spray angle for the two airflow patterns. The emission levels are far higher than for any other fuel and the effect of spray angle on NO_x emissions is considerably different. Maximum NO_x emissions with the HN airflow pattern were not measured at the widest spray angle as with other fuels, but at an intermediate angle of approximately 70 degrees. NO_x

emissions with the LN airflow pattern, which were highest at 60 and 70 degrees spray angle, were not measured at the narrowest angle because of prohibitive smoke emissions. Negligible smoke emissions were measured from all cases with the HN airflow pattern.

The observations concerning the effect of spray angle on NO_x emissions can be summarized by:

- Nitrogen-free fuels produced maximum NO_x emissions at the widest spray angle.
- The largest difference in NO_x emission between the HN and LN airflow patterns was found at the widest spray angle for the nitrogen-free fuels.
- The addition of nitrogen in the form of pyridine to distillate fuel substantially increased NO_x emissions, but it did not significantly affect the influence of spray angle on NO_x emissions.
- Results with residual oil suggest a strong interaction between spray angle and combustion airflow pattern.

5.3.1.2 The Effect of Spray Pattern

The influence of spray pattern on both NO_x and smoke emissions is shown in Figures 5-9 through 5-12 for kerosene, distillate fuel, doped distillate fuel and residual fuel oil. The influence of spray pattern appears to be dependent upon both fuel type and airflow pattern. The results can be summarized by:

- NO_x emissions obtained with nitrogen-free fuels and the HN airflow pattern were lower with the solid cone spray at narrow spray angles and higher at intermediate spray angles.
- NO_x emissions from nitrogen-free fuels with the LN airflow pattern are dependent upon fuel type; the solid cone spray gave the lowest emissions with the more volatile fuel, but higher emissions than the hollow cone spray with less volatile fuel.

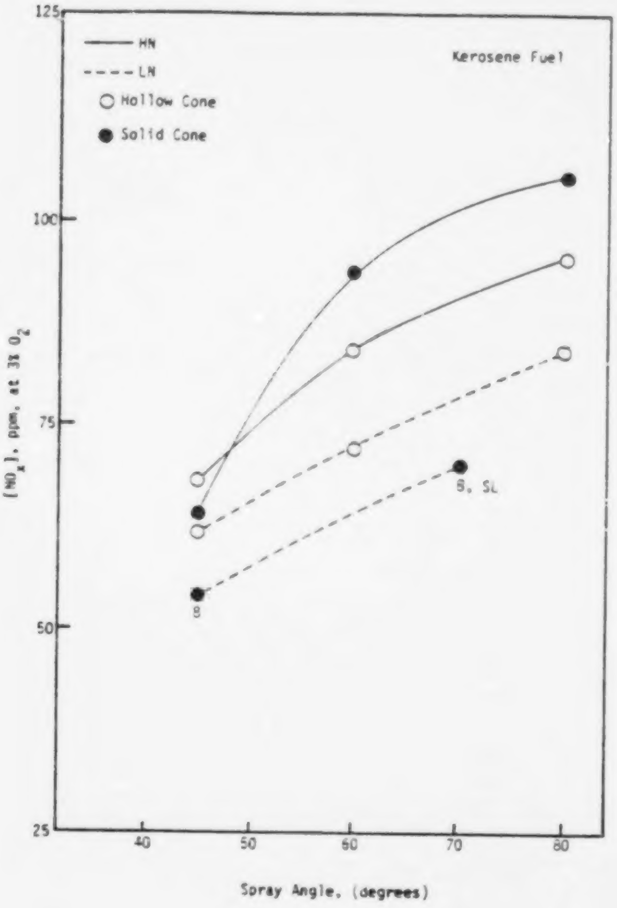

Figure 5-9. The Effect of Spray Pattern on NO$_x$/Smoke Emissions for Kerosene Fuel; HN and LN Air Pattern.

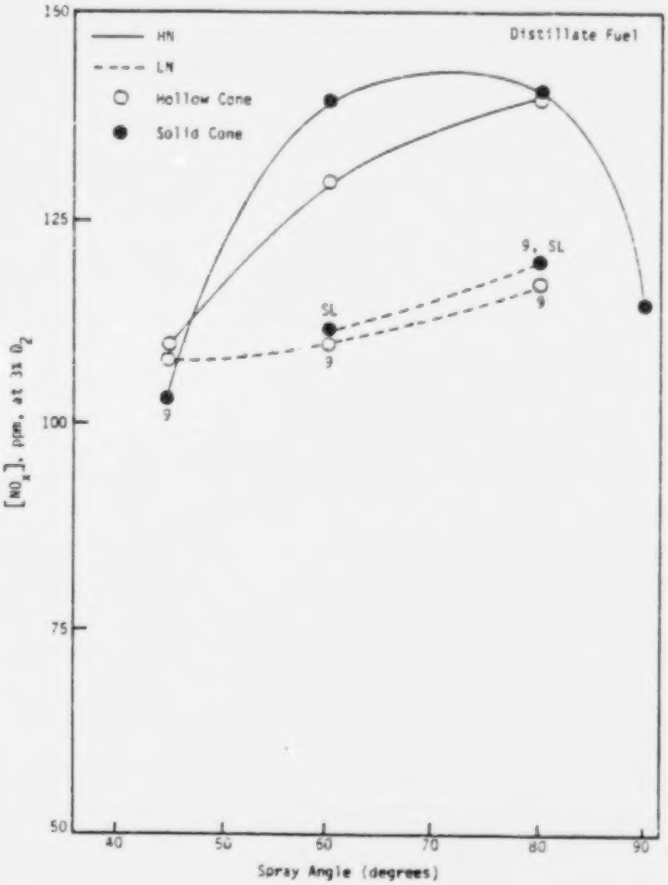

Figure 5-10. The Effect of Spray Pattern on NO_x/Smoke Emissions with Distillate Fuel; HN and LN Air Patterns, Hollow and Solid Spray Cones.

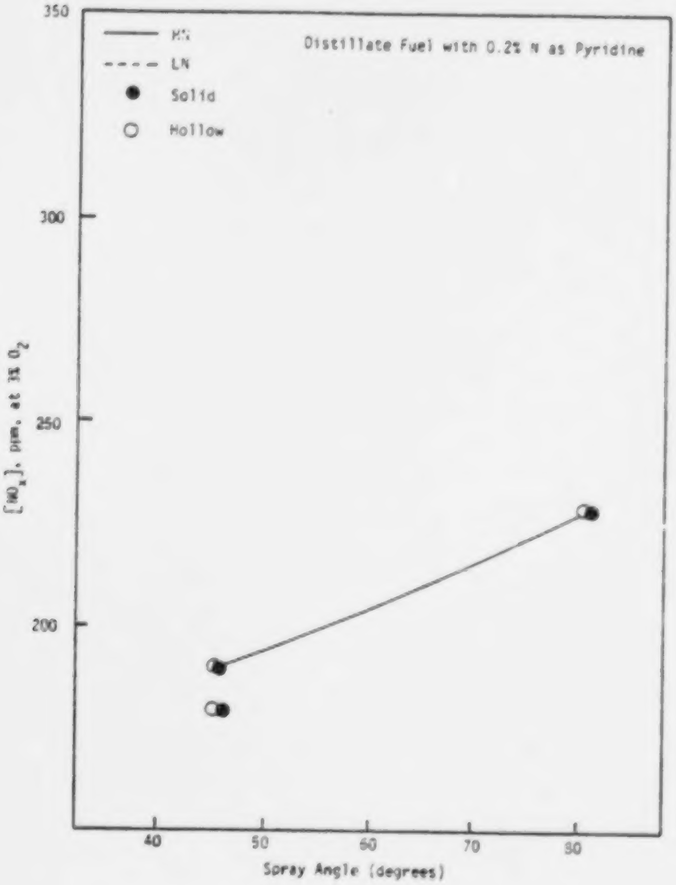

Figure 5-11. The Effect of Spray Pattern on NO_x/Smoke Emissions with Doped Distillate Fuel; HN and LN Air Patterns, Hollow and Solid Spray Cones.

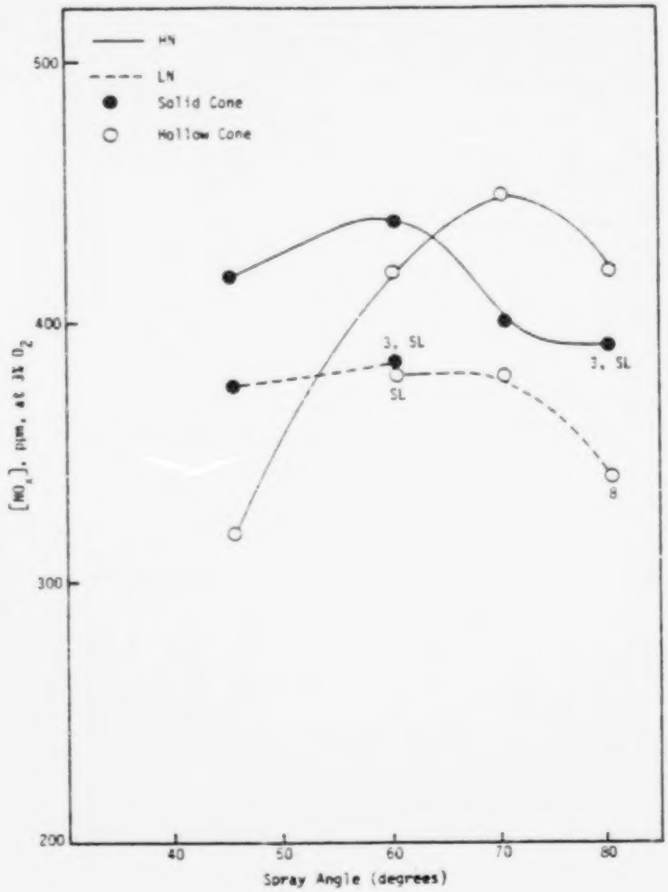

Figure 5-12. The Effect of Spray Pattern on NO_x/Smoke Emissions with No. 6 Fuel; HN and LN Air Patterns, Hollow and Solid Spray Cones.

- Surprisingly, no affect of spray pattern was observed when the fuel nitrogen was added as pyridine.
- NO_x emissions with residual fuel oil and the HN airflow pattern were found to be higher with the solid cone at narrow spray angles and lower at wide spray angles.
- Smoke emissions with residual fuel oil and the LN airflow pattern were prohibitively high from the solid cone at wide spray angles. This is in direct constrast to smoke emissions from the hollow cone which was prohibitively high at narrow spray angles.

5.3.1.3 The Effect of Nozzle Capacity

The effect of varying fuel droplet size by using different capacity nozzles for a fixed firing rate and the same four fuels is shown in Figures 5-13 through 5-20. Data are presented as a function of nozzle design capacity for the solid and hollow cones at both narrow (45-degree) and wide (80-degree) spray angles. The fuel delivery pressure measured for each nozzle appears directly above the nozzle design capacity. Figures 5-13 and 5-14 present the results for kerosene at the HN and LN airflow patterns. NO_x emission with the HN airflow pattern are independent of fuel pressure with both the narrow angle solid and hollow cone spray patterns. Measurements with the wide angle spray show that increasing the fuel pressure decreased NO_x for the solid cone pattern, but had little effect on the hollow cone spray results. Emissions with the LN airflow pattern are lower but show trends similar to those produced with the HN pattern.

The effect of fuel delivery pressure on NO and smoke emissions with distillate oil is shown in Figures 5-15 and 5-16. NO_x emissions with the HN airflow pattern and the narrow angle sprays decreased slightly with increasing fuel delivery pressure except for the hollow cone at the highest pressure. NO_x emissions from both wide angle sprays significantly decreased with increasing fuel pressure. Measurements with the LN airflow pattern were restricted to the wide angle hollow cone. All other test cases were aborted because of excessive smoke formation.

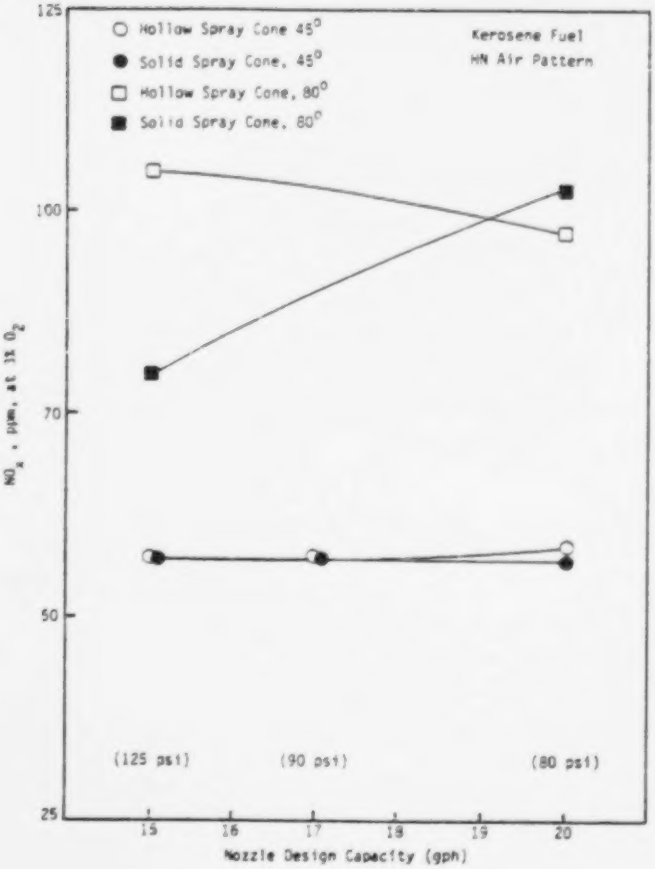

Figure 5-13. The Effect of Nozzle Design Capacity on NO_x/Smoke Emissions with Kerosene; HN Air Pattern.

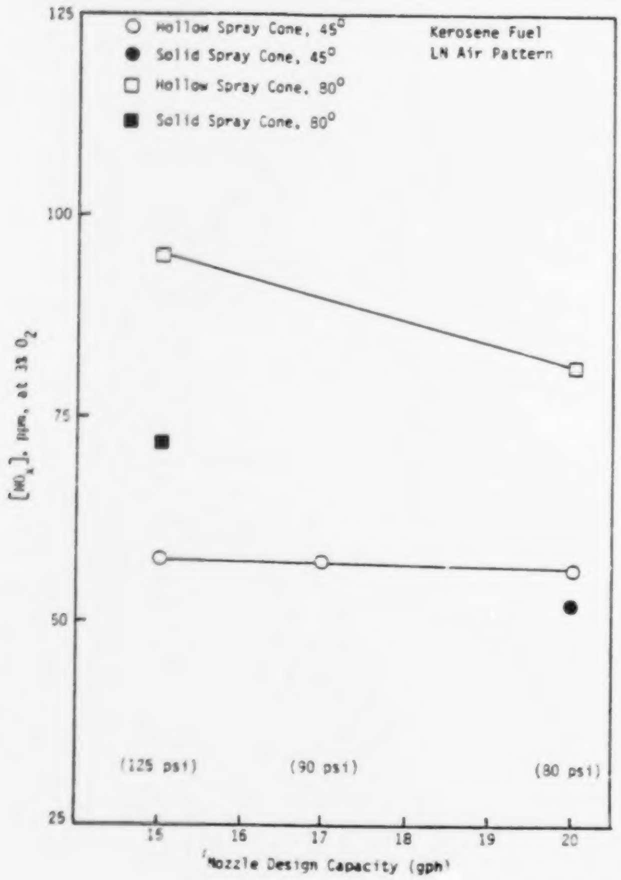

Figure 5-14. The Effect of Nozzle Design Capacity on NO_x/Smoke Emissions with Kerosene; LN Air Pattern.

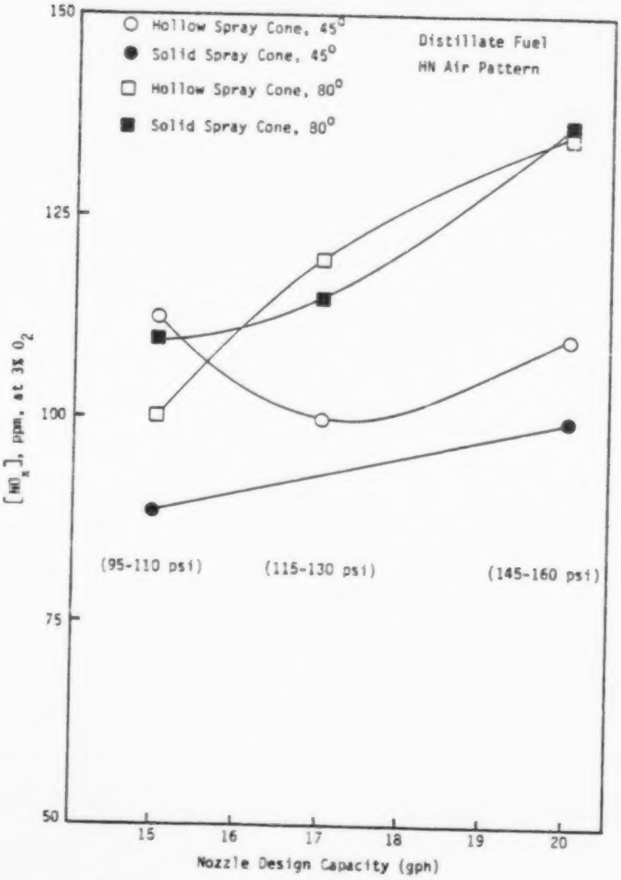

Figure 5-15. The Effect of Nozzle Design Capacity on NO_x/Smoke Emissions, Distillate Fuel, HN Air Pattern.

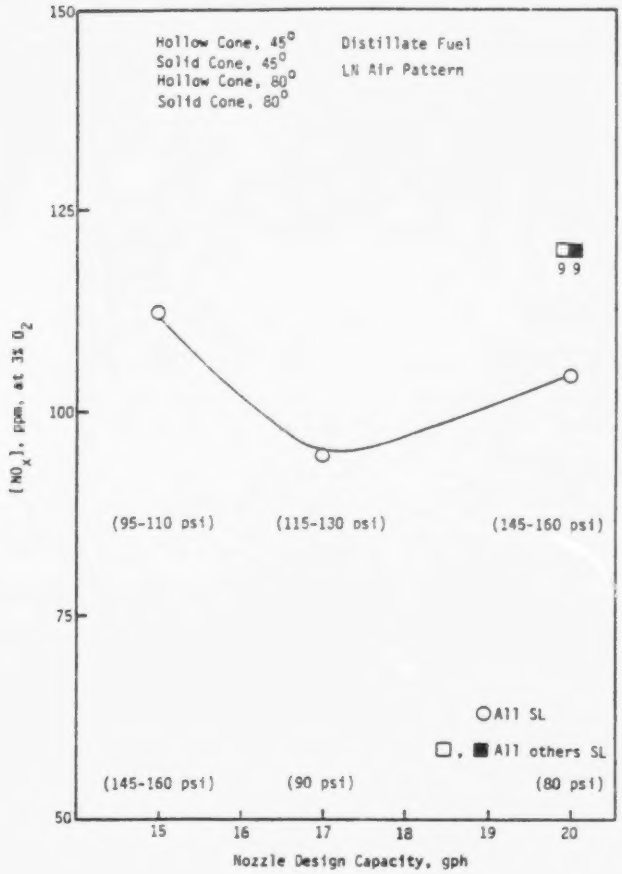

Figure 5-16. The Effect of Nozzle Design Capacity on NO_x/Smoke Emission with Distillate Fuel; LN Air Pattern.

Measurements with distillate fuel doped with pyridine shows that under some conditions NO_x emissions can be strongly affected by fuel delivery pressure. Figure 5-17 presents data for the HN airflow which shows that emissions from the wide angle hollow cone increase by over 100 ppm with elevated fuel pressure. Emissions from the wide angle solid cone are almost independent of fuel delivery pressure. The narrow angle hollow and solid cone sprays are only weakly dependent on fuel pressure and show no definite trend. Emissions with the LN airflow pattern (Figure 5-18) were found to be similar to the HN results, but somewhat lower in magnitude.

Figures 5-19 and 5-20 present the results obtained with residual fuel for the HN and LN airflow patterns. It can be seen that although there is a significant effect of fuel pressure on NO_x, no consistent trends can be identified for any of the test cases. The narrow angle hollow cone shows the largest effect of fuel pressure with the HN airflow while the narrow angle solid cone shows the largest effect with the HN airflow.

Fuel droplet size is also very dependent on liquid viscosity and for residual fuels oils this can be influenced by fuel temperature. A short test series was carried out to determine the effect of fuel temperature on NO_x and smoke emissions over a range of fuel pressure. The results shown in Figure 5-21 indicate that the effect of fuel temperature is dependent on the fuel delivery pressure. At the design fuel pressure, higher NO_x and lower smoke emissions were measured with high fuel temperature, but at elevated fuel pressure the opposite effect was measured.

The significant observations concerning the effect of nozzle capacity are:

- Thermal NO_x emissions from kerosene were found to be independent of fuel delivery pressure for narrow angle sprays, but fuel pressure had a strong effect for wide angle sprays.
- Thermal NO_x emissions from distillate fuel with the HN airflow pattern decreased with increasing fuel pressure; almost all test cases with the LN airflow were prohibited by excessive smoke emission.

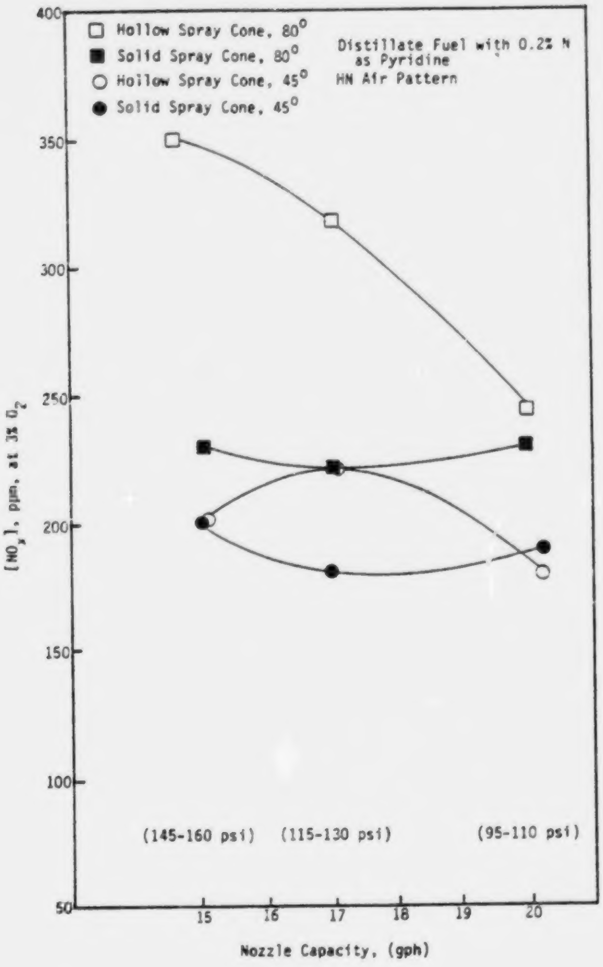

Figure 5-17. The Effect of Nozzle Design Capacity on NO$_x$/Smoke Emission; Doped Distillate Fuel, HN Air Pattern.

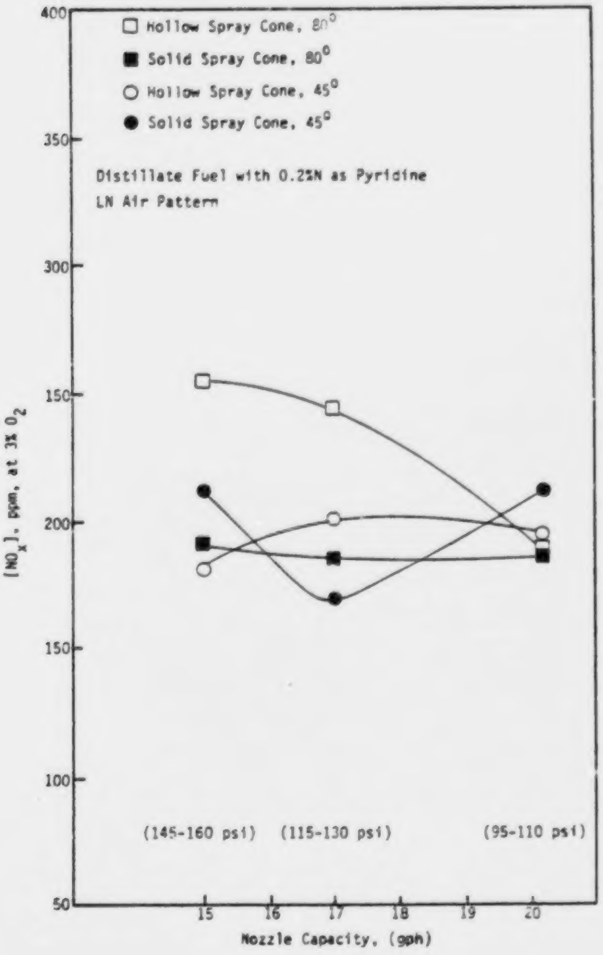

Figure 5-18. The Effect of Nozzle Design Capacity on NO_x/Smoke Emission with Doped Distillate Fuel, LN Air Pattern.

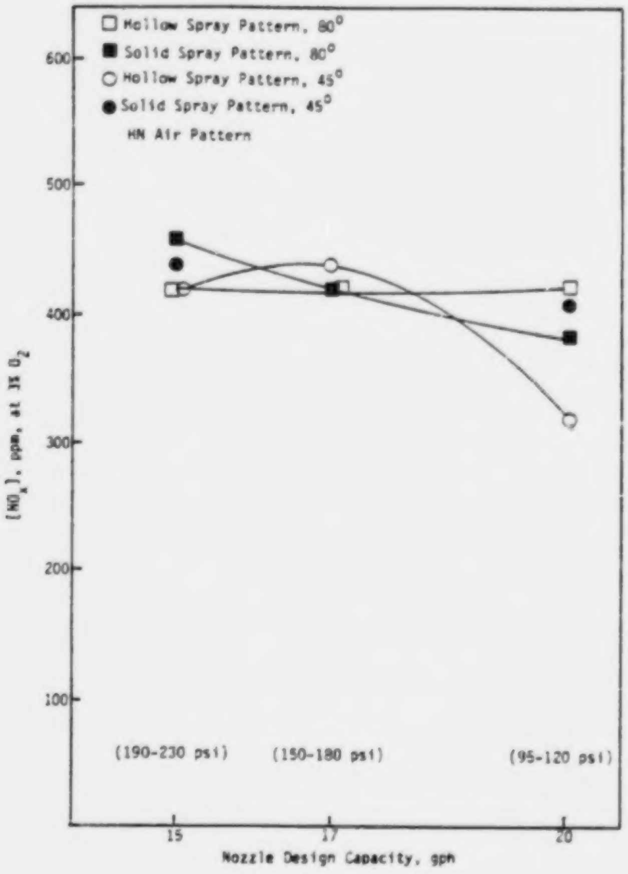

Figure 5-19. The Effect of Nozzle Design Capacity on NO_X/Smoke Emission with No. 6 Fuel; HN Air Pattern.

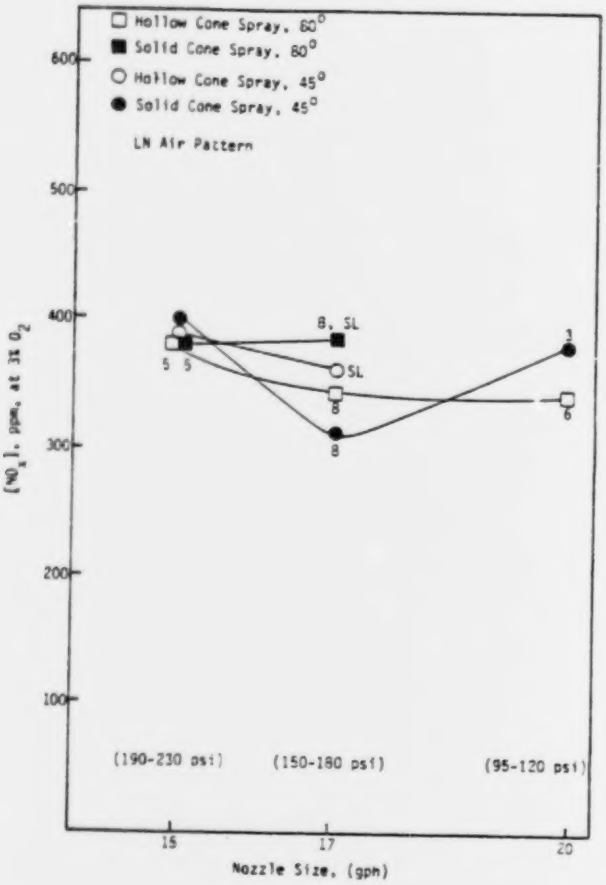

Figure 5-20. The Effect of Nozzle Size on NO$_x$/Smoke Emission with No. 6 Fuel; LN Air Pattern.

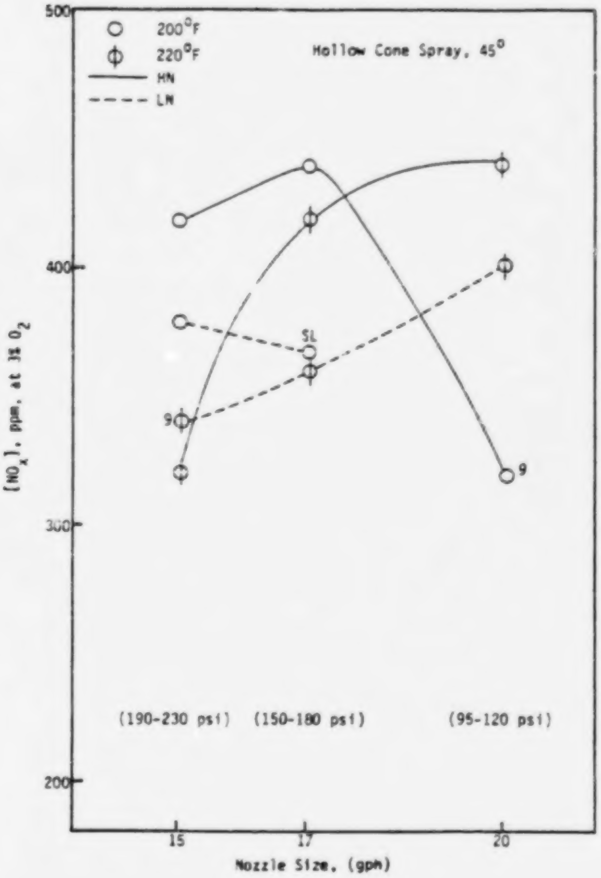

Figure 5-21. The Effect of Nozzle Size on NO_x/Smoke Emissions with No. 6 Fuel; High Fuel Temperature.

- Fuel pressure had a significant influence on NO_x emissions from distillate fuel, especially for the wide angle hollow cone spray.
- Fuel pressure had a significant influence on NO_x/smoke emissions with residual fuel oil and the effect appears to be dependent on the spray angle and type, as well as the airflow pattern.
- Increasing fuel temperature increased NO_x emissions and lowered smoke emissions at the design fuel pressure, but lowered NO_x and increased smoke at elevated fuel pressure.

5.3.2 Monarch Atomizer Characterization

Earlier EPA-supported studies on the development of combustion modification techniques to control NO_x emission from liquid fuel-fired package boilers were carried out exclusively with Monarch twin fluid atomizers. A series of tests were carried out using this nozzle (at three design capacities) in an attempt to provide information to explain earlier anomalous results and also to provide information to help plan the Phase II test program.

The results presented in Figure 5-22 for doped distillate fuel show that the effect of atomizing pressure and nozzle capacity is very dependent on the airflow pattern. NO_x emissions with the HN airflow pattern are relatively independent of both atomizing pressure and nozzle design capacity. Smoke emissions at these conditions were all negligible and the flame pattern was the characteristic HN type for all atomizing pressures. Tests with the LN airflow pattern show that both NO_x emissions and flame pattern are dependent on atomizing pressure and nozzle design capacity. At low atomizing pressures NO_x emissions were relatively high for the LN airflow pattern, smoke emissions were measurable in some cases, and the flame patterns visually resembled the HN type (short flame with strong internal recirculation zone) rather than the LN type. As atomizing air pressure was increased, the flame pattern abruptly transformed to the LN type (long, narrow flame, slow mixing in appearance) at the point where minimum NO_x was measured for each nozzle capacity. Further increases in atomizing

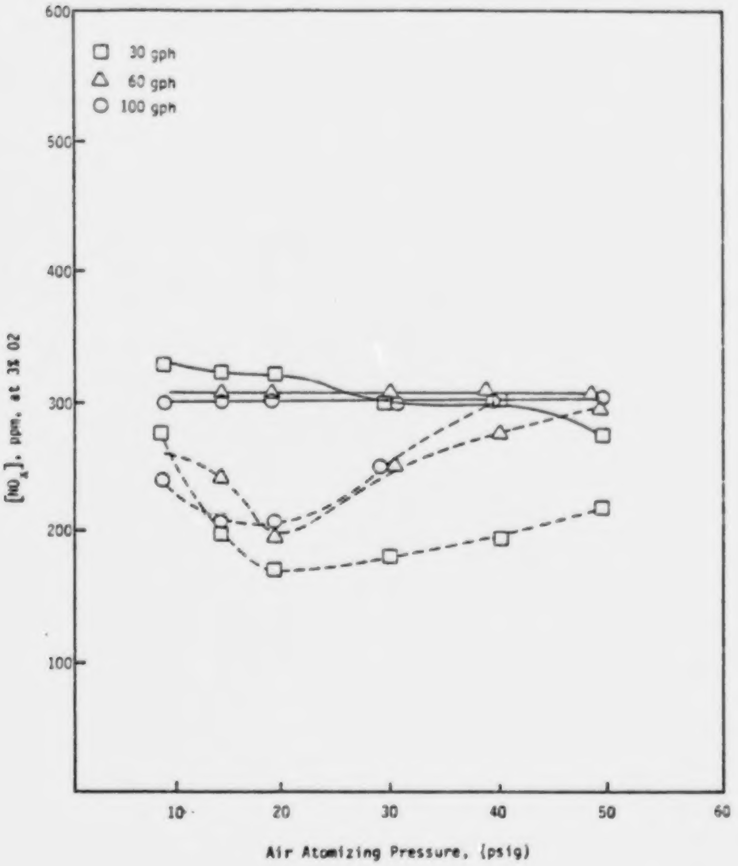

Figure 5-22. NO_x Emissions from Doped Distillate Fuel; with the Monarch Atomizers; Air Atomization, HN and LN Airflow Patterns.

pressure increased NO_x emissions, widened and shortened the flame without changing the basic flame pattern. Observations made during the cold flow spray characterization studies described in Section 2 and in Appendix 1 suggest the existence of a small recirculation zone very close to the atomizer tip induced by the pintle and swirl plate of the atomizer. The strength of this recirculation zone was observed to increase with increased atomizing pressure which causes a decrease in the effective spray angle. The sudden change in flame pattern from HN to LN as the atomizing pressure was increased suggests that there is a critical value of spray angle and momentum for the atomizer which governs the overall flame pattern for a fixed combustion airflow pattern.

The emission results obtained with steam as the atomizing medium and the pyridine-doped distillate oil differ considerably from those obtained with air atomization (see Figure 5-23). NO_x emissions were generally lower with steam than with air and almost independent of steam atomizing pressure. For the small 113 liter/hr (30 gph) nozzle, emissions were also independent of airflow pattern. For all test conditions neither the well-defined LN or HN type flame pattern was stabilized, but some unstable combination of the two was observed. Figures 5-24 and 5-25 compare the emission characteristics of these nozzles with air and steam atomization for residual fuel. With air atomization, two distinct flame patterns were observed. However, with steam as the atomizing medium, the low NO_x flame pattern could only be stabilized at high pressure for the two smaller nozzles and never for the 379 liter/hr (100 gph) nozzle.

The significant observations with the Monarch nozzle can be summarized by:

- NO_x emissions from distillate fuel and pyridine are independent of air atomizing pressure and nozzle design capacity with the HN airflow pattern, but strongly dependent for the LN airflow pattern.
- NO_x emissions from residual fuel oil with the HN airflow pattern increased with steam or air atomizing pressure except for the 227 liter/hr (60 gph) nozzle.

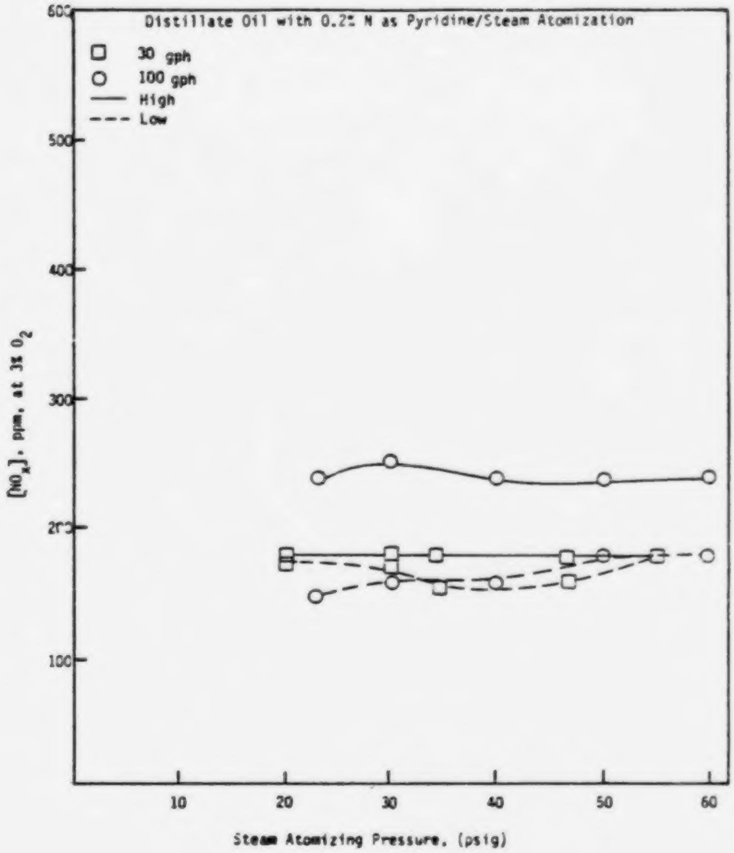

Figure 5-23. NO$_x$ and Emissions with Doped Distillate Fuel from the Monarch Atomizers; Steam Atomization; HN and LN Airflow Patterns.

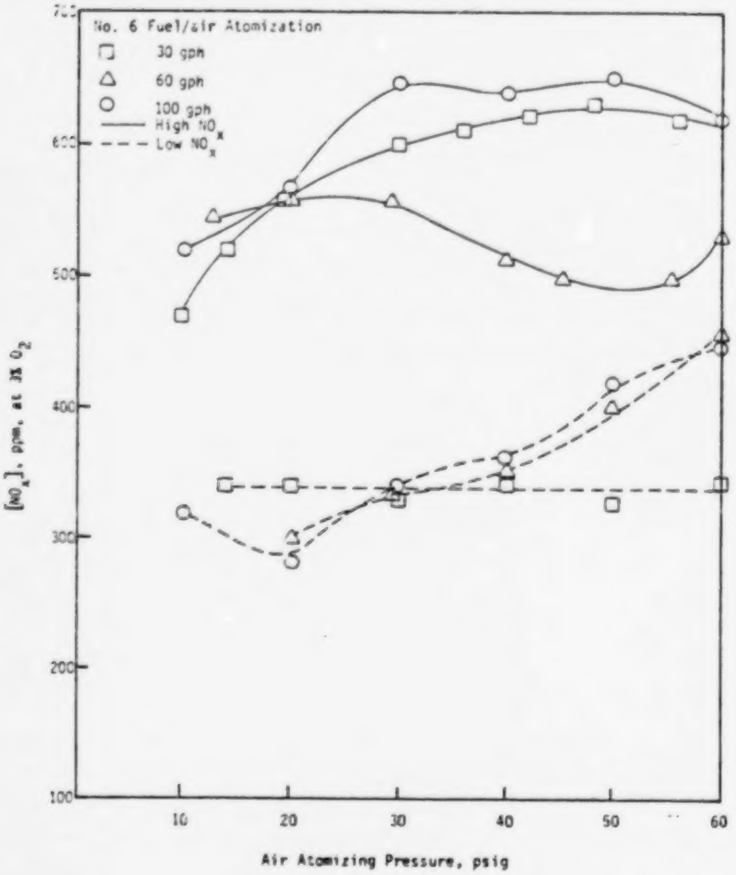

Figure 5-24. NO_x Emissions from Residual Fuel Oil with the Monarch Atomizers; Air Atomization; HN and LN Airflow Patterns.

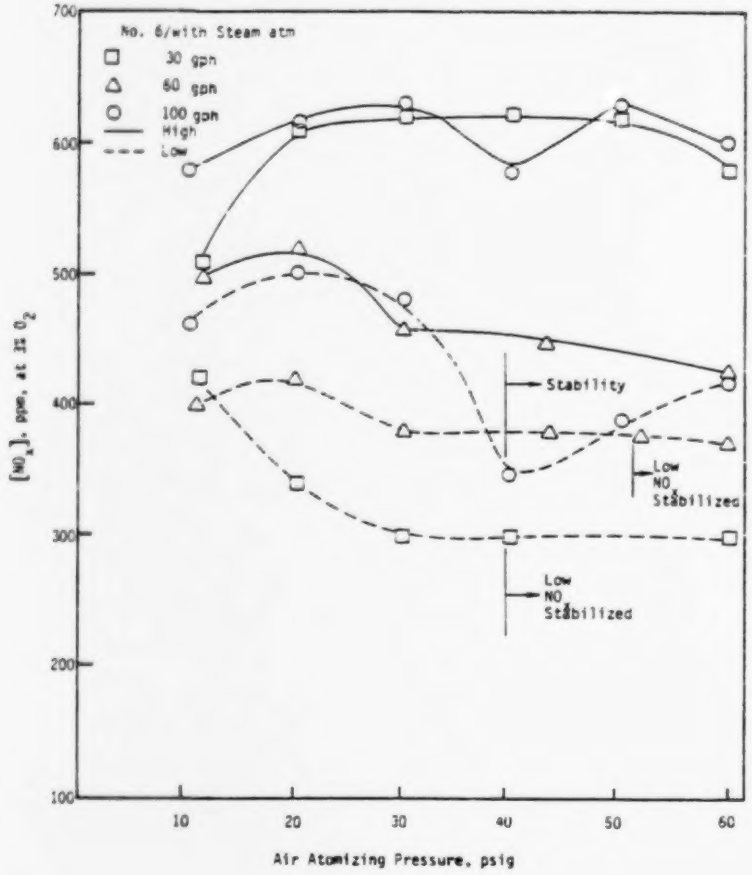

Figure 5-25. NO_x Emissions from Residual Fuel Oil with the Monarch Atomizers; Steam Atomization; HN and LN Airflow Patterns.

- The lowest NO_x emissions with residual oil were obtained with the LN airflow pattern and air atomization with the minimum atomizing pressure necessary to stabilize the LN-type flame.
- Flame pattern and NO_x emissions with the LN airflow condition with steam atomization were very dependent on nozzle design capacity and atomizing pressure.

5.4 Phase II Experimental Results

5.4.1 Experimental Conditions

The experimental studies carried out in Phase II can be divided into three sections:

- Atomizer/flow field intereaction
- Influence of fuel properties
- Staged combustion studies

The objective of the first series of experiments was to determine the extent to which atomizer design and the conditions under which it is operated affect NO_x emissions. In these experiments 14 atomizers were tested in three simple flow fields of low, medium and high swirl levels ($S = 0.21$, 0.45, 0.79) and in each flow field the atomizing air pressure was varied over a wide range. The baseline Indonesian/Malaysian oil was used and thermal fuel input of 879 kW (3×10^6 Btu/hr) was held constant throughout the tests.

The second series of tests were carried out to define the effect of fuel properties, both physical and chemical, upon NO_x emissions and to investigate the extent to which these effects are influenced by atomizer/flow field interaction. Eight fuels representing a wide range of properties and crude feedstock were tested with a number of atomizers.

The final test series was designed to investigate atomizer, swirl, and fuel effects on emissions under staged combustion conditions. The effect of primary zone stoichiometry was investigated for five nozzles and several swirl conditions with the baseline fuel. Primary zone residence time was varied for two atomizers over a range of primary stoichiometries and swirl conditions. For some of the experiments a refractory liner was inserted into the firetube downstream of the burner to investigate the effect of reduced heat loss in the primary zone.

The following subsections describe the results of each test series in the Phase II package boiler simulator investigations.

5.4.2 Experimental Results — Atomizer/Flow Field Interaction

In this section the experimental results of the first test series of Phase II testing - atomizer/flow field interaction - are presented. The purpose of this test series was to provide a comparison of NO_x and smoke emissions from 14 fuel atomizers using one residual fuel oil in three simple and reproducible combustion airflow fields.

Table 5-1 lists the atomizers which were selected for this study and the test conditions for each. For all tests in this series the Indonesian/Malaysian baseline fuel was fired at constant flow rate of 1.33 liters/min (21 gph), the atomizing fluid was air and the oil temperature at the nozzles was maintained at 299°C in each case. Excess oxygen was varied at several atomizing air pressures for each atomizer in three different swirling flow fields, ranging from weak to strong swirl. For each atomizing pressure and flow field one data point was taken with cooled flue products recirculated through the burner. The level of FGR ranged between 12 and 24 percent*. For some atomizers, the range of atomizing pressure, swirl number, and FGR was limited by flame instability, blow off or excessive smoke, and hence, these conditions were deleted from the test matrix. Flue measurements for these tests included NO_x, O_2, CO, CO_2, and Bacharach smoke number. Table 5-1 lists the 99 separate atomizer/pressure/flow field conditions which were tested.

The results of this test series concerned with atomizer screening are presented graphically in Figures 5-26 to 5-62. For each figure, open symbols represent NO_x emissions, semi-solid symbols represent NO_x emissions with FGR, and solid symbols represent Bacharach smoke number. Smoke number is assumed to be ≤ 2 where no data is given.

---

* $$\% \text{ FGR} = \frac{(\text{mass rate of recirculated products})}{(\text{mass rate of fuel + air})}$$

Table 5-1. Atomi.ers Which were Selected for this Study and the Test Conditions for Each.

	NOZZLE		REMARKS	Atomizing Air Pressure (PSIG)		
				S = 0.2	S = 0.45	S = 0.78
○	MONARCH	100 gph	ASSIST FLUID INTERNAL MISC. PINTLE	20, 30, 40	20, 30, 40	20, 30, 40
⬯		60 gph		20, 30, 40	20	20, 30, 40
□		30 gph		30, 40, 50	40	--
◦	INDUSTRIAL COMBUSTION	140-48-21	INTERNAL, MIXING CHAMBER, CENTER BODY	30, 40, 50	30	30
◊		156-48-22		30, 40, 50	--	--
⌑	DELAVAN "AIRO"	30615-16-20	SOLID CORE SPRAY	40, 50, 60	--	50, 60
∩		30615-24-25		40, 50, 60	40, 50	40, 50, 60
◇	DELAVAN SWIRL AIR	34429-2	ASSIST FLUID PINTLE	40, 50, 60	40, 50	40, 50, 60
⌂	CLEAVER BROOKS			30, 40, 50	--	30, 40, 50
✥	PEABODY	6-052-70	TWIN FLUID	25, 45, 65	25, 45, 65	25, 45, 65
◗		6-086-55		25, 45	25, 45, 65	25, 45, 65
◺		6-102-55		30,40,45,65	25, 45, 65	25, 65
△	TODD	CDS		30, 40, 50	22,30,40,50	22, 30, 50
○	SONICORE			--	5,10,15,20	5,10,15,20

kPa = (psig + 14.7)(6.895)

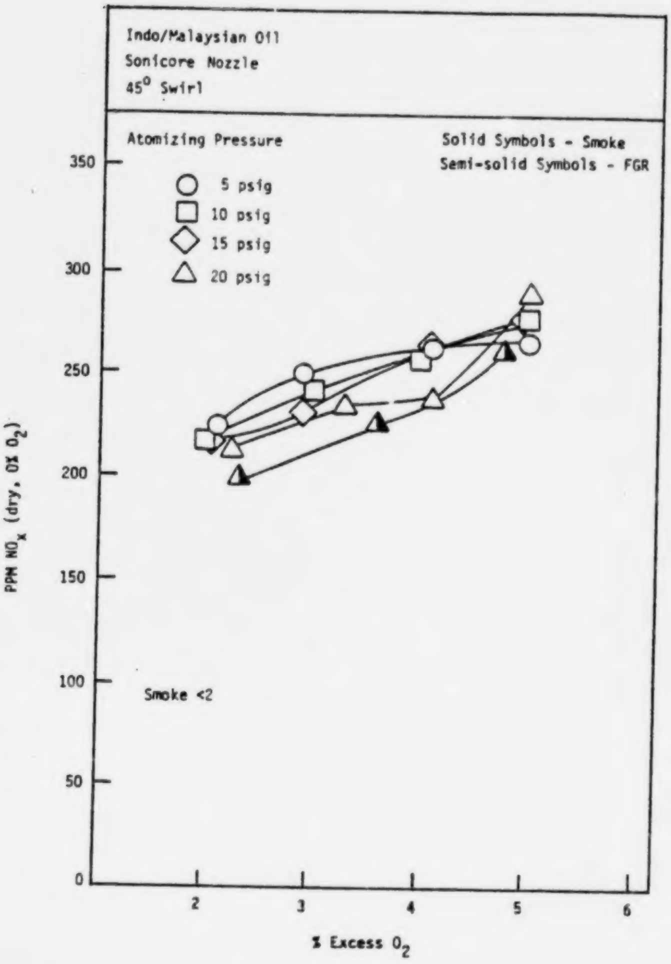

Figure 5-26. Atomizer Screening Tests - Sonicore 250T Atomizer with 45° Swirl Vanes.

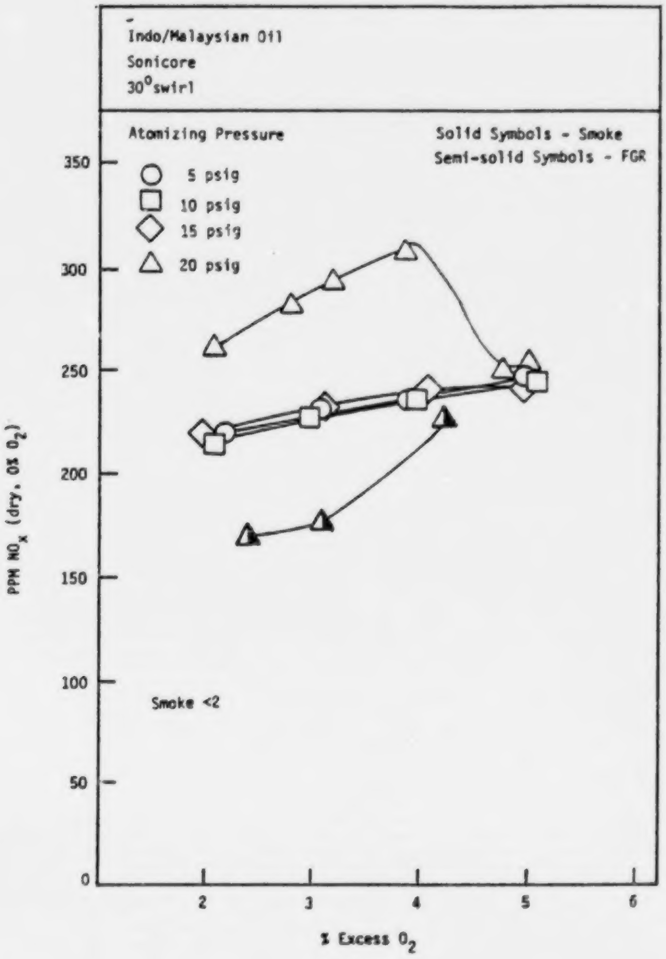

Figure 5-27. Atomizer Screening Tests - Sonicore 250T Atomizer with 30° Swirl Vanes.

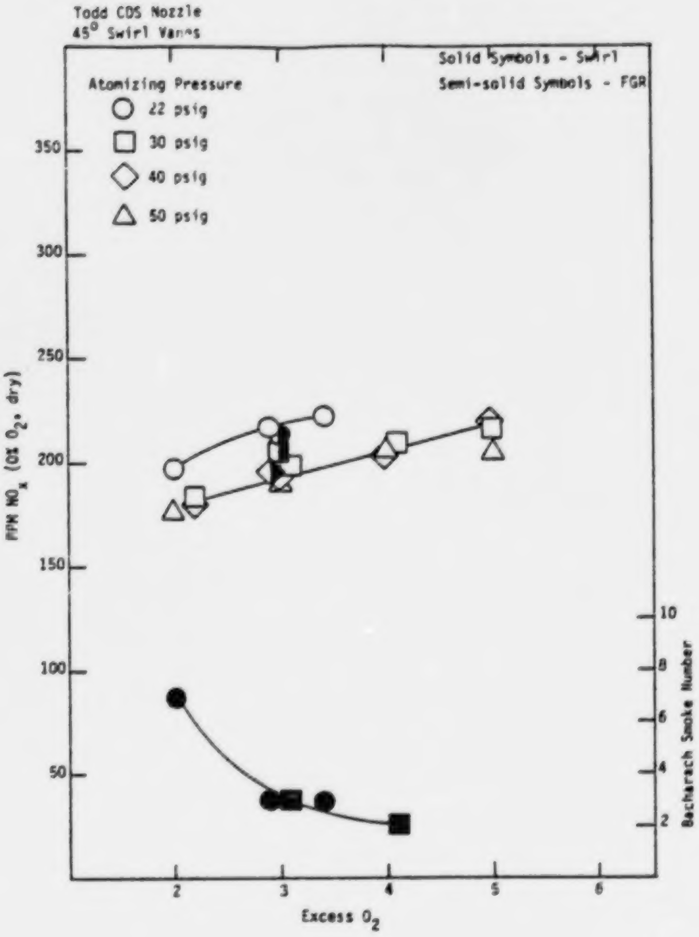

Figure 5-28. Atomizer Screening Tests - Todd CDS Atomizer with 45° Swirl Vanes.

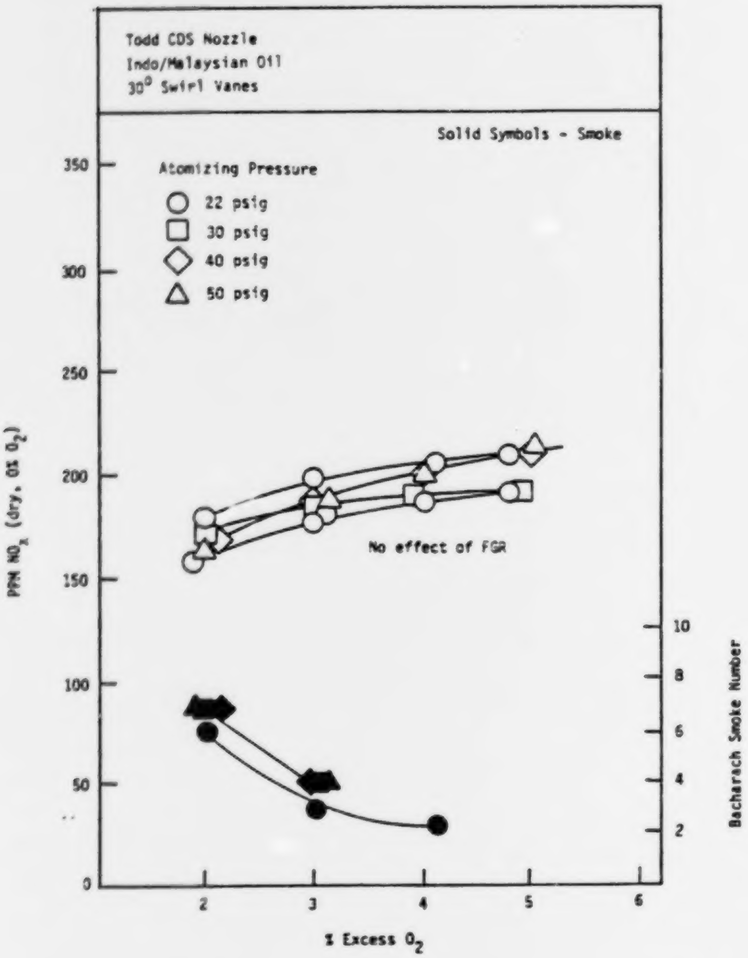

Figure 5-29. Atomizer Screening Tests - Todd CDS Nozzle with 30° Swirl Vanes.

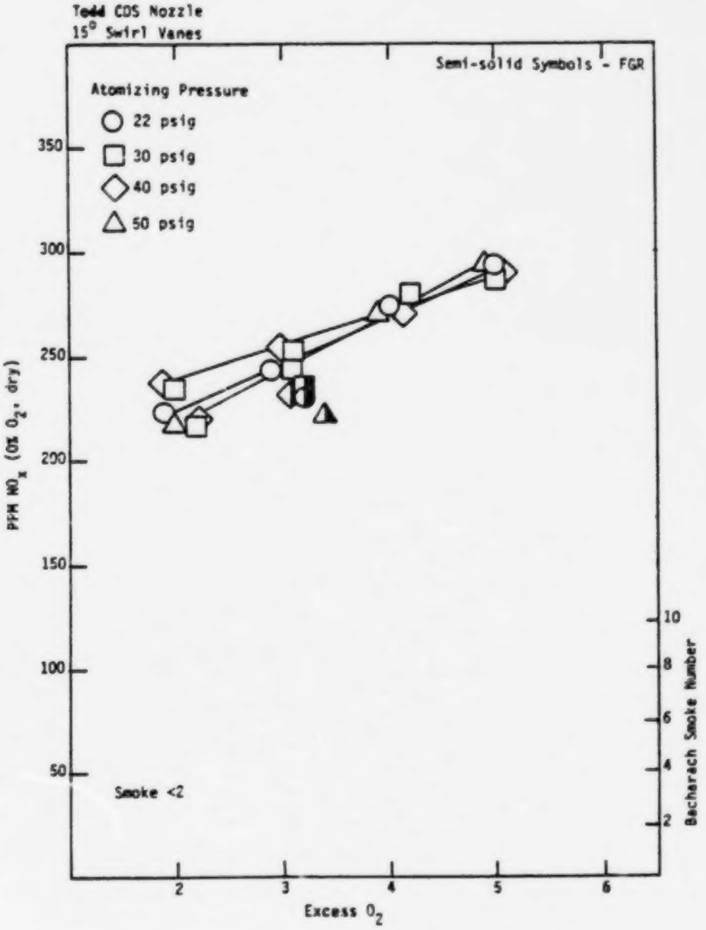

Figure 5-30. Atomizer Screening Tests - Todd CDS Atomizer with 15° Swirl Vanes.

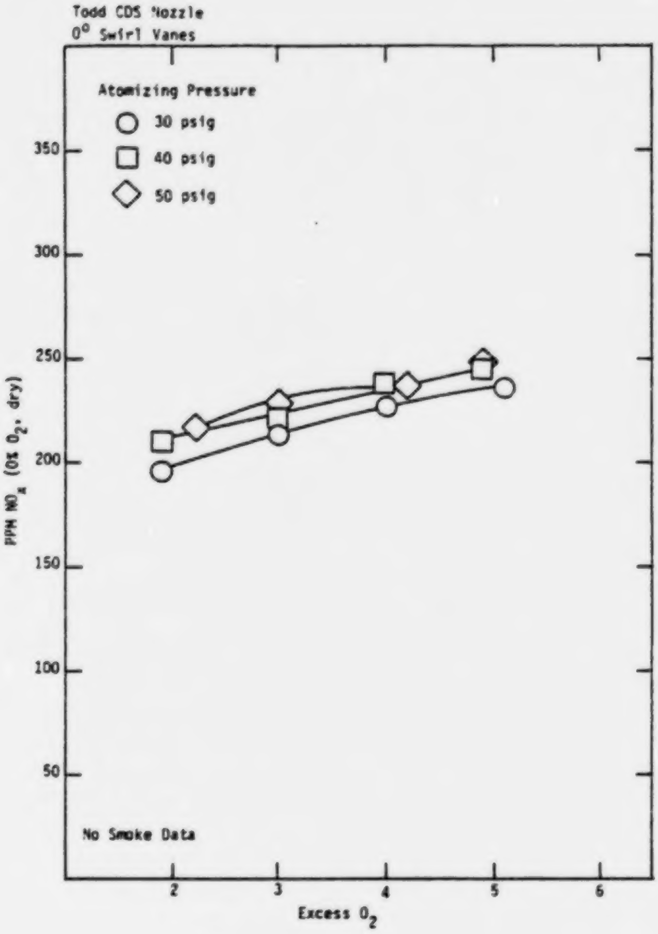

Figure 5-31. Atomizer Screening Tests - Todd CDS Atomizer with 0° Swirl Vanes.

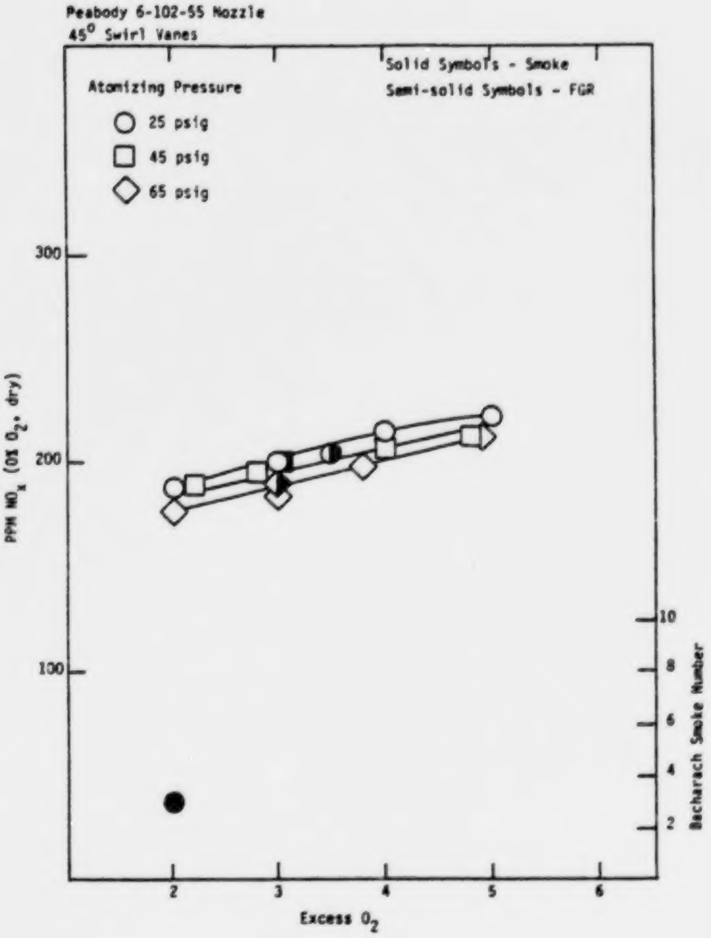

Figure 5-32. Atomizer Screening Tests - Peabody 6-102-55 with 45° Swirl Vanes.

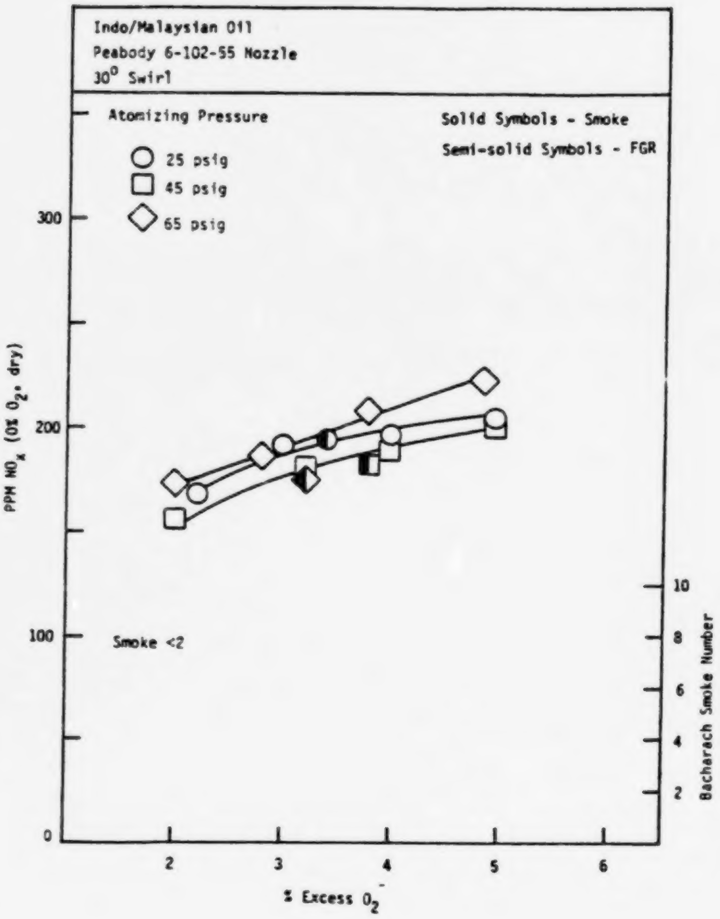

Figure 5-33. Atomizer Screening Tests - Peabody 6-102-55 with 30° Swirl Vanes.

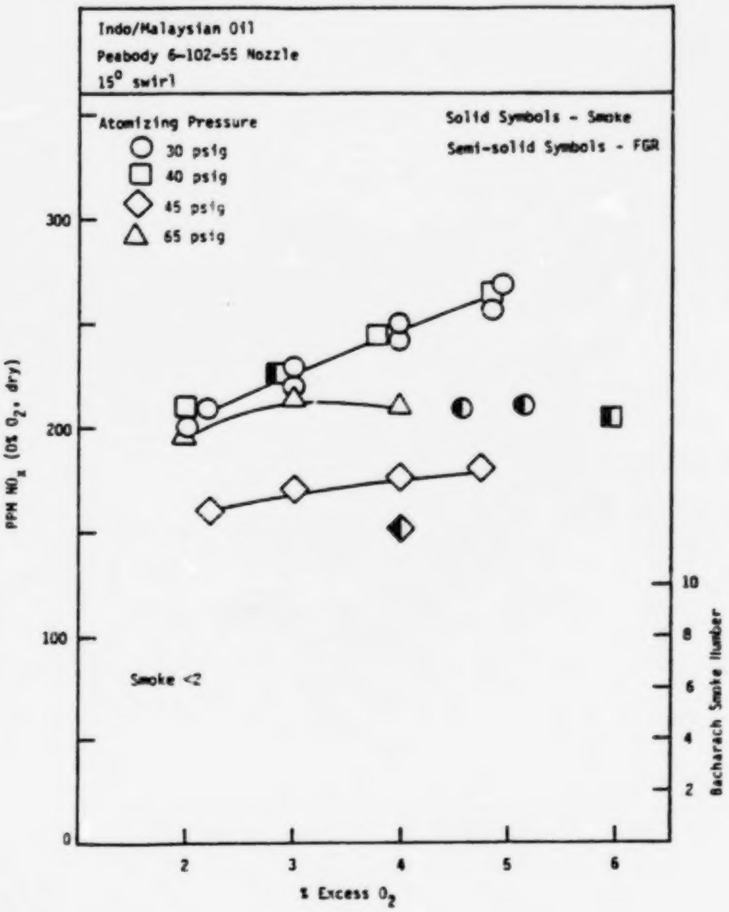

Figure 5-34. Atomizer Screening Tests - Peabody 6-102-55 with 15° Swirl Vanes.

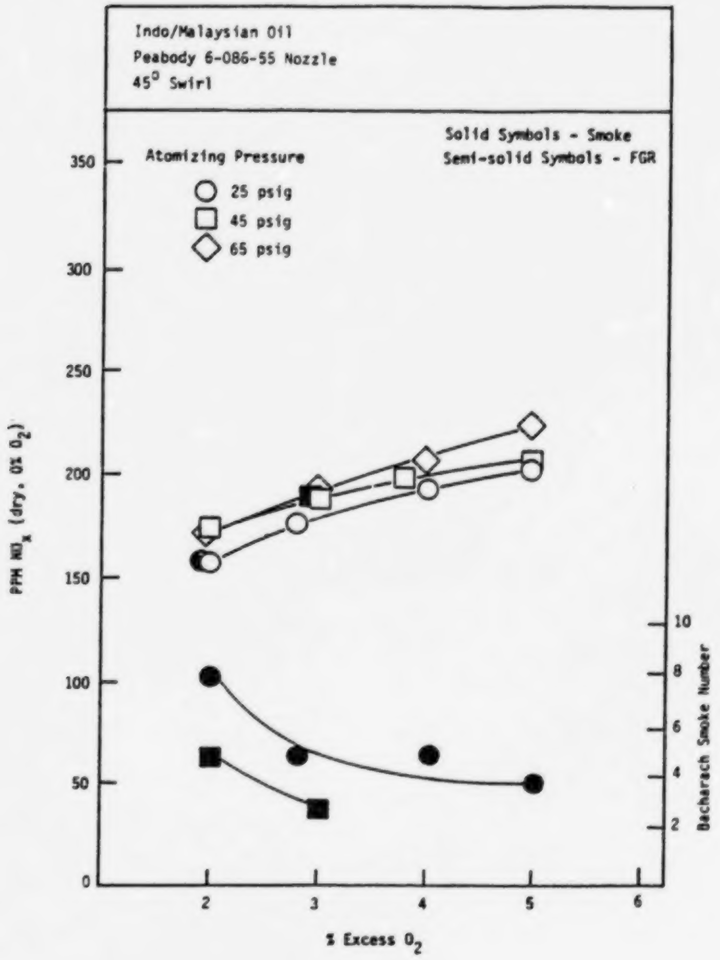

Figure 5-35. Atomizer Screening Tests - Peabody 6-086-55 with 45° Swirl Vanes.

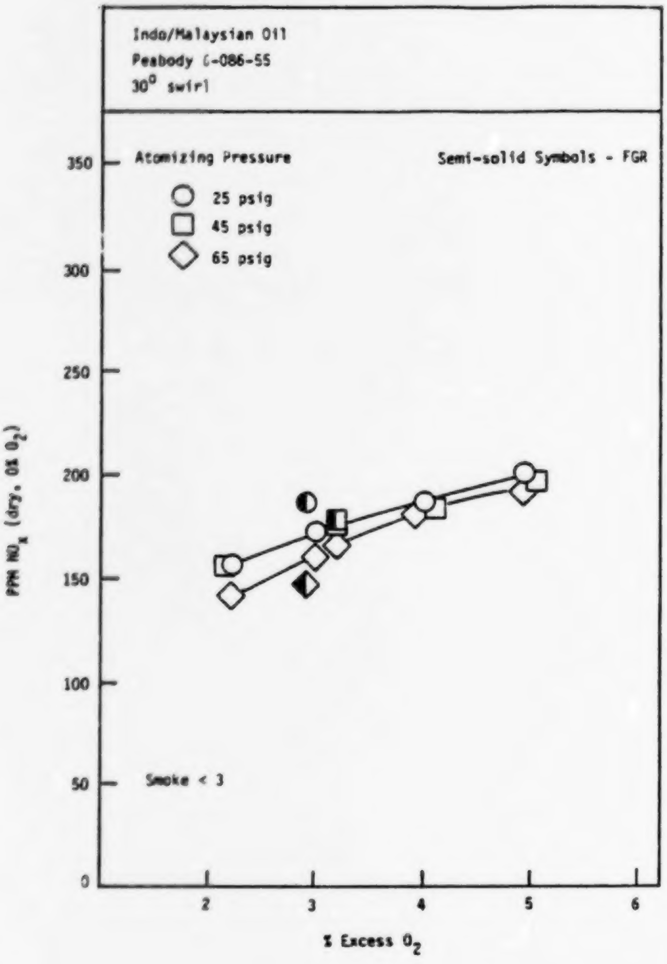

Figure 5-36. Atomizer Screening Tests - Peabody 6-086-55 with 30° Swirl Vanes.

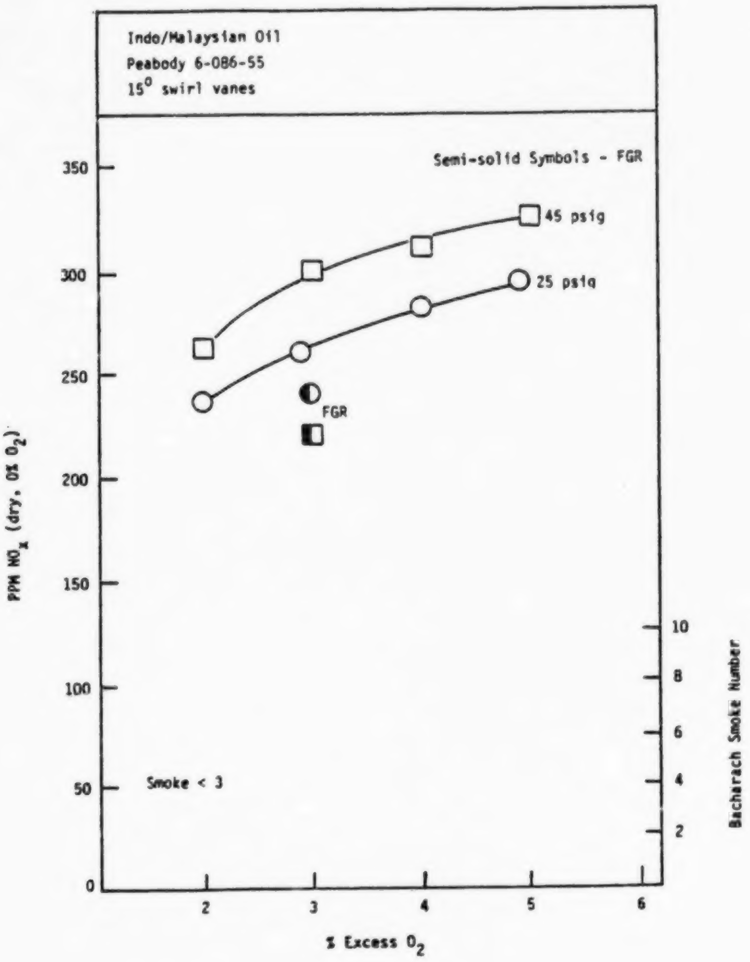

Figure 5-37. Atomizer Screening Tests - Peabody 6-096-55 with 15° Swirl Vanes.

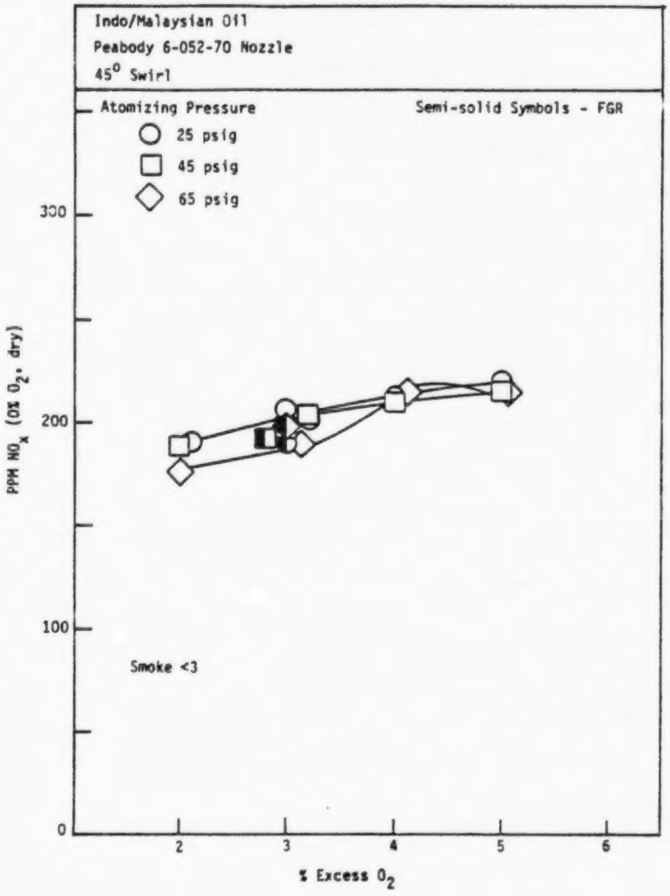

Figure 5-38. Atomizer Screening Tests - Peabody 6-052-70 with 45° Swirl Vanes.

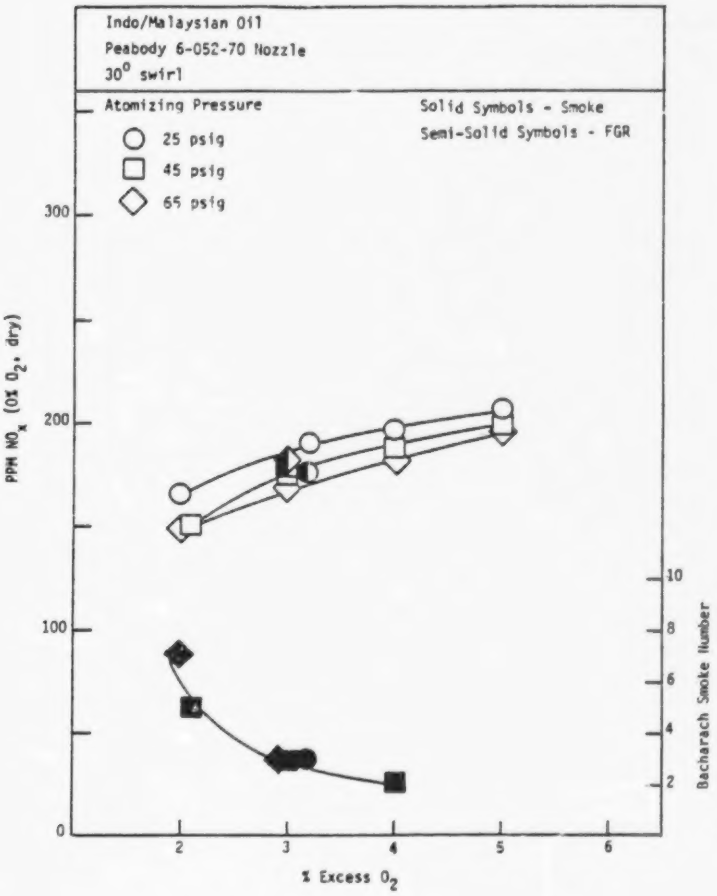

Figure 5-39. Atomizer Screening Tests - Peabody 6-052-70 with 30° Swirl Vanes.

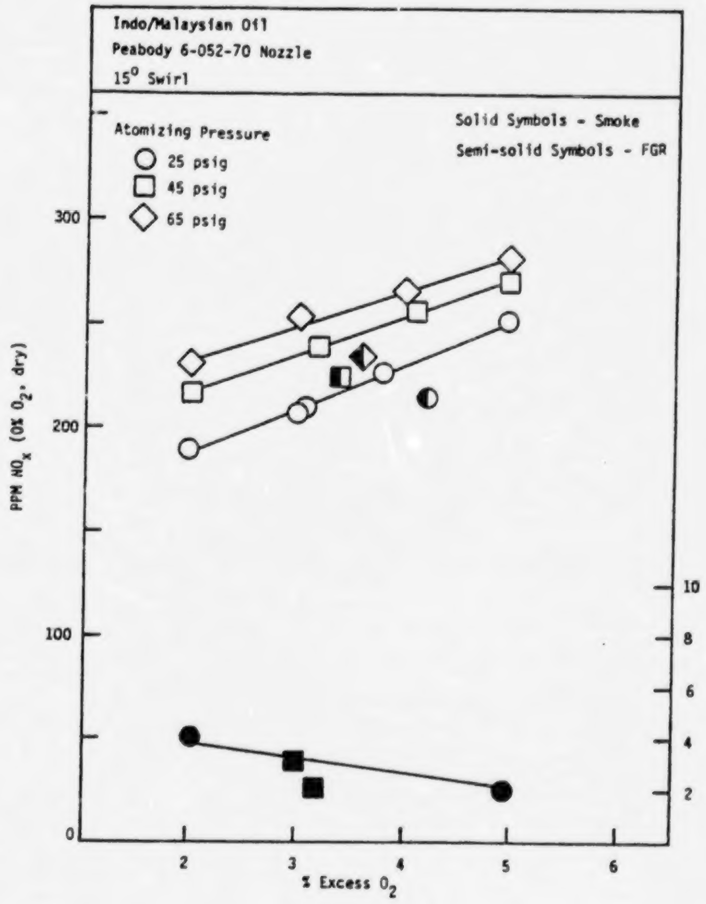

Figure 5-40. Atomizer Screening Tests - Peabody 6-052-70 with 15° Swirl Vanes.

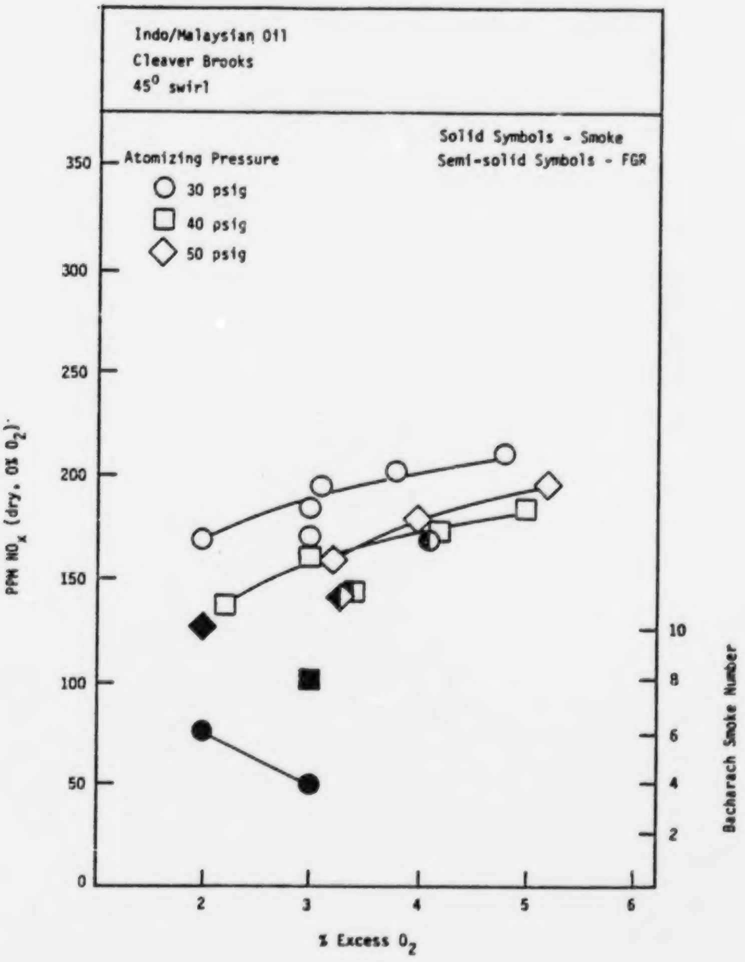

Figure 5-41. Atomizer Screening Tests - Cleaver Brooks with 45° Swirl Vanes.

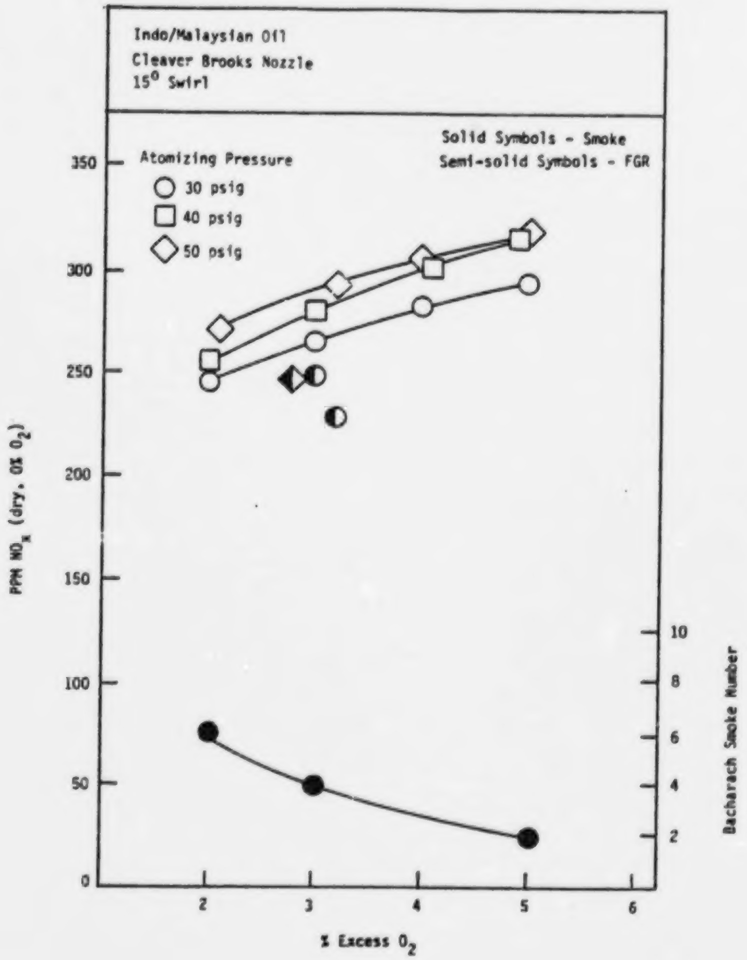

Figure 5-42. Atomizer Screening Tests - Cleaver Brooks with 15° Swirl Vanes.

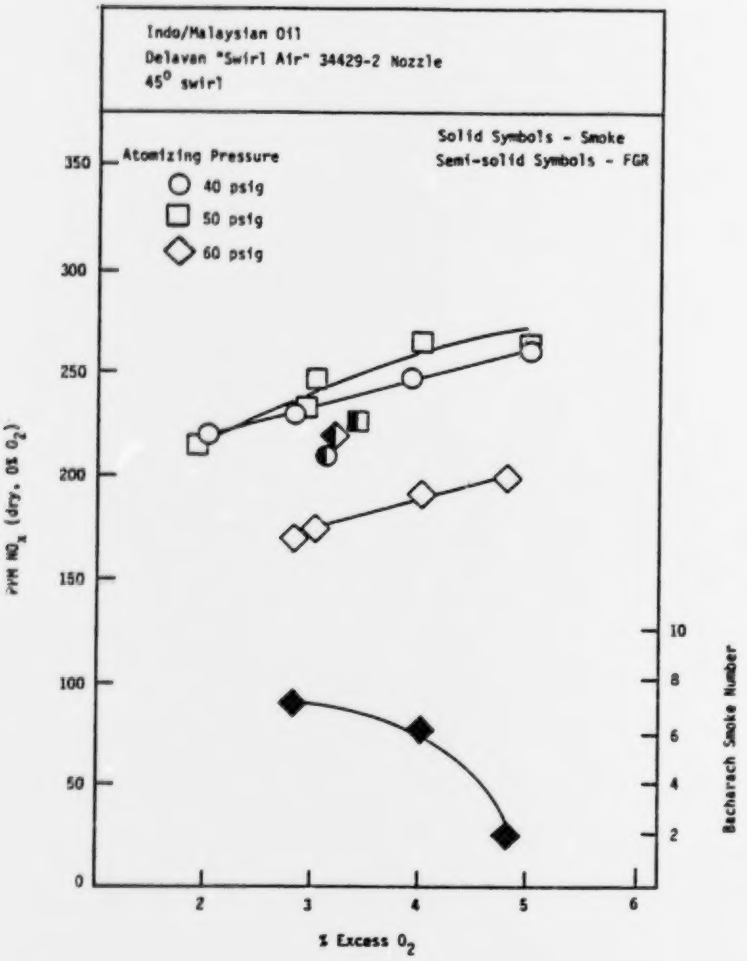

Figure 5-43. Atomizer Screening Tests - Delavan "Swirl Air" with 45° Swirl Vanes.

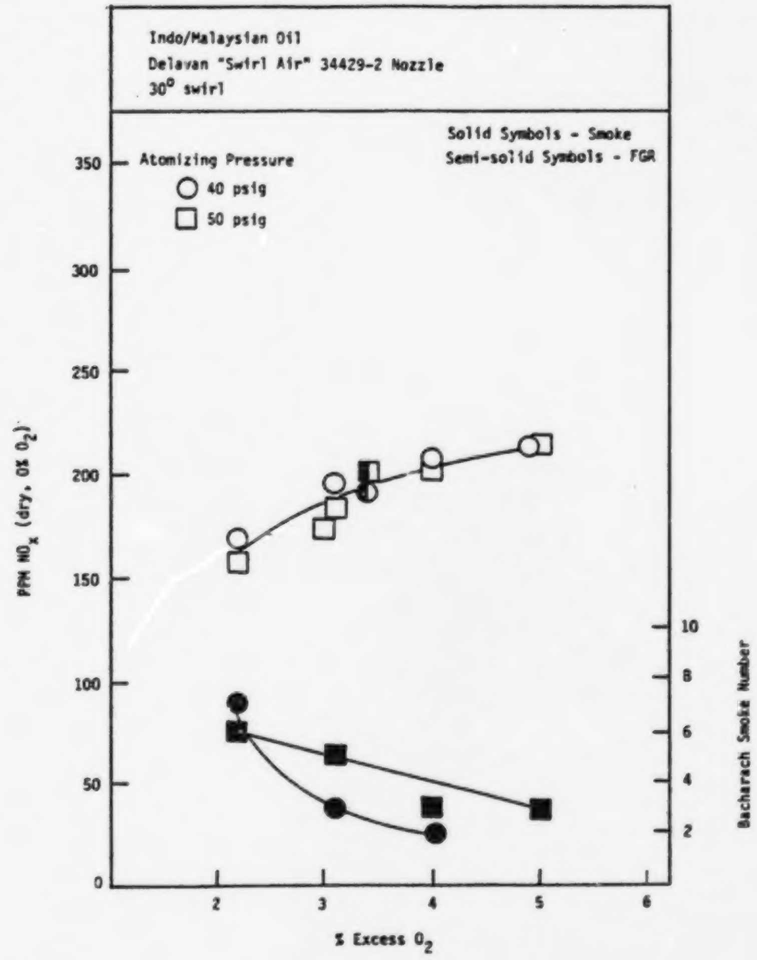

Figure 5-44. Atomizer Screening Tests - Delavan "Swirl Air" with 30° Swirl Vanes.

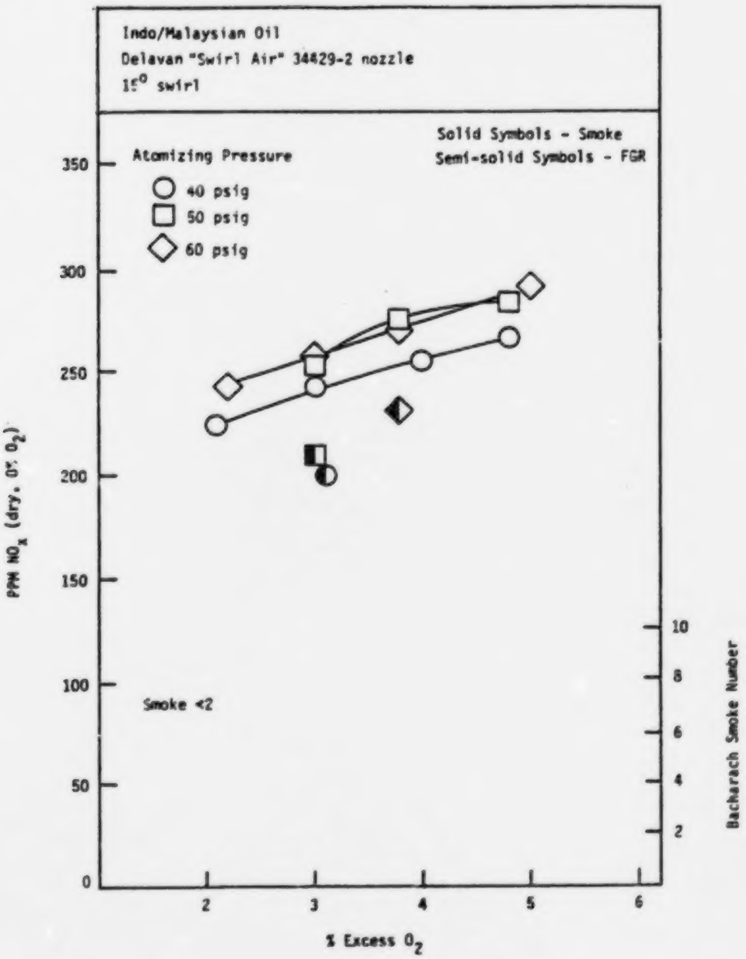

Figure 5-45. Atomizer Screening Tests - Delavan "Swirl Air" with 15° Swirl Vanes.

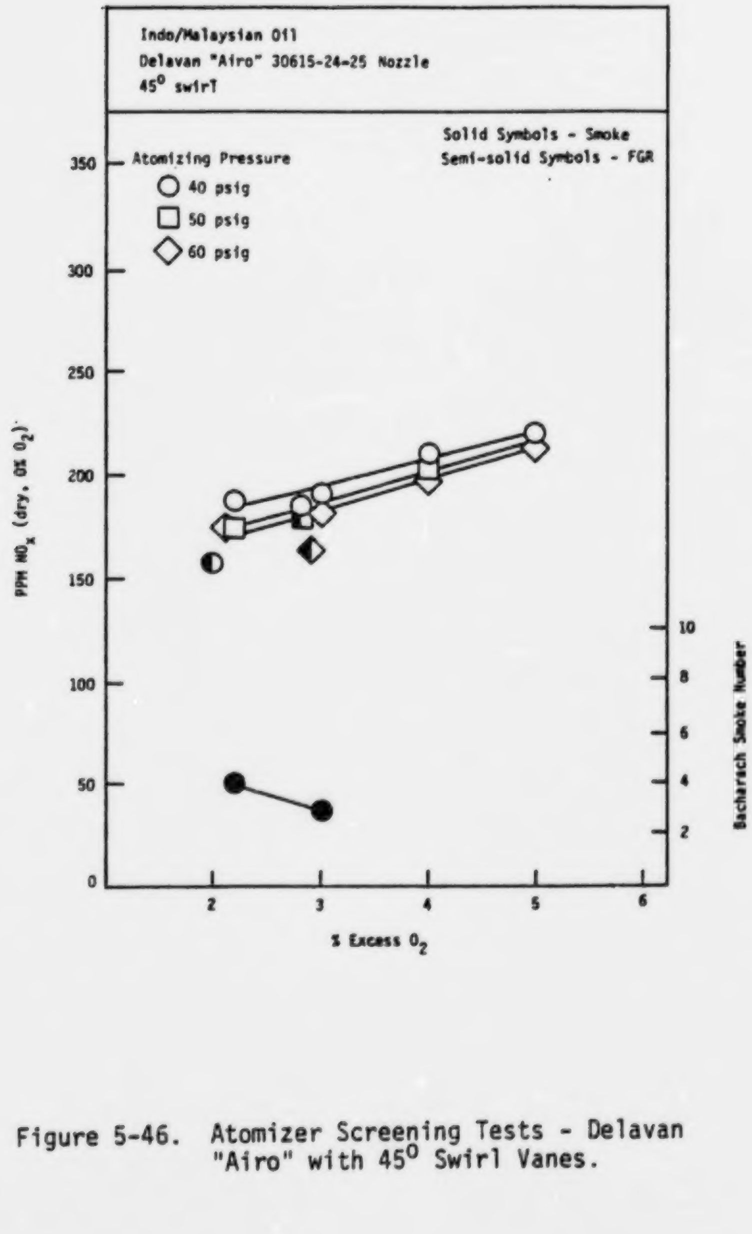

Figure 5-46. Atomizer Screening Tests - Delavan "Airo" with 45° Swirl Vanes.

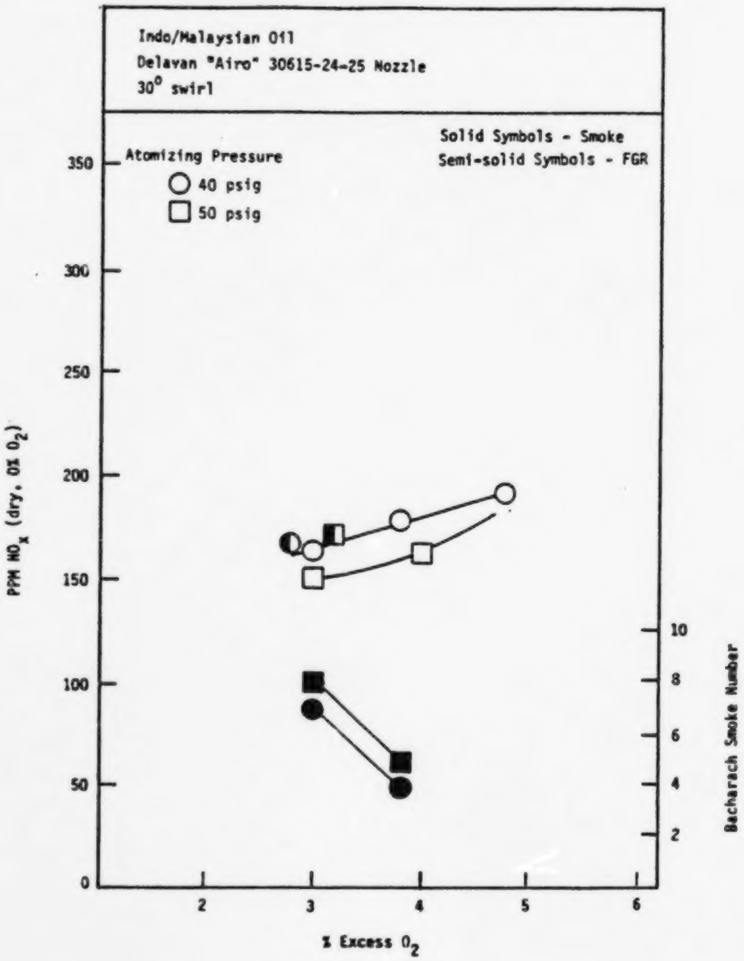

Figure 5-47. Atomizer Screening Tests - Delavan "Airo" with 30° Swirl Vanes.

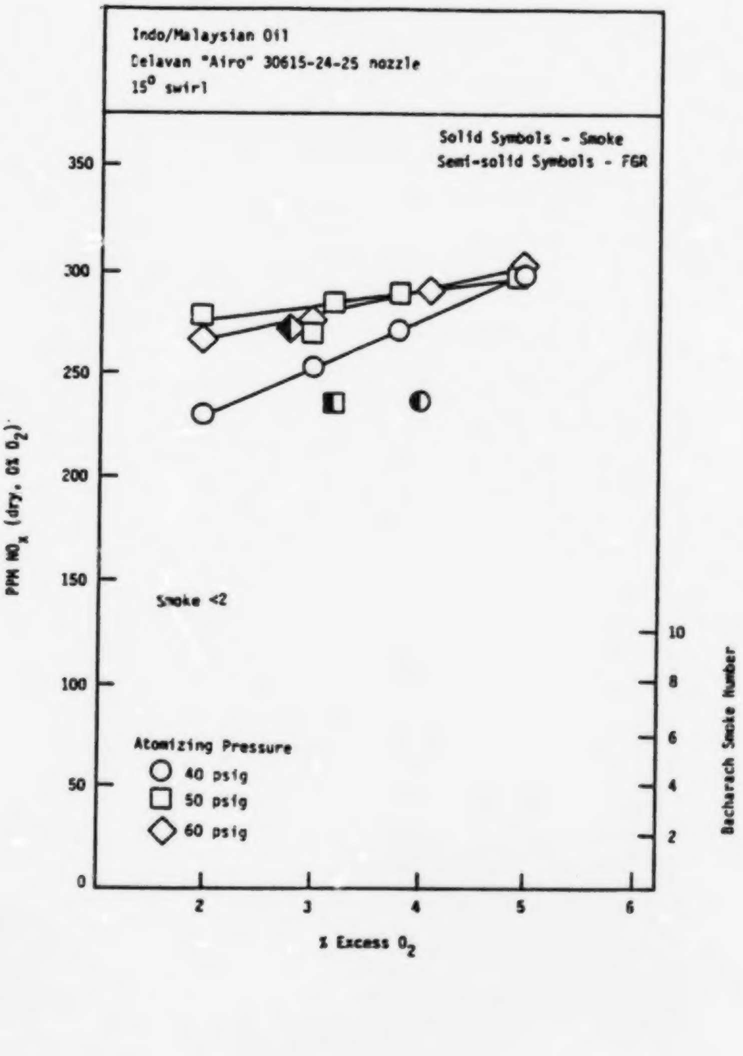

Figure 5-48. Atomizer Screening Tests - Delavan "Airo" with 15° Swirl Vanes.

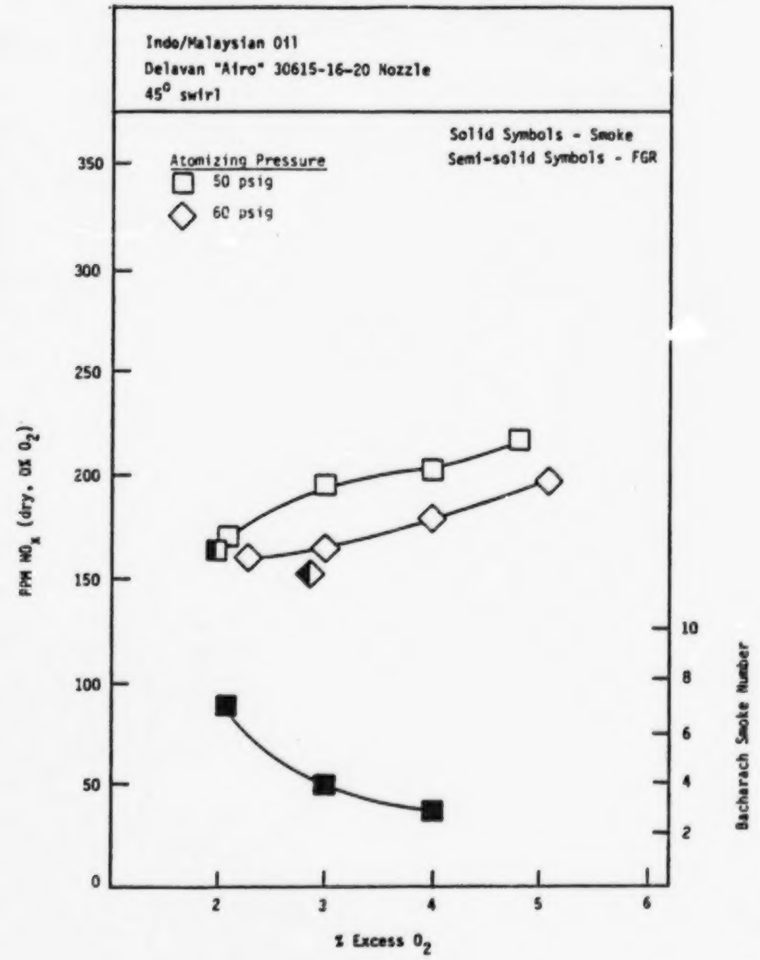

Figure 5-49. Atomizer Screening Tests - Delavan "Airo" with 45° Swirl Vanes.

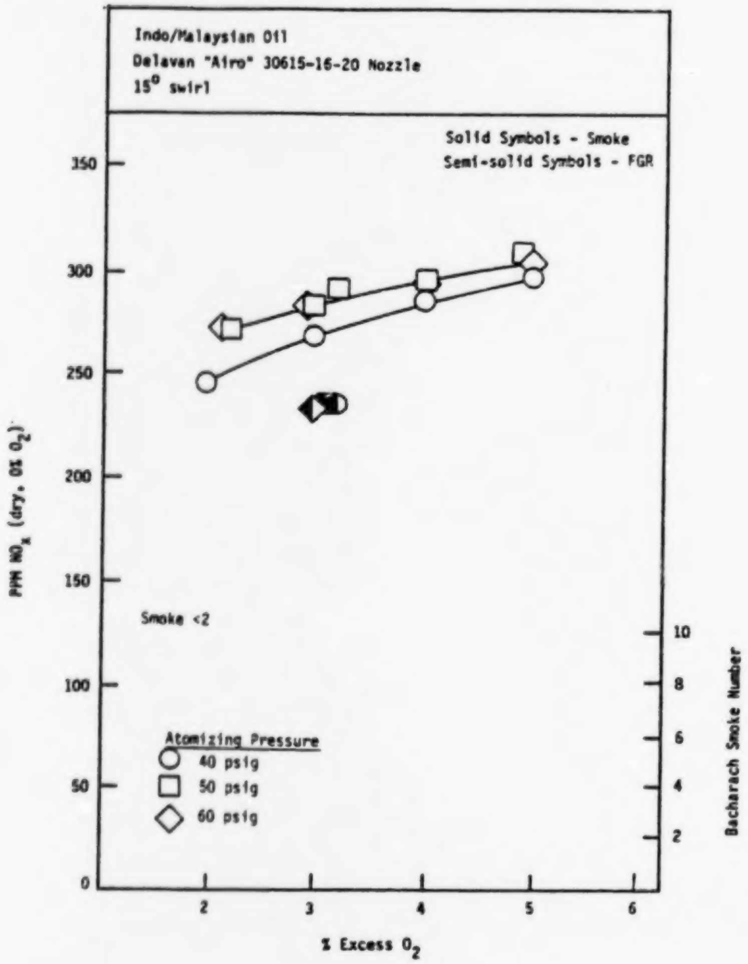

Figure 5-50. Atomizer Screening Tests - Delavan "Airo" with 15° Swirl Vanes.

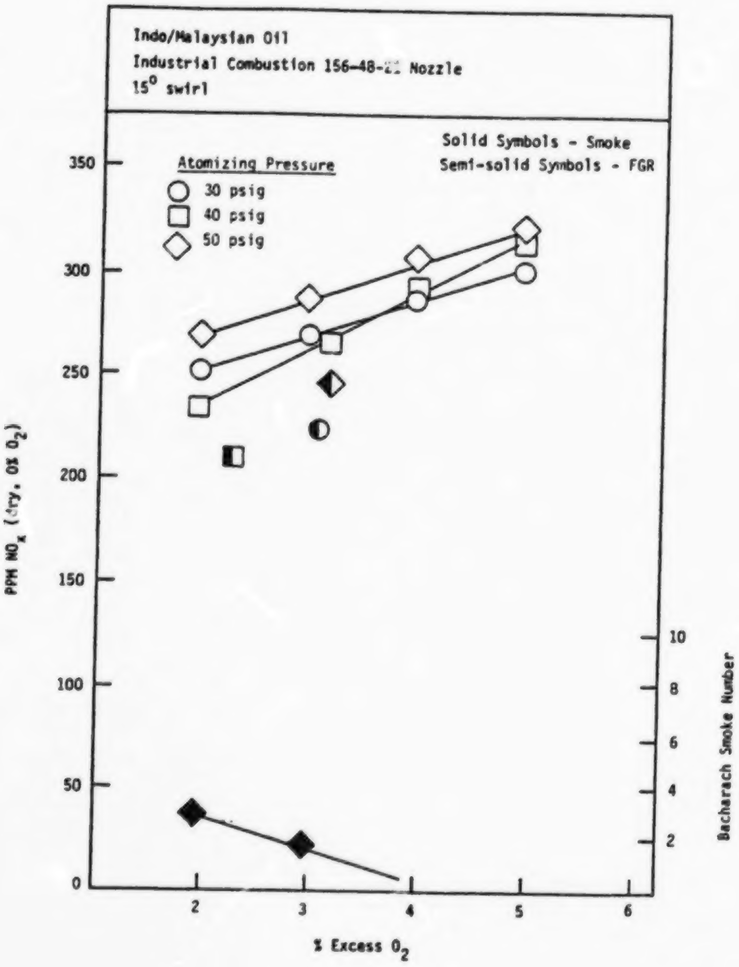

Figure 5-51. Atomizer Screening Tests - Industrial Combustion with 15° Swirl Vanes.

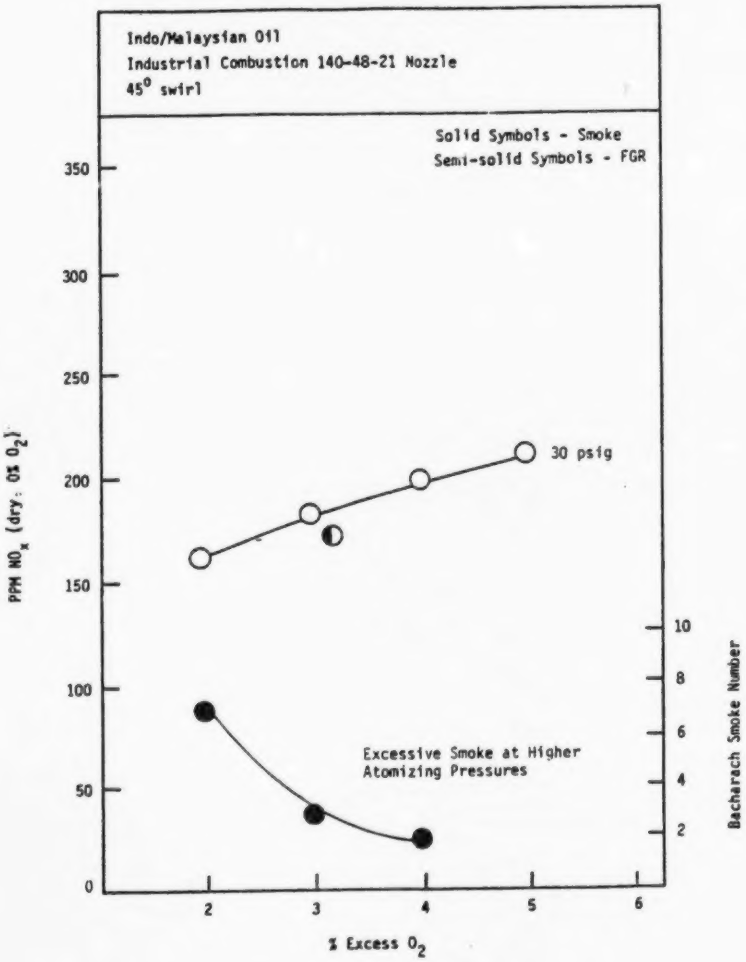

Figure 5-52. Atomizer Screening Tests - Industrial Combustion with 45° Swirl Vanes.

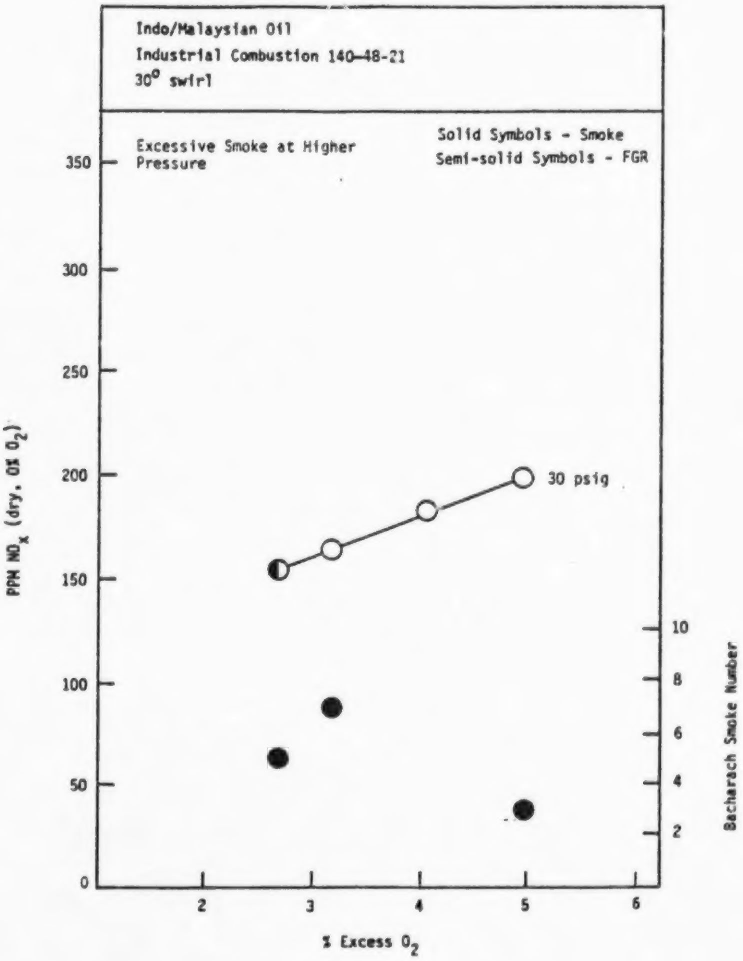

Figure 5-53. Atomizer Screening Tests - Industrial Combustion with 30° Swirl Vanes.

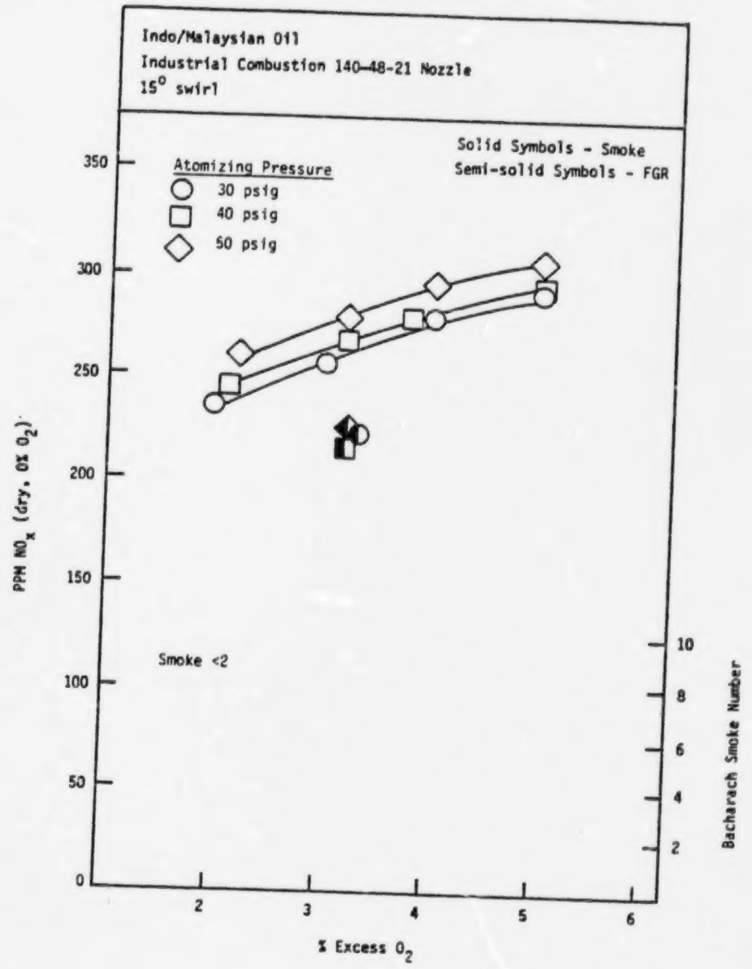

Figure 5-54. Atomizer Screening Tests - Industrial Combustion with 15° Swirl Vanes.

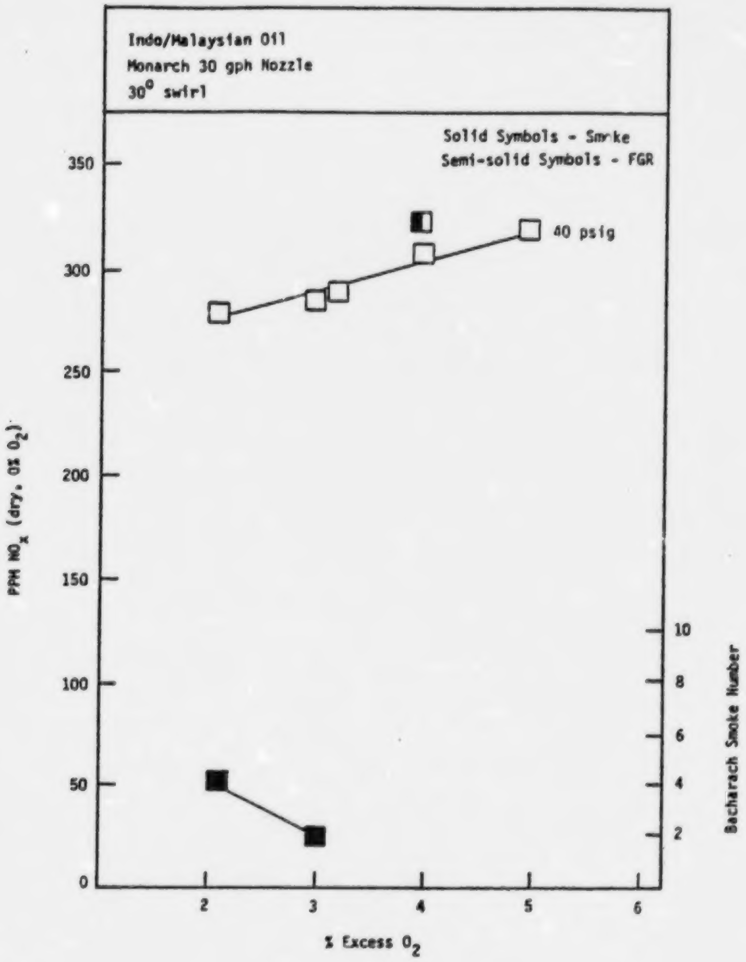

Figure 5-55. Atomizer Screening Tests - Monarch 30 gph with 30° Swirl Vanes.

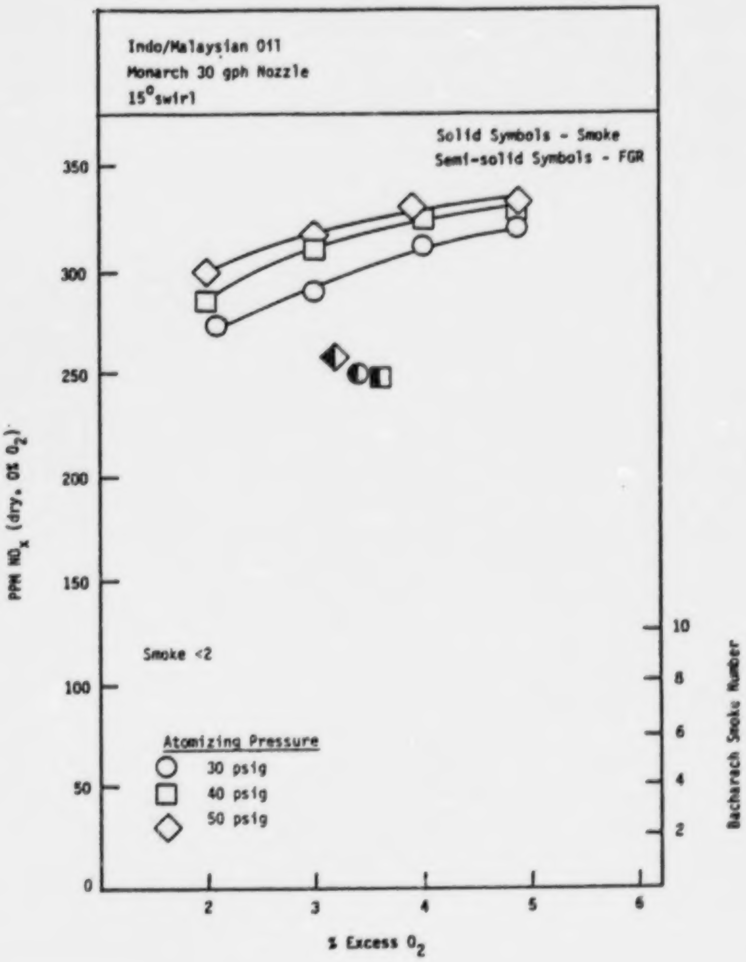

Figure 5-56. Atomizer Screening Tests - Monarch 30 gph with 15° Swirl Vanes.

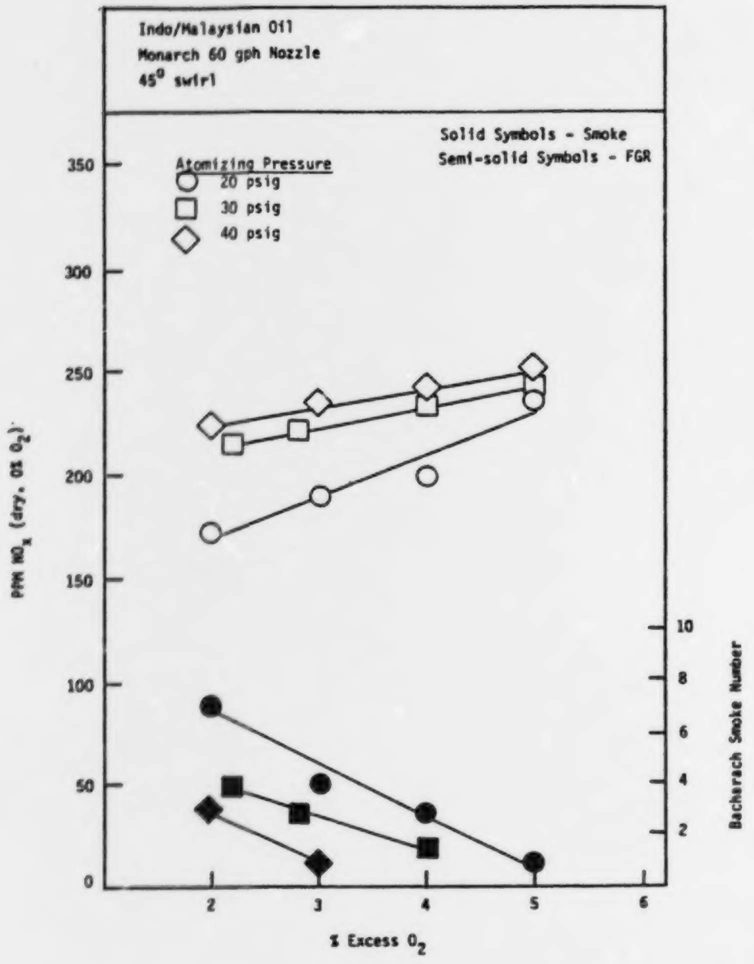

Figure 5-57. Atomizer Screening Tests - Monarch 60 gph with 45° Swirl Vanes.

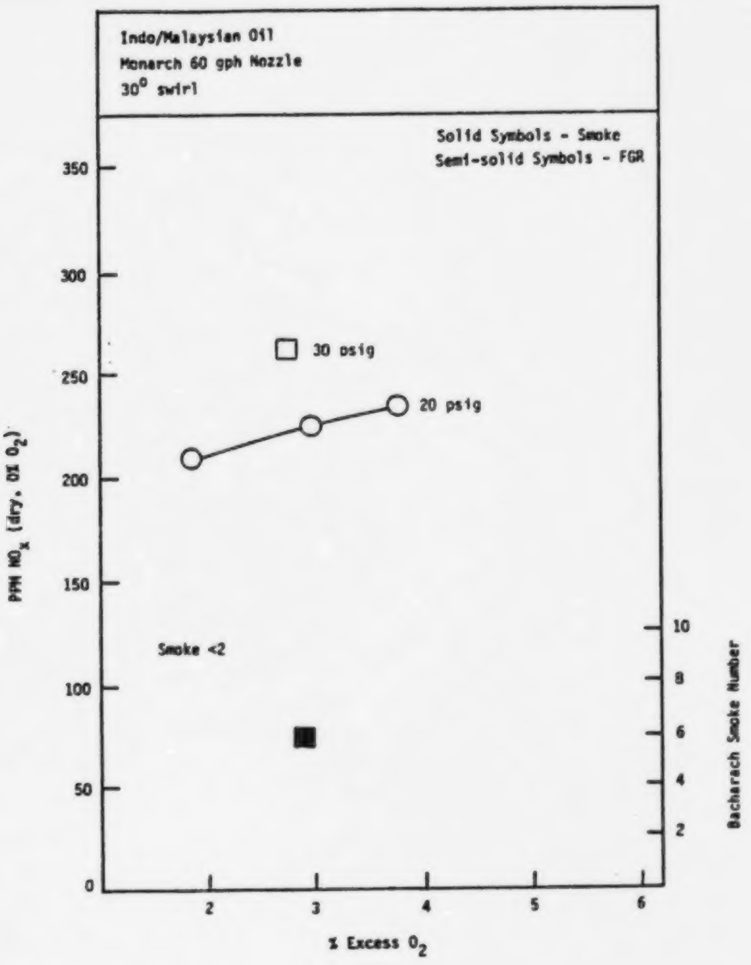

Figure 5-58. Atomizer Screening Tests - Monarch 60 gph with 30° Swirl Vanes.

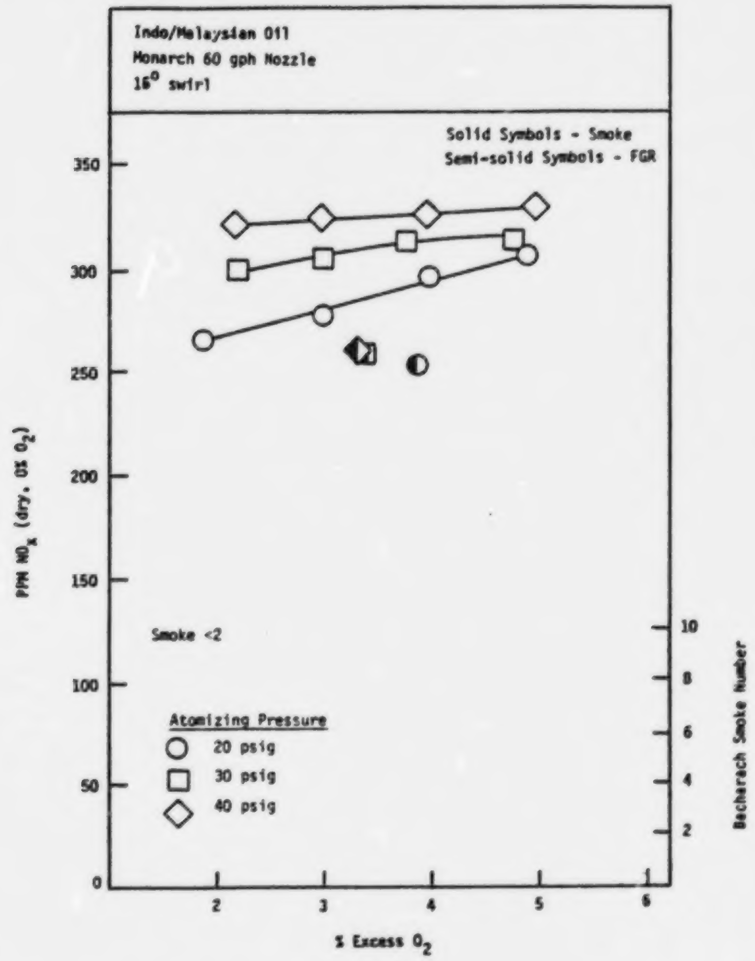

Figure 5-59. Atomizer Screening Tests - Monarch 60 gph with 15° Swirl Vanes.

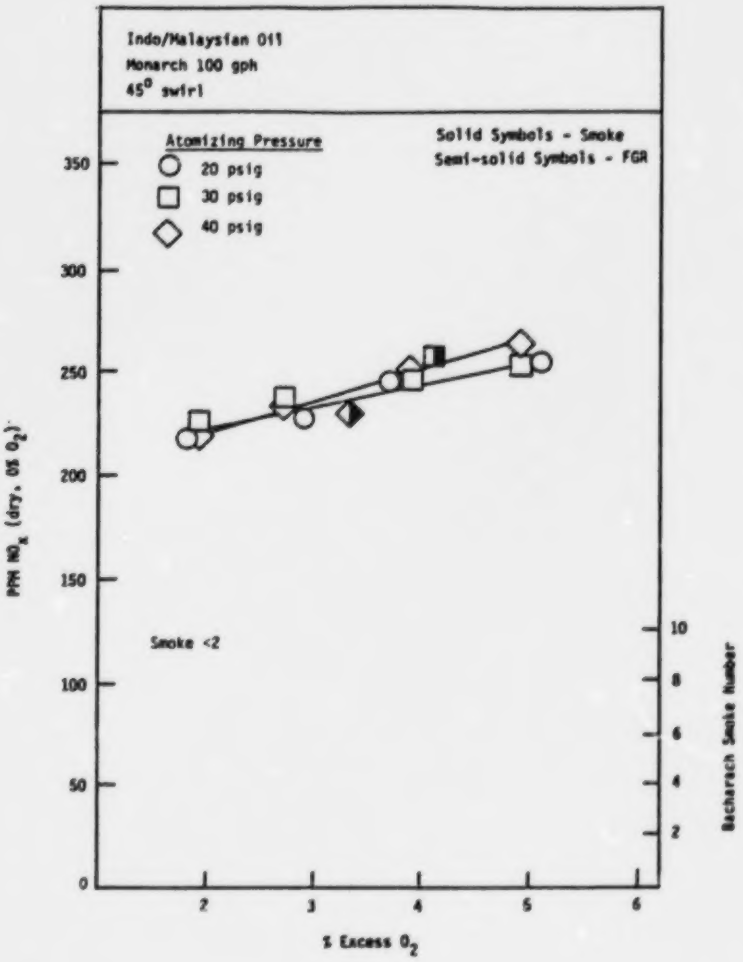

Figure 5-60. Atomizer Screening Tests - Monarch 100 gph with 45° Swirl Vanes.

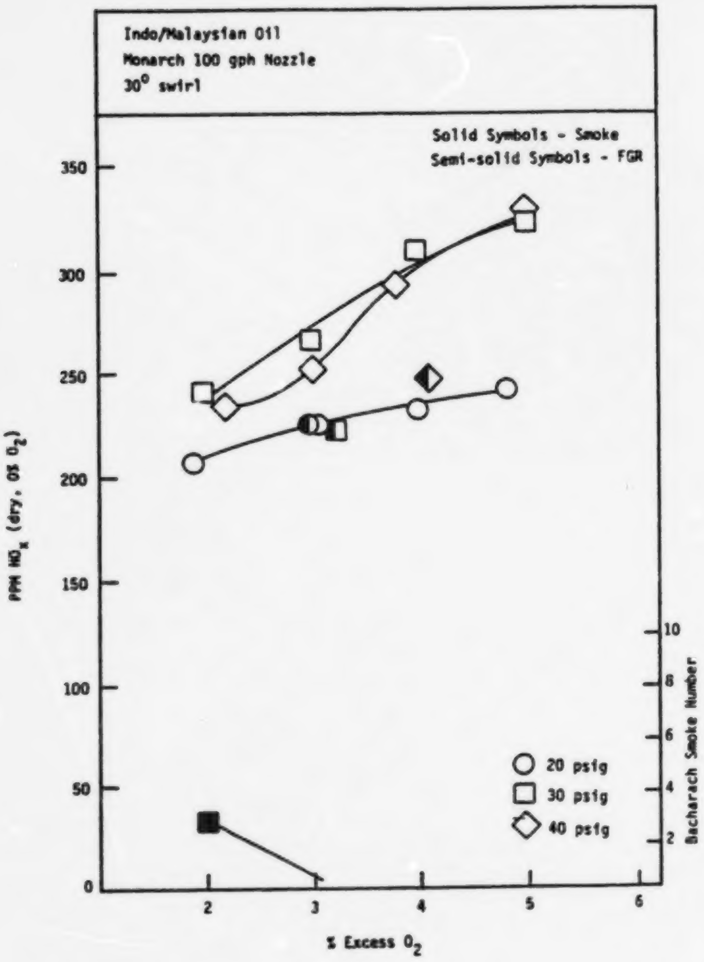

Figure 5-61. Atomizer Screening Tests - Monarch 100 gph with 30° Swirl Vanes.

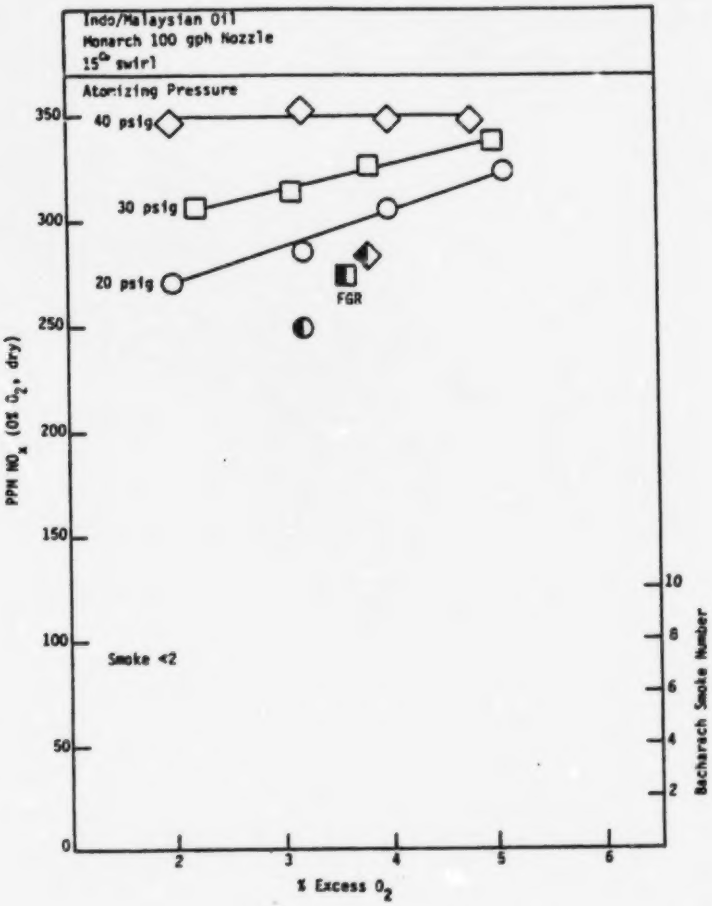

Figure 5-62. Atomizer Screening Tests - Monarch 100 gph with 15° Swirl Vanes.

5.4.2.1 Effect of Atomizers

NO_x emissions were found to depend strongly upon the particular atomizer type and operating condition in a given flow field. Figure 5-63 is a composite plot of NO_x emissions versus excess O_2 for thirteen atomizers which represent the range of emissions observed in the weakly swirling (S=0.21) flow field. Most of the atomizers produced emissions which ranged from 220 to 320 ppm of NO_x; however, some gave values as low as 160 ppm and as high as 350 ppm. Thus, atomizer design alone influenced emission levels by as much as a factor of two. The range of emissions was found to be dependent not only upon atomizer design, but also upon the swirl intensity of the flow field. Figures 5-64 and 5-65 illustrate the range of NO_x emissions which were observed for the intermediate and strongly swirling flow fields. The intermediate strength swirl field produced a range of NO_x emissions from 160 ppm to 290 ppm. The 1.9 liter/minute (30 gph) Monarch and the Sonicore 250T atomizers both produced high NO_x emissions relative to the other atomizers in this flow field. The range of emissions narrowed from 160 ppm to 260 ppm when the same atomizers were tested in the strongly swirling flow field.

5.4.2.2 Effect of Atomizing Air Pressure

Of the 14 atomizers tested, only six showed a significant effect of atomizing pressure upon NO_x emissions. Figure 5-66 shows NO_x emission versus atomizing air pressure for five atomizers with weak swirl. NO_x emission increased with increasing atomizing pressure for all atomizers with the exception of the Peabody 6-102-55 which produced a sudden drop in NO_x emission between 382 to 417 kPa (40 and 45 psig) pressure. However, entirely different effects were observed when these same atomizers were placed in more strongly swirling flow fields, and the atomizing air pressure was varied. Figure 5-67 shows NO_x versus atomizing air pressure for the strongly swirling (45-degree swirl vane) case. The two Peabody atomizers, differing in design capacity and spray angle, and the 6.3 liter/minute (100 gph) Monarch nozzle, which showed a showed a strong effect of atomizing pressure for the weakly swirling case, show no significant effect of pressure. Conversely, variations in atomizing air pressure of the Delavan "Swirl Air" nozzle produced only a slight increase in NO_x for a weakly swirling case and a sharp decrease in the strongly

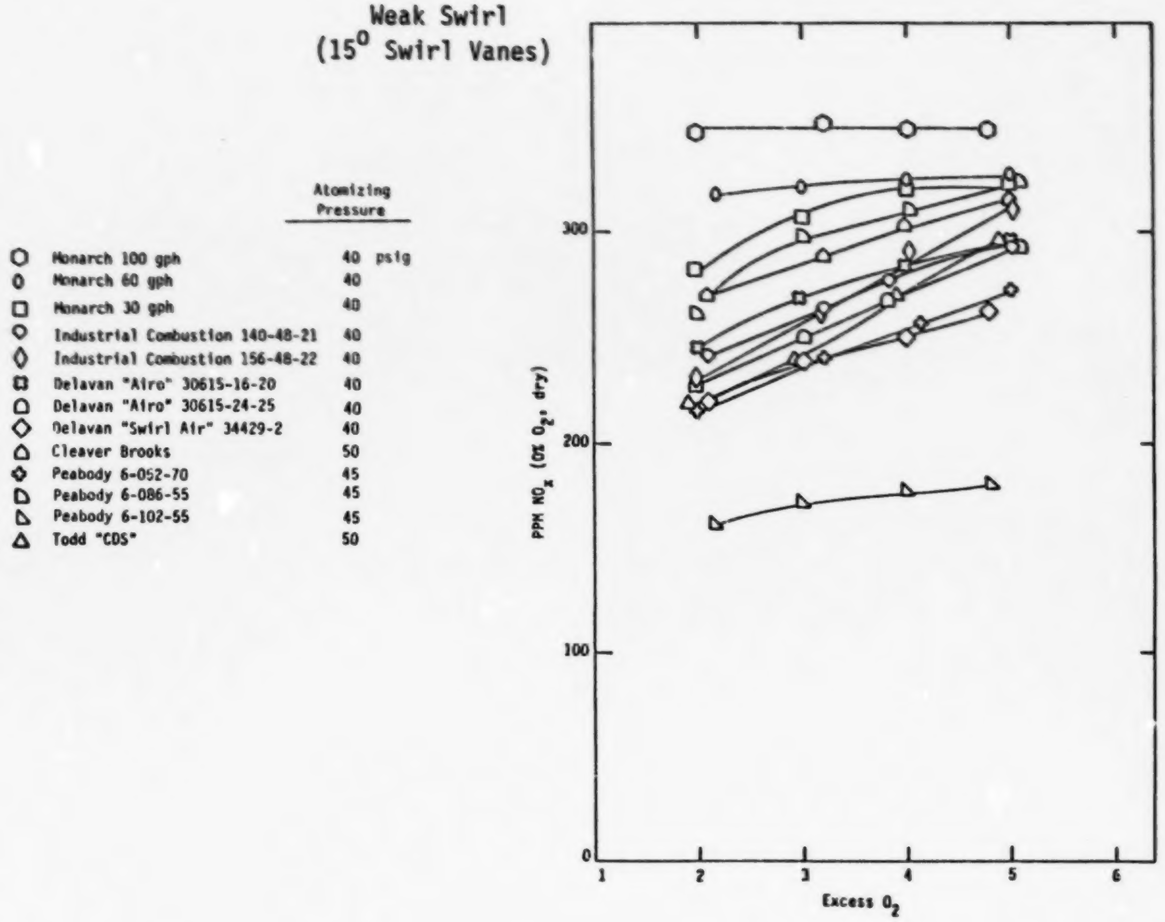

Figure 5-63. Effect of Atomizer with Weak Swirl.

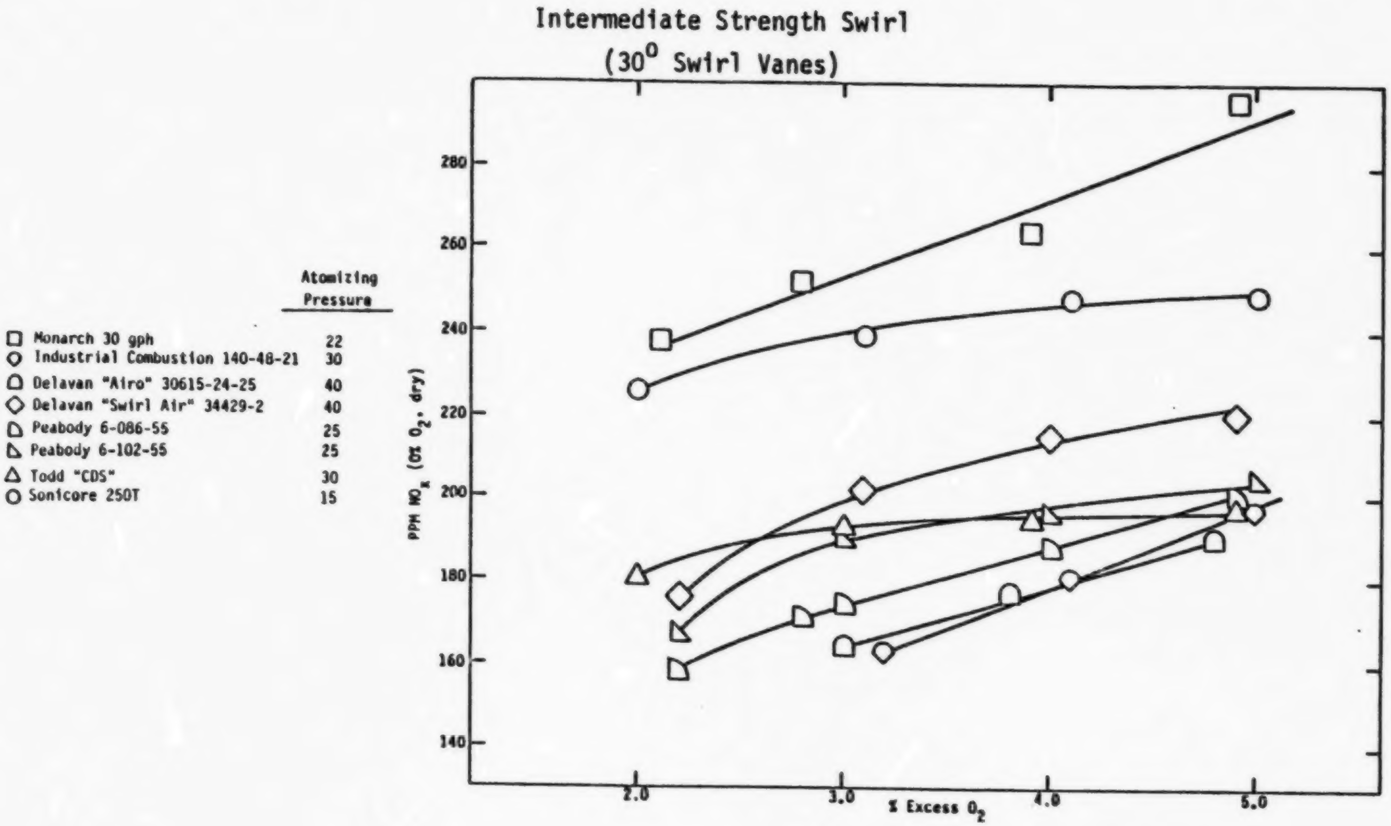

Figure 5-64. Effect of Atomizer with Intermediate Swirl.

Strong Swirl
(45° Swirl Vanes)

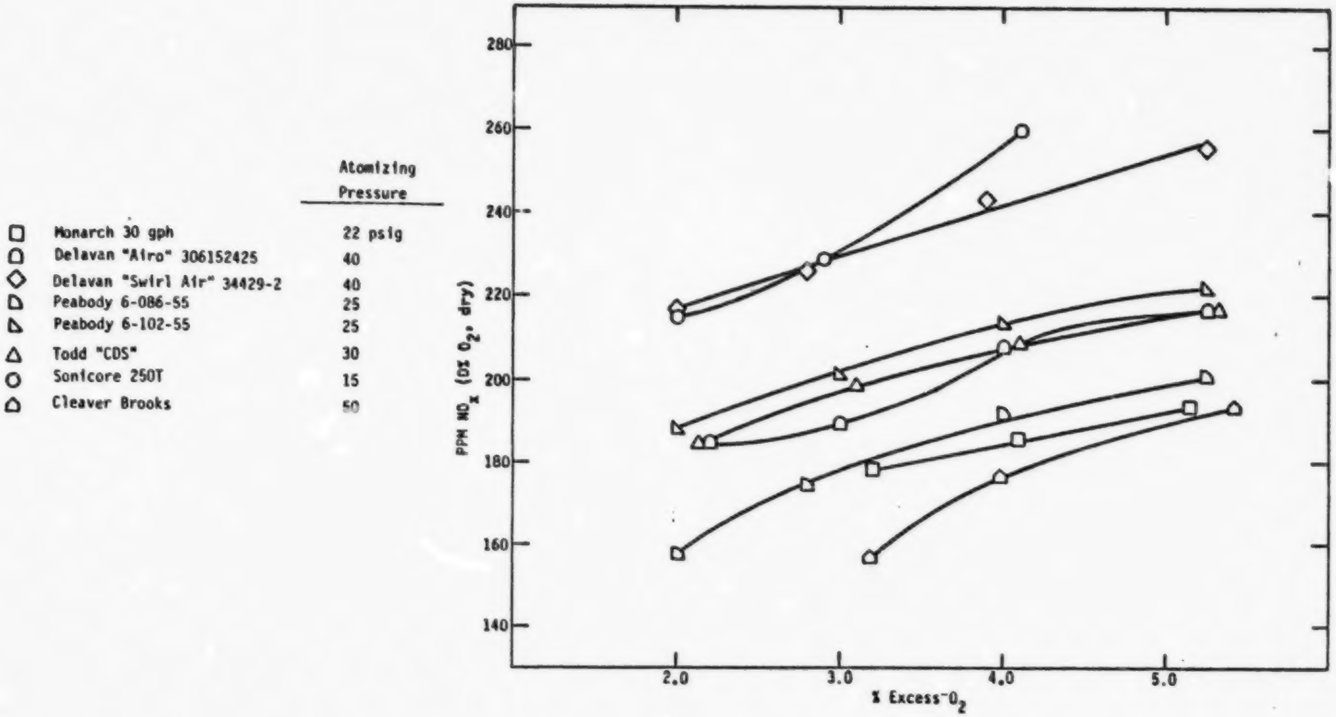

Figure 5-65. Effect of Atomizer with Strong Swirl.

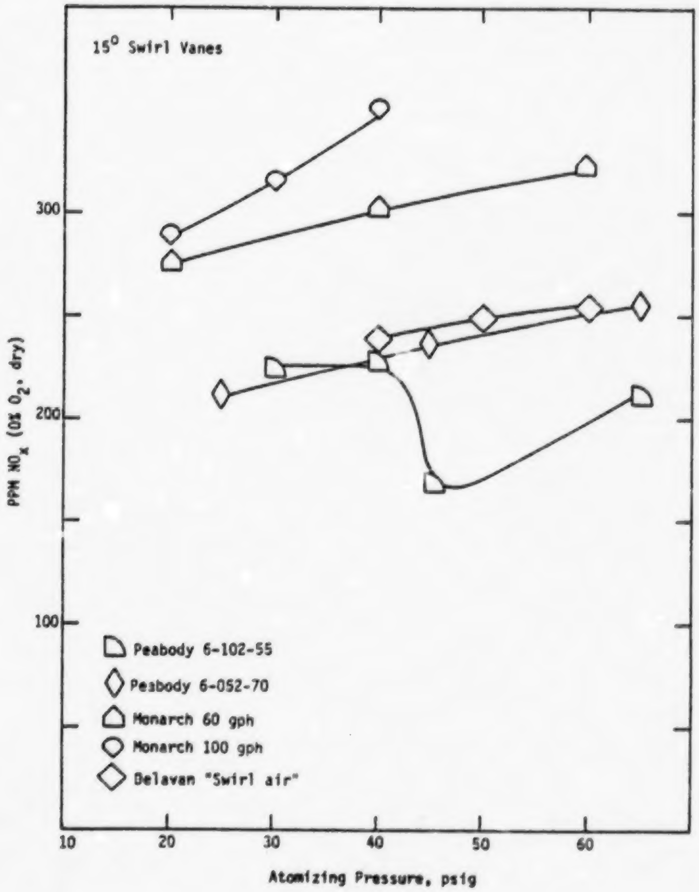

Figure 5-66. Effect of Atomizing Pressure - Weak Swirl.

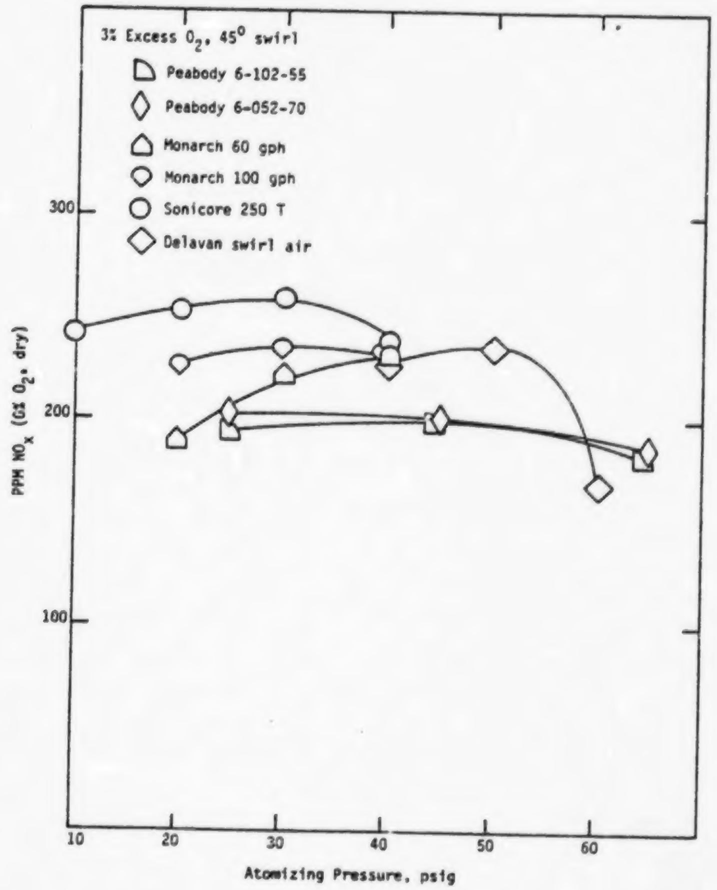

Figure 5-67. Effect of Atomizing Pressure - Strong Swirl.

swirling case. For most of the atomizers tested, atomizing air pressure did not appear to have a very significant influence on NO_x emissions. Figure 5-68 shows NO_x versus atomizing pressure for seven of the atomizers in a flow field produced with medium swirl. NO_x emissions did not vary significantly with atomizing air pressure for those atomizers shown with the exception of the 6.3 liter/minute (100 gph) Monarch nozzle. Figures 5-69 and 5-70 show the influence of swirl level and atomizing air pressure upon NO_x emission for the Todd "CDS" atomizer and the intensity of swirl has a much more significant influence on NO_x emission than atomizing air pressure for these two atomizers. A similar behavior was observed for most of the atomizers tested.

5.4.2.3 Effect of Swirl

The effect of atomizer design is strongly dependent upon the level of combustion air swirl. Figure 5-71 illustrates the extent to which swirl level affected NO_x emissions produced by the various atomizers. The weakly swirling flow field (15-degree vanes) resulted in the widest range of emission. The range of emission for the intermediate strength and strong swirl cases was approximately half that for the weak swirl case. The 45-degree swirl vanes produced a slightly narrower range than the 30-degree swirl vanes. It should be noted that the same minimum level of NO_x could be achieved at each swirl level by using the appropriate atomizer.

In Figure 5-72, NO_x emissions versus excess O_2 for a Delavan "Airo" atomizer are cross-plotted as a function of swirl. Variations in atomizing air pressure produced little effect with this atomizer, but changing the level of swirl changed NO_x emissions by nearly a factor of two. In this case, the 30-degree swirl vane produced the lowest emissions. However, with the Sonicore atomizer (Figure 5-73), the 45-degree case produced lower NO_x emissions. Figures 5-74 to 5-77 illustrate similar results for other atomizers. In general, an increase in swirl from $S = 0.2$ to $S = 0.45$ produced a significant decrease in NO_x emissions; however, a further increase to $S = 0.79$ produced only slight changes.

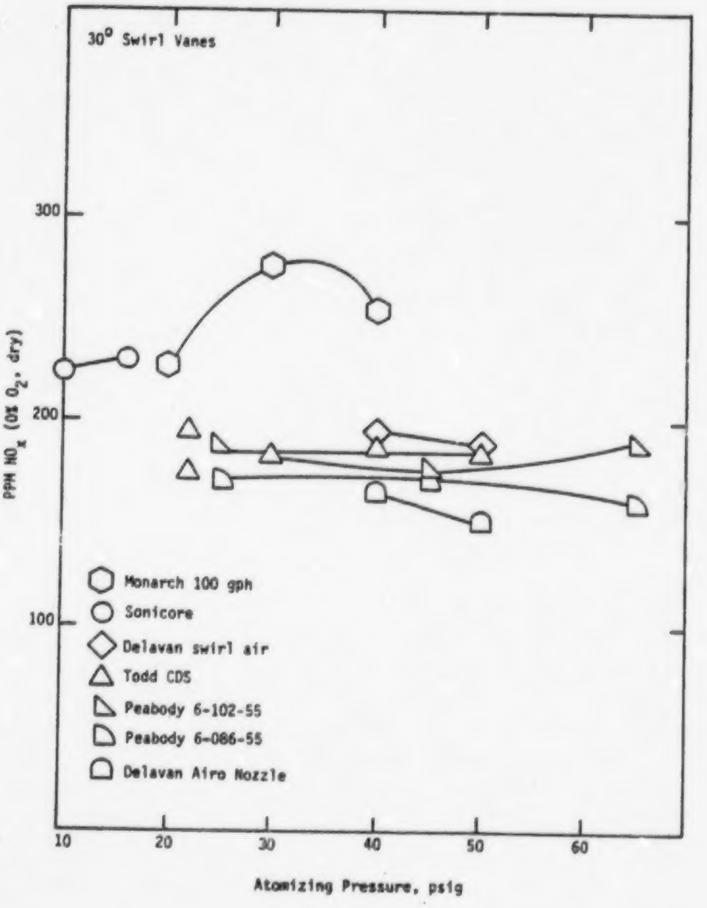

Figure 5-68. Effect of Atomizing Pressure - Intermediate Swirl.

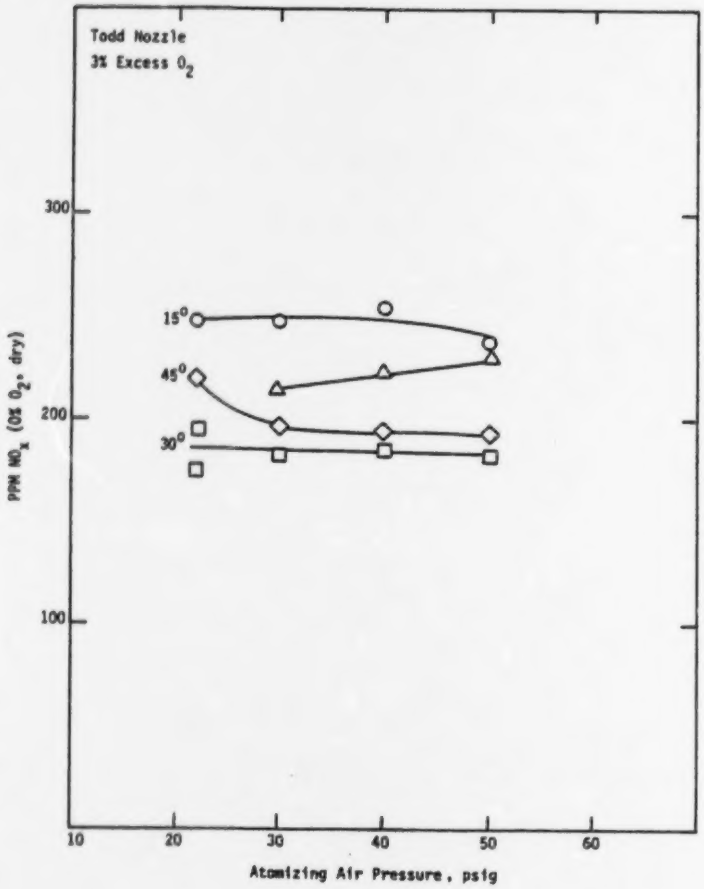

Figure 5-69. Effect of Atomizing Pressure - Todd CDS Atomizer.

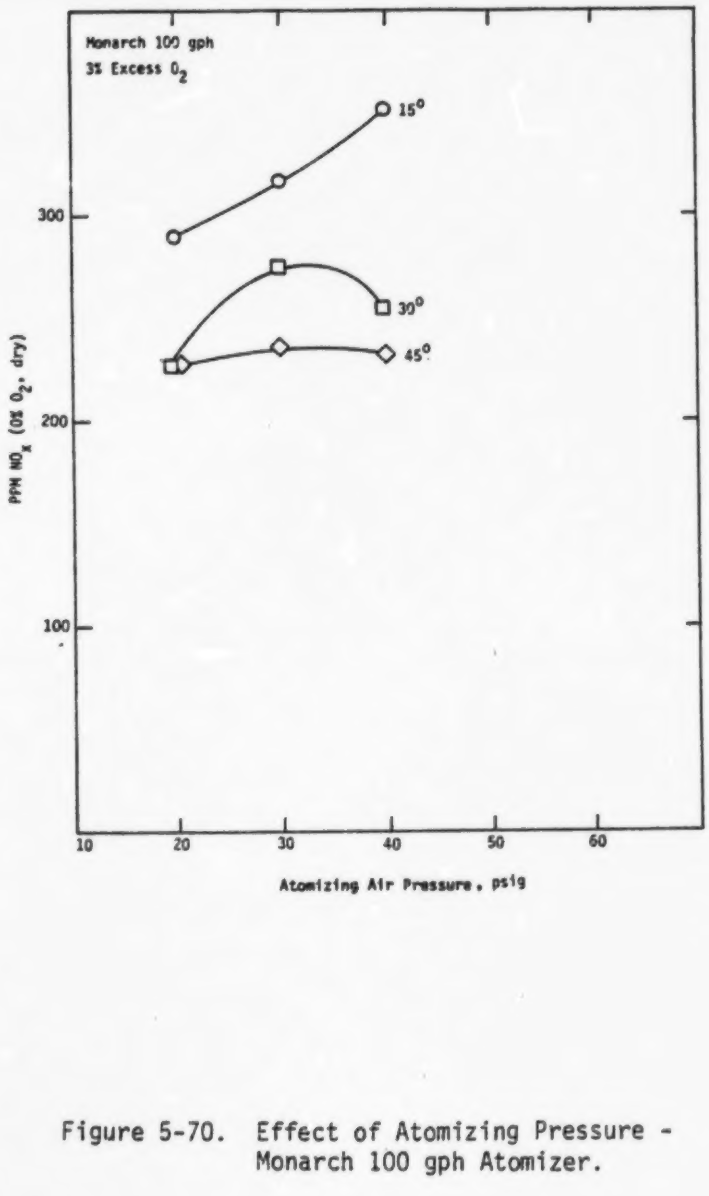

Figure 5-70. Effect of Atomizing Pressure - Monarch 100 gph Atomizer.

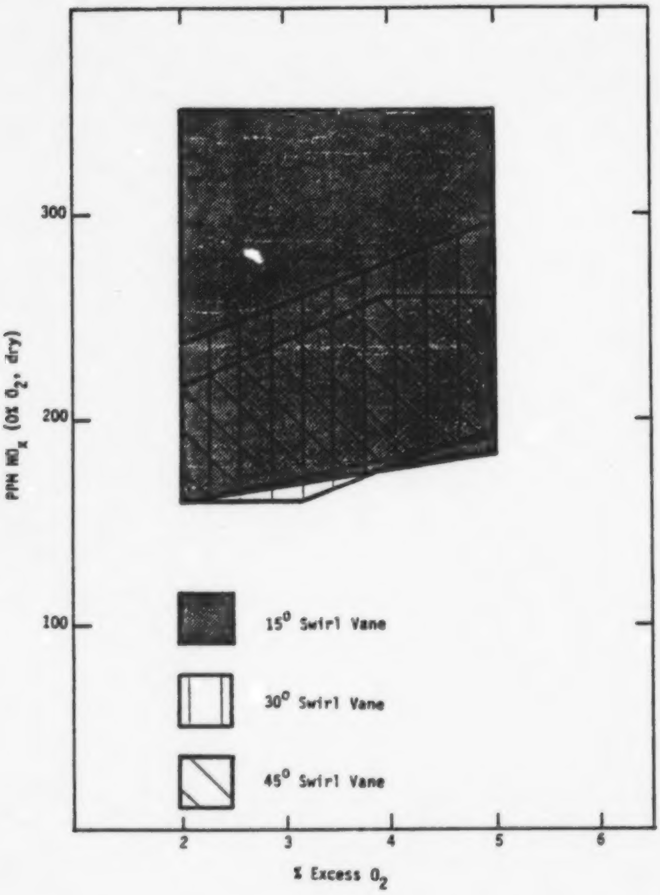

Figure 5-71. Effect of Swirl Upon NO_x Emissions.

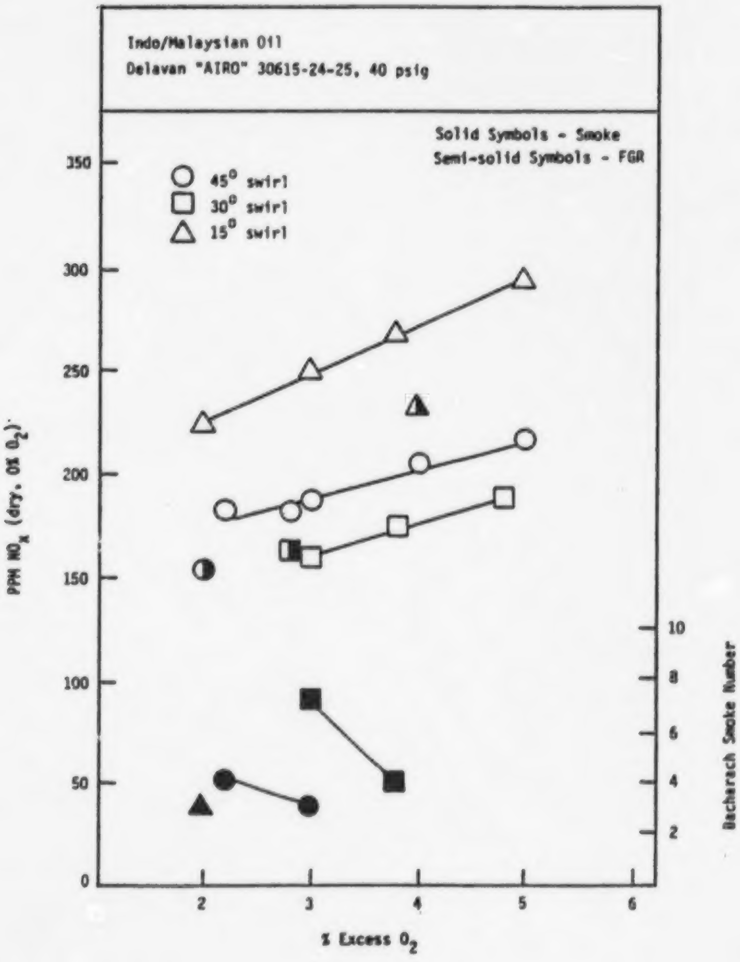

Figure 5-72. Effect of Swirl - Delavan "Airo" Atomizer.

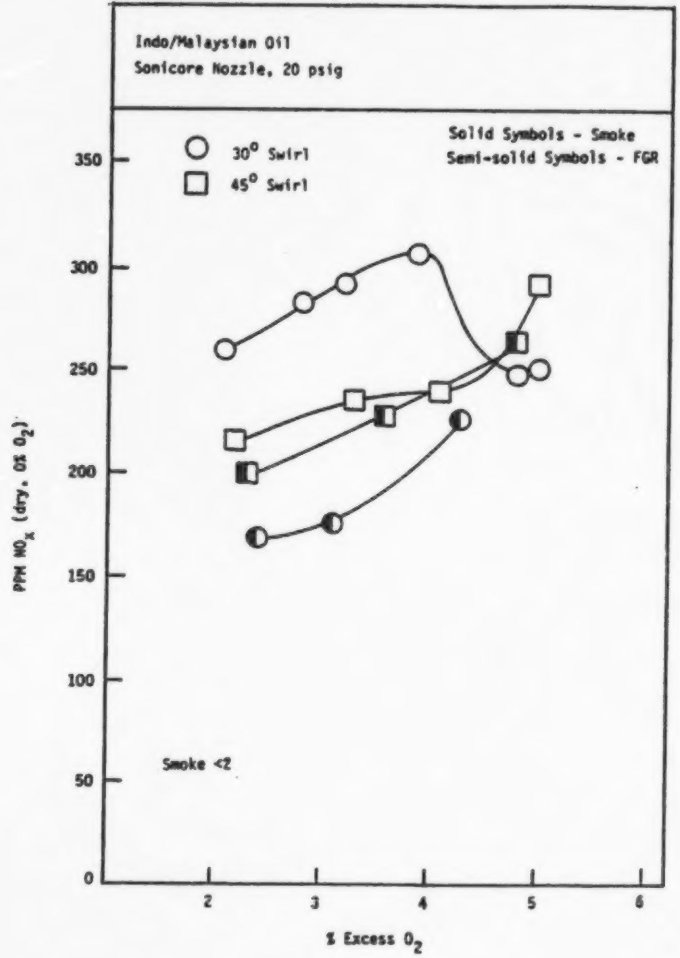

Figure 5-73. Effect of Swirl - Sonicore 250T Atomizer.

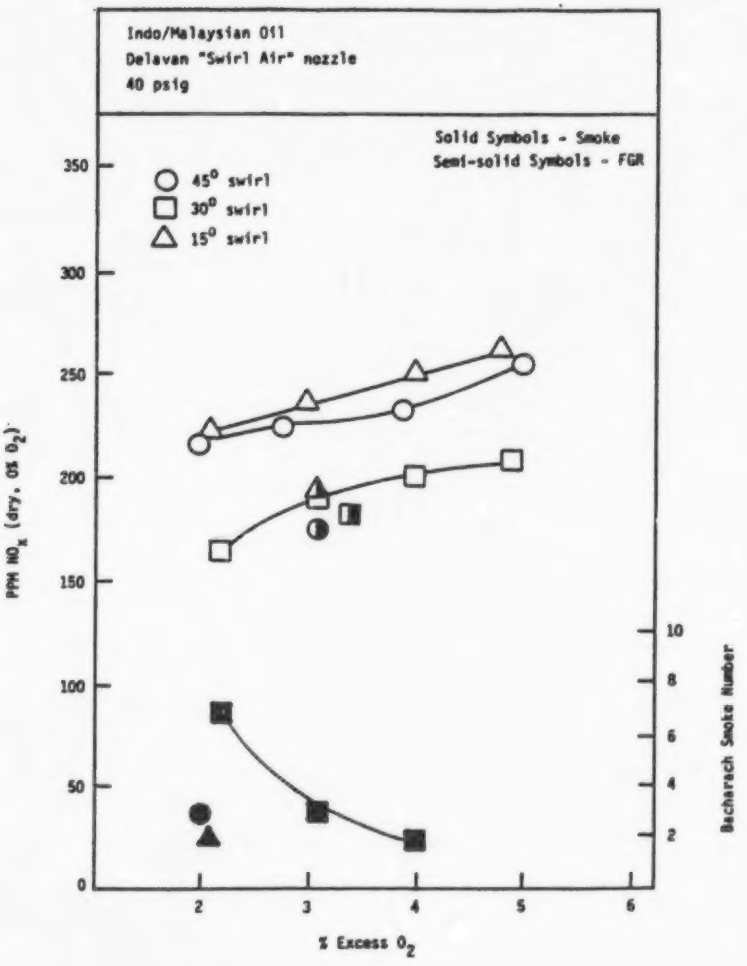

Figure 5-74. Effect of Swirl - Delavan "Swirl Air" Atomizer.

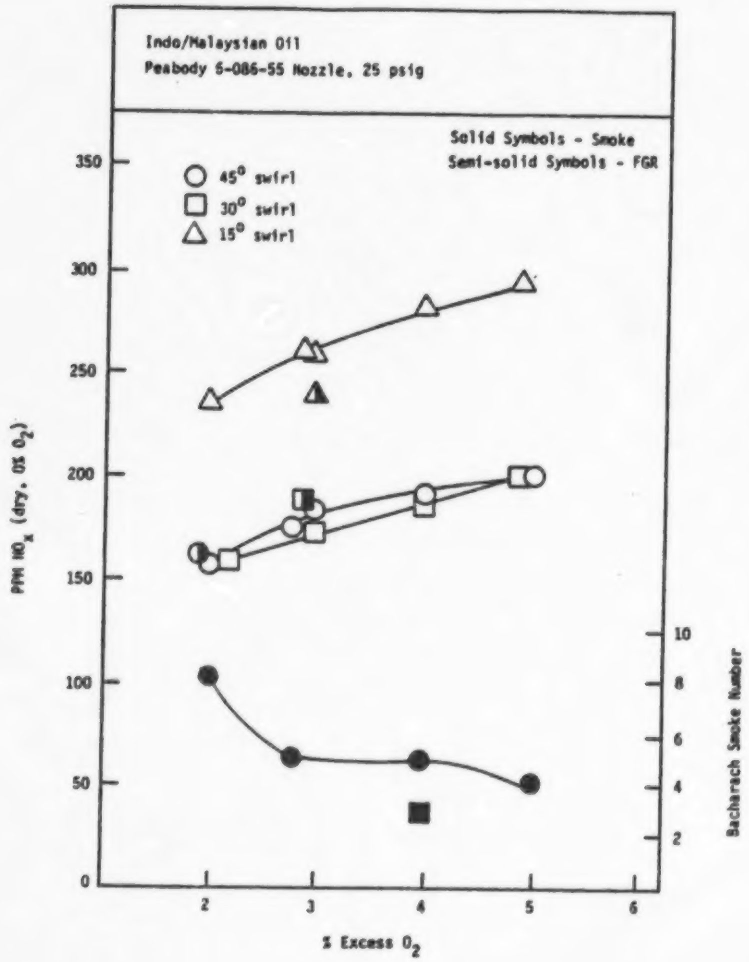

Figure 5-75. Effect of Swirl with Peabody 6-086-55 Atomizer.

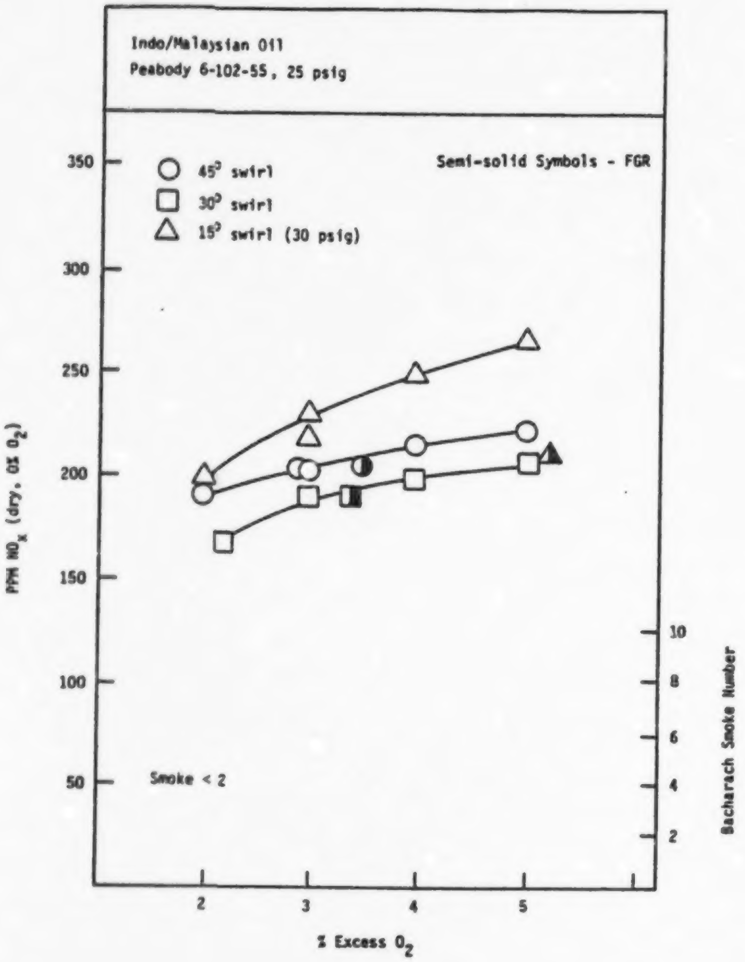

Figure 5-76. Effect of Swirl with Peabody 6-102-55 Atomizer.

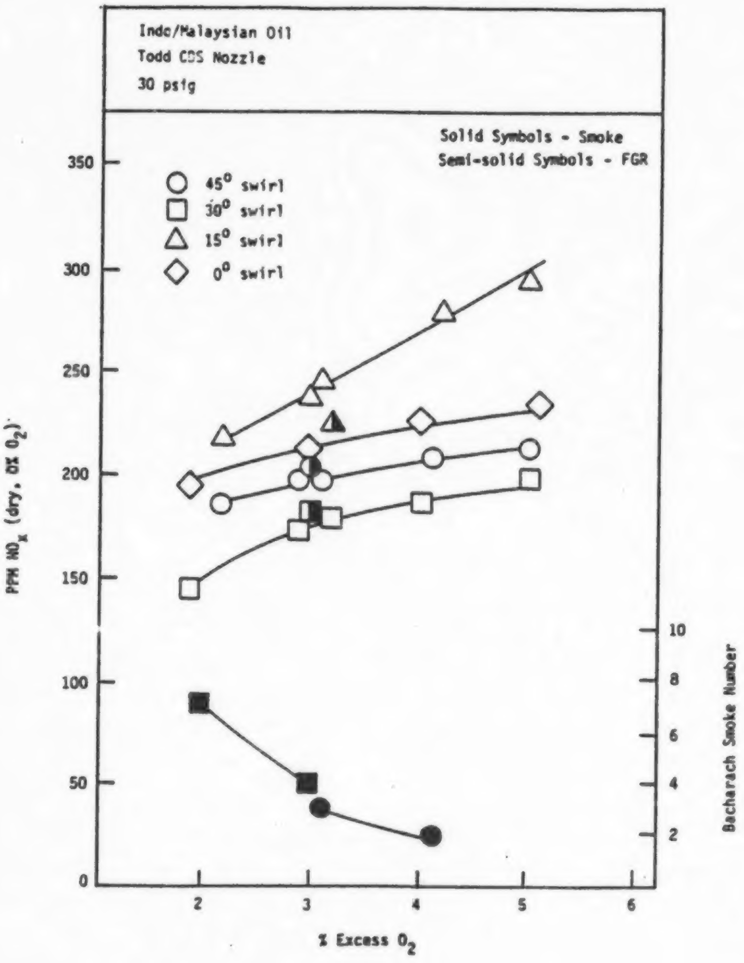

Figure 5-77. Effect of Swirl with Todd CDS Atomizer.

The influence of swirl level upon smoke emissions is illustrated in Figure 5-78. The range of smoke emissions for all the atomizers tested is summarized as a function of swirl level, and in general, the range of Bacharach Smoke Number increased with increasing swirl level. This is opposite to the trend observed for NO_x emissions presented in Figure 5-71.

5.4.2.4 Effect of Flue Gas Recirculation

In these studies the effectiveness of FGR was used to assess the influence of atomizer type and flow field upon thermal NO_x formation. For some atomizer-pressure-flow field combinations the application of FGR produced a flame which was unstable or excessively smokey, and therefore, data was not obtained at such unsuitable conditions. The amount of flue gases recirculated was also dependent upon these factors. For most of the data shown, 12 to 24 percent FGR was possible. Temperature of the cooled flue products was 79 to 104°C.

FGR produced no significant reduction of NO_x for most of the conditions tested. In some cases FGR produced higher emissions than the baseline case, attributable to increased fuel NO formation because of an increase in mixing intensity. FGR did not produce NO_x levels below the lowest level possible without FGR. Figure 5-79 illustrates NO_x levels achieved from five atomizers at two swirl levels with between 17 to 23 percent recirculation of cooled flue products. This figure indicates that atomizer design and swirl level essentially govern NO_x emissions even when FGR is applied. NO_x emissions were significantly reduced by FGR only in the case of the weakly swirling flow field, which produced relatively high emissions with most atomizers in the baseline case. FGR resulted in no significant NO_x reduction for the medium swirl case.

FGR is generally most effective when thermal NO_x accounts for a large portion of the total NO_x emissions. With nitrogen-containing residual fuels this is not generally the case, and in fact, the insensitivity of NO_x emissions to FGR and relatively cold walls of the combustor suggest that fuel NO_x accounts primarily for NO_x emissions at the lower emission range shown in Figure 5-79.

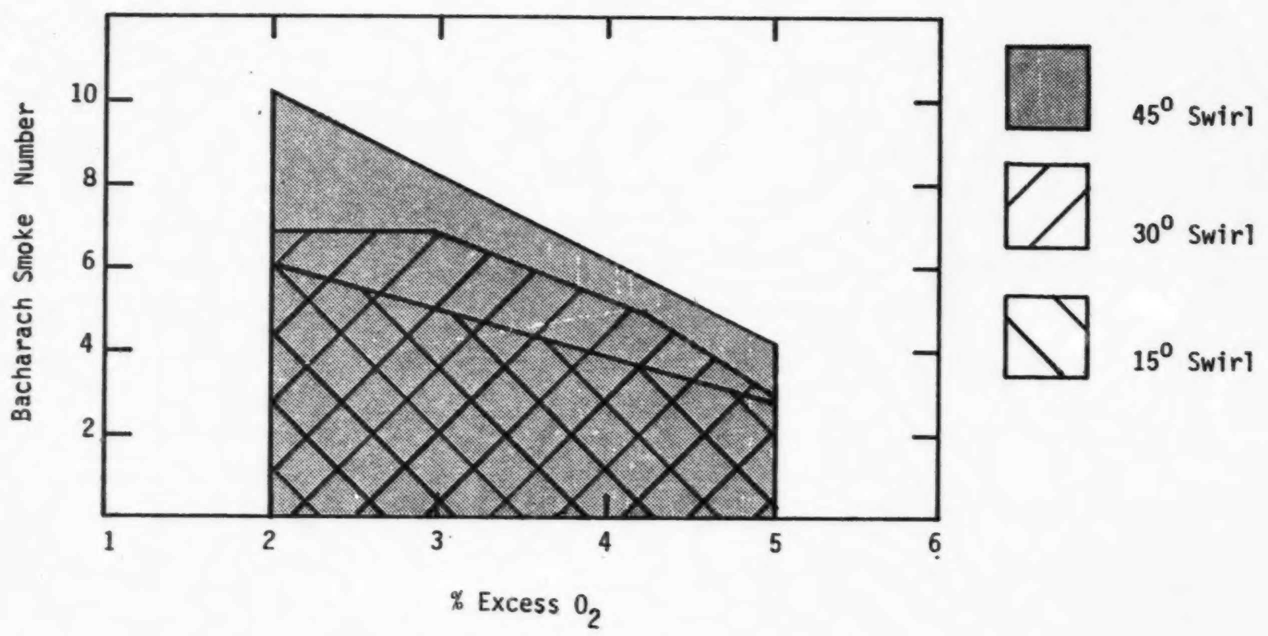

Figure 5-78. Effect of Swirl Upon Bacharach Smoke Number.

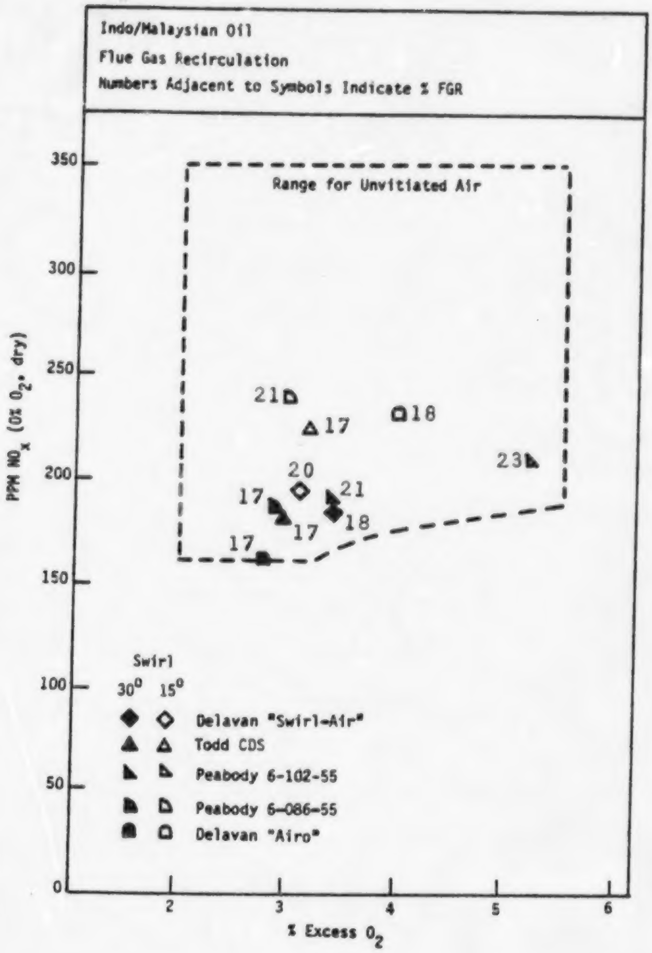

Figure 5-79. Effect of Flue Gas Recirculation.

Fuel NO_x formation in the hot, refractory-walled bench-scale furnace from the same fuel was 270 ppm. The similarity of total NO_x in the firetube simulator to fuel NO_x in the bench-scale furnace, albeit somewhat fortuitous, provides evidence that fuel NO_x accounts for most of the total NO_x from the firetube simulator, since the conversion of fuel nitrogen to NO_x is believed to be relatively insensitive to temperature. (see Figure 4-56)

5.4.2.5 Summary — Atomizer Flow Field Interaction Studies

The conclusions from the various atomizer screening studies are:

- Different atomizers produced different levels of NO_x and smoke emissions; some were strongly affected by swirl.
- Atomizer type and amount of swirl can be optimized to reduce NO_x emissions.
- Atomizer type had the greatest influence on NO_x emissions with weak swirl and the least influence with strong swirl; strong swirl produced the lowest NO_x emissions.
- Varying atomizing air pressure did not strongly affect NO_x emissions; pressure had the greatest effect with weak swirl.
- Minimum NO_x emissions from the optimum atomizer/flow field combination could not be further reduced by flue gas recirculation.

5.4.3 Fuel Composition Effects

The second series of investigations in the Phase II tests involved a comparison of NO_x emissions resulting from firing a range of residual fuels with a variety of atomizers. Excess oxygen was varied from two to five percent for each of the test conditions summarized in Table 5-2. Five oils were selected for this study with nitrogen content ranging from 0.18 to 0.77 percent, and a variation in API gravity of 21.8 to 13.2°. In addition, a shale-derived diesel fuel marine (DFM - 0.24 percent N, 33.1° API) and a crude Paraho shale oil (2.1 percent N, 20.3° API), were selected for limited testing to investigate the behavior of alternate fuels in practical

Table 5-2. Test Matrix for Fuel Composition Effects Test Series

Fuel	API Gravity	%N	Monarch 30 gph (25 psig)	Swirl Vane Angle, Degrees		Sonicore 250T (20 psig)†
				Peabody (25 psig)† 6-086-55	Todd CDS (50 psig)†	
Alaskan (Diesel)	33.1	0.007	0*	--	--	0*
Middle Eastern	19.8	0.18	30, 45	30, 45	30, 45	30, 45
Indonesian/ Malaysian	21.8	0.24	30 (30 psi)†	30, 45**	30, 45**	30, 45
DFM	33.1	0.24	--	30, 45	30, 45	--
Gulf Coast	13.2	0.36	--	--	--	30,45
Alaskan (Bunker C)	15.6	0.51	30, 45	30, 45	30, 45	30, 45
California No. 2	15.4	0.77	30, 45	30, 45	30, 45	30, 45
Crude Shale		2.10	0	--	--	0 (15 psi)†

*Data at 3 percent O_2 only - from staged combustion studies

**From atomizer/flow field screening.

†kPa = (psig + 14.7)(6.895)

combustion systems. A nitrogen-free distillate oil (Alaskan diesel - 0.007 percent N, 33.1°) was also selected to estimate thermal NO_x emission under typical experimental conditions. The results of these tests are presented graphically in Figures 5-80 to 5-96.

5.4.3.1 Effect of Fuel Nitrogen

NO_x emissions from industrial boilers are strongly dependent upon the composition of the fuel, particularly with respect to fuel nitrogen content. In these studies NO_x emissions were found to increase with increasing fuel nitrogen content in both the argon furnace and in the firetube simulator. However, the absolute level of NO_x and the dependence upon excess air was strongly influenced by swirl and by atomizer. For instance, NO_x emissions from the Sonicore atomizer (Figure 5-97) were lower with the 45-degree swirl vanes than with the 30-degree swirl vanes for each of the five fuels tested with the exception of the Middle Eastern oil. These data are plotted as a function of fuel nitrogen content, at constant excess O_2 of five percent, in Figure 5-98. For each of the two swirl levels investigated, NO_x emissions rose approximately linearly with fuel nitrogen content. However, the slope of the relationship changed with swirl level, from 572 ppm NO_x/percent N for the S=0.45 to 305 ppm NO_x/percent N for the S=0.79. This difference can be attributed to variations in fuel/air contacting causing more fuel to burn initially under oxygen-deficient conditions at the higher swirl level due to increased recirculation of burned gases. The high swirl condition will also tend to produce fuel-rich conditions in the central region of the flame which will result in reduced conversion of fuel nitrogen to NO_x.

An estimate of the contribution of thermal NO_x to total emissions can be made by extrapolating the curves of Figure 5-98 through zero percent nitrogen. For both swirl vane angels, the extrapolated curves intercept the ordinate at approximately 158 to 174 ppm NO_x. The implication from this is that the difference between the two curves is attributable to differences in the conversion of fuel-bound nitrogen to NO_x rather than differences in thermal NO_x, and emphasizes the potential for controlled-mixing burners to reduce NO_x emissions from system firing high-nitrogen residual fuels. It should not be concluded that thermal NO_x production deduced in this way represents an absolute value, only that these levels are representative of those due to thermal fixation since it is possible that the presence of fuel nitrogen species affects thermal fixation.

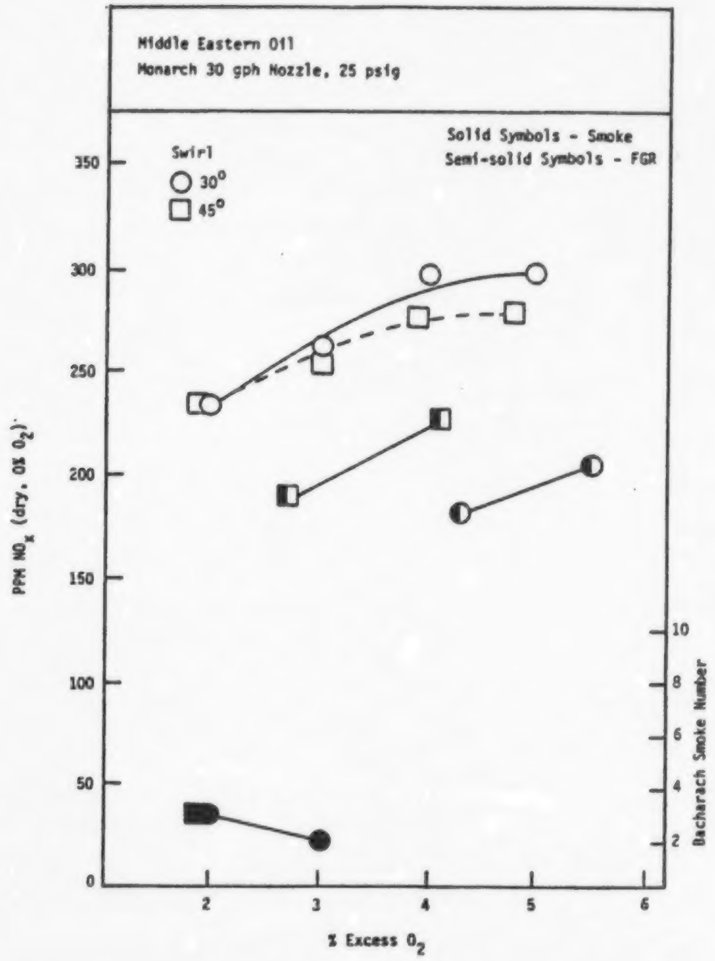

Figure 5-80. Fuel Composition Studies - Middle Eastern Oil with Monarch Atomizers.

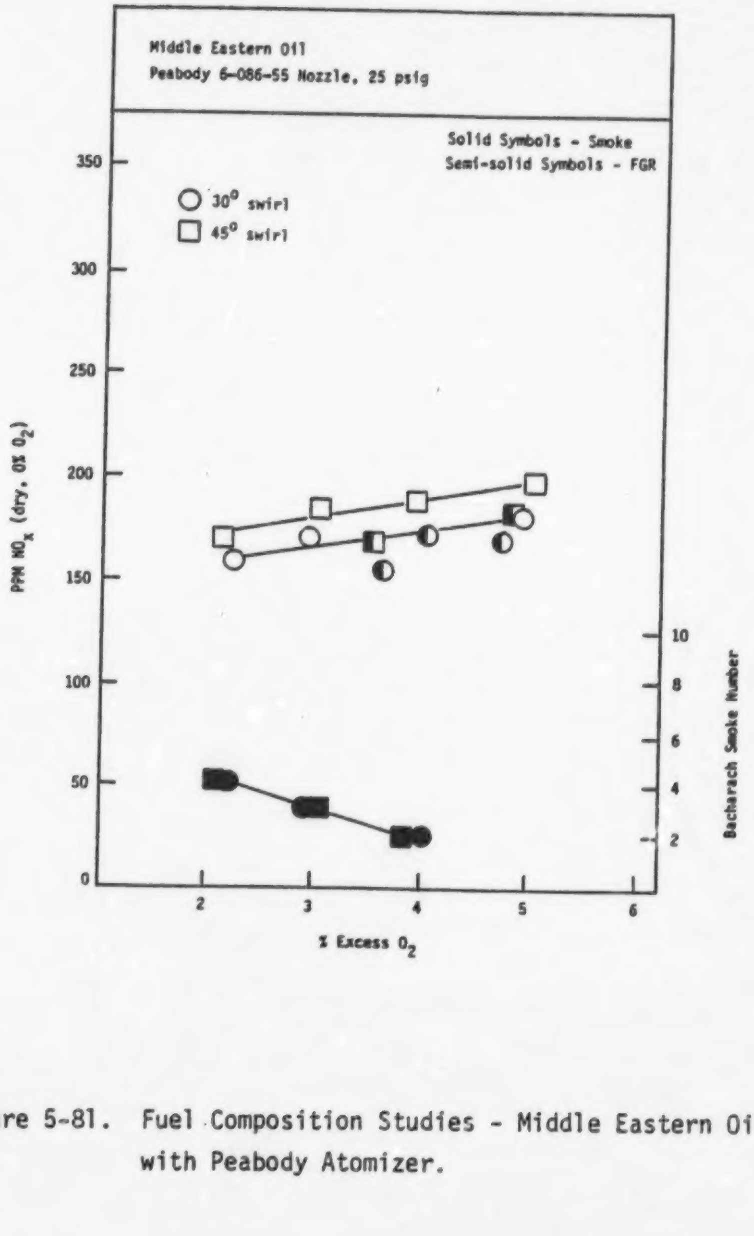

Figure 5-81. Fuel Composition Studies - Middle Eastern Oil with Peabody Atomizer.

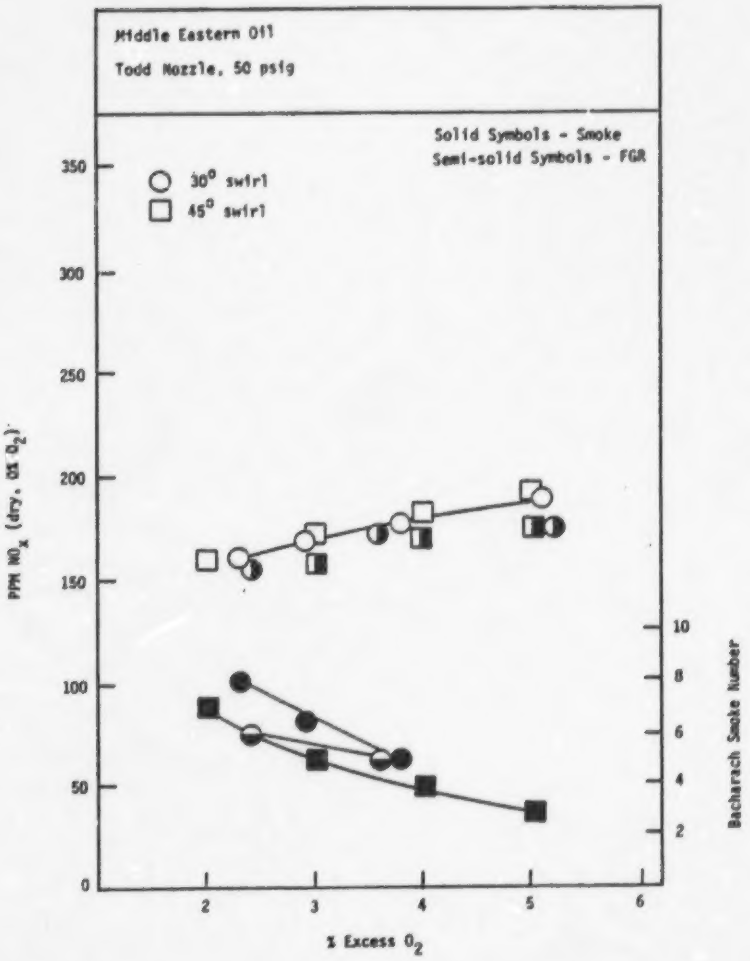

Figure 5-82. Fuel Composition Studies - Middle Eastern Oil with Todd Atomizer.

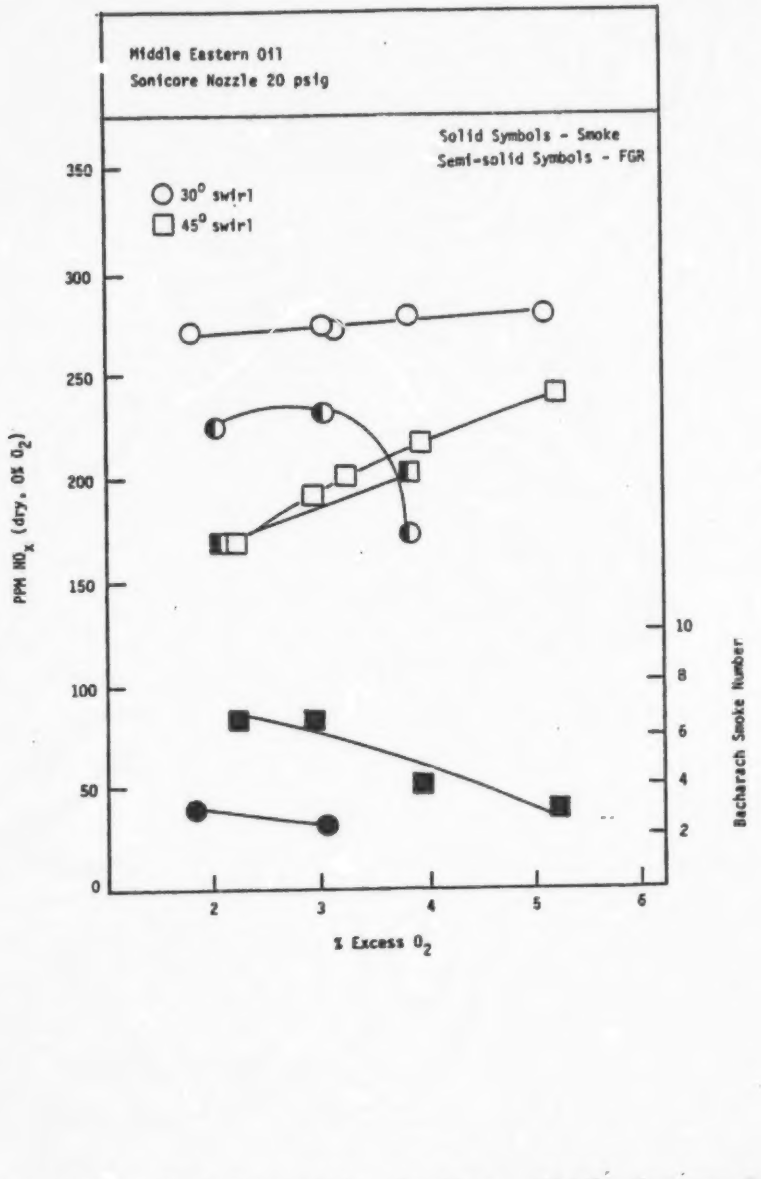

Figure 5-83. Fuel Composition Studies - Middle Eastern Oil with Sonicore Atomizers.

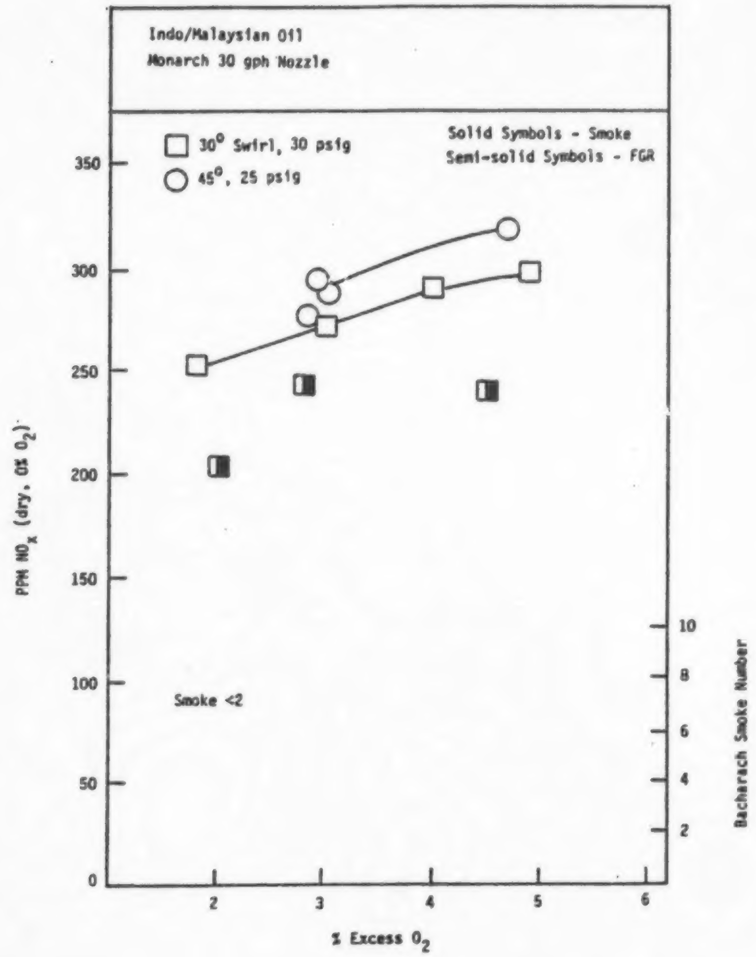

Figure 5-84. Fuel Composition Studies - Indo/Malaysian Oil with Monarch Atomizer.

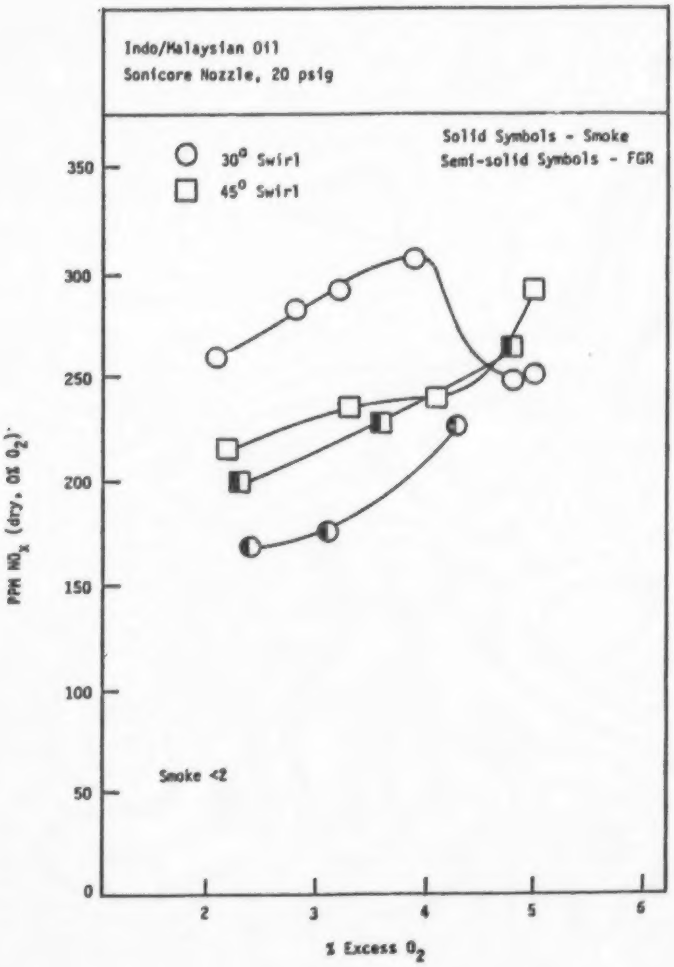

Figure 5-85. Fuel Composition Studies - Indo/Malaysian Oil with Sonicore Atomizer.

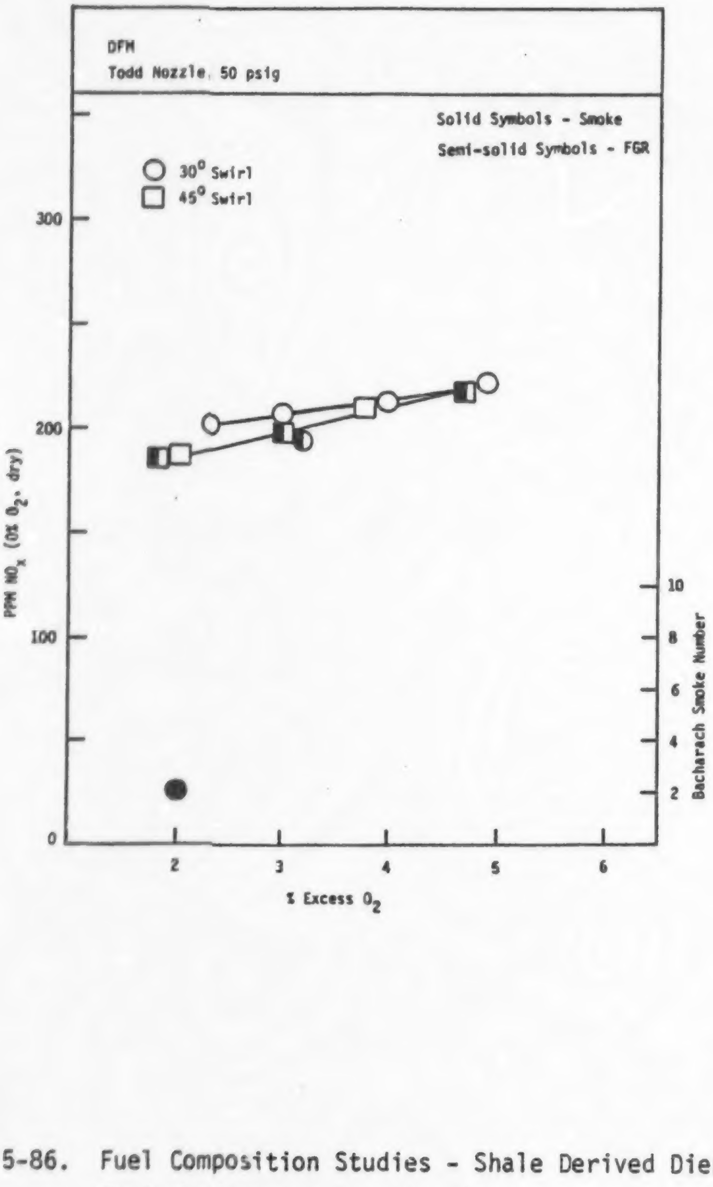

Figure 5-86. Fuel Composition Studies - Shale Derived Diesel Fuel Marine with Todd Atomizer.

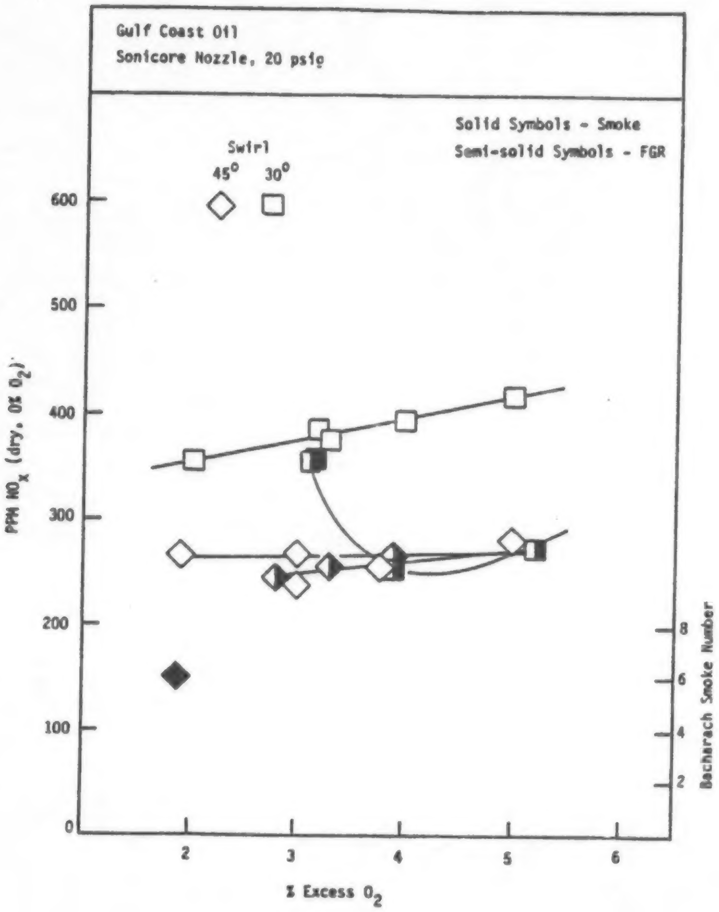

Figure 5-87. Fuel Composition Studies - Gulf Coast Oil with Sonicore Atomizers.

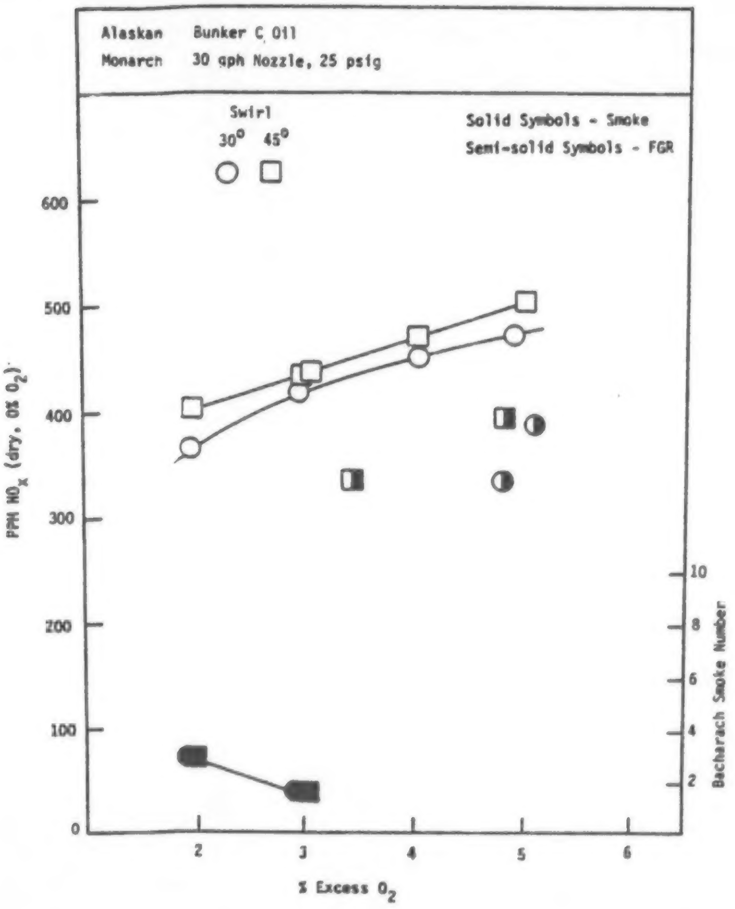

Figure 5-88. Fuel Composition Studies - Alaskan Bunker C Oil with Monarch Atomizer.

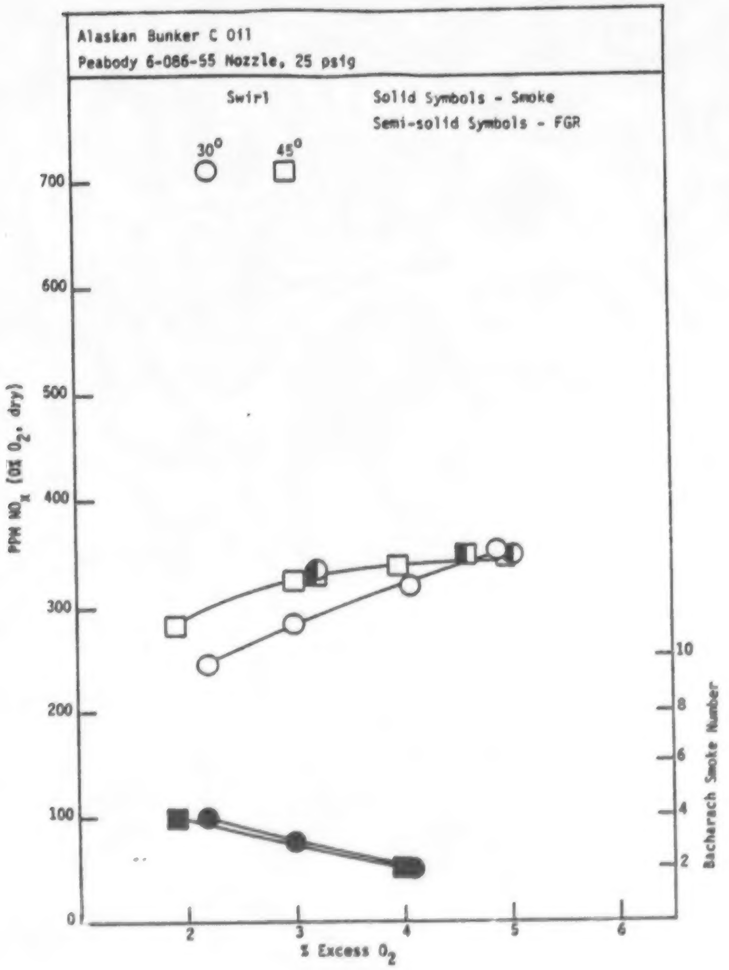

Figure 5-89. Fuel Composition Studies - Alaskan Bunker C Oil with Peabody Atomizers.

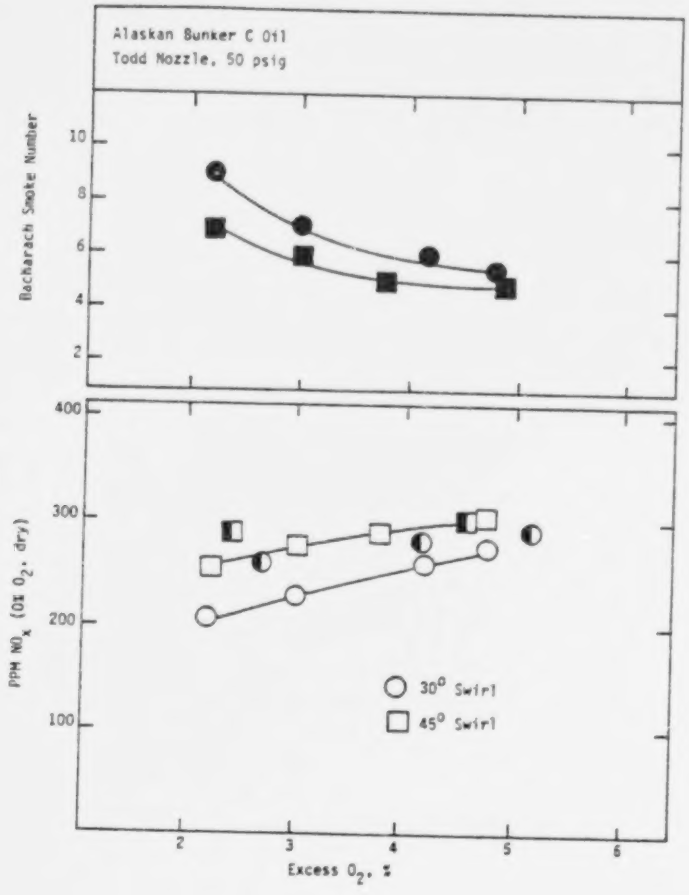

Figure 5-90. Fuel Composition Studies - Alaskan Bunker C Oil with Todd Atomizers.

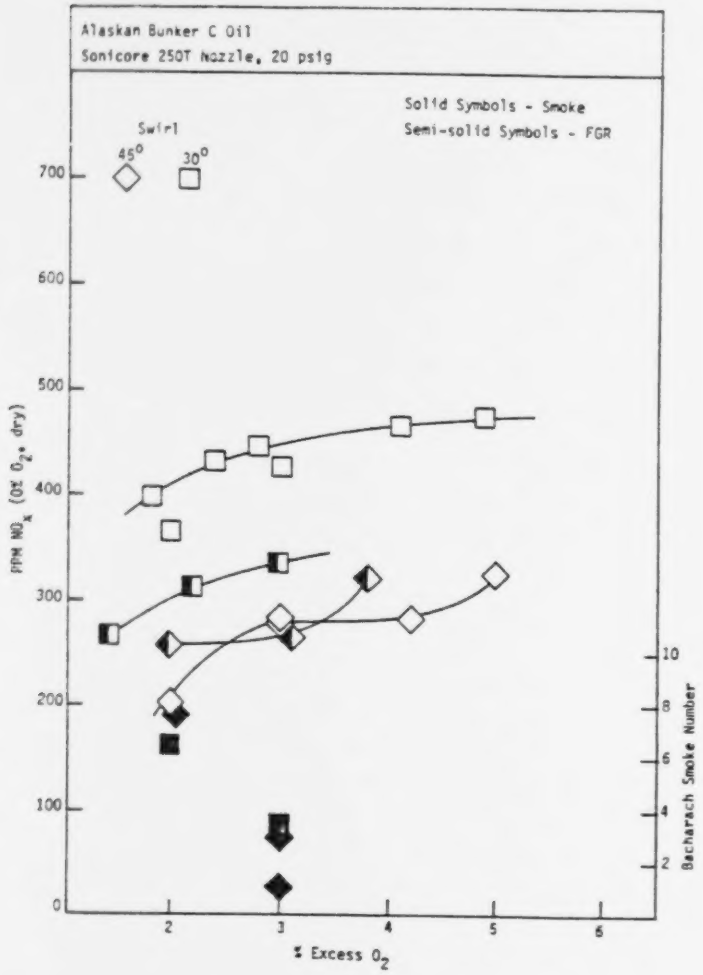

Figure 5-91. Fuel Composition Studies - Alaskan Bunker C Oil with Sonicore Atomizers.

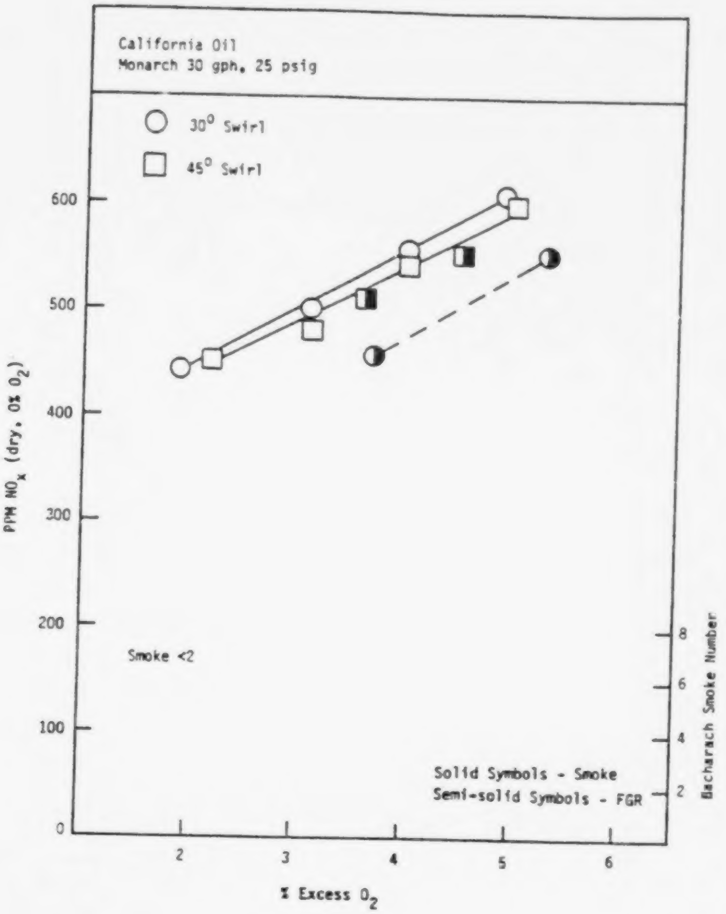

Figure 5-92. Fuel Composition Studies - California Oil with Monarch Atomizers.

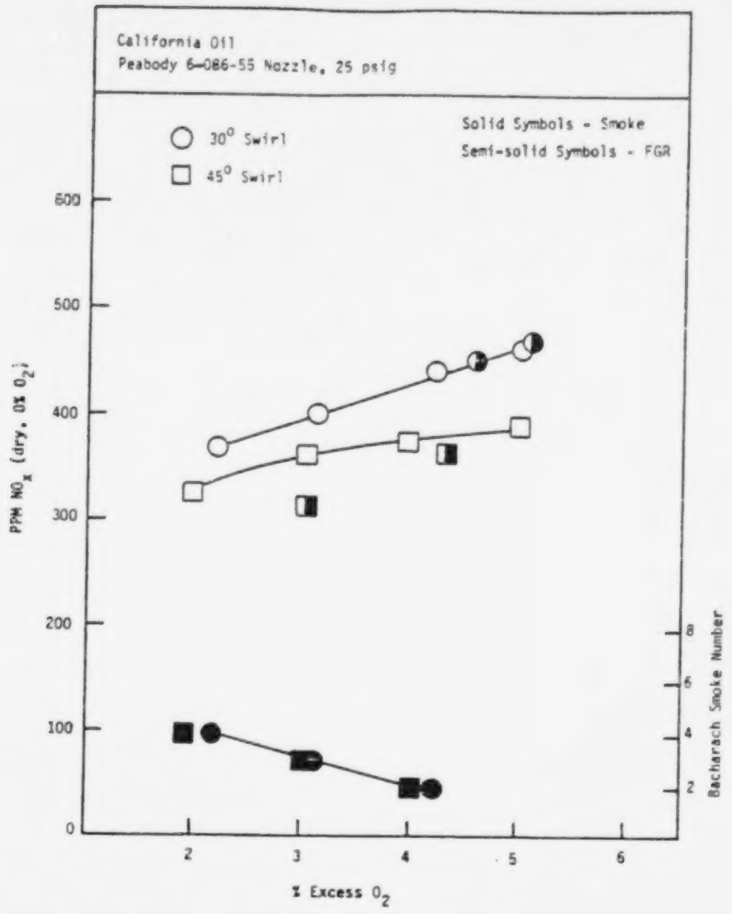

Figure 5-93. Fuel Composition Studies - California Oil with Peabody Atomizers.

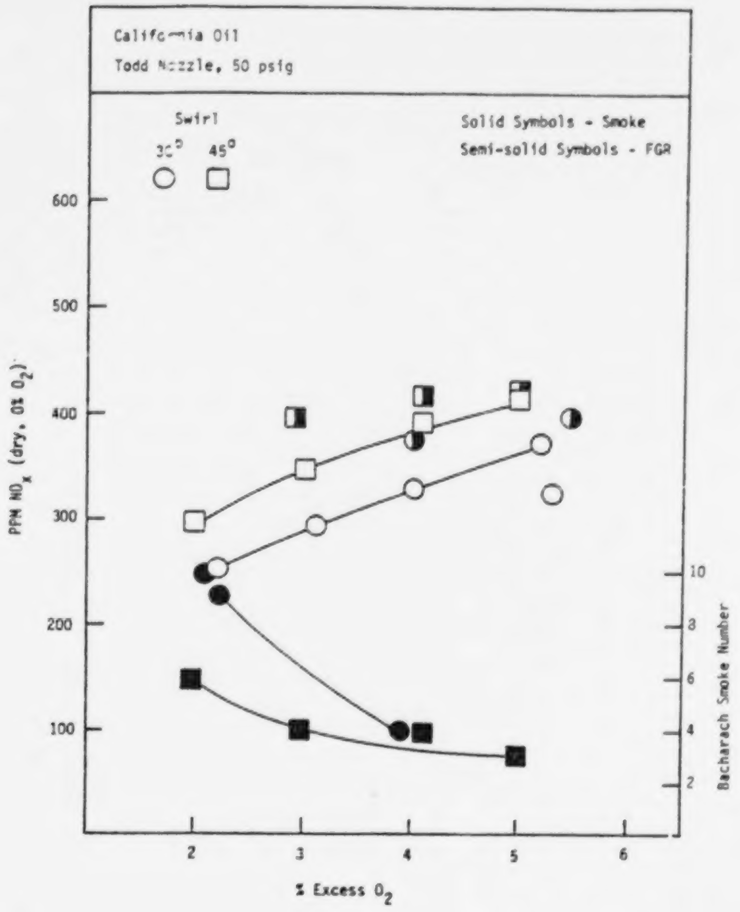

Figure 5-94. Fuel Composition Studies - California Oil with Todd Atomizer.

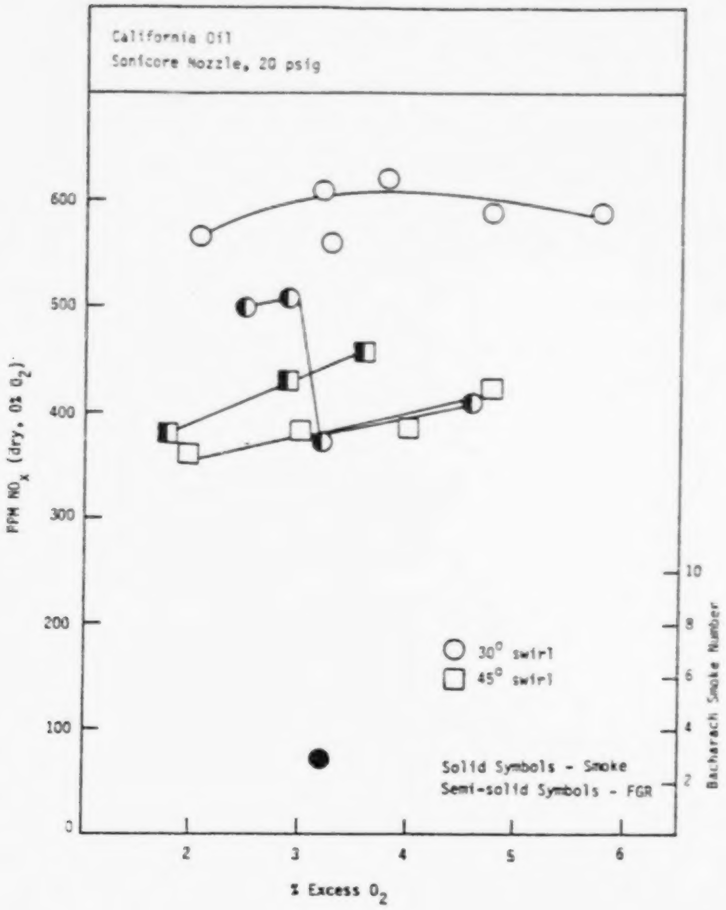

Figure 5-95. Fuel Composition Studies - California Oil with Sonicore Atomizers.

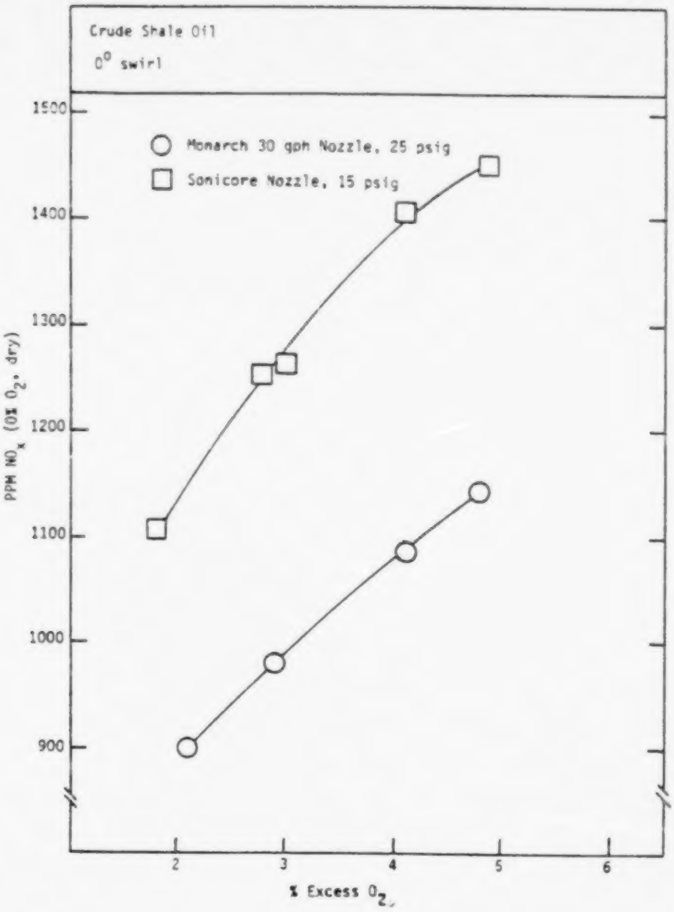

Figure 5-96. Fuel Composition Studies - Parho Process Shale Oil with Sonicore and Monarch Atomizers.

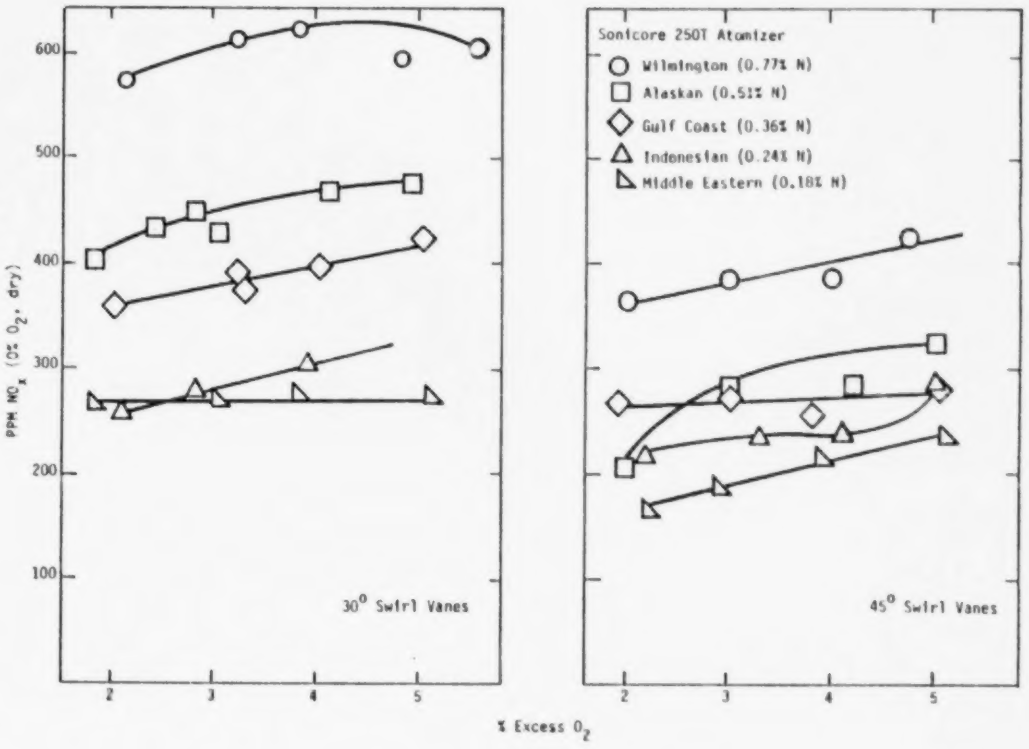

Figure 5-97. Effect of Fuel Type on NO_x Emissions.

NO_x emissions from a nitrogen-free fuel can be attributed solely to the oxidation of molecular nitrogen. A distillate diesel fuel from the Alaskan North Slope was burned in the firetube simulator to further estimate thermal NO_x emissions. One-hundred percent conversion of the fuel-bound nitrogen to NO_x will result in 11 ppm NO_x for this fuel. NO_x emissions at 16 percent excess air were 150 ppm with the Sonicore atomizer and no swirl in a slightly different combustion chamber configuration. (A short refractory liner was inserted downstream of the burner.) The difference between this level and that found by extrapolation of Figure 5-98 is slight and can be attributed to the differences in operating conditions.

A crude shale oil derived from the Paraho process was also burned in this configuration with both the Sonicore and Monarch atomizers (Figure 5-96). At 29 percent excess air (four percent O_2), NO_x emissions of 1400 ppm were observed with the Sonicore atomizer and no swirl. Figure 5-100 compares NO_x emission from the shale oil to that from the conventional residual petroleum fuels. NO_x emissions are approximately equal to that predicted from the trend observed for petroleum fuels based upon nitrogen content. This agreement may be somewhat fortuitous since the operating conditions of the burner were not exactly the same for the comparison. However, it illustrates that NO_x emissions from alternate liquid fuels can be expected to behave essentially the same way as conventional petroleum-derived fuels, and for a given combustor/flow field/atomizer combination, are dependent primarily upon fuel nitrogen content. This generalization is consistent with the results obtained in the bench-scale studies (Figure 4-47) where both total and fuel NO_x were found to be almost solely dependent upon fuel nitrogen content, regardless of the source of the fuel.

5.4.3.2 Effect of Atomizer Type

Studies with the baseline fuel demonstrated that under normal combustion conditions, NO_x emissions are dependent upon the atomizer design and the combustion airflow field. Figure 5-101 illustrates a similar influence of atomizer design and flow field for the other residual fuel oils. For each of the four atomizers NO_x emissions increased with increasing fuel

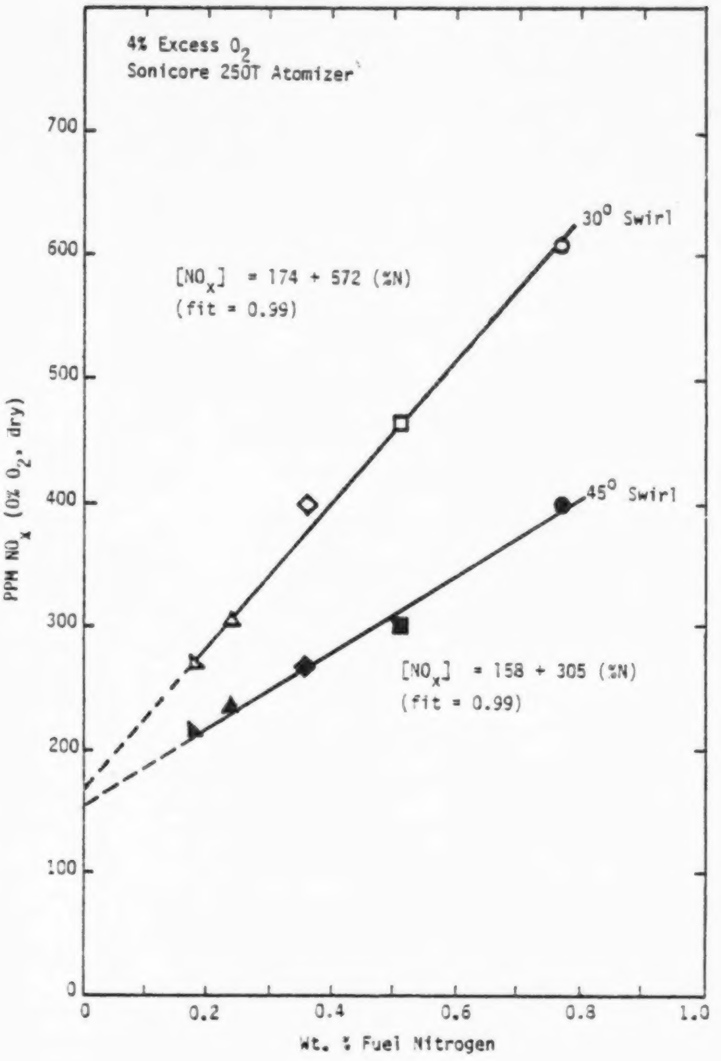

Figure 5-98. Effect of Fuel Nitrogen Content Petroleum Fuels.

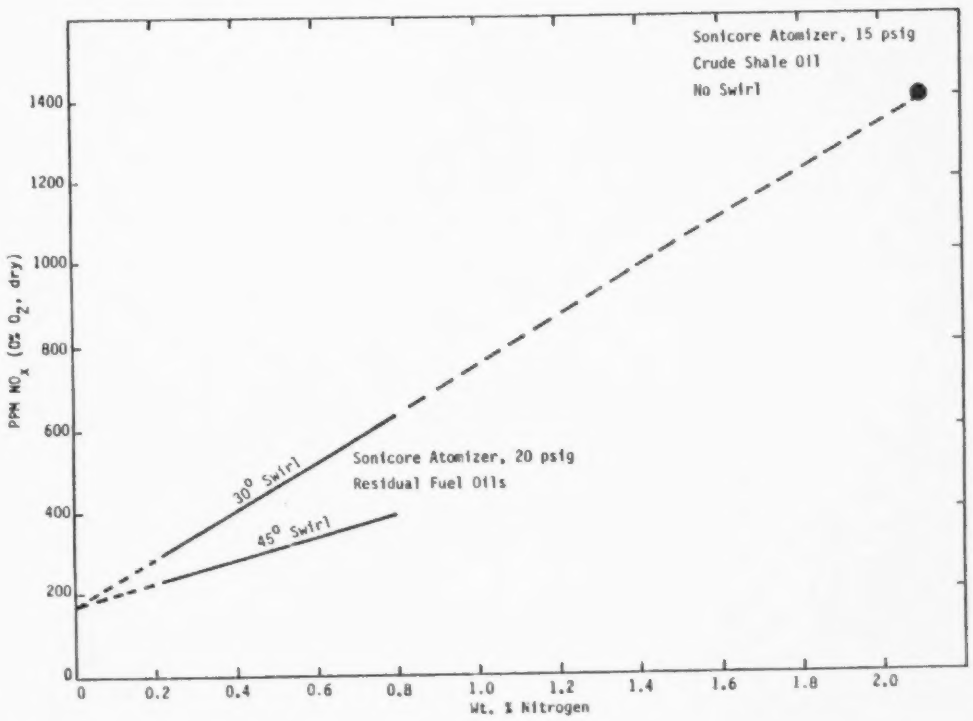

Figure 5-99. Effect of Fuel Nitrogen Content - Shale Derived Oil.

nitrogen content; however, the relationship is different for each atomizer and flow field condition. For example, the Sonicore and Monarch nozzle produced very similar dependencies of NO_x upon nitrogen content when using the 30-degree swirl vanes, but when using the 45-degree vanes the Sonicore atomizer produced much lower emissions, while the Monarch remained relatively unaffected. Extrapolation of each curve through zero percent nitrogen suggests each atomizer-flow field combination produced different amounts of thermal NO_x as well as fuel NO_x. In Figures 5-101 to 5-104, NO_x emissions versus swirl number are plotted as a function of atomizer for four residual fuel oils. With all four fuels the Sonicore appeared to be the most affected by changes in swirl and the Peabody the least affected. It can be seen that as the swirl level was increased:

- the Sonicore atomizer produced large decreases in NO_x emissions for every fuel tested;
- the Peabody atomizer produced small increases in NO_x except with the California oil;
- the Todd atomizer showed a moderate increase in NO_x emissions except with the Middle Eastern and Indonesian/Malaysian oils;
- the Monarch atomizer produced moderate decreases in NO_x except with the Alaskan and Indonesian/Malaysian oils.

It would be conjecture at this point to relate the exhaust NO_x emissions to particular atomizer characteristics and swirl level, given the complexity of the combustion field. However, each of these atomizers produced very different distributions of droplet size momentum, and trajectories which will influence local stoichiometries and mixing patterns, and hence, NO_x emissions. For instance, the Sonicore atomizer produces a very narrow distribution of fine droplets (~20 μm) which would be more easily entrained in the combustion airflow than would the larger droplets (~44 μm) produced by the Peabody atomizer. This could account for the apparent sensitivity of NO_x emissions to swirl which was observed with the Sonicore atomizer but not the Peabody.

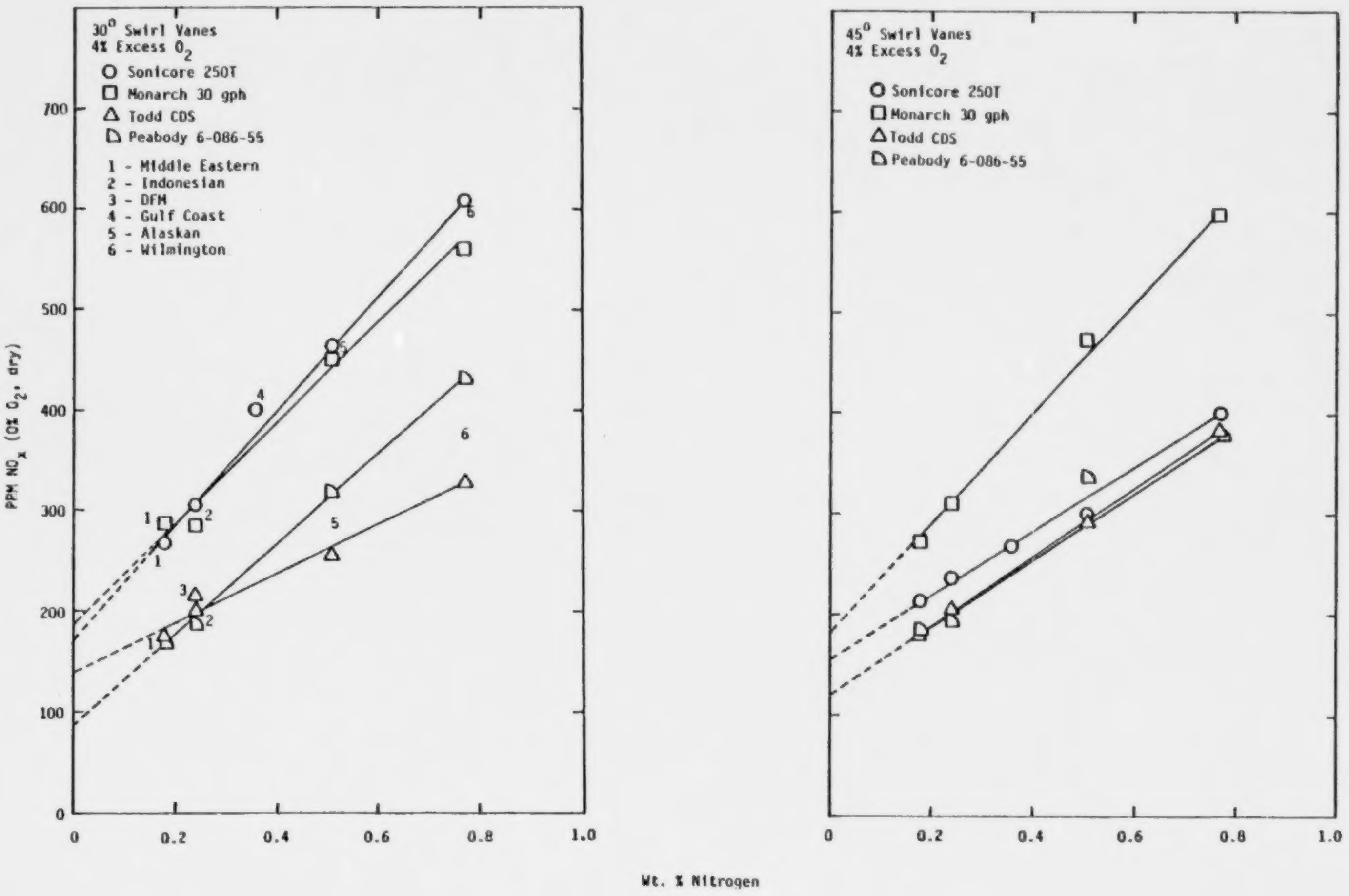

Figure 5-100. Effect of Swirl Upon Fuel Nitrogen Dependence.

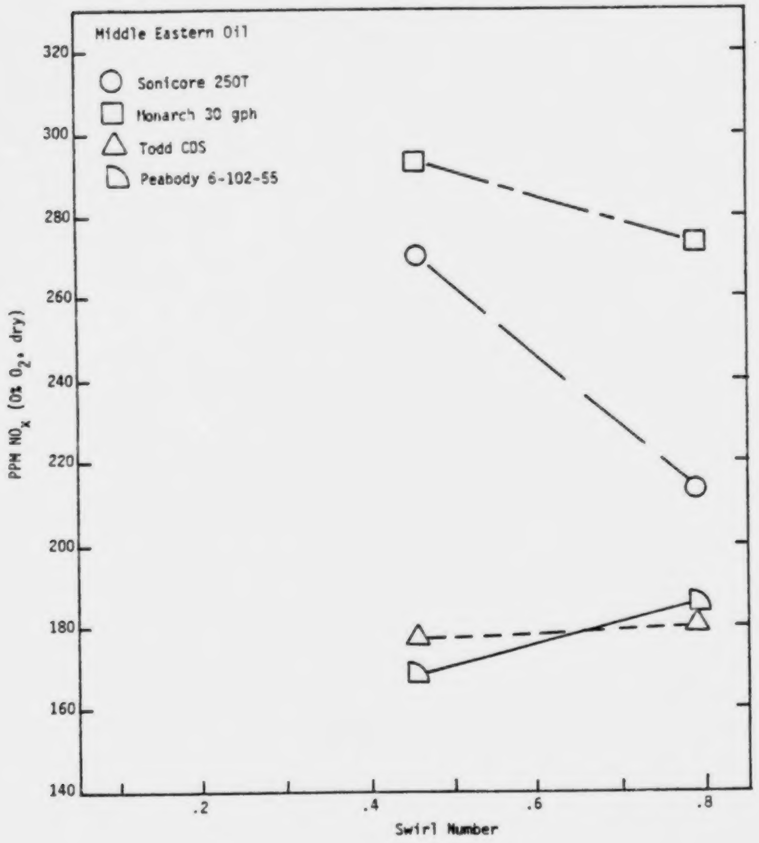

Figure 5-101. Effect of Swirl - Middle Eastern Oil.

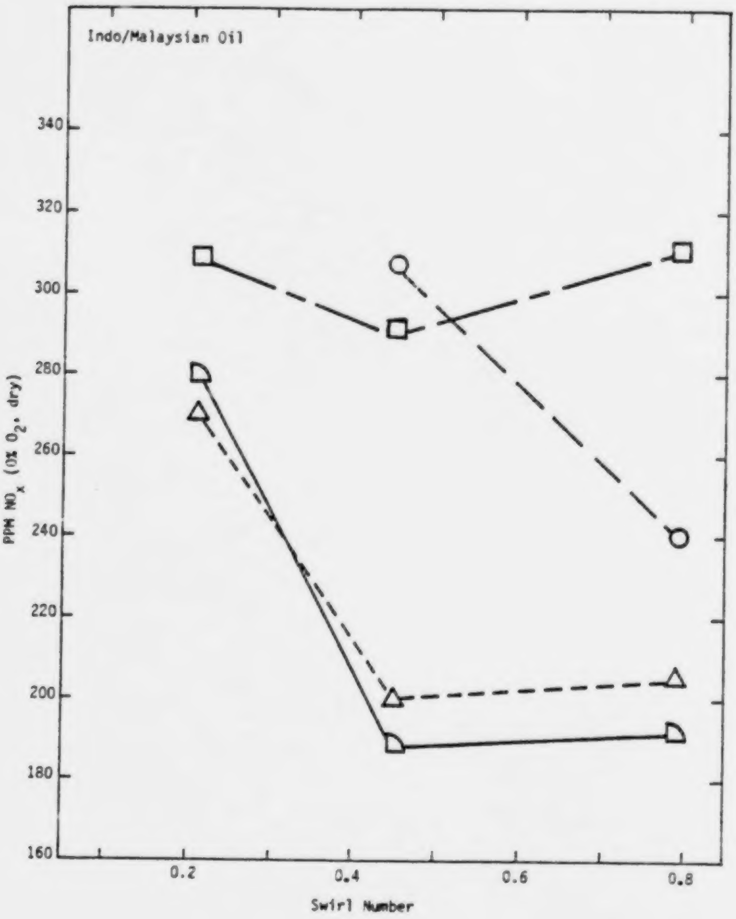

Figure 5-102. Effect of Swirl - Indo/Malaysian Oil.

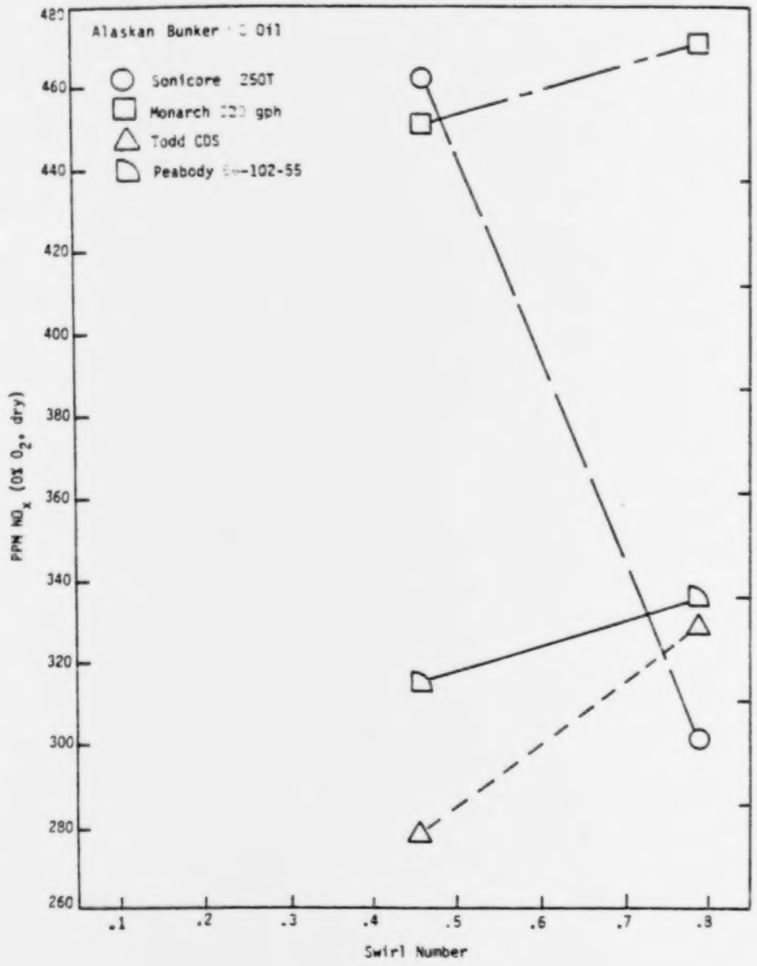

Figure 5-103. Effect of Swirl - Alaskan Bunker C Oil.

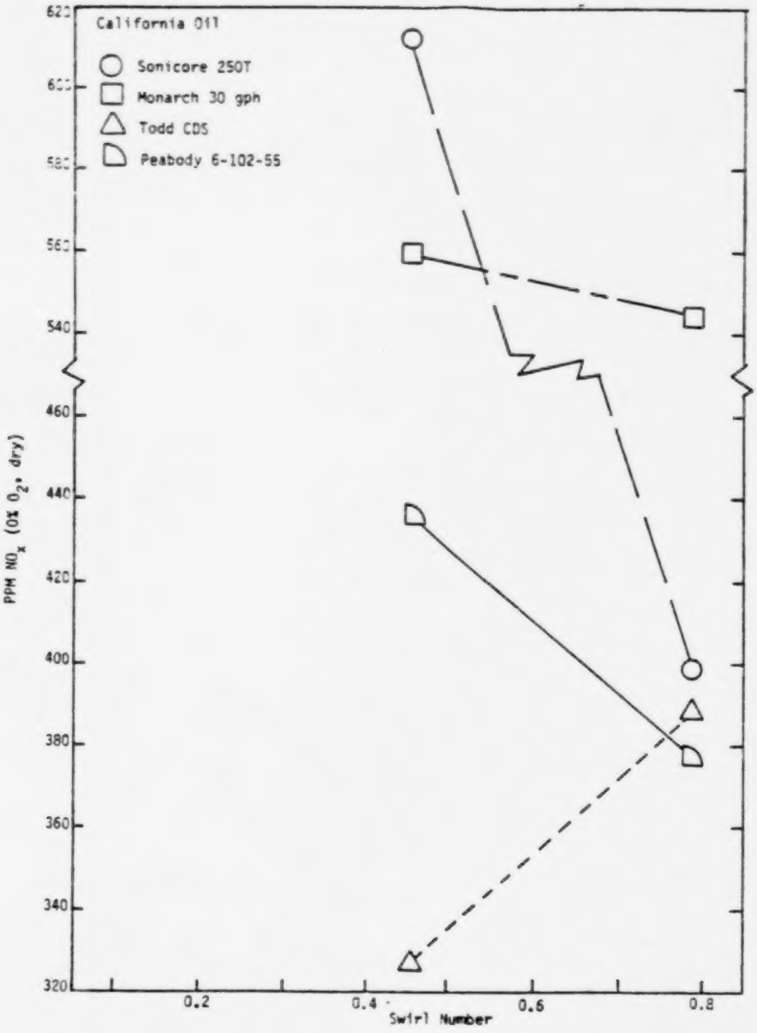

Figure 5-104. Effect of Swirl - California Oil.

It was found that smoke emissions were profoundly influenced by the atomizer and flow field combination, and no simple fuel composition parameter could be consistently related to smoke emissions. For instance, in Figure 5-105, smoke emissions versus excess oxygen from the Alaskan oil and Middle Eastern oil are compared. Asphaltene content, often an indication of the smoking tendency of a fuel, was 5.6 percent for the Alaskan oil and 3.2 percent for the Middle Eastern oil. As shown in the figure, smoke numbers were higher for the Alaskan oil than for the Middle Eastern oil with the 30-degree swirl vanes, but the converse was true with the 45-degree swirl vanes.

Figure 5-106 illustrates the range of smoke emissions observed for each of the five residual fuel oils from all the atomizers tested. Emissions were highest with the California oil when using the 30-degree swirl vanes. With the exception of the Gulf Coast oil, there did not appear to be a large difference in maximum smoke emissions between the different fuels, but there was considerable variation with swirl level, suggesting that mixing has a stronger influence than fuel type. Figure 5-107 compares maximum smoke emissions for the four atomizers and four fuels. Smoke emission as a function of atomizer and swirl was very similar with the Middle Eastern oil and Alaskan oils, for which complete data was available. In both cases, the Todd and Sonicore atomizers produced high smoke emissions and the Peabody and Monarch atomizers produced low smoke emissions. For the 45-degree swirl vanes, these atomizers produced nearly identical smoke emissions with the Middle Eastern and Alaskan oils. A similar trend was produced with the California oil.

5.4.3.3 Effect of Flue Gas Recirculation

FGR was applied in amounts of 12 to 24 percent to each atomizer-flow field-fuel combination. Figures 5-108 and 5-109 summarize the range of NO_x emissions observed for each fuel from all atomizers and flow fields with and without FGR. Generally, the application of FGR did not result in NO_x emissions lower than the range observed without FGR. For a given fuel, when NO_x emissions were low, FGR produced no further NO_x reduction, and in some cases even resulted in an increase in NO_x. Figure 5-110 presents results of FGR at two different swirl levels as a function of fuel nitrogen content

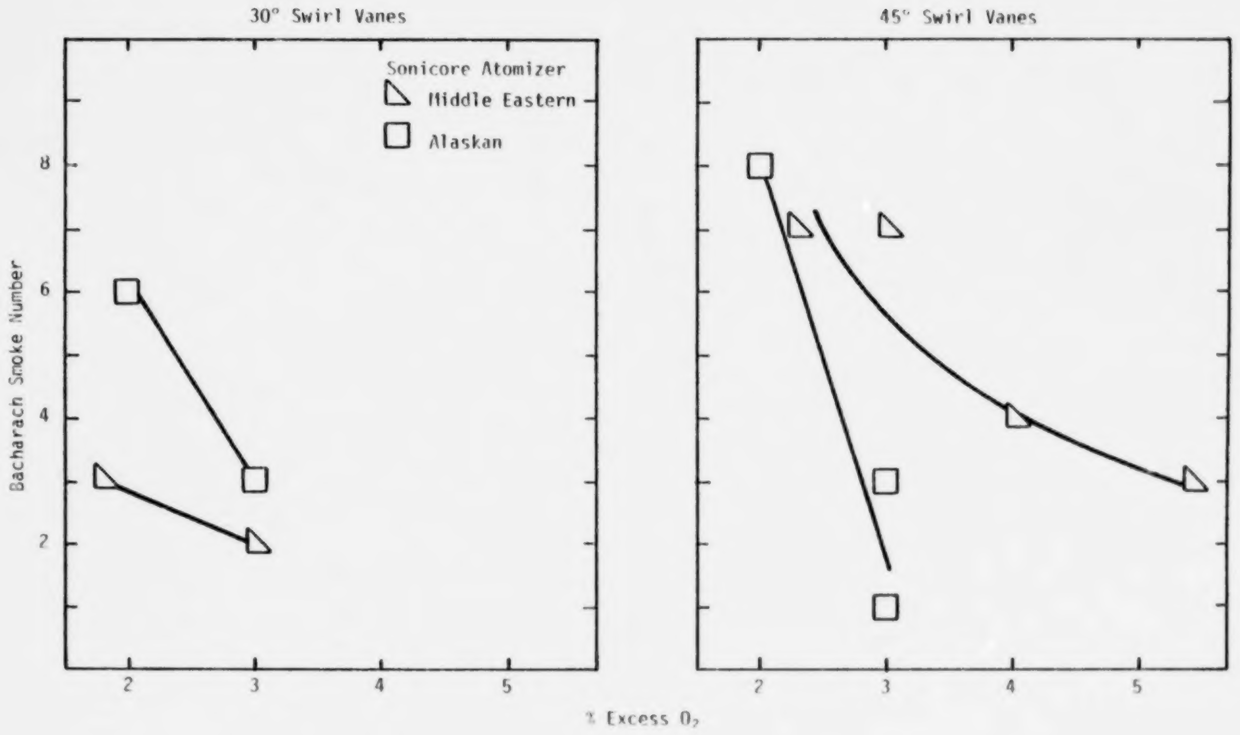

Figure 5-105. Effect of Fuel on Bacharach Smoke Number.

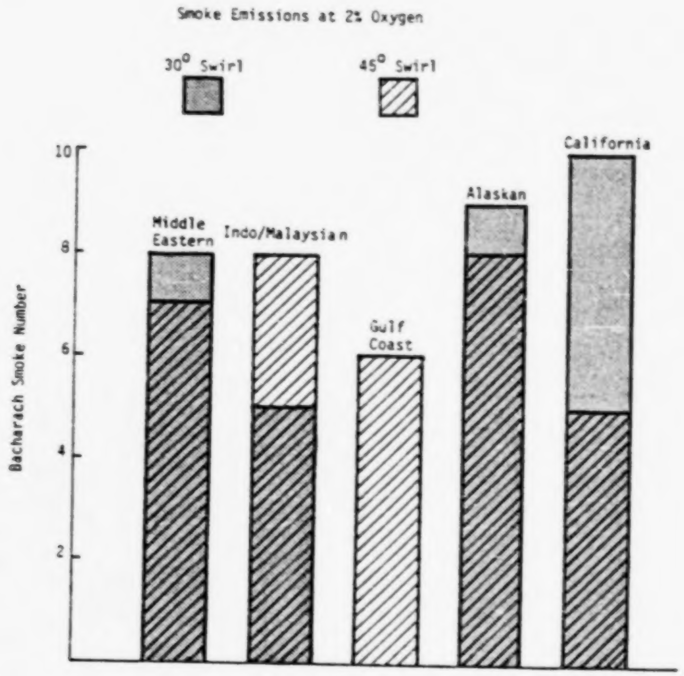

Figure 5-106. Effect of Fuel on Smoke Emissions.

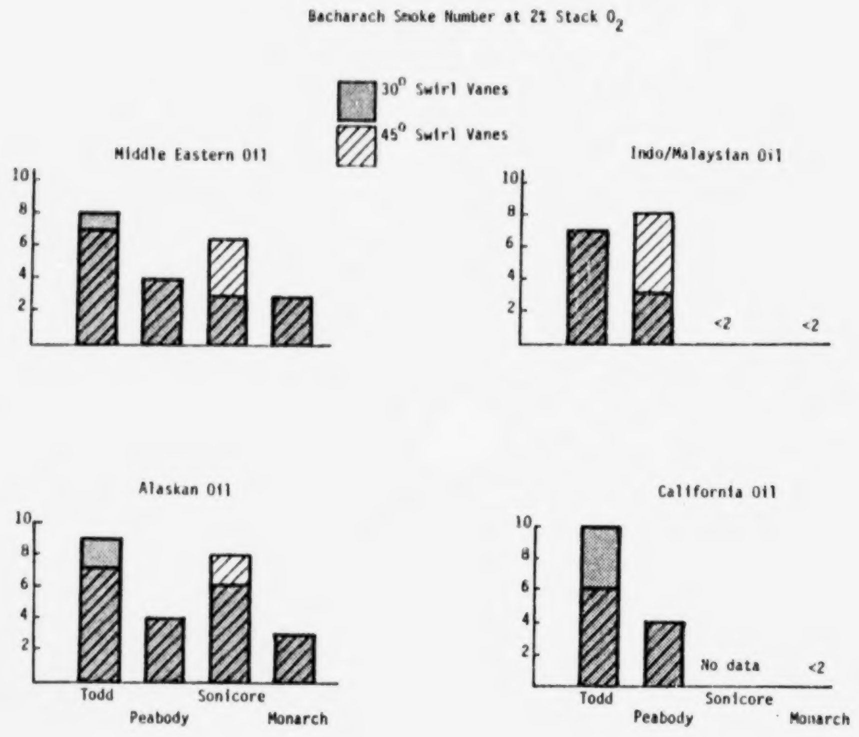

Figure 5-107. Effect of Atomizer on Smoke Emissions for Four Fuels.

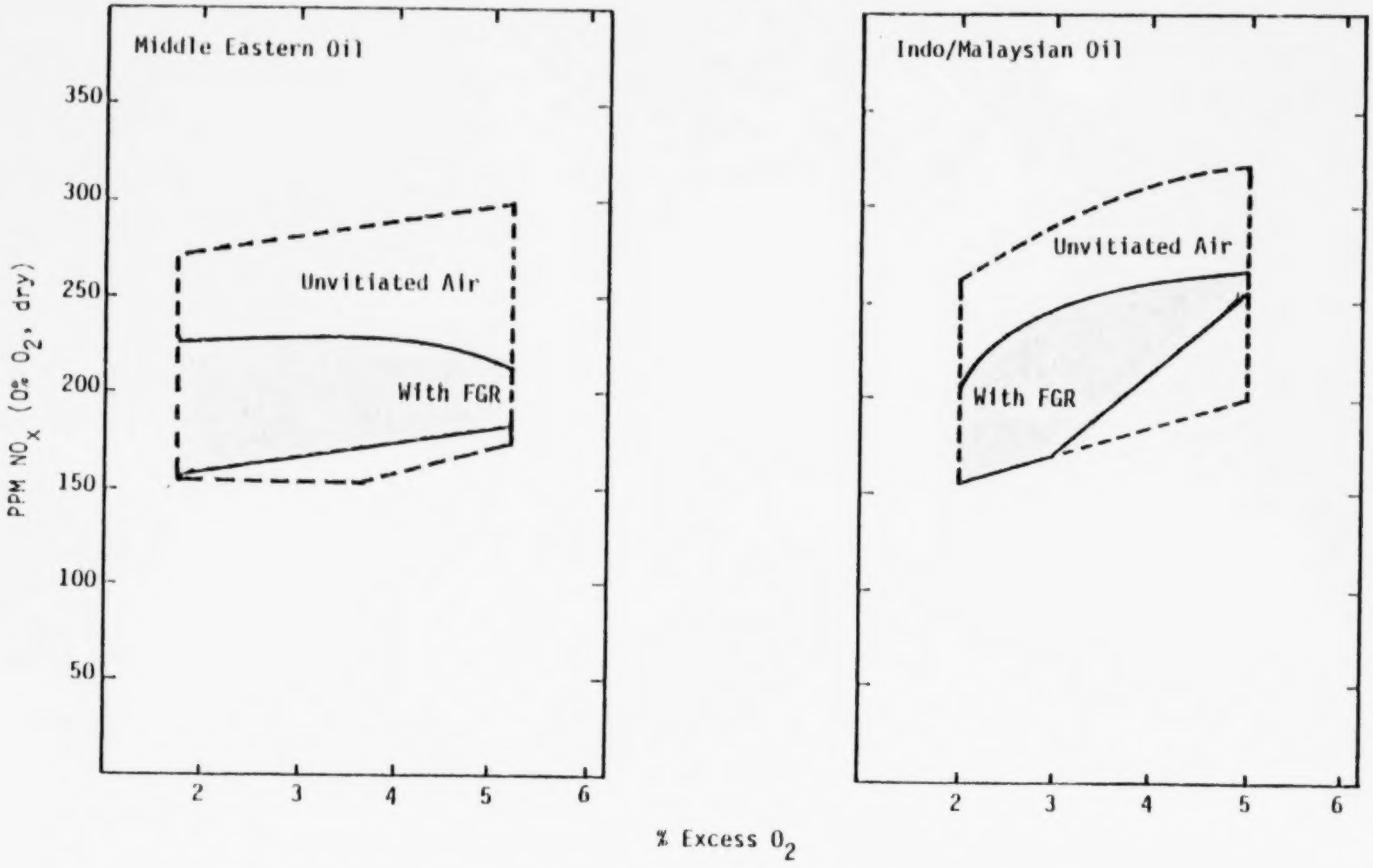

Figure 5-108. Effect of FGR - Middle Eastern Oil and Indo/Malaysian Oil.

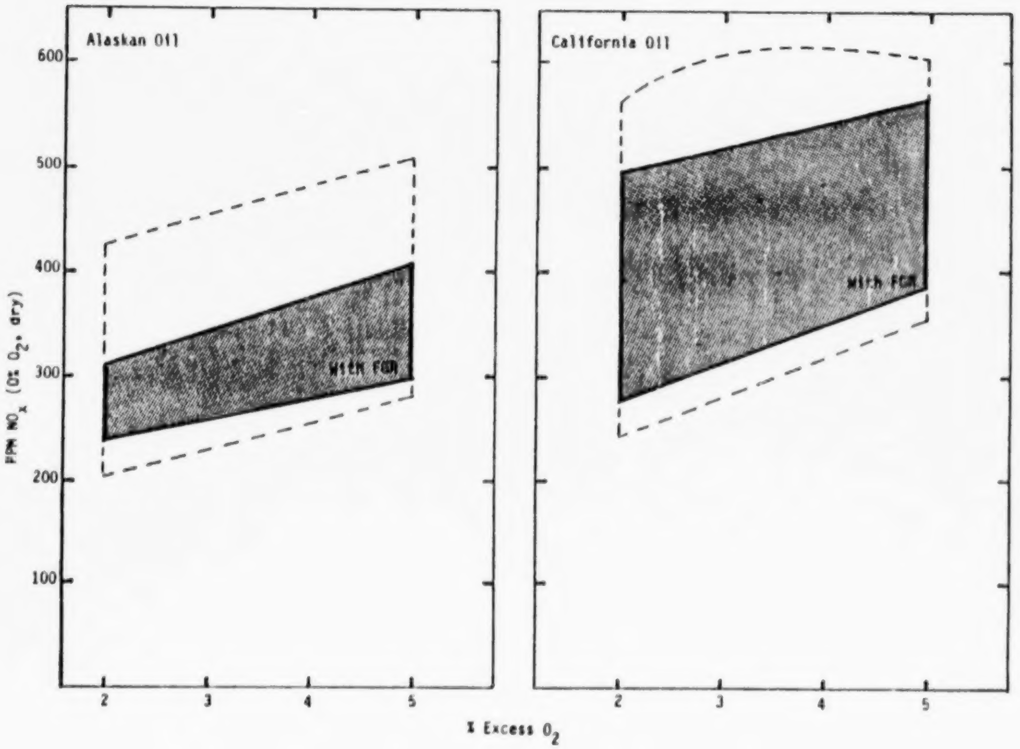

Figure 5-109. Effect of FGR - Alaskan and California Oil.

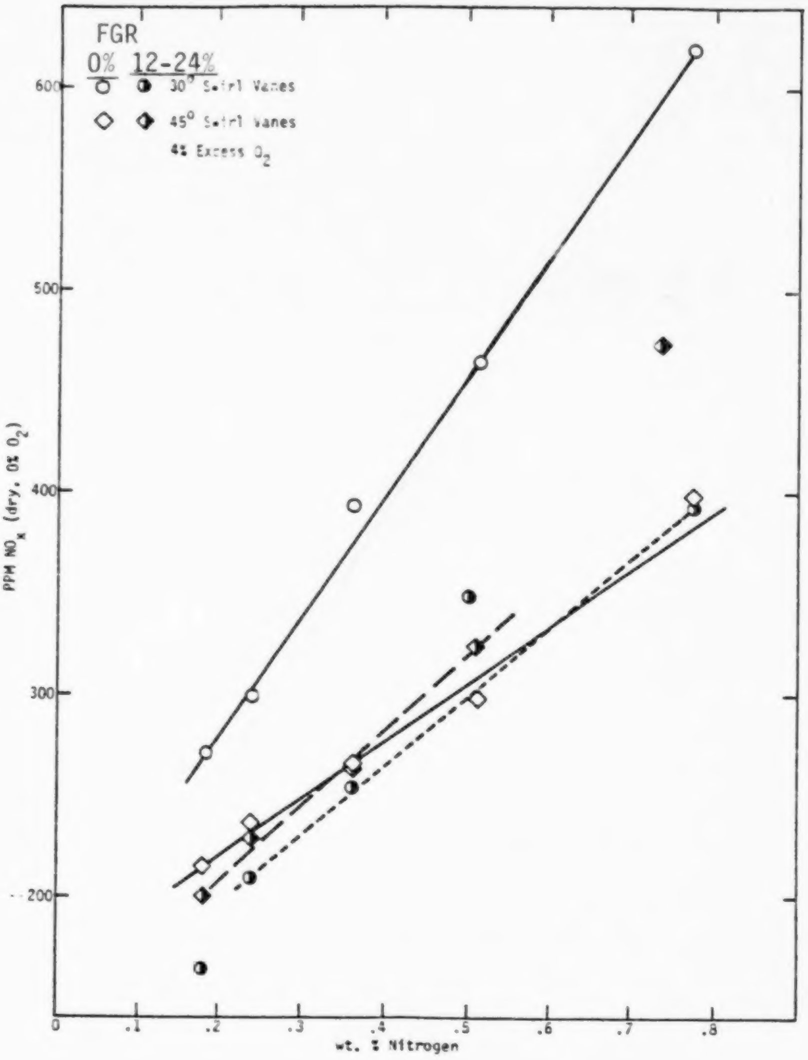

Figure 5-110. Effect of FGR Upon NO_x Emissions.

using the Sonicore atomizer. A reduction in emissions by 30 percent to 45 percent was observed for the 30-degree swirl vanes. With the 45-degree swirl vanes, FGR reduced NO_x only slightly, and in two cases even resulted in an increase in emissions. The level of NO_x with FGR was approximately equal for both swirl vane angles.

5.4.3.4 Summary — Influence of Fuel Properties

The following summarizes the results of the investigations to assess the influence of fuel properties on NO_x production under excess air conditions:

- Smoke emissions are strongly a function of the atomizer-flow field combination and only slightly dependent upon fuel type.
- NO_x emissions generally increase linearly with fuel nitrogen content for a given combustor configuration.
- Atomizer type and swirl alter the rate of increase of NO_x with fuel nitrogen content.
- FGR does not produce significant reduction of NO_x emissions from nitrogen-containing fuels.
- Fuel NO_x can account for greater than 70 percent of the total NO_x emissions produced from an 0.8 percent nitrogen residual oil.

5.4.4 Staged Combustion Studies

The final series of investigations in the Phase II testing were concerned with the effect of fuel, atomizer, and flow field upon NO_x and smoke emissions when operating under staged combustion conditions. Staged combustion is defined here as operating the burner with less than the amount of air required for combustion, then adding "secondary" air downstream of the burner to complete fuel burnout.

Table 5-3 summarizes the matrix of atomizers, fuels, and combustor conditions which were evaluated in staged combustion investigations. The

Table 5-3. Summary of Experimental Conditions - Staged Combustion Studies

Fuel	Variable	Range of Variable				
		Monarch	Sonicore	Peabody	Todd	Delavan
Indo/Malaysian	Primary Stoichiometry	0.6 - 1.16	0.6 - 1.16	0.6 - 1.16	0.6 - 1.16	0.6 - 1.16
	Overall Stoichiometry	1.6 - 1.3	1.16	1.16	1.16	1.16 - 1.30
	Residence Time	0.14 - 1.61	0.14 - 1.61	0.67	0.67	0.67
	Swirl	15, 30, 45	$0^0,15^0,30^0,45^0$	15, 30, 45	15,30, 45	15^0
	Steam Atomization	--	20 psig	--	25,50 psig	--
	FGR	--	48%	--	--	--
Alaskan (Diesel)	Primary Stoichiometry	0.6 - 1.16	0.6 - 1.16	--	--	--
	Overall Stoichiometry	1.16	1.16	--	--	--
	Residence Time	0.67	0.67	--	--	--
	Swirl	0^0	0^0	--	--	--
Alaskan (Bunker C)	Primary Stoichiometry	0.6 - 1.16	0.6 - 1.16	--	--	--
	Overall Stoichiometry	1.16	1.16	--	--	--
	Residence Time	0.67	0.67	--	--	--
	Swirl	0^0	0^0	--	--	--
Crude Shale	Primary Stoichiometry	0.6 - 1.16	0.6 - 1.16	--	--	--
	Overall Stoichiometry	1.16	1.16	--	--	--
	Residence Time	0.67	0.67	--	--	--
	Swirl	0^0	0^0	--	--	--

baseline Indonesian/Malaysian fuel was used under staged combustion conditions to evaluate the pollutant-related effects of

- atomizer type (five atomizers);
- combustion air swirl;
- first-stage stoichiometry and residence time;
- flue gas recirculation;
- two different secondary air injectors.

In addition, three other fuels ranging in nitrogen content from 0.01 to 2.1 percent were tested with the Sonicore and Monarch atomizers to study the effect of fuel nitrogen content on staged pollutant emissions. The results of these tests are presented graphically in Figures 5-111 to 5-135. Open symbols represent NO_x emissions and solid symbols, smoke emissions. Swirl level and operating conditions are indicated on each plot. Unless otherwise stated, overall excess oxygen is three percent (dry).

5.4.4.1 Effect of First-Stage Stoichiometry and Residence Time

First-stage (primary zone) stoichiometry was varied between 0.6 and 1.16 while maintaining overall excess O_2 at 3 percent with first-stage length of 122 cm for each of five atomizers using the Indonesian/Malaysian oil. In each case, NO_x emissions were found to reach a minimum with decreasing primary zone stoichiometry. Figure 5-111 shows typical results for the Sonicore atomizer with the Indonesian/Malaysian oil. NO_x emissions decrease sharply down to a primary zone stoichiometric ratio of 0.8, then rise slowly as stoichiometry of the primary zone is further decreased. Smoke emissions increased and reached a maximum at approximately the same stoichiometry as that obtained for minimum NO_x. Generally, for each atomizer and swirl combination the minimum NO_x level was reached at a primary zone stoichiometric ratio of between 0.75 and 0.85.

The effect of varying overall stoichiometry while holding primary zone stoichiometry constant is illustrated in Figures 5-112 to 5-115. NO_x emissions at five percent excess O_2 were either the same or slightly higher (~10 ppm) compared to those at three percent excess O_2. Smoke numbers were

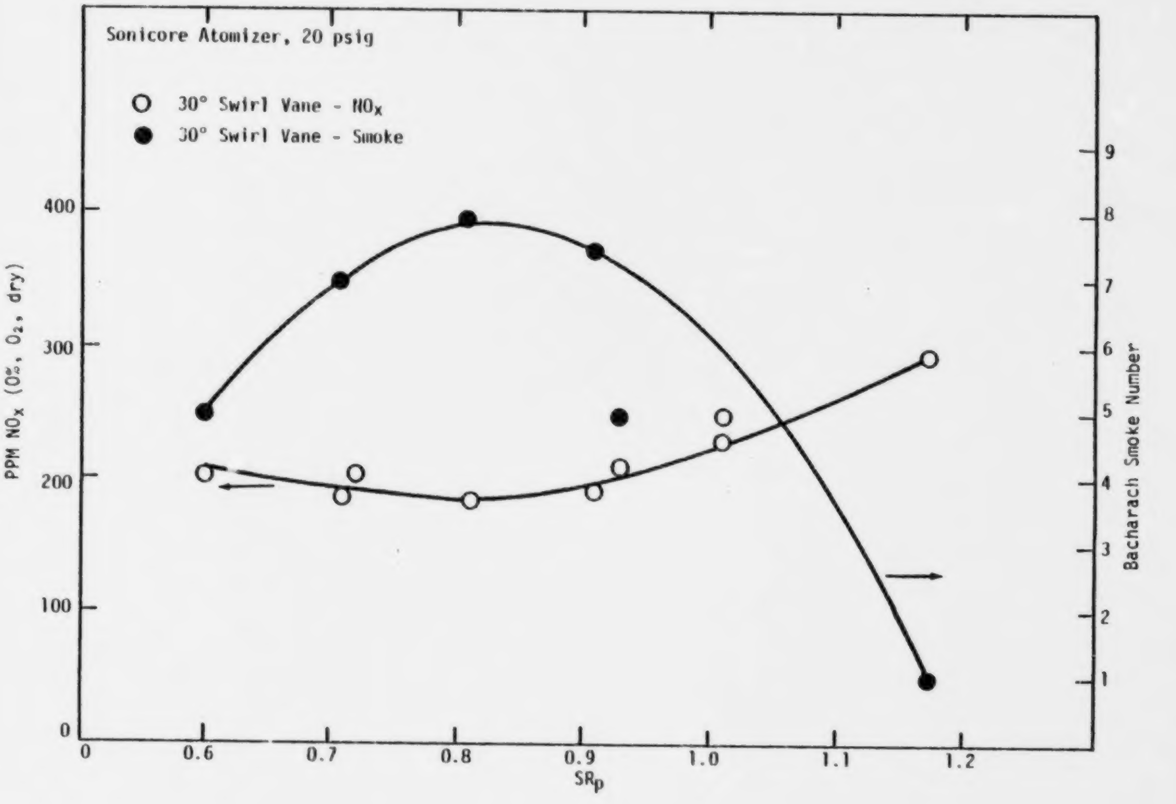

Figure 5-111. Typical Staging Results - Indo/Malaysian Oil with Sonicore Atomizer.

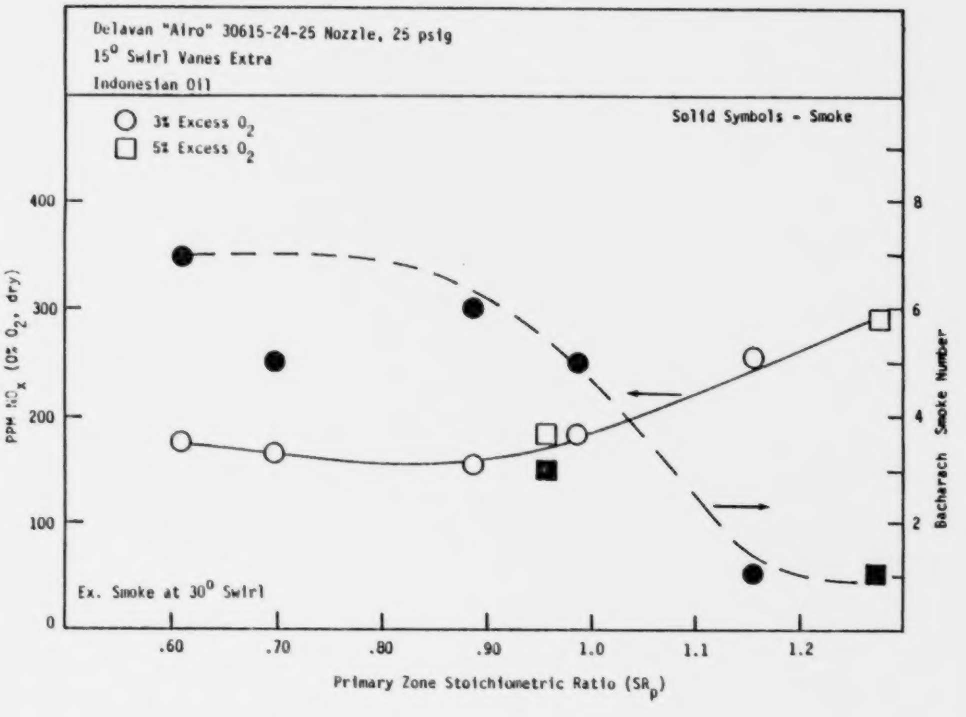

Figure 5-112. Effect of Overall Stoichiometry - Delavan "Airo" Atomizer, Weak Swirl.

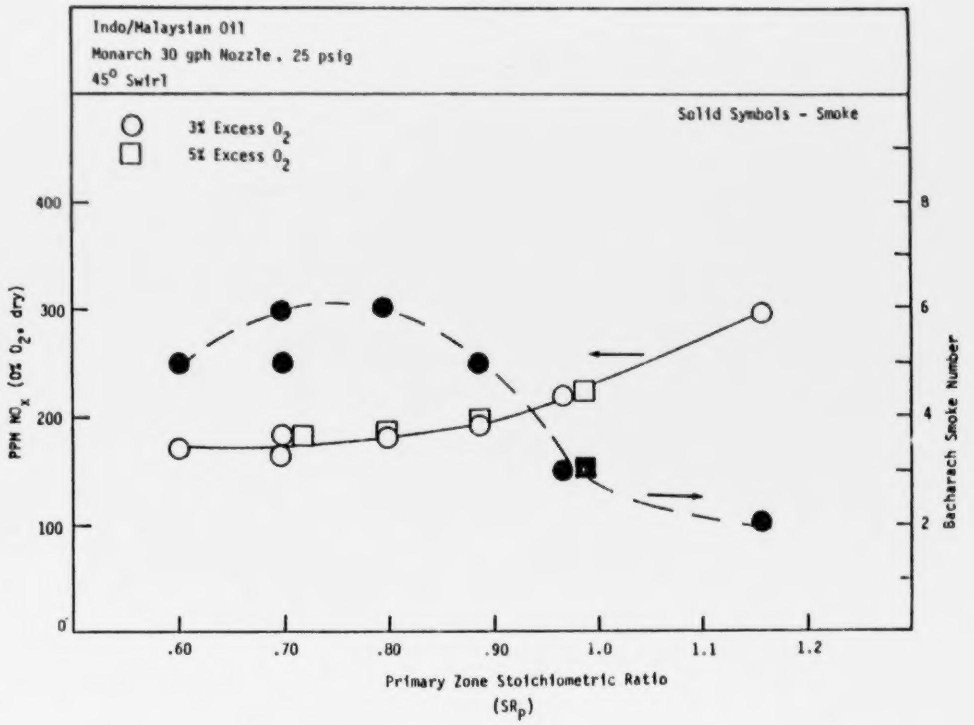

Figure 5-113. Effect of Overall Stoichiometry - Monarch Atomizer, Strong Swirl.

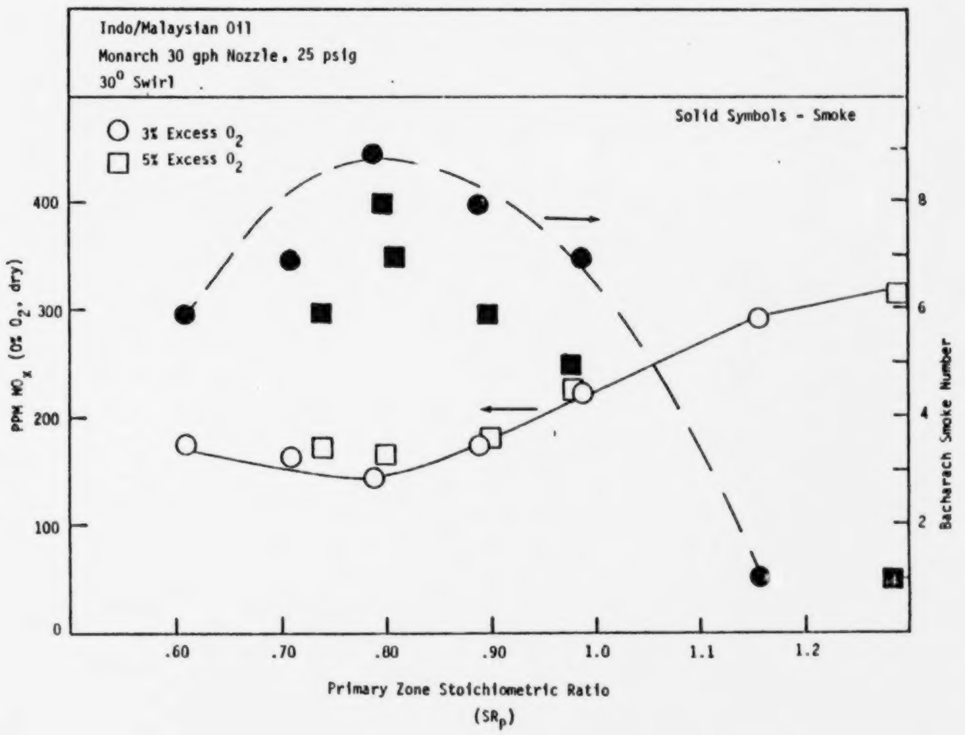

Figure 5-114. Effect of Overall Stoichiometry - Monarch Atomizer, Intermediate Swirl.

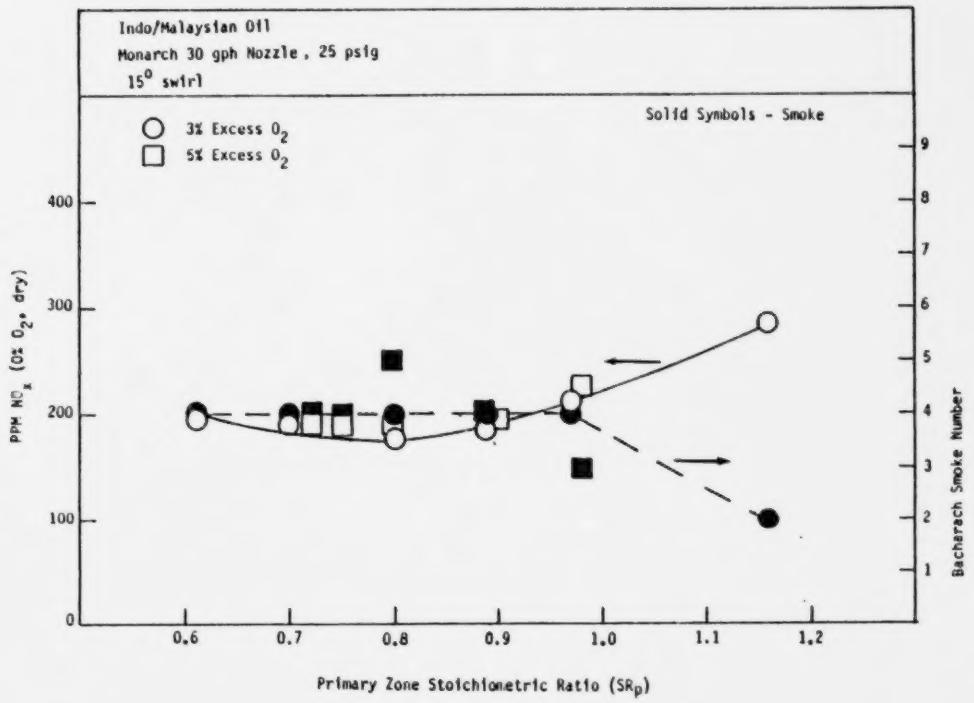

Figure 5-115. Effect of Overall Stoichiometry - Monarch Atomizer, Weak Swirl.

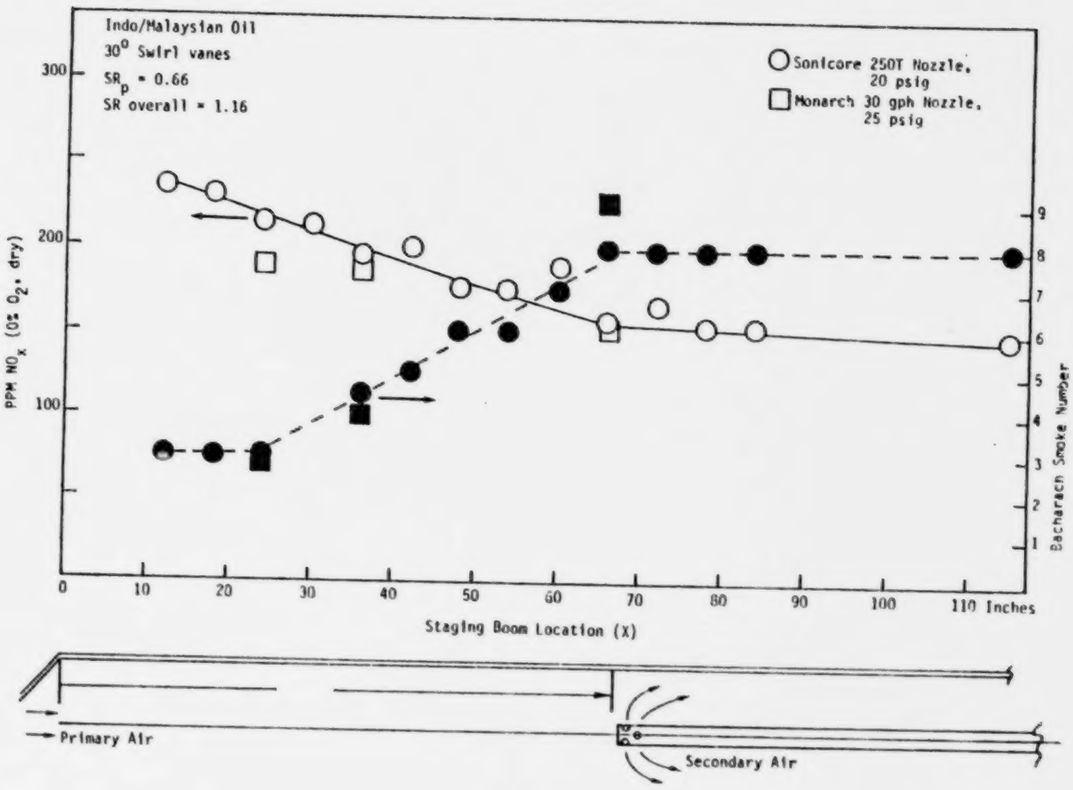

Figure 5-116. Effect of Primary Zone Residence Time, Intermediate Swirl.

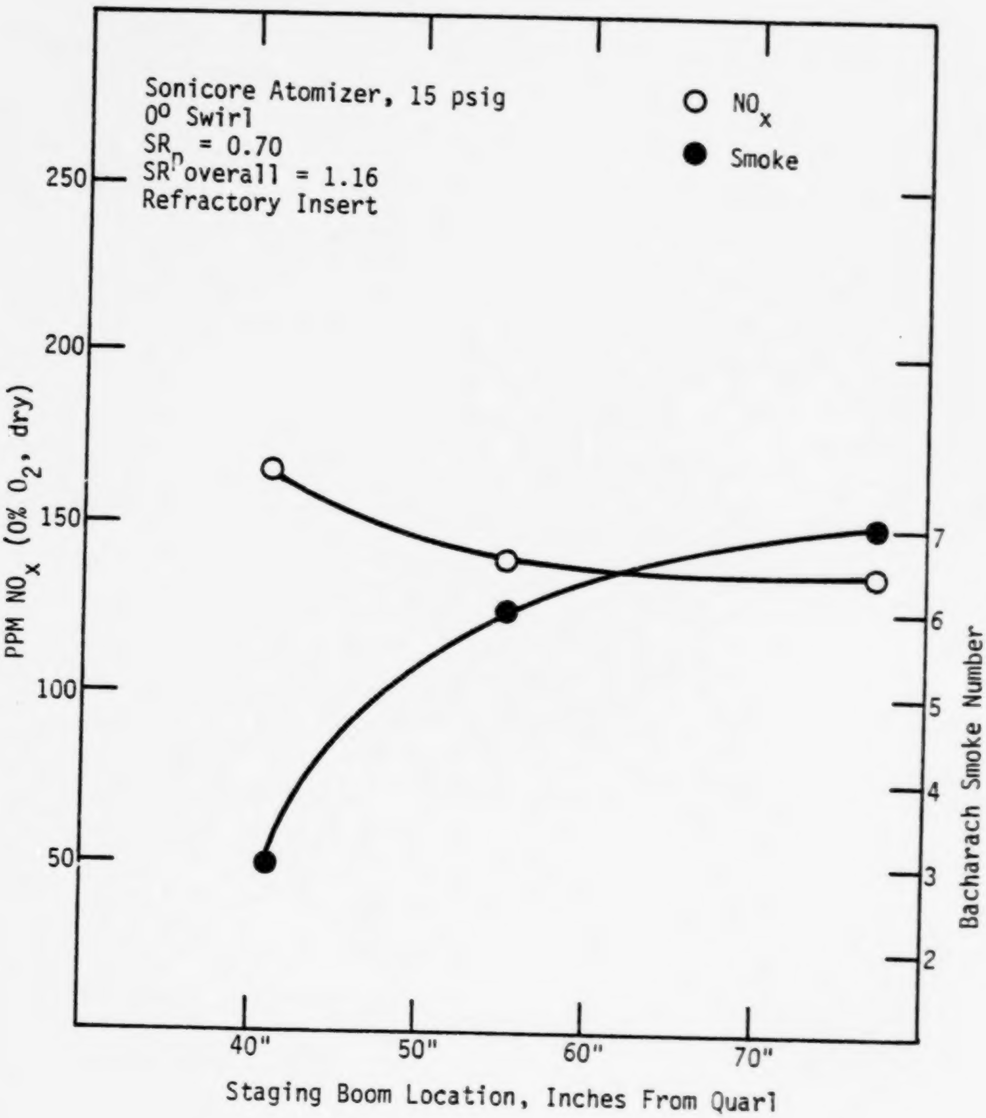

Figure 5-117. The Influence of Primary Zone Residence Time - No Swirl.

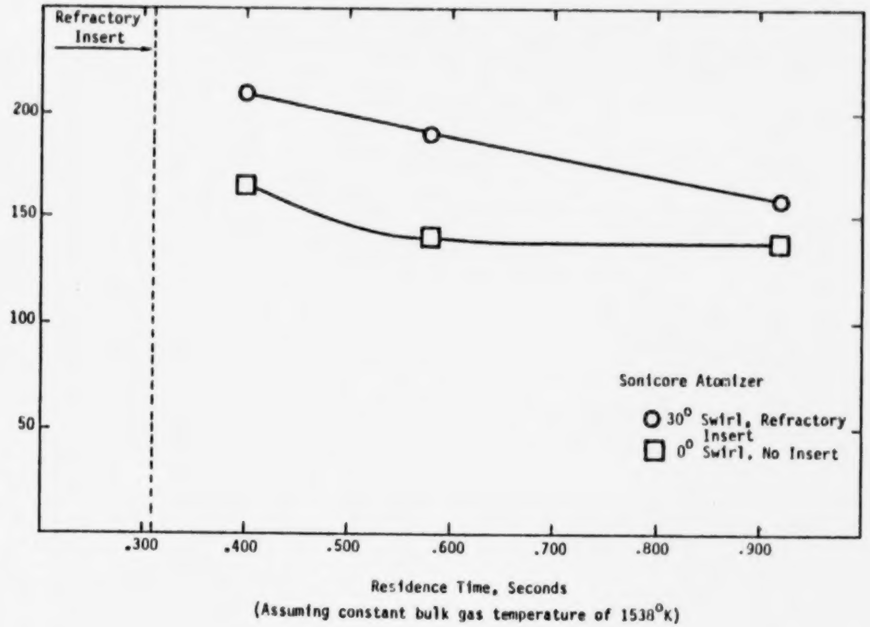

Figure 5-118. Effect of Primary Zone Residence Time.

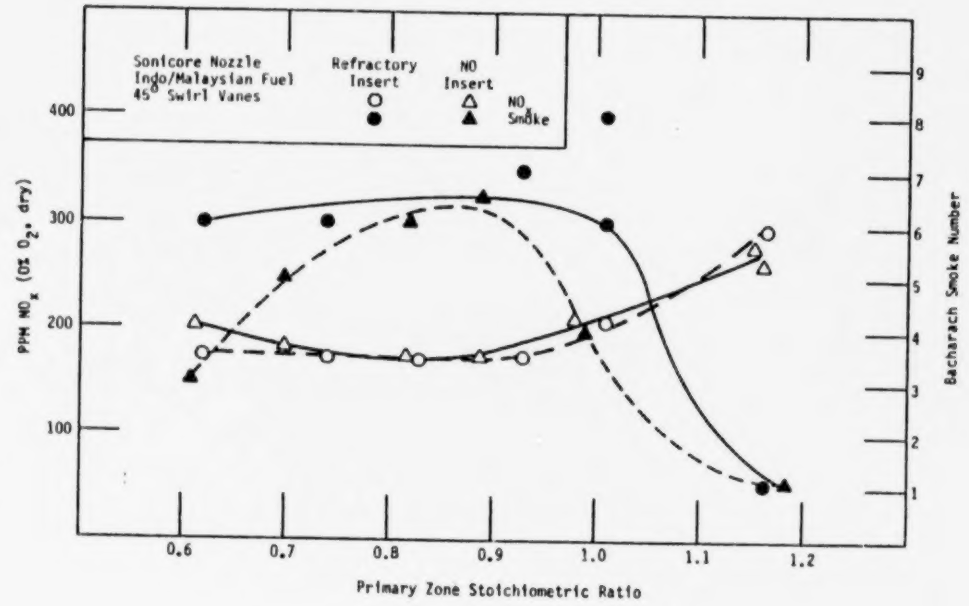

Figure 5-119. Comparison of Staged NO$_x$ Emissions with and without Refractory Liner.

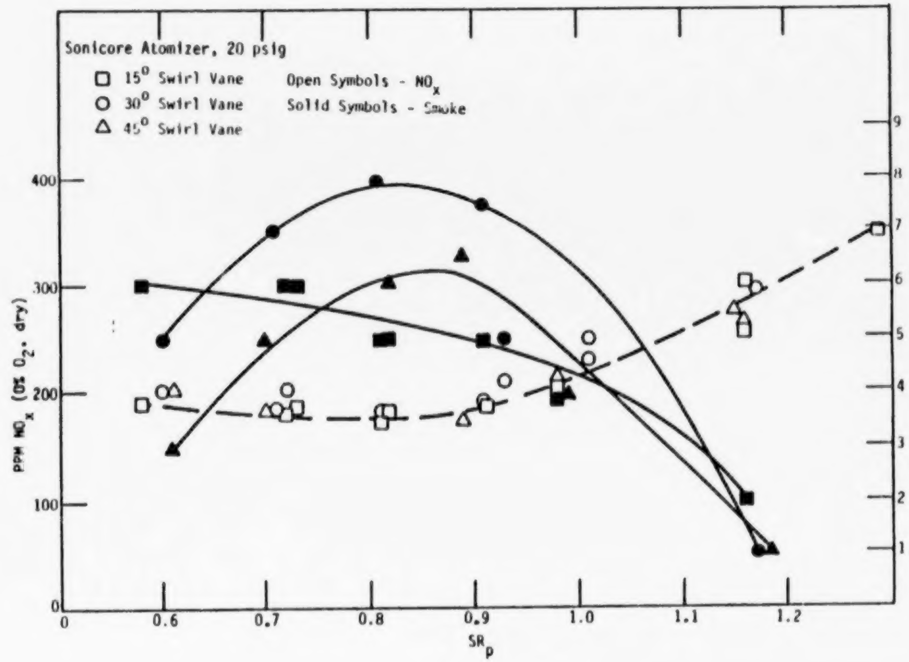

Figure 5-120. Staged Combustion Studies - Indo/Malaysian Oil with Sonicore Atomizers.

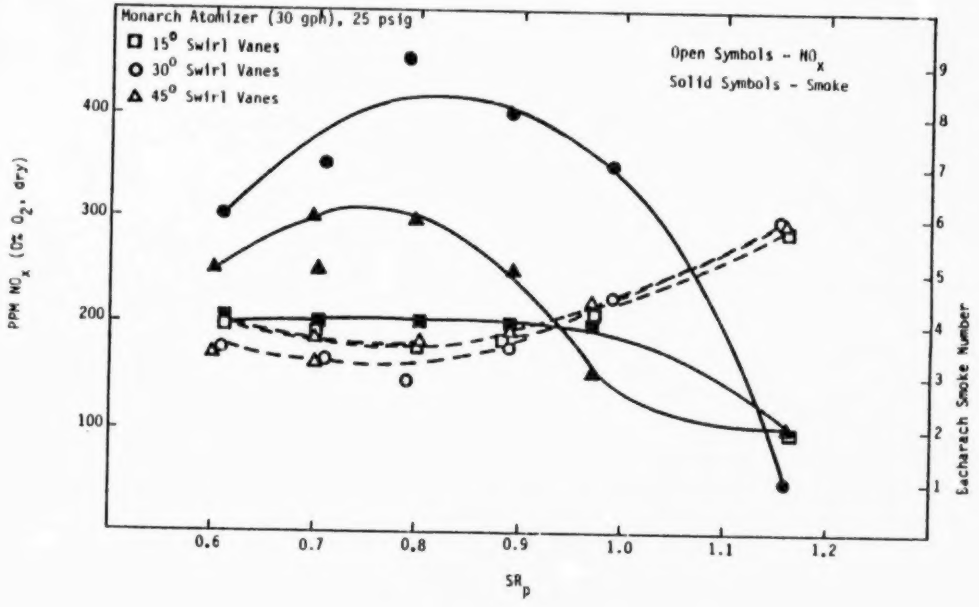

Figure 5-121. Staged Combustion Studies - Indo/Malaysian Oil with Monarch Atomizer.

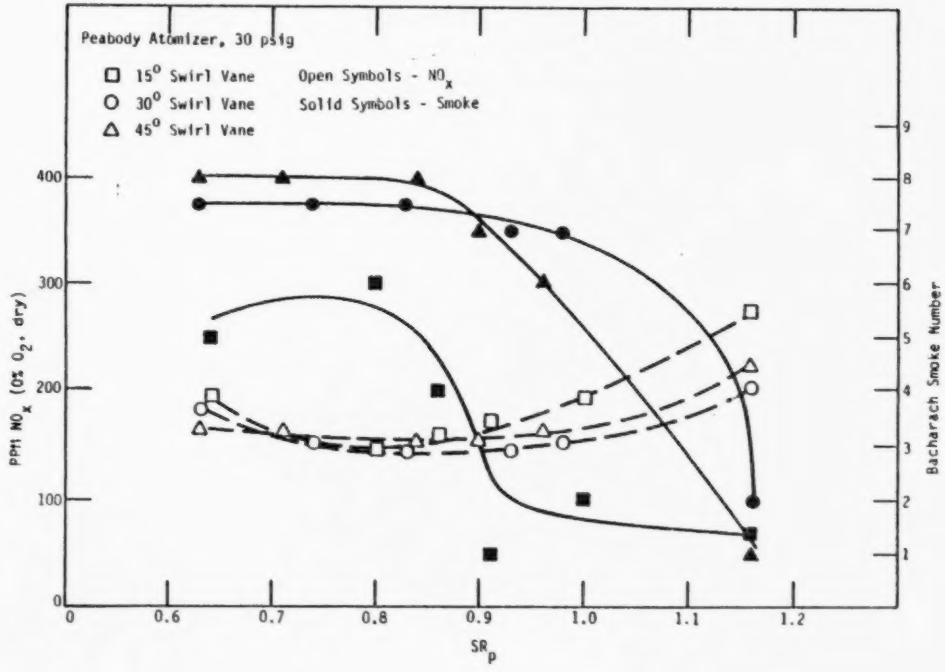

Figure 5-122. Staged Combustion Studies - Indo/Malaysian Oil with Peabody Atomizer.

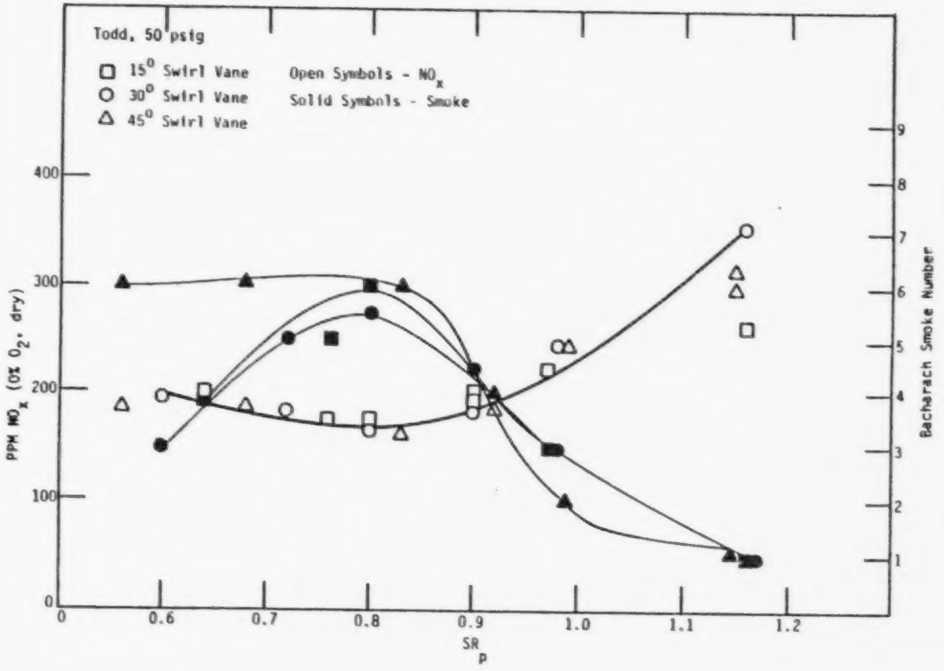

Figure 5-123. Staged Combustion Studies - Indo/Malaysian Oil With Todd Atomizer.

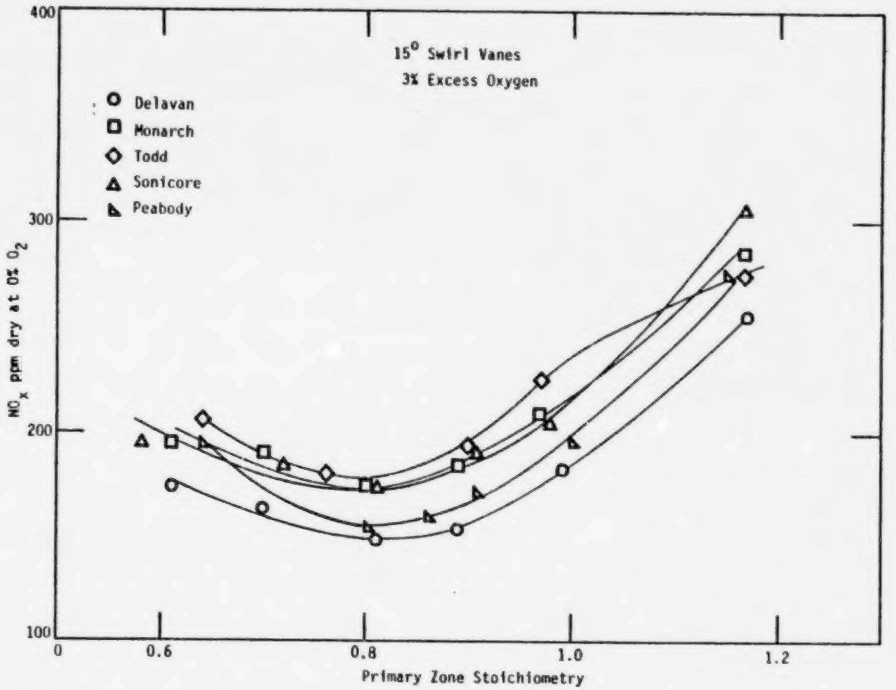

Figure 5-124. Comparison of Nozzle Performance Under Staged Combustion Conditions - Weak Swirl.

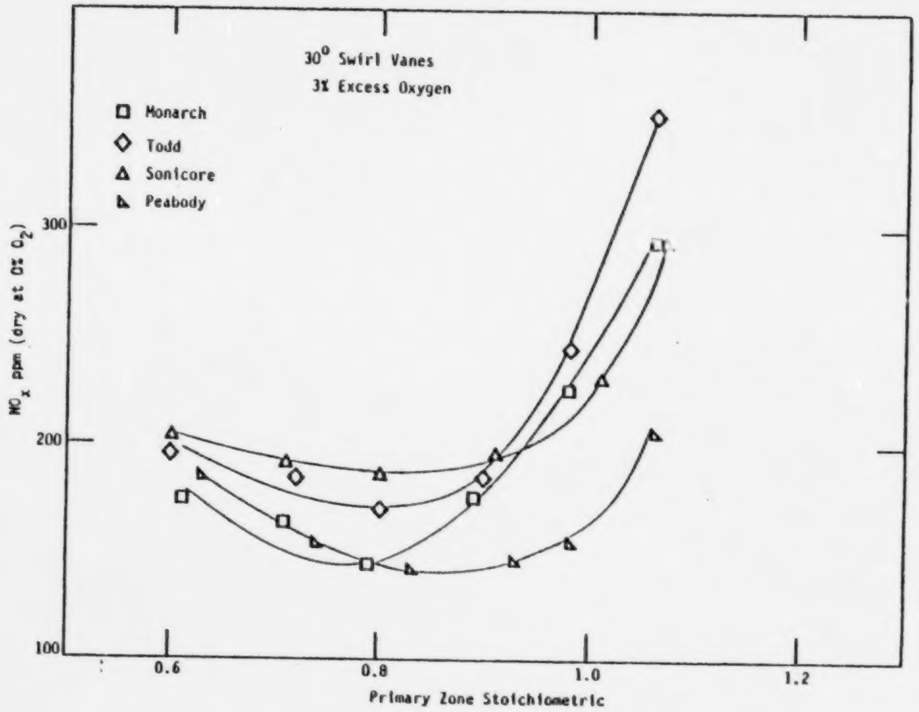

Figure 5-125. Comparison of Nozzle Performance Under Staged Combustion Conditions - Intermediate Swirl.

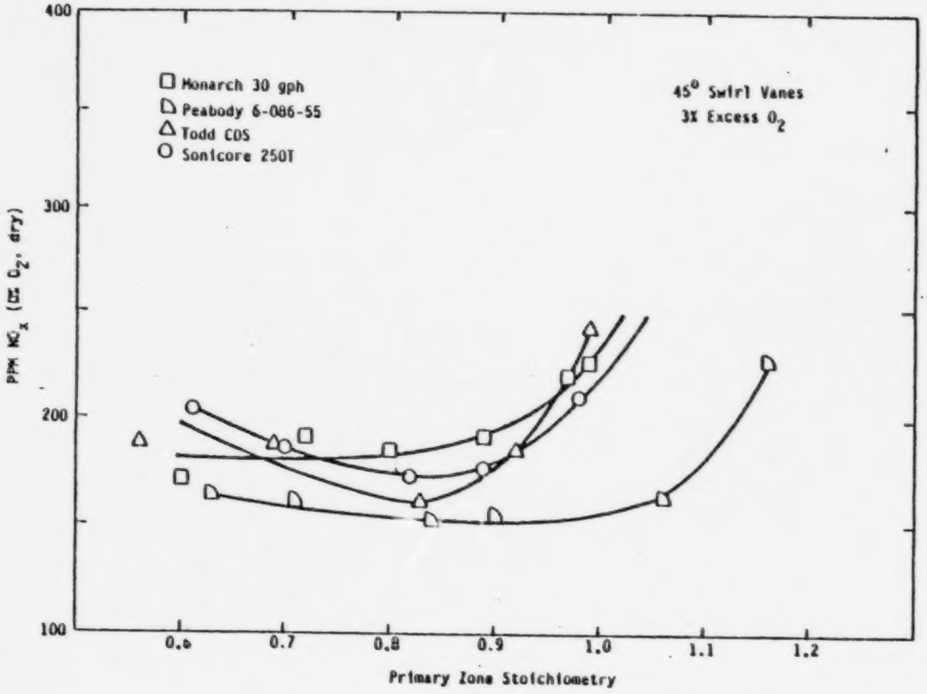

Figure 5-126. Comparison of Nozzle Performance Under Staged Combustion Conditions - Strong Swirl.

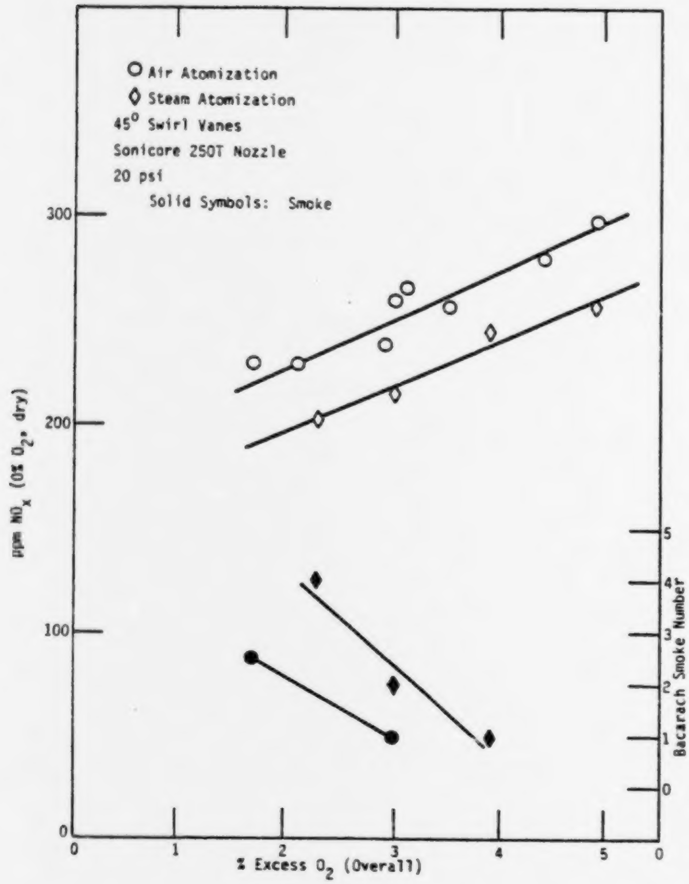

Figure 5-127. Effect of Steam Atomization - Sonicore Atomizer, Normal Combustion.

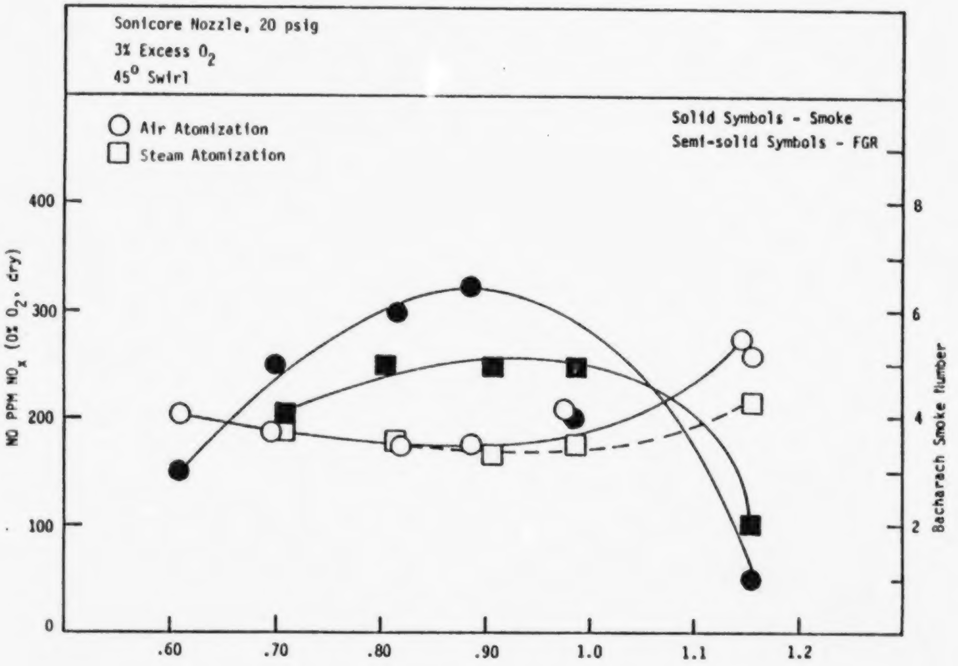

Figure 5-128. Effect of Steam Atomization - Sonicore Atomizer, Staged Combustion.

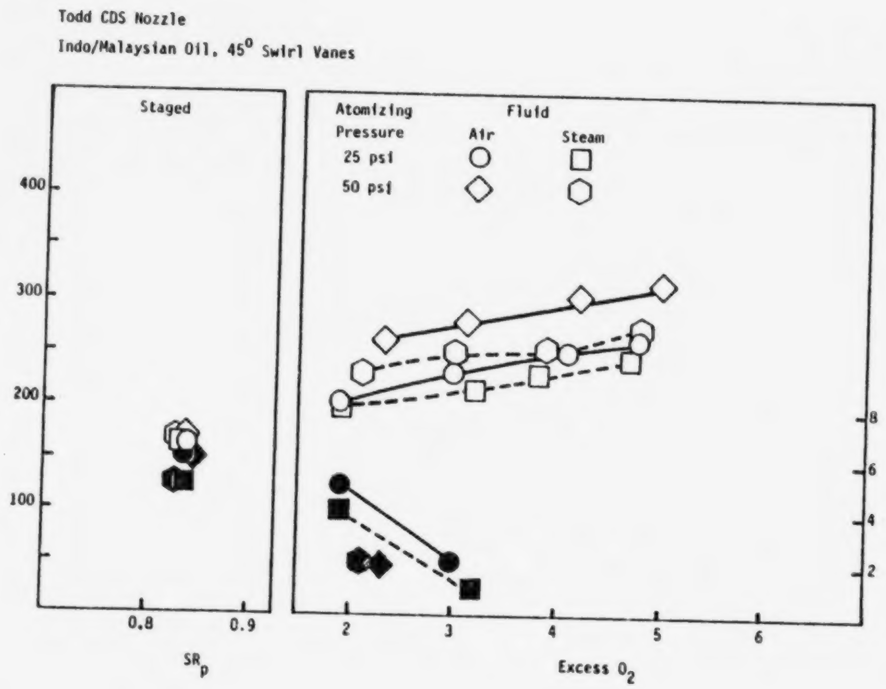

Figure 5-129. Effect of Steam Atomization - Todd Atomizer.

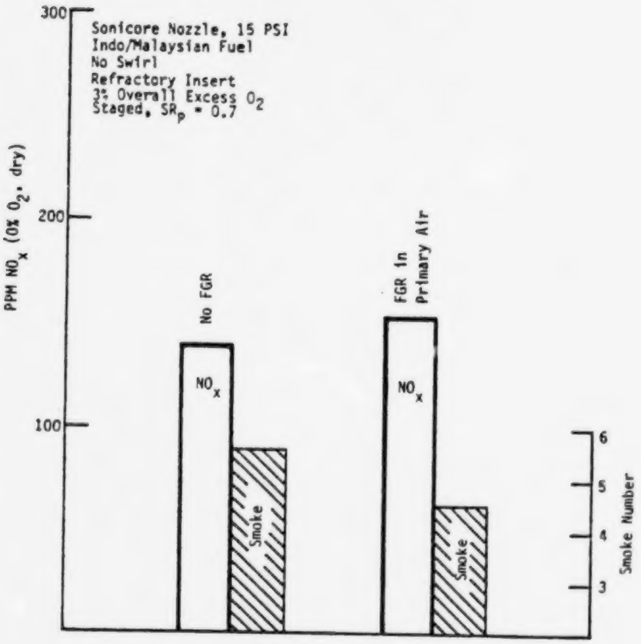

Figure 5-130. The Influence of FGR on Emissions Under Staged Combustion Conditions.

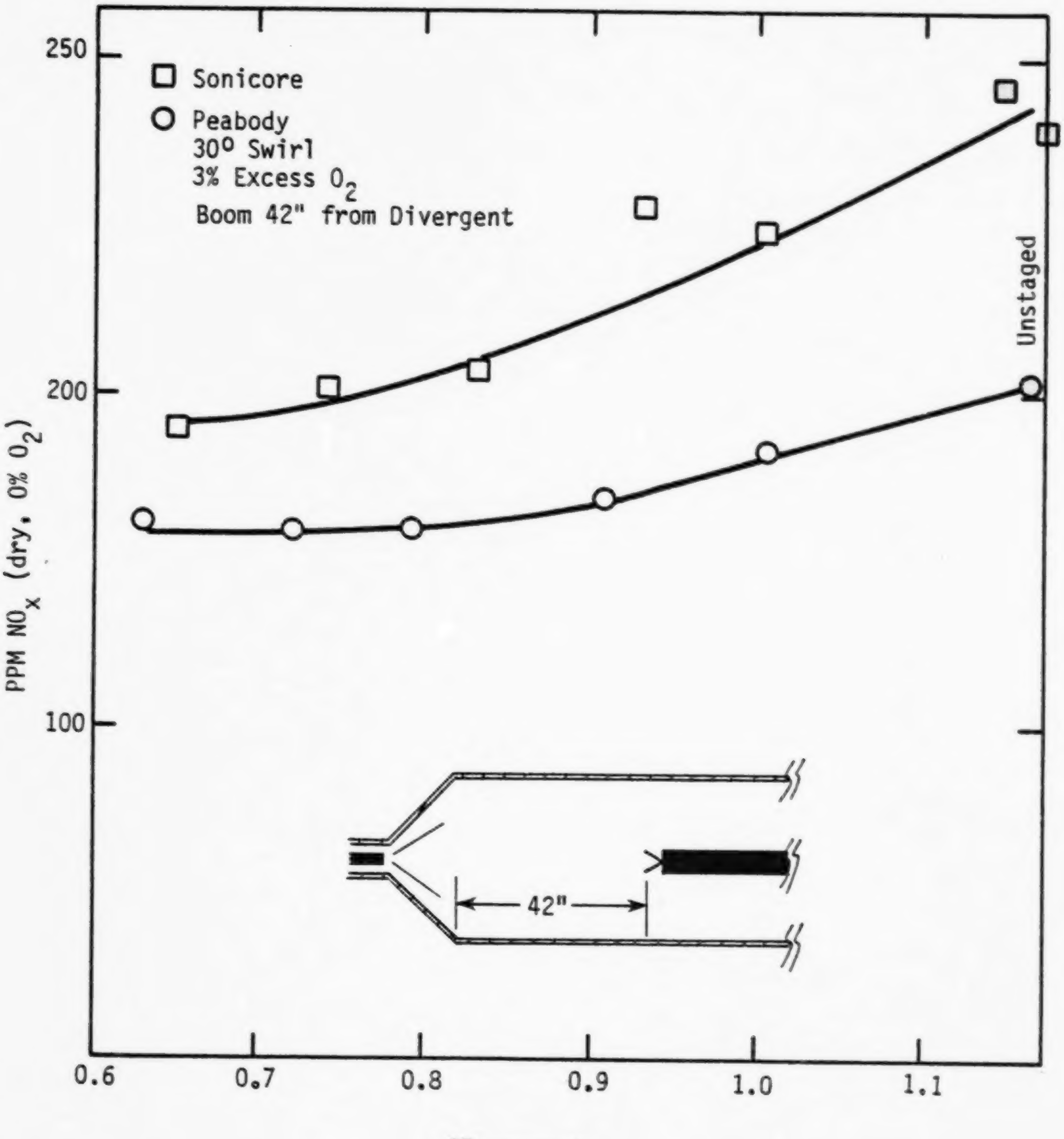

Figure 5-131. Effect of Primary Zone Stoichiometry with Conical Spreader Secondary Air Injector.

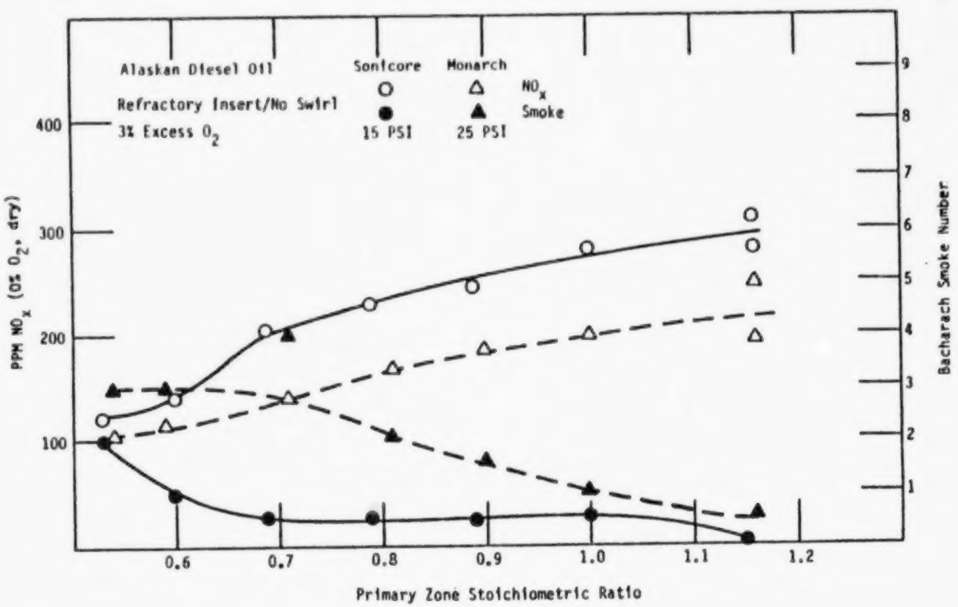

Figure 5-132. Staged Combustion Studies - Alaskan Diesel Oil.

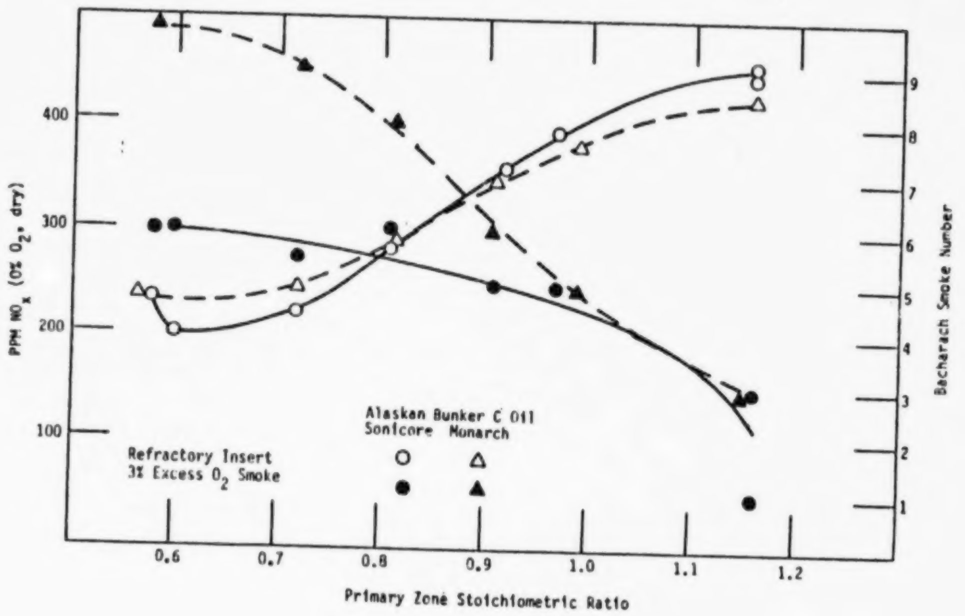

Figure 5-133. Staged Combustion Studies - Alaskan Bunker C Oil.

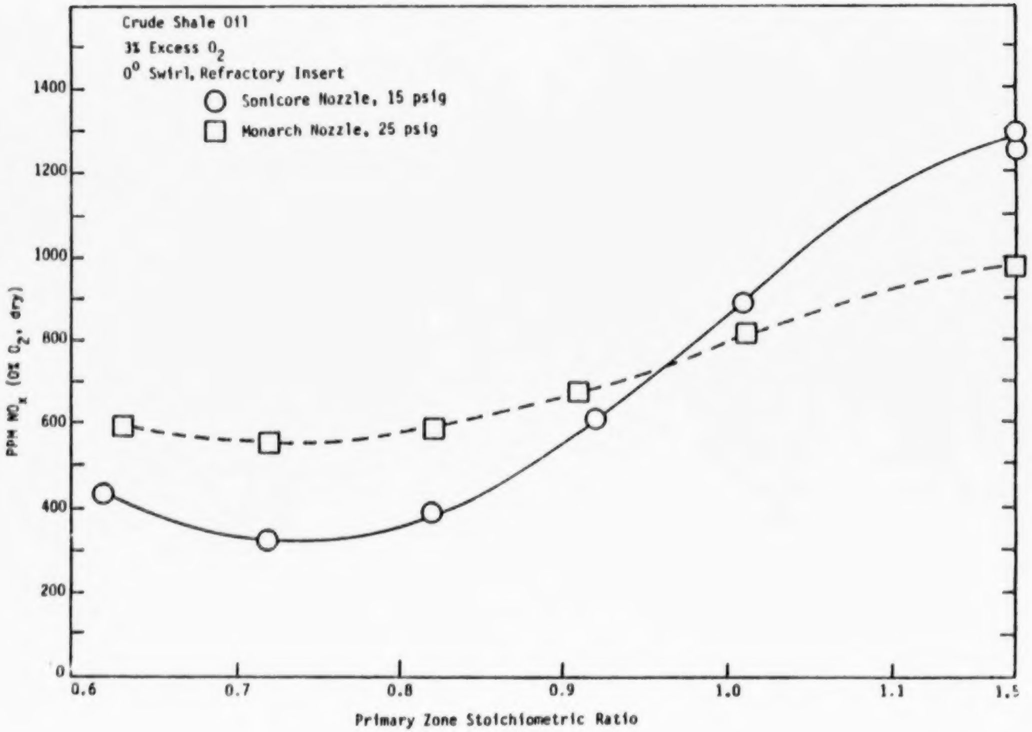

Figure 5-134. Staged Combustion Studies - Crude Shale Oil.

slightly lower at five percent excess O_2 for the Monarch atomizer with the 30-degree swirl vanes (Figure 5-114). This decrease in smoke number may be due to enhanced second-stage mixing due to higher air velocity at five percent excess O_2 or simply dilution due to the higher mass flow. In most cases pollutant emissions were the same at five percent excess O_2 as at three percent excess O_2.

The effect of varying the point of staged air injection by moving the staging boom, and therefore changing first-stage length and residence time is illustrated in Figures 5-116 to 5-118. Primary zone and overall stoichiometries were maintained constant at 0.66 and 1.16 respectively, while varying the distance between the burner and staging boom. The boom was traversed from 25 to 290 cm (10 to 114 inches) from the burner, resulting in a variation in mean residence time from approximately 0.14 to 1.61 seconds (assuming plug flow at 3×10^6 Btu/hr, $SR_p = 0.66$, and an average bulk gas temperature = 1538°K). In Figure 5-116, the effect of staging boom distance is compared for the Sonicore and Monarch atomizers with the 30° swirl vanes and Indonesian/Malaysian oil. NO_x emissions decreased with increasing residence time up to 173 cm (68 inches) from the burner, after which further retraction resulted in no further decrease in NO_x. Smoke emissions increased asymptotically to the same distance. 173 cm corresponds to a mean residence time of approximately 0.92 seconds in the primary zone. The same trend was observed with the Monarch atomizer, except for slightly lower NO_x emissions at short residence times. Figure 5-117 shows the effect of staging boom position for the Sonicore atomizer without swirl and with the refractory sleeve at a first-stage stoichiometry of 0.7. NO_x emissions were slightly lower in this case.

Staged NO_x emissions versus estimated first-stage residence time is compared for two swirl levels in Figure 5-118. A similar rate of decrease in NO_x with increasing residence time was found for swirl levels. However, the case with zero swirl reached asymptotic behavior at a shorter residence time.

Smoke emissions from the firetube simulator increased under staged combustion because soot production increases and burnout becomes more difficult.

In the bench-scale furnace smoke and visible soot emissions were generally low, and this was attributed to the high temperature and lower heat loss in the refractory tunnel furnace. Therefore, a refractory sleeve was inserted into the firetube simulator immediately downstream of the burner to reduce heat loss in the primary zone and, therefore, reduce smoke emissions under staged conditions.

Figure 5-118 presents NO_x and smoke emissions for the Sonicore atomizer, Indonesian/Malaysian fuel, and zero swirl with the refractory sleeve. NO_x emissions at four percent excess O_2 were 280 ppm, which is within the range of emissions observed without the sleeve in previous tests. Smoke emissions were less than a Bacharach smoke number of two except at low excess oxygen levels. NO_x and smoke emissions under staged conditions with and without the sleeve are compared in Figure 5-119. NO_x emissions remained virtually the same but smoke emissions appeared slightly higher when the sleeve was in place.

5.4.4.2 Effect of Swirl Level

In Figures 5-120 to 5-123 NO_x and smoke emissions versus primary stoichiometry are presented as a function of swirl vane angle for the Sonicore, Monarch, Peabody, and Todd atomizers. Variations in swirl level produced much greater variations in smoke emissions than in NO_x emissions. Lowest smoke emissions were produced with the 15^o swirl vanes for each of the four atomizers. The minimum NO_x emissions were only influenced slightly by swirl level. However, smoke number varied from four to nine for the same variation in swirl level. The lowest NO_x level coincided with the highest smoke level. These results suggest that swirl level can be optimized for a given atomizer to produce the best combination of NO_x and smoke emissions under staged conditions.

5.4.4.3 Effect of Atomizer Type

NO_x emissions versus primary zone stoichiometry are compared for the different atomizers in Figures 5-124 to 5-126 at swirl vane angles of 15, 30 and 45^o. Fifteen to 30 percent variations in the minimum NO_x levels were observed by maintaining the swirl level constant. For instance, NO_x

emissions at the intermediate swirl level varied from 150 ppm with the Delavan atomizer to 180 ppm with the Todd atomizer. The largest spread in minimum emissions was observed in the flow field produced by the 30^{o} swirl vanes (Figure 5-125), where the Peabody atomizer produced the lowest NO_x of 145 ppm and the Sonicore the highest of 185 ppm. The smallest spread was observed with the 45^{o} swirl vanes (Figure 5-126) where the lowest emissions of 155 ppm were produced by the Peabody atomizer and the highest of 185 ppm with the Monarch.

In general, although different atomizers produced different minimum NO_x levels, there was no clear ranking of the atomizers that is consistent for all three swirl levels. For instance, the Monarch atomizer produced among the highest NO_x emissions at the high and low swirl levels, yet among the lowest at the intermediate swirl. Similarly, the Todd atomizers produced the highest emissions at low swirl and nearly the lowest at high swirl. Thus, although there clearly is a large effect of atomizer type upon the effectiveness of staging in controlling NO_x emissions, the characteristics of the flow field will strongly influence not only how sensitive emissions are to changes in atomizer type, but also the absolute level of NO_x emissions which can be achieved.

Air was used as the atomizing medium for the results presented up to this point. In Figure 5-127 data are presented comparing air and steam with the Sonicore atomizer under unstaged combustion conditions. NO_x levels were slightly lower and smoke number was higher with steam as the atomizing medium. However, for comparable levels of NO_x, smoke emissions were essentially the same for steam and air. Atomizing with steam under staged combustion conditions resutled in slightly lower smoke emissions, but no change in NO_x emissions, as shown in Figure 5-128. Similar effects were observed with the Todd atomizer at two atomizing pressures (Figure 5-129).

5.4.4.4 Effect of FGR — Staged Combustion

The effect of adding cooled flue gases to the combustion air was evaluated under staged combustion conditions by recirculating 36 percent of the total mass flow through the primary airstream. This corresponds to 59 percent of the mass flow in the primary zone. The effect of FGR addition to the secondary stream was not investigated. The test conditions and results are summarized in Figure 5-130. As illustrated in the figure, the addition of FGR to the primary airstream increased NO_x emissions by approximately 15 ppm and reduced smoke number from 5.5 to 4.5. This increase in NO_x may be due to a combination of a decrease in residence time of combustion products in the primary zone, a variation in mixing intensity, and a variation in primary zone temperature.

5.4.4.5 Influence of Secondary Air Injection Geometry

Two different secondary air injector tips were tested with the baseline fuel, one with eight radial air jets, and the other which used a conical spreader to produce a sheet of air directed at 45^0 normal to the flow. The radial injector produced slightly greater NO_x reduction and was used for all the comparative investigations previously discussed. NO_x emissions versus primary stoichiometric ratio is presented in Figure 5-131 as a function of atomizer for the conical spreader injector. Minimum emissions with the Sonicore atomizer were 190 ppm and 160 ppm with the Peabody atomizer, compared with 185 and 140 ppm using the radial injector under similar test conditions. Minimum NO_x emission occurred at a primary zone stoichiometric ratio of 0.65 to 0.8 with the conical spreader injector.

5.4.4.6 Fuel Effects — Staged Combustion

In addition to the baseline fuel three other fuels were tested under staged combustion conditions: a diesel fuel, a Bunker C fuel, and a crude shale oil. Results of these experiments are presented in Figures 5-132 to 5-134. NO_x emissions from the Alaskan diesel oil (Figure 5-132) can be attributed entirely to thermal fixation of N_2 since the fuel contains only trace amounts of bound nitrogen. NO_x emissions decreased with decreasing stoichiometry and reached a minimum at a primary zone stoichiometric ratio of approximately 0.55. Minimum NO_x emissions with the Sonicore and Monarch atomizers were 60 and 50 ppm, respectively. Smoke emissions were very low, reaching a maximum smoke number of three at the worst condition. Smoke numbers with the Sonicore atomizer were lower than those achieved with the Monarch atomizer.

Results with the Alaskan Bunker C oil are presented in Figure 5-133 for the Sonicore and Monarch atomizers. In this case the Sonicore atomizer produced lower minimum NO_x emissions than did the Monarch, but higher unstaged NO_x emissions. Minimum NO_x emissions were 200 ppm and 230 ppm for the Sonicore and Monarch atomizers, respectively. Smoke emissions were very high with the Monarch atomizer (BSN>9) and acceptable (BSN=6) with the Sonicore. Similar results were obtained with the crude shale oil (Figure 5-134). In this case the Sonicore atomizer produced significantly lower minimum NO_x emissions than the Monarch and much higher unstaged emissions. Minimum NO_x emissions of approximately 325 ppm were obtained at a stoichiometric ratio of 0.75 with the Sonicore atomizer corresponding to a 75 percent reduction of NO_x. In comparison, only a 45 percent reduction was obtained using the Monarch atomizer, reaching a minimum NO_x level of 550 ppm.

5.4.4.7 Summary — Staged Combustion Studies

The results from the investigations involving staged combustion can be summarized by:

- Primary zone stoichiometry strongly governs NO_x levels achieved during staging. In general, minimum NO_x emissions were observed at a primary zone stoichiometric ratio of 0.8.
- Increasing first-stage length (hence, first-stage residence time) at constant primary zone stoichiometry decreased NO_x emissions and increased smoke emissions asymptotically to a minimum and maximum, respectively.
- Variations of atomizer and flow field produced minimum NO_x emissions from 145 to 185 ppm for the Indonesian/Malaysian oil.
- Variations of atomizing air or steam pressure produced only slight changes in minimum NO_x. Steam atomization resulted in slightly lower smoke emissions under staged combustion.

- Flue gas recirculation to the primary zone at minimum staged NO_x conditions resulted in an increase in NO_x and a reduction in smoke.
- Minimum NO_x emissions increased strongly with fuel nitrogen content up to full nitrogen levels of 0.5, and then increased only slightly as nitrogen content was increased to greater than two percent.

6.0 CONCLUSIONS

6.1 Fuel Properties

Under excess air conditions fuel nitrogen is the primary composition variable controlling fuel NO formation. NO_x emissions increase with increasing fuel nitrogen content. This conclusion can be drawn from both the pilot and the bench scale studies. As expected staged combustion drastically reduces both thermal and fuel NO_x. The NO_x reductions achieved by staged combustion were less dramatic in the pilot scale than in the bench scale experiments. Both systems indicate a very strong dependence of minimim NO_x level on fuel composition and unlike the excess air data, the minimum emissions do **not** correlate simply with total nitrogen content. Under normal operating conditions (excess air), the fuel volatility appears to have little effect on fuel NO conversion, because the spray and air distribution give a well-dispersed, rapidly mixed, heterogeneous system which appears insensitive to the rate at which the fuel nitrogen compounds are released from the liquid drops. Under staged combustion conditions however, if all the nitrogen has not been vaporized in the rich stage, then the effectiveness of the staged combustion could be reduced. To quantify the distribution of nitrogen in each of the fuels tested, vacuum distillation data were obtained by an independent laboratory. In each case, the oil was vacuum distilled into five fractions and the total mass and nitrogen content of each of the fractions was determined. Figure 6-1 shows these data plotted relative to the Essex County fuel oil as a function of distillation temperature. The data indicate that there is a large variation in the temperature at which nitrogen is evolved from the various oils, probably due to differences in the chemical speciation of the oils. Those fuels with the largest quantity of refractory nitrogen appear to be the least amenable to control by staged combustion.

6.2 Flow Field Effects

The influence of atomizer design on NO_x emissions was investigated in the pilot scale tests and Figure 6-2 presents one example of these results. The four atomizers shown with solid symbols were characterized with the laser diffraction analyzer. The Peabody and Todd nozzles produced similar dropsize

(Symbols are as defined in Figure 3-2)

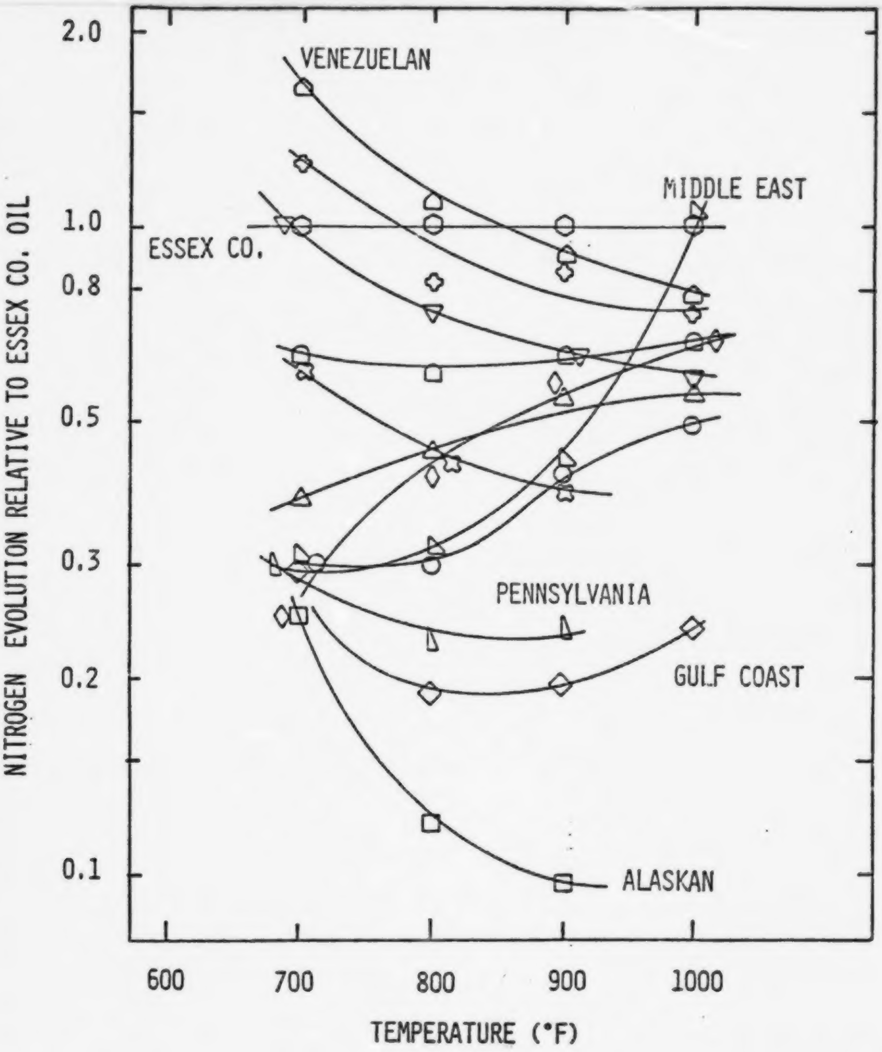

Figure 6-1. Relative Volatility of Nitrogen Species in Residual Oils.

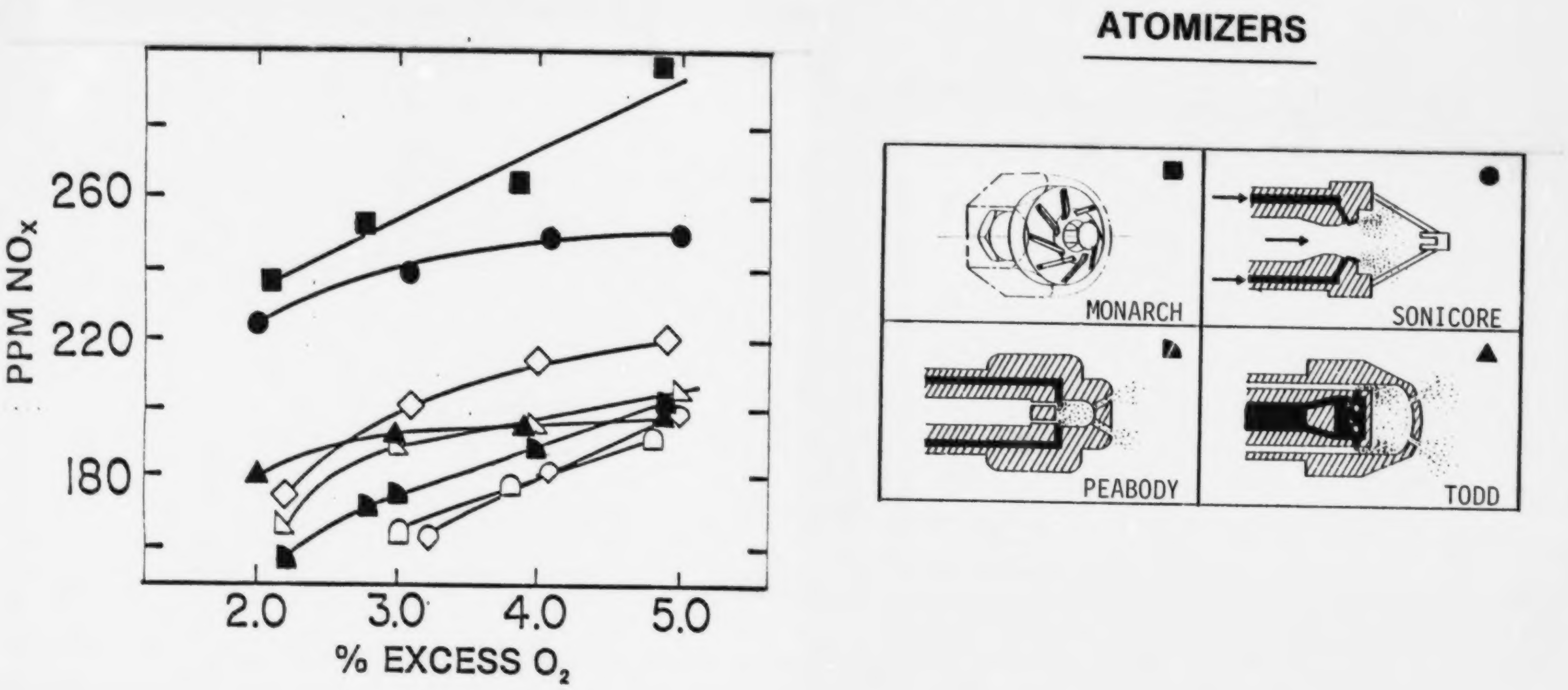

Figure 6-2. The Effect of Spray Flow Field Interactions.

distributions (mean diameter approximately 40 microns). These sprays were produced by six distinct jets. The largest mean dropsize was produced by the Monarch nozzle and the Sonicore produced the smallest.

The importance of nozzle design upon NO_x emissions is illustrated in Figure 6-3. Figure 6-3a shows data from five atomizers tested in the firetube simulator in three aerodynamically-different flow fields characterized by swirl numbers. The effect of increasing swirl is seen to be different for each atomizer. Swirl level produces a large change in NO_x emissions with the Monarch atomizer and a relatively mild change with the Delavan atomizer. The data presented in Figure 6-3b illustrates that dropsize information alone is not sufficient to correlate emissions and that flow field characteristics can be very significant with some atomizers.

The tunnel furnace experiments revealed that increasing droplet diameter by decreasing atomizing fluid flow decreases both thermal and fuel NO_x emissions under excess air conditions. Figure 6-4 shows the influence of mean droplet diameter for four different oils under staged-combustion conditions (primary zone stoichiometric ratio = 0.7). The Indonesian/Malaysian oil shows a local minimum at approximately 25 micron mean diameter in agreement with previous fundamental work.[6.5] The three light oils show a small increase in NO_x emissions with an increase in mean droplet diameter; the heavy Alaskan Bunker C was insensitive to droplet diameter.

Figure 6-5 shows analogous results from the package boiler simulator for the Alaskan diesel fuel. Unfortunately, however, the data for the ultrasonic nozzle (mean droplet diameter 22 microns) are significantly above that for the external mix, swirl-cap atomizer (mean droplet diameter 80 microns). This is in direct opposition to the influence of droplet size observed in the tunnel furnace. This apparent contradiction may be due to differences in the mass distributions of the two sprays.

Figure 6-6 shows data from package boiler simulator for both commercial nozzles with the Alaskan Bunker C oil and indicates that with this heavy oil there is apparently very little dependence on mean droplet size. This is in complete agreement with the observations in the tunnel furnace using this heavy oil. Figure 6-6 also illustrates the tradeoff between the decrease in NO_x

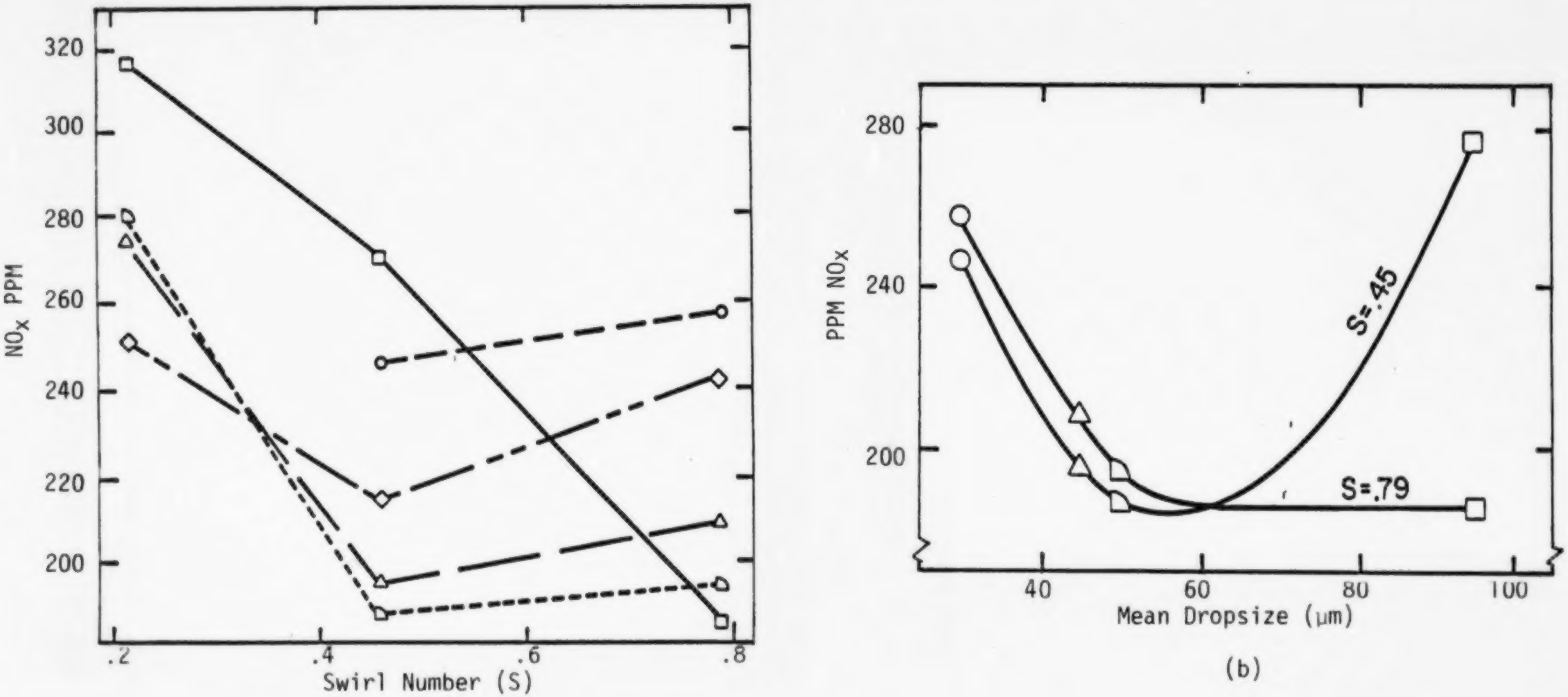

(a)

(b)

Figure 6-3. NO$_x$ Emissions as a Function of Dropsize.

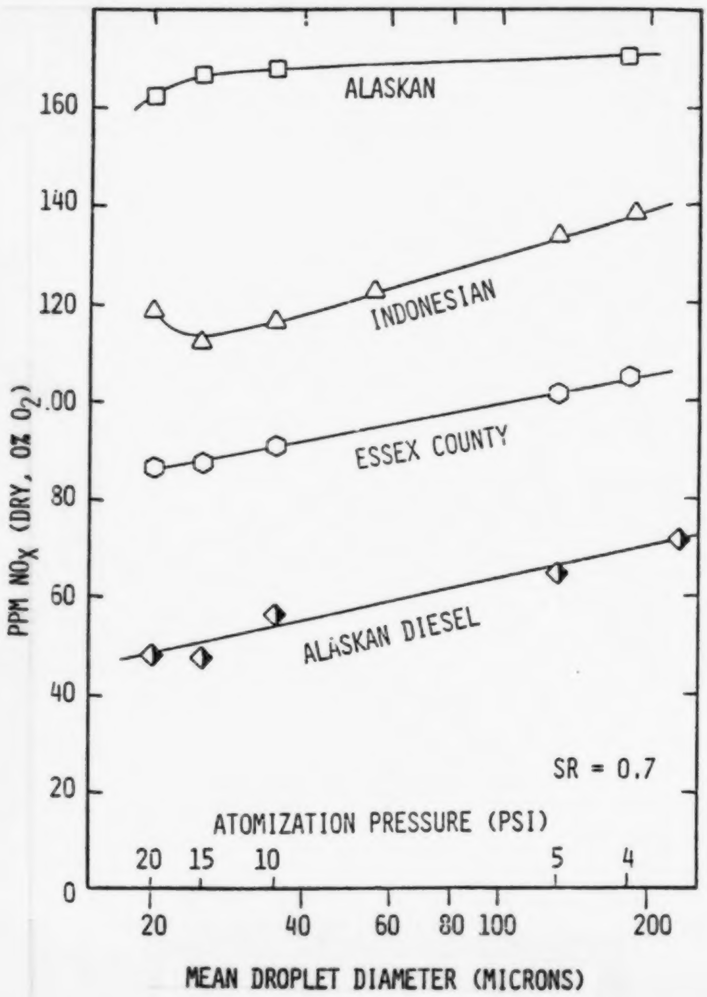

Figure 6-4. Influence of Droplet Size Under Staged-Combustion Conditions - Tunnel Furnace.

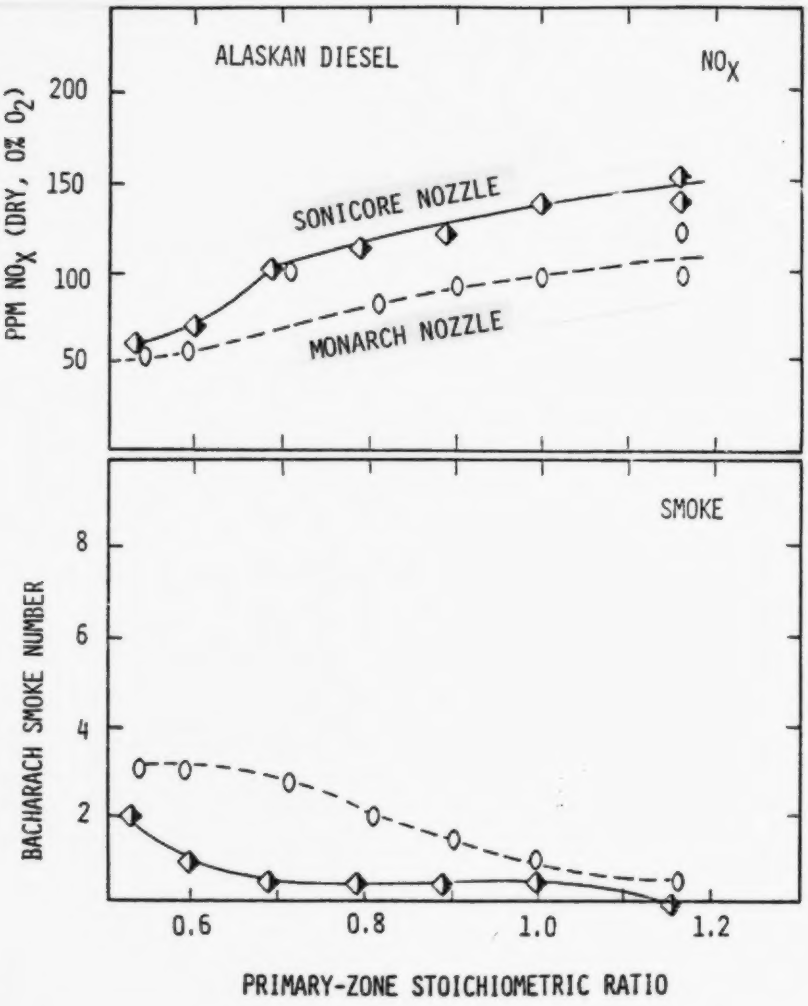

Figure 6-5. Influence of Atomizer Design - Package-Boiler Simulator - Light Oil.

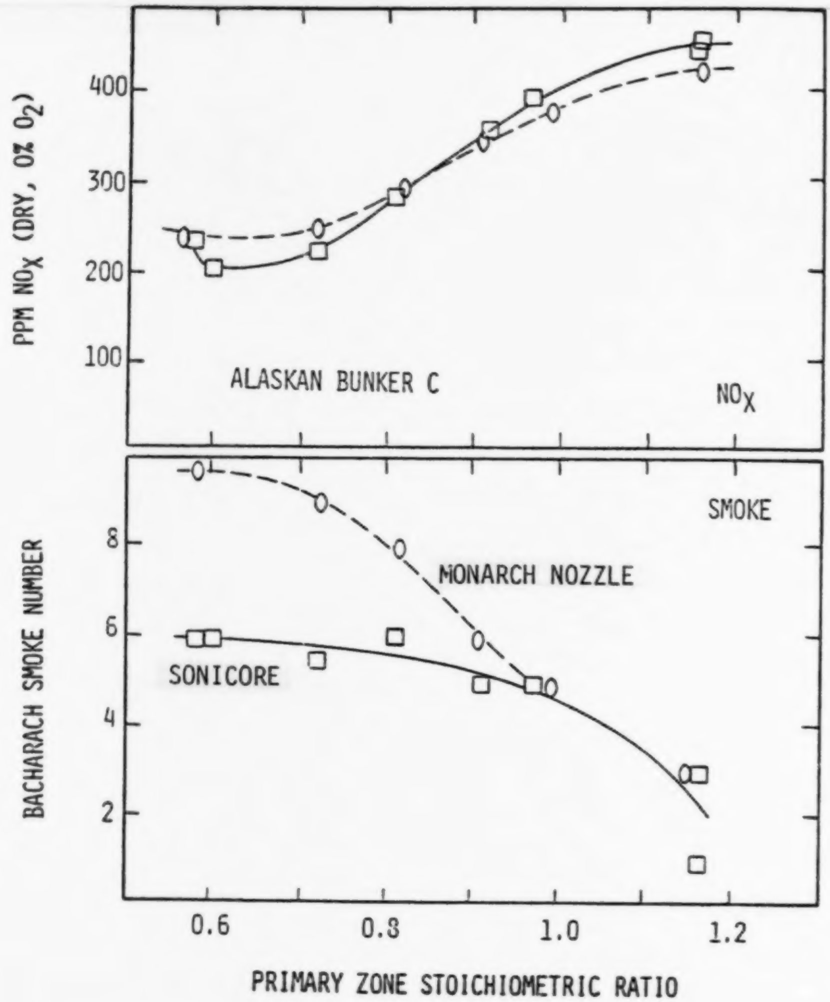

Figure 6-6. Influence of Atomizer Design - Package-Boiler Simulator - Heavy Oil.

emissions and the increase in smoke emissions as measured by Bacharach smoke number. It is significant that although there is little difference in NO_x emissions between the two nozzles, there is a dramatic difference in smoke emissions at the staged-combustion conditions. The ultrasonic atomizer, which produces a very narrow size distribution with a small mean droplet size, results in considerably less smoke than the external-mix, swirl-cap atomizer. Thus it appears that to achieve minimum emissions, with respect to both NO_x and smoke, good atomization will be required in conjunction with a staged-combustion system.

Figure 6-7 shows data from both furnace systems with the Indonesian/Malaysian oil as a function of primary zone residence time. All of these data were obtained with an overall excess oxygen of three percent and primary-zone stoichiometric ratio of 0.7. These data indicate that while the trends in the tunnel furnace are approximately the same as those in the package boiler, there is a major difference between the absolute emission levels. Laser diffraction measurements (Section 2 and Appendix I) indicate that the ultrasonic nozzles used in both systems produce approximately the same mean droplet size and size distribution. The difference in minimum emission levels is therefore believed to be the result of either scale effects (local mixing times) or thermal environment.

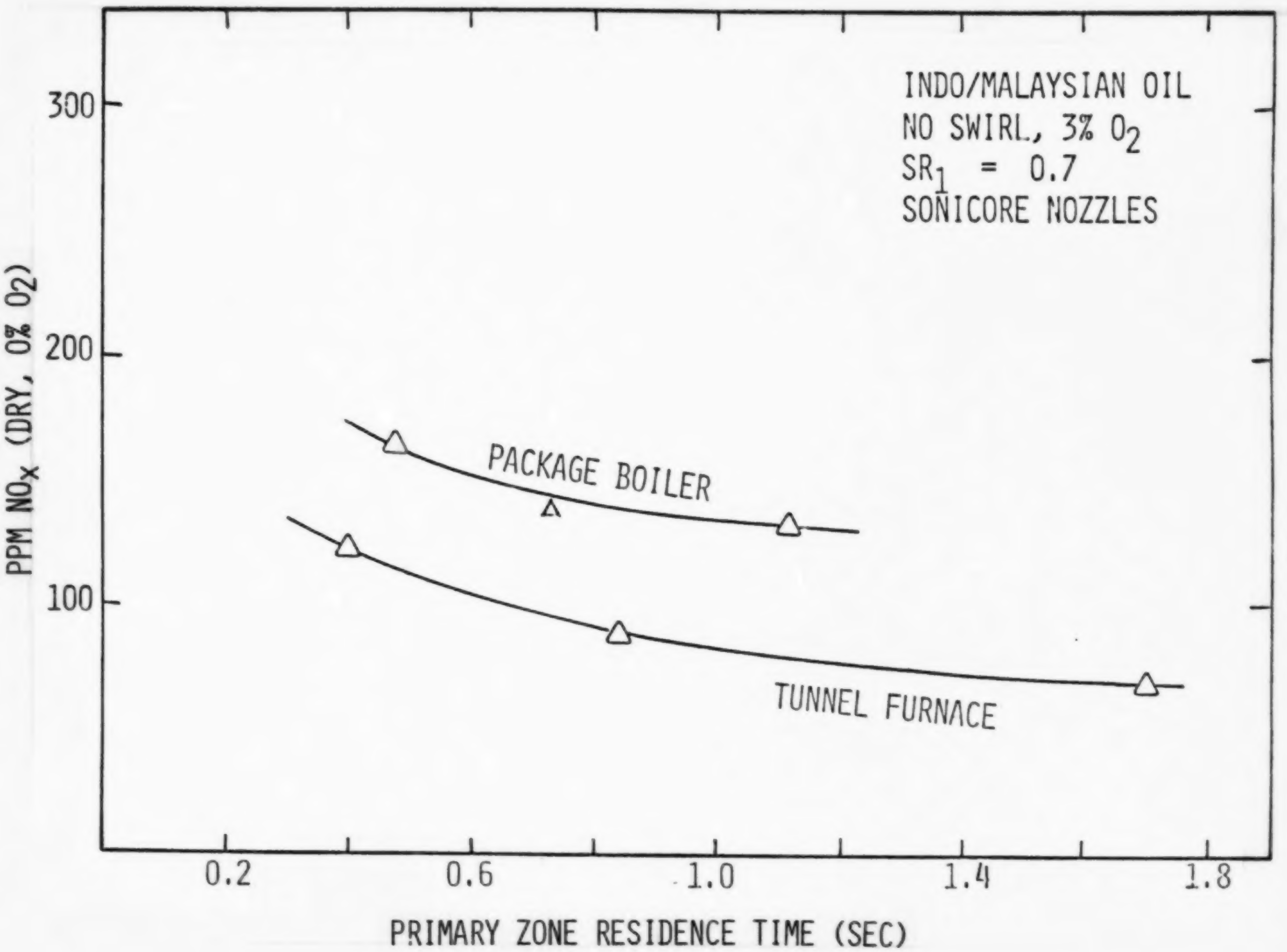

Figure 6-7. Comparison of Experimental Systems.

APPENDIX I

ATOMIZER CHARACTERIZATION

G. Flament and R. Payne

International Flame Research Foundation
IJmuiden, Holland

1.0 INTRODUCTION

This Appendix describes an investigation carried out to characterize the atomizers used in both the bench-scale and the firetube boiler simulator studies. The investigation was carried out at the International Flame Research Foundation using commercially available equipment for spray characterziation, the same nozzles as those used in the combustion studies and an isothermal spray rig.

2.0 EXPERIMENTAL SYSTEMS

This section of the report contains:

- a general description of the spray rig;
- a description of the laser diffraction technique, the principle upon which it is based, detailed of practical operation and indicates its advantages and limitations.

It must be pointed out that the application of this technique is relatively new, and thus the general arrangement of the spray rig and the laser apparatus was improved gradually during the investigation. Similarly, the assessment of the technique results from the experience gained as the work progressed.

2.1 Spray Rig

The spray rig is a box of about 1.7m high and 1.25m section. Figure 1 gives the relative positions of the spray, the laser apparatus, the sampling pipes system and other ancillary systems. It is possible to make several adjustments in order to select a certain sample of the spray or to change the atomization conditions.

2.1.1 Selection of Specific Sample of the Spray

The laser is fixed such that the beam and the axis of the spray cross each other at right angles. Assuming a conical spray with a circular symmetry, the fraction of the spray which is actually traversed by the laser beam, and therefore analyzed, is of a cylindrical shape, and this sample is situated always along a diameter of the spray. On each side of the chamber the laser beam passes through a tube (receiver tube and laser tube) the length of which is adjustable from 0 to 625mm. Therefore, the part of the spray which is actually crossed by the laser beam can be adjusted and it is possible to take the whole width of the spray (tubes completely out) or a very small part around the axis of the spray. During the measurements some air was blown through these two pipes to prevent the smallest droplets from accumulating inside the pipes and making a dense mist which would bias the measurements.

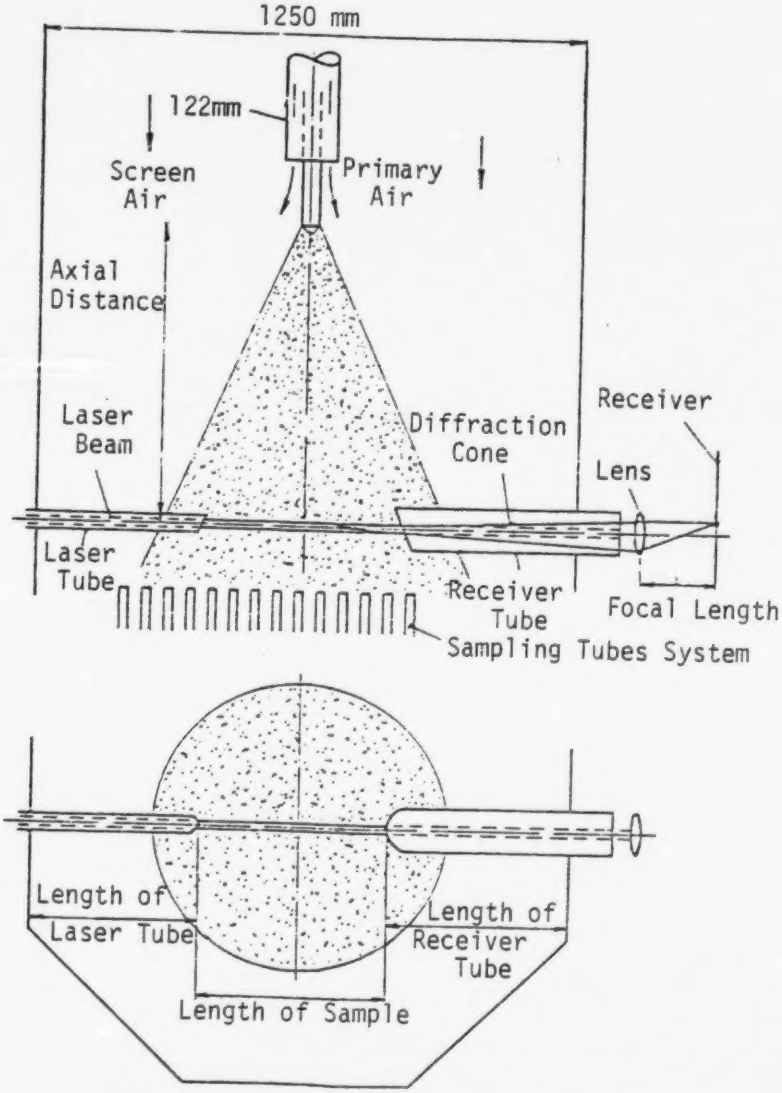

1250 mm
122mm
Screen Air
Primary Air
Axial Distance
Laser Beam
Diffraction Cone
Receiver
Lens
Laser Tube
Receiver Tube
Focal Length
Sampling Tubes System
Length of Laser Tube
Length of Receiver Tube
Length of Sample

Figure 1. Schematic of Apparatus.

The velocity of this purging air was kept very low to avoid disturbance of the spray itself.

To investigate along the axis of the spray it is possible to translate the gun itself and then to change the distance between the nozzle and the laser beam (axial distance) from 10mm up to 625mm.

2.1.2 Conditions of Atomization and Spray Environment

The oil used during the work was a light heat transfer oil whose properties at 20°C are:

- viscosity 20 cst
- surface tension 23 d/cm (23.10^{-3} N/m)
- density 866 kg/m^3

These properties correspond closely to those of a typical heavy fuel oil at a normal working preheat temperature of 120°C. The oil flow can be adjusted up to 100 kg/h and the atomizing air pressure up to 6 bars.

The rig is also equipped to provide a screen airflow all across the section with a maximum mass flow of 1900 kg/h corresponding to a velocity of 0.33 m/s and a primary airflow of 2100 kg/h corresponding to a maximum velocity of 50 m/s with the pipe of 122mm diameter.

2.1.3 Mass Distribution Measurement system

A movable sampling tube system is available to measure the mass distribution in the spray. It is made of 40 tubes of 10mm each, all aligned along a diameter of the rig. The sampling system is not perfectly isokinetic; however, by integration of the volume collected all over the spray it is possible to recalculate the total oil mass flow rate and to compare it with the input mass flow rate. The discrepancy was usually below 20 percent, and therefore, the trend given by this measurement is a good indication of the spatial mass distribution.

2.2 Laser Diffraction Droplet Size Analysis

2.2.1 Principle

The laser droplet size analyzer is based on the Fraunhofer Diffraction pattern of a laser beam by the particles moving in the beam(1). The particle cloud of a spray causes a deflection of a portion of the parallel beam and gives a conical pattern of diffracted light. Since there is a direct relation between the diameter of the particle (assumed spherical) and the angle of the light diffracted by this particle, it is possible to evaluate the diffracted light energy distribution, and thereby calculate the size distribution of a cloud of particles.

The conical diffracted light pattern is measured in the focal plane of a 300mm focal length lens by a photodetector element composed of 30 annular rings whose radii increase from 0.148 to 14.56mm. Table 1 gives a typical printout of the energy distribution measured on this photodetector.

For each ring the signal S corresponds to the measured energy with spray present and the signal B is the background measurement without spray, in such a way that (S-B) gives the real effect of the spray. Although the total light energy measured on one ring of the photodetector is the sum of the contribution of diffracted light due to all droplets, there is a strong peak for a characteristic size of droplet and qualitively it can be considered that the light energy collected on the small rings (first numbers) corresponds to a small angle of diffraction, and therefore is essentially due to the presence of big droplets in the spray. A high energy level on the last ring reveals the presence of a large number of small droplets. This is illustrated in Figure 2 which shows two different normalized energy distributions actually measured on the photodetector for a coarse spray and fine spray.

To calculate directly the droplet size distribution in the spray from the light energy distribution measured on the photodetector a system of 30 equations with 30 variables has to be solved. (Thirty rings corresponding with 30 groups of logarithmically spaced diameter of droplets.) In practice it is easier to assume a priori, a droplet size distribution in the spray

Table 1. Energy Distribution Print Out

N = 0001	S = 0085	B = 0025
N = 0002	S = 0084	B = 0025
N = 0003	S = 0094	B = 0019
N = 0004	S = 0103	B = 0017
N = 0005	S = 0116	B = 0017
N = 0006	S = 0130	B = 0015
N = 0007	S = 0148	B = 0015
N = 0008	S = 0156	B = 0014
N = 0009	S = 0161	B = 0013
N = 0010	S = 0191	B = 0014
N = 0011	S = 0197	B = 0013
N = 0012	S = 0210	B = 0015
N = 0013	S = 0215	B = 0017
N = 0014	S = 0222	B = 0022
N = 0015	S = 0226	B = 0027
N = 0016	S = 0230	B = 0026
N = 0017	S = 0231	B = 0025
N = 0018	S = 0236	B = 0024
N = 0019	S = 0232	B = 0023
N = 0020	S = 0222	B = 0024
N = 0021	S = 0203	B = 0027
N = 0022	S = 0201	B = 0033
N = 0023	S = 0179	B = 0031
N = 0024	S = 0170	B = 0031
N = 0025	S = 0148	B = 0028
N = 0026	S = 0082	B = 0025
N = 0027	S = 0021	B = 0023
N = 0028	S = 0014	B = 0021
N = 0029	S = 0014	B = 0019
N = 0030	S = 0014	B = 0019

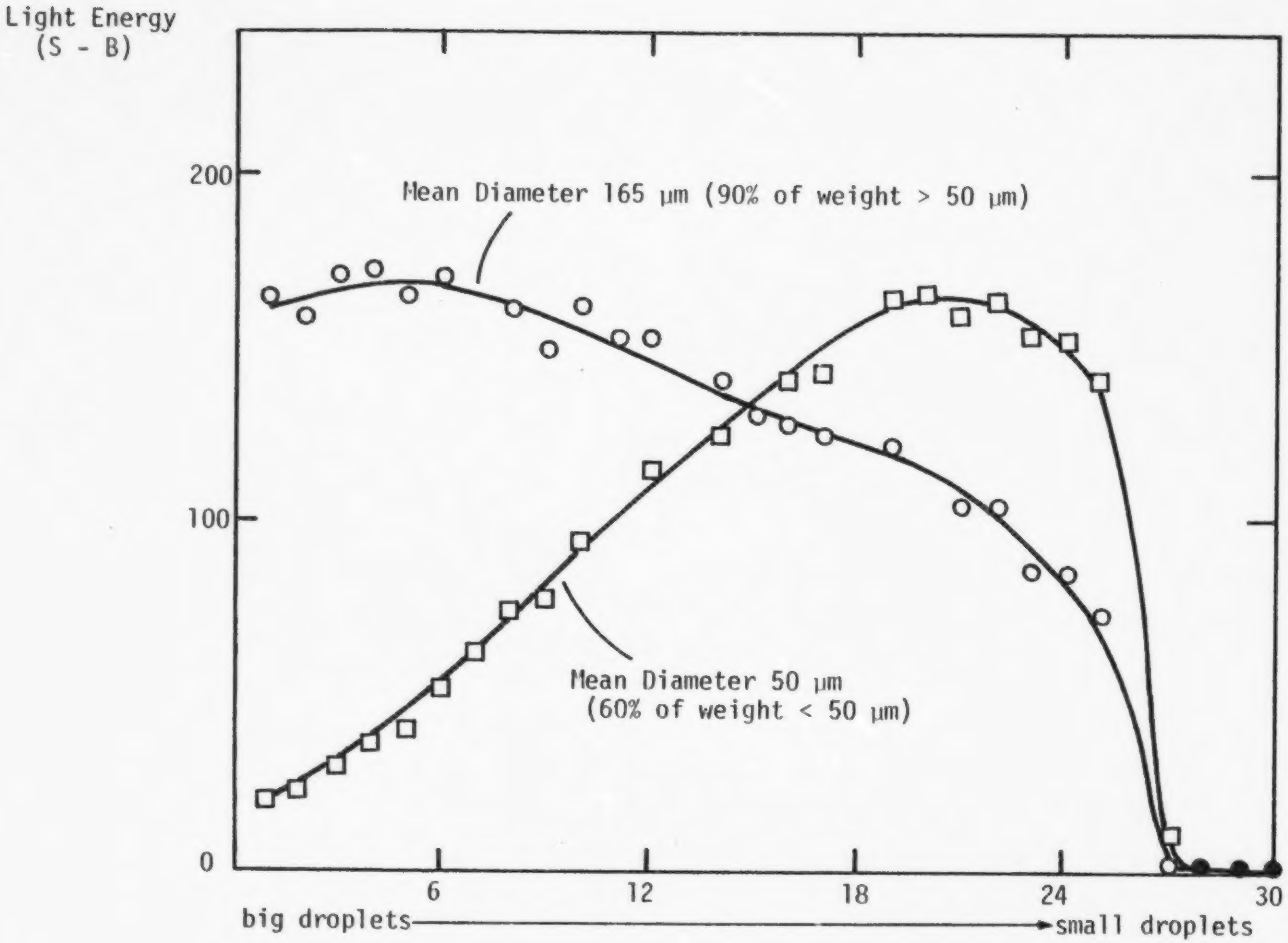

Figure 2. Light Energy Distribution for Two Different Sprays.

and to calculate with a computer the light energy distribution of the corresponding diffraction pattern. By comparison of this calculated light energy distribution with the measured one, and by iteration it is possible to determine the real droplet size distribution in the spray. This method demands the use of a relatively simple mathematical law to describe the droplet size distribuiton of the spray. The instrument delivered by Malvern is associated with a computer and the program now available uses a Rosin Rammler law.

2.2.2 The Rosin Rammler Law

The Rosin Rammler distribution is defined such that the weight or volume fraction of particles of droplets larger than size X is given by R where

$$R = e^{-\left(X/PE\right)^{W}}$$

PE is the Rosin Rammler diameter and W the Rosin Rammler exponent.

It can be seen that a weight fraction 1/e (36.8 percent) is larger than PE. W is a parameter which indicates the dispersion of the size distribution. Typical values of W for real sprays are 1.5 to 3. For a nearly monosize distribution W may be 10 or 20.

A typical result of the parameters PE and W fitted to the measured energy distribution of Table 1 is given in Table 2. First values of PE and W are selected a priori and the computer determines the light energy values which should be read on each ring of the photodetector of the droplet size distribution was following the Rosin Rammler law with PE and W. The comparison between this computed energy, called C, and the actually measured energy on each ring, called A, gives the error value E. By iteration it is possible to minimize E and the optimum values of parameters PE and W are then printed out with the corresponding detailed distribution of droplets size.

For each of the 15 particle size groups the following is given:

- the percentage in weight (P) and in number (N) for each characteristic size;
- the cumulative weight percentage R;
- C and A normalized against a maximum of 2047 (2^{11}).

Table 2. Example of Print Out of Measured Energy Distribution Fitted to Rosin Rammler Law

```
  *CO
  PE   =  +101.0 W =      + 1.9  E   =  00856898          * RE
  PE   =  + 89.0 W =      + 2.0  E   =  00735818          N: 24
  PE   =  + 87.0 W =      + 2.1  E   =  00679904
  PE   =  + 84.0 W =      + 2.2  E   =  00671188          * SE
  PE   =  + 82.0 W =      + 2.3  E   =  00682800          PE: 100
  PE   =  + 75.0 W =      + 2.4  E   =  00721246           W:1.9
  PE   =  + 71.0 W =      + 2.5  E   =  00773318
  PE   =  + 71.0 W =      + 2.6  E   =  00823580
  PE   =  + 66.0 W =      + 2.7  E   =  00891922

> PE=  + 84.0  W=        +2.2  E=  00671188

  D= +562.86 >  +261.71 P=      +0.00%  R=       +100.00%  N=        +0.00%  C=  0462  A=  0577
  D= +261.71 >  +160.29 P=      +1.59%  R=        +98.41%  N=        +0.01%  C=  0691  A=  0783
  D= +160.29 >  +112.86 P=     +13.15%  R=        +85.26%  N=        +0.16%  C=  1004  A=  1047
  D= +112.86 >   +84.29 P=     +21.78%  R=        +63.49%  N=        +0.69%  C=  1333  A=  1341
  D=  +84.29 >   +64.57 P=     +20.57%  R=        +42.91%  N=        +1.52%  C=  1675  A=  1586
  D=  +64.57 >   +50.29 P=     +15.28%  R=        +27.63%  N=        +2.45%  C=  1920  A=  1851
  D=  +50.29 >   +38.86 P=     +10.88%  R=        +16.76%  N=        +3.73%  C=  2044  A=  1949
  D=  +38.86 >   +30.29 P=      +6.70%  R=        +10.06%  N=        +4.93%  C=  1977  A=  1968
  D=  +30.29 >   +23.71 P=      +4.06%  R=         +6.00%  N=        +6.27%  C=  1807  A=  2047
  D=  +23.71 >   +18.57 P=      +2.45%  R=         +3.55%  N=        +7.89%  C=  1592  A=  1988
  D=  +18.57 >   +14.57 P=      +1.45%  R=         +2.10%  N=        +9.71%  C=  1353  A=  1684
  D=  +14.57 >   +11.43 P=      +0.86%  R=         +1.23%  N=       +11.94%  C=  1136  A=  1400
  D=  +11.43 >    +9.14 P=      +0.48%  R=         +0.76%  N=       +13.33%  C=  0931  A=  0861
  D=   +9.14 >    +7.14 P=      +0.32%  R=         +0.44%  N=       +17.83%  C=  0745  A=  0000
  D=   +7.14 >    +5.71 P=      +0.17%  R=         +0.27%  N=       +19.54%  C=  0586  A=  0000
```

2.2.3 Time Resolution of the Apparatus

The 30 rings of the photodetector are sampled sequentially by the computer and a total sweep of all rings takes 13 x 10^{-3} seconds, each ring being sampled during a basic time of 400 µs. It is interesting to multiply the number of successive sweeps in order to get an average value of the light energy distribution during a relatively long period. Figure 3 shows that by increasing the number of sweeps, the dispersion of the results which were obtained for the same conditions of atomization decreases and becomes very small when the number of sweeps is more than 100.

Thus, there is a definite advantage for the laser technique over the photographic technique in that it is possible to multiply the number of "pictures" of the spray. Spray is essentially a nonstationary phenomenon, and thus the comparison between a unique photograph and the average result of multiple sweeps taken with the laser technique may not be compatible. Measurements reported herein were carried out with 200 sweeps.

2.3 Physical Limitations

2.3.1 Limited Diameters of Small/Large Particles

The relationship between the diameter of the particle (d), the focal length of the lens (f), and the position of the peak of diffracted light energy on the photodetector (radius s) is:

$$d \times \frac{s}{f} = 0{,}277$$

Thus, for this system with a given photodetector and a 300mm focal lens the minimum diameter of detected droplet is 5.71 µm. This limitation is basically imposed by the photodetector dimensions and the focal length. There is another limitation imposed by the physical size of the detector lens and its position relative to the spray field. For small particles for which the diffraction angle is large it is possible that the diffracted cone of light may pass outside the lens, especially if these particles are far from the receiver lens.

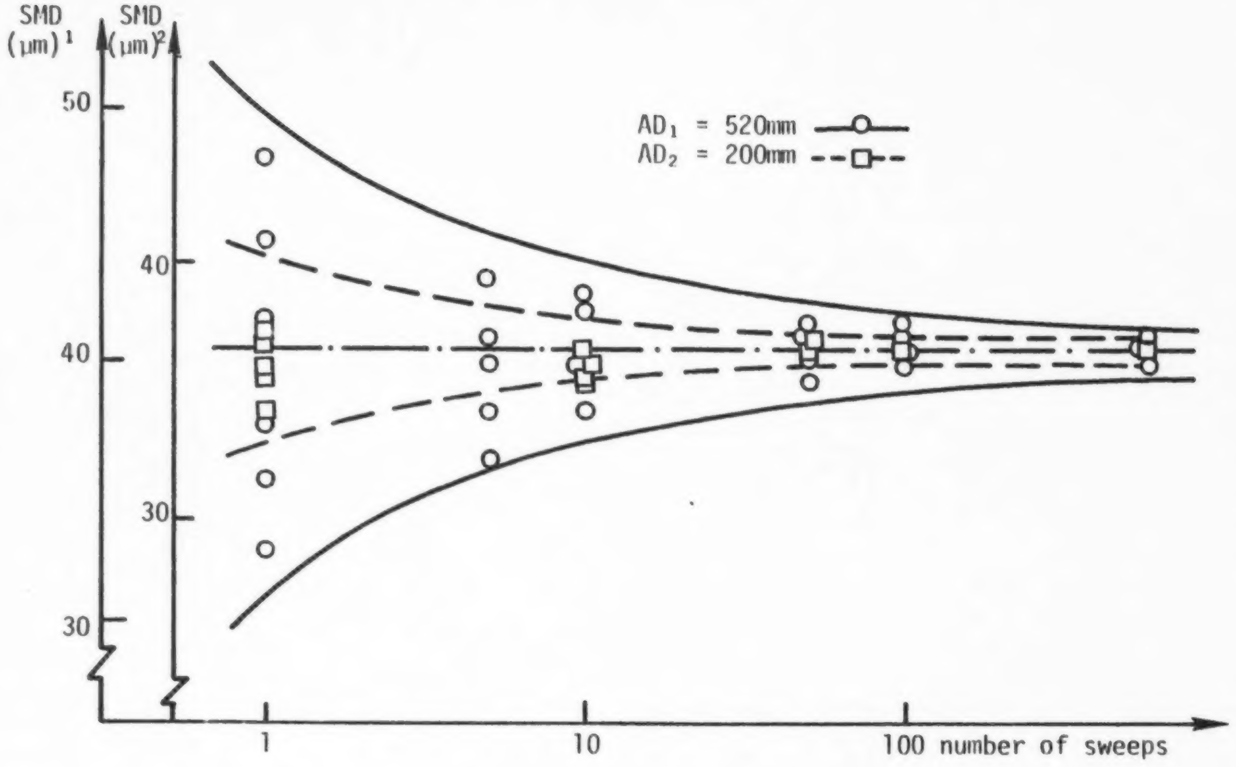

Figure 3. Influence of Number of Sweeps on Sauter Mean Diameter Calculated From Rosin Rambler Diameter.

If X is the distance between the particle and the boundary of the spray chamber opposite the receiver, the condition for a particle of diameter d to be detected is

$X > 1440 - 108{,}3\, d$ with X in mm and d in μm.

The diagram in Figure 4 represents this condition. It is obvious that this extra limitation can be stronger than the limitation due to the system itself, and is dependent on X. For instance, droplets of 7.5 μm diameter are seen only in half of the spray, and therefore, their number is biased by 100 percent. This effect can have a real importance in case of spray with a very small droplet mean diameter.

2.3.2 Density of the Spray

An important limitation common to all optical techniques is multiple scattering. If the density of the spray is very high there is some chance for the light already diffracted by a first droplet to encounter another drop. Secondary scattering will occur resulting in the light being collected at a different radial position to the unidiffracted light. When the number of secondary or multi-scattering events becomes significant, the energy distribution in the diffraction pattern is perturbed sufficiently for it to no longer comply with that predicted by the actual drop-size distribution. The instrument is equipped with a "central reading" meter which gives the percentage of light energy arriving on the center of the photodetector in order to estimate the point at which the effect of multiple scattering events becomes significant since the central reading represents undiffracted light. Some authors indicate a minimum central reading of 50 percent acceptable accuracy(2), but others claim that 90 percent is a minimum (3). It is precisely difficult to select one figure, but is is recommended to be extremely careful interpreting results when the spray obscures more than 50 percent of the transmitted light.

2.3.3 Representativeness of Spray Sample

As stated above, the drop-size distribution is measured for only that part of the spray which is actually crossed by the laser beam. In case of a

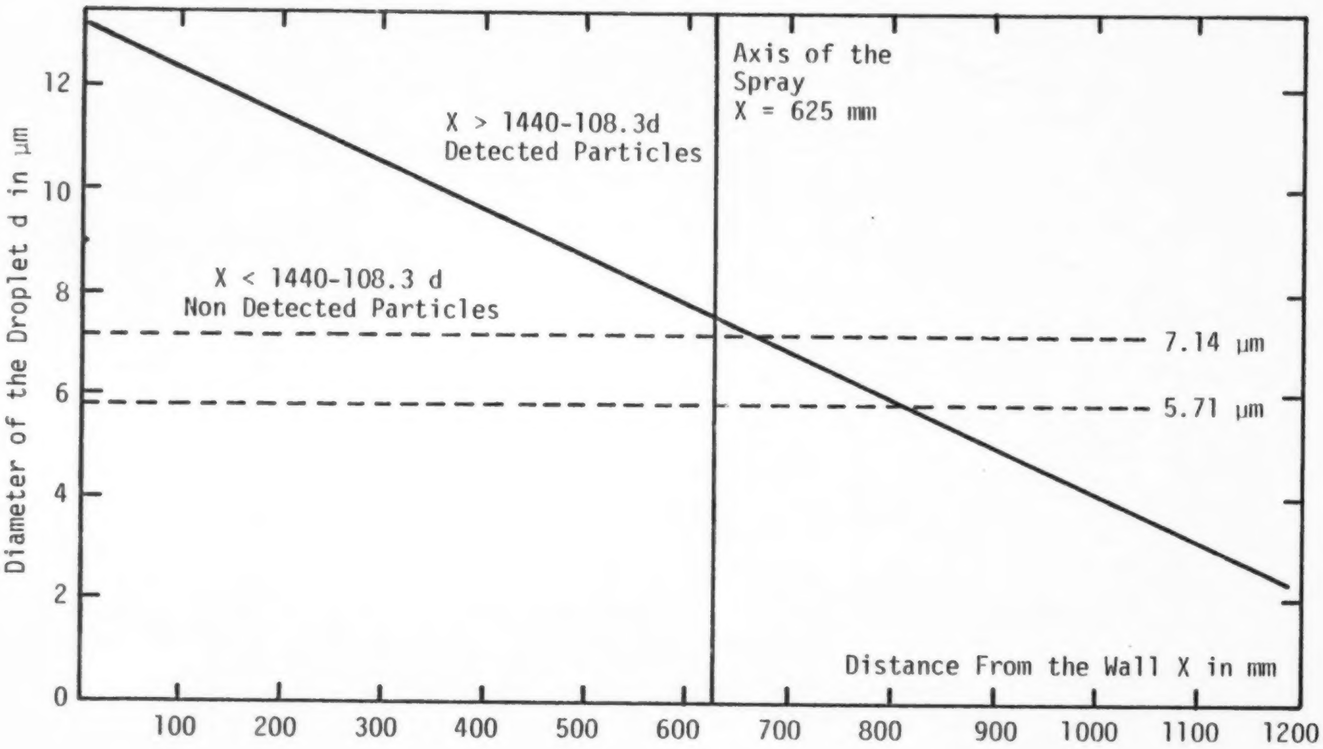

Figure 4. Limitation in Detection of Small Particles Depending Upon Their Position.

nonuniform mass distribution or of a preferential distribution of a certain size of droplets in space the problem of the representativity of the sample arises. Some simple calculations have been made to estimate the possibility of a systematic error due to the fact that the measurements are taken in a limited fraction of the spray and taking account of possible variations of both the concentration of droplets and their size as a function of radial position. The main conclusions are:

1. The droplet size mean diameter in the sampled volume is 20 percent higher than in the whole spray when large droplets are concentrated on the spray axis. This discrepancy is not affected by the spatial distribution of concentration.
2. The droplet mean diameter calculated for the restricted volume of sample is 10 percent lower than when calculated in the whole spray when small droplets are on the axis and when their concentration is higher at the periphery of the spray.
3. These trends are not systematically influence by axial distance.

From the above it can be stated that the integration along the diameter of the spray gives a reasonable estimate of the whole spray even when the spray is nonuniform.

2.4 Velocity Effects

2.4.1 Theoretical Considerations

The light energy measured on each ring of the photodetector is proportional to the number of droplets of the corresponding size which are actually present in the volume of the spray defined by the laser beam during the time of the measurement. This is, in fact, proportional to the concentration n_i of droplets of size d_i in this volume of the spray. If we call $\overline{n_i}$ the averaged number of droplets of diameter d_i per unit volume, S the section of the spray, $\overline{V}_i$ the mean velocity of the droplets of diameter d_i, the number of droplets d_i entering a certain section S_1 of the spray at an axial distance X_1 for a time Δt, will be

$$\overline{N_{i1}} = \overline{n_{i1}}\,\overline{V_{i1}}\,S_1\,\Delta t$$

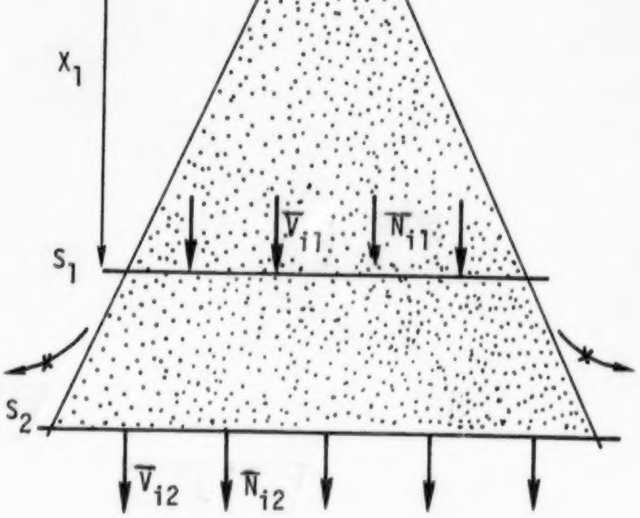

During the same time, through the section S_2, the number $\overline{N_{i2}}$ of droplets d_i has to go out from the spray

$$\overline{N_{i2}} = \overline{n_{i2}}\,\overline{V_{i2}}\,S_2\,\Delta t$$

If we assume no physical changes of droplet size (evaporation, coalescence, secondary atomization), the conservation of the fuel imposes

$$\overline{N_{i1}} = \overline{N_{i2}}$$

thus

$$\overline{n_{i1}}\,\overline{V_{i1}}\,S_1 = \overline{n_{i2}}\,\overline{V_{i2}}\,S_2$$

This relation shows that if there is any change in velocity of droplet there will be a corresponding change in their concentration, and this can alter the measurements based on concentration of droplets. Two cases are possible.

1. $\overline{V_i}\ (X) = f\ (X)$ but $\frac{\partial V_i}{\partial d_i} = 0$ (velocity if a function of axial distance, but not of droplet size)

   Since for a conical spray

   $$\frac{S_1}{S_2} = \left(\frac{X_1}{X_2}\right)^2$$

   We have

   $$\overline{n_{i2}} = \overline{n_{i1}}\ \frac{f(X_1)}{f(X_2)} \left(\frac{X_1}{X_2}\right)^2$$

   and the "weight mean diameter" (very similar to the Rosin Rammler mean diameter is:

   $$\overline{d(X_2)} = \frac{\sum_i \overline{n_{i2}}\ m_i\ d_i}{\sum_i \overline{n_{i2}}\ m_i} = \frac{\sum_i \overline{n_{i1}}\ m_i\ d_i}{\sum_i \overline{n_{i1}}\ m_i\ d_i} = \overline{d(X_1)}$$

   (with m_i = mass of a droplet $d_i = \pi/6\ d_i^{\ 3}$)

   The mean diameter is not affected by axial distance.

2. $V_i\ (X) = f\ (X,\ d_i)$ which means that the velocity variations of droplets are a function of their size. In this case we have

   $$\overline{n_{i2}} = \overline{n_{i1}}\ \frac{f\ (X_1,\ d_i)}{f\ (X_2,\ d_i)} \left(\frac{X_1}{X_2}\right)^2$$

   and

   $$\overline{d(X_2)} = \frac{\sum_i \overline{n_{i1}}\ m_i\ d_i\ \frac{f(X_1,\ d_i)}{f(C_2,\ d_i)}}{\sum_i \overline{n_{i1}}\ m_i\ \frac{f(X_1,\ d_i)}{f(X_2,\ d_i)}} \neq \overline{d(X_1)}$$

   Thus, there is a systematic effect of velocity variations of droplets on the measured mean diameter.

Since it is highly probable that initial velocity and velocity variations of droplet do depend on their size (drag forces), the second case is the most probable one.

It should be pointed out that this problem will be encountered in any technique based on concentration measurements (photographic techniques).

2.4.2 Possible Practical Velocity Effects

Figure 5 shows the effect of the screen air velocity on the Rosin Rammler mean diameter measured for two different sprays. This curve confirms the visual observations: when there is no screen air the finest components are strongly decelerated at the boundary of the spray, thereby their concentration becomes very high and they form a mist in the whole box. This stagnation of small droplets occurring in the laser beam as well, draws the mean diameter towards lower values. A screen air velocity of 0.1 m/s is sufficient to avoid the stagnation of the small droplets and to give a more realistic measurement.

Figure 6 presents the variations of "central reading" with velocity of primary air for a constant spray obtained with a Y-jet atomizer. The atomizing conditions being unchanged, it is strongly believed that the primary air effect is to entrain all the droplets at a higher velocity which decreases their concentration and the density of the optical path, and therefore, increases the part of nondiffracted light.

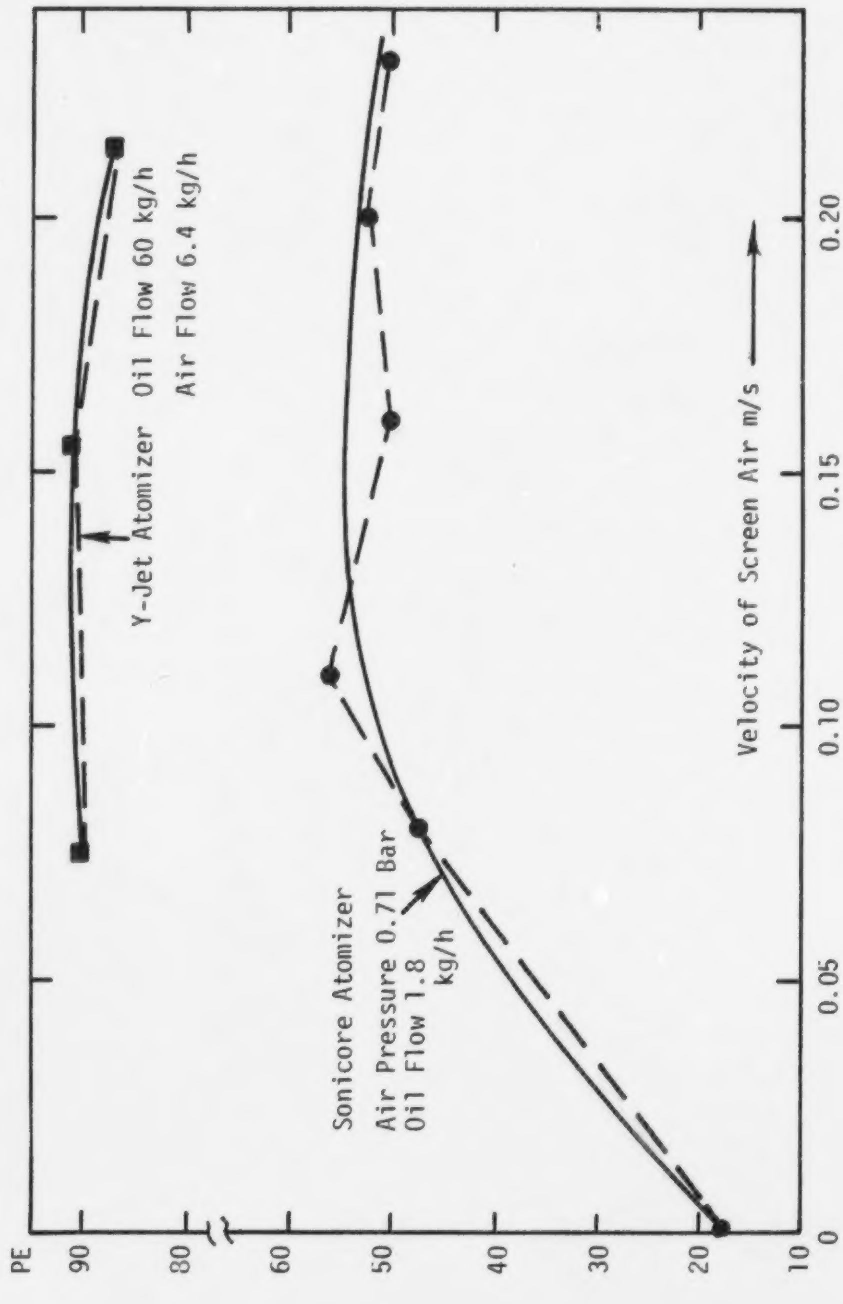

Figure 5. Effect of Screen Air Velocity on Measurement of PE.

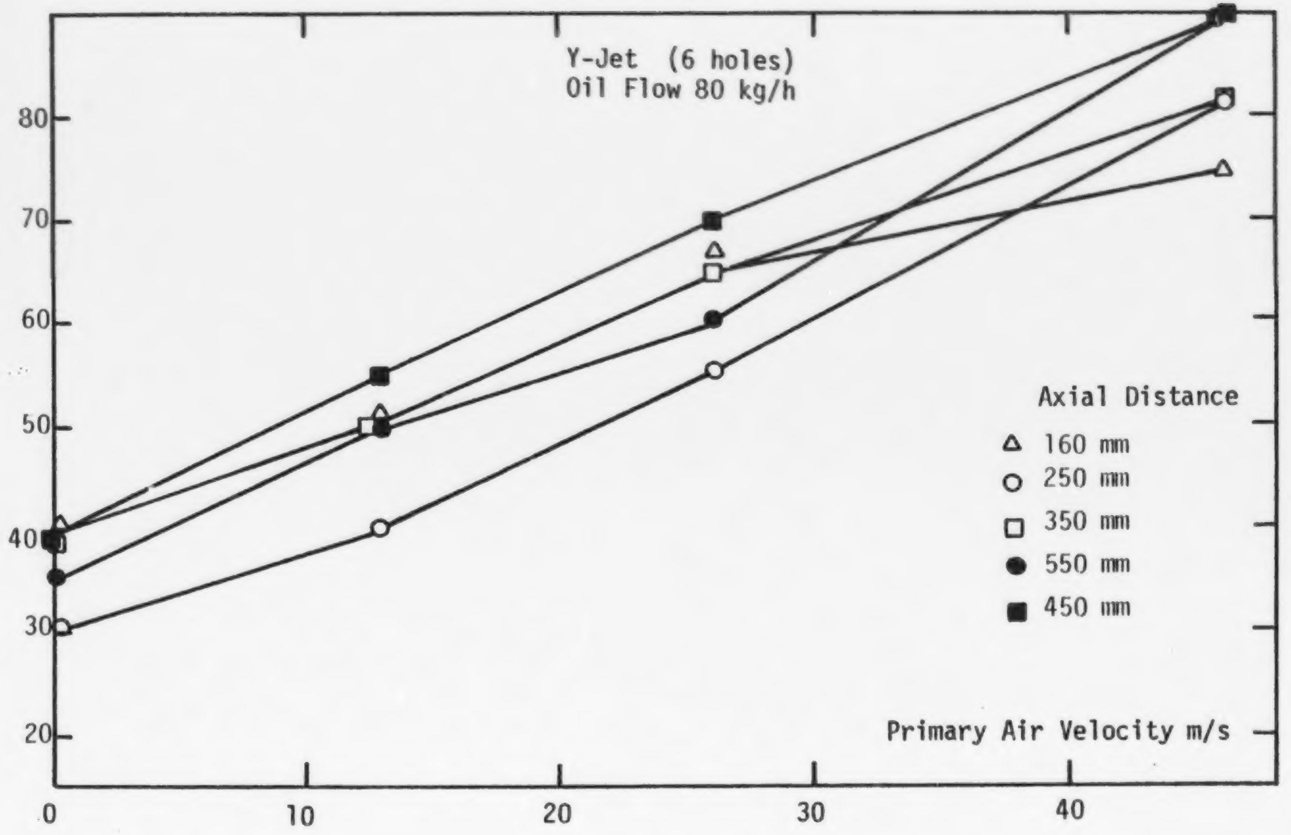

Fig. 6. Percent of Central Reading (non-diffracted light) with Changing Velocity of Primary Air.

3.0 ATOMIZER CHARACTERISTICS

Table 3 lists the six atomizers and the conditions under which they were tested and this section of the report presents the results in terms of:

- mass distribution and spray shape
- droplet size distribution at 200mm axial distance
- axial distance effect.

3.1 Mass Distribution and Shape of the Spray

Figures 7 and 8 present the results of mass distribution measurements available for all atomizers, except the Delavan siphon because the sampling system was not suitable for the very small throughput of this atomizer. All the measurements were made with the sampling tubes positioned 200 mm from the nozzle since this was the axial distance selected for general chracterization of sprays. The oil flow and atomizing air pressure were selected as nominal conditions indicated by EER.

3.1.1 Todd CDS and Peabody

Figure 7 presents the results for two of the atomizers which give a typical hollow core spray: Todd CDS and Peabody.

The theoretical limits of the sprays have been plotted assuming a perfectly conical shape with an angle given by the angle of the holes of the atomizer. This angle was estimated at 60° for Peabody and 65° for Todd.

As these two atomizers have six holes and give six discrete jets, the mass distribution is obtained for two of these individual jets which were aligned with the row of sampling tubes. It can be seen that the separation of the jets is very effective in the case of the Todd since there is almost no mass in the center of the spray and the peaks of sampled volume are quite strong and stand near the calculated limits of the spray. Thus, the trajectories of the individual jets are not bent and there is almost no interaction between the six individual jets.

For the Peabody the peaks relative to the two jets aligned with the sample tubes row are not so high, while the amount of oil in the core of the spray is significant.

Table 3. List of Atomizers, Nominal Conditions and Conditions of Tests

Atomizer Identification	Type	Range of Oil Flow kg/h	Range of Atomizing Air Pressure in Bar	Nominal Condition
Delavan Siphon	Twin fluid swirled air	1.1 → 6.9	0.2 → 2	oil: 1.0 kg/h air: 1.4 bar
Sonicore 250T	Twin fluid ultrasonic + resonator	51 → 75	0.2 → 2	oil: 75 kg/h air: 1.4 bar
Monarch	Twin fluid internal mixing, swirl chamber + pintle	51 → 75	0.7 → 4	oil: 75 kg/h air: 1.7 bar
Todd CDS 6-089-60	Twin fluid Y-jet internal mixing	51 → 75	0.5 → 4	oil: 75 kg/h air: 1.7 → 3.5 bar
Peabody 6-086-55	Twin fluid Y-jet internal mixing	51 → 75	0.5 → 4	oil: 75 kg/h air: 2 bar
Delevan Swirl Air	Twin fluid internal mixing, prefilming + pintle	51 → 75	1 → 5.7	oil: 75 kg/h air: 2 → 4 bar

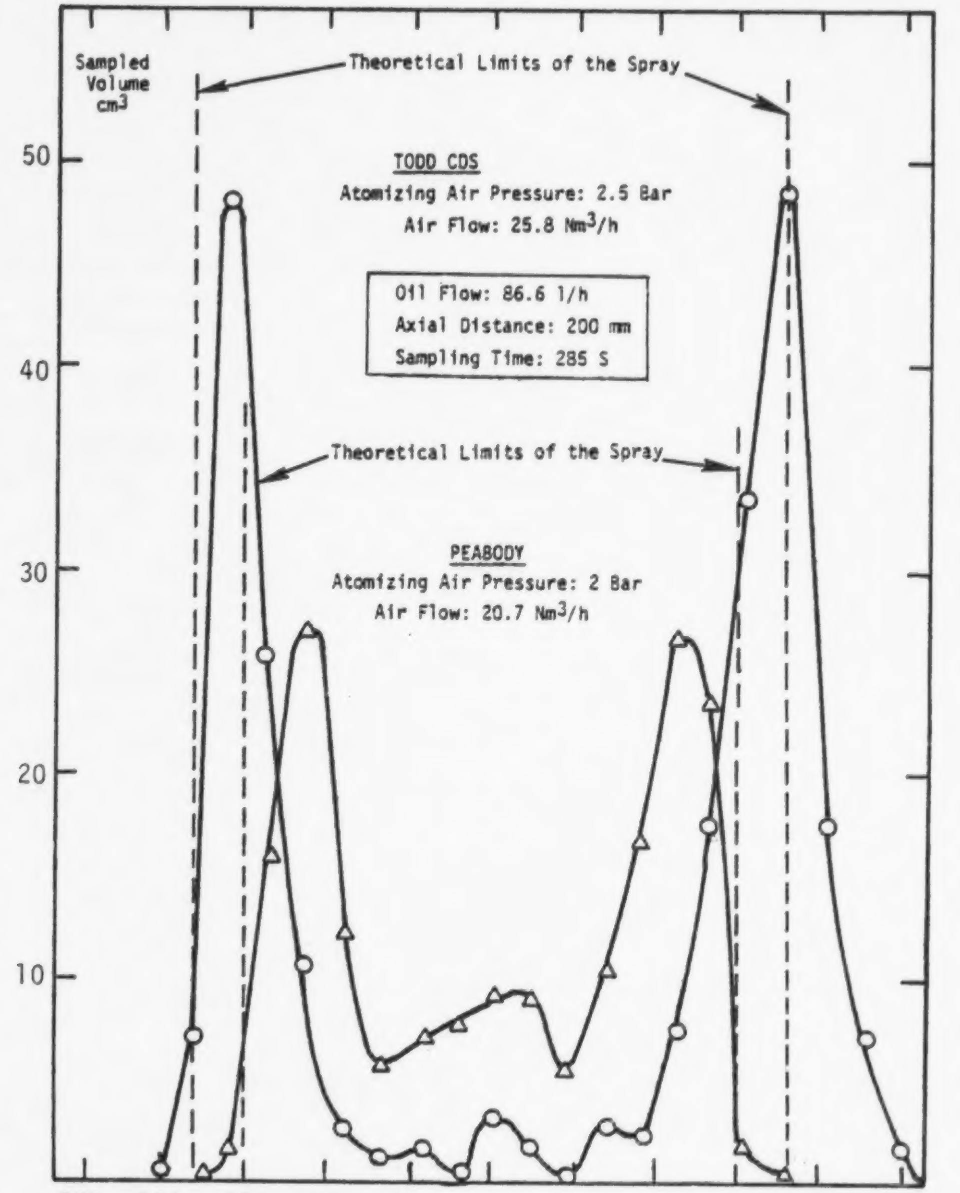

Figure 7. Volume Distributions for Two "Hollow Core" Atomizers.

In the same time the position of the peaks is not so close to the calculated limits of the spray, which means that the streamlines of the individual jets are bent towards the axis due to mutual interaction. Therefore, the spray has the shape of an umbrella and the core is closed by the spray, which probably creates an underpressure in this part due to air entrainment and a deflection of the trajectories of the initial jets towards the axis.

The two differences between the two designs are:

1. The initial angle of the holes in the cap (higher for Todd)
2. The initial distance between the holes on the cap (higher for Todd).

3.1.2 Sonicore 250T, Monarch and Delavan Swirl Air

Figure 8 presents the results for the three atomizers which give a rather full core spray: Sonicore 250T, Monarch and Delavan.

Sonicore 250T

The mass distribution clearly indicates a nonuniform spray which is possible due to the difficulty of getting good atomization for a long time because of very frequent blockages of the oil ports. However, usual observations of the spray itself indicated two basically different modes of operation with regard to the general spray form and dependent upon the atomizing air pressure, Pa. With Pa → 1.1 bar the spray angle was seen to be quite large (generally slightly greater than 100^0), with many fine droplets in the outer region of the spray. This latter point was particularly true for an air pressure of 1 bar where it was difficult to prevent a mist of fine droplets from filling the spray rig.

With an atomizing air pressure Pa → 1.2 bar the spray angle became comparatively narrow, such that beyond an axial distance of 100mm the spray remained almost cylindrical in form with a diameter of some 300mm.

Visual observations of the small Sonicore have given the same indications. With a Sonicore 312T, it appeared that even at very high atomizing air pressures

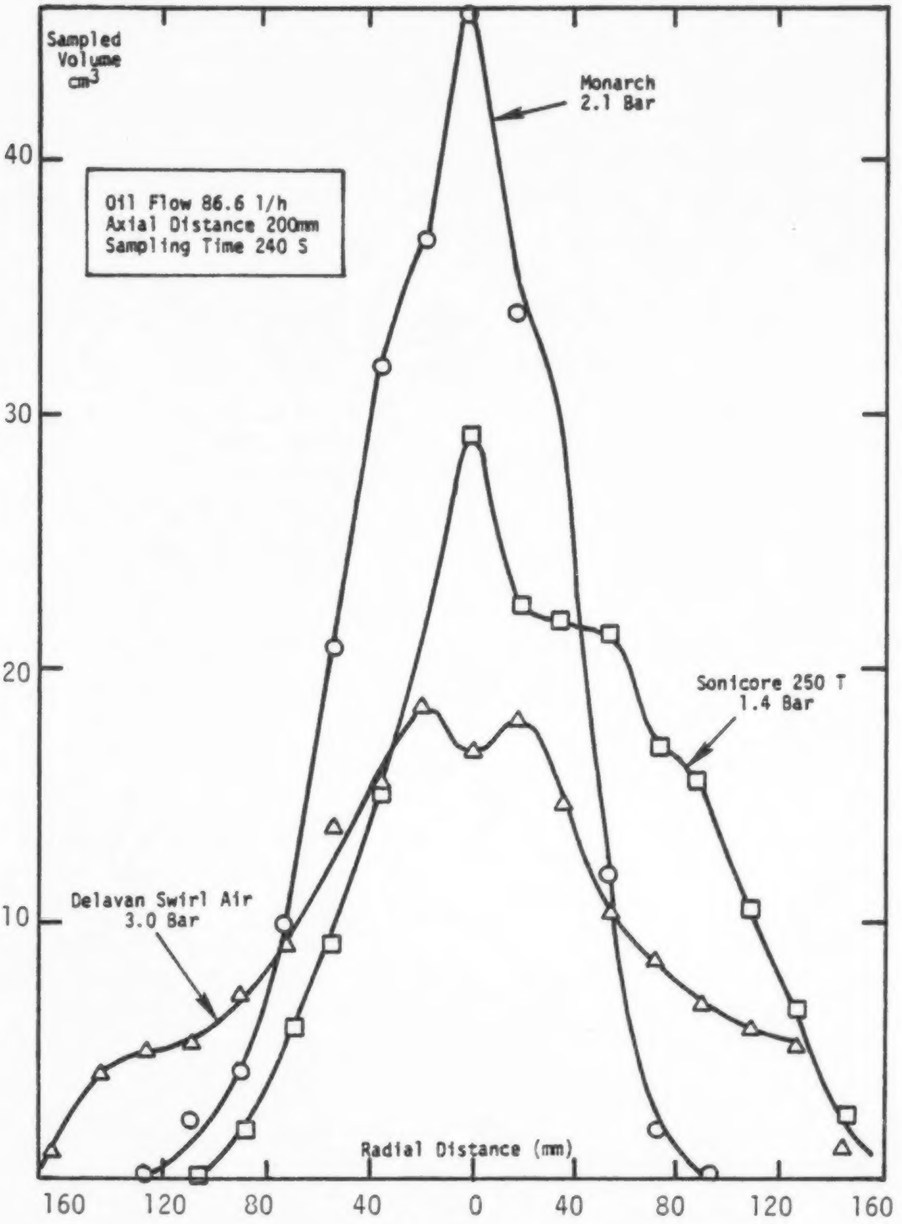

Figure 8. Volume Distributions for Three Atomizers.

the spray angle remained large and separated in three individual jets by the rods supporting the resonator. Therefore, there could be large differences between small and big Sonicore atomizer characteristics.

Delavan Swirl Air

The mass distribution shows a rather wide spray, with a relatively high flow rate around the edges. Visual observations show that the spray is perfectly conical with an angle of about 80° along the first 50 mm, but becomes more cylindrical downstream, especially for high atomizing air pressures. This is believed to be due to the presence of a small pintle at the exit of the nozzle which, in addition to the swirled air, can create a slight underpressure in the center of the spray, and therefore, deflect the trajectories of the droplets towards the axis.

Monarch

The mass distribution of the spray given by the Monarch atomizer is quite peculiar; high concentration along the axis of the spray and a resulting narrow spray while the initial angle, imposed by the cap, is 90°. This is explained by visual observations of the spray (see Figure 9).

These observations indicate the existence of a short zone of recirculating flow, located on the axis of the spray and just below the atomizer tip. This region of strong underpressure is presumably induced by the high velocity swirling airflow and extends for a distance of some 15 mm. Near the exit of the nozzle the spray has a conical shape having an angle of approximately 90°, but is rapidly deflected towards the axis with the main flow region forming a neck at a distance of some 25-30 mm. Outside of the main flow region a less dense skirt of droplets is observed as shown in Figure 9. These observations indicate why the spray does not retain its initial "hollow cone" form. It is also believed that in such a flow field the smaller oil droplets will migrate preferentially to the center of the spray, while droplets in the larger size ranges will remain in the outer regions. It was also observed that at higher atomizing air pressures the diameter of the spray is smaller in the fully developed region, although the overall characteristics of the spray remained unchanged. At an axial distance of 200 mm and for an atomizing air pressure of 2.1 bar the measured diameter of the spray was 240 mm.

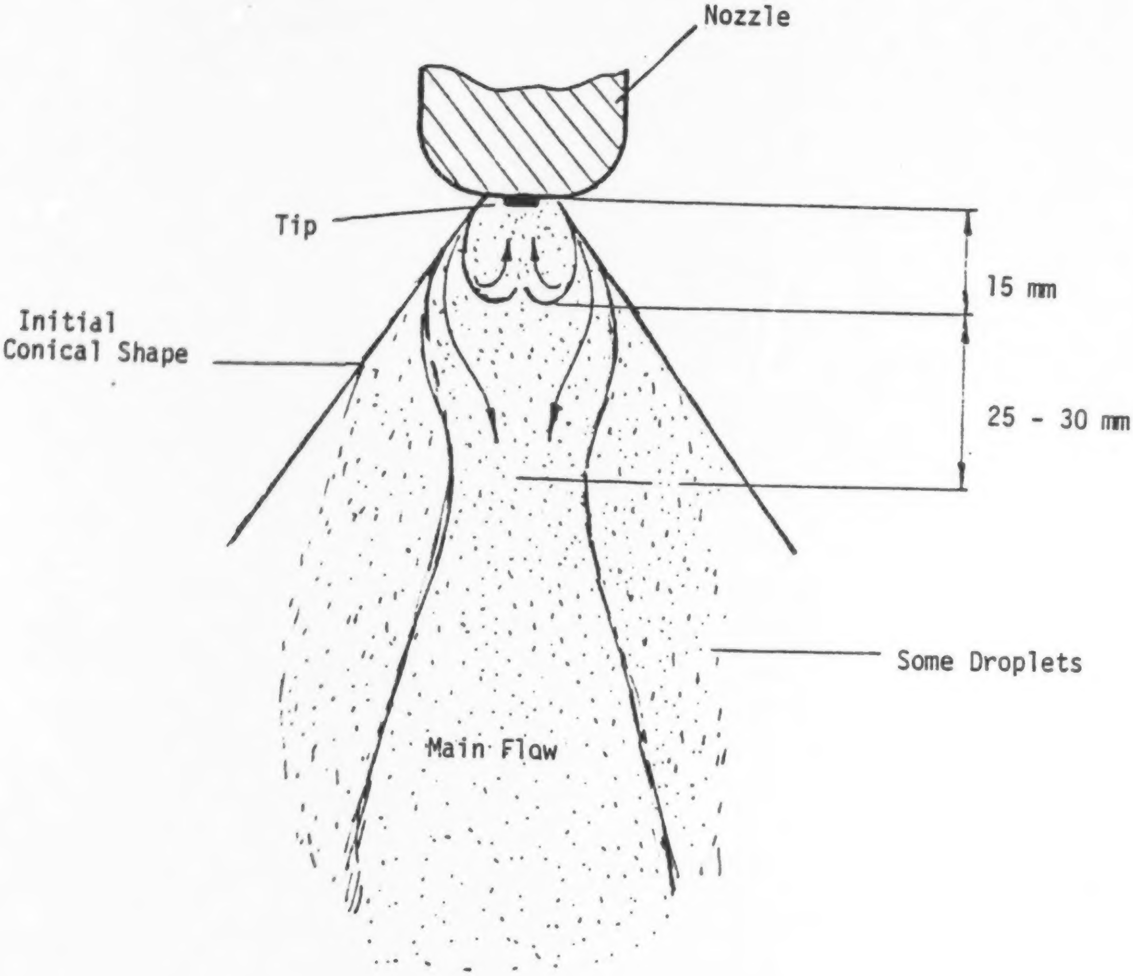
Nozzle
Tip
Initial Conical Shape
15 mm
25 - 30 mm
Some Droplets
Main Flow

Figure 9. Monarch Atomizer. Sketch of Spray with Atomizing Air Pressure 2 Bar and Very Small Oil Flow.

3.2 Droplet Size Distribution

The measurements were taken at an axial distance of 200mm and the effect of oil flow and atomizing air pressure was investigated around the nominal conditions, and within the limits indicated in Table 3.

For all atomizers the following conditions were common:

- Oil viscosity: (20 ±2) cst depending on temperature
- Oil density: 866 kg/m^3
- Air velocity:
  - -- screen air: from 0.22 to 0.33 m/s
  - -- primary air: 0

In all cases measurements were repeated at least twice for all atomizing conditions in order to check repeatability of operations.

3.2.1 Delavan Siphon

Figure 10 shows the variations of the Rosin Rammler mean diameter PE as a function of both the oil flow and the atomizing air pressure.

Figures 11 and 12 give the Rosin Rammler mean diameter PE and the Rosin Rammler exponent W as a function of the air/oil ratio, respectively.

It would appear that both PE and W are essentially dependent on air/oil ratio and almost independent of oil flow when air/oil ratio is kept constant.

For all these measurements the density of the spray remained always very low due to small throughput, and therefore the "central reading" was 100 percent, indicating an extremely low obscuration of the laser beam. For that reason the measurements were taken over the whole width of the spray.

3.2.2 Sonicore 250T

General remarks concerning the measurements:

1. This atomizer gives a rather fine spray and its density was such that in all conditions the "central reading" was too low to

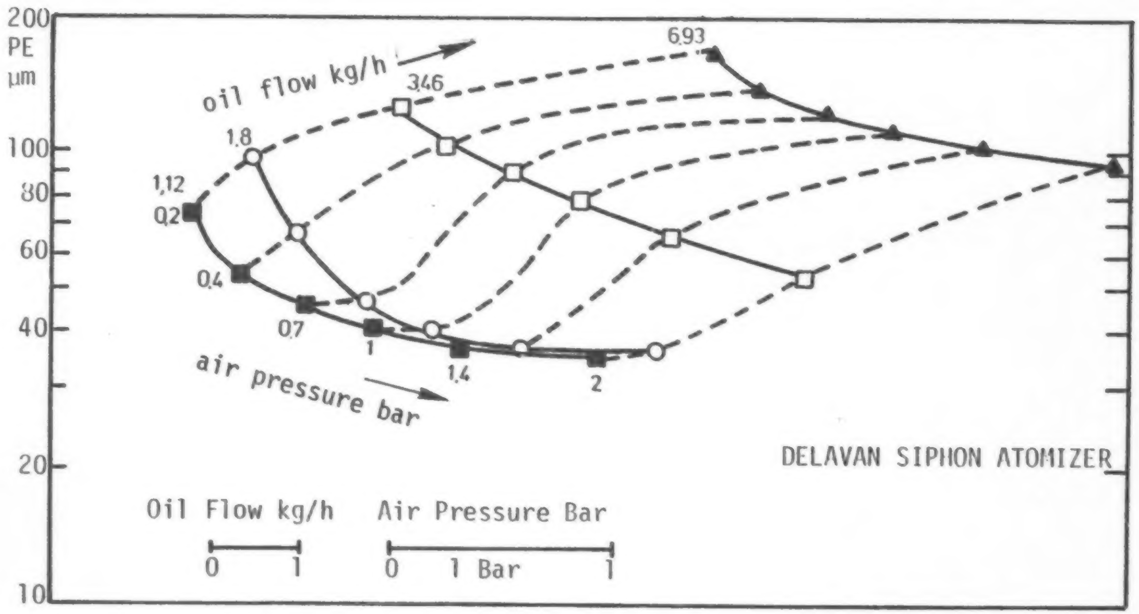

Figure 10. Effect of Oil Flow and Atomizing Air Pressure on the Measured Rosin-Rammler Mean Droplet Size (PE).

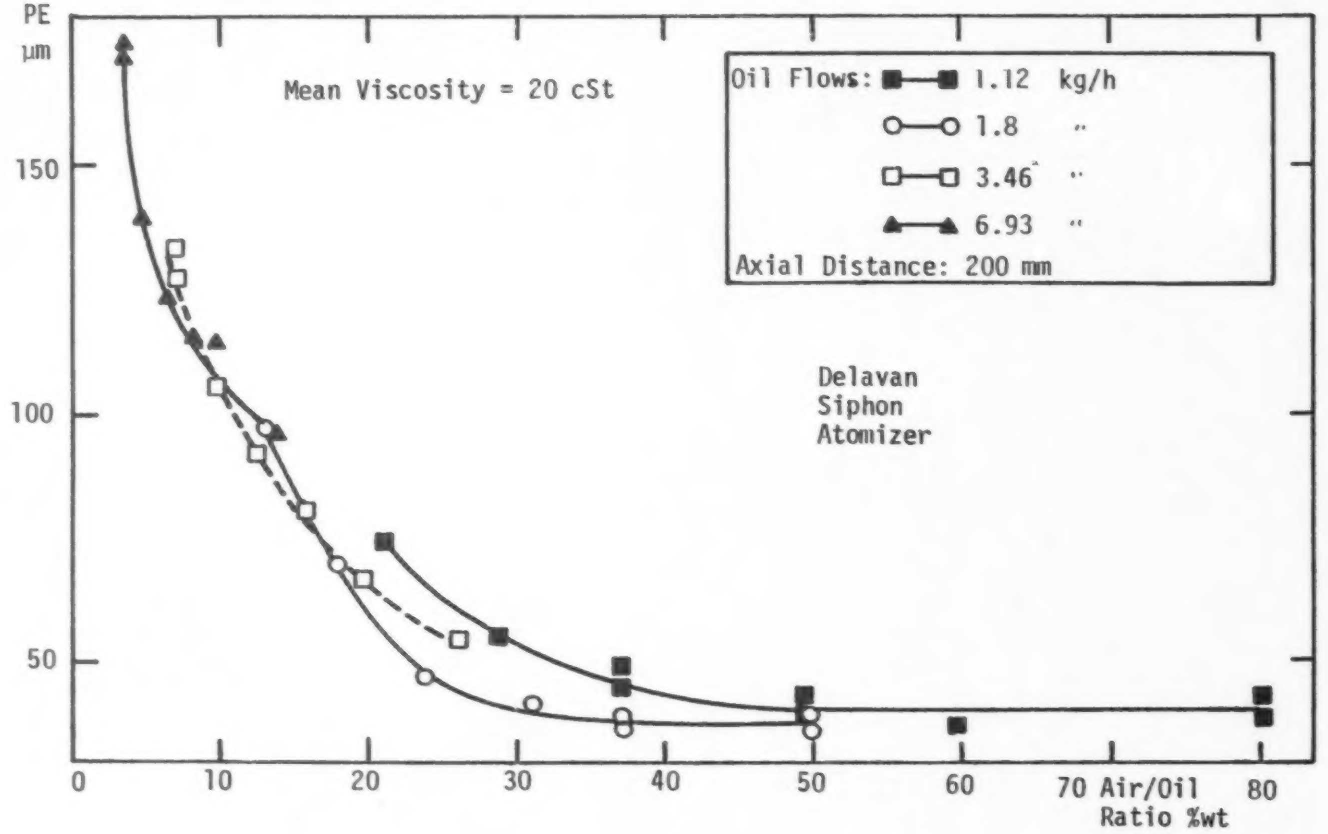

Figure 11. Rosin-Rammler Mean Diameter (PE) as a Function of the Atomising Air/Oil Ratio.

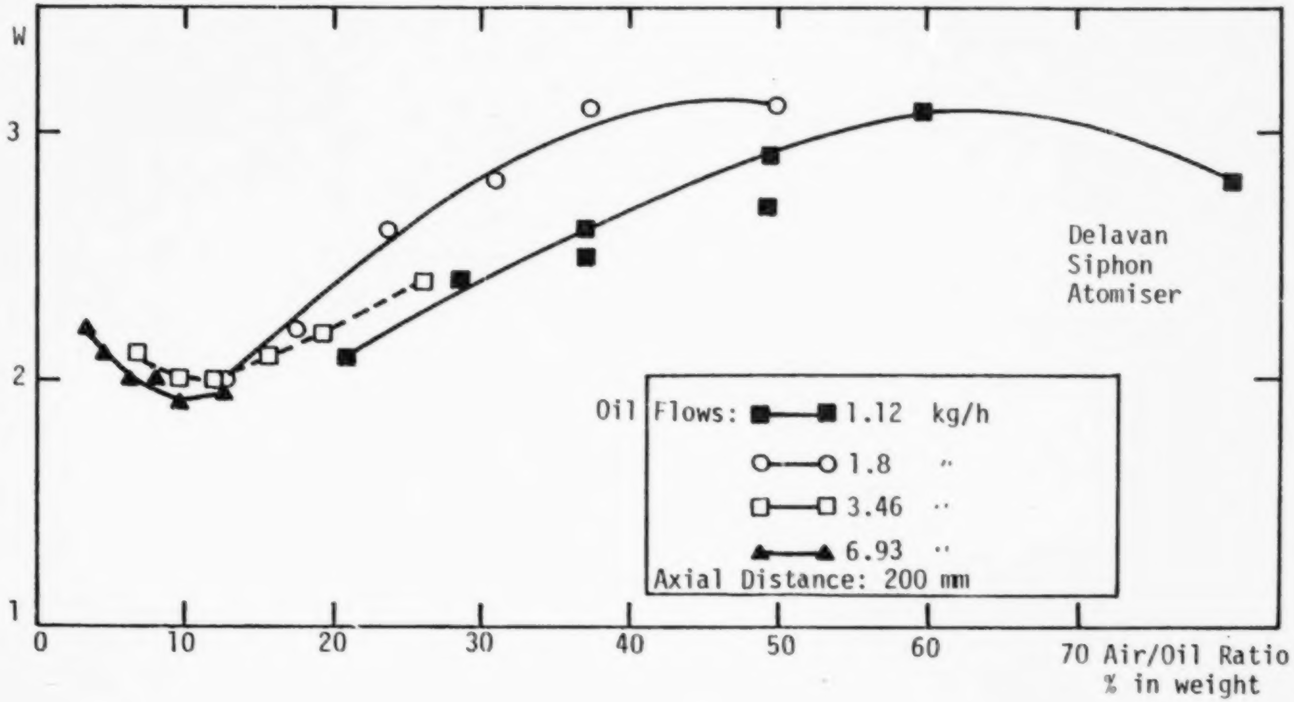

Figure 12. Rosin-Rammler Exponent (w) as a Function of the Atomizing Air/Oil Ratio.

ensure an accurate measurement. To overcome this limitation, measurements were made only through half of the spray by positioning the laser light tube on the spray axis.

2. As indicated before, the Sonicore 250T was very often blocked. The main problem was the poor repeatability of the measurements, due to an obviously poor repeatability of the atomization itself.

   Results are presented in Figures 13 and 14 and give the variations of PE and W as a function of oil flow and atomizing air pressure. Although the repeatability is not very good, they show clearly a decrease of PE together with an increase of W when atomizing air pressure reaches 1.4 bar, which means a monosize distribution of small droplets (10 μm) for the nominal conditions: 1.4 bar - 75 kg/h.

   Meanwhile, it is clear that the effect of oil flow is weak and that atomizing air pressure is the predominant parameter. At that point it is interesting to compare these results with those of the small Sonicore, and those results are presented in Figures 15 and 16.

   It can be seen that if the trends are the same for the variation of PE and W they are more clear with the small Sonicore than with the big 250T. In addition, Figures 17 and 18 give PE and W variations with atomizing parameter for the small Sonicore atomizer, but used without the resonator and with two different oil viscosities: 9 and 25 cst. The effect of oil viscosity is quite low, but the effect of the resonator seems to be quite strong. First, for the atomizer without resonator, the oil flow influences the droplet size while it had almost no effect with the normal atomizer; and second, the atomizing air pressure effect is not so strong without the resonator.

   It appears that for low atomizing air pressures the presence of this cup in the flow contributes to give a rather coarse spray, especially for low oil flows. This can be due to agglomeration

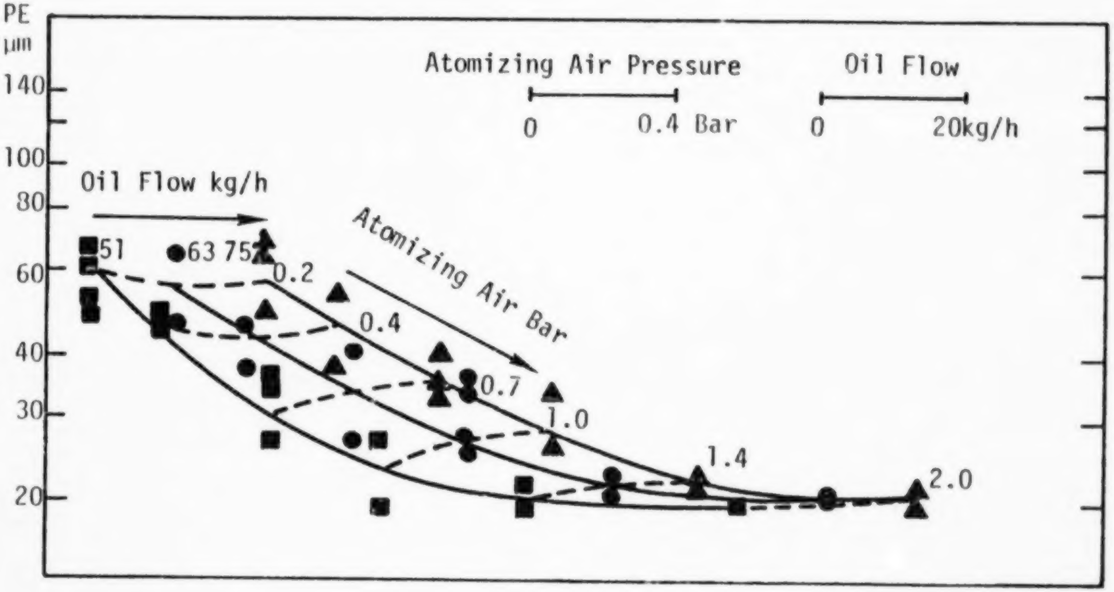

Figure 13. Sonicore 250 T. Effect of Oil Flow and Atomizing Air Pressure on Measured R.R. Exponent W. Second Trial.

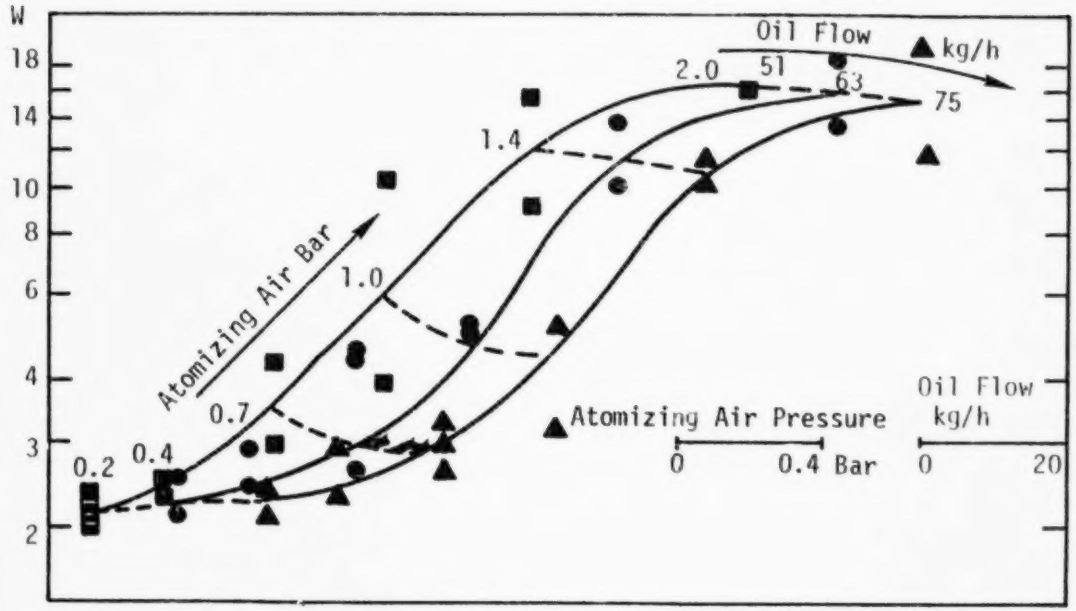

Figure 14. Sonicore 250 T. Effect of Oil Flow and Atomizing Air Pressure on Measured R.R. Exponent W. Second Trial.

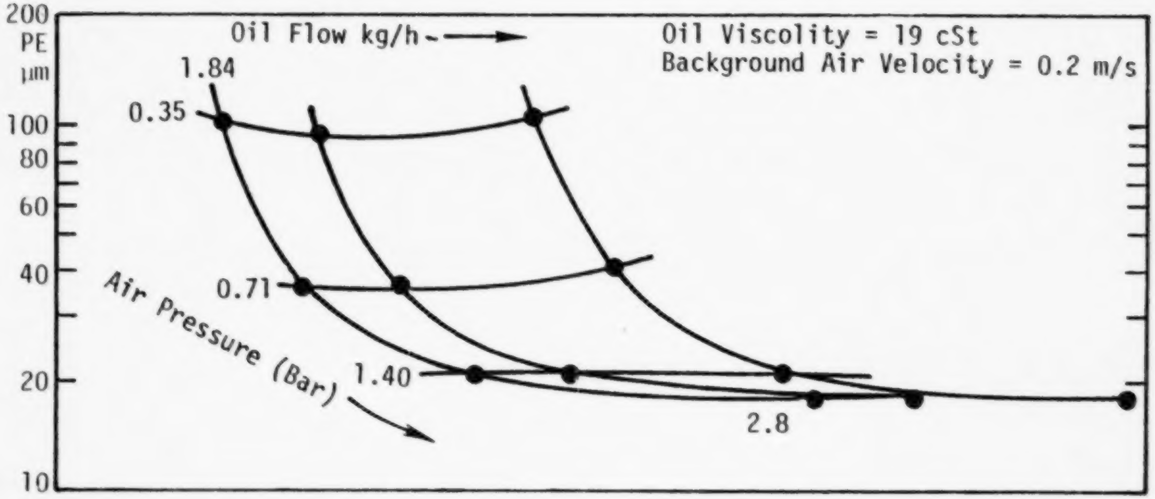

Figure 15. Sonicore Atomizer - Effect of Oil Flow and Atomizing Air Pressure on the Measured Rosin-Rammler Mean Droplet Size. (PE) (3131/2)

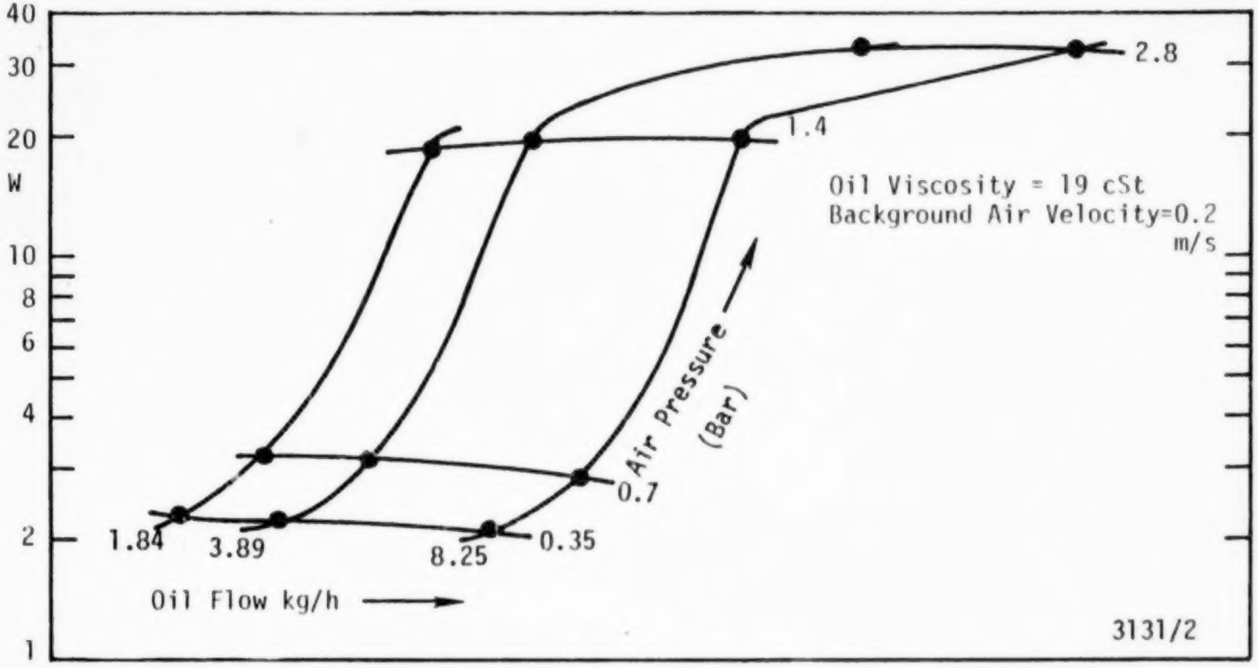

Figure 16. Sonicore Atomizer - Effect of Oil Flow and Atomizing Air Pressure on the Measured Rosin-Rammler Exponent (W).

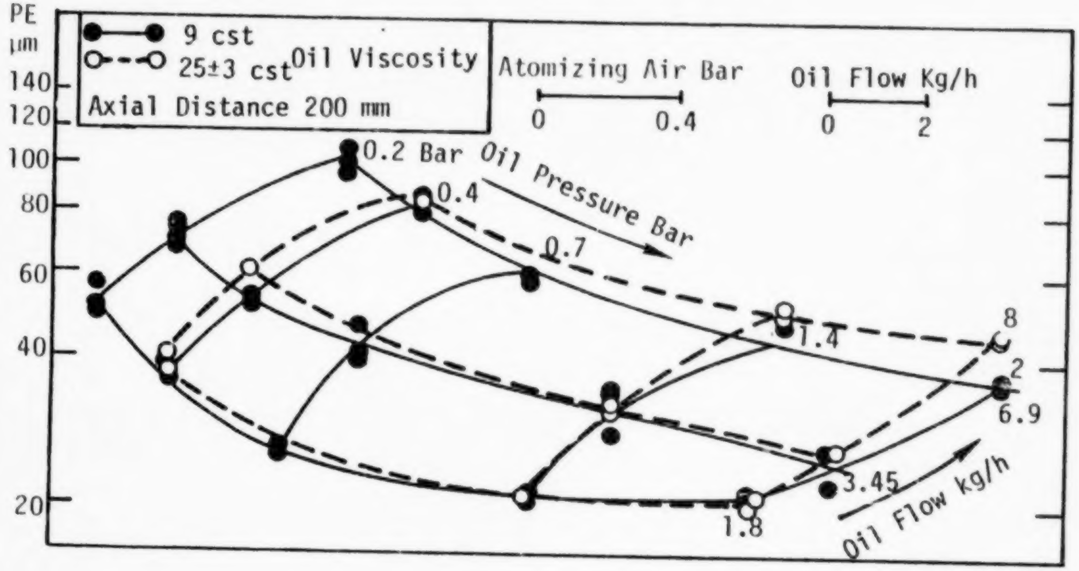

Figure 17. Small Sonicore Nozzle without Tip. Effect of Oil Flow and Antomizing Air Pressure on PE (RR Mean Diameter).

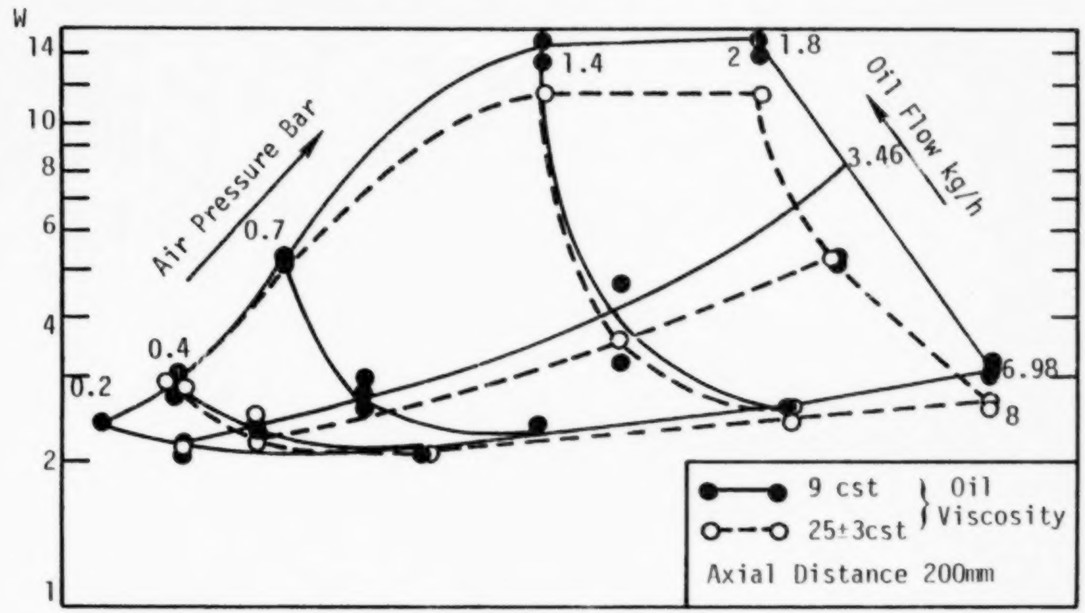

Figure 18. Small Sonicore Nozzle without Tip. Effect of Oil Flow and Atomizing Air Pressure on W (RR Exponent).

of small droplets which impinge on this cup and are not broken any more by the airflow if this one is too weak.

3.2.3 Monarch

As for the big Sonicore 250T, because of density problems all the measurements were taken with the laser light tube positioned on the spray axis. Figures 19 and 20 give the variations of PE and W as a function of atomizing air pressure and oil flow. The repeatability of the measurements was quite good as can be seen on the curves, especially when atomizing air pressure was below 2.5 bar.

The atomizing air pressure has nearly no effect on PE and W when it remains below 1.2 bar. From 1.2 bar to 3.5 bar the mean diameter decreases strongly with air pressure and reaches a minimum of about 22-30 μm depending on oil flow. In the same time W increases from 2.5 to a value which depends strongly on the oil flow: 4 with 75 kg/h of oil, but 10 with 51 kg/h. It is interesting to point out the simultaneous increase of W with the decrease of PE.

3.2.4 Todd CDS 6-089-60

As stated in Section 3.1.1, this atomizer gives a spray made of six discrete jets having an included angle of 65^0 and without any interaction between themselves. For the measurements the spray was, therefore, positioned in such a way that the laser beam was perfectly aligned with one pair of diametrically opposite jets. Most of the measurements were taken through a single jet by shielding the laser beam to the axis of the spray. Some measurements were also taken across two jets; the comparison was excellent, particularly when the atomizing air pressure was lower than three bars. Some attempts were also made to turn the gun in order to measure across one or two other jets. Again, the repeatability was very good. The relative nonrepeatability at high atomizing air pressures may be due to an unavoidable recirculation of small droplets, both outside and inside the spray. Observation showed that this mist of fine droplets built up slowly around the spray and was blown away to rebuild again after some seconds. The periodicity of this phenomenon varied, but was on the order of 20 seconds.

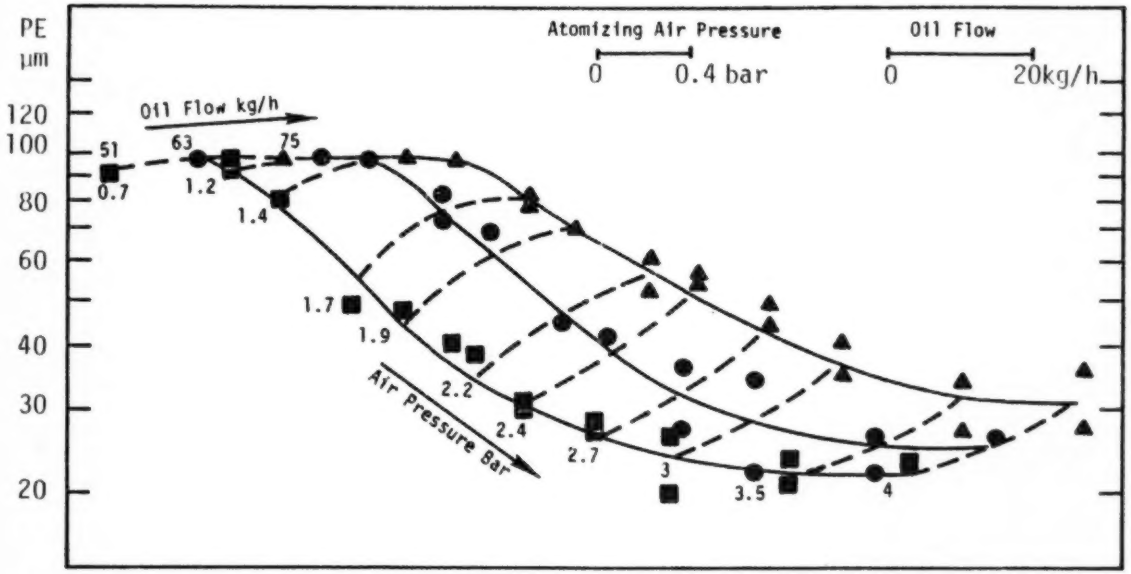

Figure 19. Monarch Atomizer. Effect of Oil Flow and Atomizing Air Pressure on the Measured R.R. Mean Diameter (PE).

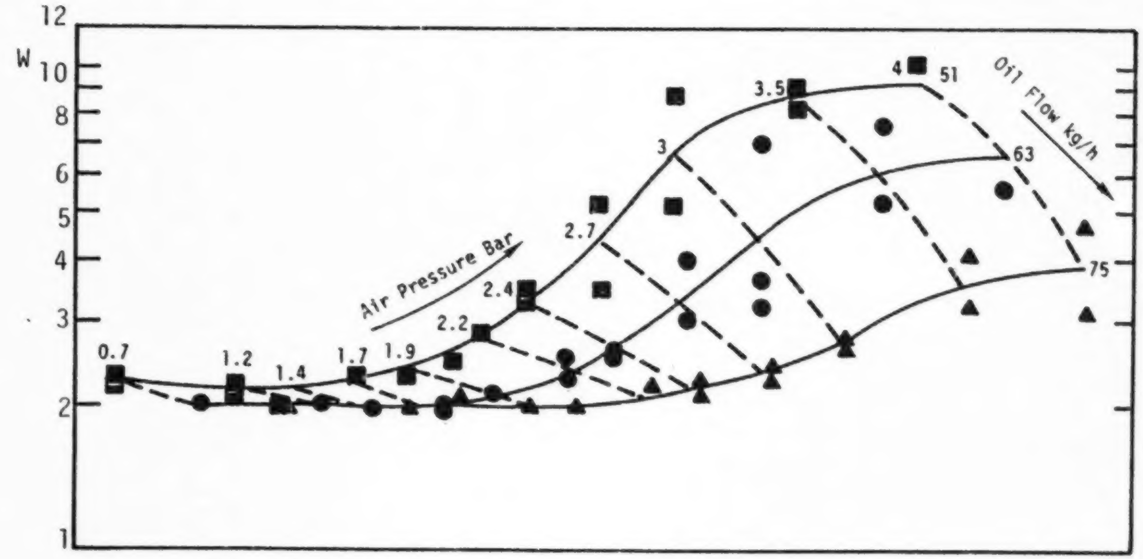

Figure 20. Monarch Atomizer. Effect of Oil Flow and Atomizing Air Pressure on the Measured R.R. Exponent W.

The effect of atomizing air pressure and oil flow on PE and W is presented in Figures 21 and 22. As for the previous atomizers, PE decreases with atomizing air pressure and W increases. The minimum of PE which is obtained for 4 bar and 51 kg/h is about 22 μm and corresponds to a high value of W: 9, which means a rather monosize spray of small droplets.

3.2.5 Peabody 6-086-55

The spray given by this atomizer is very similar to the one given by the Todd CDS. Thus, the measurements were taken in the same conditions: the laser beam was crossing only one of the six jets, as it had been proved to be quite representative of the whole spray with the previous atomizer. However, to check the similarity of the six jets measurements were repeated after an angular rotation of 60°. The repeatability was very good with this atomizer in all conditions, and even in case of high atomizing air pressures when it was impossible to avoid a slight mist of small droplets in the spray rig. The effect of atomizing air pressure and oil flow on PE and W is plotted on Figures 23 and 24.

As for the previous atomizer, the effect of atomizing air pressure is quote strong and with 4 bar we get a nearly monosize spray of small droplets (23 μm). But the difference with Todd is that PE is slightly less dependent on oil flow.

3.2.6 Delavan Swirl Air

In most cases the density of the spray was high and measurements were made through only half of the spray by positioning the laser light tube on the spray axis. However, in some particular cases measurements were taken with the whole spray in order to provide a comparison. Neglecting some of the values measured with the whole spray where spray density effects were important, the repeatability is satisfactory. Figure 25 gives the variations of PE with oil flow and atomizing air pressure. The variation of W is not presented since this exponent is relatively constant (between 1.9 and 2.7).

Figure 26 presents the variations of PE with oil flow for different atomizing air pressures. The variations of PE are quite different from those seen with other atomizers.

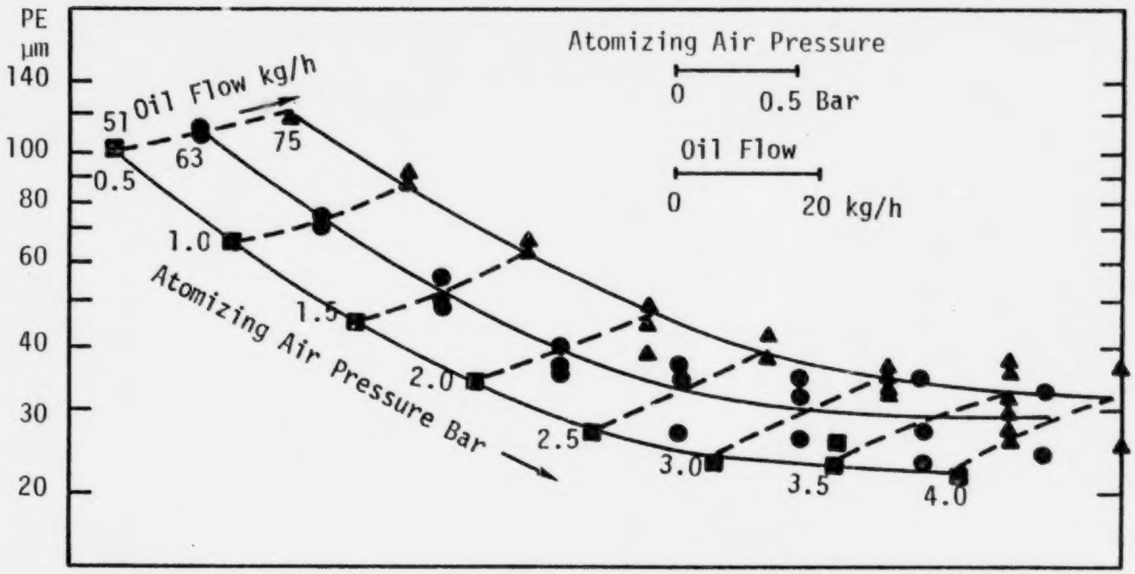

Figure 21. Todd CDS Atomizer. Effect of Oil Flow and Atomizing Air Pressure on the Measured R.R. Mean Diameter (PE)

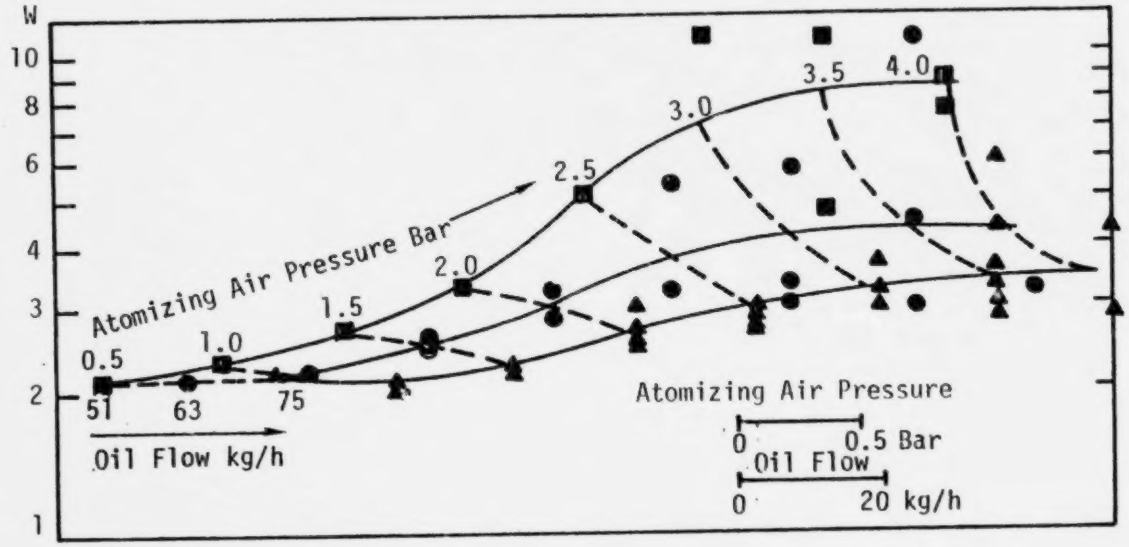

Figure 22. Todd CDS Atomizer. Effect of Oil Flow and Atomizing Air Pressure on the Measured R.R. Exponent W.

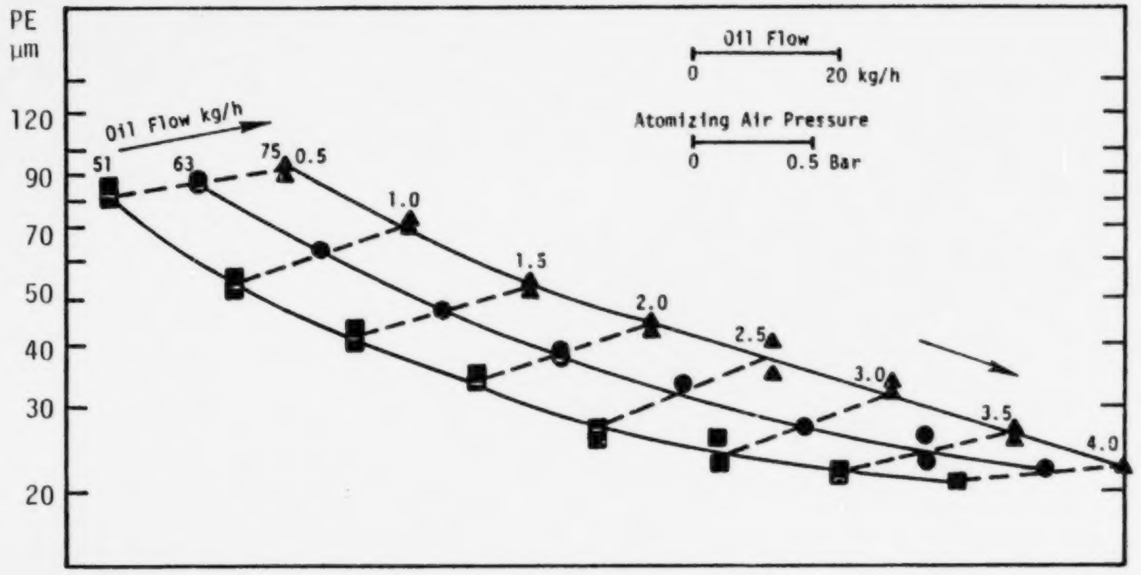

Figure 23. Peabody Atomizer. Effect of Oil Flow and Atomizing Air Pressure on the Measured R.R. Mean Diameter (PE).

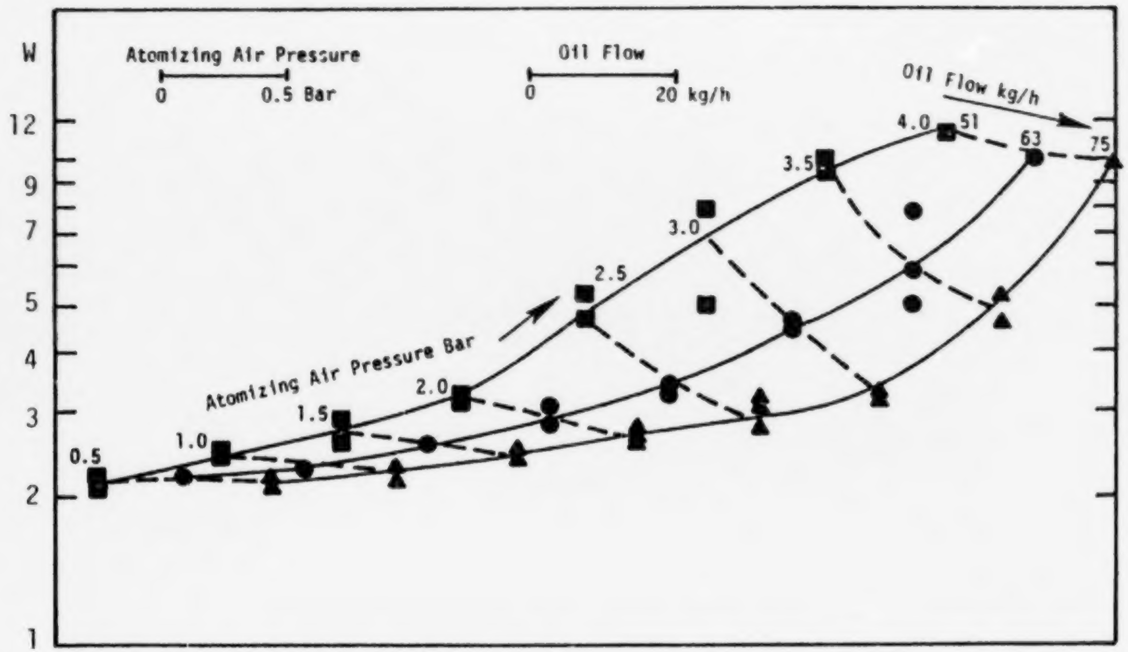

Figure 24. Peabody Atomizer. Effect of Oil Flow and Atomizing Air Pressure on the Measured R.R. Exponent W.

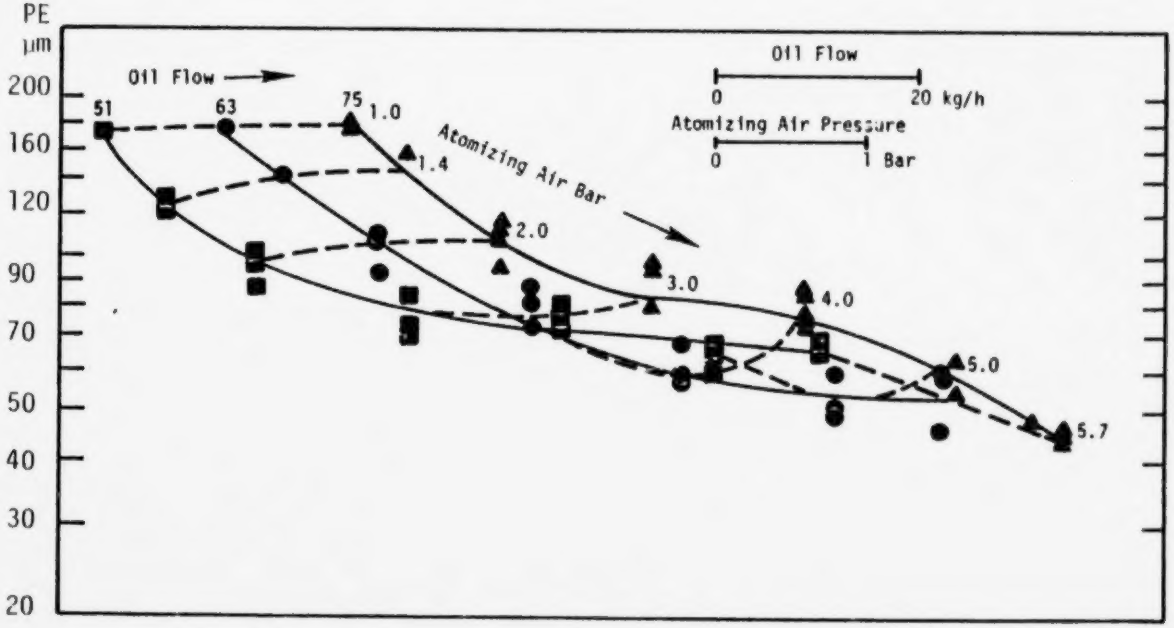

Figure 25. Delavan Swirl Air Atomizer. Effect of Oil Flow and Atomizer Air Pressure on R.R. Measured Mean Diameter.

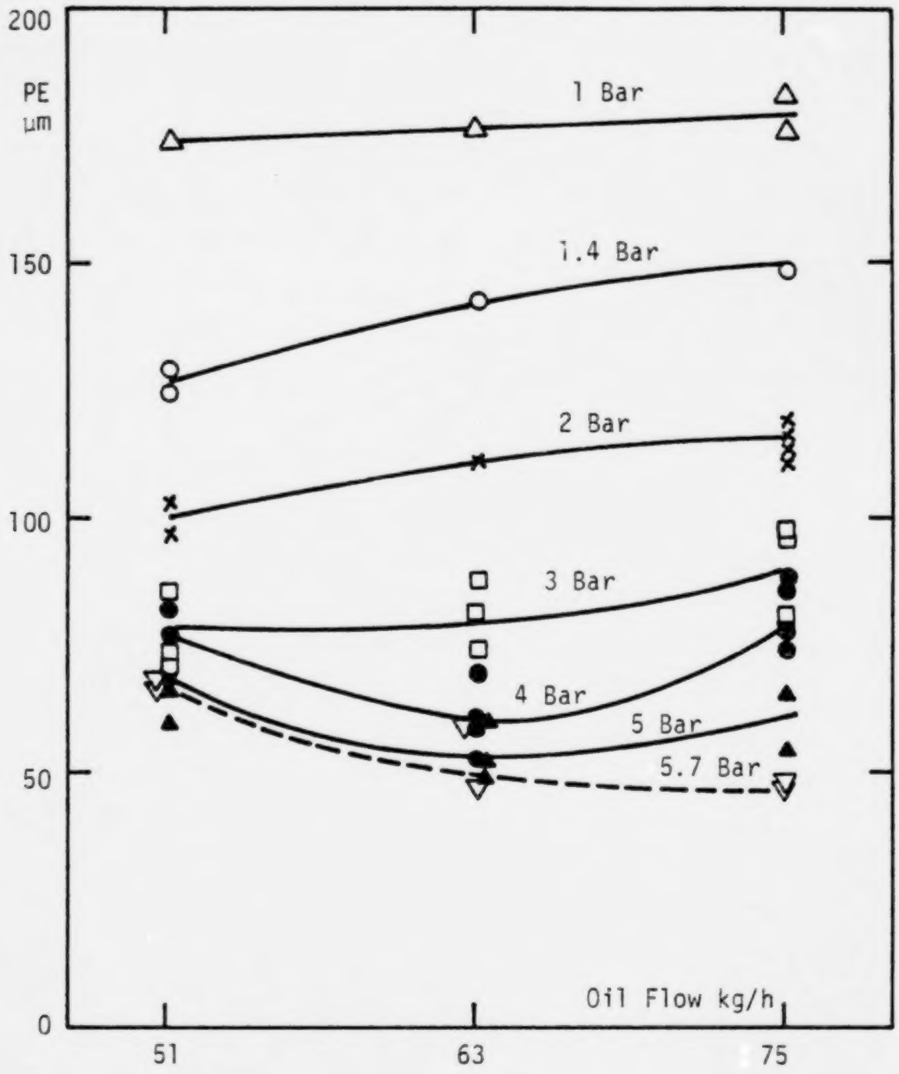

Figure 26. Delavan Swirl Air Atomizer. Effect of Oil Flow on Measured R.R. Mean Diameter PE for Atomizer Pressures.

It is especially interesting to note that the spray remains rather coarse even for high atomizing air pressures, and that PE does not decrease with oil flow in all conditions. This is probably due to the fact that the atomizer works with a low quantity of air and the design of the Delavan Swirl Air is quite different from the design of the atomizers tested before.

3.3 Axial Distance Effect

The characterization of the selected atomizers was carried out at an axial distance of 200mm. However, first experiments had shown that the measured droplet size mean diameter was strongly dependent on the axial distance between laser beam and nozzle, and for each atomizer the effect of this parameter was investigated for two or three different conditions of atomization and within the range of axial distances of 25-450mm.

3.3.1 Delavan Siphon

Axial distance effect was investigated for nominal conditions: oil flow 1.8 kg/h and atomizing air pressure 1.4 bar. Measurements were taken both in quiescent air and with a primary air velocity of 10 m/s (at burner with no swirl). Another set of atomizing conditions; oil flow 1.8 kg/h and atomizing air pressure 0.35 bar, was also selected in order to check axial distance effect of a coarser spray (70 μm at 200mm). Figure 27 gives the variations of the Rosin Rammler mean diameter with axial distance, while Figure 28 gives the corresponding variations of W.

It can be seen on Figure 27 that the measured mean diameter increases strongly with axial distance when the spray is coarse, for an atomizing air pressure of 0.35 bar. In case of a finer spray (1.4 bar) the variations of PE are following the same trend, but the effect is quite slight. The addition of primary air with a velocity of 10 m/s alters the shape of the curve which presents a strong decrease of PE close to the nozzle, and then an increase further downstream; these two parts being separated by a clear minimum at an axial distance of 80-90mm.

Figure 28, which presents the variations of W, shows a strong peak of the Rosin Rammler exponent in case of a primary air velocity of 10 m/s.

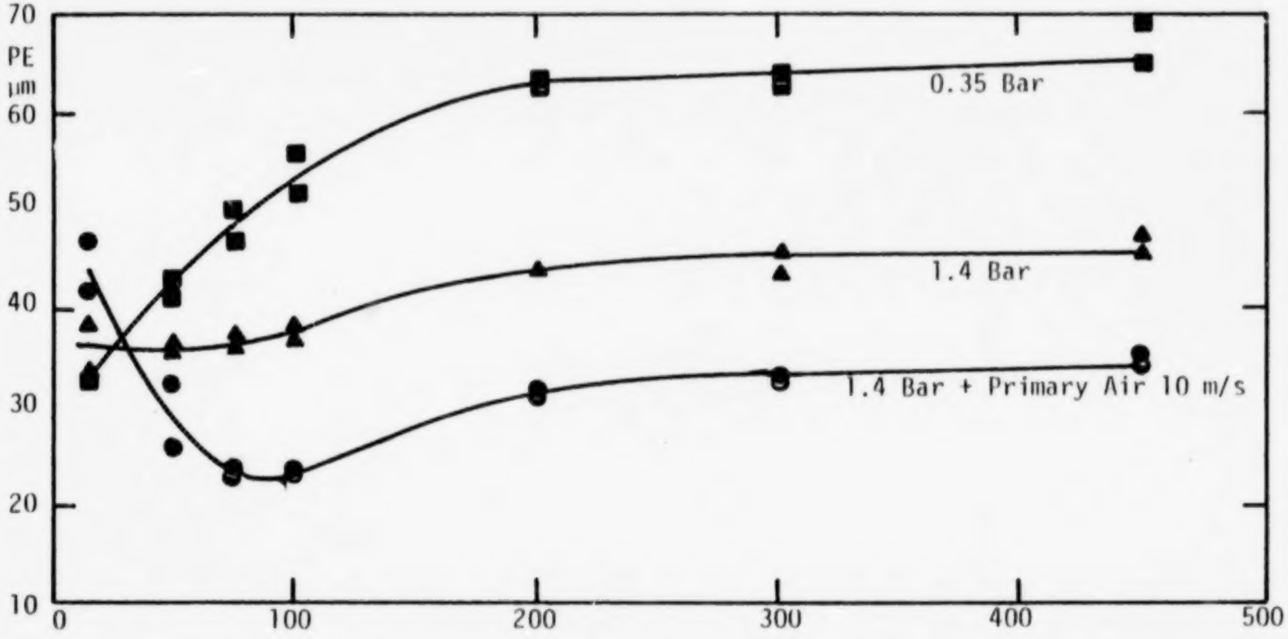

Figure 27. Delavan Siphon Nozzle. Effect of Axial Distance on PE (R.R. Mean Diameter).

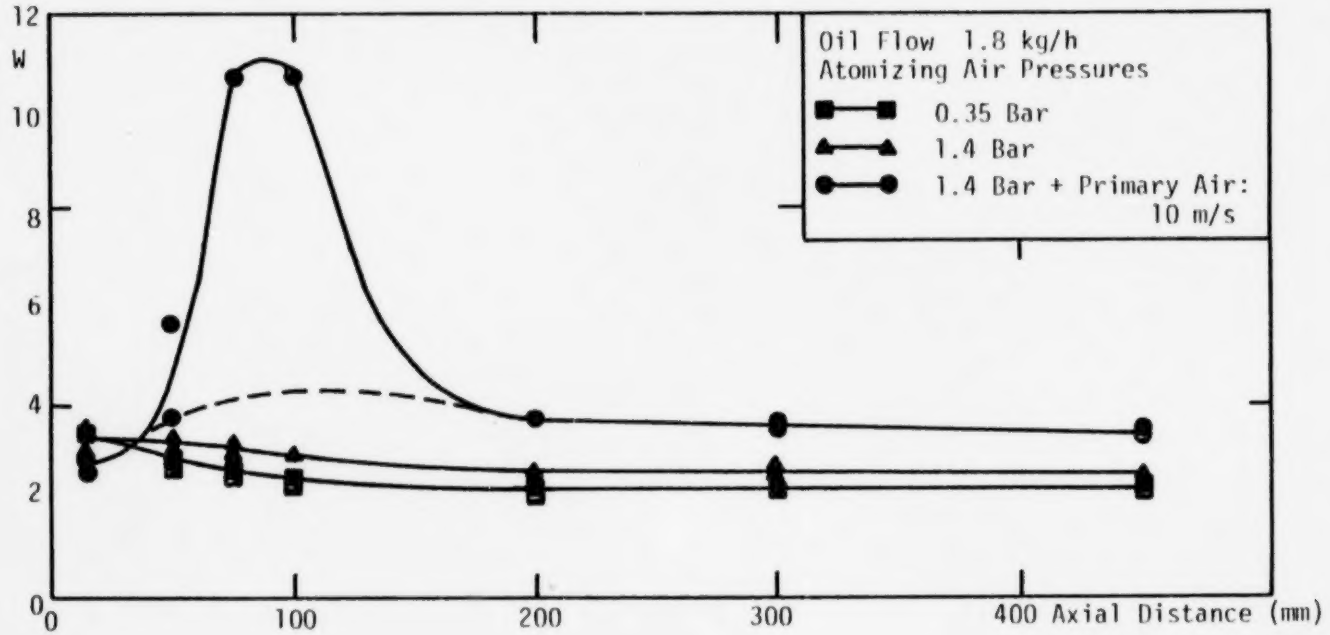

Figure 28. Delavan Siphon Nozzle. Effect of Axial Distance on W (R.R. Exponent).

By looking at the light energy distribution measured in that case on the photodetector, it can be seen that this high value of W might be artificial.

Figure 29 compares the measured light energy distribution at axial distance 90mm with different calculated energy distributions; one with the computer best answer: PE-23 µm and W=10.7, and the two others modified by manual correction. It appears that apart from the last three rings of the photodetector, corresponding to the smallest droplets, the best set of parameters should be PE=23 µm and W=3 or 5.

Since the measurements on these last three rings are usually zero due to nondetection of the finest particles (see Section 2.3.1), it is therefore better to forget the last part of the curve and to take W=4 with PE=23 µm for the best set of Rosin Rammler parameters. For that reason the corresponding curve on Figure 29 has been corrected in dotted lines.

3.3.2 Small Sonicore Without Tip

The axial distance effect has been investigated with the resonator off, and for two different oil voscisities as for droplet size distribution.

Figure 30 gives the variations of the mean diameter for four different conditions of atomization, and Figure 31 gives the variations of W.

Overall, it appears that the more coarse the spray, the stronger the increase of mean diameter with axial distance.

3.3.3 Sonicore 250T

As indicated before, the Sonicore 250T was often blocked and the measurements presented here were taken all at one time in order to keep the same conditions of atomization during the whole axial traverse, avoiding the addition of alterations of atomizing conditions with pure axial distance effect.

Thus, there can be some significant differences between measurements taken at 200mm during the axial traverse and measurements resulting from the chracterization at 200mm presented before.

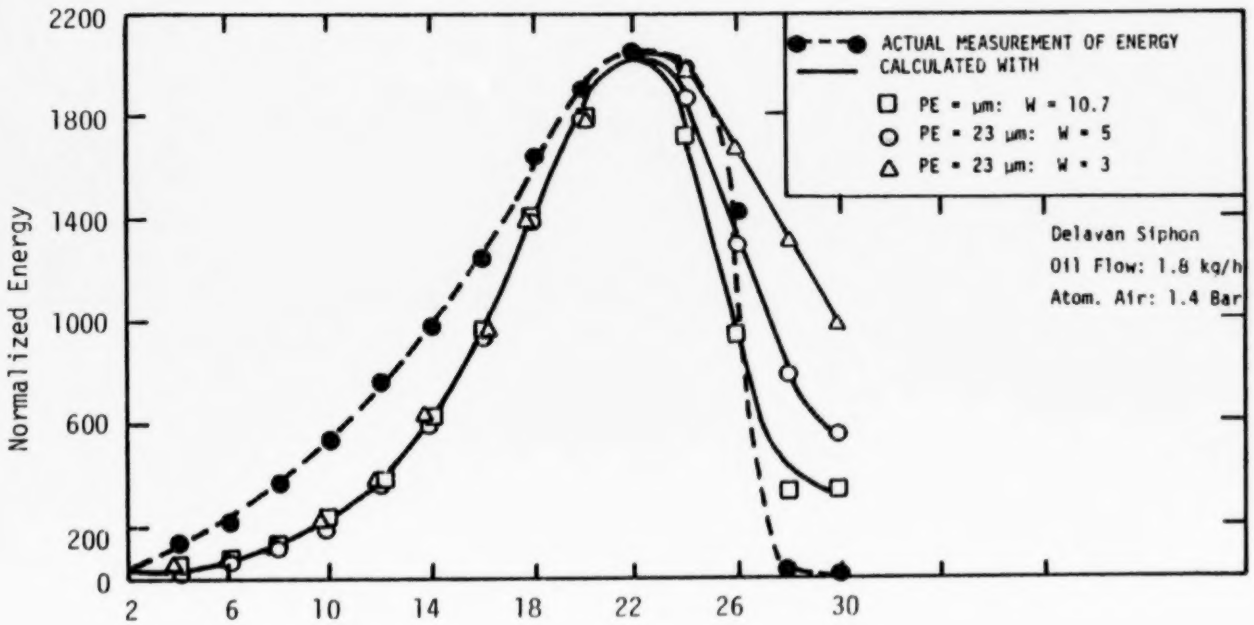

Figure 29. Normalized Energy on the Rings of the Photo Detector. Comparison Between Measured and Calculated Energy Distribution.

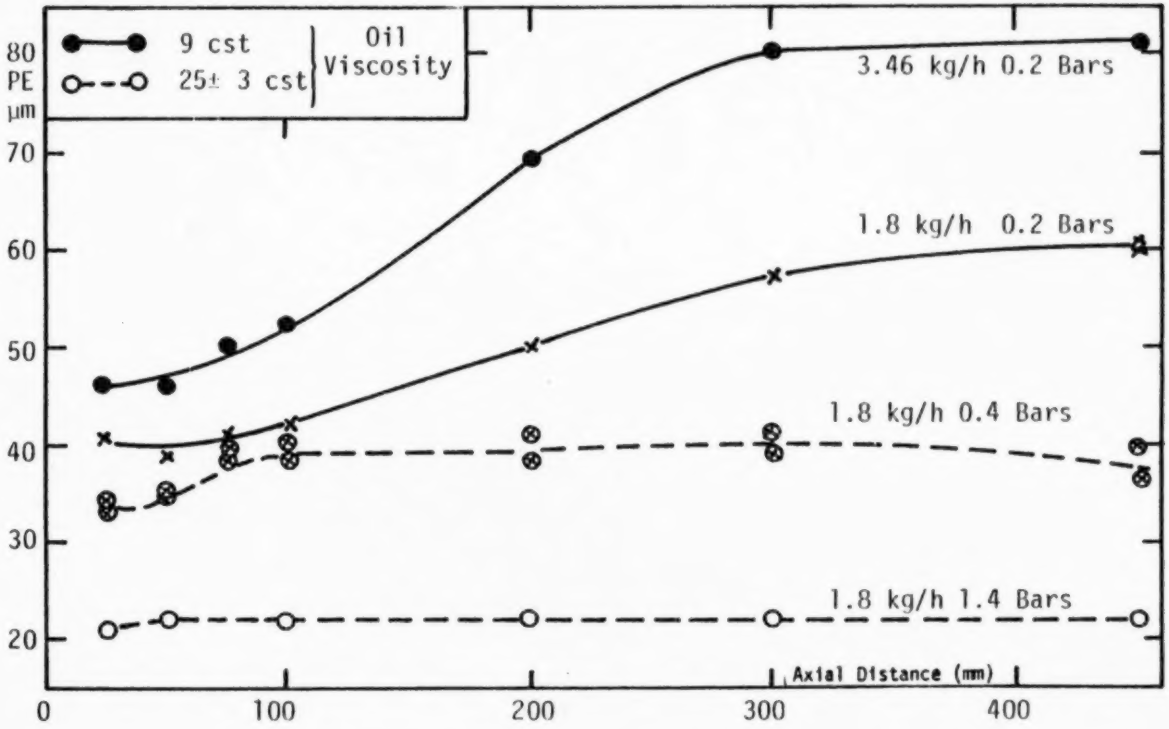

Figure 30. Small Sonicore Nozzle Without Tip. Effect of Axial Distance on PE (R.R. Mean Diameter).

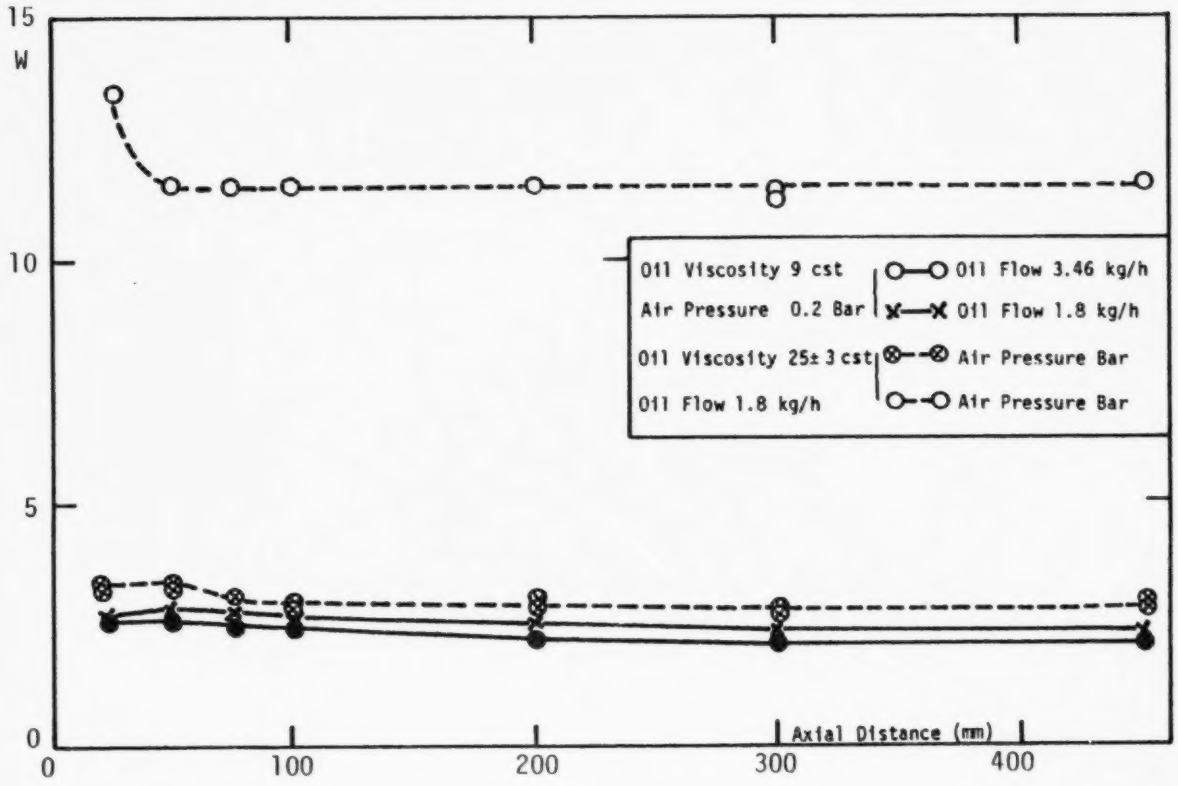

Figure 31. Small Sonicore Without Tip. Effect of Axial Distance on W (P.R. Exponent).

On the whole, the results relative to the Sonicore 250T have to be considered very carefully in absolute values and only the major trends can be considered as reliable.

Figure 32 presents the variations of Rosin Rammler diameter (PE in µm) with axial distance. The major trend is an increase of PE within an axial distance range of 60 to 450mm and as for the previous atomizer, the effect is stronger when the spray becomes more coarse. Figure 33 presents the corresponding variations of W and as for the Delavan Siphon, a detailed observation of light energy distribution reveals that the peak of W at 100mm is artificial, and that the measured spray can be better described with the set of parameters PE=23 µm, W=3. Therefore, the directly computed curves (dark lines) and the manually corrected ones (dashed lines) are plotted on Figure 33.

3.3.4 Monarch

The effect of axial distance was investigated over a range of 450mm since closer to the nozzle the density of the spray was extremely high, and therefore, it was impossible to measure across the whole spray.

Figure 34 presents the variations of the mean diameter and of the exponent with axial distance for the two atomizer conditions selected. The effect of axial distance is extremely strong with this atomizer, particularly between 50mm and 200mm, where PE increases from 25 µm to 90 µm, with almost the same rate for the two different atomizing air pressures.

In the same time W decreases strongly from a quite high value (15 for 0.7 bar and 4.7 for 1.7 bar, indicating a rather monosize spray), to a normal value, 2, indicating a scattered spray.

As for the previous atomizers, the effect is stronger in the case of the lower atomizing pressure which means a coarser spray. But this difference is significant only between 200mm and 450mm; from 50mm to 200mm the two curves are almost parallel.

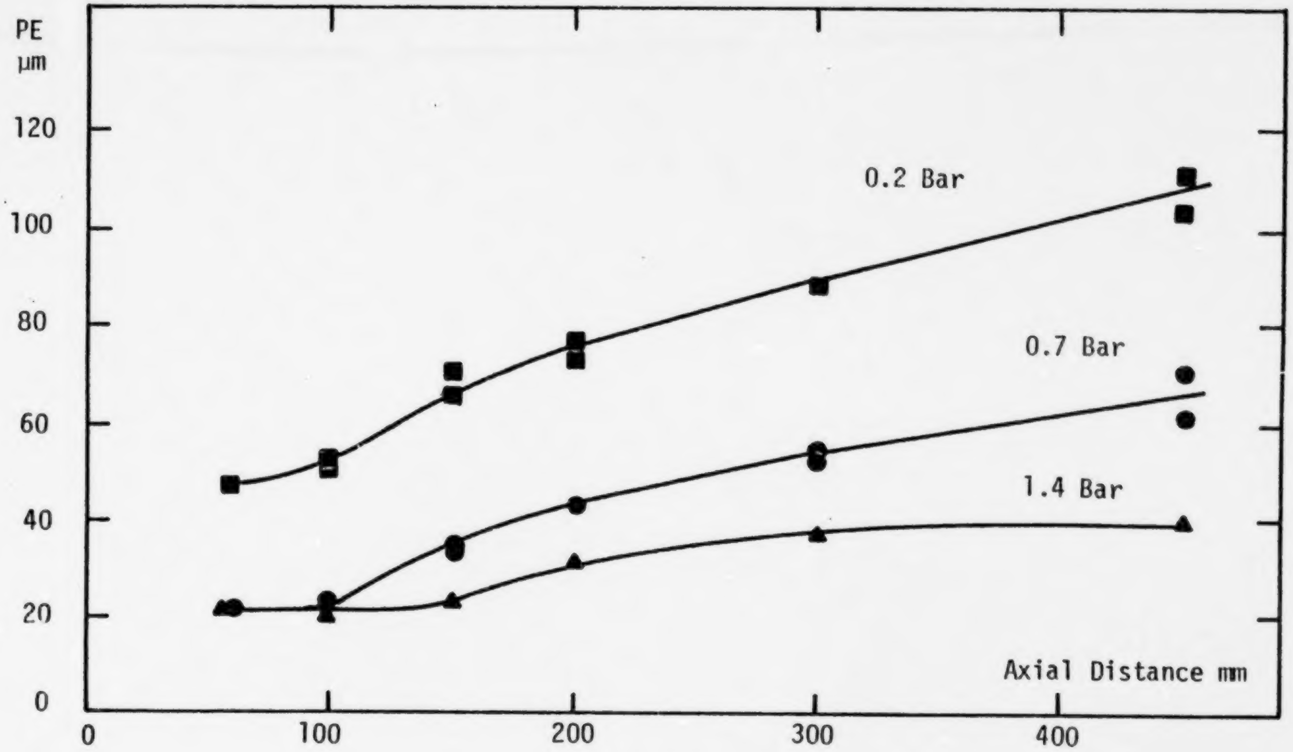

Figure 32. Sonicore 250 T. Effect of Axial Distance on Measured RoR Mean Diameter. Oil Flow = 75 kg/h.

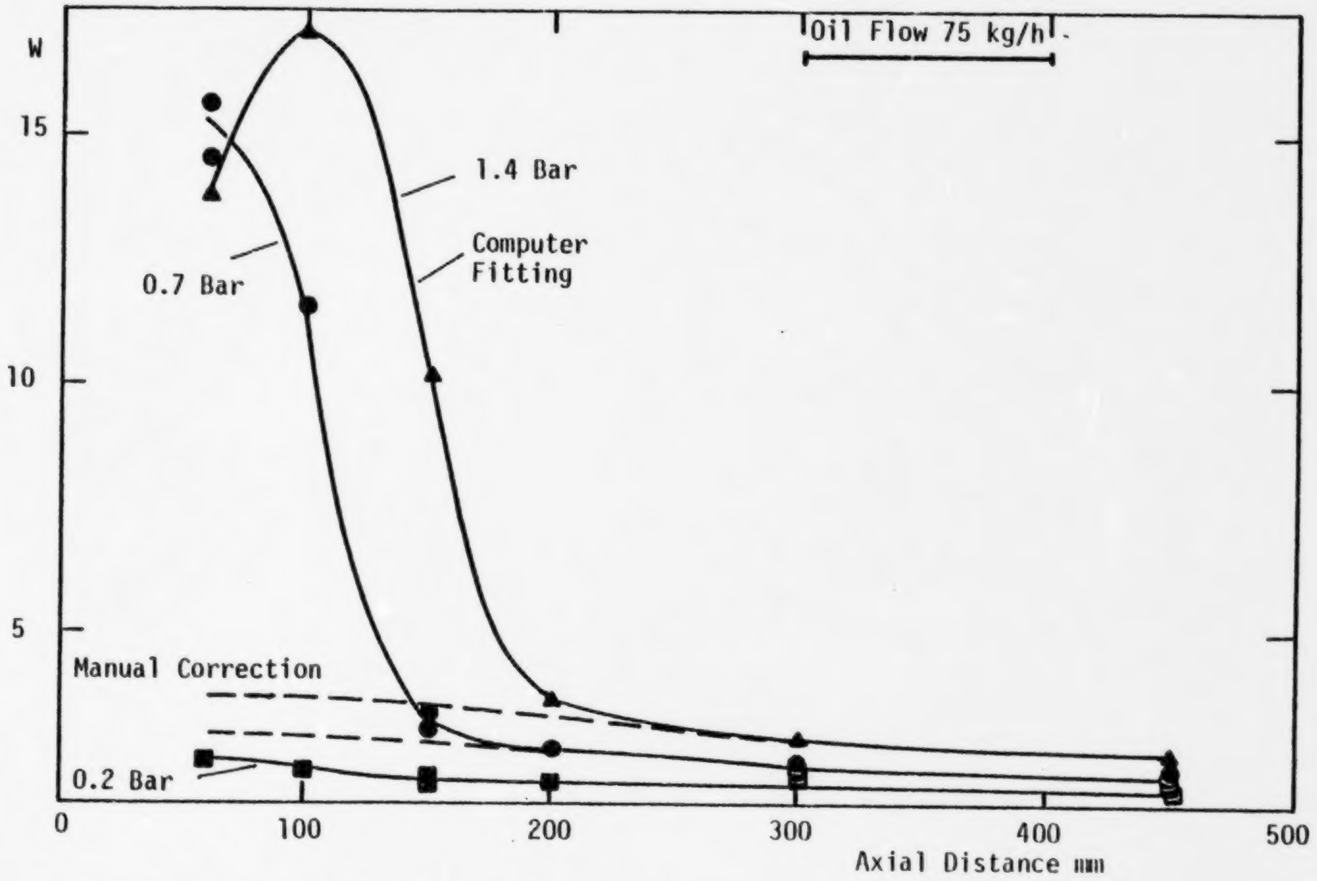

Figure 33. Sonicore 250 T. Effect of Axial Distance on Measured R.R. Exponent W.

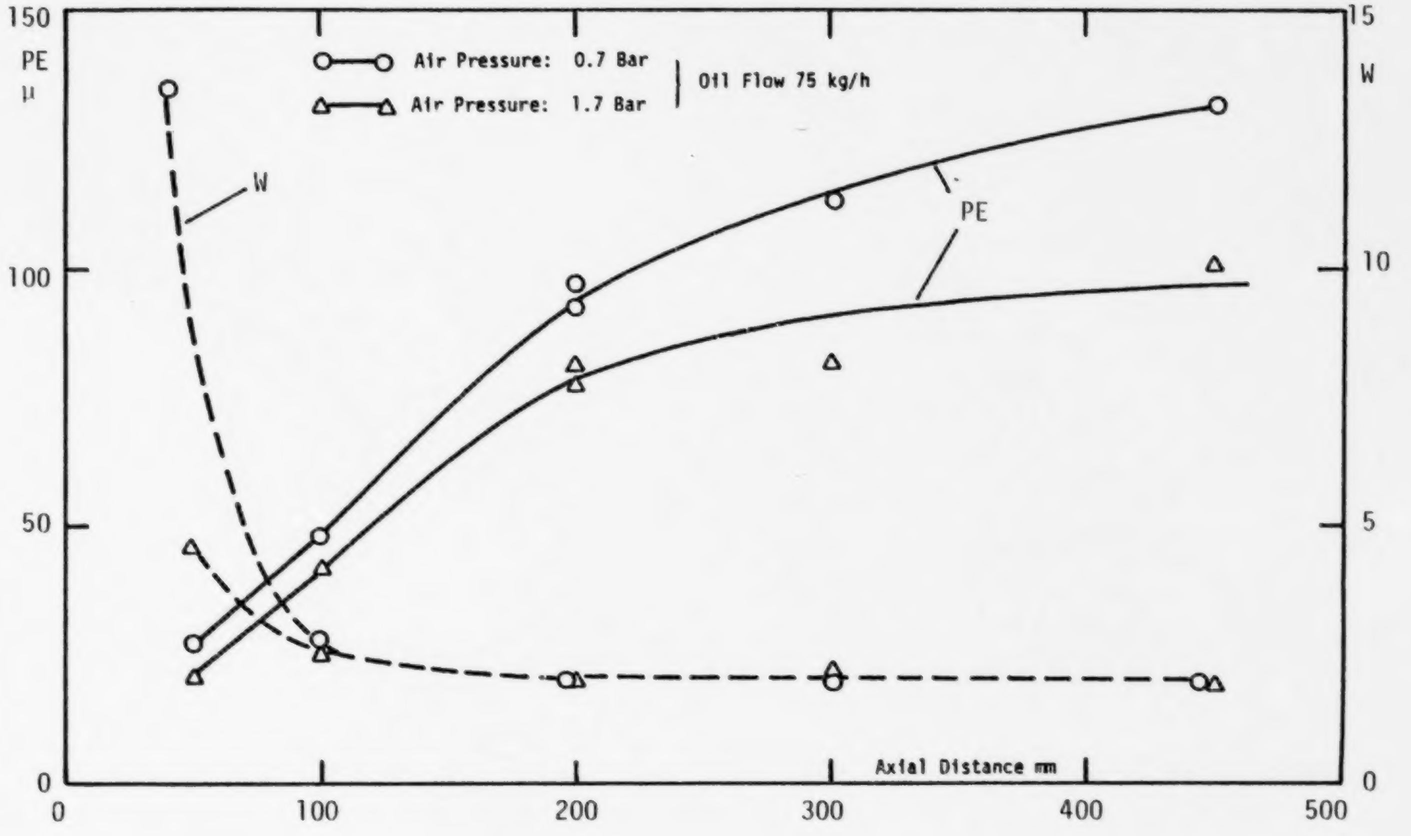

Figure 34. Monarch Atomizer. Effect of Axial Distance on Measured Mean Diameter PE and on Measured Exponent W.

It is highly probable that this very strong effect of axial distance with the Monarch must be related to the specific aerodynamic properties of this atomizer. The very strong underpressure which is present below the tip at the exit of the atomizer has been seen to be responsible for the deflection of the droplet trajectories towards the axis of the spray. It is believed that small droplets, because of their small inertia compared to the drag-forces, preferentially follow the local streamlines when the big ones keep their initial velocity and direction. Therefore, there must be a preferential decelaration of the small droplets in this recirculation zone and an accumulation of this small component in that area, giving a specially low measured mean diameter. This effect of separation of small and big droplets is confirmed by visual observations.

3.3.5 Todd CDS 6-089-60

Although the measurements were taken with only one jet since the jets are well detached with this atomizer, the very high density of the spray near the nozzle did not allow measurements in the field 0-50 mm without a high probability of error.

Figure 35 gathers the variations of measured mean diameter PE and of exponent W. As axial distance increases PE increases as well and W decreases. As for previous atomizers the increase of PE is stronger when the spray is coarser.

3.3.6 Peabody 6-086-55

As this atomizer also gives six very well detached single jets, the measurements for axial distance effect were made through one of the jets, which was very carefully positioned to cross perfectly the laser beam. The repeatability was always very good and the density such that the central reading was acceptable.

Figure 36 presents variations of mean diameter PE and exponent W. The results show a general increase of the mean diameter and of the dispersion of the droplet size distribution with increasing axial distance. The magnitude of the variations is quite similar to that observed with the Todd atomizer and confirms the similarity already mentioned between these two atomizers in terms of spray shape and droplet size characterization.

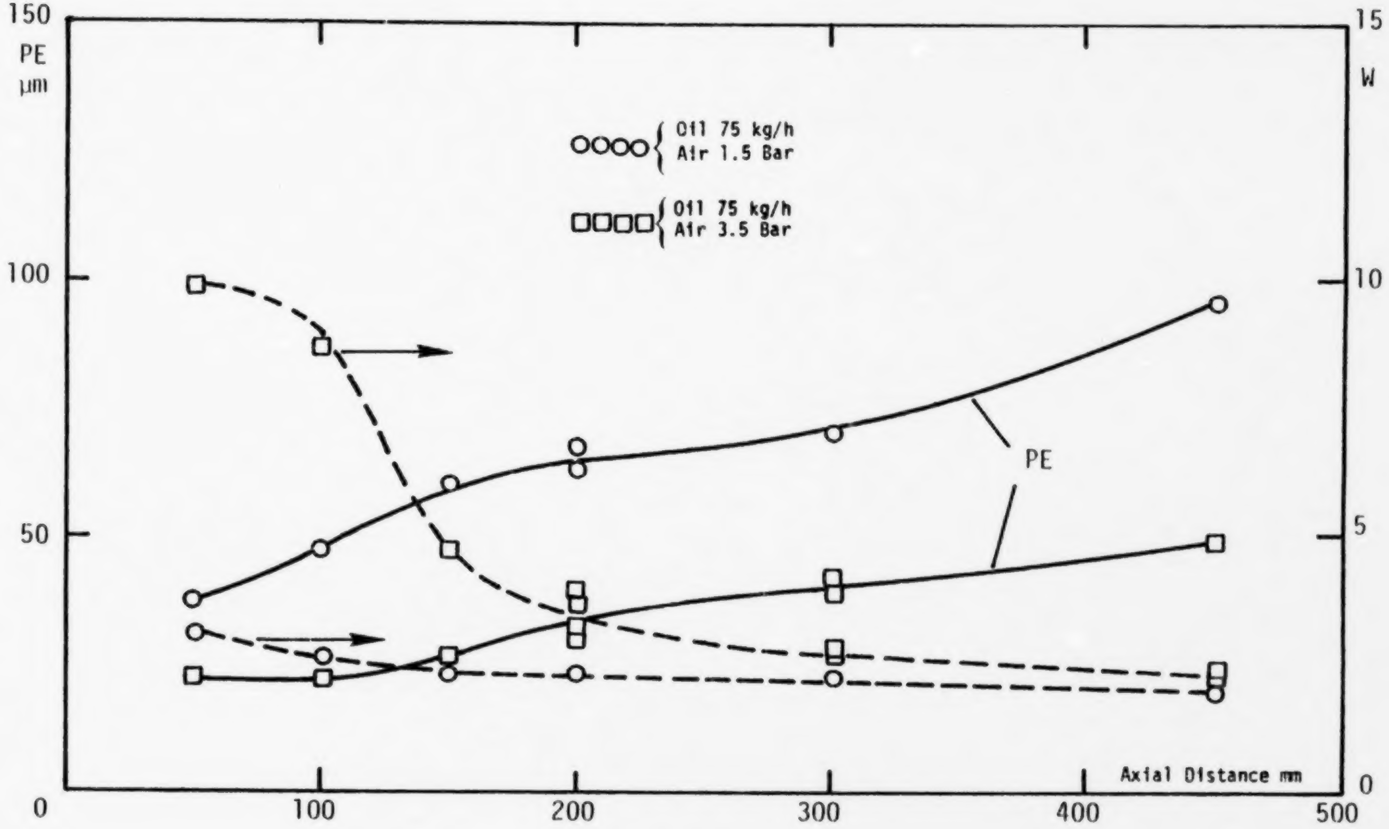

Figure 35. Todd CDS Atomizer. Effect of Axial Distance on Measured R.R. Exponent and Mean Diameter.

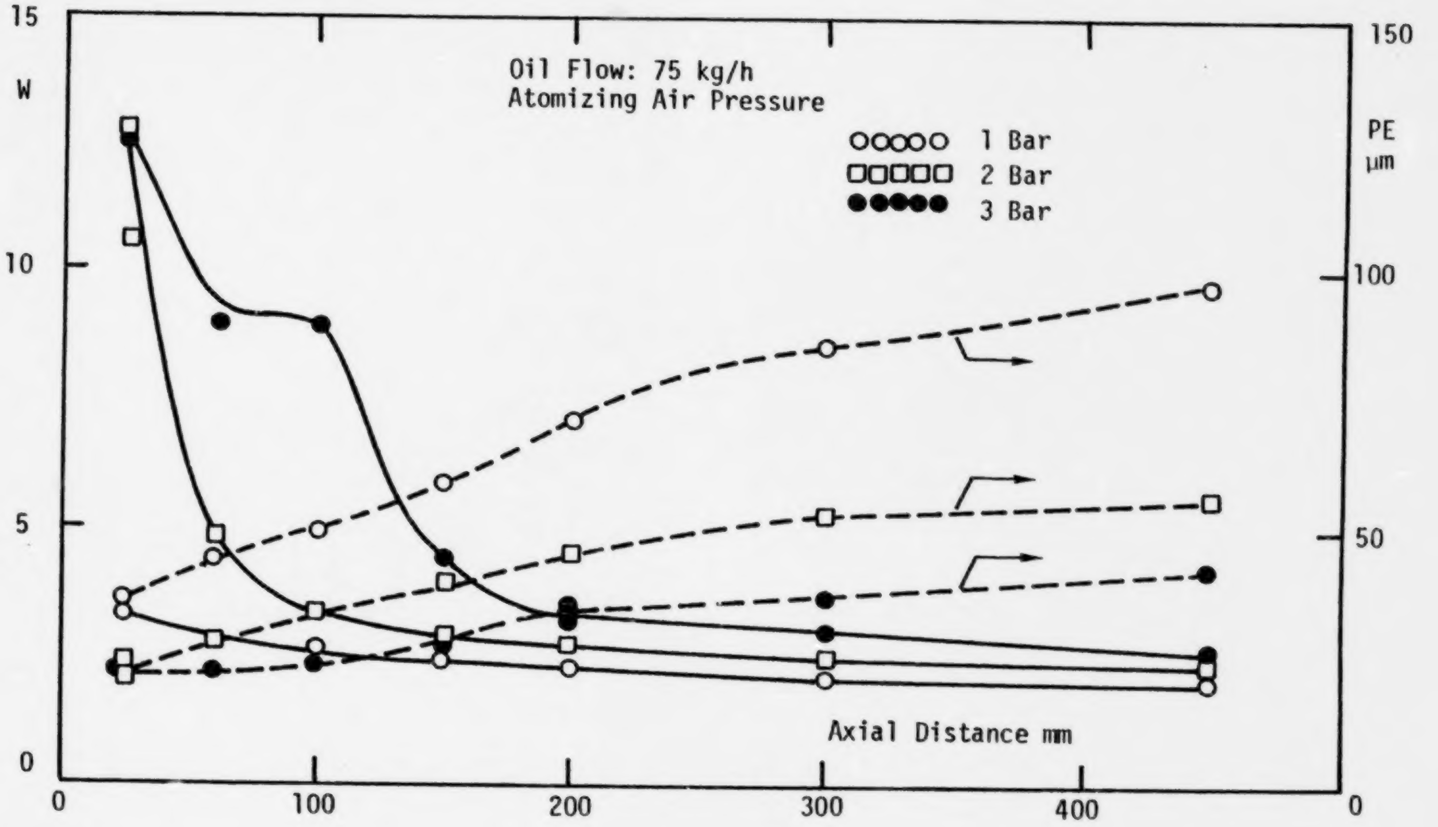

Figure 36. Peabody Atomizer. Effect of Axial Distance on R.R. Measured Exponent and Mean Diameter.

3.3.7 Delevan Swirl Air

The axial distance effect has been investigated with the operating oil flow (75 kg/h) and for two atomizing air pressures, 2 bar and 4 bar. For atomizing air pressure = 2 bar three groups of measurements were taken; two over half of the spray and one with the total spray since with this low air pressure the density of the spray was not too high.

For an air pressure of 4 bar, two groups of measurements were also taken, but both over half of the spray. The difference between the two groups of measurements taken with half spray (1 and 2 on Figure 37) is a slight shift of the laser tube.

In the case of measurements 1, this means that measurements were effectively made over a distance equal to the radius of the spray plus 5 mm. Although this error in positioning is small in itself, it is large compared to the dimensions of the spray at small axial distances.

It may be seen that the variations of PE present a minimum for a critical axial distance, which is between 50 and 100 mm, depending on conditions of atomization and measurements.

It appears that around that critical zone the results depend very much on the way the measurements were taken (half-spray, total spray, position of laser tube). The results of the same series of measurements are, however, consistent and show the same trends.

Downstream of this critical zone the results are less dependent on the conditions of measurement.

It is possible that the introduction of a tube in the spray - as the laser tube - has a significant effect on the airflow field with this atomizer, and therefore, on the spray. Far from the nozzle this effect is not important because velocities are low and the dimension of the tube is small compared to the spray diameter.

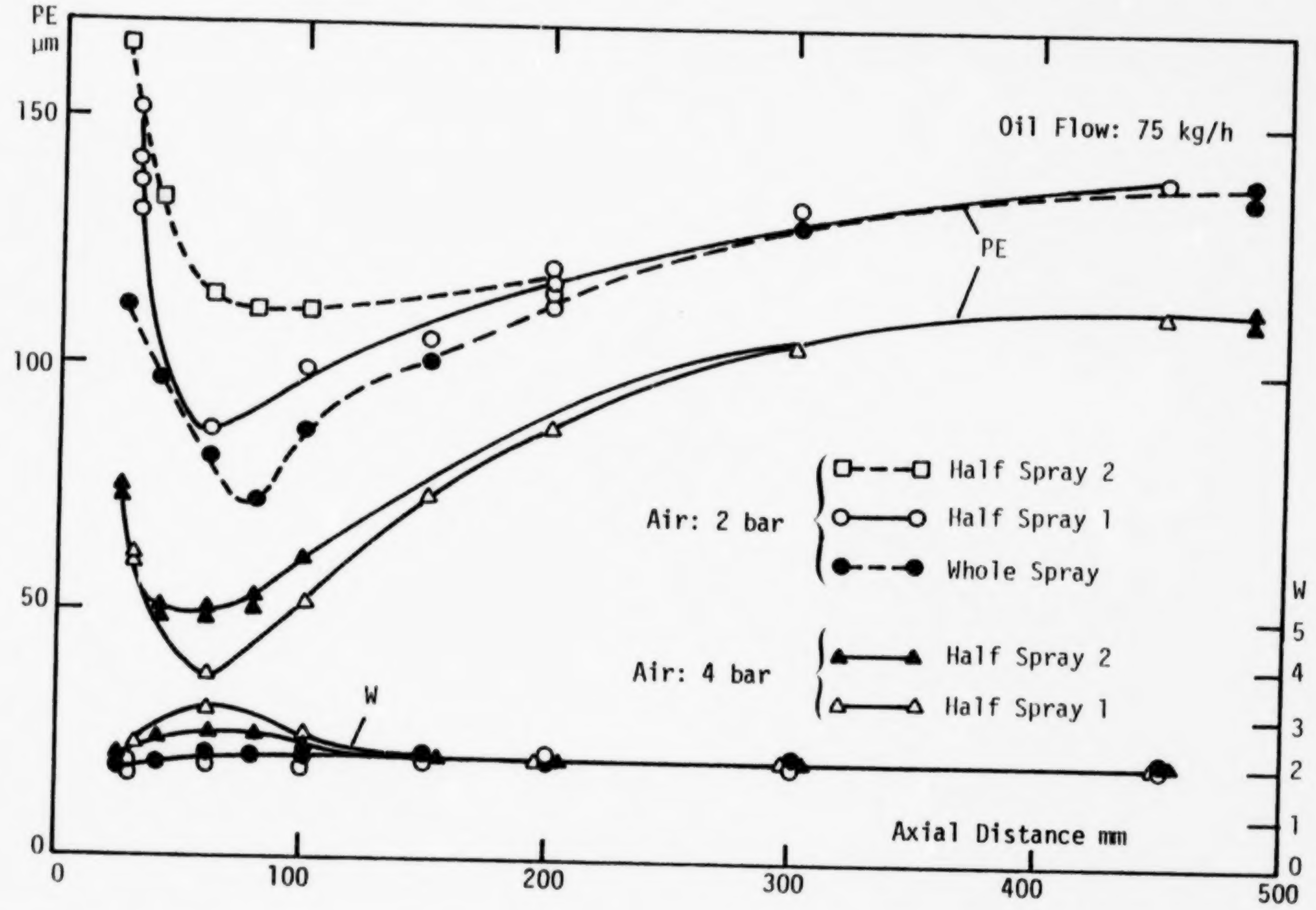

Figure 37. Delavan Swirl Air Atomizer. Effect of Axial Distance on Measured R.R. Mean Diameter PE and Exponent W.

4.0 DISCUSSION

This section of the report compared the six atomizers tested in terms of:

- spray shape and mass distribution;
- effect of air pressure, oil flow and oil pressure;
- actual droplet size distribution in operating condition;
- axial distance effect with a possible interpretation.

4.1 Spray Shape and Mass Distribution

As seen in Section 3.1, the initial shape of the spray is governed by the design of the atomizer. For example, the Todd gives a perfectly hollow core spray with six detached jets, which was expected considering the shape of the mixing chamber and the position of the mixing ports. However, it appears that the initial shape of the spray could be strongly modified by aerodynamic conditions:

- Aerodynamics of the atomizing air in case of the Monarch.
- Interaction of the spray flow with the entrained airflow in case of the Peabody, which is initially a perfectly hollow core spray with six detached jets, but reveals a significant interaction between those jets further downstream.
- Interaction of the spray flow with the airflow pattern given by a real burner in cold and hot conditions. Unfortunately, no experiments have been done in that way, except the effect of a uniform primary airflow, which was seen to alter the shape of 60^0 spray given by a Y-jet six-hole atomizer.

  As expected in that case, the initial trajectories of the droplets were bent towards the axis and after 200 mm the spray had a cylindrical shape.

4.2 Air Pressure and Oil Flow Effect of Spray Characteristics

4.2.1 Air Pressure

Figure 38 compares the effect of atomizing air pressure on measured Rosin Rammler mean diameter, for all the atomizers tested in case of operating

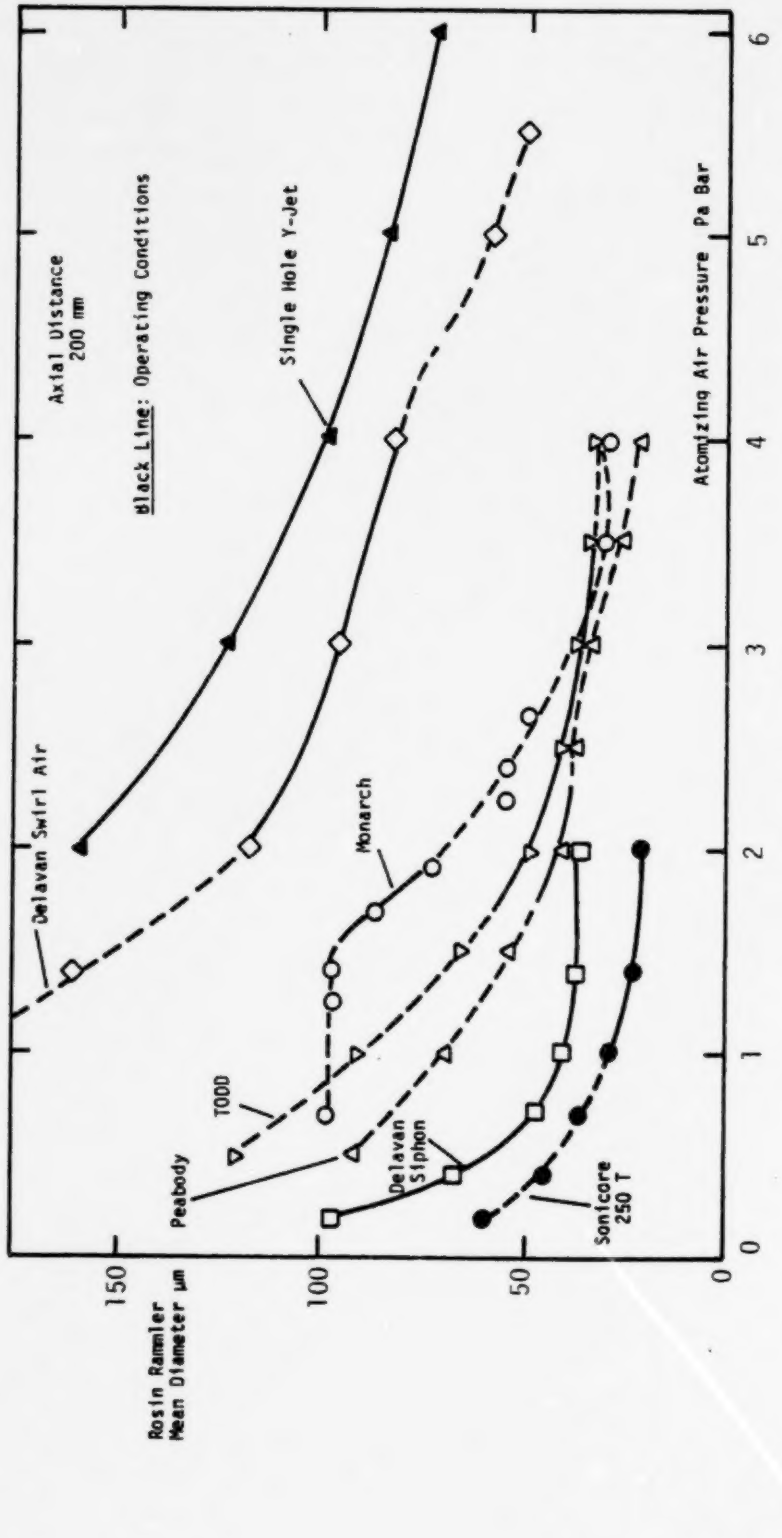

Figure 38. Effect of Atomizing Air Pressure on Rosin Rammler Mean Diameter.

oil flows; 76 kg/h for the big atomizer, and 1.8 kg/h for the Delevan siphon. Results of measurements carried out with a single hole Y-jet atomizers have been plotted on the same curve.

In all cases, as expected, increasing the atomizing air pressure decreases the droplet size mean diameter, and as we have seen in detailed results, increases the Rosin Rammler exponent, which means a rather less scattered distribution of droplet size. The minimum droplet size detected - typically 20 µm in our case - is a lower limit characteristic of the oil and of the twin fluid atomization principle, and that this limit would be reached for all droplets in case of very efficient atomization (good mixing, high shear stresses everywhere in the atomization chamber). In the case of prior atomization some big droplets could go through the atomizing air field without being broken due to the existence of some low shear stress regions.

Figure 39 tends to confirm this interpretation. It presents the variations of the droplet size mean diameter for all atomizers tested for the operating oil flow, but as a function of the ratio between atomizing air mass flow and oil flow.

Figure 39 shows that all the curves are within a narrow zone, which tends to reveal that this air/oil ratio is, in fact, the major parameter governing atomization quality, particularly at high air/oil ratio.

4.2.2 Oil Flow

For all of the atomizers tested it appears that air/oil ratio remains the most important criteria for spray characterization. However, as pointed out for Delevan siphon, when there is a significant effect of oil flow for the same air/oil ratio, the spray is always coarser with a lower oil flow.

This is an important remark, both for practical reasons and understanding of atomization.

- Practically it means that in case of turn-down, the air requirement will be relatively higher to keep approximately the same droplet size distribution.

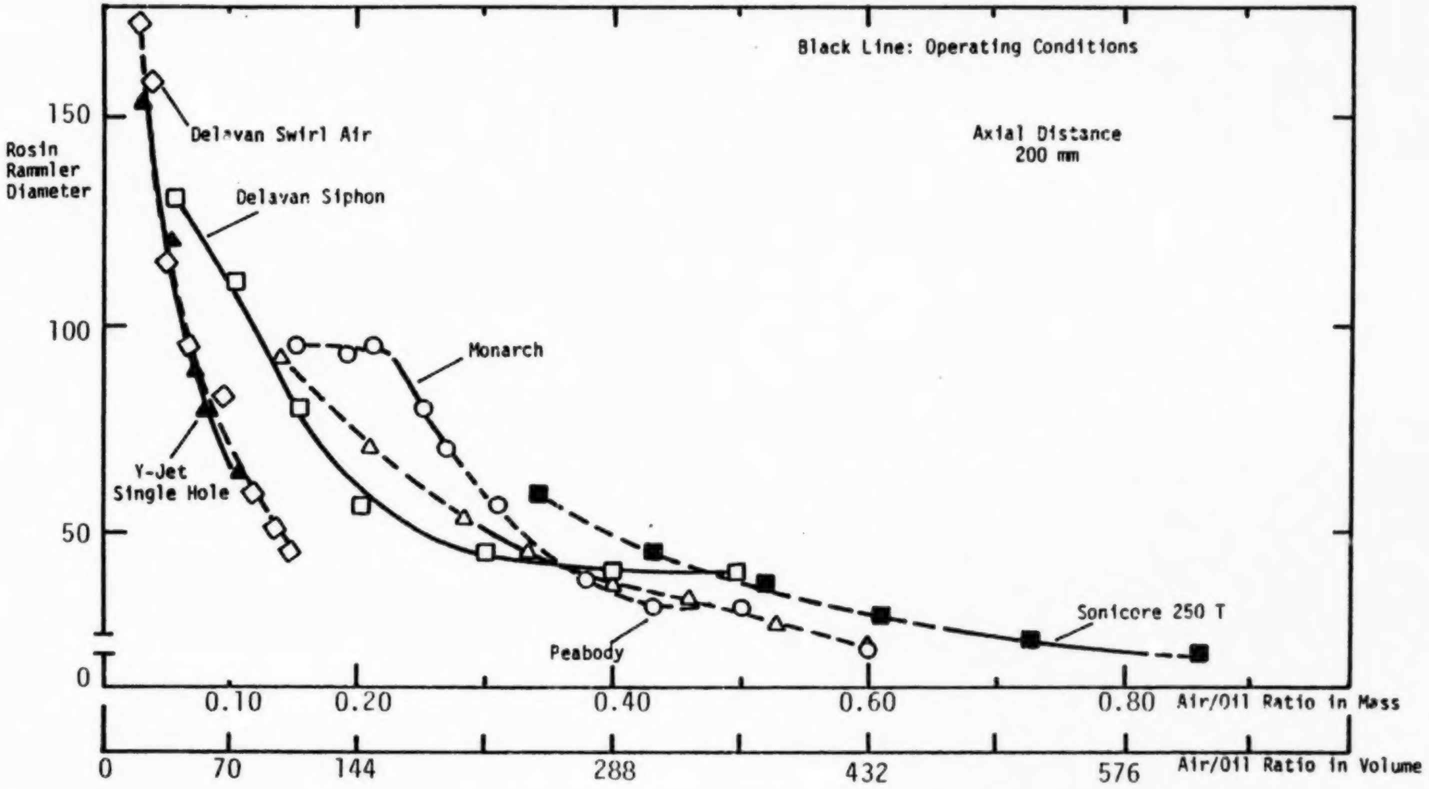

Figure 39. Effect of Air/Oil Ratio on Rosin Rammler Mean Diameter.

- This effect tends to prove that with a very low oil flow the energy requirements, i.e., air volume requirement per volume of oil, is relatively higher, probably due to worse mixing and less efficient transfer of momentum from air to oil.

4.2.3 Oil Pressure

For the atomizers which have a mixing chamber as Todd, Peabody, Delevan Siphon and Monarch, the oil pressure required to get the oil flow through the atomizer is always highly dependent on the atomizing air pressure, since there is a common counterpressure in the mixing part of the atomizer. However, for Delevan Siphon and Sonicore, the oil pressure was independent of the air pressure because the oil is injected close to the atomizer exit where the pressure is usually of the order of atmospheric pressure whatever the airflow. In that last case the oil pressure required depends only on pressure drop in the oil loop.

4.3 Actual Droplet Size Distribution in Operating Conditions

Figure 40 presents the measured droplet size distribution, in terms of fraction of weight for each range of size, for the six atomizers tested in operating conditions. We can distinguish three groups of atomizers:

- Delevan Swirl Air and Monarch, which give a rather coarse spray with a significant weight fraction of droplets bigger than 100 μm.
- Peabody, Todd and Delevan Siphon with a rather five spray and no droplets bigger than 100 μm.
- Sonicore 250T, which gives a nearly monosize spray of fine droplets; all the droplets are within the range 15 μm to 30 μm.

4.4 Axial Distance Effect

In Section 3.3 the effect of axial distance on measured mean diameter was presented. Figure 41 compares the effect of axial distance on measured droplet mean diameter for all atomizers tested in operating conditions

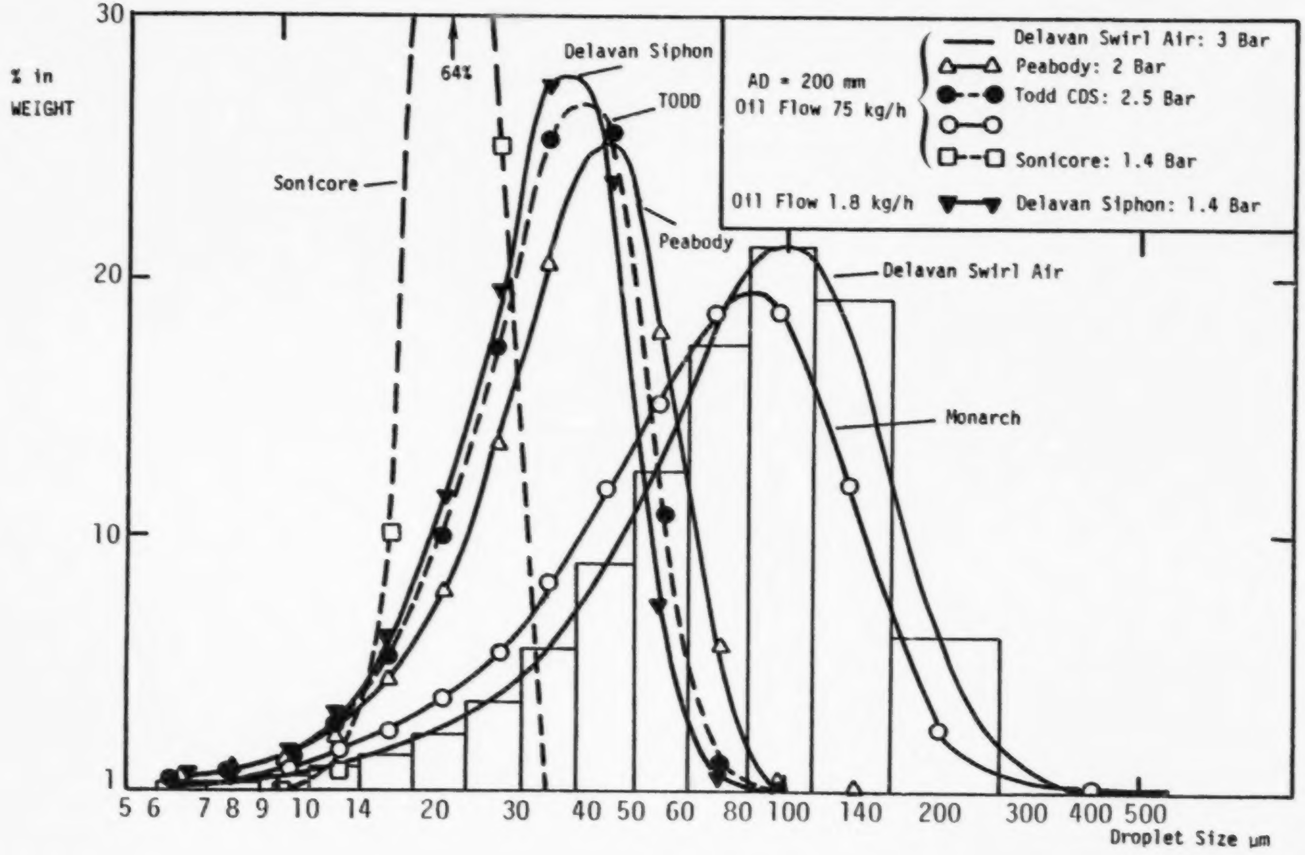

Figure 40. Droplet Size Distribution in Operating Conditions for Six Atomizers.

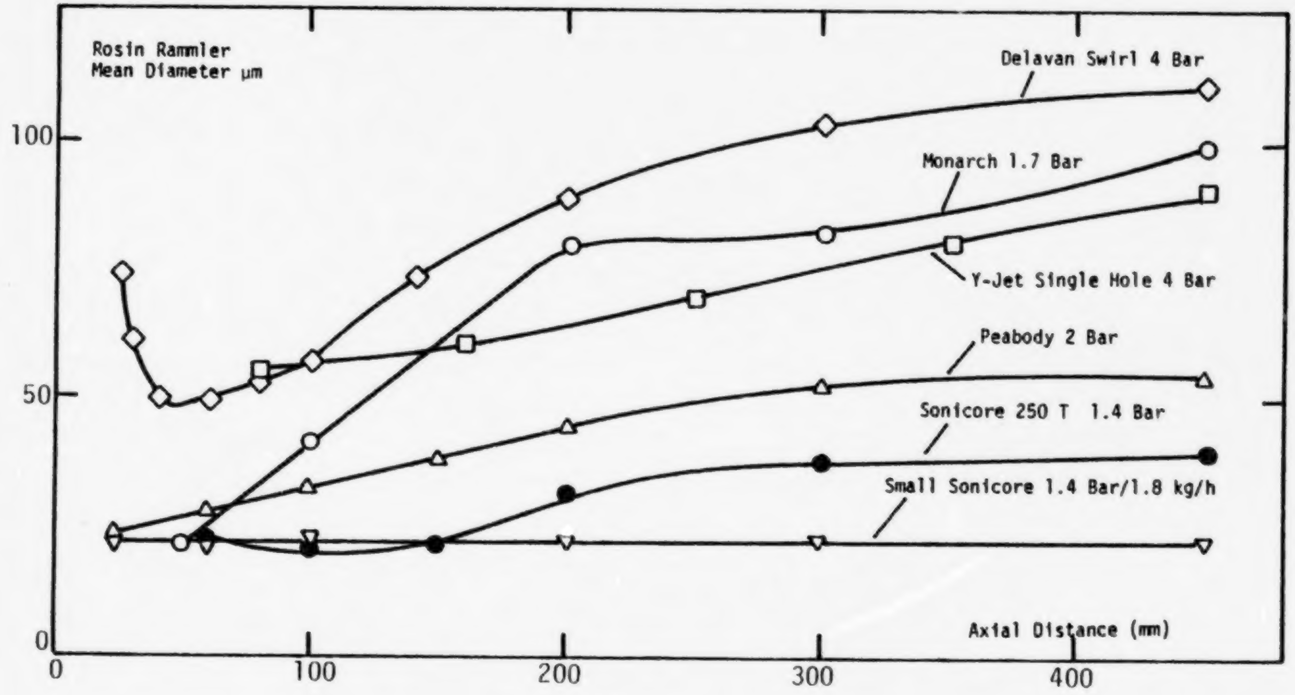

Figure 41. Effect of Axial Distance on Measured Rosin Rammler Mean Diameter.

(Todd is similar to Peabody as seen before, and Delevan Siphon is similar to Sonicore), leading to the following remarks:

- in all cases PE increases when axial distance varies from 60 to 450 mm;
- in some cases there is a minimum of PE at about 60 mm and then PE increases again when going closer to the nozzle;
- the effect can be extremely strong; from 20 m to 100 m for the Monarch atomizer;
- the effect is stronger when the spray becomes coarser. This was already noticed for each atomizer considered individually, and remains true when comparing sprays made by different atomizers. The extreme case is the small Sonicore nozzle for which there is absolutely no effect of axial distance on the measurements, and which gives a very fine monosize spray. Also, there were some doubts about the correct value of the exponent W, for some measurements taken close to the nozzle (Section 3.3), the very low values of PE measured in this axial position tends to be connected with rather high value of W, which means that at a short distance of the nozzle the spray is seen fine and monosize and this especially when far from the nozzle it is coarse and widely spread. Reasons of this strong effect could be:

Problems With the Instrument

a. Basic problem of calibration — The laser technique instrument does not require calibration; however, it has been tested by several authors(2,3,5) in conditions both of monosize flow of calibrated solid particles or with real liquid sprays.

These comparison has shown no specific trend to bias the measurements towards large or small mean diameter.

b. Multiple Scattering — Multiple scattering is a common risk for optical analysis sytems, and the limits of the instrument used for this study were not absolutely established. As the density of the spray is not constant with axial distance due to conical dispersion and velocity effects, the probability of multiple scattering in the laser beam could vary with axial distance and influence the final result. However, there are several indications that the effect of actual distance is not due to multiple scattering.

- First, there is no evidence that multiple scattering occurring in high spray density region - typically close to the nozzle as the central reading indicates - would systematically shift the measured mean diameter towards lower values and Rosin Rammler exponent towards higher values. Recent work has shown that multiple scattering tends to give a wider distribution and has almost no effect on the measured mean diameter(5).
- Second, in three cases (Delevan Swirl for two pressures) and Delevan Siphon (with primary air) the measured mean diameter increases again close to the nozzle, where the density of the spray, estimated by the central reading, is very high. Moreover, the axial distance effect has been measured with half of the spray and with the whole spray in case of Delevan Swirl, and if the absolute values of the measurements were affected (due to multiple scattering or introduction of the laser tube in the spray), the trend of the curve was the same in both cases, while density of the sample was twice with the whole spray.
- Finally, some of the results refer to a very low density spray (100 percent central reading for Delevan Siphon) and give a very strong effect of axial distance, while some other results refer to very high density sprays (Sonicore 250T, 75 kg/h, 1.4 bar) give practically no effect of axial distance.

These remarks show that there is no relationship between spray density, and therefore, the risk of multiple scattering and the influence of axial distance, which leads us to the conclusion that a real physical effect occurs in the spray.

4.4.1 Physical Effects

Physical effects responsible for changes in droplet size distribution with axial distance could be:

a. Evaporation

The preferential evaporation of the smallest droplets could make them disappear from the spray, giving a higher mean diameter.

b. Secondary Atomization and Coalescence

Secondary atomization is possible outside the atomizer, close to the nozzle and some investigators(4) have shown that it does occur in a zone which can extend up to 50 mm from the nozzle. This could be one of the reasons why PE decrease in the first 50 mm of the axial traverse. The following increase could theoretically be due to coalescence of small droplets, but there is no evidence that two small droplets impinging together will systematically give a big one, and moreover, the probability of impingement of droplets becomes very low after a certain distance due to decrease of both density of spray and differences in velocities of droplets. Therefore, changes in droplet size at the axial distances considered are difficult to explain in that way, especially for low density sprays.

c. Velocity Effects

As stated in Section 2.4, conservation of mass flow rate for each size of droplets show that any change in velocity of a packet of droplets of the same size entails a corresponding change in their apparent concentration in the mixture of air and oil which constitutes the spray.

The deceleration rates of the droplets depend upon the ratio between the drag force, porportional to the area (x R^2) and the inertia forces proportional to the volume of droplets (x R^3). Thus, for the same conditions of slipping velocity between air and droplet, the small particles should be very much more influenced by airflow than the big ones.

Thus, if the small droplets are more strongly decelerated in the area close to the nozzle than the big ones, there will be an apparent increase in their population, and this will give a smaller mean diameter. Further downstream the big droplets will be decelerated and the same phenomenon will cause the mean diameter to increase.

These qualitative considerations would confirm the shape of the curve that has been found for the Delevan Swirl Air, which presents a first decrease of PE with axial distance, a minimum at 60 mm, and a further increase.

In order to check this hypothesis, simple calculations were carried out based on the work of I. S. Habib(6).

Figure 42 presents the assumed velocities of air and droplets along the axis of the spray given by Delevan Swirl atomizer working at 4 bar, 75 kg/h of oil. Inside the atomizer the velocity of the oil flow before it is cut by high velocity air is very low; typically 1 to 5 m/s. Considering the atomizing air pressure used (4 bar), the nozzle is choked and an initial velocity of 320 m/s is assumed inside the nozzle at the point of impinging between oil and air. The airflow breaks the oil sheet and droplets are formed and then entrained, due to drag forces, at a certain velocity by the air jet. Outside the atomizer the velocity of the atomizing air decreases due to entrainment of external air (a free jet velocity decay is plotted on the same curve for comparison). The delocity decay of the spray air along the axis is assumed to be even stronger than a free jet because of momentum transfer from the airflow to the liquid droplets.

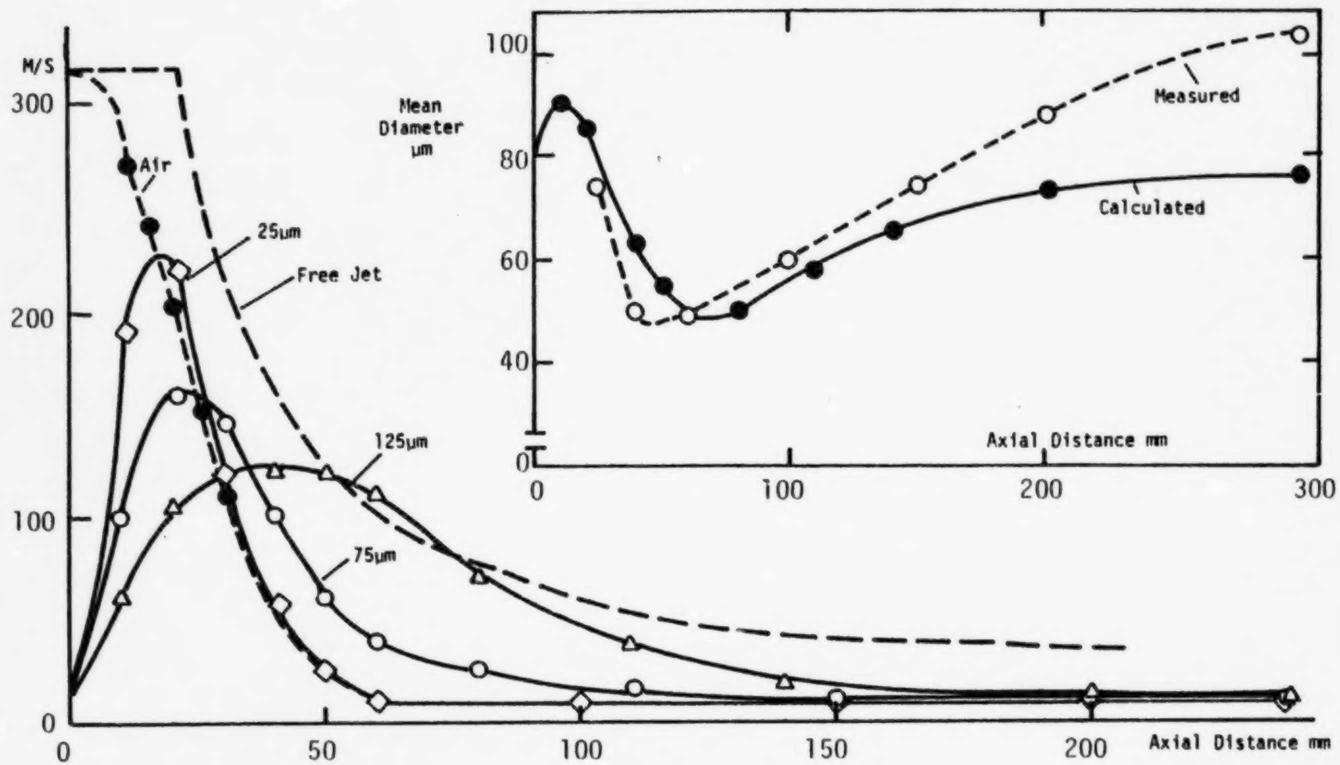

Figure 42. Effect of Axial Distance on Velocity of Droplets and On Measured Mean Diameter.

The small droplets (typical range of 25 μm) are strongly accelerated, due to low inertia, and they quickly reach the local air velocity to follow it further downstream. Meanwhile, the big droplets (75 μm) are less quickly accelerated, and reach a lower maximum velocity, slightly overshooting due to inertia and then are slightly decelerated by the low velocity airflow.

Assuming these velocity variations for three typical sizes of droplets, it is possible to calculate the corresponding variations of concentration of each size of droplets, assuming that the product velocity times concentration remains constant in the spray (Section 2.4), and provided that the spray is uniformly distributed in space and that the velocity decay is the same for all points of the spray (which is not true).

After having determined the weight fraction distribution of the three types of droplets at 60 mm in such a way that the calculated weight diameter is equal to the measured one at this specific point, it is easy to calculate the values of weight fraction distribution upstream and downstream from this point, and to calculate the weight mean diameter variations. The result is shown in the corner and compared with measurements carried out for Delevan Swirl air at 4 bars of air pressure.

The trend of the experimental curve is correctly simulated by this simple calculation. Although the "predicted" distribution does not match exactly that measured for the Delevan atomizer, the results indicate to a first approximation that under certain circumstances significant variations in mean size can be due to velocity effects.

In a real case, it is probable that the deceleration of droplets is strongly influenced by their position in the spray and could be much stronger at the periphery than along the axis, for instance. This could explain why in many instances the minimum value of PE as a function of axial distance is not observed.

4.4.2 Light Energy Distribution

The detailed analysis of the light energy distribution can help to confirm the interpretation of the effect of axial distance presented above. Assuming that the signal (S - B) recorded on a single photo element ring is proportional to the number of droplets N_i of corresponding diameter d_i which are in the spray, it is possible to have a qualitative variations of N_i with axial distance for a range of droplet diameter. This was done on Figures 43 and 44 for seven typical groupings, and corresponds to the spray produced by Delevan Swirl air at 2 bar.

It should be noted that the number of big droplets - from 85 μm to 560 μm - decreases strongly close to the nozzle, probably due to dispersion, and then increases strongly from 100 mm to 500 mm due to deceleration.

In the meantime the number of small droplets increases immediately a after the nozzle, the deceleration effect is stronger than the dispersion effect, but then reach a maximum and decreases from 100 mm to 500 mm.

The droplets which diameter are intermediate (30-50 μm) follows an intermediate curve. It is clear that the velocity effect allows a good interpretation of these curves since evaporation for instance could never lead to an increase of number of big droplets.

4.5 Suitability of the Laser Diffraction Technique for Spray Analysis

The previous discussions have shown the complexity of spray analysis and that a complete understanding of a spray requires more than a droplet size distribution. Particularly, it requires spatial distribution of velocity as a function of droplet size. The laser diffraction technique does not measure velocity, and it is a primary limitation of this technique. Other limitations are:

- density of spray: a typical limit is 100 kg/h of oil flow through the sampled volume;
- detection of very small droplets: the practical limit is 9 μm but it could be improved to 3 μm for special requirements.

However, the laser diffraction technique has some very powerful advantages, which are:

- no disturbance of the spray

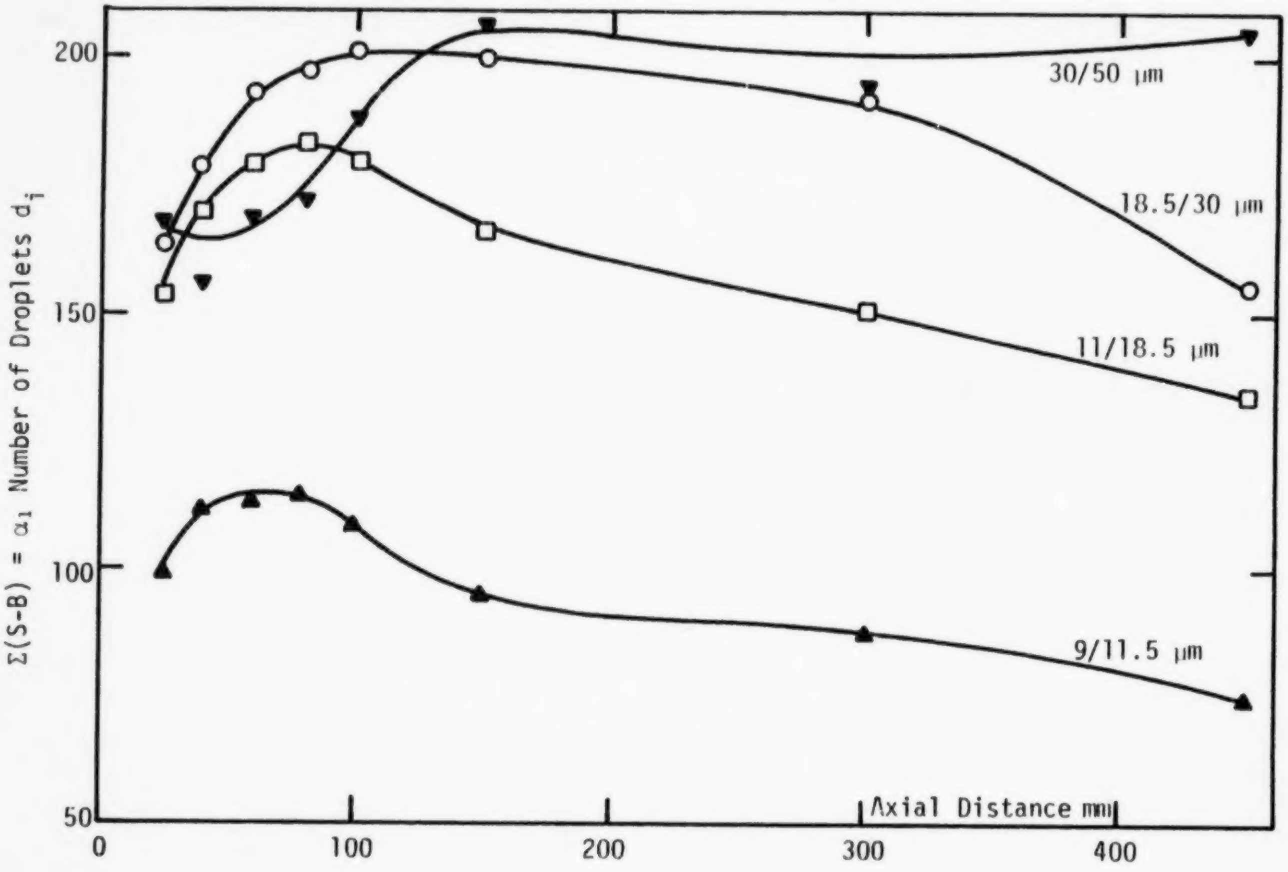

Figure 43. Variation of Light Energy Distribution With Axial Distance.

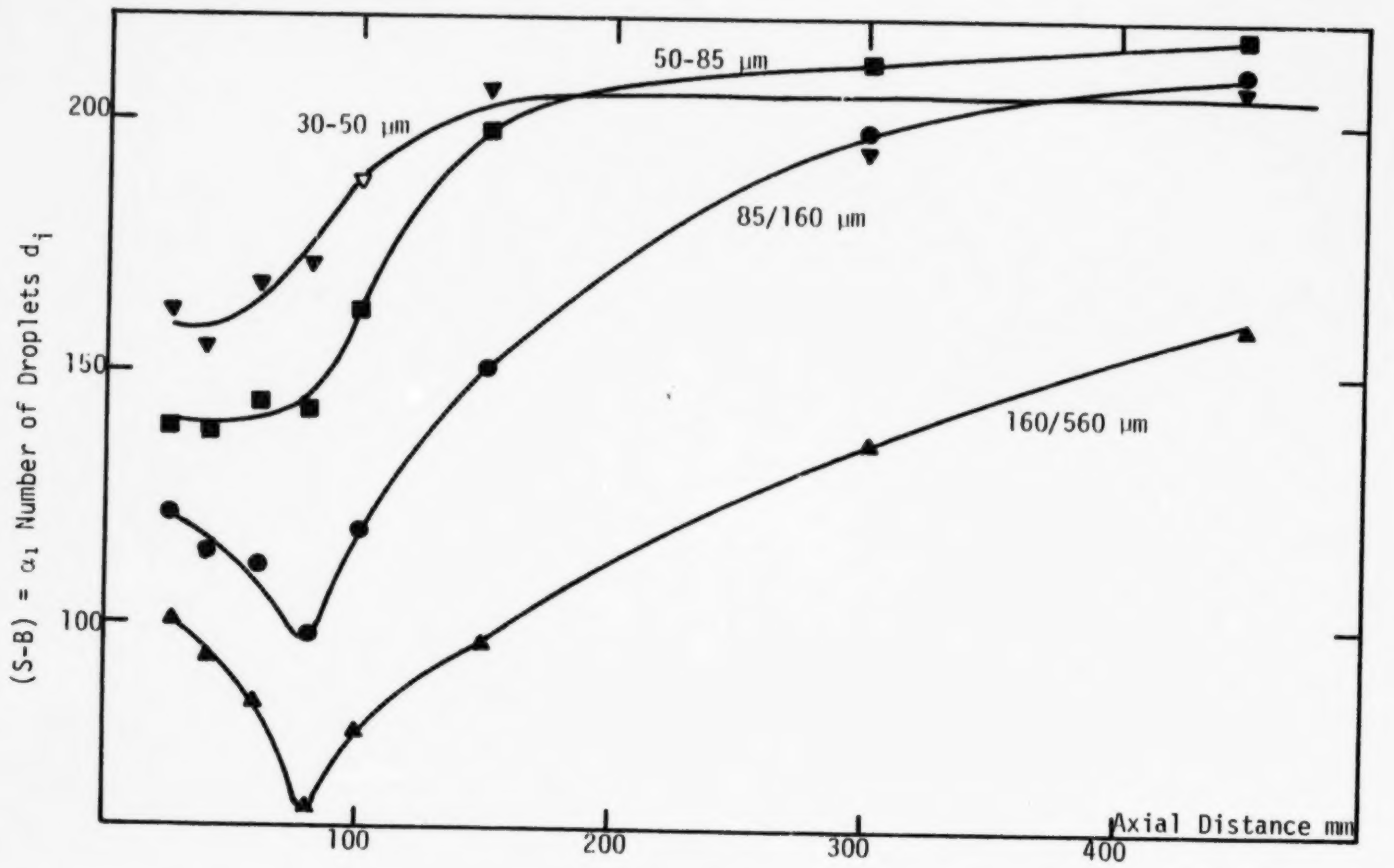

Figure 44. Variation of Light Energy Distribution with Axial Distance.

- extremely fast technique; it gives the droplet size distribution measured across the whole width of a spray very quickly.

In general, this instrument is suitable for two types of study:

1. Practical characterization of atomizers in terms of:
   - influence of atomizing parameters; oil flow, air pressure, oil type, atomizing gas type, etc., on droplet size distribution for a given atomizer;
   - design of new atomizers or improvement of existing atomizers for specific requirements as energy requirement for atomization, pollutant emissions or scaling problems.
2. Fundamental studies about dynamics of spray:
   - A complete understanding of combustion process of oil-fired systems must go through an acquisition of more fundamental knowledge of spray dynamics. The laser technique indirectly indicates some rather complex aerodynamic phenomena occurring in a spray.

5.0 GENERAL CONCLUSIONS

In conclusion, the following points may be drawn from this study:

1. A laser diffraction technique has been used to characterize six different twin fluid atomizers in terms of droplet size distribution of the spray.

   Although this technique is limited, essentially by the spray density due to multiple scattering, it appears that it is a fast accurate and reliable technique for comparative purposes.

2. The measurements taken have shown that droplet size distribution is more dependent on the ratio between the atomizing airflow rate and the oil flow rate, than on atomizer design. When this ratio is increased, the droplet size distribution becomes finer, but also less scattered and can be almost monosize (20 μm). Therefore, almost any droplet size distribution can be reached with a twin fluid atomizer by means of adjusting atomizing air pressure. A more specific property of an atomizer is probably the shape of the spray that it gives.

3. The measured mean diameter is strongly dependent upon the axial distance between the nozzle and the volume of the spray considered for measurements. This is believed to result from very strong aerodynamic effects within the spray, as preferential deceleration of the small droplets close to the nozzle or preferential spatial distribution of droplets, depending on their size.

   This means that a complete characterization of a spray requires spatial distributions under representative conditions of airflow.

REFERENCES

1. Swithenbank, J., J. M. Beér, D. S. Taylor, D. Abbot and G. C. McCreath, "A Laser Diagnostic for the Measurement of Droplet and Particulate Size Distribution", University of Sheffield, Department of Chemical Engineering and Fuel Technology, Report 1976.

2. Azzopardi, B. J. and M. L. Yeoman, "An Assessment of the Malvern Particle Size Distribution Analyzer", Engineering Sciences Division, AERE Harwell, Oxfordshire, June 1977.

3. Jones, A. R., "An Assessment of a Commercial Laser Diffraction System for Measuring Drop Sizes", Memorandum - CEGC - Research Division, Marchwood Engineering Laboratories, October 1977.

4. Mullinger, P. J. and N. A. Chigier, "The Design and Performance of Internal Mixing Multi-Jet Twin Fluid Atomizers", Journal of the Institute of Fuel (251), December 1974.

5. Negus, C and B. J. Azzopardi, "The Malvern Particle Size Distribution Analyzer: Its Accuracy and Limitations", Engineering Sciences Division, AERE Harwell, Oxfordshire, December 1978.

6. Habib, I. S., "The Interaction of a Hot Gas Flow and a Cold Liquid Spray in Channels", Journal of Heat Transfer (pp 421-426), August 1976.

APPENDIX II

LIQUID FUEL CHARACTERISTICS

In order to select the test fuels for this study, it was necessary to first review the trends in liquid fuel usage, the essentials of modern refinery processing, and the analytical characterizations of crude feedstocks. This section of the report summarizes the results of that review.

1.0 TRENDS IN LIQUID FUEL USAGE

The demand for petroleum products has grown rapidly in both volume and complexity over the past 30 years. The most spectacular area of growth has been in the use of aviation fuels where consumption has increased over 30 times from the amount used at the end of World War II. Petroleum products are the major source of energy for transportation, and are the raw materials for many of the products used throughout our economy. The demand for residual fuel oils rose substantially after World War II because of their use as a source of heat for large buildings. The continual increase in the demand for residual fuels is due in part to the fact that nuclear power generation has not developed as rapidly as was originally anticipated, and the use of low sulfur coal has not been able to absorb the increasing demand for electrical energy. During the period from 1946 to 1970, residual fuel oil experienced an overall growth rate of 2.2 percent per year. However, the annual growth for this fuel increased 4.2 percent in 1971, and over 8.9 percent in 1972.

It can be argued that the future fuel usage pattern for boilers (steam or hot water generation) will be:

- Coal - utility and large industrial units with pulverized coal firing in the larger size range and stoker firing predominating in the 50 to 250,000 lb/hr of steam range.
- Residual fuels - industrial boilers generally packaged with firing rates less than 250,000 lb/hr of steam.
- Light distillate - domestic and commercial requirements.

The choice between residual fuels and stoker firing for industrial boilers might well depend upon sulfur regulations, or upon other factors such as coal availability and fuel storage requirements. It should be remembered that there are a large number of installed industrial boilers which will be burning residual fuels for a considerable period of time. Thus, the development of low NO_x burners for residual fuel-fired boilers need not necessarily be restricted to firetube and small watertube designs. Particularly if the design of an optimum burner can be accommodated as a field retrofit.

The term residual fuel oil is used loosely by the oil industry, referring both to the heavy hydrocarbons that comprise a large portion of the natural crude oil barrel and to Nos. 5, 6 and Bunker C residual fuel oil products. Residuum is used to describe that portion of the crude oil barrel left unvaporized at 650^{o}F and normal atmospheric pressures. The terms residual fuel oil, fuel oil and residual are used synonymously to refer to the class of petroleum products sold for use as a boiler fuel. Residual fuels are produced from crude oil by a variety of refinery operations, and in many instances the refinery operates to maximize production of a particular product. However, in general, the products which dictate refinery design are relatively few in number, and the basic refinery processes are based on the large quantity products such as gasoline, jet fuel and diesel fuel. Storage and waste disposal are expensive, and it is necessary to sell or use all of the items produced from the crude even if some of the materials such as residual fuel oil must be sold at prices less than the cost of the original crude oil. In general, the lowest value of a hydrocarbon product is its heating value or fuel oil equivalent (FOE). This value is always established by location, demand, availability, combustion characteristics, sulfur content, and the price of competing fuels.

2.0 MODERN REFINERY PRACTICE

Knowledge of the physical and chemical properties of the various petroleum products is necessary in order to understand the need for different refinery processing. The products can be classified according to:

1. Low boiling point products. This classification encompasses compounds which are in the gas phase at ambient temperatures

and pressures: methane, ethane, propane, butane and corresponding olefins. These gases may be used as petrochemical feedstocks or sold as LPG.

2. Gasoline. Approximately 40 types of gasolines are manufactured by refineries, although most refiners produce gasoline in two grades, regular and premium. Gasolines are a complex mixture of hydrocarbons having a boiling range from 100 to 400°F as determined by the ASTM method. Components are blended to promote high antiknock quality, ease of starting, quick warm-up, low tendency to vapor lock, and low engine deposits.

3. Distillate Fuels. Distillate fuels can be divided into three types: jet fuels, diesel fuels and heating oils. Commercial jet fuel is a material in the kerosene boiling range, and must be clean burning. The principle distillate fuel oils for heating applications consist of No. 1 and No. 2 fuel oils. The No. 1 oil is very similar to kerosene, but generally has a higher pour point and end point. No. 2 oil is very similar to No. 2 diesel fuel, containing cracked stock and is blended from naptha, kerosene, diesel and cracked-cycle oils. The ASTM specifications for fuel oil are given in Table 1.

4. Residual Fuel Oils. Over 60 percent of the residual fuel oil used in the United States is imported. It is composed of the heaviest parts of the crude and is generally the tower bottoms from vacuum distillation. It sells for a very low price, in many instances less than the price of the crude from which it was produced, and is considered a byproduct. Critical specifications are viscosity (110 SSF at 122°F, max) and sulfur content.

Figure 1 shows the processing sequence in a modern refinery, and indicates the major process flows between operations. The crude oil is heated in a furnace and charged to an atmospheric distillation tower where it is separated into butanes and lighter wet gas, unstabilized full-range gasoline, heavy naptha, kerosene, heavy gas oil, and topped crude. The topped crude is then sent to the vacuum tower and separated into a vacuum gas oil overhead

Table 1. ASTM Fuel Oil Specifications

Grade of Fuel Oil	Flash Point deg. F.	Pour Point deg. F.	Water and Sediment, % by Volume	Carlson Residue on 10% Bottoms %	Ash % by Weight	Distillation Temperature, deg. F.			Saybolt Viscosity, acc				Kinematic Viscosity,				Gravity, deg. A.I.I.	Corrosion Copper Strip, 3 hr. at 1220F
						10% Point	10% Point	End Point	Universal at 100°F		Furol at 122°F		At 100°F		At 122°F			
	Min.	Max.	Max.	Max.	Max.	Max.	Max.	Max.	Max.	Min.	Max.	Min.	Max.	Min.	Max.	Min.	Min.	
No. 1. A distillate oil intended for vaporizing pot-type burners and other burners requiring this grade of fuel	100 or Legal	0	trace	0.15		420		625					2.2	1.4			35	
No. 2. A distillate oil for general-purpose domestic heating in burners not requiring No. 1 fuel oil	100 or Legal	201	0.10	0.35			675		40				(4.3)				26	
No. 4. An oil for burner installations not equipped with preheating facilities	130 or Legal	20	0.50		0.10				125	45			(26.4)	(5.8)				
No. 5. A residual-type oil for burner installations equipped with preheating facilities	130 or Legal		1.00		0.10					150	40			(32.1)	(81)			
No. 6. An oil for use in burners equipped with preheaters permitting a high-viscosity fuel	150		2.00								300	45			(638)	(92)		

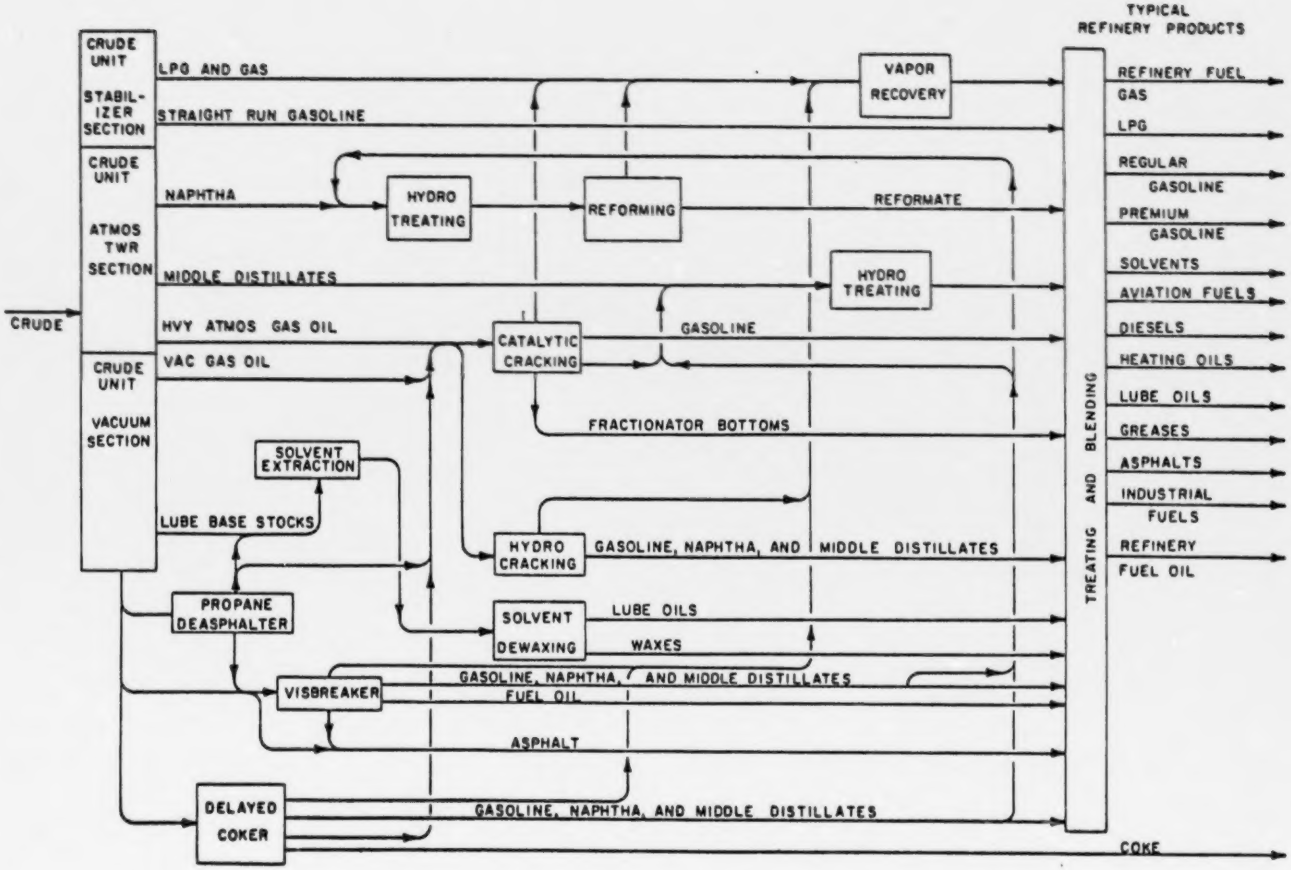
TYPICAL REFINERY PRODUCTS
CRUDE
CRUDE UNIT STABIL-IZER SECTION
CRUDE UNIT ATMOS TWR SECTION
CRUDE UNIT VACUUM SECTION
LPG AND GAS
STRAIGHT RUN GASOLINE
NAPHTHA
MIDDLE DISTILLATES
HVY ATMOS GAS OIL
VAC GAS OIL
LUBE BASE STOCKS
VAPOR RECOVERY
HYDRO TREATING
REFORMING
REFORMATE
HYDRO TREATING
CATALYTIC CRACKING
GASOLINE
FRACTIONATOR BOTTOMS
SOLVENT EXTRACTION
HYDRO CRACKING
GASOLINE, NAPHTHA, AND MIDDLE DISTILLATES
PROPANE DEASPHALTER
SOLVENT DEWAXING
LUBE OILS
WAXES
VISBREAKER
GASOLINE, NAPHTHA, AND MIDDLE DISTILLATES
FUEL OIL
ASPHALT
DELAYED COKER
GASOLINE, NAPHTHA, AND MIDDLE DISTILLATES
TREATING AND BLENDING
REFINERY FUEL GAS
LPG
REGULAR GASOLINE
PREMIUM GASOLINE
SOLVENTS
AVIATION FUELS
DIESELS
HEATING OILS
LUBE OILS
GREASES
ASPHALTS
INDUSTRIAL FUELS
REFINERY FUEL OIL
COKE

Figure 1. Schematic of a Process Sequence in a Modern Refinery

stream and reduced crude bottoms. The reduced crude bottoms from the vacuum tower are thermally cracked in a delayed coker to produce wet gas, coker gasoline, gas oil, and coke.

The atmospheric and vacuum crude unit gas oils and coker gas oil are used as feedstock for the catalytic cracking or hydrocracking units. These units crack the heavy molecules into compounds boiling in the gasoline and distillate fuel ranges. The products from the hydrocracker are saturated. The unsaturated catalytic cracking products are saturated and improved in quality by catalytic reforming or hydrotreating. The gasoline streams from the crude tower, coker, and cracking units are fed to the catalytic reformer to improve their octane numbers. The products from the catalytic reformer are blended into regular and premium gasolines for sale.

The wet gas streams from the crude unit, coker, and cracking units are frationated in the vapor recovery section into fuel gas, LPG, unsaturated hydrocarbons, normal butane, and isobutane. The fuel gas is normally burned in refinery processes and the normal butane is blended into gasoline or LPG. The unsaturated hydrocarbons and isobutane are sent to the alkylation unit for processing. This unit uses either sulfuric or hydrofluoric acid as catalyst to react olefins with isobutane to form isoparaffins boiling in the gasoline range. The product is called alkylate, and is a high-octane product blended into premium motor gasoline and aviation gasoline.

The middle distillates from the crude, coker, and cracking units are blended into diesel and jet fuels and furnace oils. In certain refineries the heavy vacuum gas oil and reduced crude from paraffinic or naphthenic base crude oils are processed into lubricating oils. After removing the asphaltenes in a propane deasphalting unit, the reduced crude bottoms are processed in a blocked operation with the heavy vacuum gas oils to produce lube-oil base stocks. The vacuum gas oils and deasphalted stocks are first solvent-extracted to remove the heavy aromatic compounds and then dewaxed to improve the pour point. They are then treated with special clays to improve their color and stability before being blended into lubricating oils.

Each refinery has its own unique processing scheme which is determined by the equipment availability, operating costs, and product demand. The optimum flow pattern for any refinery is dictated by economic considerations and no two refineries are identical in their operations. Although the Alaska pipeline will soon begin delivering crude, Western U. S. refineries cannot handle the entire flow, basically because the refineries were not constructed to deal with a sour crude. Traditionally, West Coast refiners concentrated on the light end of the barrel to optimize gasoline production, and in many instances the basic feed is a low sulfur (less than 0.3 percent) crude, whereas the North Slope crude has both a high sulfur (greater than 1 percent) and a high gravity. Refineries quite often use a blend of different crudes. As an example, ARCO's refinery at Cherry Point, Washington normally uses a blend of 18 different crudes.

3.0 FUEL OIL CHARACTERIZATION

Crude oils are physical mixtures of hydrocarbons ranging from light, short chain hydrocarbons such as LPG to moderate weight hydrocarbons such as gas oils and to long chain hydrocarbons such as residual fuel oil and waxes. The proportionate yield of each of these hydrocarbons, as well as the overall quantities of sulfur and metal contents, vary widely among crudes. Except for analysis of low boiling point compounds, no attempt is made by the refiner to analyze for all the pure components contained in crude oil. Relatively simple analytical tests are carried out on the crude, and the results of these are used with empirical correlations to evaluate the crude oils as feedstocks for a particular refinery. The more useful of these crude properties are:

1. Gravity, $^{\circ}$API. The density of petroleum oils is expressed in terms of API gravity rather than specific gravity. It is related to specific gravity in such a fashion that an increase in API gravity corresponds to a decrease in specific gravity. The units of API gravity are $^{\circ}$API and can be calculated from specific gravity by the following:

$$^{\circ}\mathrm{API} = \frac{(141.5)}{\mathrm{sp\ gr}} - 131.5$$

Both specific gravity and API gravity refer to the weight per unit volume at 60°F. Crude oil gravity may range from less than 10° API to over 50° API, but most crudes fall in the 20 to 45° API range.

2. Sulfur Content. Sulfur content and the API gravity are the two properties which have the greatest influence on the vaue of crude oil. Crudes with greater than 0.5 percent sulfur generally require more extensive processing than those with lower sulfur content. The term "sour" crude has come to mean any crude oil with a sulfur content high enough to require special processing. There is no sharp division between sour and sweet crudes, but 0.5 percent sulfur content is frequently used as the criterion.

3. Pour Point. Pour point in °F gives a rough indication of the relative paraffinicity and aromaticity of the crude. The lower the pour point, the power the paraffin content, and the greater the content of aromatics.

4. Carbon Residue. Carbon residue is determined by distillation to a coke residue in the absence of air, and is roughly related to the asphalt content of the crude and the quantity of the lubricating oil fraction that can be recovered. In general, the lower the carbon residue, the more valuable the crude.

5. Salt Content. If the salt content exceeds 10 lb/1,000 bbl of crude where the salt is expressed as NaCl, then it will be necessary to desalt the crude before processing.

6. Nitrogen Content. A high nitrogen content in the crude is undesirable becasue organic nitrogen compounds cause severe poisoning of catalysts used in processing, and crudes which contain greater than 0.25 percent by weight require special processing to remove the nitrogen.

7. Distillation Range. The boiling range of the crude gives an indication of the quantities of various products present.

8. Metals Content. The metals content of crude oils can vary from a few parts per million to more than 1,000 ppm, and in spite of their relatively low concentrations, are of considerable importance. Minute quantities of some metals (nickel, vanadium and copper) can severely affect the activities of catalysts and result in lower-value product distribution. Vanadium concentrations above 2 ppm in fuel oil can lead to severe corrosion problems and deterioration of refractory furnace lining.

Quantities of several domestic and foreign crudes are given in Table 2. In general, domestic crudes are light, yield relatively low percentages of residuum, and have low sulfur contents. Californian and Alaskan crudes are exceptions to this. Major foreign crudes from the Persian Gulf are fairly heavy and aften high in sulfur. African, Canadian and Indonesian crudes are generally sweeter and lighter. The average sulfur content of the crude refined in the U. S. will tend to increase as U. S. crude imports increase, and sulfur removal for sulfur-sensitive products will become more important. Reclassification of fireign crudes by ease of residual hydrodesulfurization, a function of nickel, vanadium and asphaltene content, yields the ranking given in Table 3.

Figure 2 shows typical API gravity residuum yield and sulfur content of 20 crudes which are currently used or expected to become important in U. S. refineries in the near future. The crudes are ranged from left to right in order of decreasing gravity, and as the gravity decreases, the average residuum yield increases and the sulfur content generally increases. Similar trends are shown in Figure 3 for average values of asphaltene content and te sum of nickel and vanadium content.

Table 2. Characteristic and Residuum Fractions (650^{0}+F) of Typical Crude Oils

	Crude Oil Specific Gravity °API	Residuum Yield (650° +F), % Liquid Volume	Crude Oil Sulfur Content, % Weight
Domestic Crude Oils			
Texas Sweet Mix	35.4	20.0	0.20
West Texas Sour	33.4	31.9	1.63
Louisiana	36.2	38.1	0.22
Oklahoma	40.2	38.3	0.21
Alaskan North Slope	27.5	53.0	0.96
California Ventura	29.7	47.6	1.56
California Wilmington	19.6	64.5	1.28
Foreign Crude Oils			
Arabian Light	34.5	43.2	1.70
Arabian Heavy	28.2	63.0	2.80
Kuwait	31.5	58.9	2.50
Nigerian Forcados	29.4	38.9	0.21
Algerian Hassi Messaoud	44.7	27.7	0.13
Iranian Light	33.9	41.0	1.40
Iranian Heavy	31.0	50.0	1.60
Lybian Amna	35.9	48.0	0.20
Lybian Brega	40.4	32.0	0.20
Indonesian Minas	35.3	59.0	0.07
Venezuelan Bachaquero	17.0	58.8	2.44
Venezuelan Tia Juana	26.3	57.8	1.51
Canadian Mixed	39.0	36.2	0.55

Table 3. Characteristics of Crude Oil Residuums Related to Ease of Catalytic Hydrodesulfurization

Ease of Desulfurization	Crude Quality	Example Crude
I. Can be desulfurized directly	Low metals, low asphaltenes	Arabian Light Kuwait Qatar
II. Can be desulfurized directly at a higher catalyst cost than I.	Moderate metals, low asphaltenes	Iranian Light Iraqi Kirkuk
III. Can be desulfurized directly, at a process severity and/or final sulfur level that is considerably higher than I.	Moderate metals, high asphaltenes	Arabian Heavy Arabian Khafji
IV. Direct processing lowers catalyst life substantially; judged uneconomical to desulfurize.	High metals, high asphaltenes	Iranian Heavy Venezuelan Tia Juana Venezuelan Bachaquero

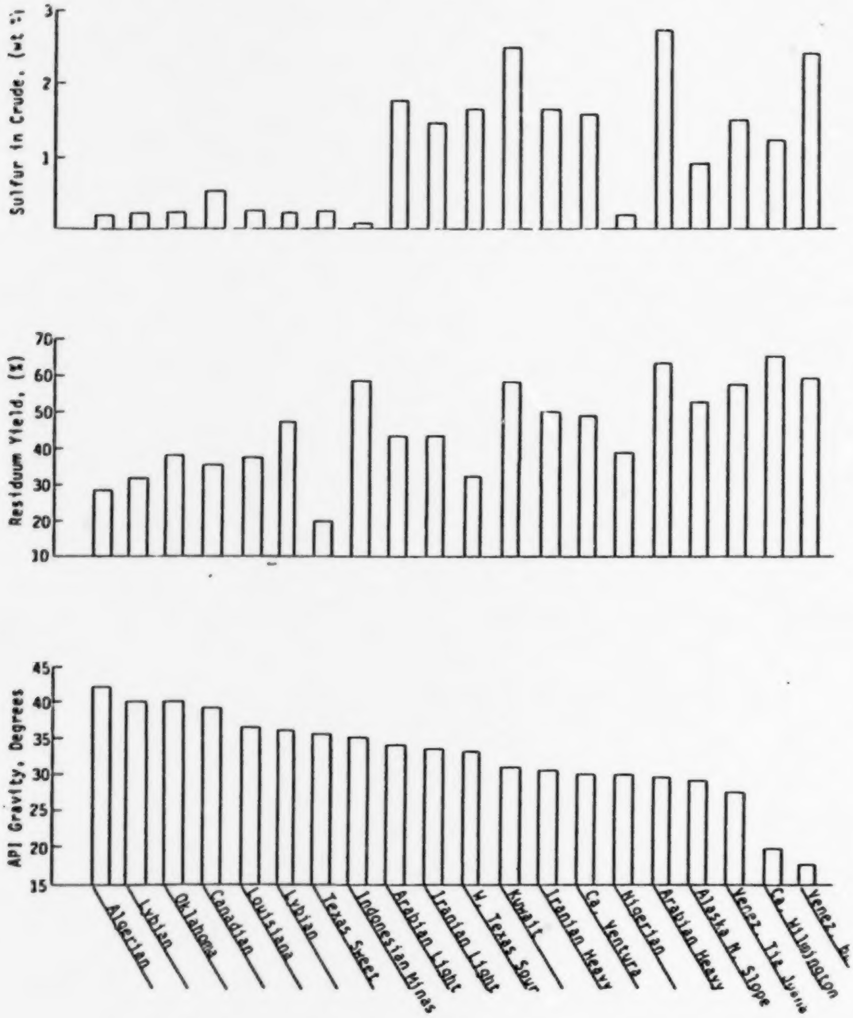

Figure 2. API Gravity, Residuum Yield, and Sulfur Content of Twenty Major Crudes

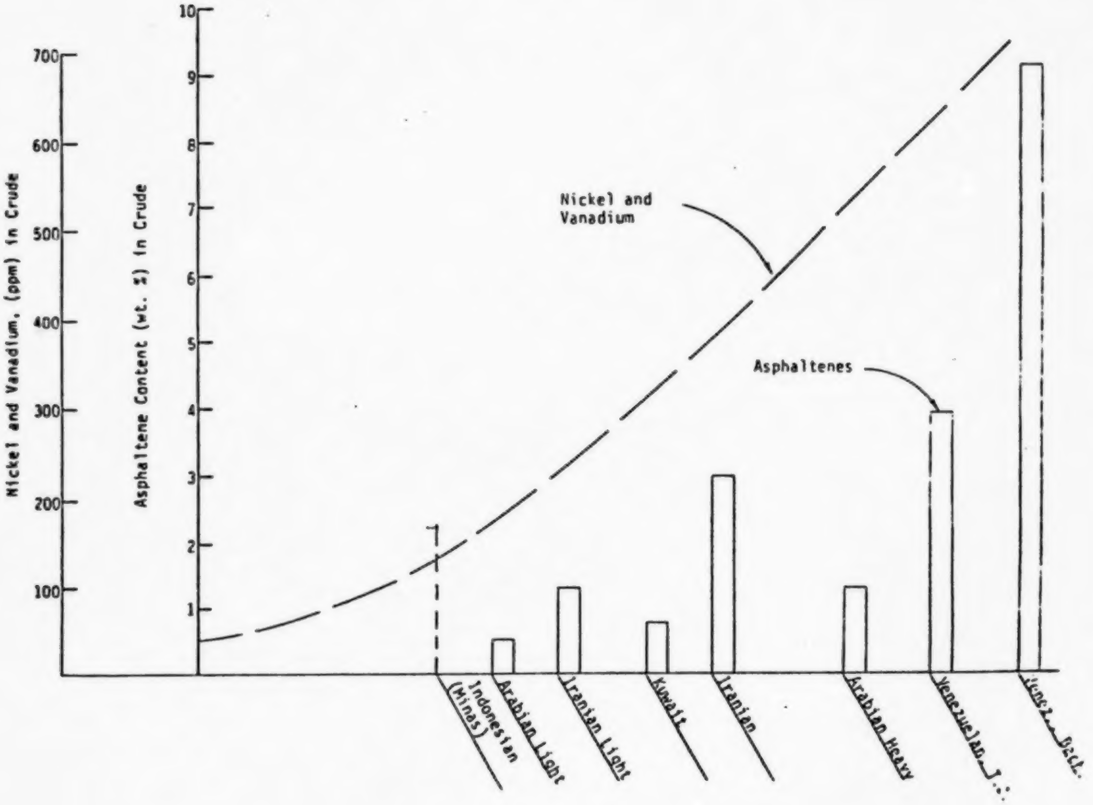

Figure 3. The Variation of Asphaltene Content and the Sum of Nickel and Vanadium Content for Crudes of Varying API Gravities